UNIVERSITY OF BIRMINGHAM
University of Birmingham Research at Birmingham

Electroweak Measurements in Electron-Positron Collisions at W-Boson-Pair Energies at LEP

The OPAL Collaboration; ALEPH Collaboration; DELPHI Collaboration; L3 Collaboration; LEP Electroweak Working Group

DOI:
10.1016/j.physrep.2013.07.004

Citation for published version (Harvard):
The OPAL Collaboration, ALEPH Collaboration, DELPHI Collaboration, L3 Collaboration & LEP Electroweak Working Group 2013, 'Electroweak Measurements in Electron-Positron Collisions at W-Boson-Pair Energies at LEP', *Physics Reports*, vol. 532, pp. 119. https://doi.org/10.1016/j.physrep.2013.07.004

Link to publication on Research at Birmingham portal

General rights
Unless a licence is specified above, all rights (including copyright and moral rights) in this document are retained by the authors and/or the copyright holders. The express permission of the copyright holder must be obtained for any use of this material other than for purposes permitted by law.

•Users may freely distribute the URL that is used to identify this publication.
•Users may download and/or print one copy of the publication from the University of Birmingham research portal for the purpose of private study or non-commercial research.
•User may use extracts from the document in line with the concept of 'fair dealing' under the Copyright, Designs and Patents Act 1988 (?)
•Users may not further distribute the material nor use it for the purposes of commercial gain.

Where a licence is displayed above, please note the terms and conditions of the licence govern your use of this document.

When citing, please reference the published version.

Take down policy
While the University of Birmingham exercises care and attention in making items available there are rare occasions when an item has been uploaded in error or has been deemed to be commercially or otherwise sensitive.

If you believe that this is the case for this document, please contact UBIRA@lists.bham.ac.uk providing details and we will remove access to the work immediately and investigate.

Download date: 28. Mar. 2024

arXiv:1302.3415v2 [hep-ex] 18 Feb 2013

EUROPEAN ORGANIZATION FOR NUCLEAR RESEARCH

CERN-PH-EP/2013-022
arXiv:1302.3415 [hep-ex]
February 14th, 2013

Electroweak Measurements in Electron-Positron Collisions at W-Boson-Pair Energies at LEP

The ALEPH Collaboration
The DELPHI Collaboration
The L3 Collaboration
The OPAL Collaboration
The LEP Electroweak Working Group[1]

Submitted to PHYSICS REPORTS

February 14th, 2013

[1] Web access at `http://www.cern.ch/LEPEWWG`

Abstract

Electroweak measurements performed with data taken at the electron-positron collider LEP at CERN from 1995 to 2000 are reported. The combined data set considered in this report corresponds to a total luminosity of about 3 fb^{-1} collected by the four LEP experiments ALEPH, DELPHI, L3 and OPAL, at centre-of-mass energies ranging from 130 GeV to 209 GeV.

Combining the published results of the four LEP experiments, the measurements include total and differential cross-sections in photon-pair, fermion-pair and four-fermion production, the latter resulting from both double-resonant WW and ZZ production as well as singly resonant production. Total and differential cross-sections are measured precisely, providing a stringent test of the Standard Model at centre-of-mass energies never explored before in electron-positron collisions. Final-state interaction effects in four-fermion production, such as those arising from colour reconnection and Bose-Einstein correlations between the two W decay systems arising in WW production, are searched for and upper limits on the strength of possible effects are obtained. The data are used to determine fundamental properties of the W boson and the electroweak theory. Among others, the mass and width of the W boson, m_{W} and Γ_{W}, the branching fraction of W decays to hadrons, $B(W \to \mathrm{had})$, and the trilinear gauge-boson self-couplings g_1^Z, κ_γ and λ_γ are determined to be:

$$
\begin{aligned}
m_{\mathrm{W}} &= 80.376 \pm 0.033 \text{ GeV} \\
\Gamma_{\mathrm{W}} &= 2.195 \pm 0.083 \text{ GeV} \\
B(W \to \mathrm{had}) &= 67.41 \pm 0.27 \text{ \%} \\
g_1^Z &= 0.984^{+0.018}_{-0.020} \\
\kappa_\gamma &= 0.982 \pm 0.042 \\
\lambda_\gamma &= -0.022 \pm 0.019 \,.
\end{aligned}
$$

Keywords: Electron-positron physics, electroweak interactions, decays of heavy intermediate gauge bosons, fermion-antifermion production, precision measurements at W-pair energies, tests of the Standard Model, radiative corrections, effective coupling constants, neutral weak current, Z boson, W boson, top quark, Higgs boson.

PACS: 12.15.-y, 13.38.-b, 13.66.-a, 14.60.-z, 14.65.-q, 14.70.-e, 14.80.-j.

Author Lists

The ALEPH, DELPHI, L3, OPAL collaborations have provided the inputs for the combined results presented in this Report. The LEP Electroweak Working Group has performed the combinations. The Working Group consists of members of the four LEP collaborations. The lists of authors from the collaborations follow.

The ALEPH Collaboration

S. Schael,[1] R. Barate,[2] R. Brunelière,[2] D. Buskulic,[2] I. De Bonis,[2] D. Decamp,[2] P. Ghez,[2] C. Goy,[2] S. Jézéquel,[2] J.-P. Lees,[2] A. Lucotte,[2] F. Martin,[2] E. Merle,[2] M.-N. Minard,[2] J.-Y. Nief,[2] P. Odier,[2] B. Pietrzyk,[2] B. Trocmé,[2] S. Bravo,[3] M.P. Casado,[3] M. Chmeissani,[3] P. Comas,[3] J.M. Crespo,[3] E. Fernandez,[3] M. Fernandez-Bosman,[3] Ll. Garrido,[3,a15] E. Grauges,[3] A. Juste,[3] M. Martinez,[3] G. Merino,[3] R. Miquel,[3] Ll.M. Mir,[3] S. Orteu,[3] A. Pacheco,[3] I.C. Park,[3] J. Perlas,[3] I. Riu,[3] H. Ruiz,[3] F. Sanchez,[3] A. Colaleo,[4] D. Creanza,[4] N. De Filippis,[4] M. de Palma,[4] G. Iaselli,[4] G. Maggi,[4] M. Maggi,[4] S. Nuzzo,[4] A. Ranieri,[4] G. Raso,[4,a24] F. Ruggieri,[4] G. Selvaggi,[4] L. Silvestris,[4] P. Tempesta,[4] A. Tricomi,[4,a3] G. Zito,[4] X. Huang,[5] J. Lin,[5] Q. Ouyang,[5] T. Wang,[5] Y. Xie,[5] R. Xu,[5] S. Xue,[5] J. Zhang,[5] L. Zhang,[5] W. Zhao,[5] D. Abbaneo,[6] A. Bazarko,[6] U. Becker,[6] G. Boix,[6,a33] F. Bird,[6] E. Blucher,[6] B. Bonvicini,[6] P. Bright-Thomas,[6] T. Barklow,[6,a26] O. Buchmüller,[6,a26] M. Cattaneo,[6] F. Cerutti,[6] V. Ciulli,[6] B. Clerbaux,[6,a23] H. Drevermann,[6] R.W. Forty,[6] M. Frank,[6] T.C. Greening,[6] R. Hagelberg,[6] A.W. Halley,[6] F. Gianotti,[6] M. Girone,[6] J.B. Hansen,[6] J. Harvey,[6] R. Jacobsen,[6] D.E. Hutchcroft,[6,a30] P. Janot,[6] B. Jost,[6] J. Knobloch,[6] M. Kado,[6,a2] I. Lehraus,[6] P. Lazeyras,[6] P. Maley,[6] P. Mato,[6] J. May,[6] A. Moutoussi,[6] M. Pepe-Altarelli,[6] F. Ranjard,[6] L. Rolandi,[6] D. Schlatter,[6] B. Schmitt,[6] O. Schneider,[6] W. Tejessy,[6] F. Teubert,[6] I.R. Tomalin,[6] E. Tournefier,[6] R. Veenhof,[6] A. Valassi,[6] W. Wiedenmann,[6] A.E. Wright,[6] Z. Ajaltouni,[7] F. Badaud,[7] G. Chazelle,[7] O. Deschamps,[7] S. Dessagne,[7] A. Falvard,[7,a20] C. Ferdi,[7] D. Fayolle,[7] P. Gay,[7] C. Guicheney,[7] P. Henrard,[7] J. Jousset,[7] B. Michel,[7] S. Monteil,[7] J.C. Montret,[7] D. Pallin,[7] J.M. Pascolo,[7] P. Perret,[7] F. Podlyski,[7] H. Bertelsen,[8] T. Fernley,[8] J.D. Hansen,[8] J.R. Hansen,[8] P.H. Hansen,[8] A.C. Kraan,[8] A. Lindahl,[8] R. Mollerud,[8] B.S. Nilsson,[8] B. Rensch,[8] A. Waananen,[8] G. Daskalakis,[9] A. Kyriakis,[9] C. Markou,[9] E. Simopoulou,[9] I. Siotis,[9] A. Vayaki,[9] K. Zachariadou,[9] A. Blondel,[10,a12] G. Bonneaud,[10] J.-C. Brient,[10] F. Machefert,[10] A. Rougé,[10] M. Rumpf,[10] M. Swynghedauw,[10] R. Tanaka,[10] M. Verderi,[10] H. Videau,[10] V. Ciulli,[11] E. Focardi,[11] G. Parrini,[11] K. Zachariadou,[11] M. Corden,[12] C. Georgiopoulos,[12] A. Antonelli,[13] M. Antonelli,[13] G. Bencivenni,[13] G. Bologna,[13,a34] F. Bossi,[13] P. Campana,[13] G. Capon,[13] F. Cerutti,[13] V. Chiarella,[13] G. Felici,[13] P. Laurelli,[13] G. Mannocchi,[13,a5] G.P. Murtas,[13] L. Passalacqua,[13] P. Picchi,[13] P. Colrain,[14] I. ten Have,[14] I.S. Hughes,[14] J. Kennedy,[14] I.G. Knowles,[14] J.G. Lynch,[14] W.T. Morton,[14] P. Negus,[14] V. O'Shea,[14] C. Raine,[14] P. Reeves,[14] J.M. Scarr,[14] K. Smith,[14] A.S. Thompson,[14] R.M. Turnbull,[14] S. Wasserbaech,[15] O. Buchmüller,[16] R. Cavanaugh,[16,a4] S. Dhamotharan,[16,a21] C. Geweniger,[16] P. Hanke,[16] G. Hansper,[16] V. Hepp,[16] E.E. Kluge,[16]

A. Putzer,[16] J. Sommer,[16] H. Stenzel,[16] K. Tittel,[16] W. Werner,[16] M. Wunsch,[16,a19] R. Beuselinck,[17] D.M. Binnie,[17] W. Cameron,[17] G. Davies,[17] P.J. Dornan,[17] S. Goodsir,[17] N. Marinelli,[17] E.B Martin,[17] J. Nash,[17] J. Nowell,[17] S.A. Rutherford,[17] J.K. Sedgbeer,[17] J.C. Thompson,[17,a14] R. White,[17] M.D. Williams,[17] V.M. Ghete,[18] P. Girtler,[18] E. Kneringer,[18] D. Kuhn,[18] G. Rudolph,[18] E. Bouhova-Thacker,[19] C.K. Bowdery,[19] P.G. Buck,[19] D.P. Clarke,[19] G. Ellis,[19] A.J. Finch,[19] F. Foster,[19] G. Hughes,[19] R.W.L. Jones,[19] N.R. Keemer,[19] M.R. Pearson,[19] N.A. Robertson,[19] T. Sloan,[19] M. Smizanska,[19] S.W. Snow,[19] M.I. Williams,[19] O. van der Aa,[20] C. Delaere,[20,a28] G.Leibenguth,[20,a31] V. Lemaitre,[20,a29] L.A.T. Bauerdick,[21] U. Blumenschein,[21] P. van Gemmeren,[21] I. Giehl,[21] F. Hölldorfer,[21] K. Jakobs,[21] M. Kasemann,[21] F. Kayser,[21] K. Kleinknecht,[21] A.-S. Müller,[21] G. Quast,[21] B. Renk,[21] E. Rohne,[21] H.-G. Sander,[21] S. Schmeling,[21] H. Wachsmuth,[21] R. Wanke,[21] C. Zeitnitz,[21] T. Ziegler,[21] J.J. Aubert,[22] C. Benchouk,[22] A. Bonissent,[22] J. Carr,[22] P. Coyle,[22] C. Curtil,[22] A. Ealet,[22] F. Etienne,[22] D. Fouchez,[22] F. Motsch,[22] P. Payre,[22] D. Rousseau,[22] A. Tilquin,[22] M. Talby,[22] M.Thulasidas,[22] M. Aleppo,[23] M. Antonelli,[23] F. Ragusa,[23] V. Büscher,[24] A. David,[24] H. Dietl,[24,a32] G. Ganis,[24,a27] K. Hüttmann,[24] G. Lütjens,[24] C. Mannert,[24] W. Männer,[24,a32] H.-G. Moser,[24] R. Settles,[24] H. Seywerd,[24] H. Stenzel,[24] M. Villegas,[24] W. Wiedenmann,[24] G. Wolf,[24] P. Azzurri,[25] J. Boucrot,[25] O. Callot,[25] S. Chen,[25] A. Cordier,[25] M. Davier,[25] L. Duflot,[25] J.-F. Grivaz,[25] Ph. Heusse,[25] A. Jacholkowska,[25,a6] F. Le Diberder,[25] J. Lefrançois,[25] A.M. Mutz,[25] M.H. Schune,[25] L. Serin,[25] J.-J. Veillet,[25] I. Videau,[25] D. Zerwas,[25] P. Azzurri,[26] G. Bagliesi,[26] S. Bettarini,[26] T. Boccali,[26] C. Bozzi,[26] G. Calderini,[26] R. Dell'Orso,[26] R. Fantechi,[26] I. Ferrante,[26] F. Fidecaro,[26] L. Foà,[26] A. Giammanco,[26] A. Giassi,[26] A. Gregorio,[26] F. Ligabue,[26] A. Lusiani,[26] P.S. Marrocchesi,[26] A. Messineo,[26] F. Palla,[26] G. Rizzo,[26] G. Sanguinetti,[26] A. Sciabà,[26] G. Sguazzoni,[26] P. Spagnolo,[26] J. Steinberger,[26] R. Tenchini,[26] C. Vannini,[26] A. Venturi,[26] P.G. Verdini,[26] O. Awunor,[27] G.A. Blair,[27] G. Cowan,[27] A. Garcia-Bellido,[27] M.G. Green,[27] T. Medcalf,[27] A. Misiejuk,[27] J.A. Strong,[27] P. Teixeira-Dias,[27] D.R. Botterill,[28] R.W. Clifft,[28] T.R. Edgecock,[28] M. Edwards,[28] S.J. Haywood,[28] P.R. Norton,[28] I.R. Tomalin,[28] J.J. Ward,[28] B. Bloch-Devaux,[29] D. Boumediene,[29] P. Colas,[29] S. Emery,[29] B. Fabbro,[29] W. Kozanecki,[29] E. Lançon,[29] M.-C. Lemaire,[29] E. Locci,[29] P. Perez,[29] J. Rander,[29] J.F. Renardy,[29] A. Roussarie,[29] J.P. Schuller,[29] J. Schwindling,[29] B. Tuchming,[29] B. Vallage,[29] S.N. Black,[30] J.H. Dann,[30] H.Y. Kim,[30] N. Konstantinidis,[30] A.M. Litke,[30] M.A. McNeil,[30] G. Taylor,[30] C.N. Booth,[31] S. Cartwright,[31] F. Combley,[31,a25] P.N. Hodgson,[31] M. Lehto,[31] L.F. Thompson,[31] K. Affholderbach,[32] E. Barberio,[32] A. Böhrer,[32] S. Brandt,[32] H. Burkhardt,[32] E. Feigl,[32] C. Grupen,[32] J. Hess,[32] G. Lutters,[32] H. Meinhard,[32] J. Minguet-Rodriguez,[32] L. Mirabito,[32] A. Misiejuk,[32] E. Neugebauer,[32] A. Ngac,[32] G. Prange,[32] F. Rivera,[32] P. Saraiva,[32] U. Schäfer,[32] U. Sieler,[32] L. Smolik,[32] F. Stephan,[32] H. Trier,[32] M. Apollonio,[33] C. Borean,[33] L. Bosisio,[33] R. Della Marina,[33] G. Giannini,[33] B. Gobbo,[33] G. Musolino,[33] L. Pitis,[33] H. He,[34] H. Kim,[34] J. Putz,[34] J. Rothberg,[34] S.R. Armstrong,[35] L. Bellantoni,[35] K. Berkelman,[35] D. Cinabro,[35] J.S. Conway,[35] K. Cranmer,[35] P. Elmer,[35] Z. Feng,[35] D.P.S. Ferguson,[35] Y. Gao,[35,a13] S. González,[35] J. Grahl,[35] J.L. Harton,[35] O.J. Hayes,[35] H. Hu,[35] S. Jin,[35] R.P. Johnson,[35] J. Kile,[35] P.A. McNamara III,[35] J. Nielsen,[35] W. Orejudos,[35] Y.B. Pan,[35] Y. Saadi,[35] I.J. Scott,[35] V. Sharma,[35] A.M. Walsh,[35] J. Walsh,[35] J. Wear,[35] J.H. von Wimmersperg-Toeller,[35] W. Wiedenmann,[35] J. Wu,[35] S.L. Wu,[35] X. Wu,[35] J.M. Yamartino,[35] G. Zobernig,[35] G. Dissertori.[36]

[1] Physikalisches Institut der RWTH-Aachen, D-52056 Aachen, Germany
[2] Laboratoire de Physique des Particules (LAPP), IN^2P^3-CNRS, F-74019 Annecy-le-Vieux Cedex, France
[3] Institut de Física d'Altes Energies, Universitat Autònoma de Barcelona, E-08193 Bellaterra (Barcelona), Spain[a7]

[4] Dipartimento di Fisica, INFN Sezione di Bari, I-70126 Bari, Italy
[5] Institute of High Energy Physics, Academia Sinica, Beijing, The People's Republic of China[a8]
[6] European Laboratory for Particle Physics (CERN), CH-1211 Geneva 23, Switzerland
[7] Laboratoire de Physique Corpusculaire, Université Blaise Pascal, IN^{2}P^3-CNRS, Clermont-Ferrand, F-63177 Aubière, France
[8] Niels Bohr Institute, 2100 Copenhagen, DK-Denmark[a9]
[9] Nuclear Research Center Demokritos (NRCD), GR-15310 Attiki, Greece
[10] Laoratoire Leprince-Ringuet, Ecole Polytechnique, IN^{2}P^3-CNRS, F-91128 Palaiseau Cedex, France
[11] Dipartimento di Fisica, Università di Firenze, INFN Sezione di Firenze, I-50125 Firenze, Italy
[12] Supercomputer Computations Research Institute, Florida State University, Tallahasee, FL-32306-4052, USA
[13] Laboratori Nazionali dell'INFN (LNF-INFN), I-00044 Frascati, Italy
[14] Department of Physics and Astronomy, University of Glasgow, Glasgow G12 8QQ,United Kingdom[a10]
[15] Utah Valley State College, Orem, UT 84058, U.S.A.
[16] Kirchhoff-Institut für Physik, Universität Heidelberg, D-69120 Heidelberg, Germany[a16]
[17] Department of Physics, Imperial College, London SW7 2BZ, United Kingdom[a10]
[18] Institut für Experimentalphysik, Universität Innsbruck, A-6020 Innsbruck, Austria[a18]
[19] Department of Physics, University of Lancaster, Lancaster LA1 4YB, United Kingdom[a10]
[20] Institut de Physique Nucléaire, Département de Physique, Université Catholique de Louvain, 1348 Louvain-la-Neuve, Belgium
[21] Institut für Physik, Universität Mainz, D-55099 Mainz, Germany[a16]
[22] Centre de Physique des Particules de Marseille, Univ Méditerranée, IN^{2}P^3-CNRS, F-13288 Marseille, France
[23] Dipartimento di Fisica, Università di Milano e INFN Sezione di Milano, I-20133 Milano, Italy.
[24] Max-Planck-Institut für Physik, Werner-Heisenberg-Institut, D-80805 München, Germany[a16]
[25] Laboratoire de l'Accélérateur Linéaire, Université de Paris-Sud, IN^{2}P^3-CNRS, F-91898 Orsay Cedex, France
[26] Dipartimento di Fisica dell'Università, INFN Sezione di Pisa, e Scuola Normale Superiore, I-56010 Pisa, Italy
[27] Department of Physics, Royal Holloway & Bedford New College, University of London, Egham, Surrey TW20 OEX, United Kingdom[a10]
[28] Particle Physics Dept., Rutherford Appleton Laboratory, Chilton, Didcot, Oxon OX11 OQX, United Kingdom[a10]
[29] CEA, DAPNIA/Service de Physique des Particules, CE-Saclay, F-91191 Gif-sur-Yvette Cedex, France[a17]
[30] Institute for Particle Physics, University of California at Santa Cruz, Santa Cruz, CA 95064, USA[a22]
[31] Department of Physics, University of Sheffield, Sheffield S3 7RH, United Kingdom[a10]
[32] Fachbereich Physik, Universität Siegen, D-57068 Siegen, Germany[a16]

[33] Dipartimento di Fisica, Università di Trieste e INFN Sezione di Trieste, I-34127 Trieste, Italy
[34] Experimental Elementary Particle Physics, University of Washington, Seattle, WA 98195 U.S.A.
[35] Department of Physics, University of Wisconsin, Madison, WI 53706, USA[a11]
[36] Institute for Particle Physics, ETH Hönggerberg, 8093 Zürich, Switzerland.

[a1] Also at CERN, 1211 Geneva 23, Switzerland.
[a2] Now at Fermilab, PO Box 500, MS 352, Batavia, IL 60510, USA
[a3] Also at Dipartimento di Fisica di Catania and INFN Sezione di Catania, 95129 Catania, Italy.
[a4] Now at University of Florida, Department of Physics, Gainesville, Florida 32611-8440, USA
[a5] Also IFSI sezione di Torino, INAF, Italy.
[a6] Also at Groupe d'Astroparticules de Montpellier, Université de Montpellier II, 34095, Montpellier, France.
[a7] Supported by CICYT, Spain.
[a8] Supported by the National Science Foundation of China.
[a9] Supported by the Danish Natural Science Research Council.
[a10] Supported by the UK Particle Physics and Astronomy Research Council.
[a11] Supported by the US Department of Energy, grant DE-FG0295-ER40896.
[a12] Now at Departement de Physique Corpusculaire, Université de Genève, 1211 Genève 4, Switzerland.
[a13] Also at Department of Physics, Tsinghua University, Beijing, The People's Republic of China.
[a14] Supported by the Leverhulme Trust.
[a15] Permanent address: Universitat de Barcelona, 08208 Barcelona, Spain.
[a16] Supported by Bundesministerium für Bildung und Forschung, Germany.
[a17] Supported by the Direction des Sciences de la Matière, C.E.A.
[a18] Supported by the Austrian Ministry for Science and Transport.
[a19] Now at SAP AG, 69185 Walldorf, Germany
[a20] Now at Groupe d' Astroparticules de Montpellier, Université de Montpellier II, 34095 Montpellier, France.
[a21] Now at BNP Paribas, 60325 Frankfurt am Mainz, Germany
[a22] Supported by the US Department of Energy, grant DE-FG03-92ER40689.
[a23] Now at Institut Inter-universitaire des hautes Energies (IIHE), CP 230, Université Libre de Bruxelles, 1050 Bruxelles, Belgique
[a24] Now at Dipartimento di Fisica e Tecnologie Relative, Università di Palermo, Palermo, Italy.
[a25] Deceased.
[a26] Now at SLAC, Stanford, CA 94309, U.S.A
[a27] Now at CERN, 1211 Geneva 23, Switzerland
[a28] Research Fellow of the Belgium FNRS
[a29] Research Associate of the Belgium FNRS
[a30] Now at Liverpool University, Liverpool L69 7ZE, United Kingdom
[a31] Supported by the Federal Office for Scientific, Technical and Cultural Affairs through the Interuniversity Attraction Pole P5/27

[a32] Now at Henryk Niewodniczanski Institute of Nuclear Physics, Polish Academy of Sciences, Cracow, Poland

[a33] Supported by the Commission of the European Communities, contract ERBFMBICT982894

[a34] Also Istituto di Fisica Generale, Università di Torino, 10125 Torino, Italy

The DELPHI Collaboration

J. Abdallah,[27] P. Abreu,[24] W. Adam,[56] P. Adzic,[13] T. Albrecht,[19] R. Alemany-Fernandez,[10] T. Allmendinger,[19] P.P. Allport,[25] U. Amaldi,[31] N. Amapane,[49] S. Amato,[53] E. Anashkin,[38] A. Andreazza,[30] S. Andringa,[24] N. Anjos,[24] P. Antilogus,[27] W-D. Apel,[19] Y. Arnoud,[16] S. Ask,[10] B. Asman,[48] J.E. Augustin,[27] A. Augustinus,[10] P. Baillon,[10] A. Ballestrero,[50] P. Bambade,[22] R. Barbier,[29] D. Bardin,[18] G.J. Barker,[58] A. Baroncelli,[41] M. Battaglia,[10] M. Baubillier,[27] K-H. Becks,[59] M. Begalli,[8] A. Behrmann,[59] K. Belous,[44] E. Ben-Haim,[27] N. Benekos,[34] A. Benvenuti,[6] C. Berat,[16] M. Berggren,[27] L. Berntzon,[48] D. Bertrand,[3] M. Besancon,[42] N. Besson,[42] D. Bloch,[11] M. Blom,[33] M. Bluj,[57] M. Bonesini,[31] M. Boonekamp,[42] P.S.L. Booth†,[25] G. Borisov,[23] O. Botner,[54] B. Bouquet,[22] T.J.V. Bowcock,[25] I. Boyko,[18] M. Bracko,[45] R. Brenner,[54] E. Brodet,[37] P. Bruckman,[20] J.M. Brunet,[9] L. Bugge,[35] B. Buschbeck,[56] P. Buschmann,[59] M. Calvi,[31] T. Camporesi,[10] V. Canale,[40] F. Carena,[10] N. Castro,[24] F. Cavallo,[6] M. Chapkin,[44] Ph. Charpentier,[10] P. Checchia,[38] R. Chierici,[29] P. Chliapnikov,[44] J. Chudoba,[14] K. Cieslik,[20] P. Collins,[10] R. Contri,[15] G. Cosme,[22] F. Cossutti,[51] M.J. Costa,[55] B. Crawley,[1] D. Crennell,[39] J. Cuevas,[36] J. D'Hondt,[3] J. Dalmau,[48] T. da Silva,[53] W. Da Silva,[27] G. Della Ricca,[51] A. De Angelis,[52] W. De Boer,[19] C. De Clercq,[3] B. De Lotto,[52] N. De Maria,[49] A. De Min,[38] L. de Paula,[53] L. Di Ciaccio,[40] A. Di Simone,[40] K. Doroba,[57] J. Drees,[59] M. Dris,[34] A. Duperrin,[29] G. Eigen,[5] T. Ekelof,[54] M. Ellert,[54] M. Elsing,[10] M.C. Espirito Santo,[24] G. Fanourakis,[13] D. Fassouliotis,[13,4] M. Feindt,[19] J. Fernandez,[43] A. Ferrer,[55] F. Ferro,[15] U. Flagmeyer,[59] H. Foeth,[10] E. Fokitis,[34] F. Fulda-Quenzer,[22] J. Fuster,[55] M. Gandelman,[53] C. Garcia,[55] Ph. Gavillet,[10] E. Gazis,[34] D. Gele,[11] R. Gokieli†,[57] B. Golob,[45,47] G. Gomez-Ceballos,[43] P. Gonçalves,[24] E. Graziani,[41] G. Grosdidier,[22] K. Grzelak,[57] J. Guy,[39] C. Haag,[19] A. Hallgren,[54] K. Hamacher,[59] K. Hamilton,[37] S. Haug,[35] F. Hauler,[19] V. Hedberg,[28] M. Hennecke,[19] H. Herr†,[10] J. Hoffman,[57] S-O. Holmgren,[48] P.J. Holt,[10] M.A. Houlden,[25] K. Hultqvist,[48] J.N. Jackson,[25] G. Jarlskog,[28] P. Jarry,[42] D. Jeans,[37] E.K. Johansson,[48] P.D. Johansson,[48] P. Jonsson,[29] C. Joram,[10] L. Jungermann,[19] F. Kapusta,[27] S. Katsanevas,[29] E. Katsoufis,[34] G. Kernel,[45] B.P. Kersevan,[45,47] U. Kerzel,[19] A. Kiiskinen,[17] B.T. King,[25] N.J. Kjaer,[10] P. Kluit,[33] P. Kokkinias,[13] V. Kostioukhine,[15] C. Kourkoumelis,[4] O. Kouznetsov,[18] Z. Krumstein,[18] M. Kucharczyk,[20] J. Lamsa,[1] G. Leder,[56] F. Ledroit,[16] L. Leinonen,[48] R. Leitner,[32] J. Lemonne,[3] V. Lepeltier†,[22] T. Lesiak,[20] J. Libby,[37] W. Liebig,[59] D. Liko,[56] A. Lipniacka,[5] J.H. Lopes,[53] J.M. Lopez,[36] D. Loukas,[13] P. Lutz,[42] L. Lyons,[37] J. MacNaughton,[56] A. Malek,[59] S. Maltezos,[34] F. Mandl,[56] J. Marco,[43] R. Marco,[43] B. Marechal,[53] M. Margoni,[38] J-C. Marin,[10] C. Mariotti,[10] A. Markou,[13] C. Martinez-Rivero,[43] J. Masik,[14] N. Mastroyiannopoulos,[13] F. Matorras,[43] C. Matteuzzi,[31] F. Mazzucato,[38] M. Mazzucato,[38] R. Mc Nulty,[25] C. Meroni,[30] W.T. Meyer,[1] E. Migliore,[49] W. Mitaroff,[56] U. Mjoernmark,[28] T. Moa,[48] M. Moch,[19] K. Moenig,[12] R. Monge,[15] J. Montenegro,[33] D. Moraes,[53] P. Morettini,[15] U. Mueller,[59] K. Muenich,[59] M. Mulders,[33] L. Mundim,[8] W. Murray,[39] B. Muryn,[21] G. Myatt,[37] T. Myklebust,[35] M. Nassiakou,[13] F. Navarria,[6] K. Nawrocki,[57] S. Nemecek,[14] R. Nicolaidou,[42] V. Nikolaenko,[11] M. Nikolenko,[18,11] A. Oblakowska-Mucha,[21] V. Obraztsov,[44] A. Olshevski,[18] A. Onofre,[24] R. Orava,[17] K. Osterberg,[17] A. Ouraou,[42] A. Oyanguren,[55] M. Paganoni,[31] S. Paiano,[6] J.P. Palacios,[25] H. Palka†,[20] Th.D. Papadopoulou,[34]

L. Pape,[10] C. Parkes,[26] F. Parodi,[15] U. Parzefall,[10] A. Passeri,[41] O. Passon,[59] V. Perepelitsa,[55] A. Perrotta,[6] A. Petrolini,[15] J. Piedra,[43] L. Pieri,[38] F. Pierre†,[42] M. Pimenta,[24] T. Podobnik,[45,47] V. Poireau,[10] M.E. Pol,[7] G. Polok,[20] P. Poropat†,[51] V. Pozdniakov,[18] N. Pukhaeva,[18] A. Pullia,[31] D. Radojicic,[37] J. Rames,[14] L. Ramler,[19] A. Read,[35] P. Rebecchi,[10] J. Rehn,[19] D. Reid,[33] R. Reinhardt,[59] P. Renton,[37] F. Richard,[22] J. Ridky,[14] I. Ripp-Baudot,[11] M. Rivero,[43] D. Rodriguez,[43] A. Romero,[49] P. Ronchese,[38] E. Rosenberg,[1] P. Roudeau,[22] T. Rovelli,[6] V. Ruhlmann-Kleider,[42] D. Ryabtchikov,[44] A. Sadovsky,[18] L. Salmi,[17] J. Salt,[55] C. Sander,[19] A. Savoy-Navarro,[27] U. Schwickerath,[10] A. Segar†,[37] R. Sekulin,[39] M. Siebel,[59] L. Simard,[42] A. Sisakian†,[18] G. Smadja,[29] O. Smirnova,[28] A. Sokolov,[44] A. Sopczak,[23] R. Sosnowski,[57] T. Spassov,[10] M. Stanitzki,[19] A. Stocchi,[22] J. Strauss,[56] B. Stugu,[5] M. Szczekowski,[57] M. Szeptycka,[57] T. Szumlak,[21] T. Tabarelli,[31] A.C. Taffard,[25] F. Tegenfeldt,[54] F. Terranova,[31] J. Thomas,[37] J. Timmermans,[33] L. Tkatchev,[18] M. Tobin,[60] S. Todorovova,[14] B. Tomé,[24] A. Tonazzo,[31] P. Tortosa,[55] P. Travnicek,[14] D. Treille,[10] G. Tristram,[9] M. Trochimczuk,[57] C. Troncon,[30] M-L. Turluer,[42] I.A. Tyapkin,[18] P. Tyapkin,[18] S. Tzamarias,[13] V. Uvarov,[44] G. Valenti,[6] P. Van Dam,[33] J. Van Eldik,[10] A. Van Lysebetten,[3] N. van Remortel,[2] I. Van Vulpen,[33] G. Vegni,[30] F. Veloso,[24] W. Venus,[39] F. Verbeure†,[2] P. Verdier,[29] V. Verzi,[40] D. Vilanova,[42] L. Vitale,[51] V. Vrba,[14] H. Wahlen,[59] A.J. Washbrook,[25] C. Weiser,[19] D. Wicke,[59] J. Wickens,[3] G. Wilkinson,[37] M. Winter,[11] M. Witek,[20] O. Yushchenko,[44] A. Zalewska,[20] P. Zalewski,[57] D. Zavrtanik,[46] V. Zhuravlov,[18] N.I. Zimin,[18] A. Zintchenko,[18] M. Zupan.[13]

[1] Department of Physics and Astronomy, Iowa State University, Ames IA 50011-3160, USA
[2] Physics Department, Universiteit Antwerpen, Universiteitsplein 1, B-2610 Antwerpen, Belgium
[3] IIHE, ULB-VUB, Pleinlaan 2, B-1050 Brussels, Belgium
[4] Physics Laboratory, University of Athens, Solonos Str. 104, GR-10680 Athens, Greece
[5] Department of Physics, University of Bergen, Allégaten 55, NO-5007 Bergen, Norway
[6] Dipartimento di Fisica, Università di Bologna and INFN, Viale C. Berti Pichat 6/2, IT-40127 Bologna, Italy
[7] Centro Brasileiro de Pesquisas Físicas, rua Xavier Sigaud 150, BR-22290 Rio de Janeiro, Brazil
[8] Inst. de Física, Univ. Estadual do Rio de Janeiro, rua São Francisco Xavier 524, Rio de Janeiro, Brazil
[9] Collège de France, Lab. de Physique Corpusculaire, IN2P3-CNRS, FR-75231 Paris Cedex 05, France
[10] CERN, CH-1211 Geneva 23, Switzerland
[11] Institut Pluridisciplinaire Hubert Curien, Université de Strasbourg, IN2P3-CNRS, BP28, FR-67037 Strasbourg Cedex 2, France
[12] Now at DESY-Zeuthen, Platanenallee 6, D-15735 Zeuthen, Germany
[13] Institute of Nuclear Physics, N.C.S.R. Demokritos, P.O. Box 60228, GR-15310 Athens, Greece
[14] FZU, Inst. of Phys. of the C.A.S. High Energy Physics Division, Na Slovance 2, CZ-182 21, Praha 8, Czech Republic
[15] Dipartimento di Fisica, Università di Genova and INFN, Via Dodecaneso 33, IT-16146 Genova, Italy
[16] Laboratoire de Physique Subatomique et de Cosmologie, Université Joseph Fourier Grenoble 1, CNRS/IN2P3, Institut Polytechnique de Grenoble, FR-38026 Grenoble Cedex, France

[17] Helsinki Institute of Physics and Department of Physics, P.O. Box 64, FIN-00014 University of Helsinki, Finland
[18] Joint Institute for Nuclear Research, Dubna, Head Post Office, P.O. Box 79, RU-101 000 Moscow, Russian Federation
[19] Institut für Experimentelle Kernphysik, Universität Karlsruhe, Postfach 6980, DE-76128 Karlsruhe, Germany
[20] Institute of Nuclear Physics PAN,Ul. Radzikowskiego 152, PL-31142 Krakow, Poland
[21] Faculty of Physics and Nuclear Techniques, University of Mining and Metallurgy, PL-30055 Krakow, Poland
[22] LAL, Univ Paris-Sud, CNRS/IN2P3, Orsay, France
[23] School of Physics and Chemistry, University of Lancaster, Lancaster LA1 4YB, UK
[24] LIP, IST, FCUL - Av. Elias Garcia, 14-1^{o}, PT-1000 Lisboa Codex, Portugal
[25] Department of Physics, University of Liverpool, P.O. Box 147, Liverpool L69 3BX, UK
[26] Dept. of Physics and Astronomy, Kelvin Building, University of Glasgow, Glasgow G12 8QQ, UK
[27] LPNHE, IN2P3-CNRS, Univ. Paris VI et VII, 4 place Jussieu, FR-75252 Paris Cedex 05, France
[28] Department of Physics, University of Lund, Sölvegatan 14, SE-223 63 Lund, Sweden
[29] Université Claude Bernard de Lyon, IPNL, IN2P3-CNRS, FR-69622 Villeurbanne Cedex, France
[30] Dipartimento di Fisica, Università di Milano and INFN-MILANO, Via Celoria 16, IT-20133 Milan, Italy
[31] Dipartimento di Fisica, Univ. di Milano-Bicocca and INFN-MILANO, Piazza della Scienza 3, IT-20126 Milan, Italy
[32] IPNP of MFF, Charles Univ., Areal MFF, V Holesovickach 2, CZ-180 00, Praha 8, Czech Republic
[33] NIKHEF, Postbus 41882, NL-1009 DB Amsterdam, The Netherlands
[34] National Technical University, Physics Department, Zografou Campus, GR-15773 Athens, Greece
[35] Physics Department, University of Oslo, Blindern, NO-0316 Oslo, Norway
[36] Dpto. Fisica, Univ. Oviedo, Avda. Calvo Sotelo s/n, ES-33007 Oviedo, Spain
[37] Department of Physics, University of Oxford, Keble Road, Oxford OX1 3RH, UK
[38] Dipartimento di Fisica, Università di Padova and INFN, Via Marzolo 8, IT-35131 Padua, Italy
[39] Rutherford Appleton Laboratory, Chilton, Didcot OX11 OQX, UK
[40] Dipartimento di Fisica, Università di Roma II and INFN, Tor Vergata, IT-00173 Rome, Italy
[41] Dipartimento di Fisica, Università di Roma III and INFN, Via della Vasca Navale 84, IT-00146 Rome, Italy
[42] DAPNIA/Service de Physique des Particules, CEA-Saclay, FR-91191 Gif-sur-Yvette Cedex, France
[43] Instituto de Fisica de Cantabria (CSIC-UC), Avda. los Castros s/n, ES-39006 Santander, Spain
[44] Institute for high energy physics, 142281 Protvino, Moscow region, Russian Federation
[45] J. Stefan Institute, Jamova 39, SI-1000 Ljubljana, Slovenia
[46] Laboratory for Astroparticle Physics, University of Nova Gorica, Kostanjeviska 16a, SI-5000 Nova Gorica, Slovenia

[47] Department of Physics, University of Ljubljana, SI-1000 Ljubljana, Slovenia
[48] Fysikum, Stockholm University, Box 6730, SE-113 85 Stockholm, Sweden
[49] Dipartimento di Fisica Sperimentale, Università di Torino and INFN, Via P. Giuria 1, IT-10125 Turin, Italy
[50] INFN,Sezione di Torino and Dipartimento di Fisica Teorica, Università di Torino, Via Giuria 1, IT-10125 Turin, Italy
[51] Dipartimento di Fisica, Università di Trieste and INFN, Via A. Valerio 2, IT-34127 Trieste, Italy
[52] Istituto di Fisica, Università di Udine and INFN, IT-33100 Udine, Italy
[53] Univ. Federal do Rio de Janeiro, C.P. 68528 Cidade Univ., Ilha do Fundão BR-21945-970 Rio de Janeiro, Brazil
[54] Department of Radiation Sciences, University of Uppsala, P.O. Box 535, SE-751 21 Uppsala, Sweden
[55] IFIC, Valencia-CSIC, and D.F.A.M.N., U. de Valencia, Avda. Dr. Moliner 50, ES-46100 Burjassot (Valencia), Spain
[56] Institut für Hochenergiephysik, Österr. Akad. d. Wissensch., Nikolsdorfergasse 18, AT-1050 Vienna, Austria
[57] Inst. Nuclear Studies and University of Warsaw, Ul. Hoza 69, PL-00681 Warsaw, Poland
[58] Now at University of Warwick, Coventry CV4 7AL, UK
[59] Fachbereich Physik, University of Wuppertal, Postfach 100 127, DE-42097 Wuppertal, Germany
[60] Now at Physik-Institut der Universität Zürich, Zürich, Switzerland
[†] Deceased

The L3 Collaboration

P.Achard[20] O.Adriani[17] M.Aguilar-Benitez[25] J.Alcaraz[25] G.Alemanni[23] J.Allaby[18] A.Aloisio[29] M.G.Alviggi[29] H.Anderhub[49] V.P.Andreev[6,34] F.Anselmo[8] A.Arefiev[28] T.Azemoon[3] T.Aziz[9] P.Bagnaia[39] A.Bajo[25] G.Baksay[26] L.Baksay[26] S.V.Baldew[2] S.Banerjee[9] Sw.Banerjee[4] A.Barczyk[49,47] R.Barillère[18] P.Bartalini[23] M.Basile[8] N.Batalova[46] R.Battiston[33] A.Bay[23] U.Becker[13] F.Behner[49] L.Bellucci[17] R.Berbeco[3] J.Berdugo[25] P.Berges[13] B.Bertucci[33] B.L.Betev[49] M.Biasini[33] M.Biglietti[29] A.Biland[49] J.J.Blaising[4] S.C.Blyth[35] G.J.Bobbink[2] A.Böhm[1] L.Boldizsar[12] B.Borgia[39] S.Bottai[17] D.Bourilkov[49] M.Bourquin[20] S.Braccini[20] J.G.Branson[41] F.Brochu[4] J.D.Burger[13] W.J.Burger[33] X.D.Cai[13] M.Capell[13] G.Cara Romeo[8] G.Carlino[29] A.Cartacci[17] J.Casaus[25] F.Cavallari[39] N.Cavallo[36] C.Cecchi[33] M.Cerrada[25] M.Chamizo[20] Y.H.Chang[44] M.Chemarin[24] A.Chen[44] G.Chen[7] G.M.Chen[7] H.F.Chen[22] H.S.Chen[7] G.Chiefari[29] L.Cifarelli[40] F.Cindolo[8] I.Clare[13] R.Clare[38] G.Coignet[4] N.Colino[25] S.Costantini[39] B.de la Cruz[25] S.Cucciarelli[33] R.de Asmundis[29] P.Déglon[20] J.Debreczeni[12] A.Degré[4] K.Dehmelt[26] K.Deiters[47] D.della Volpe[29] E.Delmeire[20] P.Denes[37] F.DeNotaristefani[39] A.De Salvo[49] M.Diemoz[39] M.Dierckxsens[2] C.Dionisi[39] M.Dittmar[49] A.Doria[29] M.T.Dova[10,♯] D.Duchesneau[4] M.Duda[1] B.Echenard[20] A.Eline[18] A.El Hage[1] H.El Mamouni[24] A.Engler[35] F.J.Eppling[13] P.Extermann[20] M.A.Falagan[25] S.Falciano[39] A.Favara[32] J.Fay[24] O.Fedin[34] M.Felcini[49] T.Ferguson[35] H.Fesefeldt[1] E.Fiandrini[33] J.H.Field[20] F.Filthaut[31] P.H.Fisher[13] W.Fisher[37] G.Forconi[13] K.Freudenreich[49] C.Furetta[27] Yu.Galaktionov[28,13] S.N.Ganguli[9] P.Garcia-Abia[25] M.Gataullin[32] S.Gentile[39] S.Giagu[39] Z.F.Gong[22] G.Grenier[24] O.Grimm[49] M.W.Gruenewald[16] V.K.Gupta[37] A.Gurtu[9] L.J.Gutay[46] D.Haas[5] D.Hatzifotiadou[8] T.Hebbeker[1] A.Hervé[18] J.Hirschfelder[35] H.Hofer[49] M.Hohlmann[26]

G.Holzner[49] S.R.Hou[44] B.N.Jin[7] P.Jindal[14] L.W.Jones[3] P.de Jong[2] I.Josa-Mutuberría[25] M.Kaur[14] M.N.Kienzle-Focacci[20] J.K.Kim[43] J.Kirkby[18] W.Kittel[31] A.Klimentov[13,28] A.C.König[31] M.Kopal[46] V.Koutsenko[13,28] M.Kräber[49] R.W.Kraemer[35] A.Krüger[48] A.Kunin[13] P.Ladron de Guevara[25] I.Laktineh[24] G.Landi[17] M.Lebeau[18] A.Lebedev[13] P.Lebrun[24] P.Lecomte[49] P.Lecoq[18] P.Le Coultre[49] J.M.Le Goff[18] R.Leiste[48] M.Levtchenko[27] P.Levtchenko[34] C.Li[22] S.Likhoded[48] C.H.Lin[44] W.T.Lin[44] F.L.Linde[2] L.Lista[29] Z.A.Liu[7] W.Lohmann[48] E.Longo[39] Y.S.Lu[7] C.Luci[39] L.Luminari[39] W.Lustermann[49] W.G.Ma[22] L.Malgeri[18] A.Malinin[28] C.Maña[25] J.Mans[37] J.P.Martin[24] F.Marzano[39] K.Mazumdar[9] R.R.McNeil[6] S.Mele[18,29] L.Merola[29] M.Meschini[17] W.J.Metzger[31] A.Mihul[11] H.Milcent[18] G.Mirabelli[39] J.Mnich[1] G.B.Mohanty[9] G.S.Muanza[24] A.J.M.Muijs[2] M.Musy[39] S.Nagy[15] S.Natale[20] M.Napolitano[29] F.Nessi-Tedaldi[49] H.Newman[32] A.Nisati[39] T.Novak[31] H.Nowak[48] R.Ofierzynski[49] G.Organtini[39] I.Pal[46]C.Palomares[25] P.Paolucci[29] R.Paramatti[39] G.Passaleva[17] S.Patricelli[29] T.Paul[10] M.Pauluzzi[33] C.Paus[13] F.Pauss[49] M.Pedace[39] S.Pensotti[27] D.Perret-Gallix[4] D.Piccolo[29] F.Pierella[8] M.Pieri[41] M.Pioppi[33] P.A.Piroué[37] E.Pistolesi[27] V.Plyaskin[28] M.Pohl[20] V.Pojidaev[17] J.Pothier[18] D.Prokofiev[34] G.Rahal-Callot[49] M.A.Rahaman[9] P.Raics[15] N.Raja[9] R.Ramelli[49] P.G.Rancoita[27] R.Ranieri[17] A.Raspereza[48] P.Razis[30] S.Rembeczki[26] D.Ren[49] M.Rescigno[39] S.Reucroft[10] S.Riemann[48] K.Riles[3] B.P.Roe[3] L.Romero[25] A.Rosca[48] C.Rosemann[1] C.Rosenbleck[1] S.Rosier-Lees[4] S.Roth[1] J.A.Rubio[18] G.Ruggiero[17] H.Rykaczewski[49] A.Sakharov[49] S.Saremi[6] S.Sarkar[39] J.Salicio[18] E.Sanchez[25] C.Schäfer[18] V.Schegelsky[34] H.Schopper[21] D.J.Schotanus[31] C.Sciacca[29] L.Servoli[33] S.Shevchenko[32] N.Shivarov[42] V.Shoutko[13] E.Shumilov[28] A.Shvorob[32] D.Son[43] C.Souga[24] P.Spillantini[17] M.Steuer[13] D.P.Stickland[37] B.Stoyanov[42] A.Straessner[20] K.Sudhakar[9] G.Sultanov[42] L.Z.Sun[22] S.Sushkov[1] H.Suter[49] J.D.Swain[10] Z.Szillasi[26,¶] X.W.Tang[7] P.Tarjan[15] L.Tauscher[5] L.Taylor[10] B.Tellili[24] D.Teyssier[24] C.Timmermans[31] S.C.C.Ting[13] S.M.Ting[13] S.C.Tonwar[9] J.Tóth[12] C.Tully[37] K.L.Tung[7] J.Ulbricht[49] E.Valente[39] R.T.Van de Walle[31] R.Vasquez[46] G.Vesztergombi[12] I.Vetlitsky[28] G.Viertel[49] M.Vivargent[4] S.Vlachos[5] I.Vodopianov[26] H.Vogel[35] H.Vogt[48] I.Vorobiev[35,28] A.A.Vorobyov[34] M.Wadhwa[5] Q.Wang[31] X.L.Wang[22] Z.M.Wang[22] M.Weber[18] S.Wynhoff[37,†] L.Xia[32] Z.Z.Xu[22] J.Yamamoto[3] B.Z.Yang[22] C.G.Yang[7] H.J.Yang[3] M.Yang[7] S.C.Yeh[45] An.Zalite[34] Yu.Zalite[34] Z.P.Zhang[22] J.Zhao[22] G.Y.Zhu[7] R.Y.Zhu[32] H.L.Zhuang[7] A.Zichichi[8,18,19] B.Zimmermann[49] M.Zöller[1]

[1] III. Physikalisches Institut, RWTH, D-52056 Aachen, Germany[§]
[2] National Institute for High Energy Physics, NIKHEF, and University of Amsterdam, NL-1009 DB Amsterdam, The Netherlands
[3] University of Michigan, Ann Arbor, MI 48109, USA
[4] Laboratoire d'Annecy-le-Vieux de Physique des Particules, LAPP,IN2P3-CNRS, BP 110, F-74941 Annecy-le-Vieux CEDEX, France
[5] Institute of Physics, University of Basel, CH-4056 Basel, Switzerland
[6] Louisiana State University, Baton Rouge, LA 70803, USA
[7] Institute of High Energy Physics, IHEP, 100039 Beijing, China[△]
[8] University of Bologna and INFN-Sezione di Bologna, I-40126 Bologna, Italy
[9] Tata Institute of Fundamental Research, Mumbai (Bombay) 400 005, India
[10] Northeastern University, Boston, MA 02115, USA
[11] Institute of Atomic Physics and University of Bucharest, R-76900 Bucharest, Romania
[12] Central Research Institute for Physics of the Hungarian Academy of Sciences, H-1525 Budapest 114, Hungary[‡]
[13] Massachusetts Institute of Technology, Cambridge, MA 02139, USA
[14] Panjab University, Chandigarh 160 014, India

[15] KLTE-ATOMKI, H-4010 Debrecen, Hungary[¶]
[16] UCD School of Physics, University College Dublin, Belfield, Dublin 4, Ireland
[17] INFN Sezione di Firenze and University of Florence, I-50125 Florence, Italy
[18] European Laboratory for Particle Physics, CERN, CH-1211 Geneva 23, Switzerland
[19] World Laboratory, FBLJA Project, CH-1211 Geneva 23, Switzerland
[20] University of Geneva, CH-1211 Geneva 4, Switzerland
[21] University of Hamburg, D-22761 Hamburg, Germany
[22] Chinese University of Science and Technology, USTC, Hefei, Anhui 230 029, China[△]
[23] University of Lausanne, CH-1015 Lausanne, Switzerland
[24] Institut de Physique Nucléaire de Lyon, IN2P3-CNRS,Université Claude Bernard, F-69622 Villeurbanne, France
[25] Centro de Investigaciones Energéticas, Medioambientales y Tecnológicas, CIEMAT, E-28040 Madrid, Spain[♭]
[26] Florida Institute of Technology, Melbourne, FL 32901, USA
[27] INFN-Sezione di Milano, I-20133 Milan, Italy
[28] Institute of Theoretical and Experimental Physics, ITEP, Moscow, Russia
[29] INFN-Sezione di Napoli and University of Naples, I-80125 Naples, Italy
[30] Department of Physics, University of Cyprus, Nicosia, Cyprus
[31] Radboud University and NIKHEF, NL-6525 ED Nijmegen, The Netherlands
[32] California Institute of Technology, Pasadena, CA 91125, USA
[33] INFN-Sezione di Perugia and Università Degli Studi di Perugia, I-06100 Perugia, Italy
[34] Nuclear Physics Institute, St. Petersburg, Russia
[35] Carnegie Mellon University, Pittsburgh, PA 15213, USA
[36] INFN-Sezione di Napoli and University of Potenza, I-85100 Potenza, Italy
[37] Princeton University, Princeton, NJ 08544, USA
[38] University of Californa, Riverside, CA 92521, USA
[39] INFN-Sezione di Roma and University of Rome, "La Sapienza", I-00185 Rome, Italy
[40] University and INFN, Salerno, I-84100 Salerno, Italy
[41] University of California, San Diego, CA 92093, USA
[42] Bulgarian Academy of Sciences, Central Lab. of Mechatronics and Instrumentation, BU-1113 Sofia, Bulgaria
[43] The Center for High Energy Physics, Kyungpook National University, 702-701 Taegu, Republic of Korea
[44] National Central University, Chung-Li, Taiwan, China
[45] Department of Physics, National Tsing Hua University, Taiwan, China
[46] Purdue University, West Lafayette, IN 47907, USA
[47] Paul Scherrer Institut, PSI, CH-5232 Villigen, Switzerland
[48] DESY, D-15738 Zeuthen, Germany
[49] Eidgenössische Technische Hochschule, ETH Zürich, CH-8093 Zürich, Switzerland

[§] Supported by the German Bundesministerium für Bildung, Wissenschaft, Forschung und Technologie.
[‡] Supported by the Hungarian OTKA fund under contract numbers T019181, F023259 and T037350.
[¶] Also supported by the Hungarian OTKA fund under contract number T026178.
[♭] Supported also by the Comisión Interministerial de Ciencia y Tecnología.
[♯] Also supported by CONICET and Universidad Nacional de La Plata, CC 67, 1900 La

Plata, Argentina.
△ Supported by the National Natural Science Foundation of China.
† Deceased.

The OPAL Collaboration

G. Abbiendi[2], K. Ackerstaff[7], C. Ainsley[5], P.F. Åkesson[7], G. Alexander[21], J. Allison[15], N. Altekamp[5], K. Ametewee[25], G. Anagnostou[1], K.J. Anderson[8], S. Anderson[11], S. Arcelli[2], S. Asai[22], S.F. Ashby[1], D. Axen[26], G. Azuelos[17], A.H. Ball[7], I. Bailey[25], E. Barberio[7,p], T. Barillari[31], R.J. Barlow[15], R. Bartoldus[3], R.J. Batley[5], S. Baumann[3], P. Bechtle[24], J. Bechtluft[13], C. Beeston[15], T. Behnke[24], K.W. Bell[19], P.J. Bell[1], G. Bella[21], A. Bellerive[6], G. Benelli[4], S. Bentvelsen[7,aa], P. Berlich[9], S. Bethke[31], O. Biebel[30], O. Boeriu[9], V. Blobel[24], I.J. Bloodworth[1], J.E. Bloomer[1], M. Bobinski[9], P. Bock[10], O. Boeriu[9], D. Bonacorsi[2], H.M. Bosch[10], M. Boutemeur[30], B.T. Bouwens[11], S. Braibant[2], P. Bright-Thomas[1], L. Brigliadori[2], R.M. Brown[19], H.J. Burckhart[7], C. Burgard[7], R. Bürgin[9], J. Cammin[3], S. Campana[4], P. Capiluppi[2], R.K. Carnegie[6], A.A. Carter[12], J.R. Carter[5], C.Y. Chang[16], D.G. Charlton[1], D. Chrisman[4], C. Ciocca[2], P.E.L. Clarke[14,bb], E. Clay[14], I. Cohen[21], J.E. Conboy[14], O.C. Cooke[15], J. Couchman[14], C. Couyoumtzelis[12], R.L. Coxe[8], A. Csilling[28], M. Cuffiani[2], S. Dado[20], C. Dallapiccola[16], M. Dallavalle[2], S. Dallison[15], S. De Jong[11,cc], A. De Roeck[7], P. Dervan[14], E.A. De Wolf[7,s], L.A. del Pozo[7], K. Desch[24], B. Dienes[29], M.S. Dixit[6], E. do Couto e Silva[11], M. Donkers[6], M. Doucet[17], J. Dubbert[30], E. Duchovni[23], G. Duckeck[30], I.P. Duerdoth[15], J.E.G. Edwards[15], P.G. Estabrooks[6], E. Etzion[21], H.G. Evans[8,dd], M. Evans[12], F. Fabbri[2], M. Fanti[2], P. Fath[10], L. Feld[9], P. Ferrari[7], F. Fiedler[30], M. Fierro[2], H.M. Fischer[3], I. Fleck[9], R. Folman[23,kk], D.G. Fong[16], M. Ford[15], M. Foucher[17], A. Frey[7], A. Fürtjes[7], D.I. Futyan[15], P. Gagnon[11], J.W. Gary[4], J. Gascon[17], S.M. Gascon-Shotkin[16,ee], G. Gaycken[24], N.I. Geddes[19], C. Geich-Gimbel[3], T. Geralis[19], G. Giacomelli[2], P. Giacomelli[2], R. Giacomelli[2], V. Gibson[5], W.R. Gibson[12], D.M. Gingrich[27], M. Giunta[4], D. Glenzinski[8,ff], J. Goldberg[20], M.J. Goodrick[5], W. Gorn[4], K. Graham[25], C. Grandi[2], E. Gross[23], J. Grunhaus[21], M. Gruwé[7], P.O. Günther[3], A. Gupta[8], C. Hajdu[28], M. Hamann[24], G.G. Hanson[4], M. Hansroul[7], M. Hapke[12], K. Harder[24], A. Harel[20], C.K. Hargrove[6], M. Harin-Dirac[4], P.A. Hart[8], C. Hartmann[3], A. Hauke[3], M. Hauschild[7], C.M. Hawkes[1], R. Hawkings[7], R.J. Hemingway[6], C. Hensel[24], M. Herndon[16], G. Herten[9], R.D. Heuer[24,y], M.D. Hildreth[7,gg], J.C. Hill[5], S.J. Hillier[1], T. Hilse[9], P.R. Hobson[33], A. Hocker[8], K. Hoffman[7], R.J. Homer[1], A.K. Honma[7], D. Horváth[28,c], K.R. Hossain[27], R. Howard[26], R.E. Hughes-Jones[15], P. Hüntemeyer[24], D.E. Hutchcroft[5], P. Igo-Kemenes[10], D.C. Imrie[25], M.R. Ingram[15], K. Ishii[22], F.R. Jacob[19], A. Jawahery[16], P.W. Jeffreys[19], H. Jeremie[17], M. Jimack[1], A. Joly[17], C.R. Jones[5], G. Jones[15], M. Jones[6], R.W.L. Jones[7,hh], U. Jost[10], P. Jovanovic[1], T.R. Junk[6,i], N. Kanaya[22], J. Kanzaki[22,u], G. Karapetian[17], D. Karlen[25], V. Kartvelishvili[15], K. Kawagoe[22], T. Kawamoto[22], R.K. Keeler[25], R.G. Kellogg[16], B.W. Kennedy[19], D.H. Kim[18], B.J. King[7], J. Kirk[26], K. Klein[10], A. Klier[23], S. Kluth[31], T. Kobayashi[22], M. Kobel[3,t], D.S. Koetke[6], T.P. Kokott[3], M. Kolrep[9], S. Komamiya[22], R.V. Kowalewski[25], T. Krämer[24], A. Krasznahorkay Jr.[29,e], T. Kress[10], P. Krieger[6,l], J. von Krogh[10], T. Kuhl[24], M. Kupper[23], P. Kyberd[12], G.D. Lafferty[15], R. Lahmann[16], W.P. Lai[18], H. Landsman[20], D. Lanske[13,*], J. Lauber[14], S.R. Lautenschlager[34], I. Lawson[25], J.G. Layter[4], D. Lazic[20], A.M. Lee[34], E. Lefebvre[17], A. Leins[30], D. Lellouch[23], J. Letts[o], L. Levinson[23], C. Lewis[14], R. Liebisch[10], J. Lillich[9], B. List[24], J. List[24], C. Littlewood[5], A.W. Lloyd[1], S.L. Lloyd[12], F.K. Loebinger[15], G.D. Long[16], M.J. Losty[6,*], J. Lu[26,b], A. Ludwig[3,t], J. Ludwig[9], A. Macchiolo[17], A. Macpherson[27,y], W. Mader[3,t], M. Mannelli[7], S. Marcellini[2], T.E. Marchant[15], C. Markus[3], A.J. Martin[12], J.P. Martin[17], G. Martinez[16], T. Mashimo[22], W. Matthews[25], P. Mättig[23,m], W.J. McDonald[27], J. McKenna[26], E.A. Mckigney[14], T.J. McMahon[1], A.I. McNab[12], R.A. McPherson[25], P. Mendez-Lorenzo[30], F. Meijers[7], W. Menges[24], S. Menke[3], F.S. Merritt[8], H. Mes[6,a], N. Meyer[24], J. Meyer[24], A. Michelini[2], S. Mihara[22], G. Mikenberg[23], D.J. Miller[14], R. Mir[23,ii], W. Mohr[9], A. Montanari[2],

T. Mori[22], M. Morii[22,jj], U. Müller[3], A. Mutter[9], K. Nagai[12], I. Nakamura[22,v], H. Nanjo[22], H.A. Neal[32], B. Nellen[3], B. Nijjhar[15], R. Nisius[31], S.W. O'Neale[1,*], F.G. Oakham[6], F. Odorici[2], H.O. Ogren[11], A. Oh[7], A. Okpara[10], N.J. Oldershaw[15], T. Omori[22], M.J. Oreglia[8], S. Orito[22,*], C. Pahl[31], J. Pálinkás[29], G. Pásztor[4,g], J.R. Pater[15], G.N. Patrick[19], J. Patt[9], M.J. Pearce[1], S. Petzold[24], P. Pfeifenschneider[13,*], J.E. Pilcher[8], J. Pinfold[27], D.E. Plane[7], P. Poffenberger[25], J. Polok[7], B. Poli[2], O. Pooth[13], A. Posthaus[3], M. Przybycień[7,n], H. Przysiezniak[27], A. Quadt[31], K. Rabbertz[7,r], D.L. Rees[1], C. Rembser[7], P. Renkel[23], H. Rick[4], D. Rigby[1], S. Robertson[25], S.A. Robins[12], N. Rodning[27], J.M. Roney[25], A. Rooke[14], E. Ros[7], S. Rosati[3], K. Roscoe[15], A.M. Rossi[2], M. Rosvick[25], P. Routenburg[27], Y. Rozen[20], K. Runge[9], O. Runolfsson[7], U. Ruppel[13], D.R. Rust[11], R. Rylko[25], K. Sachs[6], T. Saeki[22], O. Sahr[30], E.K.G. Sarkisyan[7,j], M. Sasaki[22], C. Sbarra[2], A.D. Schaile[30], O. Schaile[30], P. Scharff-Hansen[7], P. Schenk[24], J. Schieck[31], B. Schmitt[7], S. Schmitt[10], T. Schörner-Sadenius[7,z], M. Schröder[7], H.C. Schultz-Coulon[9], M. Schulz[7], M. Schumacher[3], P. Schütz[3], C. Schwick[7], W.G. Scott[19], R. Seuster[13,f], T.G. Shears[7,h], B.C. Shen[4,*], C.H. Shepherd-Themistocleous[19], P. Sherwood[14], G.P. Siroli[2], A. Sittler[24], A. Skillman[14], A. Skuja[16], A.M. Smith[7], T.J. Smith[25], G.A. Snow[16,*], R. Sobie[25], S. Söldner-Rembold[15], S. Spagnolo[19], F. Spano[8,x], R.W. Springer[27], M. Sproston[19], A. Stahl[13], M. Steiert[10], K. Stephens[15], J. Steuerer[24], B. Stockhausen[3], K. Stoll[9], D. Strom[18], R. Ströhmer[30], F. Strumia[7], L. Stumpf[25], B. Surrow[7], P. Szymanski[19], R. Tafirout[17], S.D. Talbot[1], S. Tanaka[22], P. Taras[17], S. Tarem[20], R.J. Taylor[14], M. Tasevsky[7,d], R. Teuscher[8], M. Thiergen[9], J. Thomas[14], M.A. Thomson[5], E. von Törne[3], E. Torrence[18], S. Towers[6], D. Toya[22], T. Trefzger[30], I. Trigger[7,w], Z. Trócsányi[29,e], T. Tsukamoto[22], E. Tsur[21], A.S. Turcot[8], M.F. Turner-Watson[1], I. Ueda[22], B. Ujvári[29,e], P. Utzat[10], B. Vachon25, R. Van Kooten[11], P. Vannerem[9], R. Vértesi[29,e], M. Verzocchi[16], P. Vikas[17], M. Vincter[25], E.H. Vokurka[15], C.F. Vollmer[30], H. Voss[7,q], J. Vossebeld[7,h], F. Wäckerle[9], A. Wagner[24], D. Waller[6], C.P. Ward[5], D.R. Ward[5], J.J. Ward[14], P.M. Watkins[1], A.T. Watson[1], N.K. Watson[1], P.S. Wells[7], T. Wengler[7], N. Wermes[3], D. Wetterling[10] J.S. White[25], B. Wilkens[9], G.W. Wilson[15,k], J.A. Wilson[1], G. Wolf[23], S. Wotton[5], T.R. Wyatt[15], S. Yamashita[22], G. Yekutieli[23], V. Zacek[17], D. Zer-Zion[4], L. Zivkovic[20]

[1]School of Physics and Astronomy, University of Birmingham, Birmingham B15 2TT, UK
[2]Dipartimento di Fisica dell' Università di Bologna and INFN, I-40126 Bologna, Italy
[3]Physikalisches Institut, Universität Bonn, D-53115 Bonn, Germany
[4]Department of Physics, University of California, Riverside CA 92521, USA
[5]Cavendish Laboratory, Cambridge CB3 0HE, UK
[6]Ottawa-Carleton Institute for Physics, Department of Physics, Carleton University, Ottawa, Ontario K1S 5B6, Canada
[7]CERN, European Organisation for Nuclear Research, CH-1211 Geneva 23, Switzerland
[8]Enrico Fermi Institute and Department of Physics, University of Chicago, Chicago IL 60637, USA
[9]Fakultät für Physik, Albert-Ludwigs-Universität Freiburg, D-79104 Freiburg, Germany
[10]Physikalisches Institut, Universität Heidelberg, D-69120 Heidelberg, Germany
[11]Indiana University, Department of Physics, Bloomington IN 47405, USA
[12]Queen Mary and Westfield College, University of London, London E1 4NS, UK
[13]Technische Hochschule Aachen, III Physikalisches Institut, Sommerfeldstrasse 26-28, D-52056 Aachen, Germany
[14]University College London, London WC1E 6BT, UK
[15]School of Physics and Astronomy, Schuster Laboratory, The University of Manchester M13 9PL, UK
[16]Department of Physics, University of Maryland, College Park, MD 20742, USA
[17]Laboratoire de Physique Nucléaire, Université de Montréal, Montréal, Québec H3C 3J7, Canada

[18]University of Oregon, Department of Physics, Eugene OR 97403, USA
[19]Rutherford Appleton Laboratory, Chilton, Didcot, Oxfordshire OX11 0QX, UK
[20]Department of Physics, Technion-Israel Institute of Technology, Haifa 32000, Israel
[21]Department of Physics and Astronomy, Tel Aviv University, Tel Aviv 69978, Israel
[22]International Centre for Elementary Particle Physics and Department of Physics, University of Tokyo, Tokyo 113-0033, and Kobe University, Kobe 657-8501, Japan
[23]Particle Physics Department, Weizmann Institute of Science, Rehovot 76100, Israel
[24]Universität Hamburg/DESY, Institut für Experimentalphysik, Notkestrasse 85, D-22607 Hamburg, Germany
[25]University of Victoria, Department of Physics, P O Box 3055, Victoria BC V8W 3P6, Canada
[26]University of British Columbia, Department of Physics, Vancouver BC V6T 1Z1, Canada
[27]University of Alberta, Department of Physics, Edmonton AB T6G 2J1, Canada
[28]Research Institute for Particle and Nuclear Physics, H-1525 Budapest, P O Box 49, Hungary
[29]Institute of Nuclear Research, H-4001 Debrecen, P O Box 51, Hungary
[30]Ludwig-Maximilians-Universität München, Sektion Physik, Am Coulombwall 1, D-85748 Garching, Germany
[31]Max-Planck-Institute für Physik, Föhringer Ring 6, D-80805 München, Germany
[32]Yale University, Department of Physics, New Haven, CT 06520, USA
[33]Brunel University, Uxbridge, Middlesex UB8 3PH, UK
[34]Duke University, Dept of Physics, Durham, NC 27708-0305, USA

[a] and at TRIUMF, Vancouver, Canada V6T 2A3
[b] now at University of Alberta
[c] and Institute of Nuclear Research, Debrecen, Hungary
[d] now at Institute of Physics, Academy of Sciences of the Czech Republic 18221 Prague, Czech Republic
[e] and Department of Experimental Physics, University of Debrecen, Hungary
[f] and MPI München
[g] and Research Institute for Particle and Nuclear Physics, Budapest, Hungary
[h] now at University of Liverpool, Dept of Physics, Liverpool L69 3BX, U.K.
[i] now at Fermilab, Illinois, U.S.A.
[j] and University of Texas at Arlington, USA
[k] now at University of Kansas, Dept of Physics and Astronomy, Lawrence, KS 66045, U.S.A.
[l] now at University of Toronto, Dept of Physics, Toronto, Canada
[m] current address Bergische Universität, Wuppertal, Germany
[n] now at University of Mining and Metallurgy, Cracow, Poland
[o] now at University of California, San Diego, U.S.A.
[p] now at The University of Melbourne, Victoria, Australia
[q] now at IPHE Université de Lausanne, CH-1015 Lausanne, Switzerland
[r] now at IEKP Universität Karlsruhe, Germany
[s] now at University of Antwerpen, Physics Department,B-2610 Antwerpen, Belgium; supported by Interuniversity Attraction Poles Programme – Belgian Science Policy
[t] now at Technische Universität, Dresden, Germany
[u] and High Energy Accelerator Research Organisation (KEK), Tsukuba, Ibaraki, Japan
[v] now at University of Pennsylvania, Philadelphia, Pennsylvania, USA
[w] now at TRIUMF, Vancouver, Canada
[x] now at Columbia University
[y] now at CERN

[aa] now at Nikhef, the Netherlands
[bb] now at University of Edinburgh, United Kingdom
[cc] now at University of Nijmegen, the Netherlands
[dd] now at Indiana University, USA
[ee] now at IPN Lyon, France
[ff] now at Fermilab, USA
[gg] now at University of Notre Dame, USA
[hh] now at University of Lancaster, United Kingdom
[ii] now at Technion, Haifa, Israel
[jj] now at Harvard University, USA
[kk] now at Ben-Gurion University of the Negev, Beersheba, Israel
* Deceased

In addition to the support staff at our own institutions we are pleased to acknowledge the
Department of Energy, USA,
National Science Foundation, USA,
Particle Physics and Astronomy Research Council, UK,
Natural Sciences and Engineering Research Council, Canada,
Israel Science Foundation, administered by the Israel Academy of Science and Humanities,
Benoziyo Center for High Energy Physics,
Japanese Ministry of Education, Culture, Sports, Science and Technology (MEXT) and a grant under the MEXT International Science Research Program,
Japanese Society for the Promotion of Science (JSPS),
German Israeli Bi-national Science Foundation (GIF),
Bundesministerium für Bildung und Forschung, Germany,
National Research Council of Canada,
Hungarian Foundation for Scientific Research, OTKA T-038240, and T-042864,
The NWO/NATO Fund for Scientific Research, the Netherlands.

Contents

1 Introduction **20**
1.1 LEP-II Data . . . 20
1.2 Standard-Model Processes . . . 21

2 Photon-Pair Production **26**
2.1 Introduction . . . 26
2.2 Event Selection . . . 26
2.3 Theory . . . 27
2.3.1 QED Born Cross-Section . . . 27
2.3.2 Non-QED Models . . . 27
2.3.3 Radiative Corrections . . . 29
2.3.4 Theory Uncertainty . . . 29
2.4 Combination of the Differential Cross-Section . . . 30
2.5 Combined Total Cross-Section . . . 31
2.6 Interpretation . . . 31
2.7 Conclusion . . . 37

3 Fermion-Pair Production **39**
3.1 Introduction . . . 39
3.2 Averages for Cross-Sections and Asymmetries . . . 40
3.3 Differential Cross-Sections for Muon- and Tau-Pair Final States . . . 43
3.4 Differential Cross-Sections for Electron-Positron Final States . . . 48
3.5 Interpretation . . . 53
3.5.1 Models with Z′ Bosons . . . 53
3.5.2 Contact Interactions . . . 58
3.5.3 Large Extra Dimensions . . . 61
3.5.4 Leptoquarks . . . 64
3.6 Summary . . . 64

4 Final-State Interconnection Effects **66**
4.1 Colour Reconnection . . . 66
4.1.1 Introduction . . . 66
4.1.2 Particle-Flow Measurements . . . 67
4.1.3 Determination of CR Effects Using W Mass Estimators . . . 70
4.1.4 Combination of LEP CR Measurements . . . 73
4.1.5 Summary . . . 74
4.2 Bose-Einstein Correlations . . . 74
4.2.1 Introduction . . . 74

4.2.2 Methods . . . 76
4.2.3 Distributions . . . 76
4.2.4 Results . . . 78
4.2.5 Conclusions . . . 80

5 Boson-Pair and Four-Fermion Processes 86
5.1 Introduction and Signal Definitions . . . 86
5.2 W-Pair Production . . . 88
5.2.1 Total Cross-Section Measurement . . . 89
5.2.2 Derived Quantities . . . 93
5.2.3 W Angular Distribution . . . 96
5.3 Z-Pair Production . . . 97
5.4 Z-γ^* Production . . . 100
5.5 Single-Boson Production . . . 100
5.5.1 Weν Cross-Section Measurement . . . 105
5.5.2 Zee Cross-Section Measurement . . . 105
5.6 WWγ Production . . . 112
5.7 Summary . . . 112

6 Electroweak Gauge Boson Self Couplings 114
6.1 Introduction . . . 114
6.1.1 Charged Triple Gauge Boson Couplings . . . 114
6.1.2 Neutral Triple Gauge Boson Couplings . . . 115
6.2 Combination Procedure . . . 116
6.3 Measurements . . . 118
6.4 Results . . . 119
6.4.1 Charged Triple Gauge Boson Couplings . . . 119
6.4.2 Neutral Triple Gauge Boson Couplings . . . 121
6.5 Summary and Conclusions . . . 127

7 Mass and Width of the W Boson 128
7.1 Introduction . . . 128
7.2 Determination of the W Mass at the W-Pair Production Threshold . . . 128
7.3 Measurement of Mass and Width by Direct Reconstruction . . . 129
7.3.1 Mass Reconstruction . . . 129
7.3.2 Kinematic Fitting . . . 130
7.3.3 Techniques for Determining the W-Boson Mass and Width . . . 131
7.3.4 Combination Procedure . . . 133
7.3.5 Overview of Systematic Uncertainties . . . 134
7.4 LEP Combined W-Boson Mass . . . 139
7.5 Consistency Checks . . . 140
7.6 LEP Combined W-Boson Width . . . 140
7.7 Summary . . . 141

8 Summary and Conclusions 145

Acknowledgements 146

A S-Matrix **147**
A.1 Introduction . . . 147
A.2 The S-Matrix Ansatz . . . 148
A.3 LEP-I Combination . . . 149
A.4 Discussion . . . 150
A.5 S-Matrix Combination Tables . . . 157

B Two-Fermion Combination Details **162**
B.1 Input Measurements . . . 163
B.2 Differential Cross-Section for Muon- and Tau-Pair Final States . . . 174
B.3 Differential Cross-Section for Electron-Positron Final States . . . 178

C Determination of the LEP Centre-of-Mass Energy Using Radiative-Return Events **181**

D Tests of the Colour-Reconnection Combination Procedure **186**

E Detailed Inputs and Results of LEP Four-Fermion Averages **191**

F Constraints on the Standard Model **211**
F.1 Introduction . . . 211
F.2 Measurements . . . 211
F.3 Theoretical Uncertainties . . . 214
F.4 Standard-Model Analyses . . . 214

Chapter 1

Introduction

The electron-positron collider LEP at CERN increased its collision centre-of-mass energy, $\sqrt{s}$, from the Z pole (LEP-I) up to 209 GeV during its second running phase (LEP-II) from 1995 to 2000. The four LEP experiments ALEPH, DELPHI, L3 and OPAL collected a combined total integrated luminosity of about 3 fb^{-1} in the LEP-II centre-of-mass energy range above the Z pole, 130 GeV to 209 GeV. This large dataset explores the new energy regime accessed by LEP-II with high precision, allowing new tests of the electroweak Standard Model of particle physics [1] (SM), and searches for new physics effects at higher mass scales.

Combinations of electroweak measurements performed in electron-positron collisions at Z-pole centre-of-mass energies, at LEP-I and the SLC, are reported in Reference [4]. Here, the measurements in the electroweak sector of the SM at LEP-II centre-of-mass energies are discussed, including, where necessary, studies of strong-interaction effects. Photon-pair, fermion-pair and four-fermion production processes are analysed and the results are presented in the form of total and differential cross-sections. Final-state interactions between the decay products in W-boson pair production are investigated for signals of colour reconnection and Bose-Einstein correlations. Pair-production of W bosons yields measurements of the mass, total decay width and decay branching fractions of the W boson. Together with other reactions such as single-W, single-Z, WWγ, Z-pair, Zγ and Z$\gamma\gamma$ production, the data sample allows stringent tests of the non-Abelian structure of the electroweak gauge group, by measuring triple and quartic electroweak gauge boson couplings.

1.1 LEP-II Data

In a circular accelerator such as LEP, the energy loss of the beam particles due to synchrotron radiation increases with the fourth power of the Lorentz γ factor. In order to push the LEP centre-of-mass energy beyond the Z-pole, the warm copper RF cavities used at LEP-I were replaced by superconducting RF cavities to increase the available RF power. In parallel the LEP-II centre-of-mass energy increased in steps up to a maximum of 209 GeV, reached in 2000, the final year of LEP operation. The centre-of-mass energies and the corresponding integrated luminosities collected per experiment are reported in Table 1.1. For some of the analyses described in this report, the data have been combined in different slices of centre-of-mass energies. About 0.75 fb^{-1} of integrated luminosity was recorded by each LEP experiment, for a total of about 3 fb^{-1}.

Year	Mean energy $\sqrt{s}$ [GeV]	Luminosity [pb^{-1}]
1995, 1997	130.3	6
	136.3	6
	140.2	1
1996	161.3	12
	172.1	12
1997	182.7	60
1998	188.6	180
1999	191.6	30
	195.5	90
	199.5	90
	201.8	40
2000	204.8	80
	206.5	130
	208.0	8
Total	$130 - 209$	745

Table 1.1: Centre-of-mass energies and integrated luminosities recorded by each experiment at LEP-II.

1.2 Standard-Model Processes

The various SM processes occurring at high centre-of-mass energies in electron-positron collisions and their cross-sections are shown as a function of the centre-of-mass energy in Figure 1.1.

Photon-Pair Production

The photon-pair production process, $e^+e^- \to \gamma\gamma(\gamma)$, is dominated by QED interactions. The corresponding Feynman diagrams at Born level are shown in Figure 1.2. Higher-order QED effects play a significant role but the weak interaction is negligible for the present data set. Therefore this reaction is different from the other processes discussed in this report as it provides a clean test of QED, independent of other parts of the SM.

Fermion-Pair Production

Pair-production of fermions proceeds mainly via s-channel exchange of a photon or a Z boson as shown in Figure 1.3. For energies above the Z resonance, QED radiative corrections are very large, up to several 100% of the Born cross-section. This is caused by hard initial-state radiation of photons, which lowers the centre-of-mass energy, $\sqrt{s}$, of the hard interaction down to values $\sqrt{s'}$ close to the Z mass, called radiative return to the Z. In order to probe the hard interaction at the nominal energy scale $\sqrt{s}$, cuts are applied to remove the radiative return to

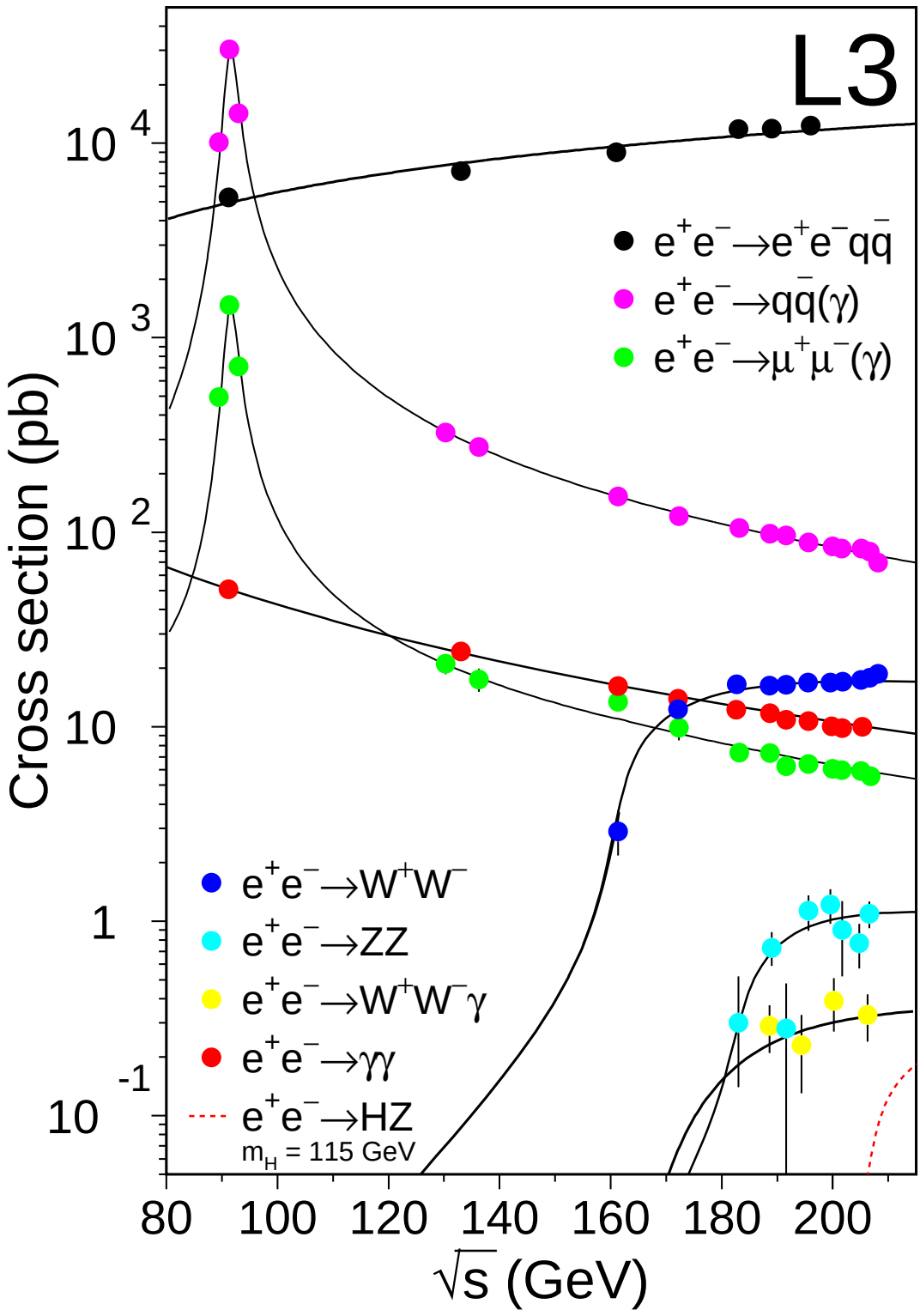


Figure 1.1: Cross-sections of electroweak SM processes. The dots with error bars show the measurements, while the continuous curves show the theoretical predictions based on the SM.

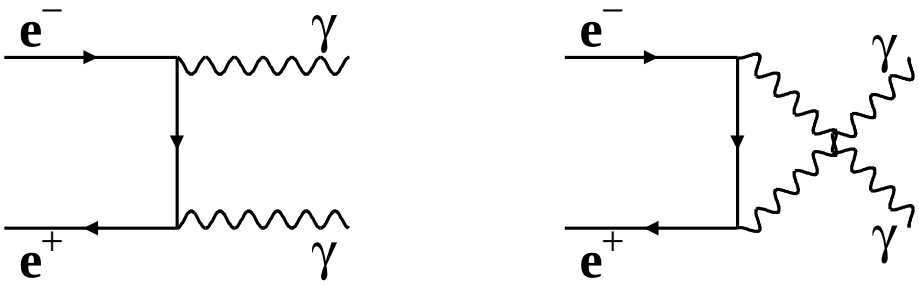


Figure 1.2: Feynman diagrams for the process $e^+e^- \to \gamma\gamma$ at the Born level.

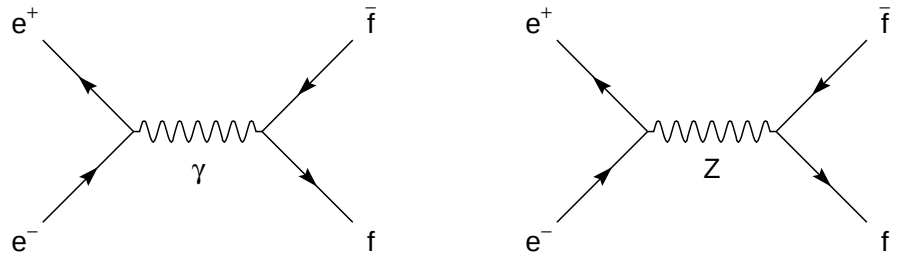


Figure 1.3: Feynman diagrams for the process $e^+e^- \to f\bar{f}$ at the Born level. For e^+e^- final states additional t-channel diagrams contribute.

the Z and only keep the high-Q^2 events. Further cuts remove non-resonant pair corrections arising from four-fermion production not included in the signal definition.

WW and ZZ Production

One of the most important processes at LEP-II consists of pair production of on-shell W bosons as shown in Figure 1.4. These events allow a determination of the mass and total decay width of the W boson. The non-Abelian nature of the electroweak gauge theory, leading to triple and quartic gauge-boson vertices such as those appearing in the two s-channel WW production diagrams, is studied and the gauge couplings are measured. Each W boson decays to a quark-antiquark pair, hadronising into jets, or to a lepton-neutrino pair, resulting in a four-fermion final state. The WW events are thus classified into fully hadronic, semileptonic and purely leptonic events. At higher centre-of-mass energies, four-fermion final states are also produced via Z-pair production, as shown in Figure 1.5.

Final-state corrections arising from the interaction between the two W decay systems, such as colour reconnection and Bose-Einstein correlations, may lead to a cross-talk effect. Such an effect potentially spoils the assignment of decay products to decaying weak bosons in terms of four-momentum, with consequences in the measurement of the W-boson mass and width in the all-hadronic channel.

Radiative corrections to W-pair production are particularly interesting as they allow the study of quartic-gauge-boson vertices as shown in Figure 1.6.

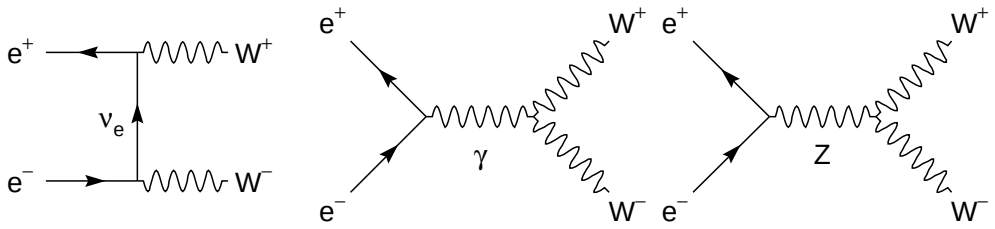


Figure 1.4: Feynman diagrams (CC03) for the process $e^+e^- \to W^+W^-$ at the Born level.



Figure 1.5: Feynman diagrams (NC02) for the process $e^+e^- \to ZZ$ at the Born level.

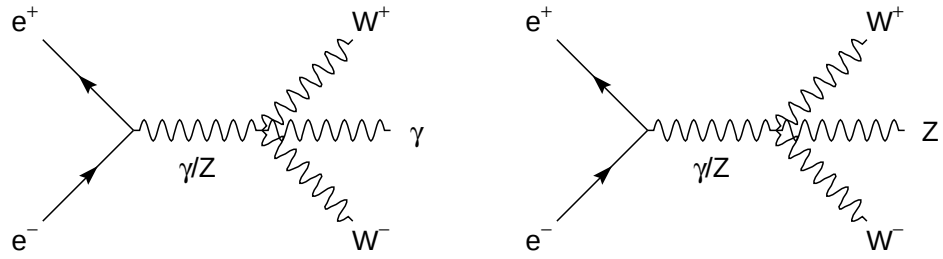


Figure 1.6: Feynman diagrams for the process $e^+e^- \to WW\gamma$ and WWZ at the Born level involving quartic electroweak-gauge-boson vertices.

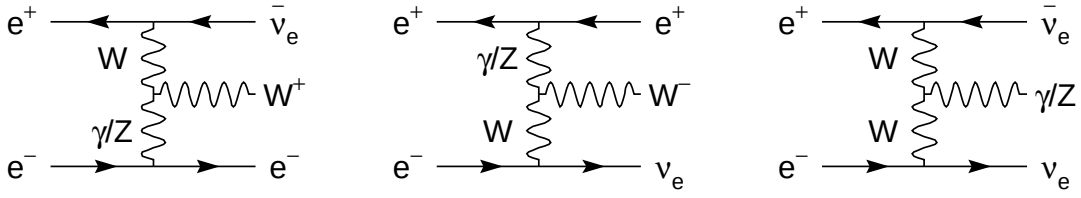


Figure 1.7: Vector-boson fusion diagrams for the single $W/Z/\gamma$ process at the Born level.

Four-Fermion Production

Besides the double-resonant WW and ZZ processes, single-resonant boson production channels such as those shown in Figure 1.7, as well as non-resonant diagrams also contribute to four-fermion production. Selections are devised to separate the various four-fermion processes, in particular WW, ZZ, single-W and single-Z production. Single-W production is sensitive to the electromagnetic gauge couplings of the W boson, as the t-channel photon exchange diagram dominates over the t-channel Z exchange diagram at LEP-II energies. Bremsstrahlung diagrams with radiation of an on-shell Z boson off an initial- or final-state fermion leg in Bhabha scattering contribute to single-Z production in the form of Zee final states.

Chapter 2

Photon-Pair Production

2.1 Introduction

The differential cross-section for the photon-pair production process $e^+e^- \to \gamma\gamma(\gamma)$ is presented here for centre-of-mass energies above 183 GeV. This process is one of the few channels at LEP energies with negligible contribution from the weak interaction. Therefore it provides a clean test of quantum electrodynamics, QED, at high energies. The combination is based on the publications [5, 6, 7, 8].

Section 2.2 gives a short overview on the event selections of the four experiments as far as they are relevant for the determination of the theory uncertainty, which is described in Section 2.3. Also the expected cross-sections from QED and other models are given. In Section 2.4 the combination of the differential cross-section is presented. The total cross-section given in Section 2.5 is derived from the differential cross-section. The results are summarised in Section 2.6.

2.2 Event Selection

The topology of this channel is very clean and the event selection, which is similar for all experiments, is based on the presence of at least two energetic clusters in the electromagnetic calorimeters (ECAL). A minimum energy of the two highest-energy ECAL clusters is required. Restrictions are made either on the acollinearity, ξ_{acol}, or on the missing longitudinal momentum, p_z. The cuts and the allowed range in polar angle, θ_i, of the observed clusters are listed in Table 2.1. The clusters are ordered by decreasing energy. In order to remove background, especially from Bhabha events, charged tracks are in general not allowed except when they can be associated to a photon conversion in one hemisphere.

Besides limited coverage of the ECAL, selection cuts to reject events with charged tracks are the main reason for a reduced signal efficiency. The effect of the different cuts depends strongly on the detector geometry. Therefore experimental systematic errors are considered uncorrelated between the experiments.

Experiment	polar angles	energies	acollinearity
ALEPH	$\lvert\cos\theta_i\rvert < 0.95$	$E_1, E_2 > 0.5 \cdot E_{\text{beam}}$	$\xi_{\text{acol}} < 20^\circ$
DELPHI	$25^\circ < \theta_i < 155^\circ$	$E_1, E_2 > 0.3 \cdot E_{\text{beam}}$	$\xi_{\text{acol}} < 50^\circ$
L3	$16^\circ < \theta_i < 164^\circ$	$E_1 + E_2 > E_{\text{beam}}$	$\xi_{\text{acol}} < 165^\circ$
OPAL	$\lvert\cos\theta_i\rvert < 0.93$	$E_1, E_2 > p_z$	–

Table 2.1: Simplified phase-space definition for the selection of $e^+e^- \to \gamma\gamma(\gamma)$ events. DELPHI does not select clusters in the range $[35^\circ, 42^\circ]$, $[88^\circ, 92^\circ]$ and $[138^\circ, 145^\circ]$. OPAL is sensitive to additional clusters up to $|\cos\theta_i| < 0.97$ ($i \geq 3$).

2.3 Theory

2.3.1 QED Born Cross-Section

The differential cross-section for the QED process $e^+e^- \to \gamma\gamma$ in lowest order is known since a long time [9]:

$$\left(\frac{d\sigma}{d\Omega}\right)_{\text{Born}} = \frac{\alpha^2}{s}\left[\frac{1+\beta^2+\beta^2\sin^2\theta}{1-\beta^2\cos^2\theta} - \frac{2\beta^4\sin^4\theta}{(1-\beta^2\cos^2\theta)^2}\right], \tag{2.1}$$

where $\sqrt{s}$ is the centre-of-mass energy. Since the emitted photons are real, with a vanishing invariant mass, the relevant scale for the fine-structure constant α is zero momentum transfer. In the following the relativistic limit for the velocity of the electron $\beta = p/E \to 1$ will be used. Since the final-state particles are identical the polar angle θ is defined such that $\cos\theta > 0$ to avoid double counting. This results in a full phase space of $\int d\Omega = 2\pi$.

Higher-order QED corrections are relevant but the lowest-order contribution involving weak couplings is negligible compared to the current experimental precision of about 1%. There is no resonance effect for this process at energies around the Z mass (LEP-I) since a spin-one vector or axial-vector particle cannot couple to two real photons. However, at the W-pair threshold there is a resonance-like effect, since the photons can be radiated off an on-shell W loop, with a dominating contribution from the triangle diagram with $WW\gamma\gamma$ coupling [10]. At such energies, corrections of up to 1.2% are expected for $\cos\theta = 0$. At the energies considered here the corrections are smaller, *e.g.*, for a centre-of-mass energy of 200 GeV they are below 0.2% at all angles, and will be neglected.

2.3.2 Non-QED Models

Various models predict deviations from the QED expectation. The simplest ansatz is the introduction of cut-off parameters $\Lambda_\pm$ as used for Bhabha and Møller scattering [12, 13]. With this formalism a short range exponential deviation is added to the Coulomb potential resulting in a differential cross-section of the form:

$$\left(\frac{d\sigma}{d\Omega}\right)_{\Lambda_\pm} = \left(\frac{d\sigma}{d\Omega}\right)_{\text{Born}} \pm \frac{\alpha^2 s}{2\Lambda_\pm^4}(1+\cos^2\theta)\,. \tag{2.2}$$

New effects can also be described by effective Lagrangian theory [14]. Here dimension-6 terms lead to anomalous eeγ couplings. The resulting deviations in the differential cross-section are similar in form to those for cut-off parameters, but with a slightly different definition of the parameter: $\Lambda_6^4 = \frac{2}{\alpha}\Lambda_+^4$. Dimension 7 and 8 Lagrangians introduce ee$\gamma\gamma$ contact interactions and result in an angular-independent term added to the Born cross-section:

$$\left(\frac{d\sigma}{d\Omega}\right)_{\Lambda'} = \left(\frac{d\sigma}{d\Omega}\right)_{\text{Born}} + \frac{s^2}{32\pi}\frac{1}{\Lambda'^6}\,. \tag{2.3}$$

The associated parameters are given by $\Lambda_7 = \Lambda'$ and $\Lambda_8^4 = m_{\text{e}}\Lambda'^3$ for dimension 7 and dimension 8 couplings, respectively.

Theories of quantum gravity in extra spatial dimensions might solve the hierarchy problem since gravitons would propagate in a compactified higher dimensional space, while other Standard Model (SM) particles are confined to the usual $3+1$ space-time dimensions [15]. While in these models the Planck mass M_D in $D = n+4$ dimensions is chosen to be at the electroweak scale, the usual Planck mass M_{Pl} in four dimensions would be $M_{\text{Pl}}^2 = R^n M_D^{n+2}$, where R is the compactification radius of the additional dimensions. Since gravitons couple to the energy-momentum tensor, their interaction with photons is as weak as that with fermions. However, the huge number of Kaluza-Klein excitation modes in the extra dimensions may give rise to observable effects. These effects depend on the scale $M_s(\sim M_D)$ which may be as low as $\mathcal{O}$(TeV). Model dependencies are absorbed in the parameter λ which is expected to be of order 1. For this analysis it is assumed that $\lambda = \pm 1$. The expected differential cross-section is given by [16]:

$$\left(\frac{d\sigma}{d\Omega}\right)_{\text{M}_\text{s}} = \left(\frac{d\sigma}{d\Omega}\right)_{\text{Born}} - \frac{\alpha s}{2\pi}\,\frac{\lambda}{M_s^4}\,(1+\cos^2\theta) + \frac{s^3}{16\pi^2}\,\frac{\lambda^2}{M_s^8}\,(1-\cos^4\theta)\,,\ \lambda = \pm 1\,. \tag{2.4}$$

Instead of an ordinary electron an excited electron e* coupling to electron and photon could be exchanged in the t-channel of the process [13, 17]. In the most general case e*eγ couplings would lead to a large anomalous magnetic moment of the electron on which strong experimental limits exist [18]. This effect can be prevented by a chiral magnetic coupling of the form:

$$\mathcal{L} = \frac{1}{2\Lambda}\bar{e^*}\sigma^{\mu\nu}\left[gf\frac{\tau}{2}W_{\mu\nu} + g'f'\frac{Y}{2}B_{\mu\nu}\right]e_L + \text{h.c.}\,, \tag{2.5}$$

where τ are the Pauli matrices and Y is the hypercharge. The model parameters are the compositeness scale Λ and the relative couplings f and f' to the gauge fields W and B with SM couplings g and g'. For the process $\text{e}^+\text{e}^- \to \gamma\gamma(\gamma)$, effects vanish in the case of $f = -f'$. For $f_\gamma = -\frac{1}{2}(f+f')$ the following cross-section results [20]:

$$\begin{aligned}\left(\frac{d\sigma}{d\Omega}\right)_{\text{e}^*} = \left(\frac{d\sigma}{d\Omega}\right)_{\text{Born}} &+ \frac{\alpha^2}{16}\frac{f_\gamma^4}{\Lambda^4}s\sin^2\theta\left[\frac{p^4}{(p^2-M_{\text{e}^*}^2)^2} + \frac{q^4}{(q^2-M_{\text{e}^*}^2)^2}\right] \\ &- \frac{\alpha^2}{2s}\frac{f_\gamma^2}{\Lambda^2}\left[\frac{p^4}{(p^2-M_{\text{e}^*}^2)} + \frac{q^4}{(q^2-M_{\text{e}^*}^2)}\right]\,,\end{aligned} \tag{2.6}$$

with $p^2 = -\frac{s}{2}(1-\cos\theta)$ and $q^2 = -\frac{s}{2}(1+\cos\theta)$. In the following it is assumed that $\Lambda = M_{\text{e}^*}$ unless stated otherwise.

2.3.3 Radiative Corrections

Radiative corrections, *i.e.*, the ratio of the next-to-leading order QED to Born level, are shown in Figure 2.1. They are determined from Monte-Carlo simulations [22], implementing a full third-order calculation including electron-mass effects. In case the third photon is below an energy cut-off, only two back-to-back photons are generated. Fourth-order effects are not included. The event angle θ is calculated as:

$$\cos\theta \;=\; \left|\sin\left(\frac{\theta_1-\theta_2}{2}\right)\right| \Big/ \sin\left(\frac{\theta_1+\theta_2}{2}\right), \tag{2.7}$$

to minimize higher order effects, where $\theta_{1,2}$ are the polar angles of the two highest-energy photons.

The correction labeled RADCOR shown in Figure 2.1 is determined from the angles $\theta_{1,2}$ of the two highest-energy photons generated without restriction on the angle. The radiative corrections depend on the selected phase space, which differs between the four experiments as listed in Table 2.1. For OPAL the radiative corrections are identical to the RADCOR distribution, apart from the edge effect, since events with a high energy photon having $|\cos\theta_i| > 0.93$ are rejected due to the cut on the longitudinal momentum. Radiative corrections for DELPHI are moderate and similar to OPAL due to the intermediate restriction on the acollinearity angle. L3 on the other hand has a very loose cut on the acollinearity angle. Thus events with only one hard photon in the accepted angle range $|\cos\theta_{2/1}| < 0.96$, the other hard photon having $0.96 < |\cos\theta_{1/2}| \simeq 1$, are selected. The event angle is calculated from the angle $\cos\theta_3$ of an observed soft photon leading to a smaller $\cos\theta$. Especially in the central region, where the cross-section is small, this leads to large corrections of up to 30%. ALEPH has a very tight cut on the acollinearity angle leading to a cross-section smaller than the Born cross-section in the central region.

2.3.4 Theory Uncertainty

For the $\gamma\gamma(\gamma)$ channel, no detailed study of the theory uncertainty, *i.e.*, the uncertainty of the third-order Monte-Carlo prediction, exists. For a QED process the higher-order effect can be estimated to be 10% ($\simeq \sqrt{\alpha}$) of the correction due to the highest calculated order. For each experiment the theory uncertainty is estimated as 10% of the radiative correction, with a minimum of 0.5%.

A Monte-Carlo study shows that despite different selections the overlap in the selected phase space is very high, for example, at $\cos\theta = 0.7$ where the third-order DELPHI cross-section is larger than the OPAL cross-section, all events in the phase space selected by OPAL are also in the phase space selected by DELPHI. This means that the common part of the correction is correlated between experiments.

For each $\cos\theta$ bin the theory error is calculated as the luminosity weighted average over the four experiments taking the correlation into account. The resulting error, listed in Tables 2.2 and 2.3, varies between 0.5% and 1.0%. The first $\cos\theta$ bin shows a larger error because DELPHI's analysis does not cover this region and thus the L3 measurements get a larger weight.

To determine limits on non-QED models these correlations are taken into account in the following way. Obviously the radiative corrections in neighbouring bins are due to the same effects and hence correlated. Forward and central region on the other hand are uncorrelated. A

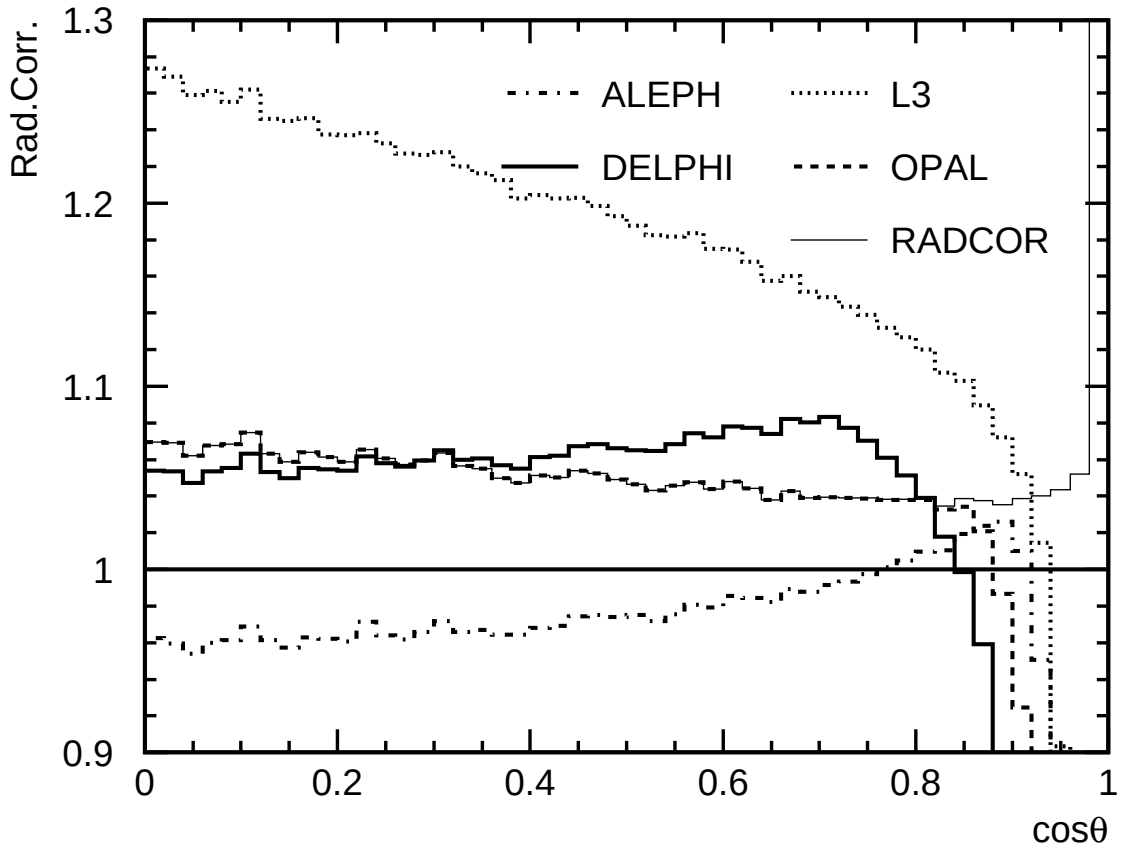


Figure 2.1: Radiative corrections for the four experiments: shown is the ratio of the full third-order RADCOR Monte-Carlo cross-section calculation with the phase-space cuts used by each experiment to the Born cross-section. The line labelled RADCOR is the ratio determined without any phase-space cuts.

detailed correlation matrix describing this situation properly is difficult to implement with a log-likelihood fit while for a χ^2 fit the available statistics are too small. To keep the log-likelihood fits of the non-QED models simple, just two independent regions are defined: barrel ($\cos\theta < 0.75$) and endcap ($\cos\theta > 0.75$). Within each region the theory error is 100% correlated, whereas the two regions are treated as uncorrelated. This simplified treatment is possible, since the theory uncertainty is smaller than the experimental systematic and statistical uncertainties.

2.4 Combination of the Differential Cross-Section

Apart from ALEPH at 183 GeV, all experiments provide the measured angular distributions in bins of $\cos\theta$, with a bin-width $B = 0.05$ for all bins except for the last one which has $B = 0.0113$. Only the $\cos\theta$-range covered differs. Besides the centre-of-mass energy $\sqrt{s_k}$ and luminosity $\mathcal{L}_k$ of each experiment k, the information includes the number of observed events $N_k^{\rm obs}$, the number of expected events $N_k^{\rm QED}$ or equivalently the correction C_k with $N_k^{\rm QED} = C_k \left(\frac{d\sigma}{d\cos\theta}\right)_{\rm Born} \mathcal{L}_k B$), as well as the experimental systematic error $\delta_k^{\rm exp}$. The experiment-dependent terms C_k correct for the different phase-space cuts reported in Table 2.1. All experiments assume an experimental systematic error which does not depend on $\cos\theta$ and hence is correlated between all bins. The

OPAL experiment introduces an additional uncorrelated experimental error $\delta^{\rm unc}$ for some bins. As explained above the experimental systematic error is uncorrelated between experiments. The resulting errors on the LEP combination are reported in Tables 2.2 and 2.3.

The effective centre-of-mass energy, $\sqrt{s}$, is determined as the luminosity weighted average, taking into account that the cross-section is proportional to $1/s$:

$$s = \mathcal{L} \Bigg/ \sum_k \frac{\mathcal{L}_k}{s_k} \ , \tag{2.8}$$

where $\mathcal{L} = \sum_k \mathcal{L}_k$. The average correction C at a given angle and energy is calculated as:

$$C = \sum_k \frac{d\sigma}{d\cos\theta}(\cos\theta_k, s_k)\mathcal{L}_k C_k \Bigg/ \frac{d\sigma}{d\cos\theta}(\cos\theta, s)\mathcal{L} \, . \tag{2.9}$$

Similarly the systematic errors are calculated, adding the contributions in quadrature. The results are given in Tables 2.2 and 2.3. The combined differential cross-section in each bin, corrected to Born level, is then calculated as:

$$\frac{d\sigma}{d\cos\theta} = \frac{N}{CB\mathcal{L}} \tag{2.10}$$

where $N = \sum_k N_k^{obs}$. The ratio of the combined cross-section and the expected Born cross-section is shown in Figure 2.2. For illustration the differential cross-section combined for all energies is shown in Figure 2.3. On average, the cross-section is slightly below the QED expectation.

2.5 Combined Total Cross-Section

The total cross-section is derived by integrating the combined differential cross-section. Since the coverage in the scattering angle varies between experiments, the total cross-section is given for two ranges, $\cos\theta < 0.9613$ and $\cos\theta < 0.90$. The latter range is covered by all four experiments. The results are shown in Figure 2.4 and are summarised in Table 2.4. For the theory error the contributions in barrel and endcap are added in quadrature. The total cross-section (especially for $\cos\theta < 0.9613$) is dominated by the very forward region, where the cross-section is strongly increasing.

2.6 Interpretation

Limits on the parameters describing the non-QED models discussed in Section 2.3.2 are determined from log-likelihood fits to the combined differential cross-section. Where possible the fit parameters are chosen such that the likelihood function is approximately Gaussian. The results of the fits are given in Table 2.5. The values of the fit parameters are about 1.5 standard deviations below the expectation, reflecting the low cross-section in the central region.

Since no significant deviations with respect to the QED expectations are found – all the parameters are compatible with zero – 95% confidence level limits are obtained by renormalising

$\cos\theta'$	N	C	theo	exp	unc	$\frac{d\sigma}{d\cos\theta}$	N	C	theo	exp	unc	$\frac{d\sigma}{d\cos\theta}$
	$\sqrt{s} = 182.692$ GeV				$\mathcal{L} = 159.4$/pb		$\sqrt{s} = 188.609$ GeV				$\mathcal{L} = 682.6$/pb	
0.029	23	0.7860	1.00	1.18	1.10	3.7	92	0.7853	1.00	1.00	0.84	3.4
0.076	39	1.0257	0.79	1.03	0.00	4.8	108	0.9321	0.79	0.80	0.00	3.4
0.126	32	0.9147	0.78	1.00	0.00	4.4	132	0.9718	0.78	0.83	0.00	4.0
0.176	32	1.0743	0.76	1.04	0.00	3.7	129	0.9473	0.76	0.81	0.00	4.0
0.226	33	0.9297	0.74	0.98	0.00	4.5	147	0.9210	0.74	0.80	0.00	4.7
0.275	41	0.9982	0.72	1.01	0.00	5.2	142	0.9539	0.72	0.82	0.00	4.4
0.326	44	0.9907	0.71	1.01	0.00	5.6	162	0.9308	0.71	0.81	0.00	5.1
0.375	37	0.9726	0.69	1.01	0.00	4.8	152	0.9207	0.69	0.82	0.00	4.8
0.426	39	0.9265	0.67	0.99	0.00	5.3	159	0.9301	0.67	0.81	0.00	5.0
0.475	37	0.9747	0.65	1.01	0.00	4.8	190	0.9351	0.65	0.80	0.00	6.0
0.525	55	0.9360	0.64	0.98	0.00	7.4	214	0.9523	0.64	0.79	0.00	6.6
0.576	55	0.9476	0.62	0.99	0.00	7.3	213	0.9380	0.62	0.80	0.00	6.7
0.626	73	0.9274	0.60	0.98	0.00	9.9	224	0.9240	0.60	0.79	0.00	7.1
0.676	70	0.9120	0.59	0.97	0.00	9.6	299	0.9198	0.59	0.79	0.00	9.5
0.726	44	0.4260	0.57	0.58	1.69	13.0	223	0.5398	0.57	0.88	1.01	12.1
0.776	53	0.4109	0.55	0.56	1.73	16.2	275	0.5295	0.55	0.89	1.02	15.2
0.826	104	0.5469	0.53	0.84	1.28	23.8	399	0.6400	0.53	0.89	0.83	18.3
0.877	197	0.7874	0.52	0.95	0.88	31.4	743	0.7959	0.52	0.82	0.66	27.4
0.928	133	0.3628	0.50	1.29	1.17	46.0	682	0.4409	0.50	1.10	0.73	45.3
0.956	35	0.2010	0.50	2.10	0.00	99.2	78	0.1426	0.50	2.10	0.00	72.8
	$\sqrt{s} = 191.597$ GeV				$\mathcal{L} = 111.8$/pb		$\sqrt{s} = 195.506$ GeV				$\mathcal{L} = 314.0$/pb	
0.029	13	0.6903	1.00	0.92	0.93	3.4	35	0.7437	1.00	1.00	0.80	3.0
0.076	22	0.9613	0.79	0.81	0.00	4.1	51	0.9882	0.79	0.84	0.00	3.3
0.126	14	0.9154	0.78	0.78	0.00	2.7	45	0.9061	0.78	0.79	0.00	3.2
0.176	18	0.9117	0.76	0.79	0.00	3.5	68	0.9401	0.76	0.84	0.00	4.6
0.226	12	0.9529	0.74	0.83	0.00	2.3	47	1.0174	0.74	0.83	0.00	2.9
0.275	30	0.9242	0.72	0.79	0.00	5.8	54	0.8987	0.72	0.80	0.00	3.8
0.326	21	0.9212	0.71	0.78	0.00	4.1	53	0.9260	0.71	0.82	0.00	3.6
0.375	26	0.9950	0.69	0.84	0.00	4.7	72	0.9005	0.69	0.80	0.00	5.1
0.426	28	0.9054	0.67	0.79	0.00	5.5	65	0.8896	0.67	0.81	0.00	4.7
0.475	29	0.9181	0.65	0.81	0.00	5.7	79	0.9573	0.65	0.81	0.00	5.3
0.525	27	0.8903	0.64	0.77	0.00	5.4	97	0.9172	0.64	0.80	0.00	6.7
0.576	29	0.9808	0.62	0.83	0.00	5.3	93	0.9437	0.62	0.82	0.00	6.3
0.626	46	0.9386	0.60	0.82	0.00	8.8	116	0.9216	0.60	0.81	0.00	8.0
0.676	41	0.9026	0.59	0.80	0.00	8.1	129	0.8611	0.59	0.78	0.00	9.5
0.726	34	0.5506	0.57	0.93	0.97	11.0	82	0.5200	0.57	0.92	0.96	10.0
0.776	43	0.5032	0.55	0.89	1.05	15.3	120	0.4941	0.55	0.92	1.00	15.5
0.826	75	0.6263	0.53	0.88	0.83	21.4	178	0.6082	0.53	0.91	0.80	18.6
0.877	108	0.7951	0.52	0.79	0.65	24.3	350	0.7900	0.52	0.79	0.61	28.2
0.928	117	0.4165	0.50	1.08	0.76	50.3	276	0.4203	0.50	1.11	0.70	41.8
0.956	16	0.1459	0.50	2.10	0.00	89.2	33	0.1492	0.50	2.10	0.00	64.0

Table 2.2: Combined differential cross-sections for $e^+e^- \to \gamma\gamma(\gamma)$. The first two numbers of each block are the centre-of-mass energy, $\sqrt{s}$, and the total luminosity, $\mathcal{L}$. The following rows list for each bin: weighted $\cos\theta$, total number of events N, correction C, theory error (theo), experimental systematic error (exp) and systematic uncorrelated error (unc). The errors are relative and given in %. The differential cross-section (in pb) is: $d\sigma/d\cos\theta(\cos\theta, \sqrt{s}) = N/C/B/\mathcal{L}$. The value listed for $\cos\theta'$ corresponds to $d\sigma/d\cos\theta(\cos\theta') \cdot B = \int_{\text{bin}} d\sigma/d\cos\theta \; d\cos\theta$.

$\cos\theta'$	N	C	theo	exp	unc	$\frac{d\sigma}{d\cos\theta}$	N	C	theo	exp	unc	$\frac{d\sigma}{d\cos\theta}$
	$\sqrt{s} = 199.504$ GeV				$\mathcal{L} = 315.2$/pb		$\sqrt{s} = 201.631$ GeV				$\mathcal{L} = 157.1$/pb	
0.029	43	0.6607	1.00	0.92	0.93	4.1	23	0.7240	1.00	0.99	0.80	4.0
0.076	44	0.8989	0.79	0.76	0.00	3.1	25	0.8865	0.79	0.78	0.00	3.6
0.126	38	0.9171	0.78	0.78	0.00	2.6	25	0.8697	0.78	0.78	0.00	3.7
0.176	38	0.9480	0.76	0.78	0.00	2.5	18	0.9562	0.76	0.84	0.00	2.4
0.226	50	0.9385	0.74	0.76	0.00	3.4	23	0.9482	0.74	0.79	0.00	3.1
0.275	57	0.9574	0.72	0.80	0.00	3.8	19	0.8910	0.72	0.76	0.00	2.7
0.326	64	0.9220	0.71	0.78	0.00	4.4	31	0.8263	0.71	0.75	0.00	4.8
0.375	64	0.9122	0.69	0.80	0.00	4.5	38	0.9389	0.69	0.81	0.00	5.2
0.426	64	0.9186	0.67	0.80	0.00	4.4	36	0.9471	0.67	0.86	0.00	4.8
0.475	67	0.9311	0.65	0.77	0.00	4.6	28	0.9213	0.65	0.79	0.00	3.9
0.525	77	0.9137	0.64	0.78	0.00	5.3	43	0.8979	0.64	0.80	0.00	6.1
0.576	94	0.9057	0.62	0.77	0.00	6.6	48	0.9472	0.62	0.82	0.00	6.5
0.626	104	0.9226	0.60	0.80	0.00	7.2	52	0.9153	0.60	0.81	0.00	7.2
0.676	111	0.8897	0.59	0.77	0.00	7.9	62	0.8703	0.59	0.78	0.00	9.1
0.726	70	0.5447	0.57	0.96	0.94	8.2	52	0.5281	0.57	0.98	0.91	12.5
0.776	108	0.5174	0.55	0.94	0.98	13.2	53	0.5151	0.55	0.97	0.93	13.1
0.826	160	0.5807	0.53	0.90	0.86	17.5	92	0.5886	0.53	0.93	0.80	19.9
0.877	307	0.8001	0.52	0.77	0.62	24.3	152	0.7988	0.52	0.79	0.58	24.2
0.928	279	0.4092	0.50	1.10	0.74	43.3	115	0.4240	0.50	1.12	0.67	34.5
0.956	28	0.1231	0.50	2.10	0.00	65.6	11	0.1197	0.50	2.10	0.00	53.2
	$\sqrt{s} = 205.279$ GeV				$\mathcal{L} = 393.3$/pb		$\sqrt{s} = 206.671$ GeV				$\mathcal{L} = 462.9$/pb	
0.029	44	0.5596	1.00	0.96	0.89	4.0	59	0.8530	1.00	0.99	0.85	3.0
0.076	64	0.9151	0.79	0.74	0.00	3.6	68	1.0029	0.79	0.89	0.00	2.9
0.126	53	0.9524	0.78	0.72	0.00	2.8	70	1.0074	0.78	0.91	0.00	3.0
0.176	51	0.9325	0.76	0.75	0.00	2.8	66	0.9777	0.76	0.87	0.00	2.9
0.226	65	0.9267	0.74	0.72	0.00	3.6	74	1.0103	0.74	0.88	0.00	3.2
0.275	50	0.9477	0.72	0.73	0.00	2.7	67	0.9818	0.72	0.87	0.00	2.9
0.326	71	0.8851	0.71	0.72	0.00	4.1	94	0.9437	0.71	0.87	0.00	4.3
0.375	63	0.9136	0.69	0.75	0.00	3.5	72	0.9200	0.69	0.92	0.00	3.4
0.426	72	0.9104	0.67	0.72	0.00	4.0	88	0.9542	0.67	0.90	0.00	4.0
0.475	62	0.9108	0.65	0.72	0.00	3.5	98	0.9776	0.65	0.88	0.00	4.3
0.525	91	0.8862	0.64	0.71	0.00	5.2	122	0.9286	0.64	0.87	0.00	5.7
0.576	97	0.9212	0.62	0.72	0.00	5.4	126	0.9500	0.62	0.88	0.00	5.7
0.626	102	0.8721	0.60	0.72	0.00	5.9	144	0.9281	0.60	0.87	0.00	6.7
0.676	150	0.8650	0.59	0.71	0.00	8.8	206	0.9089	0.59	0.86	0.00	9.8
0.726	89	0.4266	0.57	0.92	0.97	10.6	147	0.6288	0.57	0.92	0.97	10.1
0.776	105	0.3995	0.55	0.89	1.03	13.4	166	0.5891	0.55	0.90	1.02	12.2
0.826	154	0.4833	0.53	0.89	0.84	16.2	227	0.7137	0.53	0.89	0.83	13.7
0.877	345	0.7747	0.52	0.71	0.52	22.6	431	0.8173	0.52	0.86	0.72	22.8
0.928	252	0.3169	0.50	1.07	0.77	40.4	418	0.4780	0.50	1.09	0.75	37.8
0.956	24	0.0960	0.50	2.10	0.00	57.8	61	0.1490	0.50	2.10	0.00	80.4

Table 2.3: Combined differential cross-sections for $e^+e^- \to \gamma\gamma(\gamma)$. The first two numbers of each block are the centre-of-mass energy, $\sqrt{s}$, and the total luminosity, $\mathcal{L}$. The following rows list for each bin: weighted $\cos\theta$, total number of events N, correction C, theory error (theo), experimental systematic error (exp) and systematic uncorrelated error (unc). The errors are relative and given in %. The differential cross-section (in pb) is: $d\sigma/d\cos\theta(\cos\theta, \sqrt{s}) = N/C/B/\mathcal{L}$. The value listed for $\cos\theta'$ corresponds to $d\sigma/d\cos\theta(\cos\theta') \cdot B = \int_{\text{bin}} d\sigma/d\cos\theta \; d\cos\theta$.

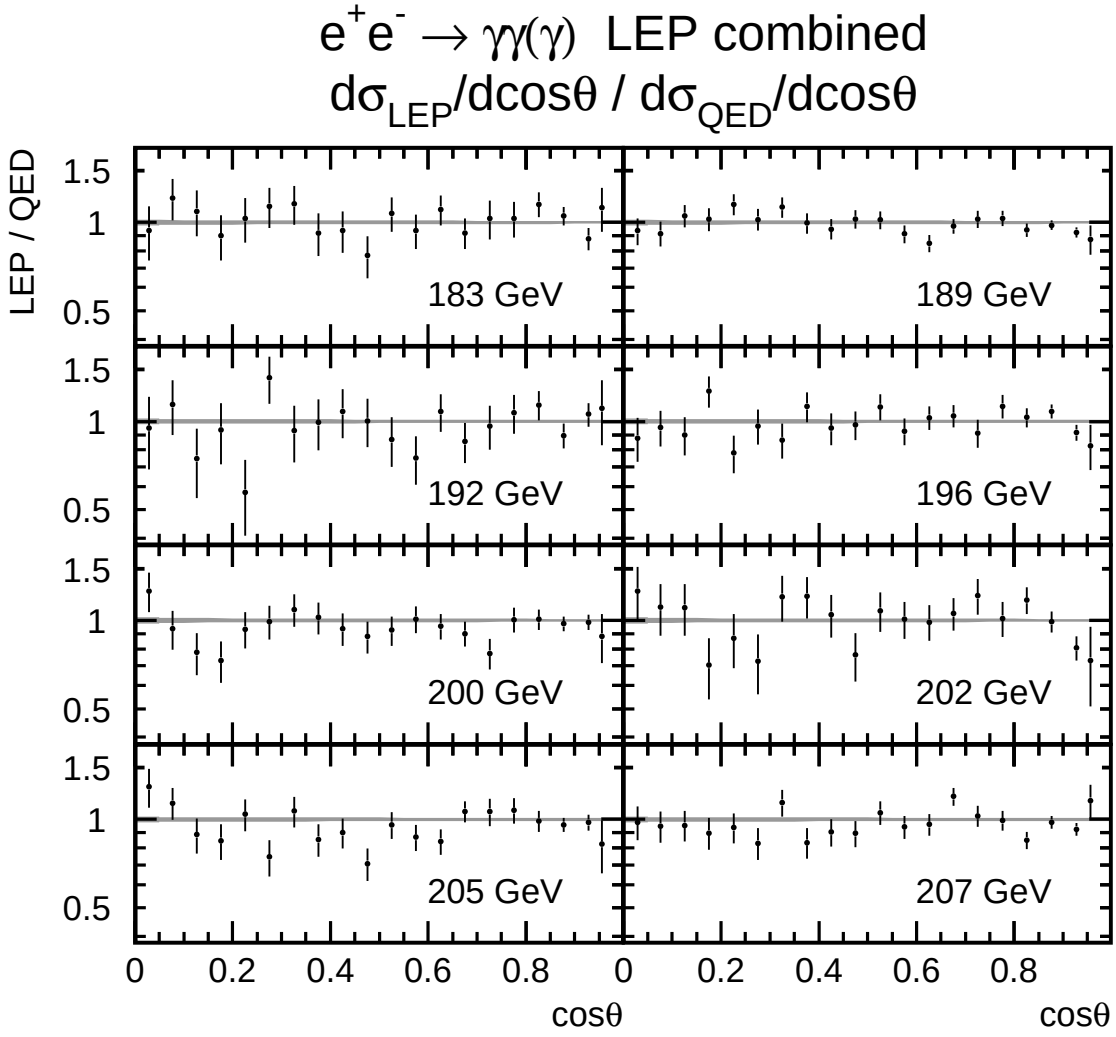


Figure 2.2: Combined differential cross-sections relative to the QED expectation. The error bars shown include the statistical and systematic experimental errors. The theory uncertainty is small, decreasing from 1.0% to 0.5% for increasing $|\cos\theta|$.

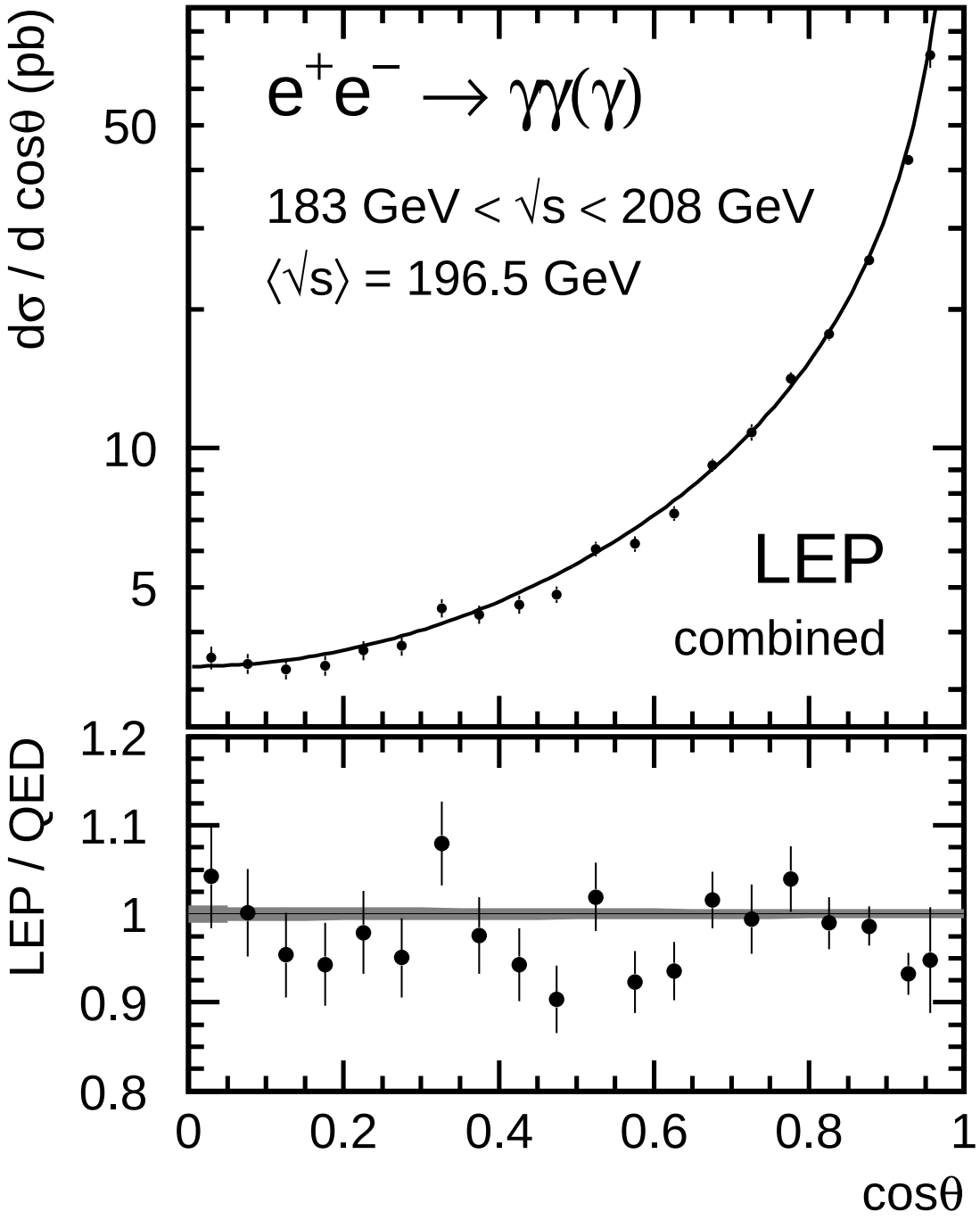


Figure 2.3: The differential cross-section combined for all energies compared to the expectation from QED. The lower plot shows the ratio of measured and expected cross-section, with the band indicating the theory error.

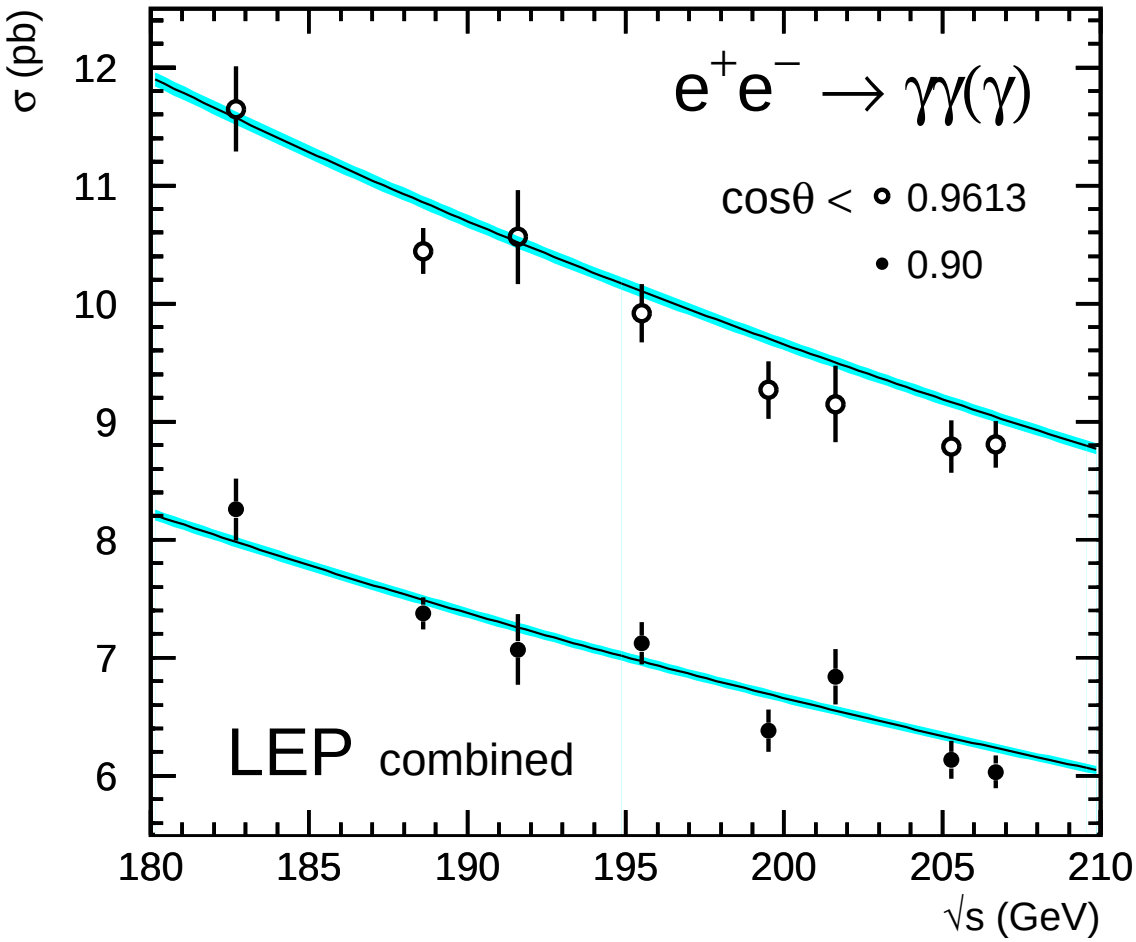


Figure 2.4: The total cross-section as a function of energy for two regions in $\cos\theta$. The error includes statistical and systematic experimental error. The theory error is shown as the band on the QED prediction.

$\sqrt{s}$ (GeV)	$\cos\theta < 0.90$ LEP	$\cos\theta < 0.90$ QED	$\cos\theta < 0.9613$ LEP	$\cos\theta < 0.9613$ QED
182.7	8.26±0.26±0.08	7.98±0.04	11.65±0.34±0.13	11.57±0.05
188.6	7.38±0.12±0.06	7.49±0.03	10.44±0.15±0.11	10.86±0.04
191.6	7.07±0.28±0.06	7.26±0.03	10.56±0.39±0.11	10.52±0.04
195.5	7.12±0.17±0.06	6.97±0.03	9.92±0.22±0.10	10.10±0.04
199.5	6.38±0.16±0.06	6.69±0.03	9.27±0.21±0.10	9.70±0.04
201.6	6.84±0.24±0.06	6.55±0.03	9.15±0.30±0.10	9.50±0.04
205.3	6.13±0.15±0.05	6.32±0.03	8.79±0.20±0.09	9.16±0.04
206.7	6.03±0.13±0.06	6.24±0.03	8.81±0.17±0.10	9.04±0.04

Table 2.4: The total cross-section (in pb) for $e^+e^- \to \gamma\gamma(\gamma)$. For the measured cross-sections (LEP) the statistical and systematic errors are given. The theory error of 0.45% (0.41%) for $\cos\theta < 0.90$ (0.9613) is quoted for the QED expectation.

Model and Fit parameter	Fit result	95% CL limit (GeV)
Cut-off parameters $\Lambda_{\pm}^{-4}$	$\left(-37^{+24}_{-23}\right) \cdot 10^{-12}$ GeV^{-4}	$\Lambda_+ > 431$ $\Lambda_- > 339$
effective Lagrangian dimension 7 Λ_7^{-6}	$\left(-2.8^{+1.8}_{-1.7}\right) \cdot 10^{-18}$ GeV^{-6}	$\Lambda_7 > 880$
effective Lagrangian dimension 6 and 8	derived from Λ_+ derived from Λ_7	$\Lambda_6 > 1752$ $\Lambda_8 > 24.3$
quantum gravity λ/M_s^4	$\left(-0.85^{+0.54}_{-0.55}\right) \cdot 10^{-12}$ GeV^{-4}	$\lambda = +1$: $M_s > 868$ $\lambda = -1$: $M_s > 1108$
excited electrons $M_{e^*}(f_\gamma = 1)$	see Figure 2.6	$M_{e^*} > 366$
$f_\gamma^2(M_{e^*} = 200$ GeV)	$-0.17^{+0.12}_{-0.12}$	$f_\gamma/\Lambda < 7.0$ TeV^{-1}

Table 2.5: Results of the fits to the differential cross-section for $e^+e^- \to \gamma\gamma(\gamma)$ and the 95% confidence level limits on the model parameters.

the probability distribution of the fit parameter to the physically allowed region, $\epsilon \geq 0$ for each Λ^+ limit and $\epsilon \leq 0$ for Λ^- limits. For limits on the coupling of an excited electron f_γ/Λ a scan over the mass M_{e^*} is performed and presented in Figure 2.5. The cross-section is nonlinear in the fit parameter only for M_{e^*}. The obtained negative log likelihood distribution is shown in Figure 2.6 and the limit is determined at 1.92 units above the minimum.

2.7 Conclusion

The differential cross-section for the photon-pair production process $e^+e^- \to \gamma\gamma(\gamma)$ was measured and found in agreement with the expectation from QED. Limits on new physics were obtained for various models. They supersede by large factors previous limits on cut-off parameters obtained from data collected at electron-positron colliders of lower centre-of-mass energies [23].

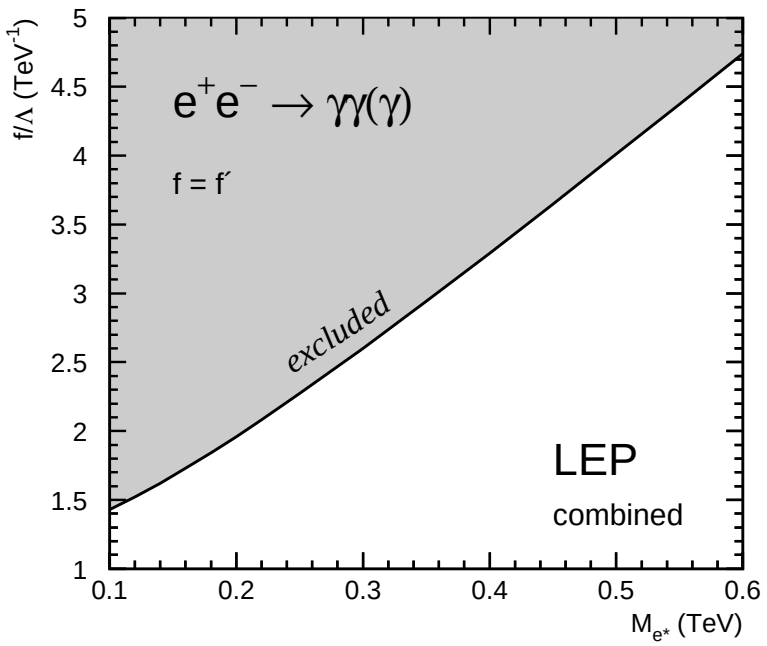


Figure 2.5: 95% CL limits on f_γ/Λ as a function of M_{e^*}. In the case of $f = f'$ it follows that $f_\gamma = -f$. It is assumed that $\Lambda = M_{e^*}$.

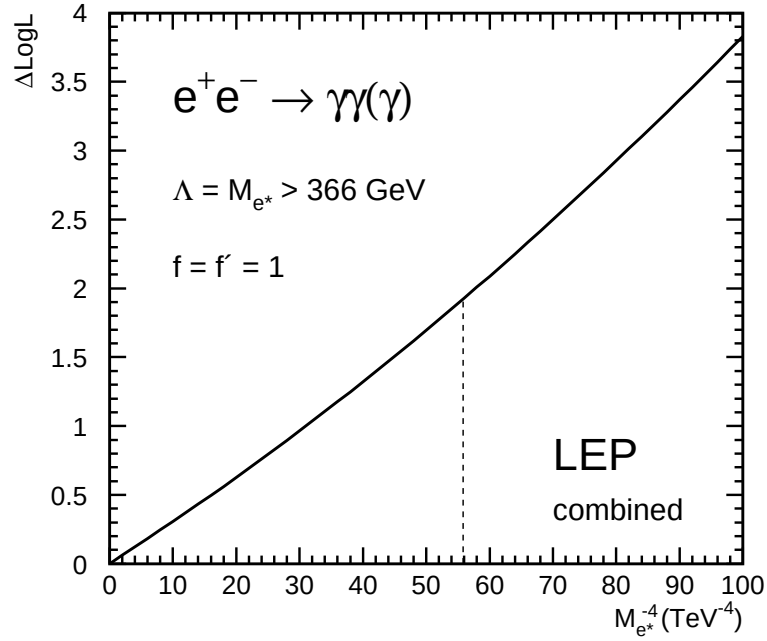


Figure 2.6: Log likelihood difference $\Delta\text{LogL} = -\ln\mathcal{L} + \ln\mathcal{L}_{\max}$ as a function of $M_{e^*}^{-4}$. The coupling is fixed at $f = f' = 1$. The value corresponding to $\Delta\text{LogL} = 1.92$ is $M_{e^*}^{-4} = 55.8$ TeV$^{-4} \to M_{e^*} = 366$ GeV.

Chapter 3

Fermion-Pair Production

3.1 Introduction

The LEP-II data were taken at centre-of-mass energies, $\sqrt{s}$, increasing from 130 GeV to 209 GeV. These energies are well above the Z-pole and the cross-sections for $e^+e^- \to f\bar{f}$ are significantly smaller than those at the Z-pole. The four LEP experiments have made measurements of the $e^+e^- \to f\bar{f}$ process over this range of energies [32, 33, 34, 35], and a combination of these data is discussed in this section.

Initial-state photon radiation is very important in analysing $e^+e^- \to f\bar{f}$. If an initial-state photon (or photons) is emitted then the effective e^+e^- centre-of-mass energy is reduced from $\sqrt{s}$ to a lower value $\sqrt{s'}$. The rate of events at a given effective energy is given by the probability to emit photons times the cross-section of $e^+e^- \to f\bar{f}$ at the reduced centre-of-mass energy $\sqrt{s'}$. For the case when $\sqrt{s'} \simeq m_Z$, corresponding to a photon energy of $E_\gamma = (s - m_Z^2)/(2\sqrt{s})$, the rate becomes very large. This part, which is called radiative return to the Z, is thus important in both the event selection and the analysis of $e^+e^- \to f\bar{f}$. For the studies reported in this section only events with a small amount of initial state radiation, *i.e.*, large $\sqrt{s'/s}$, are retained.

The cross-section for $e^+e^- \to e^+e^-$ is considerably larger than those of $e^+e^- \to \mu^+\mu^-$ and $e^+e^- \to \tau^+\tau^-$ because of the additional Feynman diagrams involving t-channel photon and Z exchange. The low angle $e^+e^- \to e^+e^-$ Bhabha scattering process is used to determine the luminosity.

In the years 1995 through 1999 LEP delivered luminosity at a number of distinct centre-of-mass energy points. In 2000 most of the luminosity was delivered close to two distinct energies, but there was also a significant fraction of the luminosity delivered in more or less a continuum of energies. To facilitate the combination of the fermion-pair measurements, the four LEP experiments divided the data collected in 2000 into two energy bins: from 202.5 to 205.5 GeV, and above 205.5 GeV. The nominal and actual centre-of-mass energies to which the LEP data are averaged for each year are given in Table 3.1.

A number of measurements of the process $e^+e^- \to f\bar{f}$ exist and are combined. The averages of cross-section and forward-backward asymmetry measurements are discussed in Section 3.2. In Section 3.3 the averages of the differential cross-section measurements, $\frac{d\sigma}{d\cos\theta}$, for the channels $e^+e^- \to \mu^+\mu^-$ and $e^+e^- \to \tau^+\tau^-$ are presented; similar averages for differential cross-sections for $e^+e^- \to e^+e^-$ are given in Section 3.4. In Section 3.5 the combined results are interpreted in terms of contact interactions, the exchange of Z′ bosons, the exchange of leptoquarks or squarks and the exchange of gravitons in large-extra-dimensions scenarios. The results are summarised in Section 3.6.

Year	Nominal Energy GeV	Actual Energy GeV	Luminosity pb^{-1}
1995	130	130.1	3
	136	136.1	3
1996	161	161.3	10
	172	172.1	10
1997	130	130.1	2
	136	136.1	2
	183	182.7	50
1998	189	188.6	170
1999	192	191.6	30
	196	195.5	80
	200	199.5	80
	202	201.7	40
2000	205	204.9	80
	207	206.5	140

Table 3.1: The nominal and actual average centre-of-mass energies for data collected during LEP-II operation in each year. The approximate average integrated luminosity analysed per experiment at each energy is also shown.

The uncorrelated systematic errors on the input measurements have been separated from the statistical errors, allowing the decomposition of the errors on the averages into statistical and systematic components. Multiplicative corrections have been used to correct measurements to the full solid angle or full s' region of the common signal definition. Additional errors have been included to account for uncertainties in these corrections.

Where comparisons with Standard Model (SM) predictions are performed, the predictions are calculated using ZFITTER [36] version 6.36 with the following input parameters:

$$m_{\mathrm{Z}} = 91.1875 \text{ GeV} \tag{3.1}$$
$$m_{\mathrm{t}} = 170.9 \text{ GeV} \tag{3.2}$$
$$m_{\mathrm{H}} = 150 \text{ GeV} \tag{3.3}$$
$$\Delta\alpha^{(5)}_{\mathrm{had}}(m^2_{\mathrm{Z}}) = 0.02758 \tag{3.4}$$
$$\alpha_{\mathrm{S}}(m_{\mathrm{Z}}) = 0.118\,. \tag{3.5}$$

3.2 Averages for Cross-Sections and Asymmetries

In this section the results of the combination of cross-sections and asymmetries are given. The individual experiments' analyses of cross-sections and forward-backward asymmetries are presented in a number of publications [46, 48, 51, 54]. Cross-section results are combined for the $\mathrm{e^+e^-} \to \mathrm{q\overline{q}}$, $\mathrm{e^+e^-} \to \mu^+\mu^-$ and $\mathrm{e^+e^-} \to \tau^+\tau^-$ channels, forward-backward asymmetry measurements are combined for the $\mu^+\mu^-$ and $\tau^+\tau^-$ final states. Events are classified according to the effective centre-of-mass energy, $\sqrt{s'}$. The averages are made for the samples of events with high effective centre-of-mass energies.

Individual experiments study different $\mathrm{f\bar{f}}$ signal definitions; corrections are applied to bring the measurements to the common signal definition:[1]

- $\sqrt{s'}$ is taken to be the mass of the s-channel propagator, with the $\mathrm{f\bar{f}}$ signal being defined by the cut $\sqrt{s'/s} > 0.85$.
- ISR-FSR photon interference is subtracted to render the propagator mass unambiguous.
- Results are given for the full 4π angular acceptance.
- Initial state non-singlet diagrams [59], see for example Figure 3.1, which lead to events containing additional fermion pairs are considered as part of the two-fermion signal. In such events, the additional fermion pairs are typically lost down the beampipe of the experiments, such that the visible event topologies are usually similar to difermion events with photons radiated from the initial state.

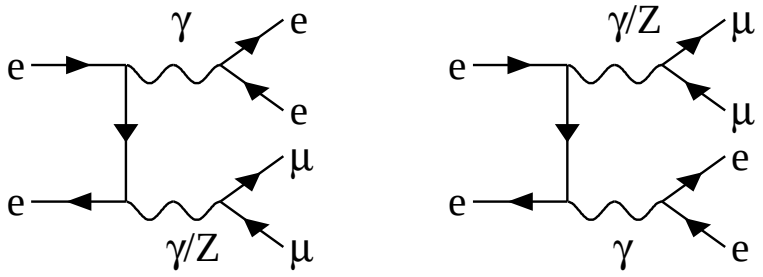


Figure 3.1: Diagrams leading to the production of initial state non-singlet electron-positron pairs in $\mathrm{e^+e^-} \to \mu^+\mu^-$, which are considered as signal in the common signal definition.

The corrections to the common signal definition were applied in two stages. First, for any measurement which used a restricted angular range or s' cut different from the default, a multiplicative correction was applied to the measurement, the associated errors, and the associated SM prediction to correct the acceptance to 4π and to the common s' cut. These corrections were calculated with ZFITTER for each centre-of-mass energy value. Although these corrections are sizable, up to 14%, they are expected to be well modelled. In the second stage an additive correction was used to correct for any other differences in signal definition (*e.g.*, use of a different s' definition, inclusion of interference between initial- and final-state radiation, treatment of four-fermion contribution) and centre-of-mass energy. The additive correction is simply the difference between the SM prediction calculated using the common signal definition, at the mean centre-of-mass energy of the measurements, and that provided by the experiment (corrected for acceptance where necessary).

Uncertainties derived from a comparison of ZFITTER with KK2f [60] are included; these are shown in Table 3.2. Additional errors are also included to account for those cases where the SM prediction provided by the experiment had used a version of ZFITTER other than the default one, or different parameters; these are shown in Table 3.3. The inclusion of these errors has a very small effect on the averages. The hadronic cross-sections change by less than 0.02%, the leptonic cross-sections by less than 0.1% and typically 0.05% and the lepton asymmetries by 0.001.

	$\sigma(\mathrm{q\overline{q}})$	$\sigma(\mu^+\mu^-)$	$\sigma(\tau^+\tau^-)$	$A_{\mathrm{FB}}(\mu^+\mu^-)$	$A_{\mathrm{FB}}(\tau^+\tau^-)$
$\cos\theta$ cut	0.0005	0.0005	0.0005	–	–
s' cut	0.0015	0.0005	0.0005	–	–
s' definition	0.002	0.001	0.001	0.0002	0.0002
ISR-FSR interference	0.002	0.002	0.002	0.005	0.005

Table 3.2: Errors derived from a comparison between ZFITTER and KK2f for variations on the standard signal definition. Values for cross-sections are given as a fraction of the corresponding cross-section; those for asymmetries are absolute.

Expt.	Energies	$\sigma(\mathrm{q\overline{q}})$	$\sigma(\mu^+\mu^-)$	$\sigma(\tau^+\tau^-)$	$A_{\mathrm{FB}}(\mu^+\mu^-)$	$A_{\mathrm{FB}}(\tau^+\tau^-)$
ALEPH	130–183	0.002	0.005	0.005	0.001	0.001
	189–207	0.002	0.003	0.003	0.0006	0.0006
DELPHI	130–207	0.00015	0.00007	0.00007	0.00002	0.00002
L3	130–189	0.002	0.005	0.005	0.005	0.005
	192–207	0.002	0.003	0.003	0.002	0.002
OPAL	130–207	0.00005	0.00005	0.00005	–	–

Table 3.3: Errors applied to account for uncertainties on the ZFITTER predictions quoted by each experiment, depending on ZFITTER version and parameter settings used by each experiment. Values for cross-sections are given as a fraction of the corresponding cross-section; those for asymmetries are absolute.

Theoretical uncertainties associated with the SM predictions for each of the measurements are not included during the averaging procedure, but must be included when assessing the compatibility of the data with theoretical predictions. The theoretical uncertainties on the SM predictions amount to 0.26% on $\sigma(\mathrm{q\overline{q}})$, 0.4% on $\sigma(\mu^+\mu^-)$ and $\sigma(\tau^+\tau^-)$, 2% on $\sigma(\mathrm{e^+e^-})$, and 0.004 on the leptonic forward-backward asymmetries [59].

The average is performed using the best linear unbiased estimator technique (BLUE) [62], which is equivalent to a χ^2 minimisation. All data from the nominal centre-of-mass energy points are averaged at the same time.

Particular care is taken to ensure that the correlations between the hadronic cross-sections are reasonably estimated. The errors are broken down into six categories, with the ensuing correlations accounted for in the combinations:

- The statistical uncertainty.
- The systematic uncertainty for the final state X which is fully correlated between energy points for that experiment.
- The systematic uncertainty for experiment Y which is fully correlated between different final states for this energy point.
- The systematic uncertainty for the final state X which is fully correlated between energy points and between different experiments.

[1]ZFITTER flags BOXD=2, CONV=2, FINR=0, INTF=0, ALEM=2.

- The systematic uncertainty which is fully correlated between energy points and between different experiments for all final states.
- The uncorrelated systematic uncertainty.

The measurements used in the combination are presented in Appendix B.1, using this decomposition of the uncertainties. Uncertainties in the hadronic cross-sections arising from fragmentation models and modelling of ISR are treated as fully correlated between experiments. Despite some differences between the models used and the methods of evaluating the errors in the different experiments, there are significant common elements in the estimation of these sources of uncertainty.

Table 3.4 gives the averaged cross-sections and forward-backward asymmetries for all energies. The χ^2/dof for the average of the LEP-II $\mathrm{f\bar{f}}$ data is 163/180, corresponding to a χ^2 probability of 81%. Most correlations are rather small, with the largest components at any given pair of energies being those between the hadronic cross-sections. The other off-diagonal terms in the correlation matrix are smaller than 10%. The correlation matrix between the averaged hadronic cross-sections at different centre-of-mass energies is given in Table 3.5.

Figures 3.2 and 3.3 show the LEP averaged cross-sections and asymmetries, respectively, as a function of the centre-of-mass energy, together with the SM predictions. There is good agreement between the SM expectations and the measurements of the individual experiments and the combined averages. The ratios of the measured cross-sections and asymmetries to the SM expectations, averaged over all energies and taking into account the correlations between the data points and the theoretical errors on the SM predictions, are given in Table 3.6. It is concluded that there is no evidence in the results of the combinations of the cross-sections and lepton forward-backward asymmetries for physics beyond the SM in the process $\mathrm{e^+e^-} \to \mathrm{f\bar{f}}$, for $\mathrm{f} = \mathrm{q}$, μ or τ.

3.3 Differential Cross-Sections for Muon- and Tau-Pair Final States

The LEP experiments have measured the differential cross-section, $\frac{\mathrm{d}\sigma}{\mathrm{d}\cos\theta}$, for the $\mathrm{e^+e^-} \to \mu^+\mu^-$ and $\mathrm{e^+e^-} \to \tau^+\tau^-$ channels for samples of events with high effective centre-of-mass energy, $\sqrt{s'/s} > 0.85$. A combination of these results is made using the BLUE technique. For some bins the number of observed events is very small, so the statistical error associated with each measurement is taken as the expected statistical error on the differential cross-section, computed from the expected number of events in each bin for each experiment. Using a Monte-Carlo simulation it has been shown that this method provides a good approximation to the exact likelihood method based on Poisson statistics.

The combination includes data from 183 GeV to 207 GeV from DELPHI and OPAL, data at 189 GeV from L3 and data from 189 GeV to 207 GeV from ALEPH. Each experiment's data are binned in 10 bins of $\cos\theta$ at each energy, using their own signal definition. The polar scattering angle, θ, is the angle of the outgoing negative lepton with respect to the incoming electron direction in the detector coordinate system. The outer acceptances of the most forward and most backward bins for which the experiments present their data are different. This was accounted for as part of the correction to a common signal definition. The ranges in $\cos\theta$ for the measurements of the individual experiments and the average are given in Table 3.7. The signal definition used corresponded to the definition given in Section 3.2.

Quantity	$\sqrt{s}$ (GeV)	Average value	SM	$\sqrt{s}$ (GeV)	Average value	SM
$\sigma(q\overline{q})$	130	82.445±2.197±0.766	83.090	192	22.064±0.507±0.107	21.259
$\sigma(\mu^+\mu^-)$	130	8.606±0.699±0.131	8.455	192	2.926±0.181±0.018	3.096
$\sigma(\tau^+\tau^-)$	130	9.020±0.944±0.175	8.452	192	2.860±0.246±0.032	3.096
$A_{fb}(\mu^+\mu^-)$	130	0.694±0.059±0.012	0.705	192	0.551±0.051±0.007	0.566
$A_{fb}(\tau^+\tau^-)$	130	0.682±0.079±0.016	0.705	192	0.590±0.067±0.008	0.565
$\sigma(q\overline{q})$	136	66.984±1.954±0.630	66.787	196	20.307±0.294±0.096	20.148
$\sigma(\mu^+\mu^-)$	136	8.325±0.692±0.109	7.292	196	2.994±0.110±0.018	2.961
$\sigma(\tau^+\tau^-)$	136	7.167±0.851±0.143	7.290	196	2.961±0.152±0.029	2.961
$A_{fb}(\mu^+\mu^-)$	136	0.707±0.061±0.011	0.684	196	0.592±0.030±0.005	0.562
$A_{fb}(\tau^+\tau^-)$	136	0.761±0.089±0.013	0.684	196	0.464±0.044±0.008	0.561
$\sigma(q\overline{q})$	161	37.166±1.063±0.398	35.234	200	19.170±0.283±0.095	19.105
$\sigma(\mu^+\mu^-)$	161	4.580±0.376±0.062	4.610	200	3.072±0.108±0.018	2.833
$\sigma(\tau^+\tau^-)$	161	5.715±0.553±0.139	4.610	200	2.952±0.148±0.029	2.832
$A_{fb}(\mu^+\mu^-)$	161	0.542±0.069±0.012	0.610	200	0.519±0.031±0.005	0.558
$A_{fb}(\tau^+\tau^-)$	161	0.764±0.061±0.013	0.610	200	0.539±0.041±0.007	0.558
$\sigma(q\overline{q})$	172	29.350±0.989±0.336	28.775	202	18.873±0.408±0.098	18.569
$\sigma(\mu^+\mu^-)$	172	3.562±0.331±0.058	3.950	202	2.709±0.146±0.017	2.766
$\sigma(\tau^+\tau^-)$	172	4.053±0.469±0.092	3.950	202	2.838±0.208±0.022	2.765
$A_{fb}(\mu^+\mu^-)$	172	0.673±0.077±0.012	0.591	202	0.547±0.045±0.005	0.556
$A_{fb}(\tau^+\tau^-)$	172	0.357±0.098±0.013	0.591	202	0.535±0.058±0.009	0.556
$\sigma(q\overline{q})$	183	24.599±0.393±0.182	24.215	205	18.137±0.282±0.087	17.832
$\sigma(\mu^+\mu^-)$	183	3.505±0.145±0.042	3.444	205	2.464±0.098±0.015	2.673
$\sigma(\tau^+\tau^-)$	183	3.367±0.174±0.049	3.444	205	2.783±0.149±0.028	2.672
$A_{fb}(\mu^+\mu^-)$	183	0.564±0.034±0.008	0.576	205	0.556±0.034±0.004	0.553
$A_{fb}(\tau^+\tau^-)$	183	0.604±0.044±0.011	0.576	205	0.618±0.040±0.008	0.553
$\sigma(q\overline{q})$	189	22.492±0.206±0.119	22.184	207	17.316±0.212±0.083	17.482
$\sigma(\mu^+\mu^-)$	189	3.150±0.075±0.016	3.207	207	2.618±0.078±0.014	2.628
$\sigma(\tau^+\tau^-)$	189	3.204±0.107±0.032	3.206	207	2.502±0.109±0.029	2.628
$A_{fb}(\mu^+\mu^-)$	189	0.571±0.020±0.005	0.569	207	0.535±0.028±0.004	0.552
$A_{fb}(\tau^+\tau^-)$	189	0.590±0.026±0.007	0.569	207	0.590±0.034±0.010	0.552

Table 3.4: Combined LEP results for the $e^+e^- \to f\overline{f}$ cross-sections (in pb) and forward-backward asymmetries; in each case the first error is statistical and the second systematic. The SM predictions are from ZFITTER.

$\sqrt{s}$	$\sqrt{s}$ (GeV)											
(GeV)	130	136	161	172	183	189	192	196	200	202	205	207
130	1.000	0.060	0.065	0.058	0.104	0.112	0.043	0.065	0.065	0.045	0.061	0.076
136	0.060	1.000	0.061	0.055	0.098	0.104	0.040	0.061	0.061	0.042	0.057	0.071
161	0.065	0.061	1.000	0.060	0.108	0.117	0.044	0.067	0.068	0.047	0.063	0.078
172	0.058	0.055	0.060	1.000	0.096	0.103	0.039	0.060	0.060	0.041	0.056	0.069
183	0.104	0.098	0.108	0.096	1.000	0.205	0.078	0.120	0.121	0.084	0.114	0.140
189	0.112	0.104	0.117	0.103	0.205	1.000	0.097	0.149	0.151	0.105	0.141	0.174
192	0.043	0.040	0.044	0.039	0.078	0.097	1.000	0.060	0.061	0.042	0.057	0.071
196	0.065	0.061	0.067	0.060	0.120	0.149	0.060	1.000	0.094	0.066	0.089	0.110
200	0.065	0.061	0.068	0.060	0.121	0.151	0.061	0.094	1.000	0.067	0.090	0.112
202	0.045	0.042	0.047	0.041	0.084	0.105	0.042	0.066	0.067	1.000	0.063	0.079
205	0.061	0.057	0.063	0.056	0.114	0.141	0.057	0.089	0.090	0.063	1.000	0.106
207	0.076	0.071	0.078	0.069	0.140	0.174	0.071	0.110	0.112	0.079	0.106	1.000

Table 3.5: The correlation coefficients between averaged hadronic cross-sections at different energies.

Channel	Ratio	Deviation
$\sigma(\mathrm{q\overline{q}})$	1.0092±0.0076	+1.21
$\sigma(\mu^+\mu^-)$	0.9936±0.0141	−0.45
$\sigma(\tau^+\tau^-)$	1.0005±0.0203	+0.02
$A_{\mathrm{FB}}(\mu^+\mu^-)$	0.9925±0.0212	−0.35
$A_{\mathrm{FB}}(\tau^+\tau^-)$	1.0246±0.0274	+0.90

Table 3.6: Comparison of measurements to SM predictions for each channel. The second column gives the mean ratio of data to prediction; the third column gives the numbers of standard deviations of the ratio from unity.

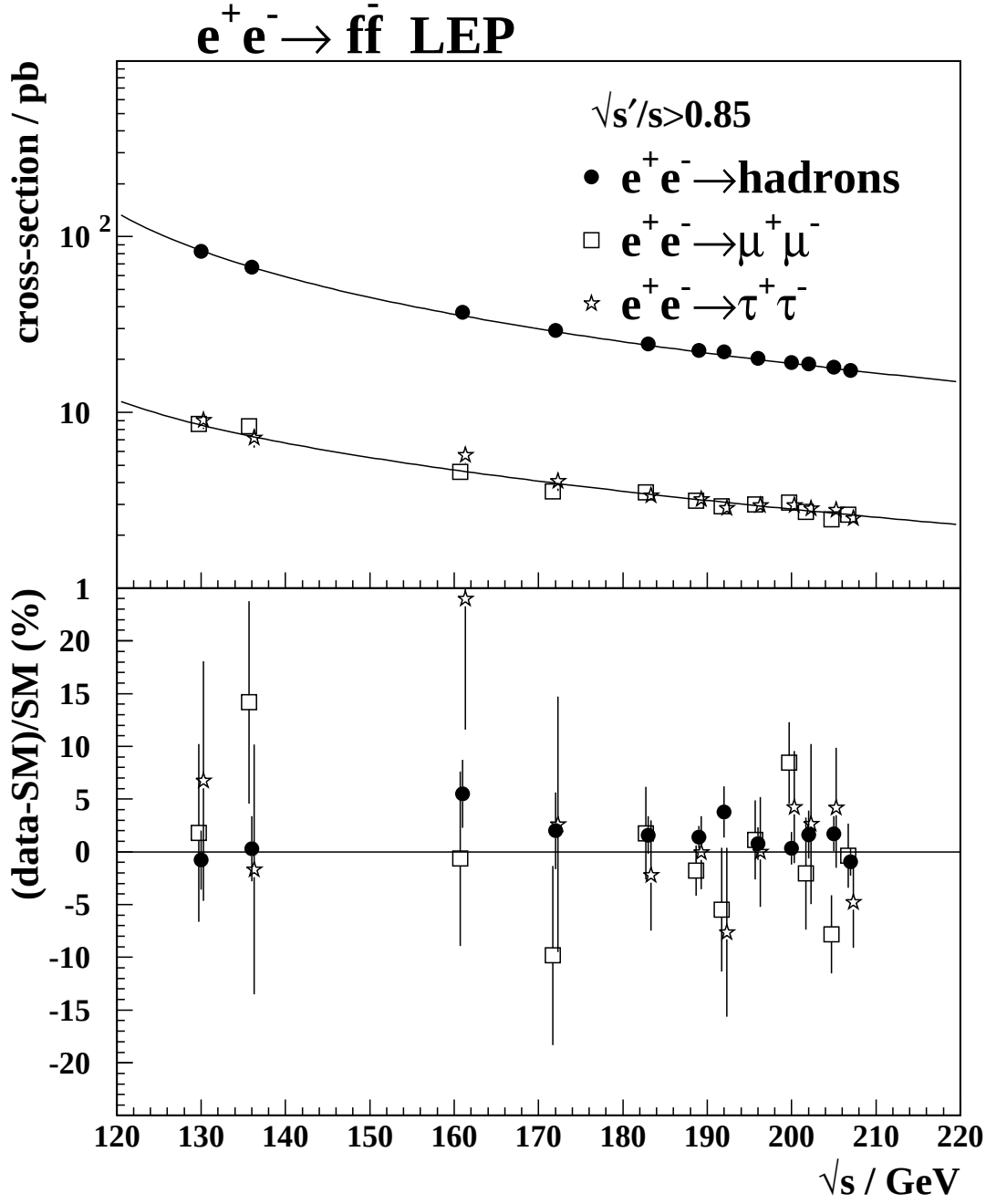


Figure 3.2: Combined LEP results on the cross-sections for $q\overline{q}$, $\mu^+\mu^-$ and $\tau^+\tau^-$ final states, as a function of centre-of-mass energy. The expectations of the SM, computed with ZFITTER, are shown as curves. The lower plot shows the difference between the data and the SM.

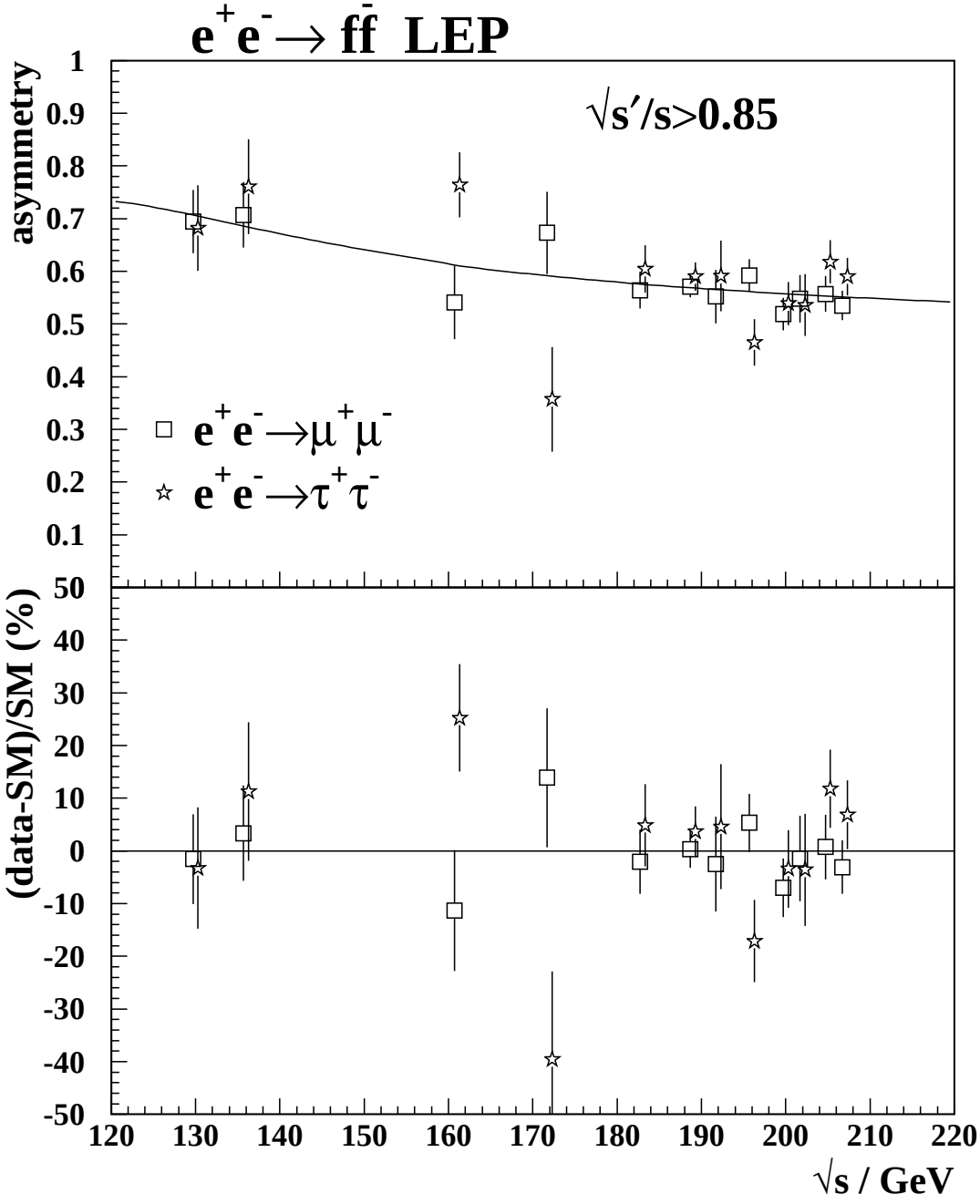


Figure 3.3: Combined LEP results on the forward-backward asymmetry for $\mu^+\mu^-$ and $\tau^+\tau^-$ final states as a function of centre-of-mass energy. The expectations of the SM computed with ZFITTER, are shown as curves. The lower plot shows differences between the data and the SM.

Experiment	$\cos\theta_{min}$	$\cos\theta_{max}$
ALEPH	-0.95	0.95
DELPHI ($e^+e^- \to \mu^+\mu^-$)	-0.97	0.97
DELPHI ($e^+e^- \to \tau^+\tau^-$)	-0.96	0.96
L3	-0.90	0.90
OPAL	-1.00	1.00
Average	-1.00	1.00

Table 3.7: The acceptances in $\cos\theta$ for which the experimental measurements at all energies are presented for combination, and the acceptance for the LEP average. For DELPHI the acceptance is shown for the different channels. For ALEPH, L3 and OPAL the acceptance is the same for muon and tau-lepton channels.

Correlated systematic errors between different experiments, channels and energies, arising from uncertainties on the overall normalisation, are considered in the averaging procedure. All data from all energies are combined in a single fit to obtain averages at each centre-of-mass energy.

The results of the averages are reported in Tables 3.8 and 3.9 and shown in Figures 3.4 and 3.5, with more details summarised in Appendix B.2. The correlations between bins in the average are less that 2% of the total error on the averages in each bin. The combination results in a χ^2 of 352.2 for 320 degrees of freedom, corresponding to a probability of 10.4%.

3.4 Differential Cross-Sections for Electron-Positron Final States

The LEP experiments have measured the differential cross-section, $\frac{d\sigma}{d\cos\theta}$ for the process $e^+e^- \to e^+e^-$ with different acollinearity cuts [32, 33, 34, 35]. The results are combined using a χ^2 fit to the measured differential cross-sections, using the experimental errors as given by the experiments. In contrast to the muon and tau-lepton channels, the higher statistics makes the use of expected errors, as discussed in Section 3.3, unnecessary here.

The combination includes data from 189 to 207 GeV, provided by ALEPH, DELPHI and OPAL. Each experiment's data are binned according to an agreed common definition, which takes into account the large forward peak of Bhabha scattering:

- 10 bins for $\cos\theta$ between 0.0 and 0.90 and
- 5 bins for $\cos\theta$ between -0.90 and 0.0

at each energy, where the polar scattering angle, θ, is the angle of the outgoing electron with respect to the incoming electron direction in the lab coordinate system. Apart from the common binning in $\cos\theta$, each experiment uses its own signal definition. The ranges in $\cos\theta$ covered by the individual experiments and the range used for the combination are given in Table 3.10. The signal definition used for the LEP average corresponds to an acollinearity cut of 10°.

Correlated systematic errors between different experiments, energies and bins at the same energy, arising from uncertainties on the overall normalisation, and from migration of events between forward and backward bins with the same absolute value of $\cos\theta$ due to uncertainties in the corrections for charge confusion, were considered in the averaging procedure.

$\cos\theta$ bin	$\sqrt{s}$ (GeV)	Average value	SM	$\sqrt{s}$ (GeV)	Average value	SM
$[-1.00, -0.80]$	183	0.197±0.183	0.547	200	0.558±0.113	0.501
$[-0.80, -0.60]$	183	0.589±0.163	0.534	200	0.376±0.098	0.478
$[-0.60, -0.40]$	183	0.807±0.174	0.627	200	0.799±0.105	0.541
$[-0.40, -0.20]$	183	1.033±0.197	0.823	200	0.817±0.118	0.689
$[-0.20, 0.00]$	183	1.178±0.236	1.121	200	1.105±0.139	0.922
$[0.00, 0.20]$	183	1.778±0.276	1.521	200	1.462±0.162	1.239
$[0.20, 0.40]$	183	2.143±0.315	2.020	200	1.849±0.185	1.640
$[0.40, 0.60]$	183	2.690±0.367	2.619	200	2.122±0.211	2.126
$[0.60, 0.80]$	183	2.916±0.420	3.314	200	2.947±0.239	2.694
$[0.80, 1.00]$	183	4.368±0.529	4.096	200	3.474±0.306	3.336
$[-1.00, -0.80]$	189	0.614±0.080	0.532	202	1.137±0.162	0.495
$[-0.80, -0.60]$	189	0.420±0.065	0.514	202	0.295±0.139	0.471
$[-0.60, -0.40]$	189	0.530±0.069	0.595	202	0.506±0.149	0.531
$[-0.40, -0.20]$	189	0.651±0.077	0.772	202	0.455±0.169	0.674
$[-0.20, 0.00]$	189	1.064±0.089	1.044	202	0.860±0.197	0.900
$[0.00, 0.20]$	189	1.313±0.111	1.411	202	1.010±0.230	1.208
$[0.20, 0.40]$	189	2.038±0.123	1.872	202	1.749±0.264	1.599
$[0.40, 0.60]$	189	2.158±0.139	2.426	202	1.844±0.299	2.072
$[0.60, 0.80]$	189	2.954±0.158	3.072	202	2.268±0.339	2.627
$[0.80, 1.00]$	189	3.795±0.216	3.799	202	3.396±0.435	3.254
$[-1.00, -0.80]$	192	0.481±0.198	0.524	205	0.621±0.113	0.485
$[-0.80, -0.60]$	192	0.384±0.173	0.504	205	0.385±0.098	0.461
$[-0.60, -0.40]$	192	0.788±0.186	0.579	205	0.382±0.104	0.517
$[-0.40, -0.20]$	192	0.581±0.212	0.748	205	0.443±0.118	0.654
$[-0.20, 0.00]$	192	1.324±0.248	1.008	205	0.891±0.137	0.870
$[0.00, 0.20]$	192	1.187±0.292	1.360	205	1.205±0.160	1.166
$[0.20, 0.40]$	192	1.932±0.334	1.803	205	1.614±0.183	1.542
$[0.40, 0.60]$	192	2.080±0.379	2.337	205	1.663±0.209	1.998
$[0.60, 0.80]$	192	3.003±0.429	2.960	205	2.097±0.237	2.534
$[0.80, 1.00]$	192	3.083±0.552	3.662	205	3.318±0.306	3.140
$[-1.00, -0.80]$	196	0.535±0.119	0.512	207	0.518±0.087	0.481
$[-0.80, -0.60]$	196	0.485±0.103	0.491	207	0.496±0.075	0.456
$[-0.60, -0.40]$	196	0.668±0.111	0.560	207	0.473±0.079	0.510
$[-0.40, -0.20]$	196	0.484±0.126	0.718	207	0.781±0.089	0.643
$[-0.20, 0.00]$	196	0.802±0.147	0.964	207	0.795±0.104	0.855
$[0.00, 0.20]$	196	1.507±0.172	1.298	207	0.995±0.121	1.145
$[0.20, 0.40]$	196	1.657±0.197	1.720	207	1.630±0.139	1.515
$[0.40, 0.60]$	196	2.303±0.223	2.229	207	2.247±0.159	1.963
$[0.60, 0.80]$	196	2.949±0.253	2.824	207	2.491±0.179	2.489
$[0.80, 1.00]$	196	3.272±0.325	3.495	207	2.995±0.231	3.086

Table 3.8: Combined LEP results for the $e^+e^- \to \mu^+\mu^-$ differential cross-sections, in pb divided by $\Delta(\cos\theta)$. The combined statistical and systematic error is shown. The SM predictions are from ZFITTER.

$\cos\theta$ bin	$\sqrt{s}$ (GeV)	Average value	SM	$\sqrt{s}$ (GeV)	Average value	SM
$[-1.00, -0.80]$	183	0.302±0.351	0.548	200	0.489±0.201	0.501
$[-0.80, -0.60]$	183	0.206±0.240	0.535	200	0.619±0.141	0.478
$[-0.60, -0.40]$	183	0.198±0.230	0.627	200	0.528±0.137	0.541
$[-0.40, -0.20]$	183	0.542±0.254	0.823	200	0.628±0.155	0.689
$[-0.20, 0.00]$	183	1.364±0.302	1.121	200	1.067±0.186	0.922
$[0.00, 0.20]$	183	1.519±0.350	1.521	200	1.130±0.214	1.239
$[0.20, 0.40]$	183	1.583±0.389	2.020	200	1.871±0.240	1.640
$[0.40, 0.60]$	183	2.296±0.450	2.619	200	2.043±0.274	2.125
$[0.60, 0.80]$	183	3.954±0.574	3.313	200	2.777±0.339	2.694
$[0.80, 1.00]$	183	4.156±0.919	4.095	200	3.437±0.523	3.336
$[-1.00, -0.80]$	189	0.389±0.123	0.532	202	0.968±0.287	0.495
$[-0.80, -0.60]$	189	0.379±0.093	0.515	202	0.322±0.189	0.471
$[-0.60, -0.40]$	189	0.485±0.089	0.595	202	0.420±0.194	0.531
$[-0.40, -0.20]$	189	0.809±0.100	0.772	202	0.731±0.220	0.674
$[-0.20, 0.00]$	189	0.848±0.118	1.044	202	0.922±0.263	0.900
$[0.00, 0.20]$	189	1.323±0.139	1.411	202	0.789±0.300	1.208
$[0.20, 0.40]$	189	1.989±0.154	1.872	202	1.953±0.341	1.599
$[0.40, 0.60]$	189	2.445±0.179	2.426	202	1.838±0.386	2.072
$[0.60, 0.80]$	189	2.467±0.225	3.071	202	3.129±0.479	2.626
$[0.80, 1.00]$	189	4.111±0.357	3.798	202	3.186±0.747	3.254
$[-1.00, -0.80]$	192	0.014±0.325	0.524	205	0.363±0.203	0.486
$[-0.80, -0.60]$	192	0.355±0.247	0.505	205	0.562±0.137	0.461
$[-0.60, -0.40]$	192	0.479±0.245	0.580	205	0.603±0.135	0.517
$[-0.40, -0.20]$	192	0.762±0.278	0.748	205	0.443±0.154	0.654
$[-0.20, 0.00]$	192	0.816±0.331	1.008	205	0.397±0.179	0.870
$[0.00, 0.20]$	192	1.609±0.385	1.360	205	1.242±0.209	1.166
$[0.20, 0.40]$	192	1.810±0.433	1.803	205	1.522±0.237	1.542
$[0.40, 0.60]$	192	2.059±0.491	2.337	205	1.846±0.268	1.998
$[0.60, 0.80]$	192	2.643±0.599	2.959	205	2.045±0.330	2.533
$[0.80, 1.00]$	192	2.575±0.935	3.661	205	4.671±0.520	3.140
$[-1.00, -0.80]$	196	0.810±0.211	0.513	207	0.272±0.145	0.481
$[-0.80, -0.60]$	196	0.738±0.147	0.491	207	0.412±0.106	0.456
$[-0.60, -0.40]$	196	0.524±0.141	0.560	207	0.534±0.104	0.510
$[-0.40, -0.20]$	196	0.688±0.162	0.718	207	0.563±0.118	0.644
$[-0.20, 0.00]$	196	0.976±0.195	0.964	207	0.683±0.140	0.855
$[0.00, 0.20]$	196	0.977±0.225	1.298	207	1.443±0.161	1.145
$[0.20, 0.40]$	196	1.648±0.252	1.719	207	1.351±0.181	1.514
$[0.40, 0.60]$	196	1.965±0.289	2.228	207	1.761±0.207	1.962
$[0.60, 0.80]$	196	2.269±0.357	2.823	207	1.655±0.255	2.489
$[0.80, 1.00]$	196	3.346±0.557	3.494	207	3.597±0.399	3.085

Table 3.9: Combined LEP results for the $e^+e^- \to \tau^+\tau^-$ differential cross-sections, in pb divided by $\Delta(\cos\theta)$. The combined statistical and systematic error is shown. The SM predictions are from ZFITTER.

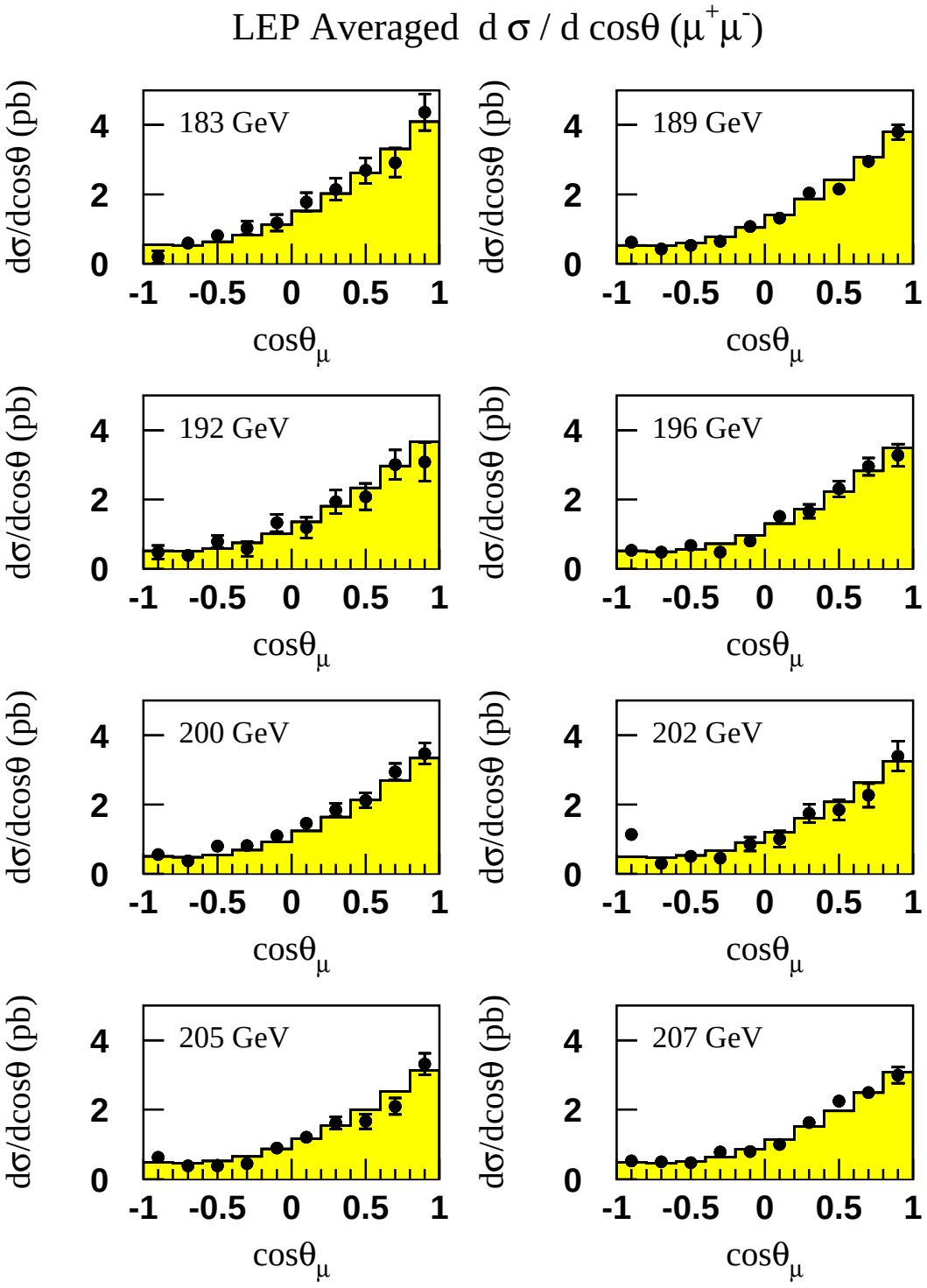


Figure 3.4: LEP averaged differential cross-sections for $e^+e^- \to \mu^+\mu^-$ at energies of 183–207 GeV. The SM predictions, shown as solid histograms, are computed with ZFITTER.

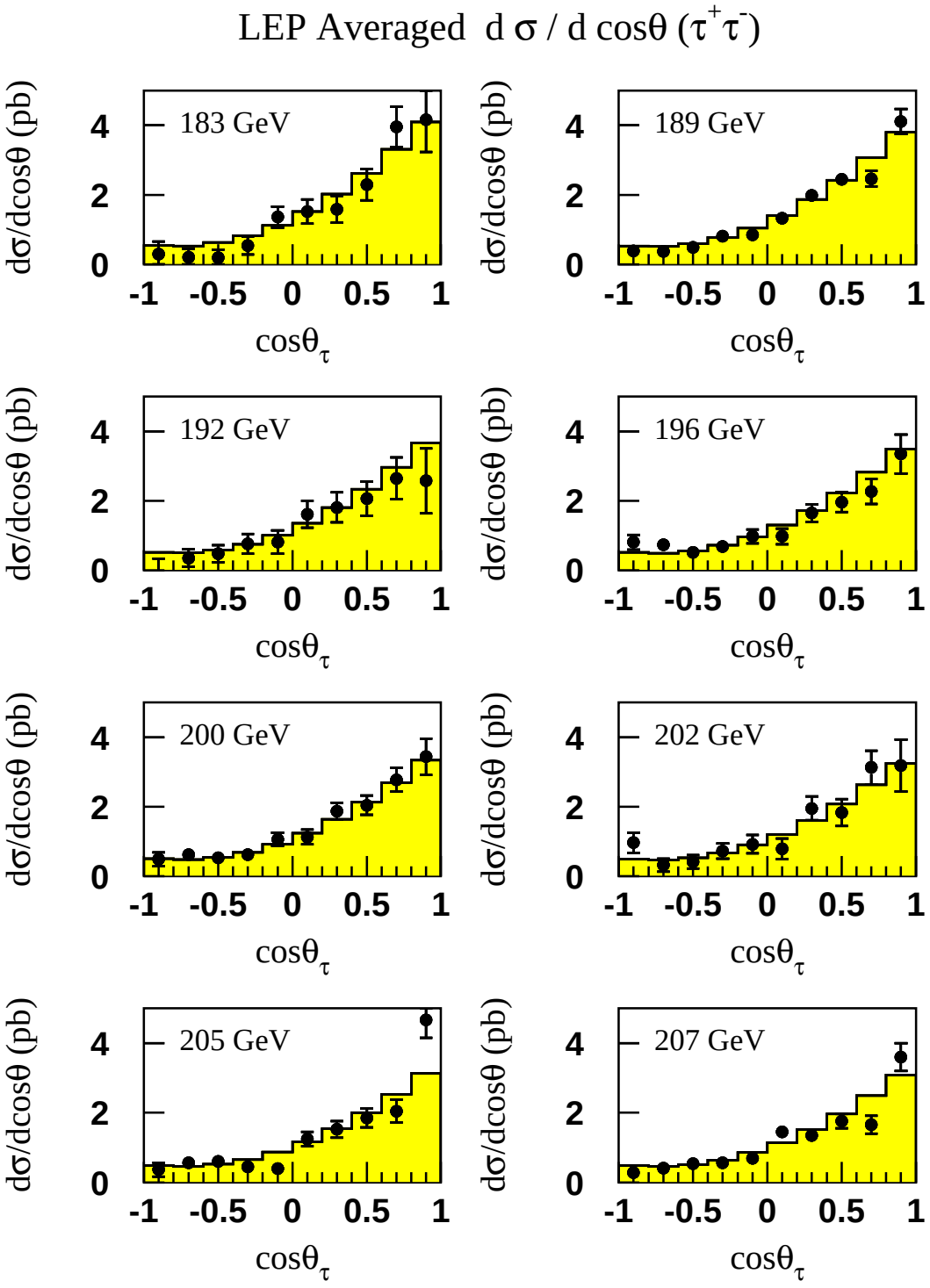


Figure 3.5: LEP averaged differential cross-sections for $e^+e^- \to \tau^+\tau^-$ at energies of 183–207 GeV. The SM predictions, shown as solid histograms, are computed with ZFITTER.

Experiment	$\cos\theta_{min}$	$\cos\theta_{max}$
ALEPH ($\sqrt{s'/s} > 0.85$)	-0.90	0.90
DELPHI (acol. $<$ 20°)	-0.72	0.72
OPAL (acol. $<$ 10°)	-0.90	0.90
Average (acol. $<$ 10°)	-0.90	0.90

Table 3.10: The acceptances for which experimental data are presented for the $e^+e^- \to e^+e^-$ channel and the acceptance for the LEP average.

An average for all energies between 189 and 207 GeV was performed. The results of the averages are reported in Tables 3.11 and 3.12 and shown in Figures 3.6 and 3.7, with more details summarised in Appendix B.3. The χ^2/dof for the average is 199.4/189, corresponding to a probability of 28.8%.

The correlations between bins in the average are well below 5% of the total error on the averages in each bin for most of the cases, and around 10% for bins close to the edges of the acceptance. The agreement between the averaged data and the predictions from the Monte-Carlo generator BHWIDE [64] is good, with a χ^2 of 85 for 90 degrees of freedom, corresponding to a probability of 63%. In conclusion, the combined results for the $e^+e^- \to e^+e^-$ channel are compatible with the SM.

3.5 Interpretation

The combined cross-section and asymmetry results are interpreted in a variety of models. They are used to place limits on the mass of a possible additional heavy neutral boson, Z′, under different assumptions. Limits on contact interactions between leptons and between leptons and quarks are obtained. The former results are of particular interest since they are inaccessible to $p\bar{p}$, pp or ep colliders. Limits are also provided on the masses of leptoquarks. The $e^+e^- \to e^+e^-$ channel is used to constrain the scale of gravity in models with extra dimensions.

3.5.1 Models with Z′ Bosons

The combined hadronic and leptonic cross-sections and the leptonic forward-backward asymmetries are used to fit the data to models including an additional, heavy, neutral boson, Z′.

New gauge bosons in the intermediate TeV scale are motivated by several theoretical approaches [65]. For instance, the breaking of Grand Unifying Theories (GUTs) based on SO(10) or E_6 symmetries may leave one or several U(1) remnants unbroken down to TeV energies, before the symmetry reduces to the SM symmetry. In the case of the E_6 model, one has the possible breaking pattern:

$$E_6 \to SO(10) \times U(1)_\psi \to SU(5) \times U(1)_\chi \times U(1)_\psi \to SM \times U(1)', \tag{3.6}$$

and the new Z′ boson corresponding to the final U(1)′ remnant is a linear combination of the gauge bosons of the two U(1) groups, $U(1)_\chi$ and $U(1)_\psi$, generated in the two-step symmetry breaking, $Z' = Z'_\chi \cos\beta + Z'_\psi \sin\beta$. The value $\beta = \arctan(-\sqrt{5/3})$ would correspond to a Z'_η originating from the direct breaking of E_6 to a rank-5 group in superstring inspired models.

$\cos\theta$ bin	$\sqrt{s}$ (GeV)	Average value	SM	$\sqrt{s}$ (GeV)	Average value	SM
$[-0.90, -0.72]$	189	1.401± 0.161	1.590	196	1.470±0.261	1.483
$[-0.72, -0.54]$	189	2.030± 0.160	1.816	196	1.527±0.221	1.695
$[-0.54, -0.36]$	189	2.162± 0.170	2.162	196	2.058±0.250	2.000
$[-0.36, -0.18]$	189	2.298± 0.186	2.681	196	2.788±0.284	2.498
$[-0.18, 0.00]$	189	4.321± 0.230	3.906	196	3.646±0.318	3.610
$[0.00, 0.09]$	189	4.898± 0.348	5.372	196	5.887±0.521	4.999
$[0.09, 0.18]$	189	6.090± 0.404	6.892	196	6.233±0.591	6.406
$[0.18, 0.27]$	189	8.838± 0.476	9.610	196	9.016±0.694	8.832
$[0.27, 0.36]$	189	12.781± 0.576	13.345	196	13.444±0.856	12.326
$[0.36, 0.45]$	189	19.586± 0.707	19.445	196	18.568±0.977	18.039
$[0.45, 0.54]$	189	30.598± 0.895	30.476	196	27.056±1.223	28.300
$[0.54, 0.63]$	189	50.488± 1.135	51.012	196	49.391±1.619	47.362
$[0.63, 0.72]$	189	95.178± 1.520	95.563	196	88.163±2.154	88.473
$[0.72, 0.81]$	189	211.427± 2.900	212.390	196	197.369±4.121	198.250
$[0.81, 0.90]$	189	679.146± 5.773	689.989	196	637.846±8.003	642.688
$[-0.90, -0.72]$	192	1.300± 0.364	1.539	200	1.483±0.245	1.420
$[-0.72, -0.54]$	192	2.099± 0.419	1.754	200	1.638±0.214	1.623
$[-0.54, -0.36]$	192	1.871± 0.385	2.091	200	2.068±0.227	1.885
$[-0.36, -0.18]$	192	1.808± 0.422	2.604	200	2.362±0.250	2.409
$[-0.18, 0.00]$	192	3.800± 0.519	3.778	200	4.251±0.313	3.435
$[0.00, 0.09]$	192	5.015± 0.891	5.205	200	5.244±0.506	4.770
$[0.09, 0.18]$	192	5.695± 0.976	6.692	200	5.888±0.571	6.157
$[0.18, 0.27]$	192	9.239± 1.175	9.242	200	8.244±0.667	8.471
$[0.27, 0.36]$	192	12.941± 1.414	12.800	200	9.506±0.736	11.773
$[0.36, 0.45]$	192	20.761± 1.807	18.776	200	16.376±0.920	17.262
$[0.45, 0.54]$	192	26.466± 2.074	29.471	200	27.000±1.214	27.117
$[0.54, 0.63]$	192	49.382± 2.671	49.338	200	44.614±1.537	45.607
$[0.63, 0.72]$	192	89.676± 3.615	92.079	200	86.454±2.060	85.143
$[0.72, 0.81]$	192	204.579± 6.760	206.087	200	190.962±3.941	190.786
$[0.81, 0.90]$	192	655.724±12.588	669.173	200	604.986±7.608	617.718

Table 3.11: Combined LEP results for the $e^+e^- \to e^+e^-$ differential cross-sections, in pb divided by $\Delta(\cos\theta)$, for $\sqrt{s}$ between 189 GeV and 200 GeV. The combined statistical and systematic error is shown. The SM predictions are from BHWIDE

$\cos\theta$ bin	$\sqrt{s}$ (GeV)	Average value	SM	$\sqrt{s}$ (GeV)	Average value	SM
$[-0.90, -0.72]$	202	1.568± 0.368	1.401	207	1.440±0.196	1.339
$[-0.72, -0.54]$	202	1.344± 0.276	1.579	207	1.426±0.163	1.517
$[-0.54, -0.36]$	202	2.107± 0.345	1.836	207	1.889±0.177	1.745
$[-0.36, -0.18]$	202	3.240± 0.406	2.361	207	2.156±0.198	2.240
$[-0.18, 0.00]$	202	2.911± 0.394	3.356	207	3.215±0.233	3.194
$[0.00, 0.09]$	202	4.603± 0.628	4.669	207	4.434±0.357	4.380
$[0.09, 0.18]$	202	6.463± 0.861	6.017	207	6.393±0.463	5.729
$[0.18, 0.27]$	202	7.457± 0.957	8.320	207	6.951±0.481	7.972
$[0.27, 0.36]$	202	11.032± 1.113	11.554	207	11.221±0.615	11.019
$[0.36, 0.45]$	202	16.428± 1.338	16.891	207	15.933±0.739	16.053
$[0.45, 0.54]$	202	27.153± 1.643	26.583	207	25.676±0.923	25.254
$[0.54, 0.63]$	202	46.490± 2.214	44.786	207	42.075±1.188	42.456
$[0.63, 0.72]$	202	87.253± 2.887	83.473	207	77.611±1.569	79.639
$[0.72, 0.81]$	202	189.026± 5.516	186.904	207	173.825±3.002	178.042
$[0.81, 0.90]$	202	599.860±10.339	605.070	207	573.637±6.024	576.688
$[-0.90, -0.72]$	205	1.102± 0.205	1.355			
$[-0.72, -0.54]$	205	1.470± 0.195	1.539			
$[-0.54, -0.36]$	205	2.050± 0.231	1.786			
$[-0.36, -0.18]$	205	2.564± 0.255	2.280			
$[-0.18, 0.00]$	205	3.410± 0.300	3.253			
$[0.00, 0.09]$	205	5.308± 0.472	4.479			
$[0.09, 0.18]$	205	5.836± 0.571	5.820			
$[0.18, 0.27]$	205	7.996± 0.635	8.077			
$[0.27, 0.36]$	205	10.607± 0.764	11.200			
$[0.36, 0.45]$	205	14.729± 0.874	16.322			
$[0.45, 0.54]$	205	26.189± 1.157	25.722			
$[0.54, 0.63]$	205	43.124± 1.497	43.217			
$[0.63, 0.72]$	205	79.255± 1.976	80.939			
$[0.72, 0.81]$	205	179.842± 3.838	180.878			
$[0.81, 0.90]$	205	587.999± 7.527	586.205			

Table 3.12: Combined LEP results for the $e^+e^- \to e^+e^-$ differential cross-sections (continued), in pb divided by $\Delta(\cos\theta)$, for $\sqrt{s}$ larger than 200 GeV. The combined statistical and systematic error is shown. The SM predictions are from BHWIDE.

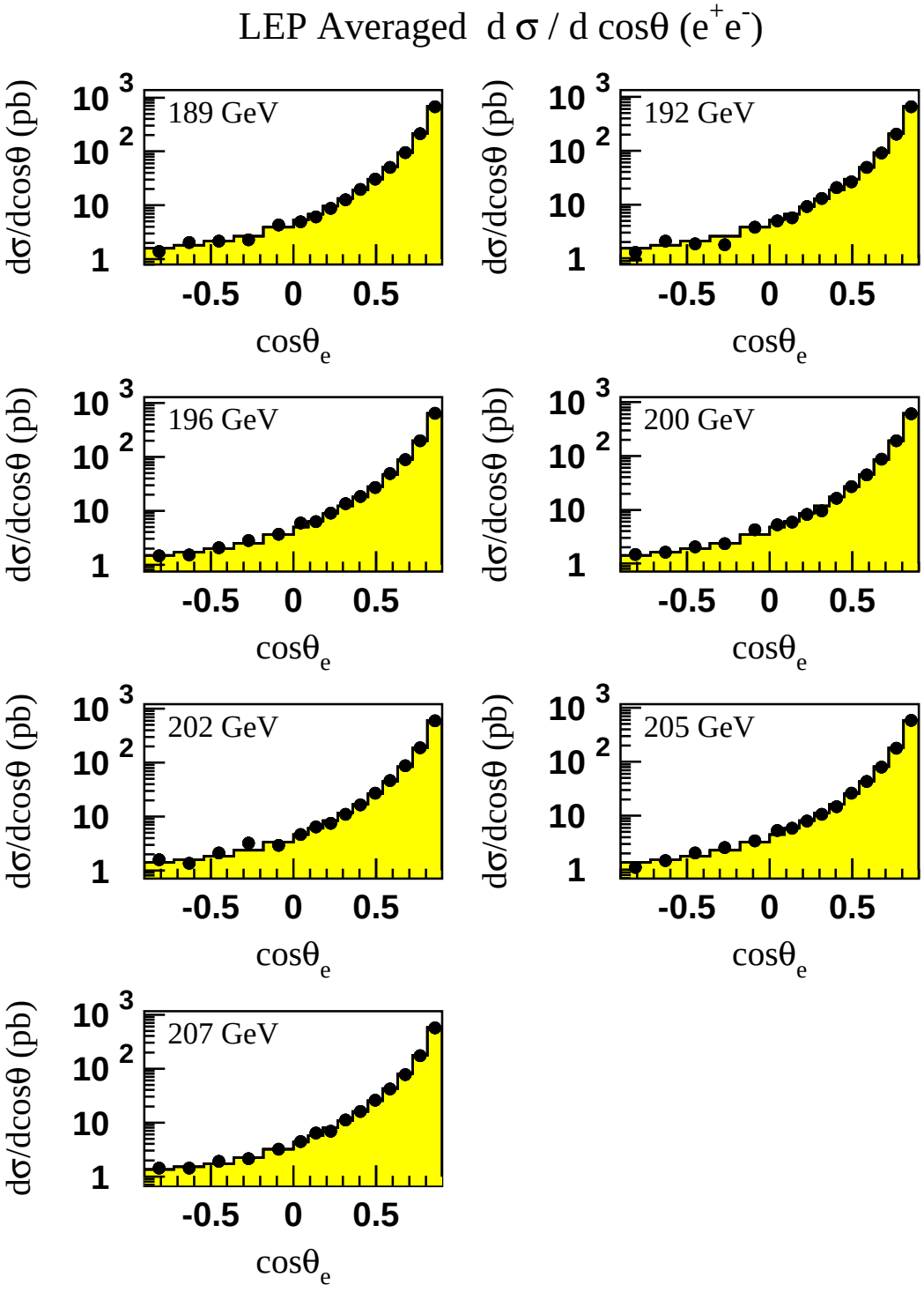


Figure 3.6: LEP averaged differential cross-sections for $e^+e^- \to e^+e^-$ at energies of 189–207 GeV. The SM predictions, shown as solid histograms, are computed with BHWIDE.

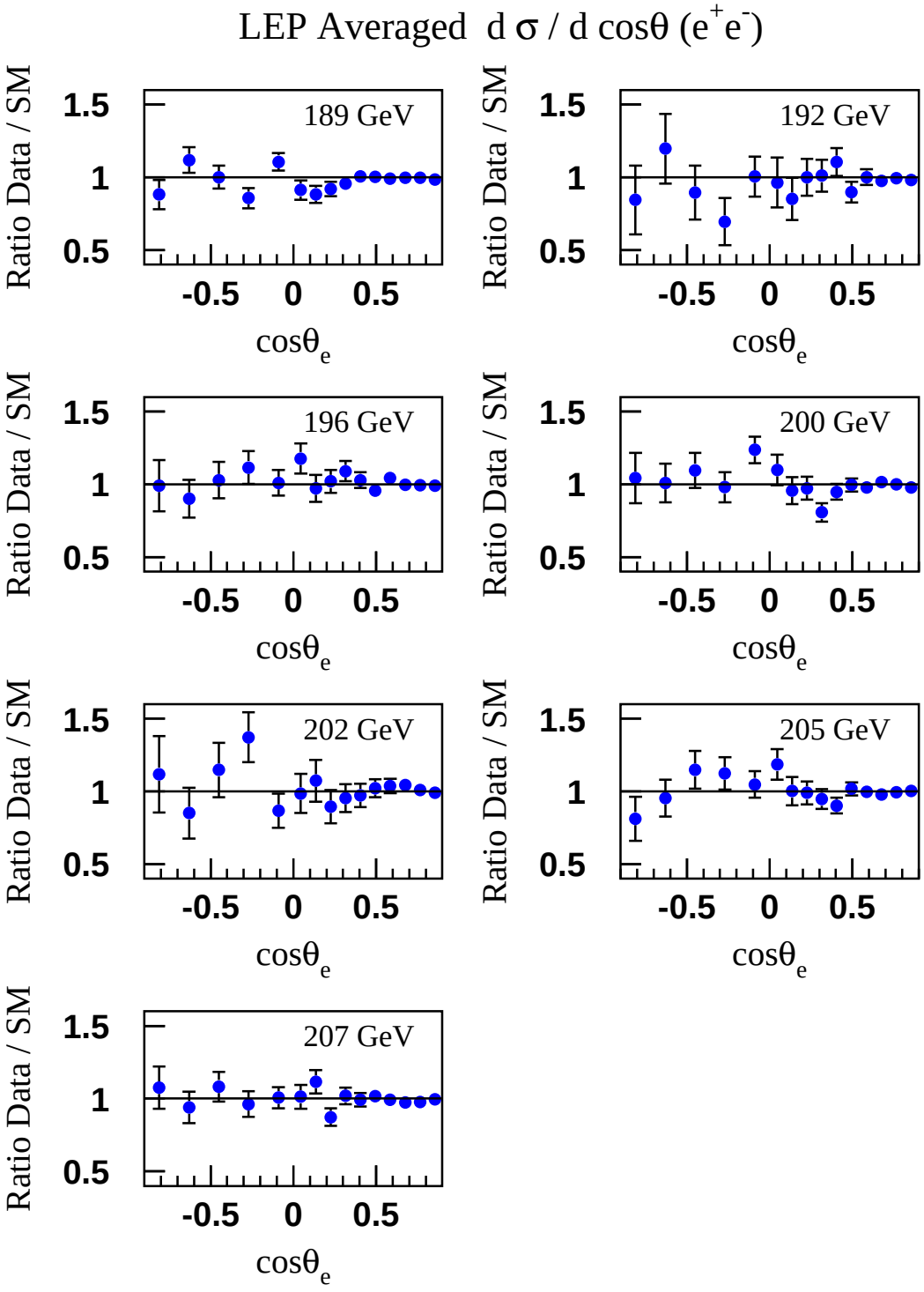


Figure 3.7: Ratio of the LEP averaged differential cross-sections for $e^+e^- \to e^+e^-$ at energies of 189–207 GeV to the SM predictions, as computed with BHWIDE.

Other options are left-right (LR) models, based on the group $SU(2)_R \times SU(2)_L \times U(1)_{B-L}$ in which the new Z'_{LR} will couple to a linear combination of the right-handed and B–L currents with a parameter:

$$\alpha_{LR}^2 = \frac{\sin^2\theta_W}{\cos^2\theta_W}\frac{g_R^2}{g_L^2} - 1\,. \tag{3.7}$$

Below the resonance, new gauge bosons appear as deviations from the SM predictions due to $\gamma - Z'$ and $Z{-}Z'$ interference terms. Fits are made to the mass of a Z', $M_{Z'}$, for Z' models varying the parameters β and α_{LR} including four special models referred to as χ, ψ, η and L-R [69] and the Sequential Standard Model (SSM) [74], which proposes the existence of a Z' with exactly the same coupling to fermions as the standard Z.

The LEP-II data alone do not significantly constrain the mixing angle between the Z and Z' fields, $\Theta_{ZZ'}$. However, results from a single experiment in which LEP-I data are used in the fit show that the mixing is consistent with zero (see for example Reference [76], giving limits of 30 mrad or less depending on the model). Hence, for these fits $\Theta_{ZZ'}$ is fixed to zero. The calculation of Z' contributions is implemented in an extension of the ZFITTER program [77].

The predictions from the Z' models are fitted to the combined LEP-II cross-section and forward-backward asymmetry measurements. In this approach the absence of Z' bosons is equivalent to infinite Z' mass or zero coupling.

No significant evidence is found for the existence of a Z' boson in any of the models. In its absence, 95% confidence level lower limits on $M_{Z'}$ are obtained with a Bayesian method with the assumption of a flat prior in the physically allowed region. The lower limits on the Z' mass are summarized in Table 3.13 and shown in Figure 3.8.

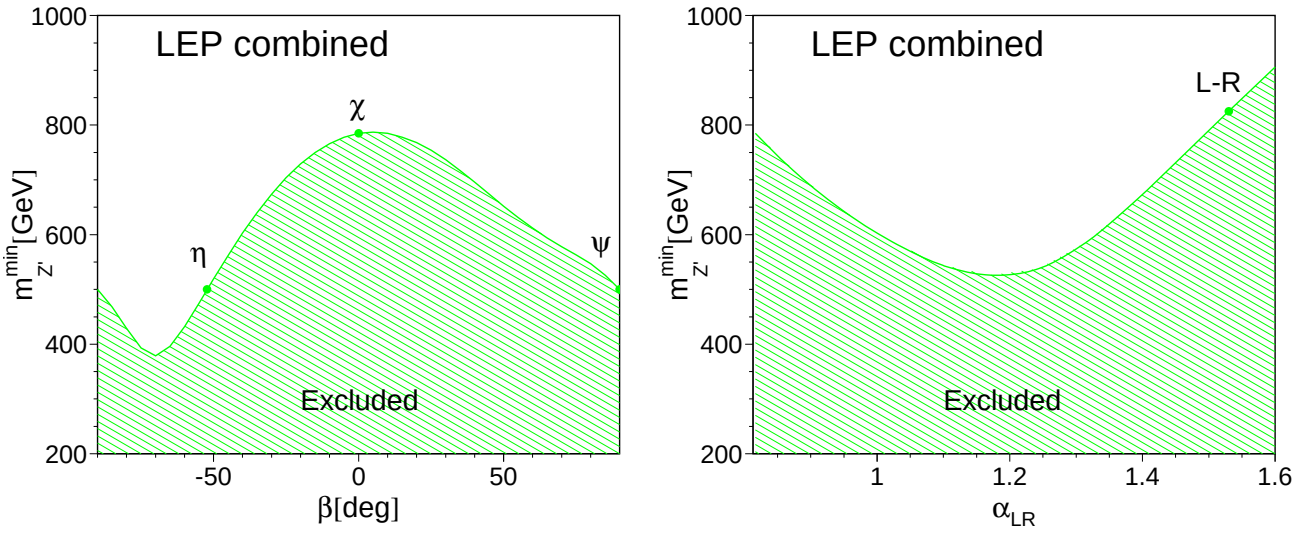


Figure 3.8: Lower limits on the Z' mass at the 95% C.L. for Z' models based on the symmetry breaking of E_6 GUT models (left plot) and on left-right models (right plot).

3.5.2 Contact Interactions

The averaged differential cross-sections for electron-pairs, the averaged cross-sections and forward-backward asymmetries for muon-pairs and tau-lepton pairs, and the hadron cross-sections are

Model	χ	ψ	η	L-R	SSM
$M_{Z'}^{limit}$ (GeV)	785	500	500	825	1760

Table 3.13: The 95% confidence level lower limits on the Z′ mass in the χ, ψ, η, L-R and SSM models.

used to search for contact interactions between leptons and between leptons and quarks.

Following Reference [79], contact interactions are parametrised by an effective Lagrangian, $\mathcal{L}_{\text{eff}}$, which is added to the SM Lagrangian and has the form:

$$\mathcal{L}_{\text{eff}} = \frac{g^2}{(1+\delta)\Lambda_{\pm}^2} \sum_{i,j=L,R} \eta_{ij} \overline{e}_i \gamma_\mu e_i \overline{f}_j \gamma^\mu f_j \,, \tag{3.8}$$

where $g^2/4\pi$ is taken to be 1 by convention, $\delta = 1(0)$ for $f = e$ ($f \neq e$), $\eta_{ij} = \pm 1$ or 0, $\Lambda_{\pm}$ is the scale of the contact interactions, e_i and f_j are left or right-handed spinors. By assuming different helicity coupling between the initial state and final state currents, a set of different models can be defined from this Lagrangian [80], with either constructive (+) or destructive (−) interference between the SM process and the contact interactions. The models and corresponding choices of η_{ij} are given in Table 3.14. The models LL, RR, VV, AA, LR, RL, V0, A0, A1 are considered here since these models lead to large deviations in the $e^+e^- \to \mu^+\mu^-$ and $e^+e^- \to \tau^+\tau^-$ channels. Potential deviations between SM predictions and measurements of the hadronic cross-section can be interpreted as new interactions occurring between electrons and a single quark flavour only, or as interaction between electrons and all quark flavours at the same time. In the former case the scale of the contact interaction is denoted by Λ_{uu} for a flavour of up type (u,c) and by Λ_{dd} for a flavour of down type (d,s,b), while for the latter the scale of the single contact interaction is denoted by Λ_{qq}.

For the purpose of fitting contact interaction models to the data, a new parameter $\varepsilon_{\pm} = 1/\Lambda_{\pm}^2$ is defined; $\varepsilon = 0$ in the limit that there are no contact interactions. This parameter is allowed to take both positive and negative values in the fits. Theoretical uncertainties on the SM predictions are taken from Reference [59], see above.

The values of ε extracted for each model are all compatible with the SM expectation $\varepsilon = 0$ within at most two standard deviations. The fitted values of ε are converted into 95% confidence level lower limits on $\Lambda_{\pm}$. The limits are obtained with a Bayesian method with the assumption of a flat prior in the physically allowed region, $\varepsilon \geq 0$ for each Λ_+ limit and $\varepsilon \leq 0$ for Λ_- limits. The results are shown in Table 3.15 and illustrated in Figure 3.9. The parameters Λ given in the last column of Table 3.15 are derived from the $\Lambda_{e^+e^-}$ values combined with the results on Λ from a combined fit to the $\mu^+\mu^-$ and $\tau^+\tau^-$ cross-sections and asymmetries.

The full correlation matrix of the differential cross-sections for electron pairs, obtained in the averaging procedure, is used in the fits. Some aspects of the combination of the LEP data on Bhabha scattering are discussed in References [81, 82, 83]). For the VV model with positive interference and assuming electromagnetic coupling strength instead of $g^2/4\pi = 1$ [82], the scale Λ can be converted to an upper limit on the electron size:

$$r_e < 1.1 \cdot 10^{-19} \text{ m}. \tag{3.9}$$

Models with stronger couplings will make this upper limit even stronger.

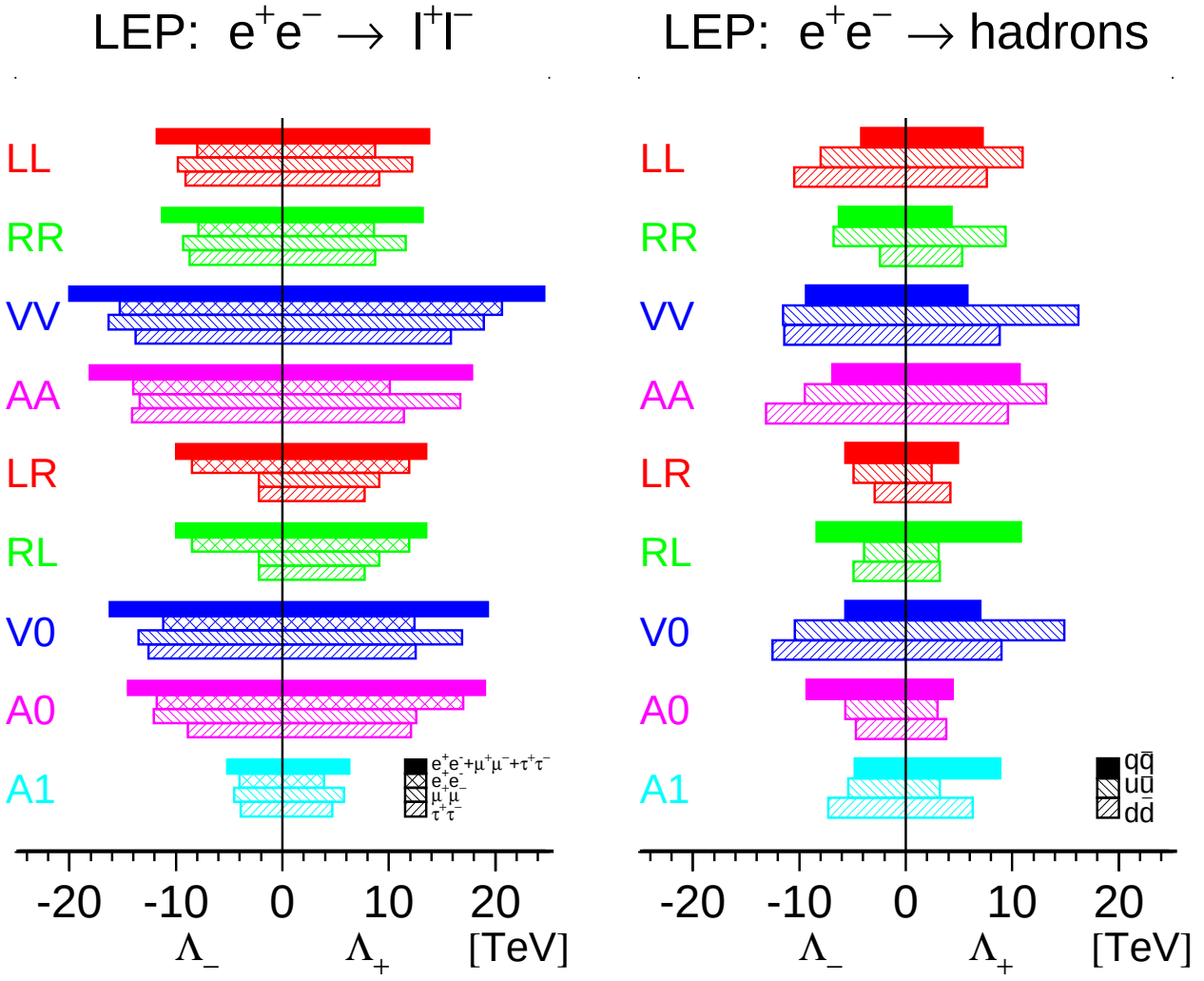


Figure 3.9: The 95% confidence limits on $\Lambda_{\pm}$, for constructive (+) and destructive interference (−) with the SM, for the contact interaction models discussed in the text. Results are shown for $e^+e^- \to e^+e^-$, $e^+e^- \to \mu^+\mu^-$, and $e^+e^- \to \tau^+\tau^-$ as well as for $e^+e^- \to u\bar{u}$, $e^+e^- \to d\bar{d}$ and $e^+e^- \to q\bar{q}$. For $e^+e^- \to \ell^+\ell^-$, universality in the contact interactions between leptons is assumed.

Model	η_{LL}	η_{RR}	η_{LR}	η_{RL}
$LL^{\pm}$	±1	0	0	0
$RR^{\pm}$	0	±1	0	0
$VV^{\pm}$	±1	±1	±1	±1
$AA^{\pm}$	±1	±1	∓1	∓1
$LR^{\pm}$	0	0	±1	0
$RL^{\pm}$	0	0	0	±1
$V0^{\pm}$	±1	±1	0	0
$A0^{\pm}$	0	0	±1	±1
$A1^{\pm}$	±1	∓1	0	0

Table 3.14: Choices of η_{ij} for different contact interaction models.

.

3.5.3 Large Extra Dimensions

An approach to the solution of the hierarchy problem has been proposed in [84], which brings close the electroweak scale $m_{EW} \sim 1$ TeV and the Planck scale $M_{Pl} = \frac{1}{\sqrt{G_N}} \sim 10^{15}$ TeV. In this framework the effective 4 dimensional M_{Pl} is connected to a new $M_{Pl(4+n)}$ scale in a (4+n) dimensional theory:

$$M_{Pl}^2 \sim M_{Pl(4+n)}^{2+n} R^n \,, \tag{3.10}$$

where there are n extra compact spatial dimensions of radius R.

In the production of fermion- or boson-pairs in e^+e^- collisions this class of models can manifest itself through virtual effects due to the exchange of gravitons (Kaluza-Klein excitations). As discussed in [87, 88, 89, 90], the exchange of spin-2 gravitons modifies in a unique way the differential cross-sections for fermion pairs, providing clear signatures. These models introduce an effective scale (ultraviolet cut-off). We will adopt the notation from [87] and call the gravitational mass scale M_s. The cut-off scale is supposed to be of the order of the fundamental gravity scale in $4 + n$ dimensions.

The parameter ε is defined as:

$$\varepsilon = \frac{\lambda}{M_s^4} \,, \tag{3.11}$$

where the coefficient λ is of order 1 and can not be calculated explicitly without knowledge of the full quantum gravity theory. In the following analysis we will assume that $\lambda = \pm1$ in order to study both the cases of positive and negative interference. To compute the deviations from the SM due to virtual graviton exchange we use the calculations [89, 88].

A fit to the $e^+e^- \to e^+e^-$ differential cross-section is performed; this channel has by far the highest sensitivity. The fitted values of ε agree well with the SM expectation, and are used to derive limits on the gravitational mass scale M_s at 95 % CL:

$$M_s > 1.09 \text{ TeV for } \lambda = +1 \,, \tag{3.12}$$

$$M_s > 1.25 \text{ TeV for } \lambda = -1 \,. \tag{3.13}$$

$e^+e^- \to \ell^+\ell^-$								
Model	Λ^-_{ee} (TeV)	Λ^+_{ee}	$\Lambda^-_{\mu\mu}$ (TeV)	$\Lambda^+_{\mu\mu}$	$\Lambda^-_{\tau\tau}$ (TeV)	$\Lambda^+_{\tau\tau}$	$\Lambda^-_{\ell^+\ell^-}$(TeV)	$\Lambda^+_{\ell^+\ell^-}$
LL	8.0	8.7	9.8	12.2	9.1	9.1	11.8	13.8
RR	7.9	8.6	9.3	11.6	8.7	8.7	11.3	13.2
VV	15.3	20.6	16.3	18.9	13.8	15.8	20.0	24.6
AA	14.0	10.1	13.4	16.7	14.1	11.4	18.1	17.8
LR	8.5	11.9	2.2	9.1	2.2	7.7	10.0	13.5
RL	8.5	11.9	2.2	9.1	2.2	7.7	10.0	13.5
V0	11.2	12.4	13.5	16.9	12.6	12.5	16.2	19.3
A0	11.8	17.0	12.1	12.6	8.9	12.1	14.5	19.0
A1	4.0	3.9	4.5	5.8	3.9	4.7	5.2	6.3

$e^+e^- \to q\bar{q}$						
Model	$\Lambda^-_{u\bar{u}}$(TeV)	$\Lambda^+_{u\bar{u}}$(TeV)	$\Lambda^-_{d\bar{d}}$(TeV)	$\Lambda^+_{d\bar{d}}$(TeV)	$\Lambda^-_{q\bar{q}}$(TeV)	$\Lambda^+_{q\bar{q}}$(TeV)
LL	8.0	11.0	10.5	7.6	4.2	7.2
RR	6.8	9.4	2.4	5.3	6.3	4.3
VV	11.5	16.2	11.4	8.8	9.4	5.8
AA	9.5	13.2	13.1	9.6	6.9	10.7
LR	4.9	2.4	2.9	4.2	5.7	4.9
RL	3.9	3.1	4.9	3.2	8.4	10.8
V0	10.4	14.9	12.5	9.0	5.7	7.0
A0	5.7	3.0	4.7	3.8	9.3	4.4
A1	5.4	3.2	7.3	6.3	4.8	8.9

Table 3.15: The 95% confidence limits on the scale, $\Lambda^{\pm}$, for constructive (+) and destructive interference (−) with the SM, for the contact interaction models discussed in the text. Results are given for $e^+e^- \to \mu^+\mu^-$, $e^+e^- \to \tau^+\tau^-$ and $e^+e^- \to e^+e^-$ as well as for $e^+e^- \to u\overline{u}$, $e^+e^- \to d\overline{d}$ and $e^+e^- \to q\overline{q}$. For $e^+e^- \to \ell^+\ell^-$, universality in the contact interactions between leptons is assumed.

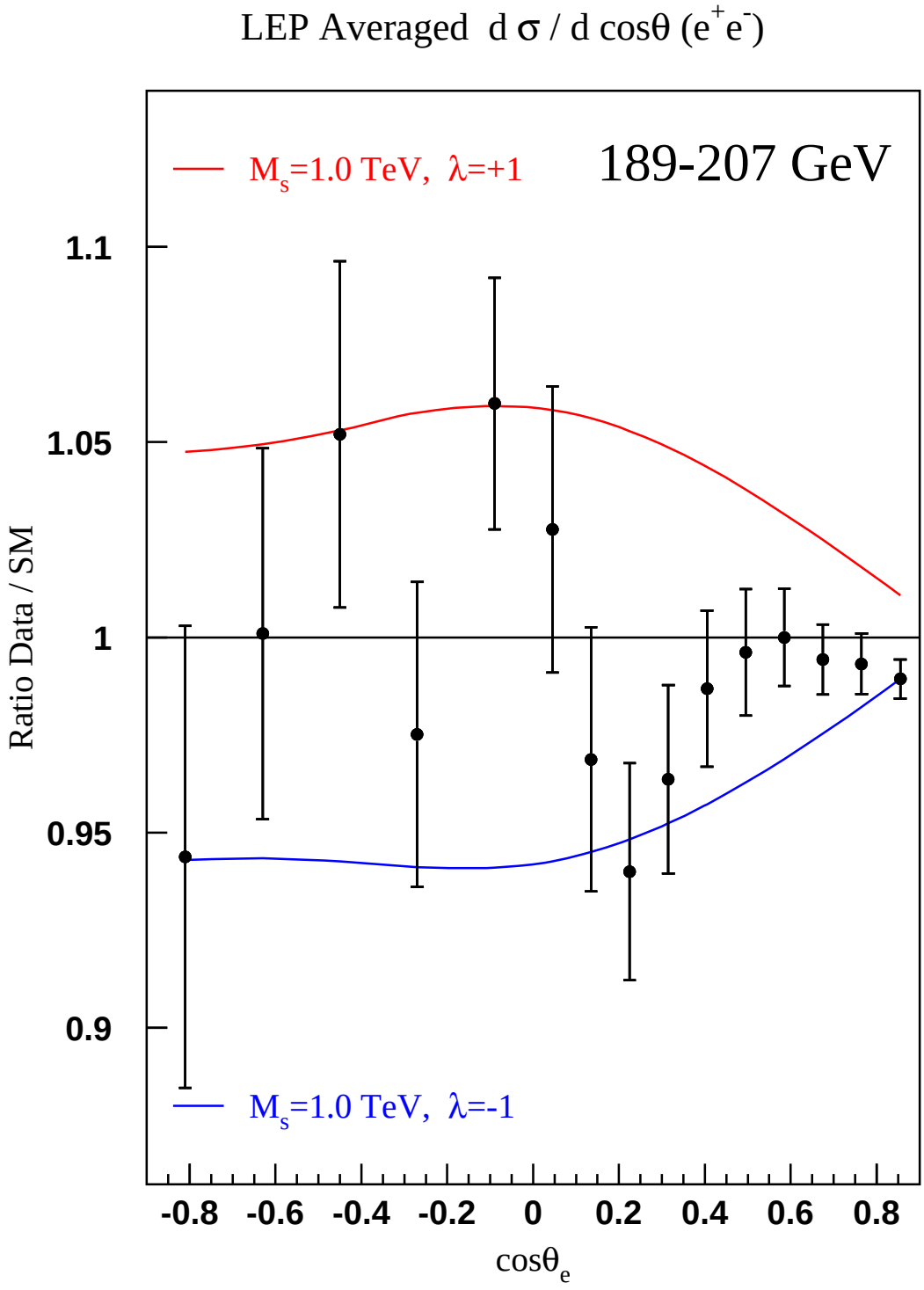


Figure 3.10: Ratio of the LEP averaged differential cross-section for $e^+e^- \to e^+e^-$ compared to the SM prediction. The effects expected from virtual graviton exchange are also shown.

An example of the analysis is shown in Figure 3.10.

The interference of virtual graviton exchange amplitudes with both t-channel and s-channel Bhabha scattering amplitudes makes this the most sensitive search channel at LEP. The results obtained here would not be strictly valid if the luminosity measurements of the LEP experiments, based on the very same process, is also be affected by graviton exchange. However, as shown in [81], the effect on the cross-section in the luminosity angular range is so small that it can safely be neglected in this analysis.

3.5.4 Leptoquarks

Leptoquarks (LQ) mediate quark-lepton transitions. They carry fermion numbers, $F = L+3B$. Following the notations in References [92] and [94], scalar leptoquarks, S_I, and vector leptoquarks, V_I, are indicated based on spin and isospin I. Isomultiplets with different hypercharges are denoted by an additional tilde. It is assumed that leptoquark couplings to quark-lepton pairs are flavour-diagonal and preserve baryon- and lepton-number. The couplings refer to $g_L,\ g_R$, according to the chirality of the lepton. In the process $e^+e^- \to q\overline{q}$ leptoquarks can be exchanged in u- or t-channel, with $F = 0$ or $|F| = 2$.

For convenience, one type of leptoquarks is assumed to be much lighter than the others. Further, experimental constraints on the product $g_L g_R$ allow separate studies of $g_L \neq 0$ or $g_R \neq 0$.

Assuming a coupling of electromagnetic strength, $g = \sqrt{4\pi\alpha}$, where α is the fine structure constant, limits on the masses of leptoquarks coupling to electrons and the first generation of quarks are derived with a Bayesian method with the assumption of a flat prior in the physically allowed region from comparisons of the theoretical predictions for the total hadronic cross-section to the LEP-II averaged measurements.

The 95% confidence level lower limits on masses m_{LQ} are summarised in Table 3.16.

LQ type	m_{LQ}^{min}(GeV)	LQ type	m_{LQ}^{min}(GeV)
$S_0(\mathrm{L}) \to \mathrm{eu}$	646	$V_{1/2}(\mathrm{L}) \to \mathrm{ed}$	348
$S_0(\mathrm{R}) \to \mathrm{eu}$	516	$V_{1/2}(\mathrm{R}) \to \mathrm{eu},\ \mathrm{ed}$	238
$\tilde{S}_0(\mathrm{R}) \to \mathrm{ed}$	256	$\tilde{V}_{1/2}(\mathrm{L}) \to \mathrm{eu}$	186
$S_1(\mathrm{L}) \to \mathrm{eu},\ \mathrm{ed}$	429	$V_0(\mathrm{L}) \to \mathrm{e\bar{d}}$	897
$S_{1/2}(\mathrm{L}) \to \mathrm{e\bar{u}}$	228	$V_0(\mathrm{R}) \to \mathrm{e\bar{d}}$	482
$S_{1/2}(\mathrm{R}) \to \mathrm{e\bar{u}},\ \mathrm{e\bar{d}}$	285	$\tilde{V}_0(\mathrm{R}) \to \mathrm{e\bar{u}}$	577
$\tilde{S}_{1/2}(\mathrm{L}) \to \mathrm{e\bar{d}}$	–	$V_1(\mathrm{L}) \to \mathrm{e\bar{u}},\ \mathrm{e\bar{d}}$	765

Table 3.16: The 95% confidence level lower limits on the LQ mass assuming $g_{L,R} = \sqrt{4\pi\alpha}$. For $\tilde{S}_{1/2}(\mathrm{L})$ no limit can be set because the contribution from this leptoquark type to the hadronic cross-section is not observable with the precision of the measurements.

3.6 Summary

A combination of the LEP-II $e^+e^- \to f\overline{f}$ cross-sections (for hadron, muon and tau-lepton final states) and forward-backward asymmetries (for muon and tau-lepton final states) from LEP

running at energies from 130 to 209 GeV is made. The results from the four LEP experiments are in good agreement with each other. The averages for all energies are shown in Table 3.4. The use of the combined fermion-pair results in an S-Matrix analysis is discussed in Appendix A. Differential cross-sections, $\frac{d\sigma}{d\cos\theta}$, for $e^+e^- \to \mu^+\mu^-$, $e^+e^- \to \tau^+\tau^-$ and $e^+e^- \to e^+e^-$ are also combined. Results are shown in Figures 3.4, 3.5 and 3.6. All results are in good agreement with the predictions of the SM.

The averaged cross-section, forward-backward asymmetry and differential cross-section results are interpreted in a variety of models. The LEP-II averaged cross-sections and lepton asymmetries are used to obtain lower limits on the mass of a possible Z' boson in different models. Limits range from 500 to 1760 GeV depending on the model. Limits on the scale of contact interactions between leptons and between electrons and quarks are determined. A full set of limits are reported in Table 3.15. Limits on the scale of gravity in models with extra dimensions ranging from 1.09 to 1.25 TeV are obtained. Limits on the masses of leptoquarks are derived from the hadronic cross-sections. The limits range from 186 to 897 GeV depending on the type of leptoquark.

Chapter 4

Final-State Interconnection Effects

At LEP-II, Final-State Interconnection (FSI) effects may exist when two colourless W or Z bosons decay hadronically, close in space-time to one another. Two phenomena are considered: Colour Reconnection (CR) and Bose-Einstein Correlations (BEC). The former is expected to appear as a consequence of the strong interaction described by non-perturbative QCD, while the latter is due to the quantum mechanical properties of those particles in the hadronic final state which follow Bose statistics. Both were observed in other physical systems [95, 99]. An additional motivation for the study of FSI effects is that they introduce potentially large systematic uncertainties in the measurement of the mass of the W boson using fully hadronic W-pair decays. The studies described here allow a better understanding of CR and BEC at LEP-II and, by constraining models and their parameters, impose limits on their quantitative effect in the W-boson mass measurement.

4.1 Colour Reconnection

4.1.1 Introduction

In $\mathrm{W^+W^-} \to \mathrm{q\overline{q}q\overline{q}}$ events, the products of the two colour singlet W decays have in general a significant space-time overlap, because the separation of their decay vertices, $\tau_W \sim 1/\Gamma_W \approx 0.1$ fm, is small compared to characteristic hadronic distance scales of ~ 1 fm. Colour reconnection, also known as colour rearrangement (CR), was first introduced in [101] and refers to a reorganization of the colour flow between the decay products of the two W bosons. A precedent for such effects is set by colour suppressed B meson decays, *e.g.* $B \to J/\psi K$, where there is "cross-talk" between the two original colour singlets, $\bar{\mathrm{c}}$+s and c+spectator [101, 102].

QCD interference effects between the colour singlets in $\mathrm{W^+W^-}$ decays during the perturbative phase are expected to be small, affecting the W mass by $\sim (\frac{\alpha_\mathrm{S}}{\pi N_\mathrm{colours}})^2\Gamma_W \sim \mathcal{O}(1\text{ MeV})$ [102]. In contrast, non-perturbative effects involving soft gluons with energies less than Γ_W may be significant, with effects on m_W of $\sim \mathcal{O}(10\text{ MeV})$. To estimate the impact of this phenomenon, a variety of phenomenological models have been developed [102, 103, 104, 105, 106, 107]. These models differ mainly in the detailed mechanism of CR and hadronisation, and in the fraction of reconnected events.

Some of the models can also be tested at the Z peak in three-jet events. The analyses [108, 109, 110] showed that the ARIADNE model type 1 [103], and similar the the Rathsman/GAL model [107] with default parameter settings, is not consistent with the data. Colour rearrangement in W-pair events could, however, also be caused by additional reconnection

mechanisms. The combination presented here concentrates on the SK1 model [102] in which the probability for reconnection to occur in an event is given by $p_{\mathrm{reco}} = 1 - \exp(-\mathcal{I}k_I)$. The quantity $\mathcal{I}$ is the space-time overlap integral between the colour flux tubes that are stretched between quarks and gluons originating from the perturbative phase of the two hadronic W decays, and k_I is an adjustable parameter of the SK1 model, thus allowing to vary the fraction of reconnected events in the Monte-Carlo simulation. Figure 4.1 shows the reconnection probability, p_{reco} as a function of the model parameter k_I, for an SK1 Monte-Carlo event sample generated at a centre-of-mass energy of 189 GeV, and used by all LEP experiments as part of the combination procedure. By varying k_I, the SK1 model results can be compared to other models which have a fixed reconnection probability, such as the ARIADNE model type 2 [103] and HERWIG [104]. In the context of W mass measurements, it is observed [111, 112, 113, 114] that all models behave similarly when adjusted to the same reconnection fraction. The HERWIG CR model assumes a reconnection probability of 1/9 counting the possible colour rearrangements, while the ARIADNE-2 reconnection probability is about 22% at a centre-of-mass energy of 189 GeV.

Many observables have been studied in the search for an experimental signature of colour reconnection. The inclusive properties of events such as the mean charged particle multiplicity, distributions of thrust, rapidity, transverse momentum and $\ln(1/x_p)$, where x_p is the scaled particle momentum, are found to have limited sensitivity [115, 116]. The effects of CR are predicted to be numerically larger in these observables when only higher mass hadrons such as kaons and protons are considered [117]. However, experimental investigations [116] find no significant gain in sensitivity due to the low production rate of such particles in W decays.

Eventually, two methods were developed which yield a sensitive handle on CR effects in hadronic W decays: the so-called "particle-flow" method [118, 120], and the influence of CR on the W-boson mass reconstructed as a function of the particle momentum threshold and when applying different jet algorithms. These two are described in the following and their combined results are presented.

4.1.2 Particle-Flow Measurements

In the analogy with the "string effect" analysis in 3-jet $\mathrm{e^+e^-} \to \mathrm{q\overline{q}g}$ events [121], the particle-flow method has been investigated by the DELPHI, L3 and OPAL collaborations [128, 129, 115]. In these analyses, pairs of jets in $\mathrm{W^+W^-} \to \mathrm{q\overline{q}q\overline{q}}$ events are associated with the decay of a W, after which four jet-jet regions are chosen: two corresponding to jets sharing the same W parent (intra-W), and two in which the parents differ (inter-W). As there is a two-fold ambiguity in the assignment of inter-W regions, the configuration having the smaller sum of inter-W angles is chosen.

Particles are projected onto the planes defined by these jet pairs and the particle density constructed as a function of ϕ, the projected angle relative to one jet in each plane. To account for the variation in the opening angles, ϕ_0, of the jet-jet pairs defining each plane, the particle densities in ϕ are constructed as functions of normalized angles, $\phi_r = \phi/\phi_0$, by a simple rescaling of the projected angles for each particle, event by event. Particles having projected angles ϕ smaller than ϕ_0 in at least one of the four planes are considered further. This gives particle densities, $\frac{1}{N_{\mathrm{event}}}\frac{\mathrm{d}n}{\mathrm{d}\phi_r}$, in four regions with ϕ_r in the range from 0 to 1, and where n and N_{event} are the number of particles and events, respectively.

As the particle density reflects the colour flow in an event, CR models predict a change in the relative particle densities between inter-W and intra-W regions. On average, colour

reconnection is expected to affect the particle densities of both inter-W regions in the same way and so they are added together, as are the two intra-W regions. The observable used to quantify such changes, R_N, is defined:

$$R_N = \frac{\frac{1}{N_{\rm event}} \int_{0.2}^{0.8} \frac{{\rm d}n}{{\rm d}\phi_r}({\rm intra-W}){\rm d}\phi_r}{\frac{1}{N_{\rm event}} \int_{0.2}^{0.8} \frac{{\rm d}n}{{\rm d}\phi_r}({\rm inter-W}){\rm d}\phi_r} \,. \tag{4.1}$$

As the effects of CR are expected to be enhanced for low momentum particles far from the jet axes, the range of integration excludes jet cores ($\phi_r \approx 0$ and $\phi_r \approx 1$). The precise upper and lower limits are optimized by model studies of predicted sensitivity.

The DELPHI, L3 and OPAL experiments have developed their own variation on this analysis, differing primarily in the selection of $\mathrm{W^+W^-} \to \mathrm{q\overline{q}q\overline{q}}$ events. In DELPHI [128] and L3 [129], events are selected in a very particular configuration ("topological selection") by imposing restrictions on the jet-jet angles and on the jet-resolution parameter for the three- to four-jet transition (Durham [130] or Luclus [134] schemes). This leads to more planar events than those in an inclusive $\mathrm{W^+W^-} \to \mathrm{q\overline{q}q\overline{q}}$ sample and the association between jet pairs and W bosons is given by the relative angular separation of the jets. The overall efficiency for selecting signal events ranges between 12% and 22% with purities of 70-85%. The efficiency to assign the correct jets to the parent W's amounts to 70-91%. Data samples with small signal efficiency typically have the highest purity and best efficiency for correct jet assignment. The OPAL [115] event selection is based on their W mass analysis. Assignment of pairs of jets to W's follows the procedure used in measuring $m_{\rm W}$, using a multivariate algorithm [114] with an overall efficiency for selecting $\mathrm{W^+W^-} \to \mathrm{q\overline{q}q\overline{q}}$ events of 40%, a signal purity of 86%, and an efficiency for correctly assigning jets to parent W's of 90%, albeit with a less planar topology and hence a more complicated colour flow.

The data are corrected bin-by-bin for background contamination in the inter-W and intra-W regions separately. The possibility of CR effects existing in background processes is neglected because the background is dominated by $\mathrm{e^+e^-} \to \mathrm{q\overline{q}}$ events and the $\mathrm{ZZ} \to \mathrm{q\overline{q}q\overline{q}}$ background, in which CR effects may also be present, is at the level of 2% only.

The measured values of R_N are compared after they have been normalized using a common sample of Monte-Carlo events, processed using the detector simulation and particle-flow analysis of each experiment. The ratio, r, is constructed:

$$r = \frac{R_N^{\rm data}}{R_N^{\rm no-CR}} \,, \tag{4.2}$$

where $R_N^{\rm data}$ and $R_N^{\rm no-CR}$ are the values of R_N measured by each experiment in data and in a common sample of events simulated without CR. In the absence of CR, all experiments should find r consistent with unity. The default no-CR sample used for this normalization consists of $\mathrm{e^+e^-} \to \mathrm{W^+W^-}$ events produced using the KORALW [139] event generator and hadronised using the JETSET [140] model.

The common Monte-Carlo samples used in the combination are only available at a single centre-of-mass energy, $E_{\rm cm}$, of 188.6 GeV. The R_N are however measured at each centre-of-mass energy separately, in both real data and Monte-Carlo simulations. The predicted variation of R_N with centre-of-mass energy is determined by each experiment using its own samples of simulated $\mathrm{e^+e^-} \to \mathrm{W^+W^-}$ events, with hadronisation performed using the no-CR JETSET

	Experiment	
R_N	L3	OPAL
Data	0.8436 ± 0.0217	1.2426 ± 0.0248
JETSET	0.8622 ± 0.0037	1.2910 ± 0.0028
SK1 (100%)	0.7482 ± 0.0033	1.0780 ± 0.0028
HERWIG	0.8822 ± 0.0038	1.3110 ± 0.0029
ARIADNE	0.8754 ± 0.0037	1.2860 ± 0.0028
Systematics	L3	OPAL
Intra-W BEC	0.0017	0.0017
$e^+e^- \to q\overline{q}$ shape	0.0086	0.0104
$\sigma(e^+e^- \to q\overline{q})$	0.0071	0.0024
$ZZ \to q\overline{q}q\overline{q}$ shape	} 0.0020	0.0018
$\sigma(ZZ \to q\overline{q}q\overline{q})$		0.0009
Detector effects	0.0016	0.0142
$E_{\rm cm}$ dependence	0.0020	0.0005

Table 4.1: Particle-flow measurements compared to Monte-Carlo predictions for the SK1 CR model and different hadronisation models, together with systematic uncertainties, provided by L3 and OPAL for the CR combination.

model. The evolutions of R_N are parametrised by second order polynomial functions in $E_{\rm cm}$ and are detailed in References [128, 129, 115]. The R_N measured in data are subsequently extrapolated by each experiment to the reference energy of 188.6 GeV.

Input from a particle-flow measurement is provided by L3 and OPAL in terms of measured R_N and corresponding ΔR_N for different systematic variations of the analysis or different Monte Carlo modelling [129, 115]. They are shown in Table 4.1. DELPHI provides their results in terms of likelihood functions, which are discussed below. Systematic uncertainties due to Bose-Einstein correlations are limited to the level which is compatible with the LEP measurement of BEC (see Chapter 4.2). Scale uncertainties on the main background processes $e^+e^- \to q\overline{q}$ and $ZZ \to q\overline{q}q\overline{q}$, and hadronisation uncertainties, which are derived from the spread of R_N for the JETSET, ARIADNE and HERWIG hadronisation models are also taken into account. For these uncertainties the smallest of each systematic uncertainty of L3 and OPAL is taken as correlated, the remaining part as uncorrelated. Detector effects and the extrapolation to a single centre-of-mass energy, as well as the uncertainty of the 4-jet background shape of $e^+e^- \to q\overline{q}$ events with multi-gluon emission, are assumed to be uncorrelated.

The scaled measurements of L3 and OPAL, $r_1^{\rm data} = r_L^{\rm data}$ and $r_2^{\rm data} = r_O^{\rm data}$, are combined by minimizing a χ^2 function which depends on the model parameter k_I through the model dependence of $r_i(k_I)$:

$$\begin{aligned}\chi^2_r(k_I, c_1, c_2) \;=\; & \sum_{i,j=1,2} \Big\{ \left(r_i^{\rm data} - r_i(k_I) + c_i\delta_{i,r}\right) \left(C_r^{-1}\right)_{ij} \\ & \qquad \cdot \left(r_j^{\rm data} - r_j(k_I) + c_j\delta_{j,r}\right) \Big\} \\ & + \sum_{m,n=1,2} c_m \left(C_c^{-1}\right)_{mn} c_n \,. \end{aligned} \tag{4.3}$$

The covariance matrix, C_r, is constructed from only the uncorrelated uncertainties and is ac-

tually diagonal. Correlated uncertainties are introduced by varying each measurement $r_i^{\rm data}$ with an additive term $c_i\delta_{i,r}$, where $\delta_{i,r}$ is the correlated part of the uncertainty on $r_i^{\rm data}$, and c_i are auxiliary variables. The second term in the χ^2_r function introduces correlations between the auxiliary variables, so that the systematic uncertainties $\delta_{i,r}$ also become effectively correlated. This procedure is equivalent to the so-called profile likelihood method with correlated nuisance parameters, see, *e.g.*, [141] and references therein. The correlation matrix $(C_c^{-1})_{mn}$ is constructed such that the uncertainty and central value of k_I is exactly identical to the result obtained with a classical and full covariance matrix C_r. The best agreement is found for a correlation coefficient of 0.50 between the auxiliary parameters. This more complicated prescription is used to combine this result with other CR inputs, which are provided in terms of likelihood functions.

To be able to vary k_I continuously in the minimization, the SK1 model predictions of $r_i(k_I)$ are described by a parametrised, phenomenological function:

$$\begin{aligned} r_i(k_I) &= 1 + a_{i,1}\frac{k_I}{k_I+b_i} + a_{i,2}\left(\frac{k_I}{k_I+b_i}\right)^2 + a_{i,3}\left(\frac{k_I}{k_I+b_i}\right)^4 \\ &\quad + \frac{a_{i,4}}{(1+k_I)} - a_{i,4}\ . \end{aligned} \tag{4.4}$$

By construction, $r_i(k_I)$ is equal to 1 in the limit $k_I \to 0$, *i.e.*, when no CR effects are present. The parameters, $a_{i,j}$ and b_i ($i = 1, 2, j = 1, \ldots, 4$), of the function are adjusted to fit the $r_i(k_I)$ dependence determined in the SK1 Monte-Carlo simulation by L3 and OPAL, which are shown in Table D.1 of Appendix D. The terms $\frac{k_I}{k_I+b}$ are motivated by the approximate description of the functional shape of the reconnection probability, $p_{\rm reco}(k_I)$.

With this parameter set, the function and the Monte-Carlo simulations agree within less than one statistical standard deviation, as shown in Figure 4.1. The best fitting parameter values are listed in Table D.2.

The DELPHI experiment also performed a particle-flow analysis [128]. The result is represented in terms of two likelihood functions, $L_{\rm p-flow,}D{\rm ,full}(k_I)$ and $L_{\rm p-flow,}D{\rm ,uncorr}(k_I)$, where the former contains all systematic uncertainties and the latter only uncorrelated systematic uncertainties. These likelihoods are transformed into $\Delta\chi^2(k_I) = -2\log L(k_I)$ values, which are smoothed by cubic splines and then used in the combination. To treat correlations with other inputs properly, a systematic variation, $\delta_{\rm p-flow,}D(k_I)$, of k_I is introduced such that the full $\Delta\chi^2_{\rm p-flow,}D{\rm ,full}(k_I)$ can be reproduced in the following way from the uncorrelated $\Delta\chi^2_{\rm p-flow,}D{\rm ,uncorr}(k_I)$ using an auxiliary variable c_3:

$$\Delta\chi^2_{\rm p-flow,}D{\rm ,corr}(k_I) = \min_{c_3}\left\{\Delta\chi^2_{\rm p-flow,}D{\rm ,uncorr}(k_I + c_3\delta_{\rm p-flow,}D(k_I)) + c_3^2\right\}\ . \tag{4.5}$$

The combined minimisation of $\Delta\chi^2_{\rm p-flow,}D{\rm ,corr}(k_I, c_3)$ with respect to k_I and c_3 is equivalent to a minimisation of $\Delta\chi^2_{\rm p-flow,}D{\rm ,full}(k_I)$ with respect to k_I only. The best agreement between the full description and this procedure is obtained for $\delta_{\rm p-flow,}D(k_I) = 0.246 + (0.754)^2 k_I$, which is shown in Figure 4.2. The advantage of this method is again the possibility to correlate c_3 with systematic uncertainties from other CR inputs.

4.1.3 Determination of CR Effects Using W Mass Estimators

A second very sensitive observable for CR is the variation of the reconstructed W-boson mass in fully hadronic events when applying different particle momentum thresholds and jet algorithms

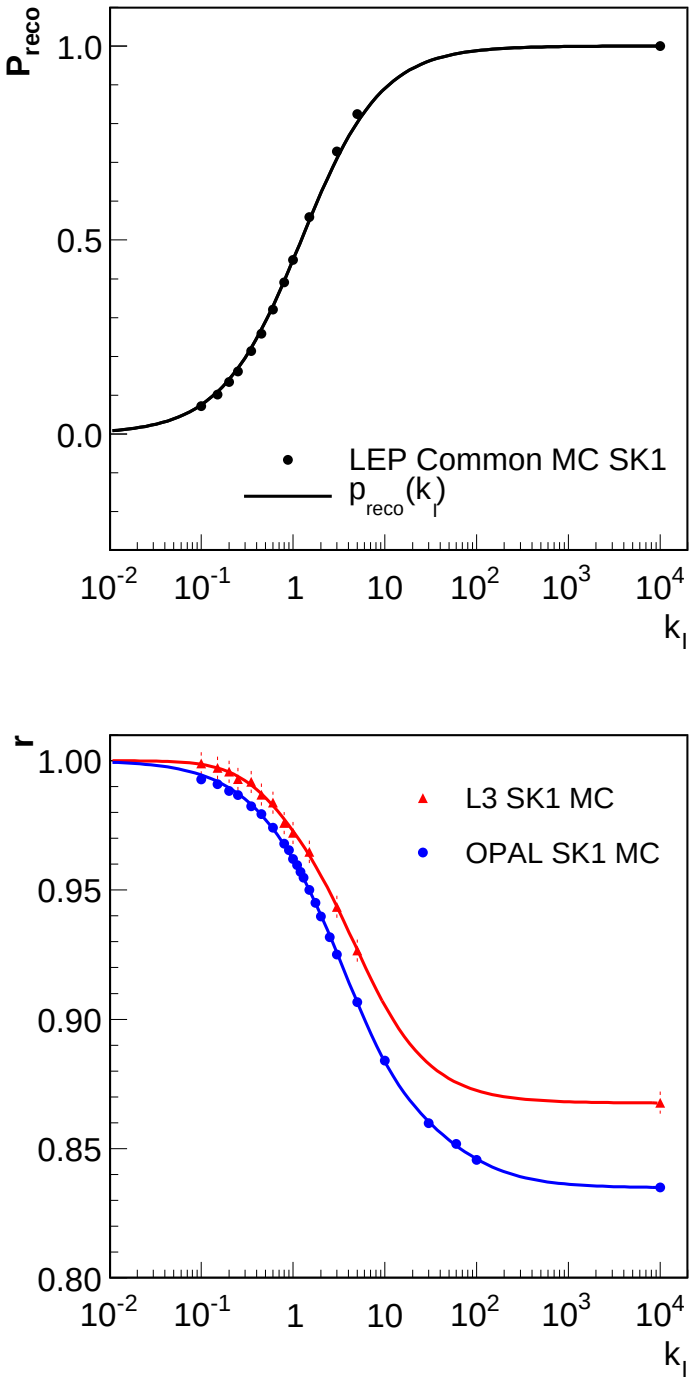


Figure 4.1: Top: Reconnection probability as a function of the SK1 model parameter, k_I, together with an approximate curve $p_{\rm reco}(k_I)$ to guide the eye. Bottom: Monte-Carlo calculation and parametrisation of the particle-flow ratio, $r(k_I)$, for L3 and OPAL, shown as triangles and circles, respectively.

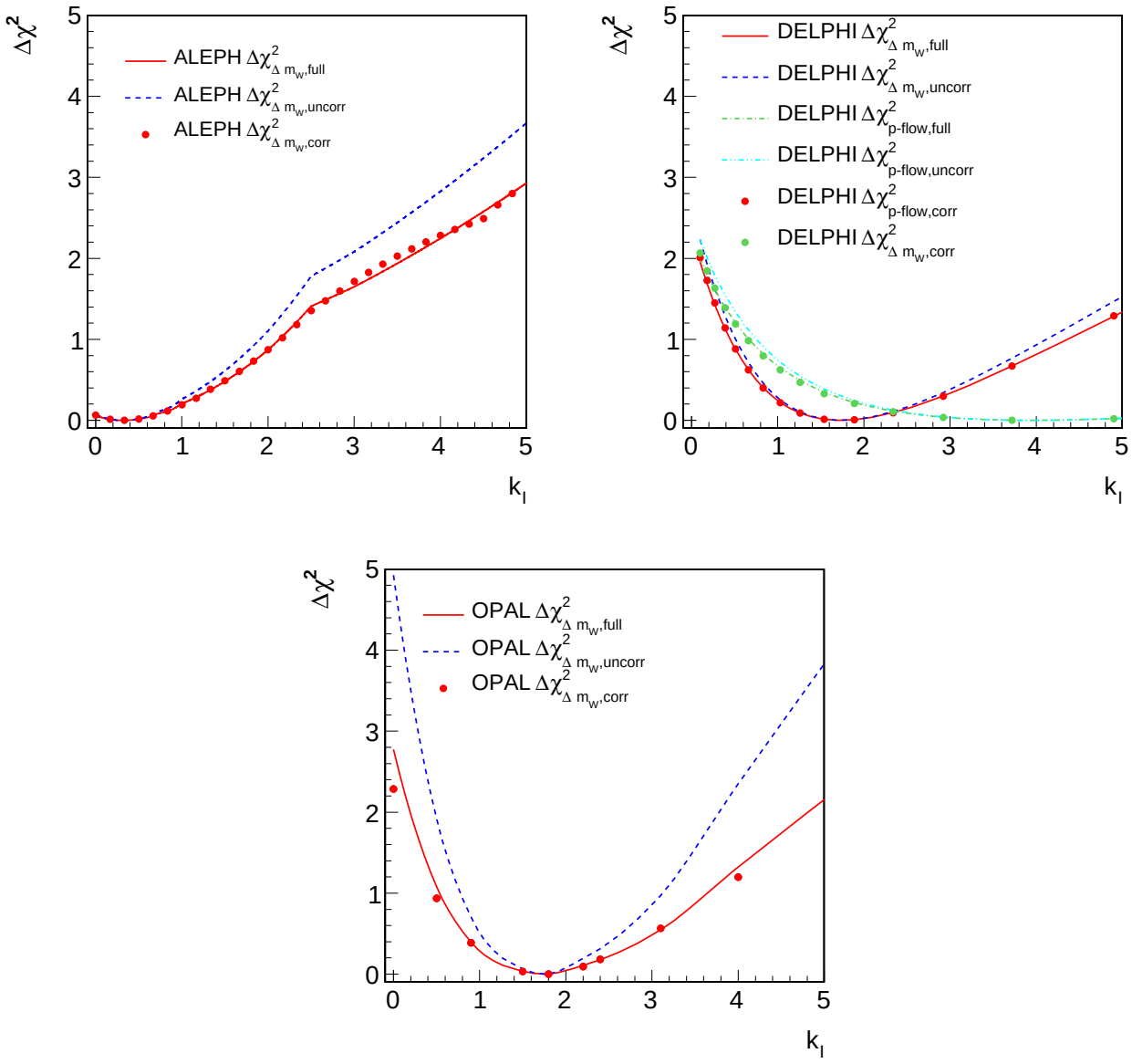


Figure 4.2: Comparison of $\Delta\chi^2$ distributions for CR measurements from particle-flow and mass estimator differences, Δm_{W}, by the ALEPH, DELPHI and OPAL experiments. Distributions are shown when all uncertainties (continuous lines) and only uncorrelated uncertainties (dashed lines) are taken into account. The full-uncertainty curves are compared to the $\Delta\chi^2$ distribution when the variation of the parametrised uncertainty $\delta(k_I)$ is used to introduce the correlated part of the systematic uncertainties (circles).

at event reconstruction. As pointed out before, CR influences mostly the particle-flow between jets and hence the low momentum component of the hadronic jets. Thus, estimators of m_{W} in which the jet-defining parameters are chosen to enhance or reduce the weight given to such low momentum particles allow an observable to be constructed which is sensitive to the presence or absence of CR. To measure the effect of CR, the mass difference, Δm_{W}, of two estimators is determined in data and compared to the mass difference predicted by a certain CR model. Since only mass *differences* are used to measure CR, the correlation with the actual W mass measurement is small, in the order of 10% [111, 128, 114].

The ALEPH experiment studied the dependence of m_{W} as a function of a momentum threshold, p_{cut}, of the jet particles and of the cone radius R of the jets, which were constructed using the Durham-PE algorithm [130]. The p_{cut} thresholds were varied between 1 GeV and 3 GeV and the radius between 0.4 rad and 1.0 rad. DELPHI compared the m_{W} value from the standard W mass analysis with alternative estimators applying a cone cut at $R = 0.5$ rad and a particle momentum cut at 2 GeV, applying again the Durham jet clustering algorithm [130] in combination with an iterative cone algorithm in order to estimate the direction of the modified jets. OPAL found that their optimal CR sensitivity is for the comparison between an analysis with a particle momentum cut at 2.5 GeV and an alternative one in which the jet particles are weighted according to a factor p^{κ}, with $\kappa = -0.5$. The Durham jet clustering algorithm [130] is used to calculate the modified jet directions.

The ALEPH, DELPHI and OPAL inputs are provided in terms of $\Delta\chi^2$ curves with complete systematic uncertainties and with only the uncorrelated part, $\Delta\chi^2_{\Delta m_{\mathrm{W}},i,\mathrm{full}}(k_I)$ and $\Delta\chi^2_{\Delta m_{\mathrm{W}},i,\mathrm{uncorr}}(k_I)$, respectively. Cubic splines are used to interpolate between the provided data points. Correlations are again not taken directly from the input function, $\Delta\chi^2_{\Delta m_{\mathrm{W}},i,\mathrm{full}}(k_I)$, but are introduced by varying k_I with additional uncertainties $\pm\delta(k_I)$ using auxiliary variables c_i:

$$\Delta\chi^2_{\Delta m_{\mathrm{W}},A,\mathrm{corr}}(k_I) = \min_{c_4}\left\{\Delta\chi^2_{\Delta m_{\mathrm{W}},A,\mathrm{uncorr}}(k_I + c_4\delta_{\Delta m_{\mathrm{W}},A}(k_I)) + c_4^2\right\}, \tag{4.6}$$

$$\Delta\chi^2_{\Delta m_{\mathrm{W}},D,\mathrm{corr}}(k_I) = \min_{c_5}\left\{\Delta\chi^2_{\Delta m_{\mathrm{W}},D,\mathrm{uncorr}}(k_I + c_5\delta_{\Delta m_{\mathrm{W}},D}(k_I)) + c_5^2\right\}, \tag{4.7}$$

$$\Delta\chi^2_{\Delta m_{\mathrm{W}},O,\mathrm{corr}}(k_I) = \min_{c_6}\left\{\Delta\chi^2_{\Delta m_{\mathrm{W}},O,\mathrm{uncorr}}(k_I + c_6\delta_{\Delta m_{\mathrm{W}},O}(k_I)) + c_6^2\right\}. \tag{4.8}$$

The parametrisations of $\delta_{\Delta m_{\mathrm{W}},i}(k_I)$ follow step-wise linear functions and are listed in Appendix D. The original input of ALEPH, DELPHI and OPAL is shown in Figure 4.2 and compared to the $\Delta\chi^2_{\Delta m_{\mathrm{W}},i,\mathrm{corr}}(k_I)$ functions using the prescription described above. Good agreement is observed.

The main correlated systematic uncertainties which are taken into account are from comparisons of hadronisation models, background scale and shape uncertainties, as well as Bose-Einstein correlations. Detector effects and corrections of the 4-jet background are taken as uncorrelated. The original ALEPH analysis [111] does not consider uncertainties due to the BEC effect. Therefore, the corresponding $\delta_{\Delta m_{\mathrm{W}},A}(k_I))$ values are scaled up by 11%, which is derived from an additional dedicated systematic study.

4.1.4 Combination of LEP CR Measurements

The LEP measurements of CR using the particle-flow method and the mass estimator differences are combined using the following total $\Delta\chi^2$ function:

$$
\begin{aligned}
\Delta\chi^2(k_I, c_1, \ldots, c_6) \;=\; & \sum_{i,j=1,2} \left\{ (r_i^{\text{data}} - r_i(k_I) + c_i\delta_{i,r}) \left(C_r^{-1}\right)_{ij} (r_j^{\text{data}} - r_j(k_I) + c_j\delta_{j,r}) \right\} \\
& + \Delta\chi^2_{\text{p-flow},D,\text{uncorr}}(k_I + c_3\delta_{\text{p-flow},D}(k_I)) \\
& + \Delta\chi^2_{\Delta m_{\text{W}},A,\text{uncorr}}(k_I + c_4\delta_{\Delta m_{\text{W}},A}(k_I)) \\
& + \Delta\chi^2_{\Delta m_{\text{W}},D,\text{uncorr}}(k_I + c_5\delta_{\Delta m_{\text{W}},D}(k_I)) \\
& + \Delta\chi^2_{\Delta m_{\text{W}},O,\text{uncorr}}(k_I + c_6\delta_{\Delta m_{\text{W}},O}(k_I)) \\
& + \sum_{m,n=1}^{6} c_m \left(C_c^{-1}\right)_{mn} c_n \,, \qquad (4.9)
\end{aligned}
$$

which is constructed from the ingredients presented above. It is minimized with respect to k_I and the auxiliary parameters $c_1, \ldots, c_6$, which are correlated through the covariance matrix C_c. In the LEP combination, the correlation coefficients are set to 0.5, motivated by the full covariance matrix of the R_N measurements, where the correlated systematic uncertainties are reduced to only the common part in each pair of measurements.

As a cross-check, the CR measurements of each collaboration are combined, and the best k_I values as well as their uncertainties are extracted using the procedure described above. All results of the individual experiments [111, 128, 129, 114] could be adequately reproduced, with small deviations being attributed to known systematic effects covered by the assigned uncertainties. More details can be found in the Appendix D.

The $\Delta\chi^2$ curves obtained for each experiment are shown in Figure 4.3, together with the LEP result. Combining all LEP data yields:

$$
k_I \;=\; 1.26^{+0.84}_{-0.64}\,. \qquad (4.10)
$$

This result corresponds to a preferred reconnection probability of 51% at a centre-of-mass energy of 189 GeV in the SK1 model. Absence of CR can not be excluded, but is disfavoured by LEP at more than two standard deviations.

4.1.5 Summary

A combination of the LEP particle-flow and W-mass estimator results is presented, using the entire LEP-II data sample. The data exclude with 6.9 standard deviations an extreme version of the SK-I model in which colour reconnection has been forced to occur in essentially all events. The combination procedure has been generalized to the SK-I model as a function of its reconnection probability. The combined data are described best by the model in which 51% of events at 189 GeV are reconnected, corresponding to $k_I = 1.26$. The LEP data disfavour the no-CR hypothesis at 99.5% confidence level, deviating from it by 2.8 standard deviations. The 68% confidence level range for k_I is determined to be $0.62 \leq k_I \leq 2.10$.

4.2 Bose-Einstein Correlations

4.2.1 Introduction

The LEP experiments have studied the strength of particle correlations between two hadronic systems obtained from W-pair decays occurring close in space-time at LEP-II. The work

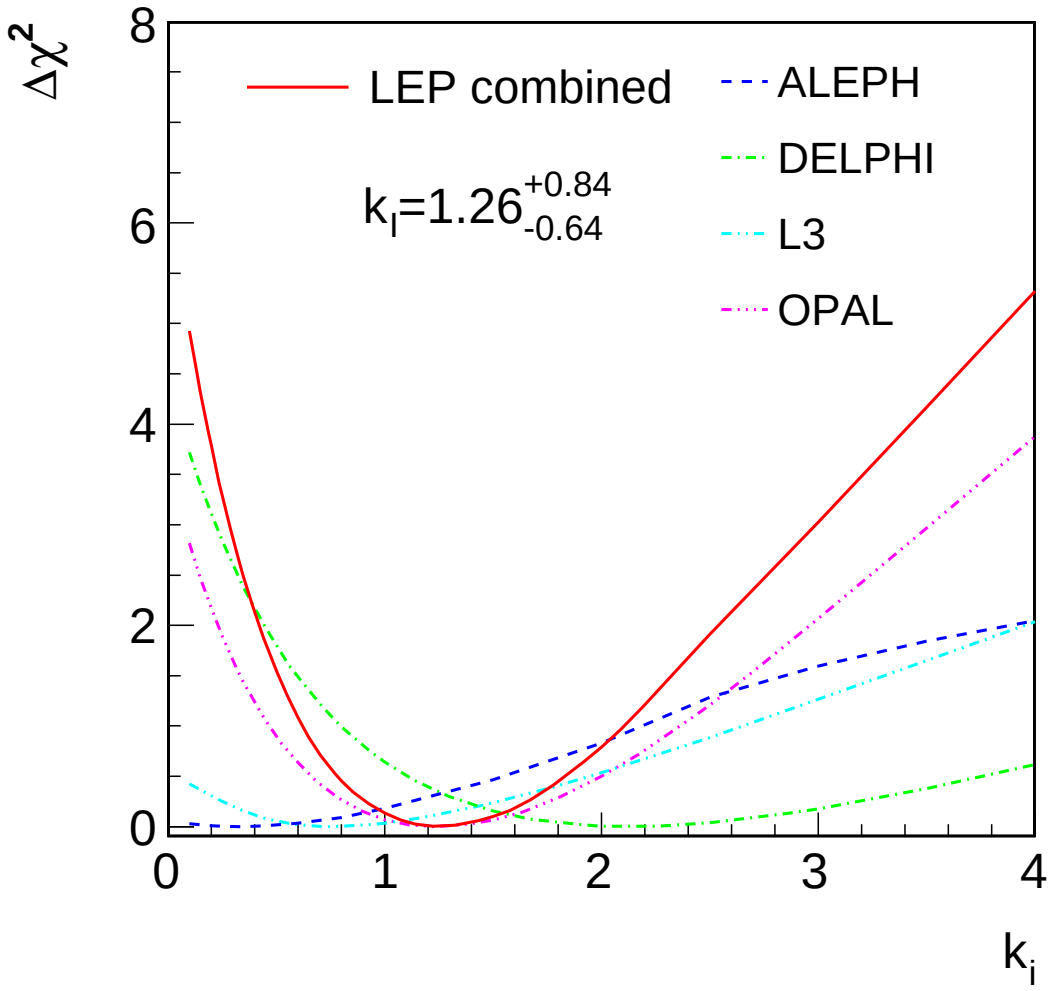


Figure 4.3: Individual and LEP combined $\Delta\chi^2$ curves for the measurement of the CR parameter k_I in the SK1 model.

presented in this section is focused on so-called Bose-Einstein correlations (BEC), *i.e.*, the enhanced probability of production of pairs (multiplets) of identical mesons close together in phase space. The effect is readily observed in particle physics, in particular in hadronic decays of the Z boson, and is qualitatively understood as a result of quantum-mechanical interference originating from the symmetry of the amplitude of the particle production process under exchange of identical mesons.

The presence of correlations between hadrons coming from the decay of a W-pair, in particular those between hadrons originating from different W bosons, can affect the direct reconstruction of the mass of the initial W bosons. The measurement of the strength of these correlations can be used to constrain the corresponding systematic uncertainty in the W mass measurement.

4.2.2 Methods

The principal method [142], called "mixing method", used in the measurement is based on the direct comparison of 2-particle spectra from genuine hadronic W-pair events, WW $\rightarrow \mathrm{q\bar{q}q\bar{q}}$, and from mixed WW events. The latter are constructed by mixing the hadronic sides of two semileptonic W-pair events, WW $\rightarrow \mathrm{q\bar{q}}\ell\nu$, first used in [143]. Such a reference sample has the advantage of reproducing the correlations between particles belonging to the same W boson, while the particles from different W bosons are uncorrelated by construction.

This method gives a model-independent estimate of the interplay between the two hadronic systems, for which BEC and also colour reconnection are considered as dominant sources. The possibility of establishing the strength of inter-W correlations in a model-independent way is rather unique; most correlations do carry an inherent model dependence on the reference sample. In the present measurement, the model dependence is limited to the background subtraction.

4.2.3 Distributions

The two-particle correlations are evaluated using two-particle densities defined in terms of the 4-momentum transfer $Q = \sqrt{-(p_1 - p_2)^2}$, where p_1, p_2 are the 4-momenta of the two particles:

$$\rho_2(Q) = \frac{1}{N_{ev}} \frac{dn_{pairs}}{dQ} \,. \tag{4.11}$$

Here n_{pairs} stands for the number of like-sign (unlike-sign) 2-particle permutations.[1] In the case of two stochastically independent hadronically decaying W bosons the two-particle inclusive density is given by:

$$\rho_2^{WW} \;=\; \rho_2^{W^+} + \rho_2^{W^-} + 2\rho_2^{mix}, \tag{4.12}$$

where ρ_2^{mix} can be expressed via the single-particle inclusive density $\rho_1(p)$ as:

$$\rho_2^{mix}(Q) \;=\; \int d^4p_1 d^4p_2 \rho^{W^+}(p_1)\rho^{W^-}(p_2)\delta(Q^2 + (p_1 - p_2)^2)\delta(p_1^2 - m_\pi^2)\delta(p_2^2 - m_\pi^2). \tag{4.13}$$

Assuming further that:

$$\rho_2^{W^+}(Q) \;=\; \rho_2^{W^-}(Q) \;=\; \rho_2^{W}(Q), \tag{4.14}$$

one obtains for the case of two stochastically independent hadronically decaying W bosons:

$$\rho_2^{WW}(Q) \;=\; 2\rho_2^{W}(Q) + 2\rho_2^{mix}(Q). \tag{4.15}$$

[1] For historical reasons, the number of particle permutations rather than combinations is used in formulas, leading to a factor 2 in front of ρ_2^{mix} in Equation 4.12. The experimental statistical errors are, however, based on the number of particle pairs, *i.e.*, 2-particle combinations.

In the mixing method, ρ_2^{mix} is obtained by combining two hadronic W systems from two different semileptonic W-pair events. The direct search for inter-W BEC is done using the difference of 2-particle densities:

$$\Delta\rho(Q) \;=\; \rho_2^{WW}(Q) - 2\rho_2^{W}(Q) - 2\rho_2^{mix}(Q), \tag{4.16}$$

or, alternatively, their ratio:

$$D(Q) \;=\; \frac{\rho_2^{WW}(Q)}{2\rho_2^{W}(Q) + 2\rho^{mix}(Q)} \;=\; 1 + \frac{\Delta\rho(Q)}{2\rho_2^{W}(Q) + 2\rho^{mix}(Q)}. \tag{4.17}$$

Given the definition of the genuine inter-W correlations function $\delta_I(Q)$ [144], it can be shown that

$$\delta_I(Q) \;=\; \frac{\Delta\rho(Q)}{2\rho_2^{mix}(Q)}. \tag{4.18}$$

To disentangle the BEC effects from other possible correlation sources (such as energy-momentum conservation or colour reconnection), which are supposed to be the same for like-sign and unlike-sign charge pairs, the double difference:

$$\delta\rho(Q) = \Delta\rho^{like-sign}(Q) - \Delta\rho^{unlike-sign}(Q), \tag{4.19}$$

or the double ratio,

$$d(Q) = D^{like-sign}(Q)/D^{unlike-sign}(Q), \tag{4.20}$$

is analyzed.

The event mixing procedure may introduce artificial distortions, or may not fully account for some detector effects or for correlations other than BEC. Most of these possible effects are treated in the Monte-Carlo simulation without inter-W BEC. Therefore they are reduced by using the double ratio or the double difference:

$$D'(Q) \;=\; \frac{D(Q)_{data}}{D(Q)_{MC,nointer}}\;, \qquad \Delta\rho'(Q) \;=\; \Delta\rho(Q)_{data} - \Delta\rho(Q)_{MC,nointer}\;, \tag{4.21}$$

where $D(Q)_{MC,nointer}$ and $\Delta\rho(Q)_{MC,nointer}$ are derived from a MC without inter-W BEC.

In addition to the mixing method, ALEPH [145] also uses the double ratio of like-sign pairs ($N_\pi^{++,--}(Q)$) and unlike-sign pairs $N_\pi^{+-}(Q)$ corrected with Monte-Carlo simulations without BEC effects:

$$R^*(Q) \;=\; \left(\frac{N_\pi^{++,--}(Q)}{N_\pi^{+-}(Q)}\right)^{data} \Bigg/ \left(\frac{N_\pi^{++,--}(Q)}{N_\pi^{+-}(Q)}\right)^{MC}_{noBE}. \tag{4.22}$$

In analyses based on $\Delta\rho(Q)$, $\delta\rho(Q)$ or $\delta_I(Q)$, a deviation from zero indicates the presence of inter-W correlations, whereas for studies of $D(Q)$, $D'(Q)$ or $d(Q)$, the corresponding signature is a deviation from unity. For $R^*(Q)$, a difference between data and the Monte-Carlo prediction excluding inter-W BEC is studied.

4.2.4 Results

The four LEP experiments have published results applying the mixing method to the full LEP-II data sample. As examples, the distributions of $\Delta\rho'$ measured by ALEPH [146], δ_I measured by DELPHI [147], D and D' measured by L3 [148] and D measured by OPAL [149] are shown in Figures 4.4, 4.5, 4.6 and 4.7, respectively. In addition ALEPH have published results using R^* [145]. The centre-of-mass energies, luminosities and the number of events used for the different measurements are listed in Table 4.2.

	$\sqrt{s}$	Luminosity	Number of events	
	[GeV]	[pb^{-1}]	WW $\to$ q$\bar{\text{q}}$q$\bar{\text{q}}$	WW $\to$ q$\bar{\text{q}}\ell\nu$
ALEPH	183-209	683	6155	4849
DELPHI	189-209	550	3252	2567
L3	189-209	629	5100	3800
OPAL	183-209	680	4470	4533
ALEPH R*	172-189	242	2021	-

Table 4.2: The centre-of-mass energies, luminosities and the number of events used for the different measurements.

A simple combination procedure is available through a χ^2 average of the numerical results of each experiment [145, 146, 147, 148, 149] with respect to a specific BEC model under study, here based on comparisons with various tuned versions of the LUBOEI model [140, 150]. The tuning is performed by adjusting the parameters of the model to reproduce correlations in samples of Z and semileptonic W decays, and applying identical parameters to the modelling of inter-W correlations (so-called "fullBE" scenario). In this way the tuning of each experiment takes into account detector systematic uncertainties in the track measurements.

An important advantage of the combination procedure used here is that it allows the combination of results obtained using different analyses. The combination procedure assumes a linear dependence of the observed size of BEC on various estimators used to analyse the different distributions. It is also verified that there is a linear dependence between the measured W mass shift and the values of these estimators [113]. The estimators are: the integral of the $\Delta\rho(Q)$ distribution (ALEPH, L3, OPAL); the parameter Λ when fitting the function $N(1+\delta Q)(1+\Lambda\exp(-k^2Q^2))$ to the $D'(Q)$ distribution, with N fixed to unity (L3), or δ fixed to zero and k fixed to the value obtained from a fit to the full BEC sample (ALEPH); the parameter Λ when fitting the function $N(1+\delta Q)(1+\Lambda\exp(-Q/R))$ to the $D(Q)$, $D(Q)'$ and d distributions, with R fixed to the value obtained from a fit to the full BEC sample (OPAL); the parameter Λ when fitting the function $\Lambda\exp(-RQ)(1+\epsilon RQ)+\delta(1+\frac{\rho_2^W}{\rho_2^{mix}})$ to the δ_I distribution, with R and ϵ fixed to the value obtained from a fit to the full BEC sample (DELPHI); and finally the integral of the term describing the BEC part, $\int\lambda\exp(-\sigma^2Q^2)$, when fitting the function $\kappa(1+\epsilon Q)(1+\lambda\exp(-\sigma^2Q^2))$ to the $R^*(Q)$ distribution (ALEPH).

The size of the correlations for like-sign pairs of particles measured in terms of these estimators is compared with the values expected in the model with and without inter-W correlations in Table 4.3. Table 4.4 summarizes the normalized fractions of the model seen.

For the combination of the above measurements one has to take into account correlations between them. Correlations between results of the same experiment are strong and are not

Analysis	Data–noBE	stat.	syst.	corr. syst.	fullBE–noBE	Ref.
ALEPH (fit to D')	**-0.004**	**0.011**	**0.014**	**0.003**	**0.081**	[146]
ALEPH (integral of $\Delta\rho$)	-0.127	0.143	0.199	0.044	0.699	[146]
ALEPH (fit to R^*)	-0.004	0.0062	0.0036	negligible	0.0177	[145]
DELPHI (fit to δ_I)	**$+0.72$**	**0.29**	**0.17**	**0.070**	**1.40**	[147]
L3 (fit to D')	**$+0.008$**	**0.018**	**0.012**	**0.0042**	**0.103**	[148]
L3 (integral of $\Delta\rho$)	$+0.03$	0.33	0.15	0.055	1.38	[148]
OPAL (integral of $\Delta\rho$)	-0.01	0.27	0.23	0.06	0.77	[149]
OPAL (fit to D)	**$+0.040$**	**0.038**	**0.038**	**0.017**	**0.120**	[149]
OPAL (fit to D')	$+0.042$	0.042	0.047	0.019	0.123	[149]
OPAL (fit to d)	-0.017	0.055	0.050	0.003	0.133	[149]

Table 4.3: An overview of the results from different measurements described in Section 4.2.3: the difference between the measured correlations and the model without inter-W correlations (data–noBE), the corresponding statistical (stat.) and total systematic (syst.) errors, the correlated systematic error contribution (corr. syst.), and the difference between "fullBE" and "noBE" scenario. The measurements used in the combination are highlighted.

Analysis	Fraction of model	stat.	syst.
ALEPH (fit to D')	**-0.05**	**0.14**	**0.17**
ALEPH (integral of $\Delta\rho$)	-0.18	0.20	0.28
ALEPH (fit to R^*)	-0.23	0.35	0.20
DELPHI (fit to δ_I)	**$+0.51$**	**0.21**	**0.12**
L3 (fit to D')	**$+0.08$**	**0.17**	**0.12**
L3 (integral of $\Delta\rho$)	$+0.02$	0.24	0.11
OPAL (integral of $\Delta\rho$)	-0.01	0.35	0.30
OPAL (fit to D)	**$+0.33$**	**0.32**	**0.32**
OPAL (fit to D')	$+0.34$	0.34	0.38
OPAL (fit to d)	-0.13	0.41	0.38

Table 4.4: The measured size of BEC expressed as the relative fraction of the model with inter-W correlations (see Equation 4.23 and Table 4.3). The measurements used in the combination are highlighted.

available. Varying these correlations and combining the three ALEPH measurements, for example, one obtains normalized fractions of the model seen very close to those of the most precise measurement. Therefore, for simplicity, the combination of the most precise measurements of each experiment is made here: D' from ALEPH, δ_I from DELPHI, D' from L3 and D from OPAL. In this combination only the uncertainties in the understanding of the background contribution in the data are treated as correlated between experiments (denoted as "corr. syst." in Table 4.3). The combination via a fit using MINUIT gives:

$$\frac{\text{data} - \text{model(noBE)}}{\text{model(fullBE)} - \text{model(noBE)}} = 0.17 \pm 0.095(stat.) \pm 0.085(sys.) = 0.17 \pm 0.13 \ , \quad (4.23)$$

where "noBE" includes correlations between decay products of each W, but not the ones between decay products of different Ws and "fullBE" includes all the correlations. A $\chi^2/\text{dof} = 3.5/3$ of the fit is observed. The measurements and their average are shown in Figure 4.8. The measurements used in the combination are marked with an arrow. The results of LEP experiments are in good agreement.

4.2.5 Conclusions

The LUBOEI model of BEC between pions from different W bosons is disfavoured. The 68% confidence level (CL) upper limit on these correlations is $0.17 + 0.13 = 0.30$. This result can be translated into a 68% CL upper limit on the shift of the W mass measurements due to the BEC between particles from different Ws, Δm_{W}, assuming a linear dependence of Δm_{W} on the size of the correlation. For the specific BE model investigated, LUBOEI, a shift of -35 MeV in the W mass is obtained at full BEC strength. The W mass analysis techniques applied are, however, optimized to reduce colour reconnection effects on m_{W} which also has the effect of reducing the mass shift due to BEC. A combination of the reduced shifts reported by the LEP experiments [151, 152, 153, 154] gives a shift of -23 MeV in the W mass at full BEC strength. Thus the 68% CL upper limit on the magnitude of the mass shift within the LUBOEI model is: $|\Delta m_{\mathrm{W}}| = 0.30 \times 23$ MeV $= 7$ MeV.

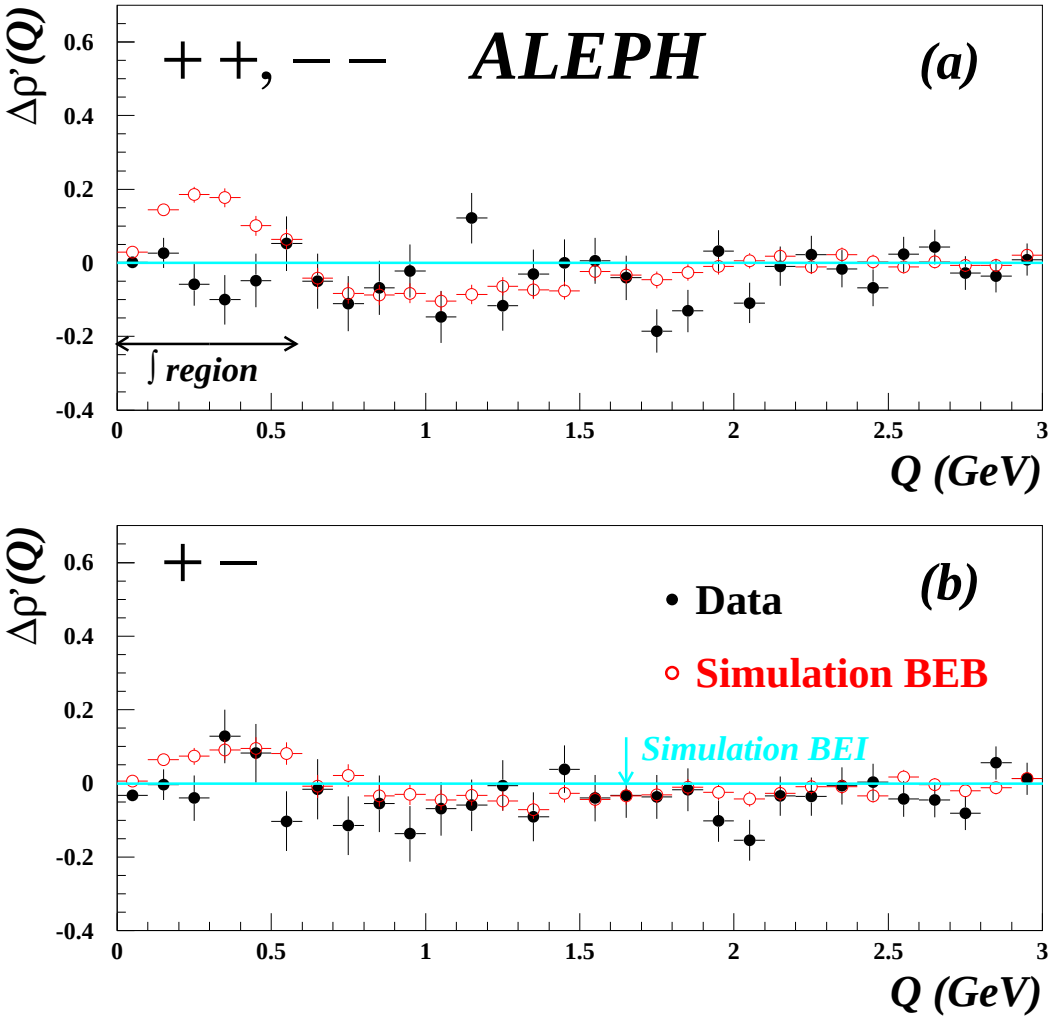


Figure 4.4: Distribution of the quantity $\Delta\rho'$ for like- and unlike-sign pairs as a function of Q as measured by the ALEPH collaboration [146]. BEI stands for the case in which Bose-Einstein correlations do not occur between decay products of different W bosons, and BEB if they do.

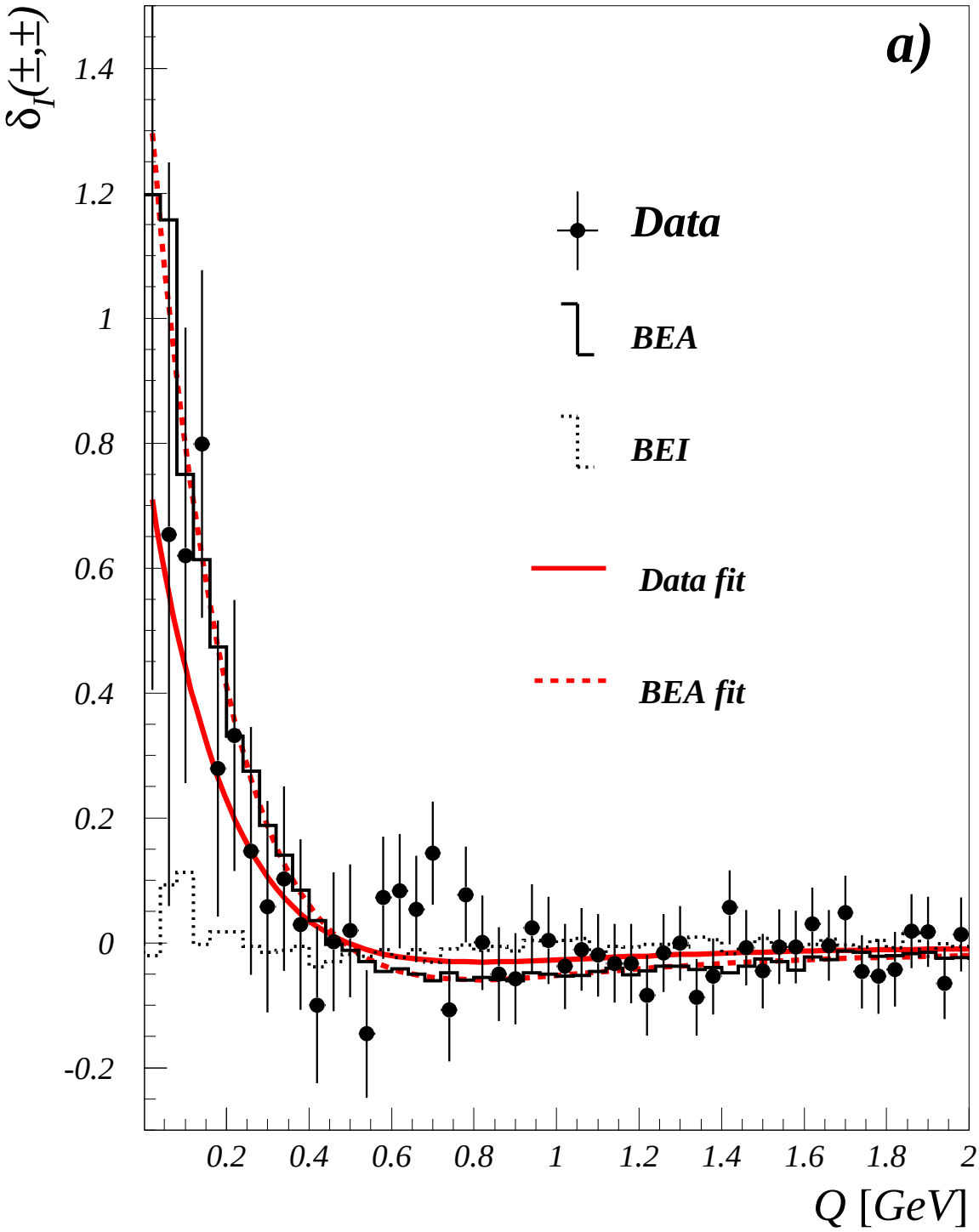


Figure 4.5: Distributions of the quantity δ_I for like-sign pairs as a function of Q as measured by the DELPHI collaboration [147]. The solid line shows the fit results. BEI stands for the case in which Bose-Einstein correlations do not occur between decay products of different W bosons, and BEA if they do.

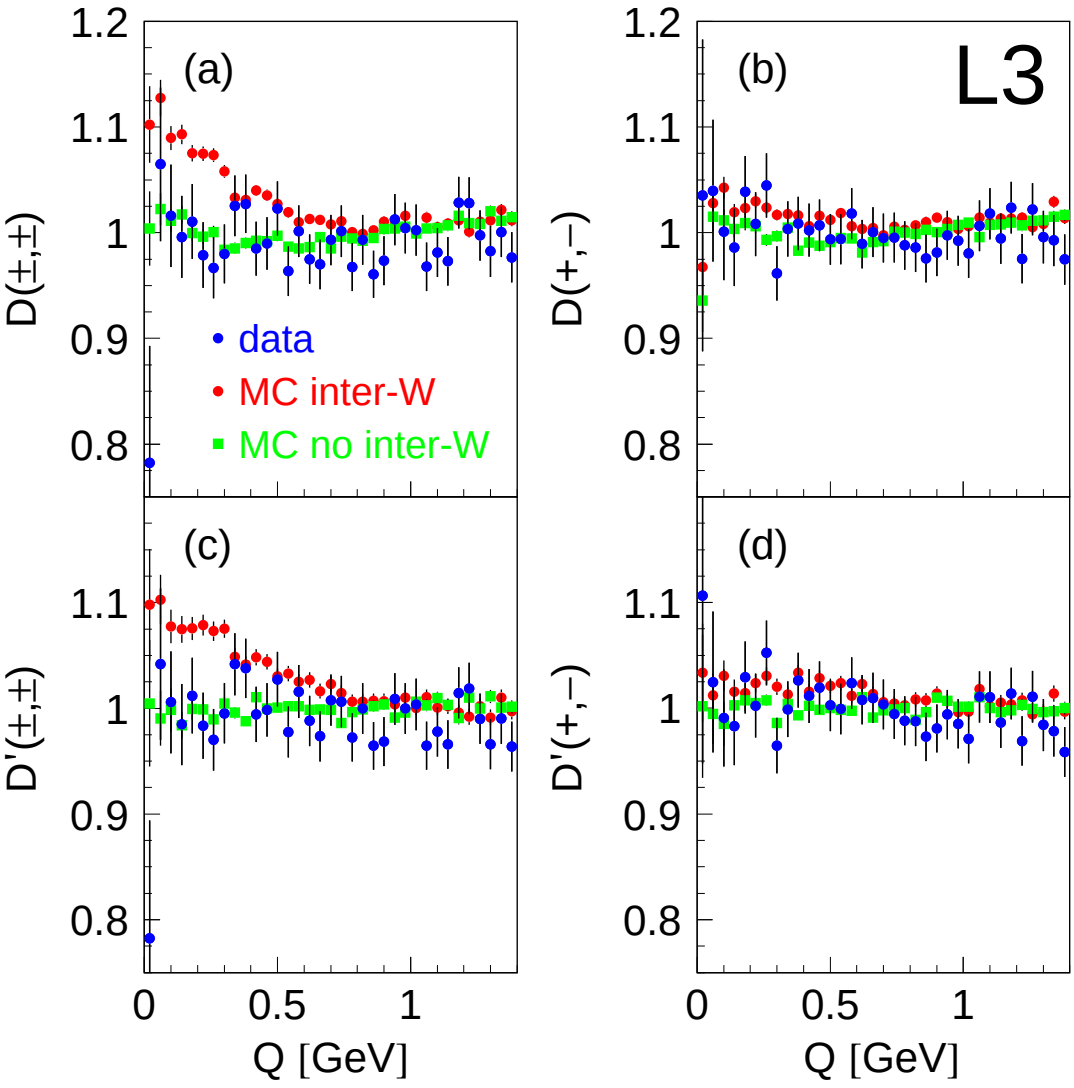


Figure 4.6: Distributions of the quantity D and D' for like- and unlike-sign pairs as a function of Q as measured by the L3 collaboration [148].

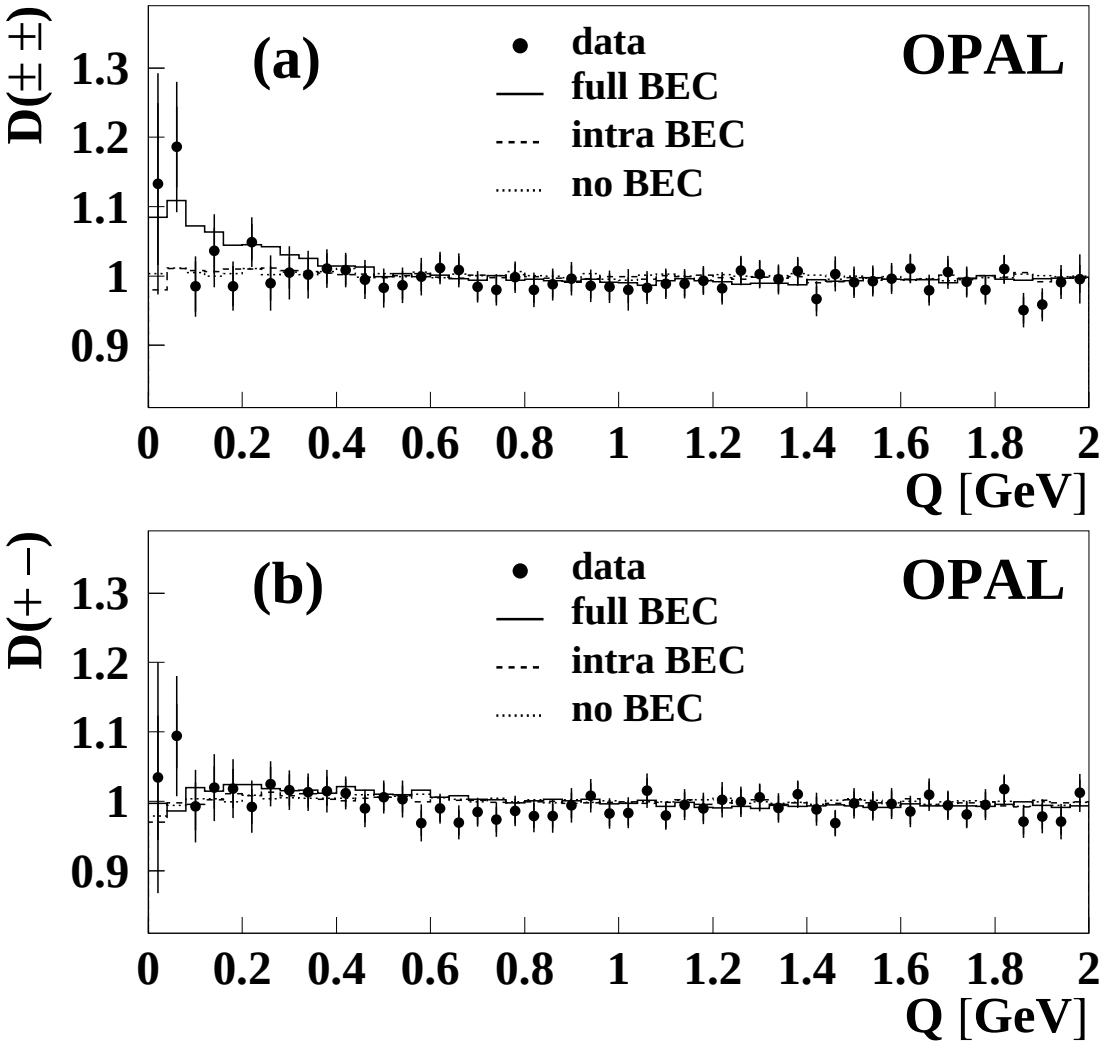


Figure 4.7: Distribution of the quantity D for like- and unlike-sign pairs as a function of Q as measured by the OPAL collaboration [149].

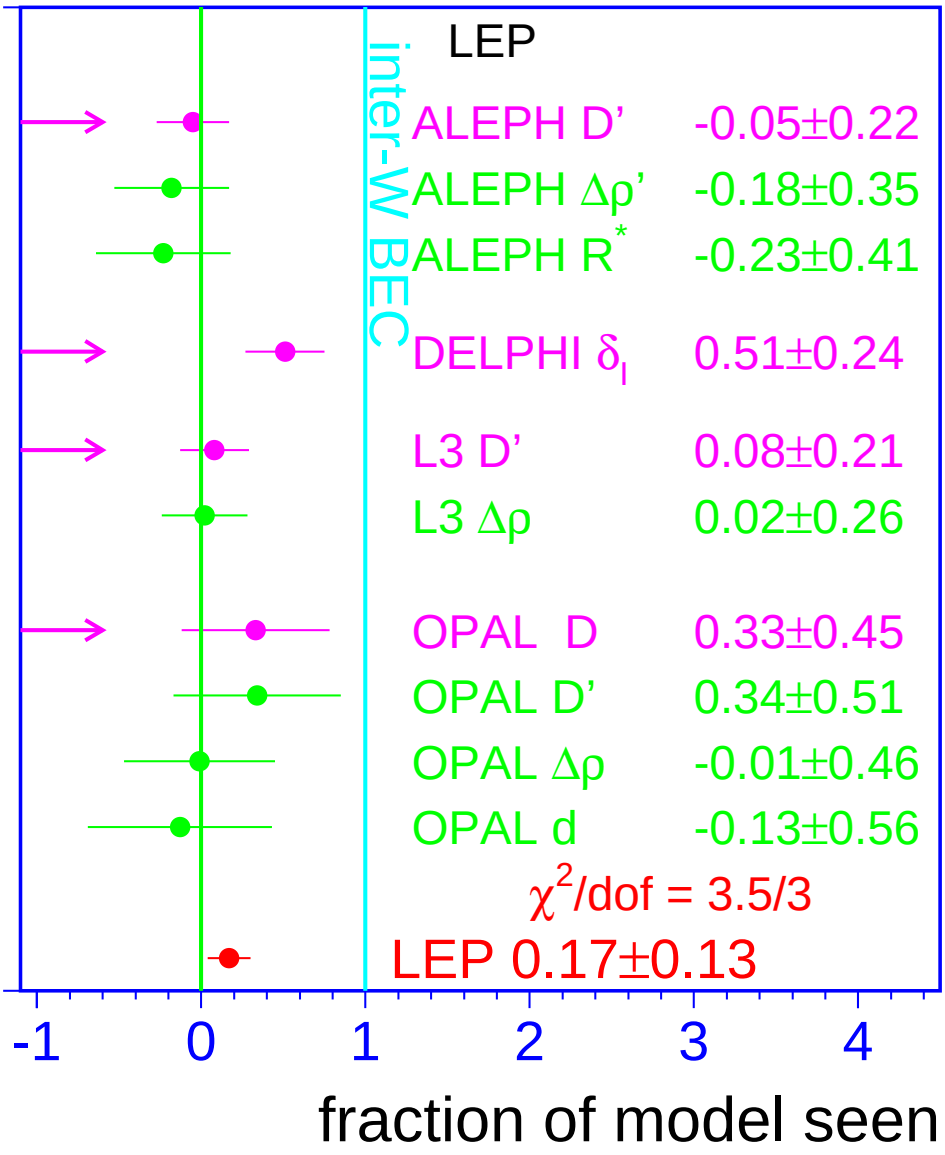


Figure 4.8: Measured BEC expressed as the relative fraction of the model with inter-W correlations. The arrows indicate the measurements used in the combination. The LEP combination is shown at the bottom.

Chapter 5

Boson-Pair and Four-Fermion Processes

5.1 Introduction and Signal Definitions

Cross-section measurements at LEP-II are essential because they allow many direct and indirect tests of the Standard Model (SM). W-pair production and decay, certainly the most interesting manifestation of four-fermion production, is directly related to fundamental parameters of the model, such as the W-boson mass at the production threshold energy and to the non-Abelian gauge structure of the theory. The W-decay branching fractions and the value of $|V_{cs}|$ can be directly extracted from a cross-section measurement. A broader investigation of four-fermion production in several regions of phase space also brings additional information on the boson-fermion coupling structure, on the effect of radiative corrections and on the possible presence of new physics.

This chapter summarizes the combination of final results of the four LEP experiments on four-fermion production cross-sections. The signals, with the exception of WW and ZZ, are defined on the basis of their final states together with cuts to enhance certain regions of phase space. For WW and ZZ, a diagrammatic definition is used for the sake of simplicity, even though this corresponds to a non gauge invariant definition. In what follows we will use terms such as "singly resonant" or "doubly resonant", indicating regions of the phase space rather than a process itself.

The most interesting regions of the four-fermion phase space that are measured at LEP and for which a combination is performed, are summarized as:

- **WW:** defined as the CC03 component of the four-fermion processes, involving s-channel γ and Z exchange and t-channel ν exchange (see Figure 1.4).

- **ZZ:** in analogy with the definition of W-pair production, Z-pair production is defined as the subset of NC02 Feynman diagrams having two resonant Z bosons (see Figure 1.5).

- **Zγ^*:** defined for final states with two fermion-antifermion pairs, at least one being leptonic (electrons or muons). To properly consider only singly resonant regions, it is required that one and only one of the invariant masses of the couples satisfies: $|m_{ff'} - m_Z| < 2\Gamma_Z$, where $m_{ff'}$ is the invariant mass of the two same-flavour fermions. In case of four identical leptons all oppositely charged couples have to be considered. Moreover the following final state dependent phase-space cuts have been introduced:

- eeqq, $\mu\mu$qq: $|\cos\theta_\ell| < 0.95$, $m_{\ell\ell} > 5$ GeV, $m_{qq} > 10$ GeV, ℓ =e,μ
- $\nu\nu$qq: $m_{qq} > 10$ GeV
- $\nu\nu\ell\ell$: $m_{\ell\ell} > 10$ GeV, $m_{\ell\nu} > 90$ GeV or $m_{\ell\nu} < 70$ GeV, ℓ =e,μ
- $\ell_1\ell_1\ell_2\ell_2$: $|\cos\theta_{\ell_1\ell_2}| < 0.95$, $m_{\ell_1\ell_1} > 5$ GeV, $m_{\ell_2\ell_2} > 5$ GeV, ℓ =e,μ

- **Weν:** considered as the complete t-channel subset of Feynman diagrams contributing to $e\nu_e f\bar{f}'$ final states, with additional cuts to exclude the regions of phase space dominated by multiperipheral diagrams, where the cross-section calculation is affected by large uncertainties. The phase space cuts are (charge conjugation is implicit): $m_{q\bar{q}} > 45$ GeV for the $e\nu q\bar{q}$ final states, $E_\ell > 20$ GeV for the $e\nu l\nu$ final states with $\ell = \mu$ or τ, and finally $|\cos\theta_{e^-}| > 0.95$, $|\cos\theta_{e^+}| < 0.95$ and $E_{e^+} > 20$ GeV for the $e\nu e\nu$ final states (see Figure 1.7).

- **Zee:** defined considering only the ee$q\bar{q}$ and ee$\mu\mu$ final states. The following phase space cuts are applied to enhance the signal: $m_{q\bar{q}}(m_{\mu\mu}) > 60$ GeV, and in addition: $\theta_{e^-} < 12°$, $12° < \theta_{e^+} < 120°$ and $E_{e^+} > 3$ GeV when the positron is visible, or $\theta_{e^+} > 168°$, $60° < \theta_{e^-} < 168°$ and $E_{e^-} > 3$ GeV when the electron is visible. This definition assumes the electron direction to be $+z$ and the positron direction to be $-z$.

- **WWγ:** it is defined as the part of the $e^+e^- \to W^+W^-\gamma$ process compatible with charged currents, *i.e.*, including the final states $udud\gamma$, $cscs\gamma$, $udcs\gamma$, $ud\ell\nu\gamma$, $cs\ell\nu\gamma$, $\ell\nu\ell\nu\gamma$, assuming a diagonal CKM matrix. The following phase-space cuts are applied to enhance the signal: $E_\gamma > 5$ GeV, $|\cos\theta_\gamma| < 0.95$, $\cos\theta_{\gamma,f} < 0.9$, the invariant mass of the W-decay fermion pairs between $m_W - 2\Gamma_W$ and $m_W + 2\Gamma_W$ (see Figure 1.6).

The cross-sections are determined from a fit to the number of observed events in data, knowing the signal efficiencies corresponding to the above signal definitions, and the expected accepted backgrounds, from Monte-Carlo simulations.

The LEP cross-section combination is performed in a fit to the $N=N_{exp}\times N_{\sqrt{s}}$ experimental inputs, where N_{exp} identifies the number of LEP experiments providing input for the measurement and $N_{\sqrt{s}}$ is the number of energy points provided. The method used is the Best Linear Unbiased Estimate method (BLUE) described in [62]. In the fits, inter-experiment and inter-energy correlations of the systematic errors are taken into account, dividing the sources according to their correlation and assuming for each either 0% or 100% correlation strength for simplicity. After building the appropriate N×N correlation matrix for the measurements, the χ^2 minimisation fit is performed by matrix algebra and is cross-checked with the use of Minuit [155].

The numbers shown here represent the combination of cross-section values and derived quantities such as branching fractions or differential distributions. For each measurement, the collaborations provided input in agreement with the conventions used to define the signal and to split the systematic uncertainties: small differences may therefore appear between the values quoted here and those published by the experiments. The combinations are performed for the whole LEP-II period, that includes data from e^+e^- collisions from $\sqrt{s} = 183$ GeV up to $\sqrt{s} = 207$ GeV. The energy binning chosen and the corresponding average integrated luminosity per experiment at each energy point are shown in Table 5.1; they result from a combination of the luminosity in the hadronic and leptonic channels, therefore small changes from the values published by individual experiments may be present.

	ALEPH		DELPHI		L3		OPAL		LEP
Year	$\sqrt{s}$ [GeV]	$\mathcal{L}$ [pb^{-1}]	$\sqrt{s}$ [GeV]	$\mathcal{L}$ [pb^{-1}]	$\sqrt{s}$ [GeV]	$\mathcal{L}$ [pb^{-1}]	$\sqrt{s}$ [GeV]	$\mathcal{L}$ [pb^{-1}]	$\sqrt{s}$ [GeV]
1997	182.66	56.81	182.65	52.08	182.68	55.46	182.68	57.38	182.67
1998	188.63	174.21	188.63	154.07	188.64	176.77	188.63	183.04	188.63
1999	191.58	28.93	191.58	24.84	191.60	29.83	191.61	29.33	191.59
1999	195.52	79.86	195.51	74.04	195.54	84.15	195.54	76.41	195.53
1999	199.52	86.28	199.51	82.31	199.54	83.31	199.54	76.58	199.52
1999	201.63	41.89	201.64	40.01	201.75	37.18	201.65	37.68	201.67
2000	204.86	81.41	204.86	75.66	204.82	79.01	204.88	81.91	204.85
2000	206.53	133.21	206.55	129.95	206.57	139.12	206.56	138.54	206.55

Table 5.1: Summary of luminosity and luminosity-weighted centre-of-mass energies, per year, of the four LEP experiments, and final LEP averaged energy.

The structure of this chapter is as follows: in Section 5.2 the W-pair production is described and the combined results on cross-sections, W branching fractions, $|V_{cs}|$ and W polar-angle distributions are presented. Sections 5.3 and 5.4 concern neutral current boson production and present combined results on ZZ and Zγ^* cross-sections, respectively. The combination of single boson production cross-sections is reported in Section 5.5. All the presented results are compared to recent theoretical predictions, many of which were developed in the framework of the LEP-II Monte-Carlo workshop [156].

5.2 W-Pair Production

The signal definition has been given in Section 5.1. W-pair production is investigated via all possible final states arising in the decay of the two W bosons. According to the different decays, three topologically different final states can arise: the fully hadronic, where both W bosons decay into quarks, characterised by high multiplicity of the final state; the mixed hadronic-leptonic, also called semileptonic, with the presence of an isolated and energetic lepton and hadronic decay products of the second W; and the fully leptonic, with the production of two acoplanar leptons. The SM branching fractions for these final states are, respectively, 0.456, 0.349, and 0.105 [36]. There are ten experimentally distinguishable final states: $q\overline{q}q\overline{q}$, $q\overline{q}\mu^+\nu$, $q\overline{q}e^+\nu$, $q\overline{q}\tau^+\nu$, $\mu^+\nu\tau^-\nu$, $e^+\nu\tau^-\nu$, $\tau^+\nu\tau^-\nu$, $\mu^+\nu e^-\nu$, $\mu^+\nu\mu^-\nu$, $e^+\nu e^-\nu$. Charge conjugation is assumed everywhere.

Event selections are generally based on Neural Network approaches to separate the signals from the major backgrounds, which arise mainly from $q\bar{q}(\gamma)$ events in the fully hadronic final state, while four-fermion backgrounds are also important in the other channels. Typical selection efficiencies range from 80% to 90% in the fully hadronic channel, from 70% to 90% in the various semileptonic channels and about 70% in the fully leptonic ones. The purest channels (95%) are the semileptonic ones with electrons or muons in the final state. Details on the event selections and experimental performances can be found in [157, 158, 159, 160].

5.2.1 Total Cross-Section Measurement

From the number of WW selected events in data, knowing the expected background and the efficiency on the signal, the production cross-section is extracted through likelihood fits. Cross-sections are then combined, accounting for the correlation of the systematic errors as shown in Table 5.2. The inputs used for the combinations are given in Table E.1, with the details on the composition of the systematic error in terms of correlated components shown in Table E.2. For this analysis, the SM W-decay branching fractions are assumed; see Section 5.2.2 for the measurement of these branching fractions.

Source	LEP correlation	Energy correlation
Theory uncertainties on signal	Yes	Yes
Theory uncertainties on backgrounds	Yes	Yes
Theory uncertainty on luminosity	Yes	Yes
Experimental uncertainties on luminosity	No	Yes
Detector effects	No	Yes
Monte-Carlo statistics	No	No

Table 5.2: Grouping of systematic uncertainties into those correlated among experiments and those correlated among different energies. The theory uncertainties on the signal include fragmentation effects, radiative corrections and final state interaction effects.

The measured statistical errors are used for the combination; after building the full 32×32 covariance matrix for the measurements, the χ^2 minimisation fit is performed by matrix algebra, as described in Ref. [62], and is cross-checked using Minuit [155].

The results from each experiment for the W-pair production cross-section are shown in Table 5.3, together with the LEP combination at each energy. All measurements assume SM values for the W decay branching fractions. The combined LEP cross-sections at the eight energies are all positively correlated, see Table E.3, with correlations ranging from 6% to 19%.

Figure 5.1 shows the combined LEP W-pair cross-section measured as a function of the centre–of–mass energy. The experimental results are compared with the theoretical calculations from YFSWW [161, 167] and RACOONWW [168] between 155 and 215 GeV using $m_{\mathrm{W}} = 80.35$ GeV. The two programs have been extensively compared and agree at a level better than 0.5% at the LEP-II energies [156]. The calculations above 170 GeV, based for the two programs on the so-called leading-pole (LPA) or double-pole (DPA) approximations [156], have theoretical uncertainties decreasing from 0.7% at 170 GeV to about 0.4% at centre–of–mass energies larger than 200 GeV[1], while in the threshold region, where the programs use an improved Born approximation, a larger theoretical uncertainty of 2% is assigned. This theoretical uncertainty is represented by the blue band in the figure. The cross-sections are sensitive to the W-boson mass, such that an error of 50 MeV on the W mass would translate into additional errors of 0.1% (3.0%) on the cross-section predictions at 200 GeV (161 GeV), respectively. All results, up to the highest centre–of–mass energies, are in agreement with the two theoretical predictions

[1] The theoretical uncertainty $\Delta\sigma/\sigma$ on the W-pair production cross-section calculated in the LPA/DPA above 170 GeV can be parametrised as $\Delta\sigma/\sigma = (0.4 \oplus 0.072 \cdot t_1 \cdot t_2)\%$, where $t_1 = (200 - 2 \cdot m_{\mathrm{W}})/(\sqrt{s} - 2 \cdot m_{\mathrm{W}})$ and $t_2 = (1 - (\frac{2 \cdot M_{\mathrm{W}}}{200})^2)/(1 - (\frac{2 \cdot M_{\mathrm{W}}}{\sqrt{s}})^2)$.

$\sqrt{s}$	WW Cross-Section [pb]				
[GeV]	ALEPH	DELPHI	L3	OPAL	LEP
161.3	4.23 ± 0.75	$3.61\ ^{+\ 0.99}_{-\ 0.87}$	$2.89\ ^{+\ 0.82}_{-\ 0.71}$	$3.62\ ^{+\ 0.94}_{-\ 0.84}$	3.69 ± 0.45
172.1	$11.7\ \pm 1.3$	$11.4\ \pm 1.4$	$12.3\ \pm 1.4$	$12.3\ \pm 1.3$	$12.0\ \pm 0.7$
182.7	15.86 ± 0.63	16.07 ± 0.70	16.53 ± 0.72	15.45 ± 0.62	15.92 ± 0.34
188.6	15.78 ± 0.36	16.09 ± 0.42	16.17 ± 0.41	16.24 ± 0.37	16.05 ± 0.21
191.6	17.10 ± 0.90	16.64 ± 1.00	16.11 ± 0.92	15.93 ± 0.86	16.42 ± 0.47
195.5	16.60 ± 0.54	17.04 ± 0.60	16.22 ± 0.57	18.27 ± 0.58	16.99 ± 0.29
199.5	16.93 ± 0.52	17.39 ± 0.57	16.49 ± 0.58	16.29 ± 0.55	16.77 ± 0.29
201.6	16.63 ± 0.71	17.37 ± 0.82	16.01 ± 0.84	18.01 ± 0.82	16.98 ± 0.40
204.9	16.84 ± 0.54	17.56 ± 0.59	17.00 ± 0.60	16.05 ± 0.53	16.81 ± 0.29
206.6	17.42 ± 0.43	16.35 ± 0.47	17.33 ± 0.47	17.64 ± 0.44	17.20 ± 0.24

Table 5.3: W-pair production cross-section from the four LEP experiments and combined values at all recorded centre-of-mass energies. The measurements above 175 GeV have been combined in a single fit, taking into account inter-experiment as well as inter-energy correlations of systematic errors, with a χ^2/dof of 26.6/24. The fit at 161.3 GeV (172.1 GeV) has a χ^2/dof of 1.3/3 (0.22/3).

considered and listed in Table E.4. In the lower part of the figure, the data are also compared with hypothetical predictions for which W-pair production happens in absence of one or two of the CC03 diagrams. The need for the diagram with a ZWW vertex is a spectacular confirmation of the non-Abelian nature of the electroweak SM.

The agreement between the measured W-pair cross-section, $\sigma_{\rm WW}^{\rm meas}$, and its expectation according to a given theoretical model, $\sigma_{\rm WW}^{\rm theo}$, can be expressed quantitatively in terms of their ratio:

$$\mathcal{R}_{\rm WW} = \frac{\sigma_{\rm WW}^{\rm meas}}{\sigma_{\rm WW}^{\rm theo}}, \tag{5.1}$$

averaged over the measurements performed by the four experiments at different energies in the LEP-II region. The above procedure has been used to compare the measurements at the eight energies between 183 GeV and 207 GeV with the predictions of GENTLE [173], KORALW [174, 167], YFSWW [161, 167] and RACOONWW [168]. The measurements at 161 GeV and 172 GeV have not been used in the combination because they were performed using data samples of low statistics and because of the high sensitivity of the cross-section to the value of the W mass at these energies.

The combination of the ratio $\mathcal{R}_{\rm WW}$ is performed using as input from the four experiments the 32 cross-sections measured at each of the eight energies. These are then converted into 32 ratios by dividing them by the theoretical predictions listed in Table E.4. The full 32×32 covariance matrix for the ratios is built taking into account the same sources of systematic errors used for the combination of the W-pair cross-sections at these energies.

The small statistical errors on the theoretical predictions at the various energies, taken as fully correlated for the four experiments and uncorrelated between different energies, are

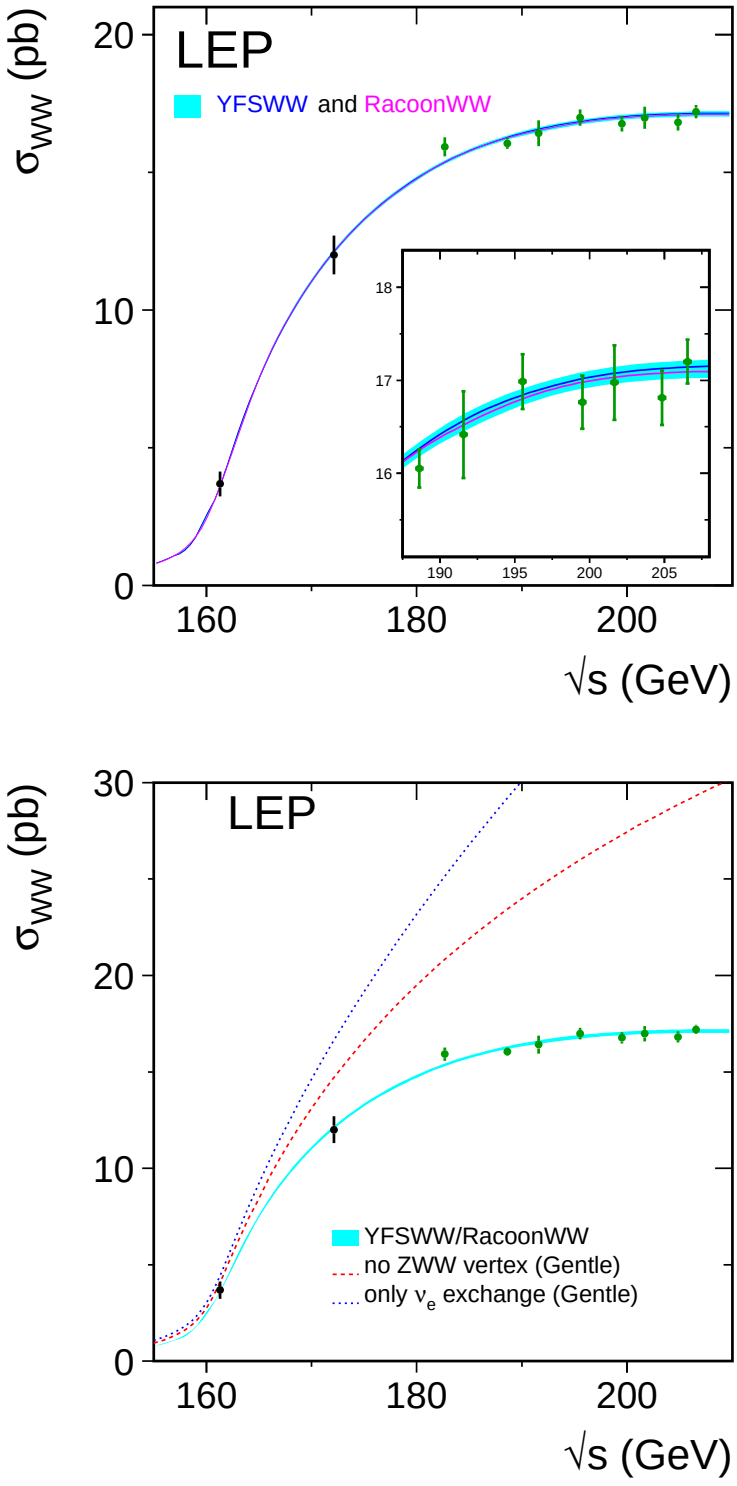


Figure 5.1: Measurements of the W-pair production cross-section, compared to the predictions of RACOONWW [168] and YFSWW [161, 167]. The shaded area represents the uncertainty on the theoretical predictions, estimated as $\pm 2\%$ for $\sqrt{s} < 170$ GeV and ranging from 0.7 to 0.4% above 170 GeV. The W mass is fixed at 80.35 GeV; its uncertainty is expected to give a significant contribution only at threshold energies.

$\sqrt{s}$ [GeV]	$\mathcal{R}_{\mathrm{WW}}^{\mathrm{YFSWW}}$	$\mathcal{R}_{\mathrm{WW}}^{\mathrm{RACOONWW}}$
182.7	1.037 ± 0.022	1.036 ± 0.023
188.6	0.987 ± 0.013	0.988 ± 0.013
191.6	0.991 ± 0.028	0.994 ± 0.029
195.5	1.009 ± 0.018	1.011 ± 0.019
199.5	0.985 ± 0.017	0.987 ± 0.018
201.6	0.994 ± 0.023	0.997 ± 0.024
204.9	0.982 ± 0.017	0.984 ± 0.018
206.6	1.003 ± 0.014	1.007 ± 0.015
χ^2/dof	26.6/24	26.6/24
Average	0.995 ± 0.008	0.997 ± 0.008
χ^2/dof	32.2/31	32.0/31

Table 5.4: Ratios of LEP combined W-pair cross-section measurements to the expectations according to YFSWW [161, 167] and RACOONWW [168]. For each of the two models, two fits are performed, one to the LEP combined values of $\mathcal{R}_{\mathrm{WW}}$ at the eight energies between 183 GeV and 207 GeV, and another to the LEP combined average of $\mathcal{R}_{\mathrm{WW}}$ over all energies. The results of the fits are given in the table together with the resulting χ^2/dof. The fits take into account inter-experiment as well as inter-energy correlations of systematic errors.

also translated into errors on the individual measurements of $\mathcal{R}_{\mathrm{WW}}$. The theoretical errors on the predictions, due to the physical and technical precision of the generators used, are not propagated to the individual ratios but are used when comparing the combined values of $\mathcal{R}_{\mathrm{WW}}$ to unity. For each of the four models considered, two fits are performed: in the first, eight values of $\mathcal{R}_{\mathrm{WW}}$ at the different energies are extracted, averaged over the four experiments; in the second, only one value of $\mathcal{R}_{\mathrm{WW}}$ is determined, representing the global agreement of measured and predicted cross-sections over the whole energy range.

The results of the fits to $\mathcal{R}_{\mathrm{WW}}$ for YFSWW and RACOONWW are given in Table 5.4, with more details given in Table E.5. As already qualitatively noted from Figure 5.1, the LEP measurements of the W-pair cross-section above threshold are in very good agreement with the predictions and can test the theory at the level of better than 1%. In contrast, the predictions from GENTLE and KORALW are about 3% too high with respect to the measurements due to the lack of LPA/DPA corrections; the equivalent values of $\mathcal{R}_{\mathrm{WW}}$ in those cases are, respectively, 0.970 ± 0.008 and 0.976 ± 0.008. The results of the fits for YFSWW and RACOONWW are also shown in Figure 5.2, where relative errors of 0.5% on the cross-section predictions have been assumed. For simplicity the energy dependence of the theory error on the W-pair cross-section has been neglected in the figure. The main differences between the predictions of YFSWW/RACOONWW and GENTLE/KORALW arise from non-leading $\mathcal{O}(\alpha)$ electroweak radiative corrections to the W-pair production process and non-factorisable corrections, which are included (in the LPA/DPA leading-pole/double-pole approximation [156]) in both YFSWW and RACOONWW, but not in GENTLE and KORALW. The data clearly prefer the computations which more precisely include $\mathcal{O}(\alpha)$ radiative corrections.

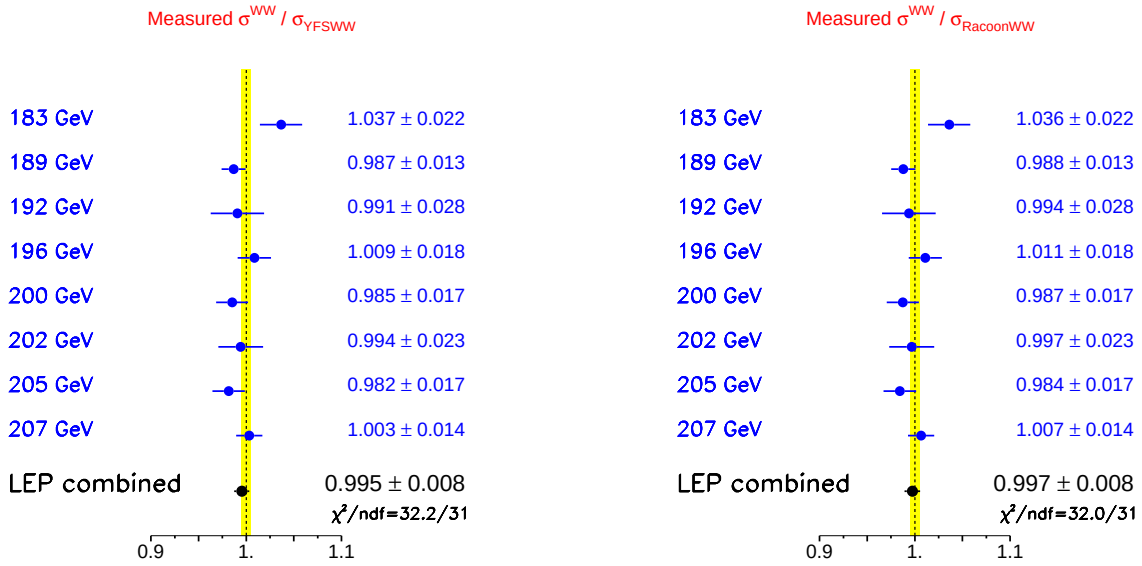


Figure 5.2: Ratios of LEP combined W-pair cross-section measurements to the expectations calculated with YFSWW [161, 167] and RACOONWW [168] The yellow bands represent constant relative errors of 0.5% on the two cross-section predictions.

5.2.2 Derived Quantities

From the cross-sections of the individual WW decay channels, each experiment determined the values of the W branching fractions, with and without the assumption of lepton universality [2]. In the fit with lepton universality, the branching fraction to hadrons is determined from that to leptons by constraining the sum to unity. In building the full 12×12 covariance matrix, the same correlations of the systematic errors as used for the cross-section measurements are assumed. The detailed inputs to LEP and the correlation matrices are reported in Table E.6.

The results from each experiment are reported in Table 5.5 together with the LEP combination and shown in Figure 5.3. The results of the fit which does not assume lepton universality show a negative correlation of 20.1% (12.2%) between the $W \to \tau\overline{\nu}_\tau$ and $W \to e\overline{\nu}_e$ ($W \to \mu\overline{\nu}_\mu$) branching fractions, while between the electron and muon decay channels there is a positive correlation of 13.5%.

From the results on the leptonic branching fractions an excess of the branching fraction $W \to \tau\overline{\nu}_\tau$ with respect to the other leptons is evident. The excess can be quantified by the pair-wise ratios of the branching fractions, which represent a test of lepton universality in the decay of on-shell W bosons:

[2] In what follows any effects from lepton masses on W partial widths are neglected given their small size.

	Lepton non–universality			Lepton universality
Experiment	$\mathcal{B}(\mathrm{W} \to \mathrm{e}\overline{\nu}_{\mathrm{e}})$ [%]	$\mathcal{B}(\mathrm{W} \to \mu\overline{\nu}_{\mu})$ [%]	$\mathcal{B}(\mathrm{W} \to \tau\overline{\nu}_{\tau})$ [%]	$\mathcal{B}(\mathrm{W} \to \mathrm{hadrons})$ [%]
ALEPH	10.78 ± 0.29	10.87 ± 0.26	11.25 ± 0.38	67.13 ± 0.40
DELPHI	10.55 ± 0.34	10.65 ± 0.27	11.46 ± 0.43	67.45 ± 0.48
L3	10.78 ± 0.32	10.03 ± 0.31	11.89 ± 0.45	67.50 ± 0.52
OPAL	10.71 ± 0.27	10.78 ± 0.26	11.14 ± 0.31	67.41 ± 0.44
LEP	10.71 ± 0.16	10.63 ± 0.15	11.38 ± 0.21	67.41 ± 0.27
χ^2/dof	6.3/9			15.4/11

Table 5.5: Summary of W branching fractions derived from W-pair production cross-sections measurements up to 207 GeV centre–of–mass energy.

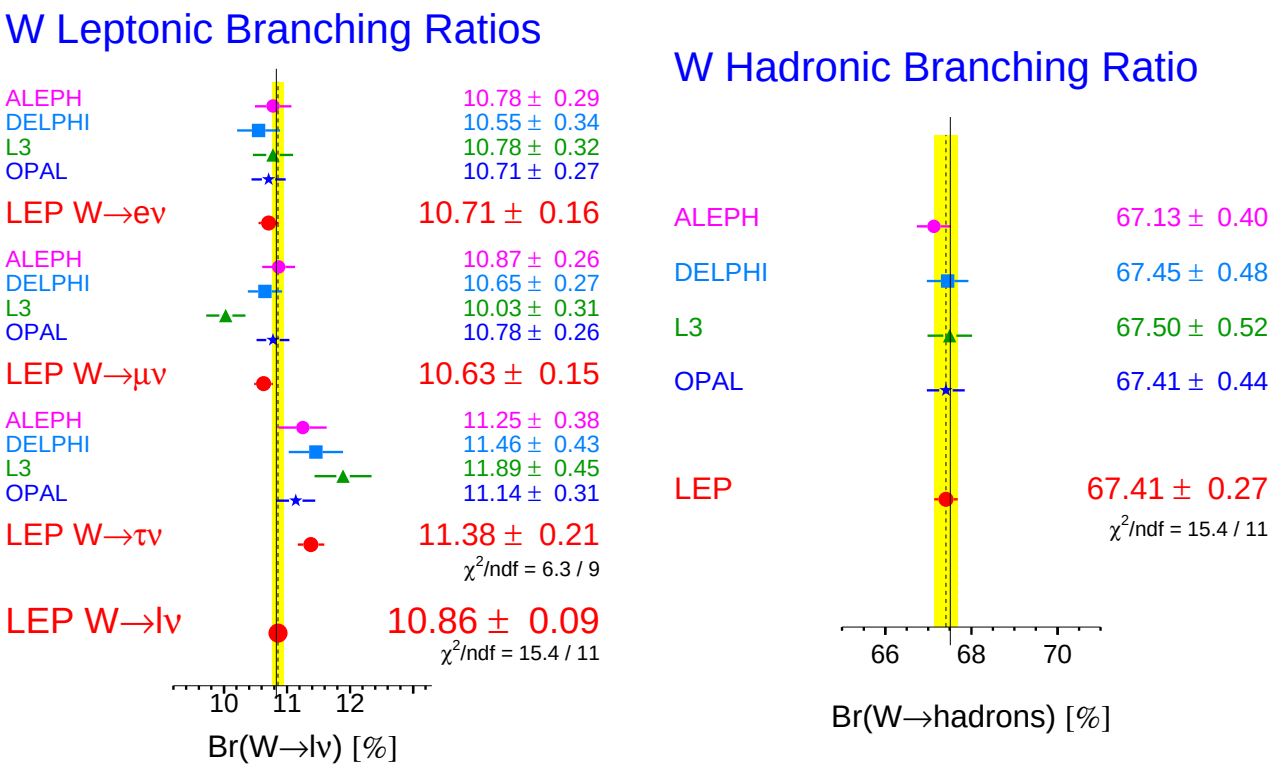


Figure 5.3: Leptonic and hadronic W branching fractions, as measured by the experiments, and the LEP combined values according to the procedures described in the text.

$$\mathcal{B}(\mathrm{W} \to \mu\overline{\nu}_\mu) \,/\, \mathcal{B}(\mathrm{W} \to \mathrm{e}\overline{\nu}_\mathrm{e}) \;=\; 0.993 \pm 0.019\,, \tag{5.2}$$

$$\mathcal{B}(\mathrm{W} \to \tau\overline{\nu}_\tau) \,/\, \mathcal{B}(\mathrm{W} \to \mathrm{e}\overline{\nu}_\mathrm{e}) \;=\; 1.063 \pm 0.027\,, \tag{5.3}$$

$$\mathcal{B}(\mathrm{W} \to \tau\overline{\nu}_\tau) \,/\, \mathcal{B}(\mathrm{W} \to \mu\overline{\nu}_\mu) \;=\; 1.070 \pm 0.026\,. \tag{5.4}$$

The branching fraction of W into taus with respect to that into electrons and muons differs by more than two standard deviations, where the correlations have been taken into account. The branching fractions of W into electrons and into muons agree well. Assuming only partial lepton universality the ratio between the tau fractions and the average of electrons and muons can also be computed:

$$2\mathcal{B}(\mathrm{W} \to \tau\overline{\nu}_\tau) \,/\, (\mathcal{B}(\mathrm{W} \to \mathrm{e}\overline{\nu}_\mathrm{e}) + \mathcal{B}(\mathrm{W} \to \mu\overline{\nu}_\mu)) \;=\; 1.066 \pm 0.025 \tag{5.5}$$

resulting in an agreement at the level of 2.6 standard deviations only, with all correlations included.

If overall lepton universality is assumed (in the massless assumption), the hadronic branching fraction is determined to be $67.41 \pm 0.18(\mathrm{stat.}) \pm 0.20(\mathrm{syst.})\%$, while the leptonic branching fraction is $10.86 \pm 0.06(\mathrm{stat.}) \pm 0.07(\mathrm{syst.})\%$. These results are consistent with the SM expectations of 67.51% and 10.83% [36], respectively. The systematic error receives equal contributions from the correlated and uncorrelated sources.

Within the SM, the branching fractions of the W boson depend on the six matrix elements $|\mathrm{V}_{\mathrm{qq}'}|$ of the Cabibbo–Kobayashi–Maskawa (CKM) quark mixing matrix not involving the top quark. In terms of these matrix elements, the leptonic branching fraction of the W boson $\mathcal{B}(\mathrm{W} \to \ell\overline{\nu}_\ell)$ is given by

$$\frac{1}{\mathcal{B}(\mathrm{W} \to \ell\overline{\nu}_\ell)} \;=\; 3\left\{1 + \left[1 + \frac{\alpha_\mathrm{s}(\mathrm{M}_\mathrm{W}^2)}{\pi}\right] \sum_{\substack{i\,=\,(u,\,c),\\ j\,=\,(d,\,s,\,b)}} |\mathrm{V}_{ij}|^2\right\}, \tag{5.6}$$

where $\alpha_\mathrm{s}(\mathrm{M}_\mathrm{W}^2)$ is the strong coupling constant and fermion mass effects are negligible. Taking $\alpha_\mathrm{s}(\mathrm{M}_\mathrm{W}^2) = 0.119 \pm 0.002$ [178], and using the experimental knowledge of the sum $|\mathrm{V}_{\mathrm{ud}}|^2 + |\mathrm{V}_{\mathrm{us}}|^2 + |\mathrm{V}_{\mathrm{ub}}|^2 + |\mathrm{V}_{\mathrm{cd}}|^2 + |\mathrm{V}_{\mathrm{cb}}|^2 = 1.0544 \pm 0.0051$ [178], the above result can be interpreted as a measurement of $|\mathrm{V}_{\mathrm{cs}}|$ which is the least well determined of these matrix elements:

$$|\mathrm{V}_{\mathrm{cs}}| \;=\; 0.969 \,\pm\, 0.013.$$

The error includes a contribution of 0.0006 from the uncertainty on α_s and a 0.003 contribution from the uncertainties on the other CKM matrix elements, the largest of which is that on $|\mathrm{V}_{\mathrm{cd}}|$. These uncertainties are negligible in the error of this determination of $|\mathrm{V}_{\mathrm{cs}}|$, which is dominated by the experimental error of 0.013 arising from the measurement of the W branching fractions.

5.2.3 W Angular Distribution

In addition to measuring the total W^+W^- cross-section, the LEP experiments produce results for the differential cross-section, $d\sigma_{WW}/d\cos\theta_W$, where θ_W is the polar angle of the produced W^- with respect to the e^- beam direction. The LEP combination of these measurements will allow future theoretical models which predict deviations in this distribution to be tested against the LEP data in a direct and, as far as possible, model-independent manner. To reconstruct the $\cos\theta_W$ distribution it is necessary to identify the charges of the decaying W bosons. This can only be performed without significant ambiguity when one of W-boson decays via $W \to e\nu$ or $W \to \mu\nu$, in which case the lepton provides the charge tag. Consequently, the combination of the differential cross-section measurements is performed for the $q\overline{q}e\nu$ and $q\overline{q}\mu\nu$ channels combined. Selected $q\overline{q}\tau\nu$ events are not considered due to the larger backgrounds and difficulties in determining the tau lepton charge in the case where not all charged decay products are detected.

The measured $q\overline{q}e\nu$ and $q\overline{q}\mu\nu$ differential cross-sections are corrected to correspond to the CC03 set of diagrams with the additional constraint that the charged lepton is more than 20° away from the e^+e^- beam direction, $|\theta_{\ell^\pm}| > 20^\circ$. This angular requirement corresponds approximately to the experimental acceptance of the four LEP experiments and also greatly reduces the difference between the full $4f$ cross-section and the CC03 cross-section by reducing the contribution of t-channel diagrams in the $q\overline{q}e\nu$ final state[3]. The angle $\cos\theta_W$ is reconstructed from the four-momenta of the fermions from the W^- decay using the ECALO5 photon recombination scheme[156], a prescription for combining photons to a close-by charged fermion.

The LEP combination is performed in ten bins of $\cos\theta_W$. Because the differential cross-section distribution evolves with $\sqrt{s}$, reflecting the changing relative $s-$ and $t-$ channel contributions, the LEP data are divided into four $\sqrt{s}$ ranges: 180 GeV$-$184 GeV, 184 GeV$-$194 GeV, 194 GeV $-$ 204 GeV, and 204 GeV $-$ 210 GeV. It has been verified for each $\sqrt{s}$ range that the differences in the differential cross-sections at the mean value of $\sqrt{s}$ compared to the luminosity-weighted sum of the differential cross-sections reflecting the actual distribution of the data across $\sqrt{s}$ are negligible compared to the statistical errors.

The experimental resolution in LEP on the reconstructed values of $\cos\theta_W$ is typically 0.15-0.20. When simulating W-pair production, a significant migration between generated and reconstructed bins of $\cos\theta_W$ is observed. The effects of bin-to-bin migration are not explicitly unfolded, instead each experiment obtains the cross-section in the i^{th} bin of the differential distribution, σ_i, from

$$\sigma_i = \frac{N_i - b_i}{\epsilon_i \mathcal{L}}, \tag{5.7}$$

where:

- N_i is the observed number of $q\overline{q}e\nu/q\overline{q}\mu\nu$ events reconstructed in the ith bin of the $\cos\theta_W$ distribution.

[3]With this requirement the difference between the total four-fermion (CC20 [156]) and double-resonant (CC03) $q\overline{q}e\nu$ cross-section is approximately 3.5 %, as opposed to 24.0 % without the lepton angle requirement. For the $q\overline{q}\mu\nu$ channel the difference between the total four-fermion (CC10 [156]) and double-resonant (CC03) cross-section is less than 1 % in both cases.

b_i is the expected number of background events in bin i. The contribution from four-fermion background is treated as in each of the experiments' W^+W^- cross-section analyses.

ϵ_i is the Monte-Carlo efficiency in bin i, defined as $\epsilon_i = S_i/G_i$ where S_i is the number of selected CC03 MC $q\overline{q}\ell\nu_\ell$ events reconstructed in bin i and G_i is the number of MC CC03 $q\overline{q}e\nu/q\overline{q}\mu\nu$ events with generated $\cos\theta_W$ (calculated using the ECALO5 recombination scheme) lying in the ith bin ($|\theta_{\ell^\pm}| > 20^\circ$). Selected $q\overline{q}\tau\nu$ events are included in the numerator of the efficiency.

This bin-by-bin efficiency correction method has the advantages of simplicity and that the resulting σ_i are uncorrelated. The main disadvantage of this procedure is that bin-by-bin migrations between generated and reconstructed $\cos\theta_W$ are corrected purely on the basis of the SM expectation and may potentially be biased. The validity of the simple correction procedure was tested by considering a range of deviations from the SM. Specifically, the SM $\cos\theta_W$ distribution was reweighted, in turn, by factors of $1 + 0.1(\cos\theta_W - 1)$, $1 - 0.2\cos^2\theta_{W^-}$, $1 + 0.2\cos^2\theta_{W^-}$ and $1 - 0.4\cos^8\theta_{W^-}$, and data samples generated corresponding to the combined LEP luminosity. These reweighting functions represent deviations which are large compared to the statistics of the combined LEP measurements. The bin-by-bin correction method was found to result in good χ^2 distributions when the extracted $\cos\theta_W$ distributions were compared with the underlying generated distribution (*e.g.* the worst case gave a mean χ^2 of 11.3 for the 10 degrees of freedom corresponding to the ten $\cos\theta_W$ bins), and no significant bias was found in these tests.

For the LEP combination the systematic uncertainties on measured differential cross-sections are broken down into two terms: uncertainties which are fully correlated between bins and experiments and errors which are correlated between bins but uncorrelated between experiments. This procedure reflects the fact that the dominant systematic errors affect the overall normalisation of the measured distributions rather than the shape.

The detailed inputs provided by the four LEP experiments are reported in Tables E.7, E.8, E.9 and E.10. Table 5.6 presents the combined LEP results. In the table the bin-by-bin error breakdown is also reported. The result is also shown in Figure 5.4, where the combined data are superimposed on the four-fermion theory predictions calculated with KandY [167] and RACOONWW [168], which are indistinguishable on the plot scale. The agreement of data and calculations is generally very good, with an apparent under-fluctuation of data with respect to the central values of the theory predictions in the last bin of the 194 GeV − 204 GeV energy range.

5.3 Z-Pair Production

The signal definition has been given in Section 5.1. Z-pair production shows several similarities to W-pair production. The different final states depend on the decay of the heavy bosons: it is possible to have four quarks, two quarks and two leptons or four leptons in the final state. The signatures are very clean and the main background is represented by WW production.

The approaches used by the experiments for the selection are based on Neural Network techniques. The final states studied involve both the hadronic and leptonic decays of the Z boson, where invisible decays are included when accompanied by a charged decay. The selection efficiencies depend significantly on the final state, ranging from 25% to 60%, with purities from 30% to 70% [179, 180, 181, 182]. The main backgrounds include four-fermion production, di-leptonic and QCD final states.

$\cos\theta_{W^-}$ bin i	1	2	3	4	5	6	7	8	9	10
$\sqrt{s}$ range: $180-184$ GeV				$\mathcal{L} = 163.90$ pb^{-1}					Weighted $\sqrt{s} = 182.66$ GeV	
σ_i (pb)	0.502	0.705	0.868	1.281	1.529	2.150	2.583	2.602	4.245	5.372
$\delta\sigma_i$ (pb)	0.114	0.129	0.143	0.203	0.195	0.244	0.270	0.254	0.367	0.419
$\delta\sigma_i$(stat) (pb)	0.112	0.128	0.142	0.202	0.194	0.241	0.267	0.249	0.362	0.413
$\delta\sigma_i$(syst) (pb)	0.016	0.017	0.018	0.023	0.024	0.036	0.040	0.049	0.059	0.073
$\sqrt{s}$ range: $184-194$ GeV				$\mathcal{L} = 587.95$ pb^{-1}					Weighted $\sqrt{s} = 189.09$ GeV	
σ_i (pb)	0.718	0.856	1.009	1.101	1.277	1.801	2.215	2.823	4.001	5.762
$\delta\sigma_i$ (pb)	0.074	0.079	0.086	0.088	0.094	0.123	0.140	0.151	0.179	0.223
$\delta\sigma_i$(stat) (pb)	0.073	0.078	0.084	0.085	0.091	0.119	0.135	0.144	0.169	0.208
$\delta\sigma_i$(syst) (pb)	0.015	0.015	0.018	0.023	0.023	0.031	0.035	0.046	0.060	0.081
$\sqrt{s}$ range: $194-204$ GeV				$\mathcal{L} = 605.05$ pb^{-1}					Weighted $\sqrt{s} = 198.38$ GeV	
σ_i (pb)	0.679	0.635	0.991	1.087	1.275	1.710	2.072	2.866	4.100	6.535
$\delta\sigma_i$ (pb)	0.079	0.065	0.084	0.088	0.096	0.116	0.126	0.158	0.185	0.236
$\delta\sigma_i$(stat) (pb)	0.078	0.064	0.083	0.085	0.094	0.112	0.122	0.152	0.175	0.220
$\delta\sigma_i$(syst) (pb)	0.012	0.013	0.016	0.021	0.021	0.029	0.033	0.043	0.059	0.085
$\sqrt{s}$ range: $204-210$ GeV				$\mathcal{L} = 630.51$ pb^{-1}					Weighted $\sqrt{s} = 205.92$ GeV	
σ_i (pb)	0.495	0.602	0.653	1.057	1.240	1.707	2.294	2.797	4.481	7.584
$\delta\sigma_i$ (pb)	0.058	0.066	0.069	0.094	0.093	0.115	0.140	0.143	0.187	0.262
$\delta\sigma_i$(stat) (pb)	0.057	0.065	0.068	0.091	0.090	0.111	0.137	0.136	0.175	0.244
$\delta\sigma_i$(syst) (pb)	0.012	0.013	0.015	0.021	0.022	0.030	0.033	0.045	0.064	0.096

Table 5.6: Combined W^- differential angular cross-section in the 10 angular bins for the four chosen energy intervals. For each energy range, the sum of the measured integrated luminosities and the luminosity-weighted centre-of-mass energy is reported. The results per angular bin in each of the energy interval are then presented: σ_i indicates the average of $d[\sigma_{WW}(BR_{e\nu}+BR_{\mu\nu})]/d\cos\theta_{W^-}$ in the i-th bin of $\cos\theta_{W^-}$, with a bin width of 0.2. For each bin, the values of the total, statistical and systematic errors are reported. All values are given in pb.

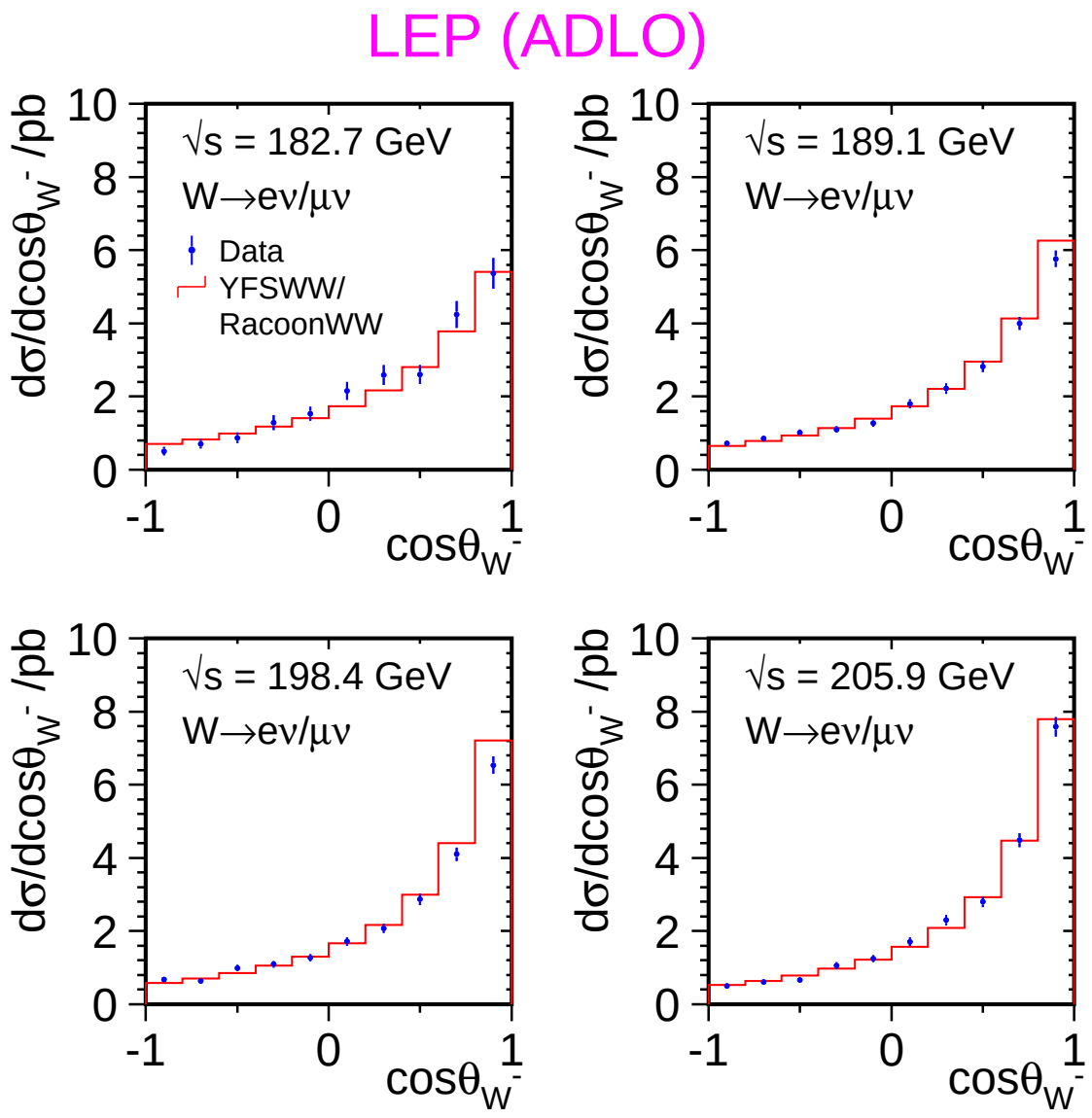


Figure 5.4: LEP combined $d[\sigma_{WW}(BR_{e\nu}+BR_{\mu\nu})]/d\cos\theta_{W^-}$ distributions for the four chosen energy intervals. The combined values (points) are superimposed on the four-fermion predictions from KandY and RACOONWW.

The LEP combination is performed applying the same technique as used for the WW cross-section measurement. The symmetrised expected statistical error of each analysis is used, to avoid biases due to the limited number of selected events. The detailed inputs from the experiments are reported in Table E.11. The results of the individual experiments are summarized in Table 5.7, together with the LEP averages. The composition of the systematic error in terms of correlated components is shown in Table E.12. The cross-sections used for the combination are determined by the experiments using the frequentist approach, without assuming any prior for the value of the cross-section itself.

The measurements are shown in Figure 5.5 as a function of the LEP centre–of–mass energy, where they are compared to the YFSZZ [183] and ZZTO [184] predictions as listed in Table E.13. Both these calculations have an estimated uncertainty of 2% [156]. The data do not show any significant deviation from the theoretical expectations.

In analogy with the W-pair cross-section, a value for $\mathcal{R}_{\mathrm{ZZ}}$ can also be determined: its definition and the procedure of the combination follows those described for $\mathcal{R}_{\mathrm{WW}}$. The data are compared with the YFSZZ and ZZTO predictions; Table 5.8, with more details given in Table E.14, reports the combined values of $\mathcal{R}_{\mathrm{ZZ}}$ at each energy and combined, and Figure 5.6 shows them in comparison to unity, where the $\pm 2\%$ error on the theoretical ZZ cross-section is shown as a yellow band. The experimental accuracy on the combined value of $\mathcal{R}_{\mathrm{ZZ}}$ is about 5%.

5.4 Z-γ^* Production

The signal definition has been given in Section 5.1. The study of these final states is also relevant for the measurement of neutral gauge couplings. The LEP collaborations did not provide a complete analysis of all possible Zγ^* final states. While ALEPH and OPAL did not present any results on Zγ^*, DELPHI provided results for the $\nu\nu$qq, $\ell\ell$qq, $\ell\ell\ell\ell$ and qqqq final states [185], and L3 provided results for the $\nu\nu$qq, $\ell\ell$qq, $\ell\ell\nu\nu$, and $\ell\ell\ell\ell$ channels [186], where $\ell = \mathrm{e}, \mu$. Final states containing τ leptons were not studied. The combination reported here has been performed using data from the final states provided by both DELPHI and L3, namely $\nu\nu$qq, $\mu\mu$qq and eeqq.

To increase the statistics the cross-sections were determined using the full data sample at an average LEP-II centre-of-mass energy. Table 5.9 presents the measured cross-sections, where the expected statistical errors were used for the combination. As noted in Section 5.1, the $Z\gamma^*$ signal has been defined by mass and angular cuts specific to each of the contributing channels, and the comparison of the combined LEP cross-section with the theoretical prediction, calculated with `grc4f` [187] and shown in the last section of Table 5.9, has been made by imposing the same cuts on each of the experimental and simulated samples included in the combination. The results agree well with the expectations.

5.5 Single-Boson Production

The study of singly resonant final states finds its motivations in the comparison with SM calculations in a delicate region of the 4-f phase space, where the treatment of ISR or fermion loop corrections can induce large corrections, up to several percent, to the total cross-section. These processes are also very sensitive to the value of α_{QED}. Moreover, single W production also brings information on possible anomalous WWγ couplings.

$\sqrt{s}$	ZZ cross-section [pb]				
(GeV)	ALEPH	DELPHI	L3	OPAL	LEP
182.7	$0.11\ ^{+\ 0.16}_{-\ 0.12}$	$0.35\ ^{+\ 0.20}_{-\ 0.15}$	0.31 ± 0.17	$0.12\ ^{+\ 0.20}_{-\ 0.18}$	0.22 ± 0.08
188.6	$0.67\ ^{+\ 0.14}_{-\ 0.13}$	$0.52\ ^{+\ 0.12}_{-\ 0.11}$	0.73 ± 0.15	$0.80\ ^{+\ 0.15}_{-\ 0.14}$	0.66 ± 0.07
191.6	$0.62\ ^{+\ 0.40}_{-\ 0.33}$	$0.63\ ^{+\ 0.36}_{-\ 0.30}$	0.29 ± 0.22	$1.29\ ^{+\ 0.48}_{-\ 0.41}$	0.67 ± 0.18
195.5	$0.73\ ^{+\ 0.25}_{-\ 0.22}$	$1.05\ ^{+\ 0.25}_{-\ 0.22}$	1.18 ± 0.26	$1.13\ ^{+\ 0.27}_{-\ 0.25}$	1.00 ± 0.12
199.5	$0.91\ ^{+\ 0.25}_{-\ 0.22}$	$0.75\ ^{+\ 0.20}_{-\ 0.18}$	1.25 ± 0.27	$1.05\ ^{+\ 0.26}_{-\ 0.23}$	0.95 ± 0.12
201.6	$0.71\ ^{+\ 0.32}_{-\ 0.27}$	$0.85\ ^{+\ 0.33}_{-\ 0.28}$	0.95 ± 0.39	$0.79\ ^{+\ 0.36}_{-\ 0.30}$	0.81 ± 0.18
204.9	$1.20\ ^{+\ 0.28}_{-\ 0.26}$	$1.03\ ^{+\ 0.23}_{-\ 0.20}$	$0.77\ ^{+\ 0.21}_{-\ 0.19}$	$1.07\ ^{+\ 0.28}_{-\ 0.25}$	0.98 ± 0.13
206.6	$1.05\ ^{+\ 0.22}_{-\ 0.21}$	$0.96\ ^{+\ 0.16}_{-\ 0.15}$	$1.09\ ^{+\ 0.18}_{-\ 0.17}$	$0.97\ ^{+\ 0.20}_{-\ 0.19}$	1.00 ± 0.09

Table 5.7: Z-pair production cross-sections from the four LEP experiments and combined values for the eight centre-of-mass energies between 183 GeV and 207 GeV. The χ^2/dof of the combined fit is 14.5/24.

$\sqrt{s}$(GeV)	$\mathcal{R}_{\mathrm{ZZ}}^{\mathrm{ZZTO}}$	$\mathcal{R}_{\mathrm{ZZ}}^{\mathrm{YFSZZ}}$
182.7	0.857 ± 0.320	0.857 ± 0.320
188.6	1.017 ± 0.113	1.007 ± 0.111
191.6	0.865 ± 0.226	0.859 ± 0.224
195.5	1.118 ± 0.134	1.118 ± 0.134
199.5	0.974 ± 0.126	0.970 ± 0.126
201.6	0.805 ± 0.174	0.800 ± 0.174
204.9	0.934 ± 0.122	0.928 ± 0.121
206.6	0.948 ± 0.092	0.938 ± 0.091
χ^2/dof	14.5/24	14.5/24
Average	0.966 ± 0.052	0.960 ± 0.052
χ^2/dof	17.4/31	17.4/31

Table 5.8: Ratios of LEP combined Z-pair cross-section measurements to the expectations according to ZZTO [184] and YFSZZ [183]. The results of the combined fits are given together with the resulting χ^2/dof. Both fits take into account inter-experiment as well as inter-energy correlations of systematic errors.

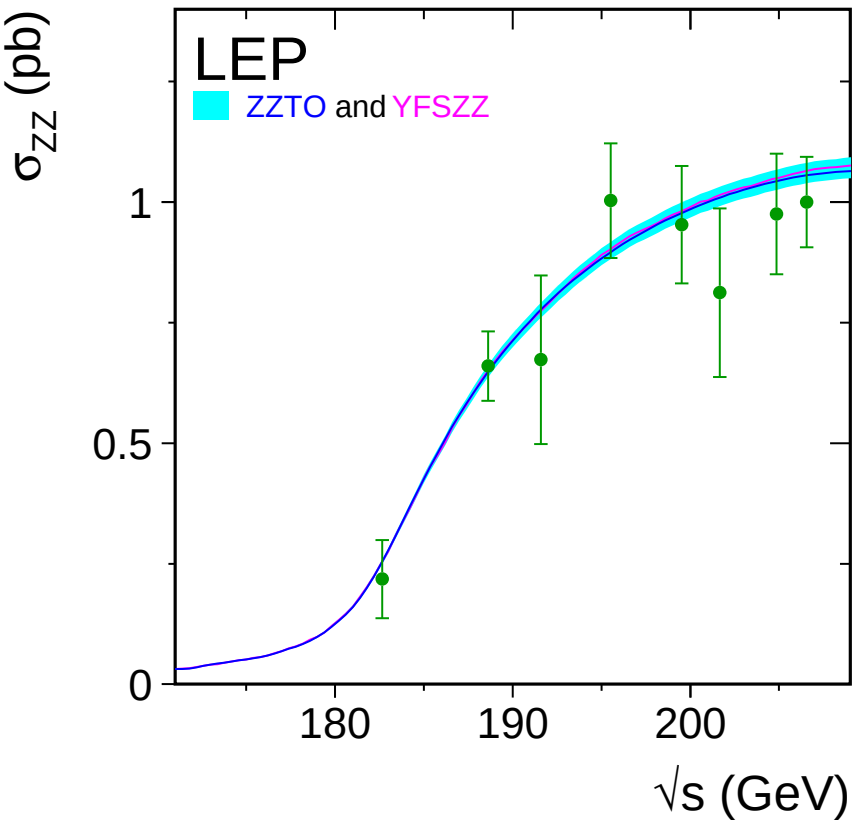


Figure 5.5: Measurements of the Z-pair production cross-section, compared to the predictions of YFSZZ [183] and ZZTO [184]. The shaded area represents the ±2% uncertainty on the predictions.

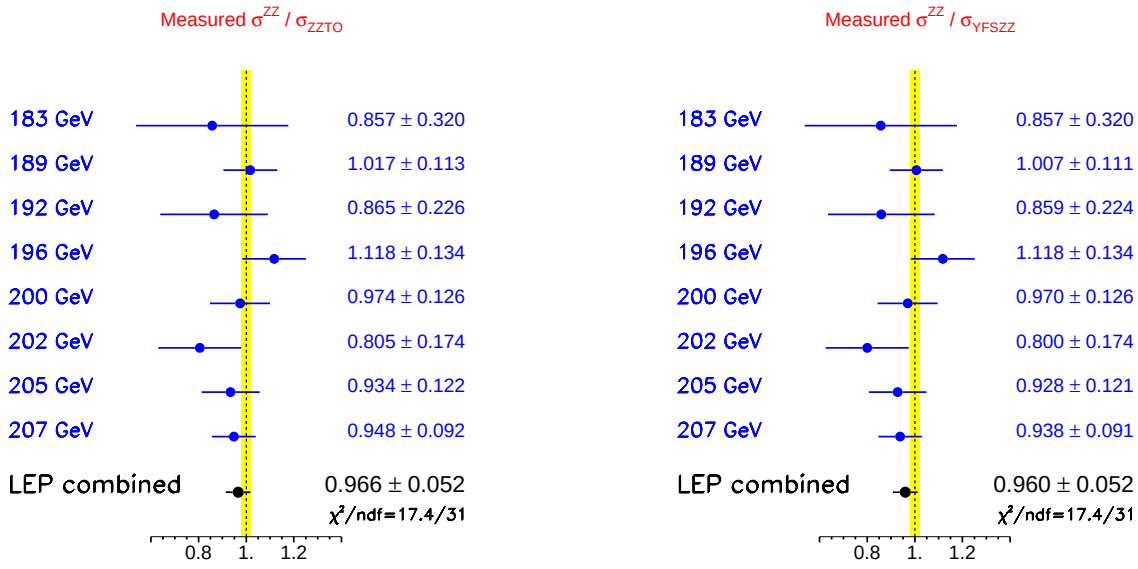


Figure 5.6: Ratios of LEP combined Z-pair cross-section measurements to the expectations according to ZZTO [184] and YFSZZ [183] The yellow bands represent constant relative errors of 2% on the two cross-section predictions.

Channel	$\sqrt{s}$ [GeV]	L [pb^{-1}]	σ [pb]	$\delta\sigma_{\rm stat}$ [pb]	$\delta\sigma^{\rm unc}_{\rm syst}$ [pb]	$\delta\sigma^{\rm cor}_{\rm syst}$ [pb]	$\delta\sigma_{\rm MC}$ [pb]
DELPHI							
$\nu\nu$qq	197.1	666.7	0.042	$^{+0.022}_{-0.014}$	0.008	0.002	0.042
$\mu\mu$qq	197.1	666.7	0.031	$^{+0.013}_{-0.011}$	0.004	0.001	0.016
eeqq	197.1	666.7	0.063	$^{+0.018}_{-0.016}$	0.009	0.001	0.016
L3							
$\nu\nu$qq	196.7	679.4	0.072	$^{+0.047}_{-0.041}$	0.004	0.016	0.046
$\mu\mu$qq	196.7	681.9	0.040	$^{+0.018}_{-0.016}$	0.002	0.003	0.017
eeqq	196.7	681.9	0.100	$^{+0.024}_{-0.022}$	0.004	0.007	0.020
LEP combined							
Channel	$\sqrt{s}$ [GeV]	L [pb^{-1}]	σ [pb]	$\delta\sigma_{\rm stat}$ [pb]	$\delta\sigma_{\rm syst}$ [pb]	$\delta\sigma_{\rm tot}$ [pb]	$\sigma_{\rm theory}$ [pb]
$\nu\nu$qq	196.9	679.4	0.055	0.031	0.008	0.032	0.083
$\mu\mu$qq	196.9	681.9	0.035	0.012	0.003	0.012	0.042
eeqq	196.9	681.9	0.079	0.012	0.005	0.013	0.059

Table 5.9: Zγ^* measurements by the experiments and combined LEP measurements. The columns show, respectively, the channel, the luminosity-weighted centre-of-mass energy, the luminosity, the measured cross-section, the measured statistical error, the systematic contribution uncorrelated between experiments, the systematic contribution correlated between experiments and the expected statistical error from the simulation. For the LEP combination the full systematic error and the total error are given and the last column presents the theory expectation with `grc4f` [187].

Single boson production at LEP is mostly realised via t-channel processes, where either the incident electron or positron maintains its direction, escaping undetected along the beam and thus generating missing momentum along the z axis. Single W and single Z production then proceed dominantly via the vector boson fusion process illustrated in Figure 1.7 or via Bremsstrahlung processes. In the case of single W production in the W $\to$ e$\overline{\nu}_{\rm e}$ final state, the W is detected either by its hadronic decay producing two jets, or by its leptonic decay producing a single charged lepton; single Z production in the Z $\to$ e$^+$e$^-$ final state is identified from an electron recoiling against two fermions (quarks or leptons) coming from the Z decay.

The selection of these events is particularly difficult because of the relatively low cross-section of the signal and because of the presence of large backgrounds in these phase space regions. Particularly large backgrounds arise from radiative $q\bar{q}$ production or $\gamma\gamma$ scattering. The analyses, mostly based on sequential cuts on kinematic variables, have an efficiency which depends on the considered final state and ranges typically from 35% to 60% [190, 191, 192, 193, 194]. These references describe results on single-boson production using selection criteria which are specific to the individual experiments. The results shown below are derived from a common selection procedure using the criteria listed in Section 5.1.

5.5.1 Weν Cross-Section Measurement

The signal definition has been given in Section 5.1. The LEP combination of the single-W production cross-section is performed using the expected statistical errors, given the limited statistical precision of the single measurements. The correlation of the systematic errors in energy and among experiments is properly taken into account. The hadronic and the total single-W cross-sections are combined independently, as the former is less contaminated by $\gamma\gamma$ interaction contributions. The details on the input measurements are summarised in Tables E.15 and E.16.

The hadronic single-W results and combinations are reported in Table 5.10 and Figure 5.7. The total single-W results, for all decay modes and combinations are listed in Table 5.11 and Figure 5.8. In the two figures, the measurements are compared with the expected values from WPHACT [195] and `grc4f` [187], listed in Table E.17. In Figure 5.7, the predictions of WTO [198], which includes fermion-loop corrections for the hadronic final states, have also been included. As discussed more in detail in [156], the theoretical predictions are scaled upward to correct for the implementation of QED radiative corrections at the wrong energy scale s. The full correction of 4%, derived from comparison with the theoretical predictions from SWAP [202], is conservatively taken as a systematic error. This uncertainty dominates the $\pm 5\%$ theoretical error currently assigned to these predictions, represented by the shaded area in Figures 5.7 and 5.8. All results, up to the highest centre–of–mass energies, are in agreement with the theoretical predictions.

The agreement can also be appreciated in Table 5.12, where the values of the ratio between measured and expected cross-section values according to the computations of `grc4f` and WPHACT are reported, with additional details listed in Table E.18. The combination is performed accounting for the energy and experiment correlations of the systematic sources. The results are also presented in Figure 5.9.

5.5.2 Zee Cross-Section Measurement

The signal definition has been given in Section 5.1. The combination of results is performed with the same technique used for the other channels. The results include the hadronic and the leptonic channels and all the centre–of–mass energies from 183 to 209 GeV from the ALEPH [190], DELPHI [191] and L3 [203] Collaborations. The OPAL results [204] are not included in the combination as they were not provided according to the common signal definition.

Tables 5.13 and 5.14, with details summarised in Table E.19, present the inputs from the experiments and the corresponding LEP combinations in the muon and hadronic channel, respectively. The $ee\mu\mu$ cross-section is already combined in energy by the individual experiments to increase the statistics of the data. The combination takes into account the correlation of the energy and experimental systematic errors. The results in the hadronic channel are compared with the predictions of WPHACT and `grc4f`, listed in Table E.20, in Figure 5.10 as a function of the centre–of–mass energy.

The same data are expressed as ratios of the measured to the predicted cross-section, listed in Table 5.15, with details on the decomposition of the systematic error reported in Table E.21, and shown in Figure 5.11. The accuracy of the combined ratio is about 7% with three experiments contributing to the average.

$\sqrt{s}$ (GeV)	Single-W hadronic cross-section (pb)			
	ALEPH	DELPHI	L3	LEP
182.7	$0.44\ ^{+\ 0.29}_{-\ 0.24}$	$0.11\ ^{+\ 0.31}_{-\ 0.14}$	$0.58\ ^{+\ 0.23}_{-\ 0.20}$	0.42 ± 0.15
188.6	$0.33\ ^{+\ 0.16}_{-\ 0.15}$	$0.57\ ^{+\ 0.21}_{-\ 0.20}$	$0.52\ ^{+\ 0.14}_{-\ 0.13}$	0.47 ± 0.09
191.6	$0.52\ ^{+\ 0.52}_{-\ 0.40}$	$0.30\ ^{+\ 0.48}_{-\ 0.31}$	$0.84\ ^{+\ 0.44}_{-\ 0.37}$	0.56 ± 0.25
195.5	$0.61\ ^{+\ 0.28}_{-\ 0.25}$	$0.50\ ^{+\ 0.30}_{-\ 0.27}$	$0.66\ ^{+\ 0.25}_{-\ 0.23}$	0.60 ± 0.14
199.5	$1.06\ ^{+\ 0.30}_{-\ 0.27}$	$0.57\ ^{+\ 0.28}_{-\ 0.26}$	$0.37\ ^{+\ 0.22}_{-\ 0.20}$	0.65 ± 0.14
201.6	$0.72\ ^{+\ 0.39}_{-\ 0.33}$	$0.67\ ^{+\ 0.40}_{-\ 0.36}$	$1.10\ ^{+\ 0.40}_{-\ 0.35}$	0.82 ± 0.20
204.9	$0.34\ ^{+\ 0.24}_{-\ 0.21}$	$0.99\ ^{+\ 0.33}_{-\ 0.31}$	$0.42\ ^{+\ 0.25}_{-\ 0.21}$	0.54 ± 0.15
206.6	$0.64\ ^{+\ 0.21}_{-\ 0.19}$	$0.81\ ^{+\ 0.23}_{-\ 0.22}$	$0.66\ ^{+\ 0.20}_{-\ 0.18}$	0.69 ± 0.12

Table 5.10: Single-W hadronic production cross-section from the LEP experiments and combined values for the eight energies between 183 and 207 GeV, in the hadronic decay channel of the W boson. The χ^2/dof of the combined fit is 13.2/16.

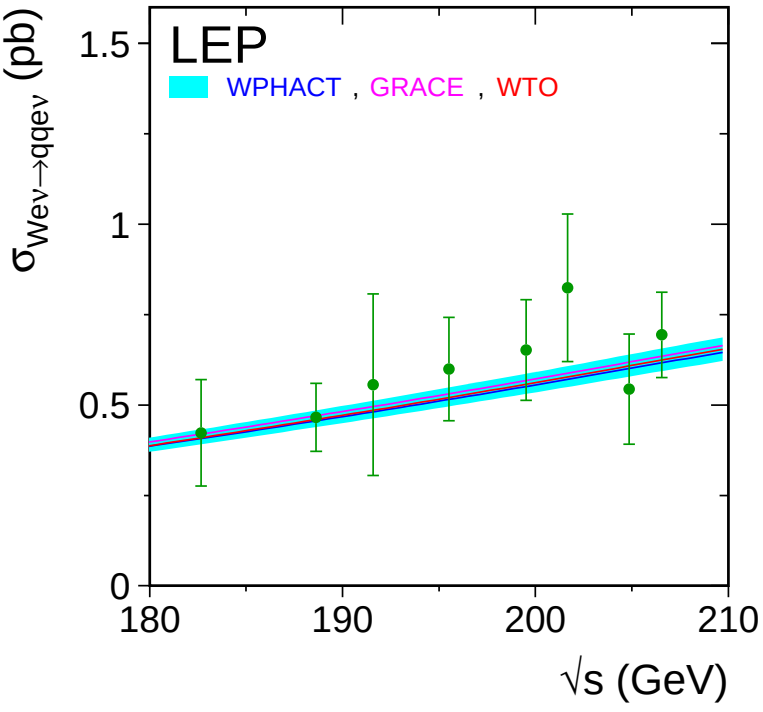


Figure 5.7: Measurements of the single-W production cross-section in the hadronic decay channel of the W boson, compared to the predictions of WTO [198], WPHACT [195] and `grc4f` [187]. The shaded area represents the ±5% uncertainty on the predictions.

$\sqrt{s}$ (GeV)	Single-W total cross-section (pb)			
	ALEPH	DELPHI	L3	LEP
182.7	$0.60\ ^{+\ 0.32}_{-\ 0.26}$	$0.69\ ^{+\ 0.42}_{-\ 0.25}$	$0.80\ ^{+\ 0.28}_{-\ 0.25}$	0.70 ± 0.17
188.6	$0.55\ ^{+\ 0.18}_{-\ 0.16}$	$0.75\ ^{+\ 0.23}_{-\ 0.22}$	$0.69\ ^{+\ 0.16}_{-\ 0.15}$	0.66 ± 0.10
191.6	$0.89\ ^{+\ 0.58}_{-\ 0.44}$	$0.40\ ^{+\ 0.55}_{-\ 0.33}$	$1.11\ ^{+\ 0.48}_{-\ 0.41}$	0.81 ± 0.28
195.5	$0.87\ ^{+\ 0.31}_{-\ 0.27}$	$0.68\ ^{+\ 0.34}_{-\ 0.38}$	$0.97\ ^{+\ 0.27}_{-\ 0.25}$	0.85 ± 0.16
199.5	$1.31\ ^{+\ 0.32}_{-\ 0.29}$	$0.95\ ^{+\ 0.34}_{-\ 0.30}$	$0.88\ ^{+\ 0.26}_{-\ 0.24}$	1.05 ± 0.16
201.6	$0.80\ ^{+\ 0.42}_{-\ 0.35}$	$1.24\ ^{+\ 0.52}_{-\ 0.43}$	$1.50\ ^{+\ 0.45}_{-\ 0.40}$	1.17 ± 0.23
204.9	$0.65\ ^{+\ 0.27}_{-\ 0.23}$	$1.06\ ^{+\ 0.37}_{-\ 0.32}$	$0.78\ ^{+\ 0.29}_{-\ 0.25}$	0.80 ± 0.17
206.6	$0.81\ ^{+\ 0.22}_{-\ 0.20}$	$1.14\ ^{+\ 0.28}_{-\ 0.25}$	$1.08\ ^{+\ 0.21}_{-\ 0.20}$	1.00 ± 0.14

Table 5.11: Single-W total production cross-section from the LEP experiments and combined values for the eight energies between 183 and 207 GeV. The χ^2/dof of the combined fit is 8.1/16.

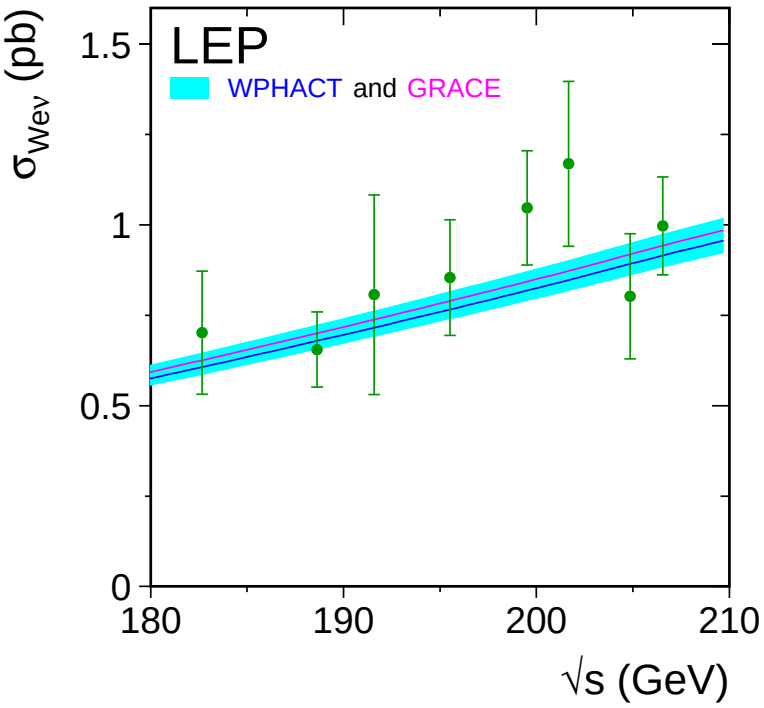


Figure 5.8: Measurements of the single-W total production cross-section, compared to the predictions of WPHACT [195] and `grc4f` [187]. The shaded area represents the ±5% uncertainty on the predictions.

$\sqrt{s}$(GeV)	$\mathcal{R}_{\mathrm{We}\nu}^{\mathtt{grc4f}}$	$\mathcal{R}_{\mathrm{We}\nu}^{\mathrm{WPHACT}}$
182.7	1.122 ± 0.272	1.157 ± 0.281
188.6	0.936 ± 0.149	0.965 ± 0.154
191.6	1.094 ± 0.373	1.128 ± 0.385
195.5	1.081 ± 0.203	1.115 ± 0.210
199.5	1.242 ± 0.187	1.280 ± 0.193
201.6	1.340 ± 0.261	1.380 ± 0.269
204.9	0.873 ± 0.189	0.899 ± 0.195
206.6	1.058 ± 0.143	1.089 ± 0.148
χ^2/dof	8.1/16	8.1/16
Average	1.058 ± 0.078	1.090 ± 0.080
χ^2/dof	12.1/23	12.1/23

Table 5.12: Ratios of LEP combined total single-W cross-section measurements to the expectations according to `grc4f` [187] and WPHACT [195]. The resulting averages over energies are also given. The averages take into account inter-experiment as well as inter-energy correlations of systematic errors.

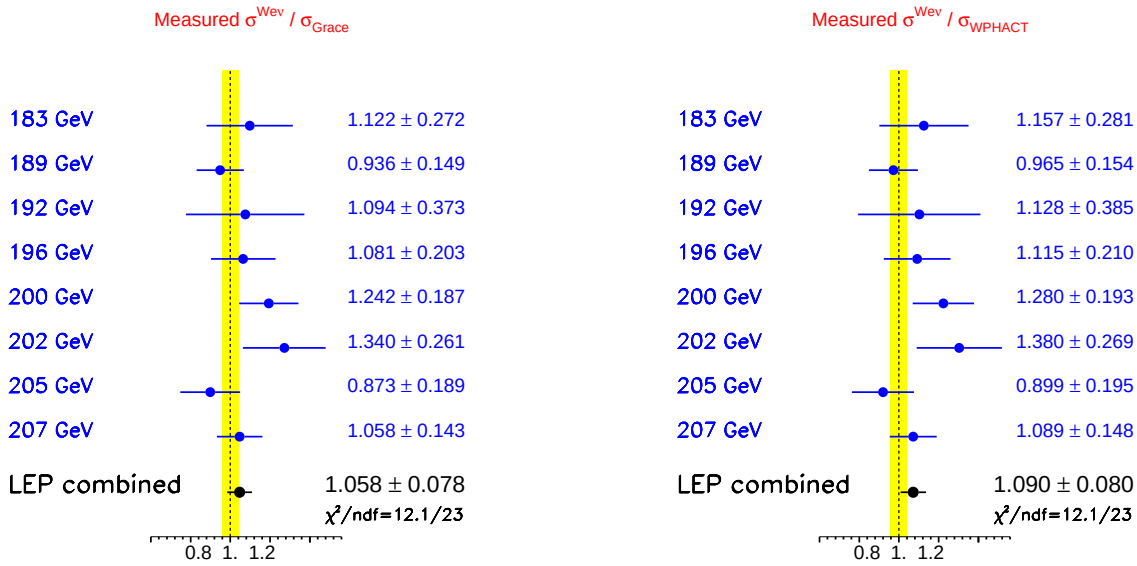


Figure 5.9: Ratios of LEP combined total single-W cross-section measurements to the expectations according to `grc4f` [187] and WPHACT [195]. The yellow bands represent constant relative errors of 5% on the two cross-section predictions.

	Single-Z cross-section into muons(pb)			
	ALEPH	DELPHI	L3	LEP
Av. $\sqrt{s}$(GeV)	196.67	197.10	196.60	196.79
$\sigma_{\mathrm{Zee}\to\mu\mu\mathrm{ee}}$	0.055 ± 0.016	$0.070\ ^{+\ 0.023}_{-\ 0.019}$	0.043 ± 0.013	0.057 ± 0.009

Table 5.13: Energy averaged single-Z production cross-section into muons from the LEP experiments and the LEP combined value.

$\sqrt{s}$	Single-Z hadronic cross-section (pb)			
(GeV)	ALEPH	DELPHI	L3	LEP
182.7	$0.27\ ^{+\ 0.21}_{-\ 0.16}$	$0.56\ ^{+\ 0.28}_{-\ 0.23}$	$0.51\ ^{+\ 0.19}_{-\ 0.16}$	0.45 ± 0.11
188.6	$0.42\ ^{+\ 0.14}_{-\ 0.12}$	$0.64\ ^{+\ 0.16}_{-\ 0.14}$	$0.55\ ^{+\ 0.11}_{-\ 0.10}$	0.53 ± 0.07
191.6	$0.61\ ^{+\ 0.39}_{-\ 0.29}$	$0.63\ ^{+\ 0.40}_{-\ 0.30}$	$0.60\ ^{+\ 0.26}_{-\ 0.21}$	0.61 ± 0.15
195.5	$0.72\ ^{+\ 0.24}_{-\ 0.20}$	$0.66\ ^{+\ 0.22}_{-\ 0.19}$	$0.40\ ^{+\ 0.13}_{-\ 0.11}$	0.55 ± 0.10
199.5	$0.60\ ^{+\ 0.21}_{-\ 0.18}$	$0.57\ ^{+\ 0.20}_{-\ 0.17}$	$0.33\ ^{+\ 0.13}_{-\ 0.11}$	0.47 ± 0.10
201.6	$0.89\ ^{+\ 0.35}_{-\ 0.28}$	$0.19\ ^{+\ 0.21}_{-\ 0.16}$	$0.81\ ^{+\ 0.27}_{-\ 0.23}$	0.67 ± 0.13
204.9	$0.42\ ^{+\ 0.17}_{-\ 0.15}$	$0.37\ ^{+\ 0.18}_{-\ 0.15}$	$0.56\ ^{+\ 0.16}_{-\ 0.14}$	0.47 ± 0.10
206.6	$0.70\ ^{+\ 0.17}_{-\ 0.15}$	$0.69\ ^{+\ 0.16}_{-\ 0.14}$	$0.59\ ^{+\ 0.12}_{-\ 0.11}$	0.65 ± 0.08

Table 5.14: Single-Z hadronic production cross-section from the LEP experiments and combined values for the eight energies between 183 and 207 GeV. The χ^2/dof of the combined fit is 13.0/16.

$\sqrt{s}$(GeV)	$\mathcal{R}_{\mathrm{Zee}}^{\mathtt{grc4f}}$	$\mathcal{R}_{\mathrm{Zee}}^{\mathrm{WPHACT}}$
182.7	0.871 ± 0.219	0.876 ± 0.220
188.6	0.982 ± 0.126	0.990 ± 0.127
191.6	1.104 ± 0.275	1.112 ± 0.277
195.5	0.964 ± 0.167	0.972 ± 0.168
199.5	0.809 ± 0.165	0.816 ± 0.167
201.6	1.126 ± 0.222	1.135 ± 0.224
204.9	0.769 ± 0.160	0.776 ± 0.162
206.6	1.062 ± 0.124	1.067 ± 0.125
χ^2/dof	13.0/16	13.0/16
Average	0.955 ± 0.065	0.962 ± 0.065
χ^2/dof	17.1/23	17.0/23

Table 5.15: Ratios of LEP combined single-Z hadronic cross-section measurements to the expectations according to `grc4f` [187] and WPHACT [195]. The resulting averages over energies are also given. The averages take into account inter-experiment as well as inter-energy correlations of systematic errors.

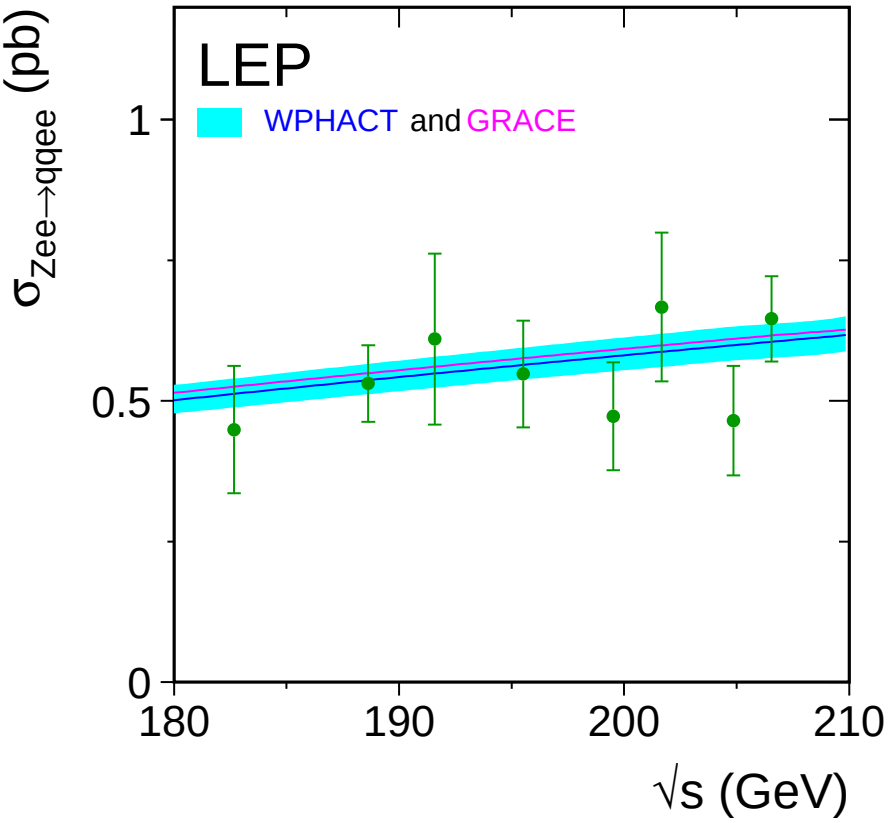


Figure 5.10: Measurements of the single-Z hadronic production cross-section, compared to the predictions of WPHACT [195] and `grc4f` [187]. The shaded area represents the ±5% uncertainty on the predictions.

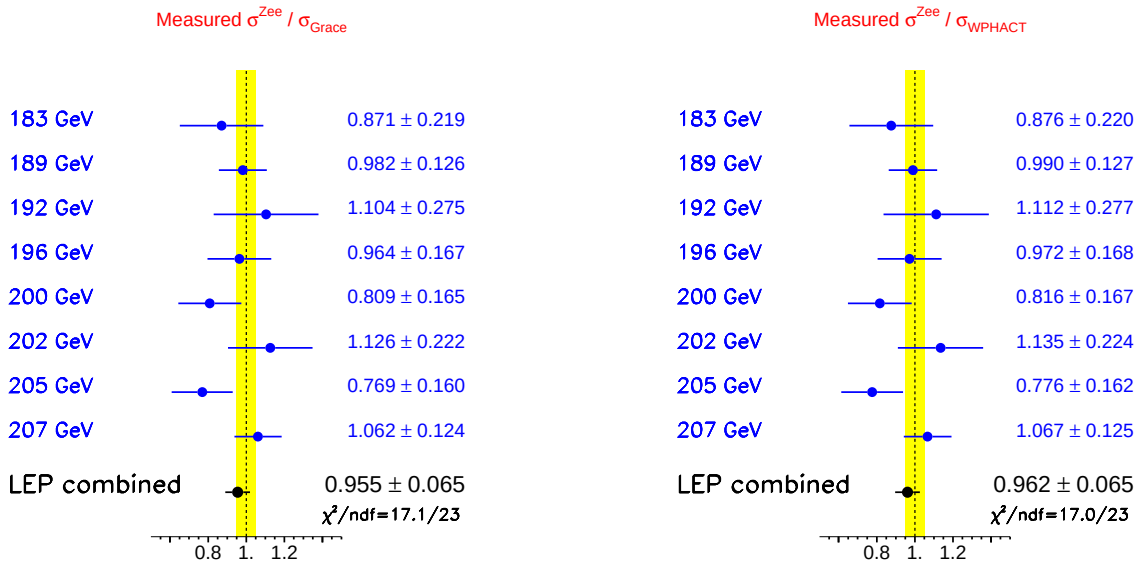


Figure 5.11: Ratios of LEP combined single-Z hadronic cross-section measurements to the expectations according to `grc4f` [187] and WPHACT [195]. The yellow bands represent constant relative errors of 5% on the two cross-section predictions.

5.6 WWγ Production

The signal definition has been given in Section 5.1. The study of photon production in association with a W-boson pair is important for testing the sector of quartic gauge couplings. In order to increase the statistical accuracy, the LEP combination is performed in energy intervals rather than at each energy point; they are defined according to the LEP-II running periods where more statistics were accumulated. The luminosity-weighted centre–of–mass energy per interval is determined in each experiment and then combined to obtain the corresponding value for each energy interval. Table 5.16 reports those energies and the cross-sections measured by the experiments that are used in this combination [206, 207, 208], together with the combined LEP values.

Figure 5.12 shows the combined data points compared with the cross-section calculated with EEWWG [209] and RACOONWW. The RACOONWW prediction is shown in the figure without any theory error band.

5.7 Summary

This chapter has summarised the final LEP results in terms of four-fermion cross-sections and derived quantities. The WW cross-section has been measured precisely at LEP-II energies. The measurements clearly favour those theoretical predictions which properly include O(α) electroweak corrections, thus showing that the SM can be tested at the loop level at LEP-II.

In general the results are in good agreement with the SM predictions, both in the charged current and in the neutral current sector. A small anomaly in the W decay branching fractions, favouring W decays into $\tau\nu_\tau$ compared to the other lepton families, is observed in the data. This excess is above two standard deviations in the measured branching fractions into both $e\nu_e$ and $\mu\nu_\mu$.

$\sqrt{s}$ (GeV)	WWγ cross-section (pb)			
	DELPHI	L3	OPAL	LEP
188.6	0.05 ± 0.08	0.20 ± 0.09	0.16 ± 0.04	0.15 ± 0.03
194.4	0.17 ± 0.12	0.17 ± 0.10	0.17 ± 0.06	0.17 ± 0.05
200.2	0.34 ± 0.12	0.43 ± 0.13	0.21 ± 0.06	0.27 ± 0.05
206.1	0.18 ± 0.08	0.13 ± 0.08	0.30 ± 0.05	0.24 ± 0.04

Table 5.16: WWγ production cross-section from the LEP experiments and combined values for the four energy bins.

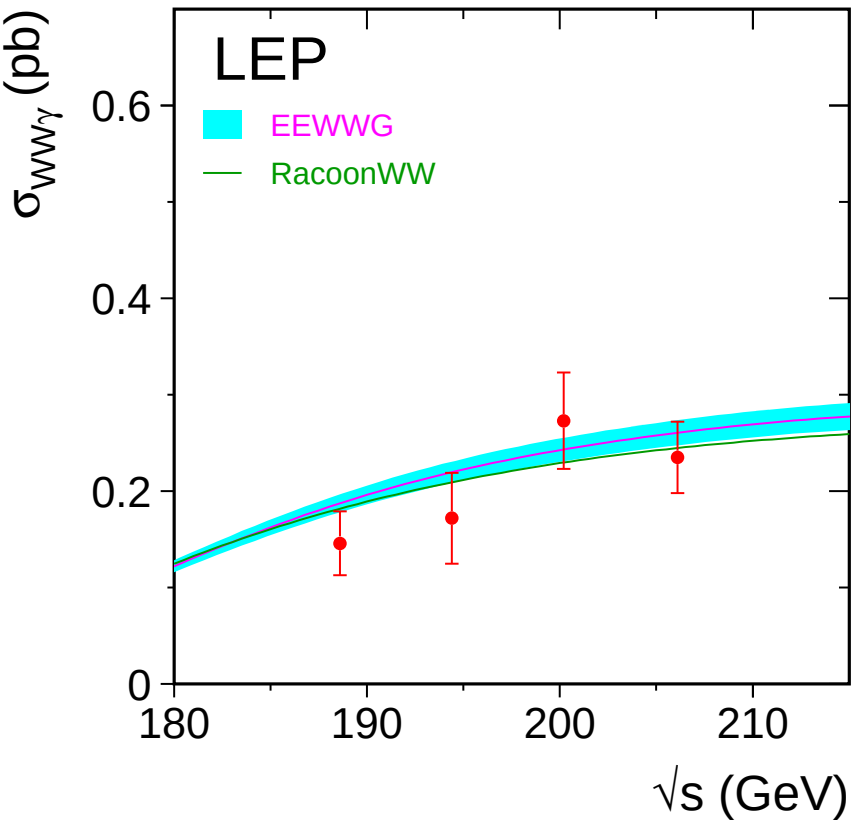


Figure 5.12: Measurements of the WWγ production cross-section, compared to the predictions of EEWWG [209] and RACOONWW [168]. The shaded area in the EEWWG curve represents the $\pm 5\%$ uncertainty on the predictions.

Chapter 6

Electroweak Gauge Boson Self Couplings

6.1 Introduction

The measurement of gauge boson couplings and the search for possible anomalous contributions due to the effects of new physics beyond the Standard Model (SM) are among the principal physics aims at LEP-II [210]. Combined results on triple gauge boson couplings are presented here.

The W-pair production process, $e^+e^- \to W^+W^-$, involves the charged triple gauge boson vertices between the W^+W^- and the Z or photon shown in Figure 1.4. During LEP-II operation, about 10,000 W-pair events were collected by each experiment. Single W ($e\nu W$) and single photon ($\nu\bar{\nu}\gamma$) production at LEP are also sensitive to the $WW\gamma$ vertex, see Figure 1.7. Results from these channels are also included in the combination for some experiments; the individual references should be consulted for details. The Monte-Carlo calculations, RacoonWW [168] and YFSWW [161, 167], incorporate an improved treatment of $O(\alpha_{em})$ corrections to WW production. The corrections affect the measurements of the charged TGCs in W-pair production. Results including these $O(\alpha_{em})$ corrections have been submitted from all four LEP collaborations ALEPH [211], DELPHI [212], L3 [213] and OPAL [214].

At centre-of-mass energies exceeding twice the Z boson mass, pair production of Z bosons is kinematically allowed. Here, one searches for the possible existence of triple vertices involving only neutral electroweak gauge bosons. Such vertices could also contribute to $Z\gamma$ production. In contrast to triple gauge boson vertices with two charged gauge bosons, purely neutral gauge boson vertices do not occur at tree level in the SM of electroweak interactions.

The expected total and differential cross-sections of these processes depend on the values of the triple gauge couplings, allowing their measurements by comparing Monte-Carlo simulations to the data. In contrast to the analysis of electroweak gauge boson self-couplings performed at hadron colliders, no form-factor term scaling the bare couplings is applied in the analysis of the LEP data.

6.1.1 Charged Triple Gauge Boson Couplings

The parametrisation of the charged triple gauge boson vertices is described in References [210, 215, 216, 217]. The most general Lorentz invariant Lagrangian which describes the triple gauge boson interaction has fourteen independent complex couplings, seven describing the $WW\gamma$

vertex and seven describing the WWZ vertex. Assuming electromagnetic gauge invariance as well as C and P conservation, the number of independent TGCs reduces to five. A common set is $\{g_1^{\rm Z}, \kappa_\gamma, \kappa_{\rm Z}, \lambda_\gamma, \lambda_{\rm Z}\}$, with SM values of $g_1^{\rm Z} = \kappa_\gamma = \kappa_{\rm Z} = 1$ and $\lambda_\gamma = \lambda_{\rm Z} = 0$. The parameters proposed in [210] and used by the LEP experiments are $g_1^{\rm Z}$, κ_γ and λ_γ with the gauge constraints:

$$\kappa_{\rm Z} = g_1^{\rm Z} - (\kappa_\gamma - 1)\tan^2\theta_{\rm W}\,, \tag{6.1}$$

$$\lambda_{\rm Z} = \lambda_\gamma\,, \tag{6.2}$$

where θ_W is the weak mixing angle. In an effective Lagrangian approach, all three of the remaining independent couplings, $g_1^{\rm Z}$, κ_γ and λ_γ, receive contributions from operators of dimension six or greater. The couplings are considered as real, with the imaginary parts fixed to zero. Note that the measured coupling values themselves and not their deviation from the SM values are quoted. LEP combinations are made in single-parameter fits, in each case setting the other TGCs to their SM value.

The coupling $g_1^{\rm Z}$ describes the overall strength of the WWZ coupling. The photonic couplings κ_γ and λ_γ are related to the magnetic and electric properties of the W boson. One can write the lowest order terms for a multipole expansion describing the W-γ interaction as a function of κ_γ and λ_γ. For the magnetic dipole moment, μ_W, and the electric quadrupole moment, q_W, one obtains:

$$\mu_W = \frac{e}{2m_W}\left(1 + \kappa_\gamma + \lambda_\gamma\right)\,, \tag{6.3}$$

$$q_W = -\frac{e}{m_W^2}\left(\kappa_\gamma - \lambda_\gamma\right)\,. \tag{6.4}$$

The inclusion of $O(\alpha_{em})$ corrections in the Monte-Carlo calculations has a considerable effect on the charged TGC measurement. Both the total cross-section and the differential distributions are affected. The cross-section is reduced by $1-2\%$ depending on the energy. For the differential distributions, the effects are naturally more complex. The polar $\rm W^-$ production angle carries most of the information on the TGC parameters; its shape is modified to be more forwardly peaked. In a fit to data, the $O(\alpha_{em})$ effect manifests itself as a negative shift of the obtained TGC values with a magnitude of typically -0.015 for λ_γ and $g_1^{\rm Z}$ and -0.04 for κ_γ.

6.1.2 Neutral Triple Gauge Boson Couplings

There are two classes of Lorentz invariant structures associated with neutral TGC vertices which preserve $U(1)_{em}$ and Bose symmetry, as described in [216, 224].

The first class refers to anomalous $\rm Z\gamma\gamma^*$ and $\rm Z\gamma Z^*$ couplings which are accessible at LEP in the process $\rm e^+e^- \to Z\gamma$. The parametrisation contains eight couplings: h_i^V with $i = 1, ..., 4$ and $V = \gamma$,Z. The superscript $V = \gamma$ refers to $\rm Z\gamma\gamma^*$ couplings and superscript $V =$Z refers to $\rm Z\gamma Z^*$ couplings. The photon and the Z boson in the final state are considered as on-shell particles, while the third boson at the vertex, the s-channel internal propagator, is off shell. The couplings h_1^V and h_2^V are CP-odd while h_3^V and h_4^V are CP-even.

The second class refers to anomalous $\rm ZZ\gamma^*$ and $\rm ZZZ^*$ couplings which are accessible at LEP-II in the process $\rm e^+e^- \to ZZ$. This anomalous vertex is parametrised in terms of four couplings: f_i^V with $i = 4, 5$ and $V = \gamma$,Z. The superscript $V = \gamma$ refers to $\rm ZZ\gamma^*$ couplings and

the superscript $V = \mathrm{Z}$ refers to ZZZ^* couplings. Both Z bosons in the final state are assumed to be on-shell, while the third boson at the triple vertex, the s-channel internal propagator, is off-shell. The couplings f_4^V are CP-odd whereas f_5^V are CP-even.

In an effective Lagrangian approach, the couplings h_1^V, h_3^V, f_4^V, f_5^V receive contributions from operators of dimension six or greater, while the lowest-dimension operators contributing to h_2^V and h_4^V have dimension eight. Note that the h_i^V and the f_i^V couplings are independent of each other. They are assumed to be real and they vanish at tree level in the SM. Results on neutral gauge boson couplings are reported for single- and two-parameter fits.

6.2 Combination Procedure

The combination is based on the individual likelihood functions from the four LEP experiments. Each experiment provides the negative log likelihood, $\log \mathcal{L}$, as a function of the coupling parameters to be combined. The single-parameter analyses are performed fixing all other parameters to their SM values. For the charged TGCs, the gauge constraints listed in Section 6.1.1 are always enforced. Either the $\log \mathcal{L}$ curves were available in numerical form or they have been treated as parabolic according to the respective publication. Details of the individual measurements entering the combination are summarized below.

The $\log \mathcal{L}$ functions from each experiment include statistical as well as those systematic uncertainties which are considered as uncorrelated between experiments. In all combinations, the individual $\log \mathcal{L}$ functions are combined. It is necessary to use the $\log \mathcal{L}$ functions directly in the combination, since in some cases they are not parabolic, and hence it is not possible to properly combine the results by simply taking weighted averages of the measurements.

The main contributions to the systematic uncertainties that are uncorrelated between experiments arise from detector effects, background in the selected signal samples, limited Monte-Carlo statistics and the fitting method. Their importance varies for each experiment and the individual references should be consulted for details.

In the neutral TGC sector, the main correlated systematic uncertainties arise from the theoretical cross-section prediction in ZZ and Zγ-production, about 2% for ZZ and about 1% (2%) in the $\mathrm{q\overline{q}}\gamma$ ($\nu\bar{\nu}\gamma$) channel. The effect of a correlated treatment has been estimated in earlier measurements to be negligible. Hence this and all other correlated sources of systematic errors, such as those arising from the LEP beam energy, are for simplicity treated as uncorrelated. The combination is performed by adding the $\log \mathcal{L}$ curves of the individual experiments.

In the charged TGC sector, systematic uncertainties considered correlated between the experiments are summarised in Table 6.1: the theoretical cross-section prediction, σ, which is 0.5% for W-pair production and 5% for single W production, hadronisation effects (HAD), the final state interactions, namely Bose-Einstein correlations (BEC) and colour reconnection (CR), and the uncertainty in the radiative corrections themselves (LPA). The latter was the dominant systematic error in previous combinations, where we used a conservative estimate, namely the full effect from applying the $O(\alpha_{em})$ corrections. Analyses on the subject are available from several LEP experiments, based on comparisons of fully simulated events using two different leading-pole approximation schemes (LPA-A and LPA-B, [225] and references therein). In addition, the availability of comparisons of the generators incorporating $O(\alpha_{em})$ corrections, RacoonWW and YFSWW [168, 161, 167], makes it possible to perform a more realistic estimation of this effect and its uncertainty. In general, the TGC shift measured in the comparison of the two generators is found to be larger than the effect from the different LPA schemes. This improved estimation, while still being conservative, reduces the systematic

Source	g_1^Z	κ_γ	λ_γ
σ_{WW} prediction	0.003	0.018	0.002
σ_W prediction	-	0.003	0.001
Hadronisation	0.003	0.005	0.004
Bose-Einstein Correlation	0.002	0.003	0.002
Colour Reconnection	0.003	0.005	0.002
$O(\alpha_{em})$ correction	0.002	0.014	0.002

Table 6.1: The systematic uncertainties considered correlated between the LEP experiments in the charged TGC combination and their effect on the combined fit results for the charged TGC parameters.

uncertainty from $O(\alpha_{em})$ corrections by about a third for g_1^Z and λ_γ and roughly halves it for κ_γ, compared to the full $O(\alpha_{em})$ correction. The application of this reduced systematic error renders the charged TGC measurements statistics dominated. In case of the charged TGCs, the systematic uncertainties considered correlated between the experiments amount to 32% of the combined statistical and uncorrelated uncertainties for λ_γ and g_1^Z, while for κ_γ they amount to 57%, indicating again that the measurements of λ_γ, g_1^Z and κ_γ are limited by data statistics.

The combination procedure [226] used for the charged TGCs allows the combination of statistical and correlated systematic uncertainties, independently of the analysis method chosen by the individual experiments. The combination uses the likelihood curves and correlated systematic errors submitted by each of the four experiments. The procedure is based on the introduction of an additional free parameter to take into account the systematic uncertainties, which are treated as shifts on the fitted TGC value, and are assumed to have a Gaussian distribution. A simultaneous minimisation of both parameters, TGC and systematic error, is performed.

In detail, the combination proceeds in the following way: the set of measurements from the LEP experiments ALEPH, DELPHI, OPAL and L3 is given with statistical and uncorrelated systematic uncertainties in terms of likelihood curves: $-\log\mathcal{L}^A_{stat}(x)$, $-\log\mathcal{L}^D_{stat}(x)$ $-\log\mathcal{L}^L_{stat}(x)$ and $-\log\mathcal{L}^O_{stat}(x)$, respectively, where x is the coupling parameter in question. Also given are the shifts for each of the five totally correlated sources of uncertainty mentioned above; each source S leads to systematic errors σ^S_A, σ^S_D, σ^S_L and σ^S_O.

Additional parameters Δ^S are included in order to take into account a Gaussian distribution for each of the systematic uncertainties. The procedure then consists in minimising the function:

$$-\log\mathcal{L}_{total} = \sum_{E=A,D,L,O} \log\mathcal{L}^E_{stat}(x - \sum_S(\sigma^S_E\Delta^S)) + \sum_S \frac{(\Delta^S)^2}{2} \tag{6.5}$$

where x and Δ_S are the free parameters, and the sums run over the four experiments E and the correlated systematic errors S discussed above and listed in Table 6.1. The resulting uncertainty on x takes into account all sources of uncertainty, yielding a measurement of the coupling with the error representing statistical and systematic sources. The projection of the minima of

the log-likelihood as a function of x gives the combined log-likelihood curve including statistical and systematic uncertainties. The advantage over the scaling method used previously is that it treats systematic uncertainties that are correlated between the experiments correctly, while not forcing the averaging of these systematic uncertainties into one global LEP systematic uncertainties scaling factor. In other words, the (statistical) precision of each experiment gets reduced by its own correlated systematic errors, instead of an averaged LEP systematic error. The method has been cross-checked against the scaling method, and was found to give comparable results. The inclusion of the systematic uncertainties leads to small differences, as expected by the improved treatment of correlated systematic errors. A similar behaviour is seen in Monte-Carlo comparisons of these two combination methods [227]. Furthermore, it was shown that the minimisation-based combination method used for the charged TGCs agrees with the method based on optimal observables, where systematic effects are included directly in the mean values of the optimal observables (see [227]), for any realistic ratio of statistical to systematic uncertainties. Further details on the combination method can be found in [226].

In the following, single-parameter fits are presented for the TGC parameters g_1^{Z}, κ_γ, λ_γ, h_i^V and f_i^V, while results from two-parameter fits are also given for $(f_4^\gamma, f_4^{\mathrm{Z}})$ and $(f_5^\gamma, f_5^{\mathrm{Z}})$. For results quoted in numerical form, the one standard deviation uncertainties (68% confidence level) are obtained by taking the coupling values for which $\Delta \log \mathcal{L} = +0.5$ above the minimum. The 95% confidence level (C.L.) limits are given by the coupling values for which $\Delta \log \mathcal{L} = +1.92$ above the minimum. For multi-parameter analyses, the two dimensional 68% C.L. contour curves for any pair of couplings are obtained by requiring $\Delta \log \mathcal{L} = +1.15$, while for the 95% C.L. contour curves $\Delta \log \mathcal{L} = +3.0$ is required. Since the results on the different parameters and parameter sets are obtained from the same data sets, they cannot themselves be combined when looking at models establishing additional relations between these couplings.

6.3 Measurements

The combined results presented here are obtained from charged and neutral electroweak gauge boson coupling measurements as discussed above. The individual references should be consulted for details about the data samples used.

The charged TGC analyses of ALEPH, DELPHI, L3 and OPAL use data collected at LEP-II with centre-of-mass energies up to 209 GeV. These analyses use different channels, typically the semileptonic and fully hadronic W-pair decays [211, 212, 228, 229, 230, 213, 214]. The full data set is analysed by all four experiments. Anomalous TGCs affect both the total production cross-section and the shape of the differential cross-section as a function of the polar W^- production angle. The relative contributions of each helicity state of the W bosons are also changed, which in turn affects the distributions of their decay products. The analyses presented by each experiment make use of different combinations of each of these quantities. In general, however, all analyses use at least the expected variations of the total production cross-section and the W^- production angle. Results from $e\nu\mathrm{W}$ and $\nu\bar{\nu}\gamma$ production are included by some experiments. Single-W production is particularly sensitive to κ_γ, thus providing information complementary to that from W-pair production.

The h-coupling analyses of ALEPH, DELPHI and L3 use data collected at LEP-II with centre-of-mass energies of up to 209 GeV. The OPAL measurements use the data at 189 GeV only. The results of the f-couplings are obtained from the whole data set above the ZZ-production threshold by all experiments. The experiments already pre-combine different processes and final states for each of the couplings. All analyses use measurements of the total

cross-sections of Zγ and ZZ production and the differential distributions in the determination of the h_i^V couplings [231, 232, 233, 234] and the f_i^V couplings [231, 232, 235, 236], while DELPHI also includes $Z\gamma^*$ data in the determination of both sets of couplings.

6.4 Results

We present results from the four LEP experiments on the various electroweak gauge boson couplings, and their combination. The results quoted for each individual experiment are calculated using the methods described in Section 6.2. Therefore they may differ slightly from those reported in the individual references, as the experiments in general use other methods to combine the data from different channels and to include systematic uncertainties. In particular for the charged couplings, experiments using a combination method based on optimal observables (ALEPH, OPAL) obtain results with small differences compared to the values given by our combination technique. These small differences have been studied in Monte-Carlo tests and are well understood [227]. For the h-coupling results from OPAL and DELPHI, a slightly modified estimate of the systematic uncertainty due to the theoretical cross-section prediction is responsible for slightly different limits compared to the published results.

6.4.1 Charged Triple Gauge Boson Couplings

The individual analyses and results of the experiments for the charged couplings are described in [211, 212, 228, 229, 230, 214]. The results of single-parameter fits from each experiment are shown in Table 6.2, where the errors include both statistical and systematic effects. The individual $\log \mathcal{L}$ curves and their sum are shown in Figure 6.1. The results of the combination are given in Table 6.3. A list of the systematic errors treated as fully correlated between the LEP experiments, and their shift on the combined fit result were given in Table 6.1. The combined results agree well with the SM expectation.

Parameter	ALEPH	DELPHI	L3	OPAL	SM
g_1^Z	$0.996^{+0.030}_{-0.028}$	$0.975^{+0.035}_{-0.032}$	$0.965^{+0.038}_{-0.037}$	$0.985^{+0.035}_{-0.034}$	1
κ_γ	$0.983^{+0.060}_{-0.060}$	$1.022^{+0.082}_{-0.084}$	$1.020^{+0.075}_{-0.069}$	$0.899^{+0.090}_{-0.084}$	1
λ_γ	$-0.014^{+0.029}_{-0.029}$	$0.001^{+0.036}_{-0.035}$	$-0.023^{+0.042}_{-0.039}$	$-0.061^{+0.037}_{-0.036}$	0

Table 6.2: The measured central values and one standard deviation errors obtained by the four LEP experiments for the charged TGC parameters. In each case the parameter listed is varied while the remaining two are fixed to their SM values (also shown). Both statistical and systematic errors are included. The values given here differ slightly from the ones quoted in the individual contributions from the four LEP experiments, as a different combination method is used. See text in section 6.2 for details.

Parameter	68% C.L.	95% C.L.	SM
g_1^Z	$+0.984^{+0.018}_{-0.020}$	[0.946, 1.021]	1
κ_γ	$+0.982^{+0.042}_{-0.042}$	[0.901, 1.066]	1
λ_γ	$-0.022^{+0.019}_{-0.019}$	[−0.059, 0.017]	0

Table 6.3: The combined results for the 68% C.L. errors and 95% C.L. intervals obtained for the charged TGC parameters from the four LEP experiments. In each case the parameter listed is varied while the other two are fixed to their SM values (also shown). Both statistical and systematic errors are included.

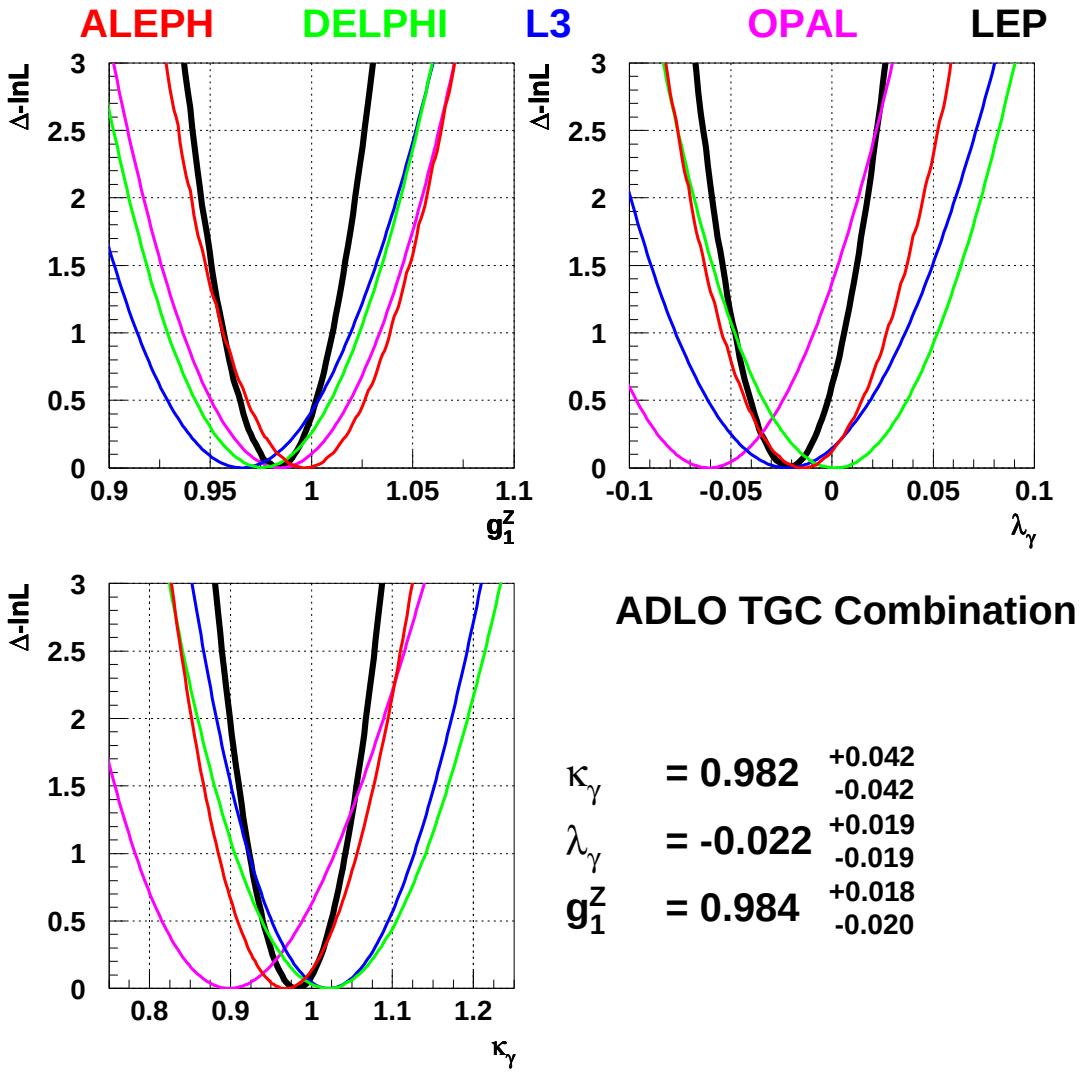


Figure 6.1: The log $\mathcal{L}$ curves of the four experiments (thin lines) and the LEP combined curve (black line) for the three charged TGCs g_1^Z, κ_γ and λ_γ. In each case, the minimal log $\mathcal{L}$ value is subtracted.

6.4.2 Neutral Triple Gauge Boson Couplings

The individual analyses and results of the experiments for the h-couplings are described in [232, 233, 234]. The results from DELPHI, L3 and OPAL, and the LEP combination, are shown in Table 6.4, where the errors include both statistical and systematic uncertainties. The individual $\log \mathcal{L}$ curves and their sum are shown in Figures 6.2 and 6.3. The results agree with the SM expectation.

Parameter	DELPHI	L3	OPAL	LEP
h_1^γ	$[-0.14,\ 0.14]$	$[-0.06,\ 0.06]$	$[-0.11,\ 0.11]$	$[-0.05,\ 0.05]$
h_2^γ		$[-0.05,\ 0.02]$	$[-0.08,\ 0.08]$	$[-0.04,\ 0.02]$
h_3^γ	$[-0.05,\ 0.04]$	$[-0.06,\ 0.00]$	$[-0.16,\ -0.01]$	$[-0.05,\ -0.00]$
h_4^γ		$[-0.00,\ 0.04]$	$[0.01,\ 0.13]$	$[0.01,\ 0.05]$
h_1^Z	$[-0.23,\ 0.23]$	$[-0.15,\ 0.14]$	$[-0.19,\ 0.19]$	$[-0.12,\ 0.11]$
h_2^Z		$[-0.09,\ 0.08]$	$[-0.13,\ 0.13]$	$[-0.07,\ 0.07]$
h_3^Z	$[-0.30,\ 0.16]$	$[-0.22,\ 0.11]$	$[-0.27,\ 0.12]$	$[-0.19,\ 0.06]$
h_4^Z		$[-0.07,\ 0.15]$	$[-0.08,\ 0.17]$	$[-0.04,\ 0.13]$

Table 6.4: The 95% C.L. intervals ($\Delta \log \mathcal{L} = 1.92$) in the neutral TGC parameters h_i^V measured by the DELPHI, L3 and OPAL, and the LEP combined values. In each case the parameter listed is varied while the remaining ones are fixed to their SM values ($h_i^V = 0$). Both statistical and systematic uncertainties are included. DELPHI did not interpret its measurements in terms of neutral gauge couplings of dimension 8 operators, hence does not enter in the combination for $h_{2/4}^V$.

The individual analyses and results of the experiments for the f-couplings are described in [231, 232, 235, 236]. The single-parameter results for each experiment and the LEP combination are shown in Table 6.5, where the errors include both statistical and systematic uncertainties. The individual $\log \mathcal{L}$ curves and their sum are shown in Figure 6.4. Three experiments, ALEPH, L3 and OPAL, contributed data to two-parameter fits to the TGC pairs (f_4^γ, f_4^Z) and (f_5^γ, f_5^Z). The two-parameter results including the LEP combination are shown in Table 6.6, where the errors include both statistical and systematic uncertainties. The 68% C.L. and 95% C.L. contour curves resulting from the combinations of the two-dimensional likelihood curves are shown in Figures 6.5 and 6.6. The couplings agree with the SM expectation.

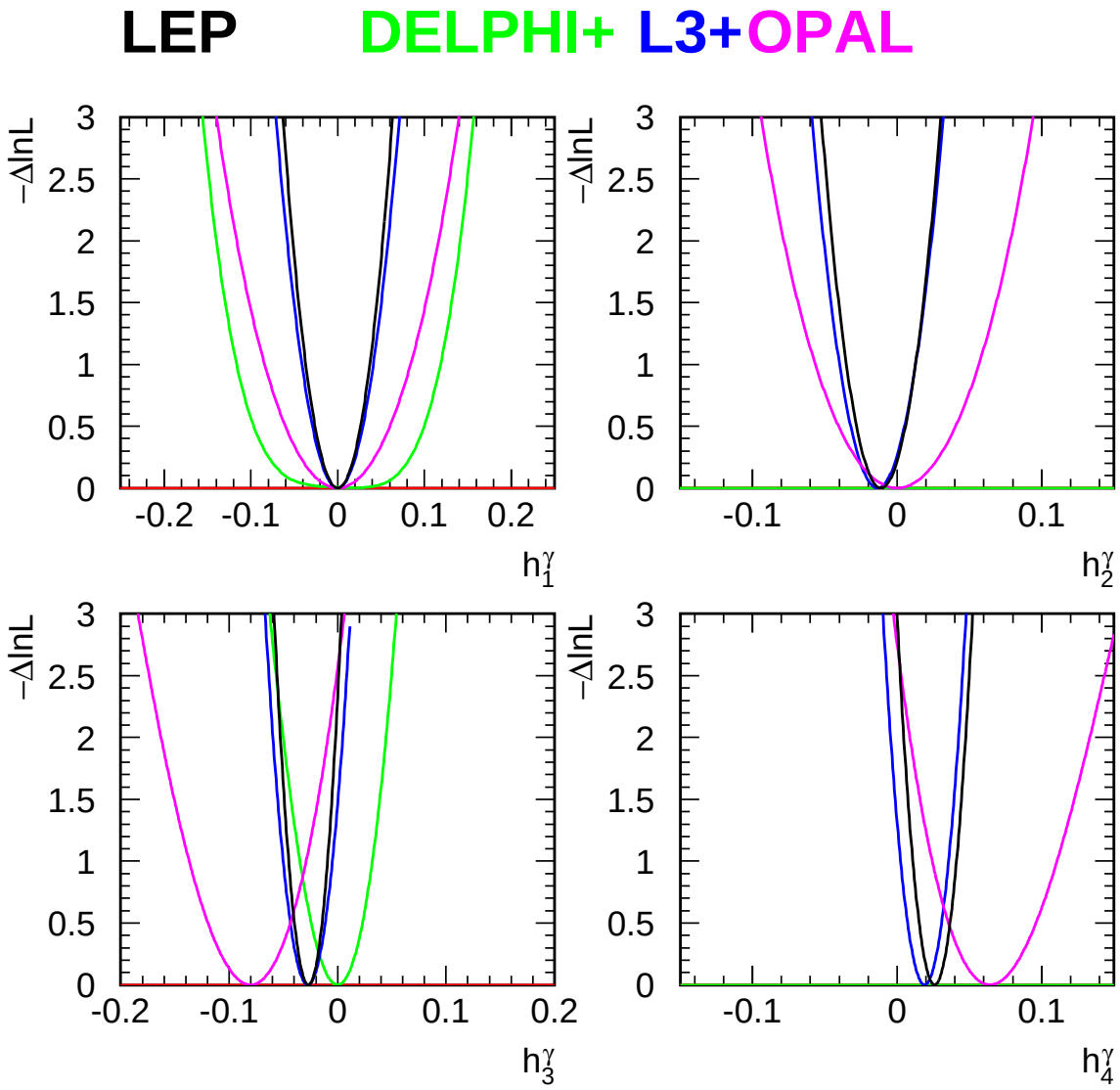


Figure 6.2: The $\log \mathcal{L}$ curves of DELPHI, L3, and OPAL experiments and the LEP combined curve for the four neutral TGCs h_i^γ, $i = 1, 2, 3, 4$. In each case, the minimal value is subtracted. Note, DELPHI did not interpret its measurements in terms of neutral gauge couplings of dimension 8 operators, hence does not enter in the combination for $h_{2/4}^V$.

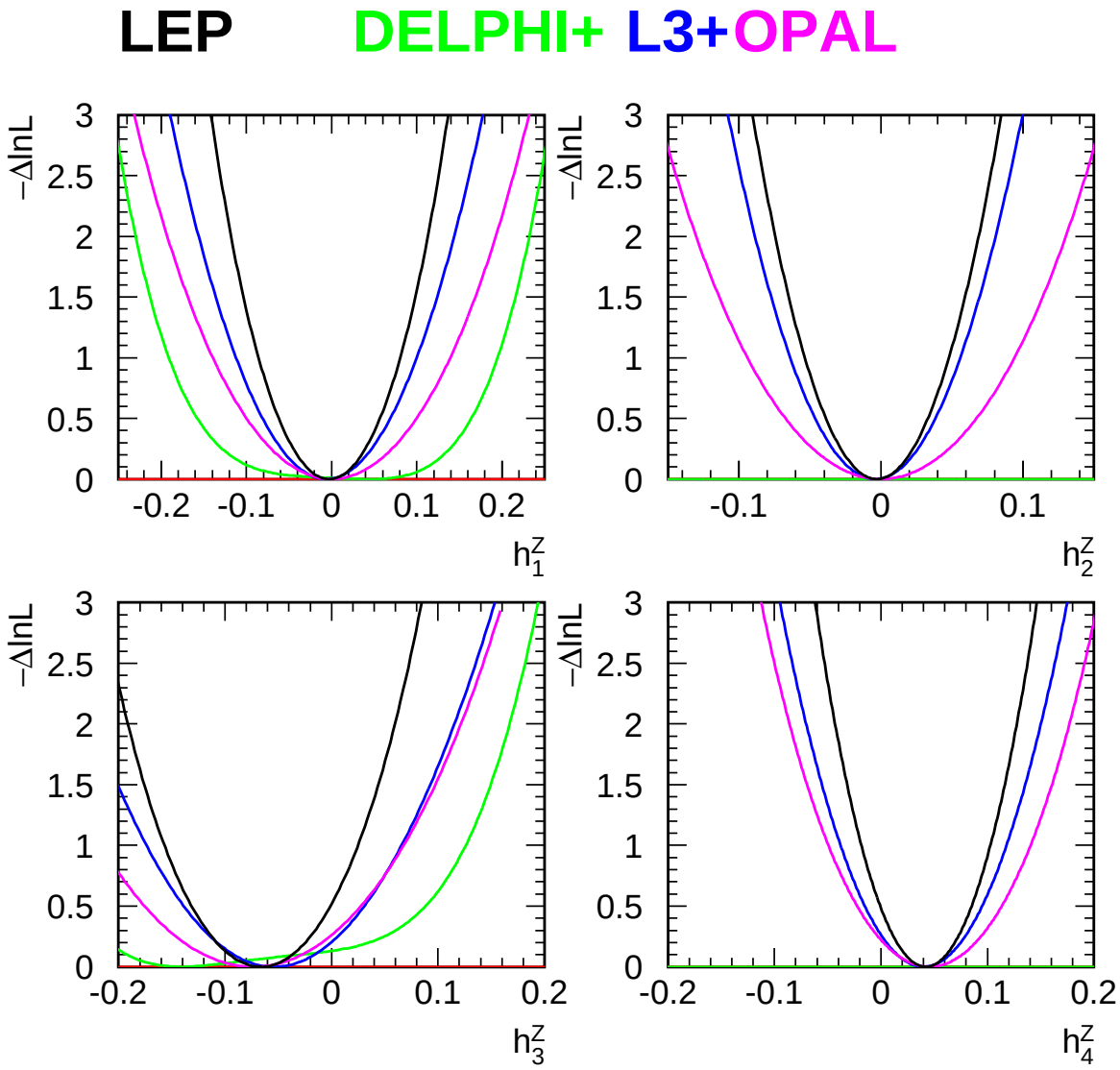


Figure 6.3: The $\log \mathcal{L}$ curves of the DELPHI, L3, OPAL experiments and the LEP combined curve for the four neutral TGCs h_i^Z, $i = 1, 2, 3, 4$. In each case, the minimal value is subtracted. Note, DELPHI did not interpret its measurements in terms of neutral gauge couplings of dimension 8 operators, hence does not enter in the combination for $h_{2/4}^V$.

Parameter	ALEPH	DELPHI	L3	OPAL	LEP
f_4^γ	$[-0.32,\ 0.33]$	$[-0.23,\ 0.25]$	$[-0.28,\ 0.28]$	$[-0.32,\ 0.33]$	$[-0.17,\ 0.19]$
f_4^Z	$[-0.53,\ 0.54]$	$[-0.40,\ 0.42]$	$[-0.48,\ 0.46]$	$[-0.45,\ 0.58]$	$[-0.28,\ 0.32]$
f_5^γ	$[-0.73,\ 0.74]$	$[-0.52,\ 0.48]$	$[-0.39,\ 0.47]$	$[-0.71,\ 0.59]$	$[-0.35,\ 0.32]$
f_5^Z	$[-1.18,\ 1.19]$	$[-0.38,\ 0.62]$	$[-0.35,\ 1.03]$	$[-0.94,\ 0.25]$	$[-0.34,\ 0.35]$

Table 6.5: The 95% C.L. intervals ($\Delta \log \mathcal{L} = 1.92$) in the neutral TGC parameters f_i^V measured by ALEPH, DELPHI, L3 and OPAL, and the LEP combined values. In each case the parameter listed is varied while the remaining ones are fixed to their SM values ($f_i^V = 0$). Both statistical and systematic uncertainties are included.

Parameter	ALEPH	L3	OPAL	LEP	Correlations	
f_4^γ	$[-0.29,\ 0.25]$	$[-0.28,\ 0.28]$	$[-0.32,\ 0.33]$	$[-0.20,\ 0.18]$	1.00	-0.33
f_4^Z	$[-0.43,\ 0.44]$	$[-0.48,\ 0.46]$	$[-0.47,\ 0.58]$	$[-0.29,\ 0.32]$	-0.33	1.00
f_5^γ	$[-0.59,\ 0.57]$	$[-0.53,\ 0.62]$	$[-0.67,\ 0.62]$	$[-0.40,\ 0.38]$	1.00	-0.20
f_5^Z	$[-0.90,\ 0.78]$	$[-0.47,\ 1.39]$	$[-0.95,\ 0.33]$	$[-0.56,\ 0.36]$	-0.20	1.00

Table 6.6: The 95% C.L. intervals ($\Delta \log \mathcal{L} = 1.92$) in the neutral TGC parameters f_i^V in two-parameter fits measured by ALEPH, L3 and OPAL, and the LEP combined values. In each case the two parameters listed are varied while the remaining ones are fixed to their SM values ($f_i^V = 0$). Both statistical and systematic uncertainties are included. Since the shape of the log-likelihood is not parabolic, there is some ambiguity in the definition of the correlation coefficients and the values quoted here are approximate.

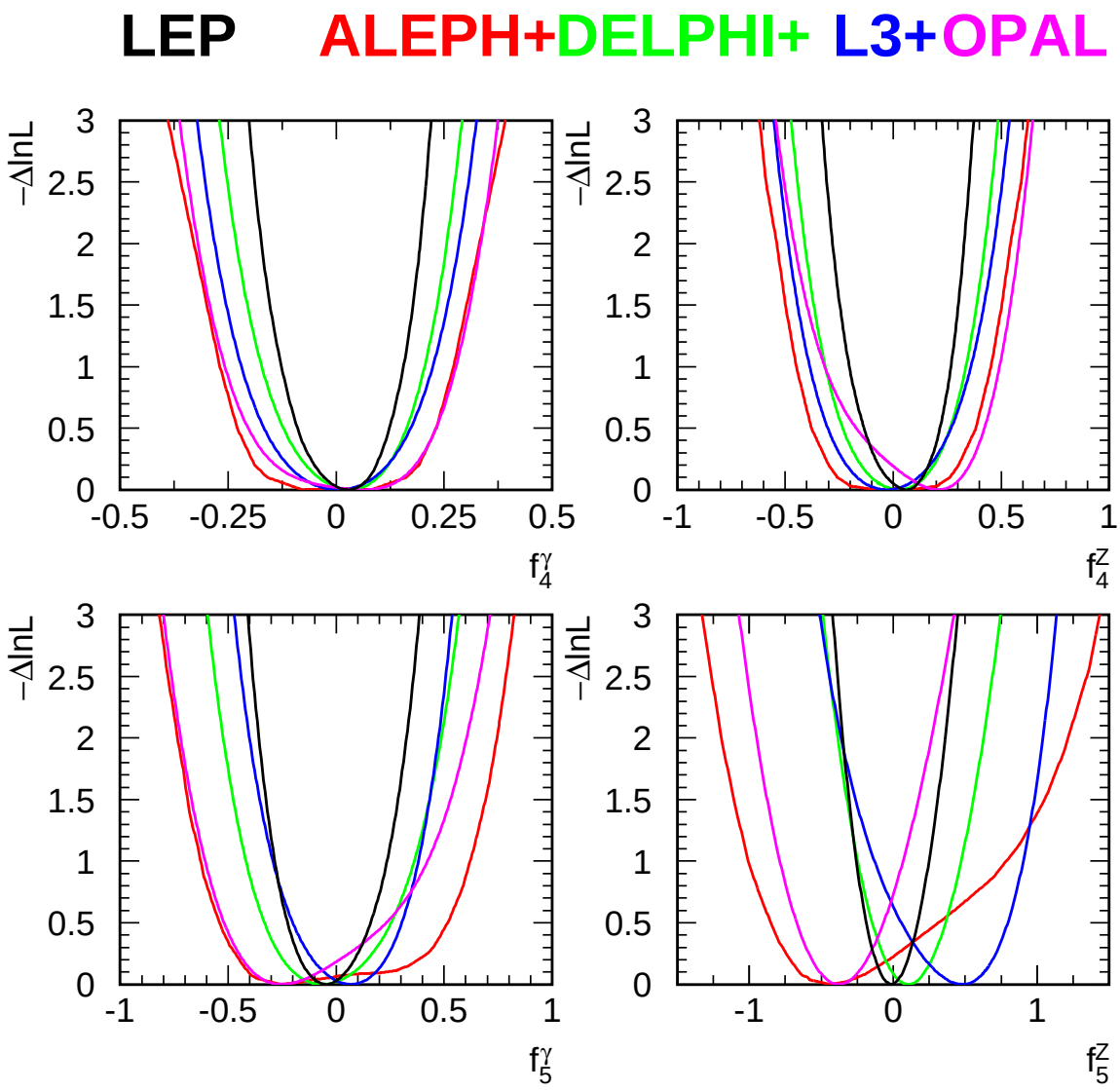


Figure 6.4: The $\log \mathcal{L}$ curves of the four experiments, and the LEP combined curve for the four neutral TGCs f_i^V, $V = \gamma, Z$, $i = 4, 5$. In each case, the minimal value is subtracted.

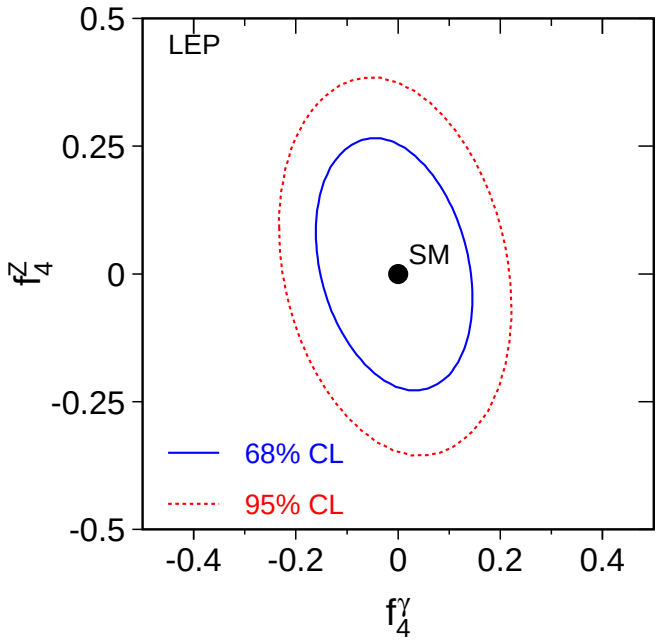


Figure 6.5: Contour curves of 68% C.L. and 95% C.L. in the plane of the neutral TGC parameters (f_4^γ, f_4^Z) showing the LEP combined result to which ALEPH, L3 and OPAL contributed.

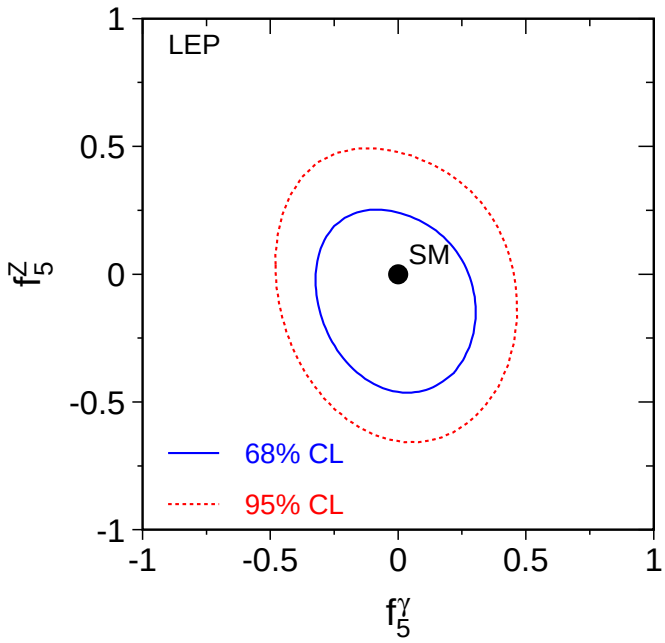


Figure 6.6: Contour curves of 68% C.L. and 95% C.L. in the plane of the neutral TGC parameters (f_5^γ, f_5^Z) showing the LEP combined result to which ALEPH, L3 and OPAL contributed.

6.5 Summary and Conclusions

Combinations of charged and neutral triple gauge boson couplings were made, based on results from the four LEP experiments ALEPH, DELPHI, L3 and OPAL. No deviation from the SM prediction is seen for any of the electroweak gauge boson couplings studied. While the existence of charged TGCs was experimentally verified already early on by the measurement of the total WW cross-section, see also Chapter 5, their values have now been measured with an accuracy of 0.02 to 0.04, and found to be in agreement with the SM expectation. As an example, these data allow the Kaluza-Klein theory [237], in which $\kappa_\gamma = -2$, to be excluded [238]. No evidence of the existence of neutral TGCs are found, limiting their magnitude to less than 0.05 to 0.35 depending on coupling.

Chapter 7

Mass and Width of the W Boson

7.1 Introduction

The mass of the W boson is a fundamental parameter in particle physics. Together with the Z-boson mass, it sets the energy scale of electroweak symmetry breaking. Both masses are closely related to the weak mixing angle. At LEP, the W-boson mass is determined by measuring the cross-section of W-boson pairs at the production threshold, from the leptonic decay spectrum of the W boson, and by directly reconstructing W boson decays. The latter method is the more precise one. It also allows a determination of the total decay width of the W boson. Direct measurements of W-boson mass and width are also performed at the Tevatron $\mathrm{p\bar{p}}$ collider [239, 240, 241, 242].

7.2 Determination of the W Mass at the W-Pair Production Threshold

The SM cross-section of the reaction $\mathrm{e^+e^-} \rightarrow \mathrm{W^+W^-}$ shows a typical threshold behaviour close to a centre-of-mass energy that corresponds to twice the W mass. In the threshold region the cross-section rises in proportion to the velocity of the W bosons produced, which is approximately given by $\beta = \sqrt{1 - 4m_{\mathrm{W}}^2/s}$, neglecting radiative corrections and finite width effects. Thus, a measurement of the production cross-section at a given centre-of-mass energy is directly related to the W boson mass. The intrinsic precision of this method is similar to the direct-reconstruction method, described below. However, since LEP predominantly operated at higher centre-of-mass energies in order to search for new physics as well as to make precise electroweak measurements, the data collected at threshold energies corresponds to only 3% of the full data set (see Table 1.1).

Using Monte-Carlo simulations, the centre-of-mass energy where the cross-section is most sensitive to m_{W} was determined to be $\sqrt{s} = 161$ GeV, but data at 172-183 GeV were also analysed to extract m_{W} from the measured cross-section. Each LEP experiment compared the measured cross-sections at each centre-of-mass energy to the m_{W} dependent SM prediction calculated using the GENTLE program [173]. The results of the four LEP experiments combined for the different centre-of-mass energies [243, 152, 244, 245] are shown in Table 7.1. Owing to the dependence of the theory cross-section on the mass for a given centre-of-mass energy, both the extracted mass and its uncertainty decrease with increasing measured cross-sections.

Systematic uncertainties from hadronisation and fragmentation effects in hadronically de-

Threshold Analysis	
Experiment	m_{W}[GeV]
ALEPH	80.20 ± 0.34
DELPHI	$80.45^{+0.45}_{-0.41}$
L3	$80.78^{+0.48}_{-0.42}$
OPAL	$80.40^{+0.46}_{-0.43}$

Table 7.1: W mass measurements from the $\mathrm{W^+W^-}$ threshold cross-section at $\sqrt{s} = 161 - 183$ GeV [243, 152, 244, 245]. The uncertainties include statistical and systematic contributions.

caying W bosons, radiative corrections, final-state interactions are all negligible compared to the statistical uncertainty of the measurement. Combining all LEP W-pair threshold data yields:

$$m_{\mathrm{W}}(\text{threshold}) = 80.42 \pm 0.20 \pm 0.03(E_{\mathrm{LEP}}) \text{ GeV} , \tag{7.1}$$

where the uncertainty due to the LEP centre-of-mass energy [246] is given separately. The treatment of systematic uncertainties is further detailed below.

7.3 Measurement of Mass and Width by Direct Reconstruction

7.3.1 Mass Reconstruction

The mass and total decay width of the W boson is determined with high precision by reconstructing directly the decay products of the two W bosons, mainly in the fully hadronic, $\mathrm{W^+W^-} \to \mathrm{q\overline{q}q\overline{q}}$, and semi-leptonic, $\mathrm{W^+W^-} \to \mathrm{q\overline{q}}\ell\nu_\ell$, decay channels.

The $\mathrm{W^+W^-} \to \ell\nu_\ell\ell\nu_\ell$ decay also contains information on m_{W} when analysing the leptonic energy spectrum or reconstructing an approximated mass of the decaying W bosons, as performed by the OPAL collaboration [248]. However, the intrinsic statistical precision dominates the total uncertainty and OPAL determines a value of:

$$m_{\mathrm{W}}(\ell\nu_\ell\ell\nu_\ell) = 80.41 \pm 0.41(\text{stat.}) \pm 0.13(\text{syst.}) \text{ GeV} , \tag{7.2}$$

analysing data at centre-of-mass energies between 183 GeV and 209 GeV. It is interesting to compare this result with those from the other decay channels, since systematic uncertainties from hadronic W decays are absent. Within the given precision it agrees well with the W mass measurements in $\mathrm{W^+W^-} \to \mathrm{q\overline{q}q\overline{q}}$ and $\mathrm{W^+W^-} \to \mathrm{q\overline{q}}\ell\nu_\ell$ events discussed below. For the purpose of the LEP combination, OPAL combines the measurements in the fully leptonic channel at each run period with the semi-leptonic results.

The $\mathrm{W^+W^-} \to \mathrm{q\overline{q}q\overline{q}}$ decays are reconstructed from hadronic jets observed in the final state, formed from measured particle tracks and energy depositions in the calorimeters. Different jet

clustering algorithms are applied, *e.g.*, the Durham [130], Diclus [249], and Cambridge [250] algorithms. Depending on the choice of clustering parameters, additional gluon radiation may be resolved, so that not only pairs of jets, but also five-jet topologies are reconstructed. Similarly, initial-state photon radiation (ISR) and final-state photon radiation (FSR) may be detected by a calorimetric cluster consistent with an electromagnetic shower shape and without a matched track in a given angular cone around the photon candidate. Such reconstruction methods improve the detailed knowledge of the event kinematics and therefore the resolution in the reconstructed masses of the decaying W bosons. The correct reconstruction of the fully hadronic final state is further complicated by combinatorial ambiguities to pair the reconstructed jets to the W decays. In case of four jets there are three possible combinations. For five-jet topologies this number increases to 15. The ambiguity is treated differently by the four LEP experiments. ALEPH selects only one combination in their analyses, using a pairing probability that is based on the CC03 matrix element evaluated for the reconstructed jets [151]. The other experiments use a W-mass estimator which combines all pairings that have a high probability to be correct [152, 153, 154]. The pairings are weighted accordingly in the combined mass likelihood. In this way, a maximum of information is retained for the subsequent mass extraction method. For DELPHI, the weights are based on the polar angle of the reconstructed W boson, the sum of jet charges of each jet combination and the transverse momentum of the gluon jet in five-jet events [152]. L3 exploits the probability of a kinematic fit [153], while OPAL uses a neural network trained with the above-mentioned variables and the reconstructed mass differences of the W bosons [154]. The fully hadronic data samples are furthermore separated into 4-jet and 5-jet sub-samples (L3), or all possible jet configurations, also with different clustering schemes, and properly weighted in the final m_{W} and Γ_{W} analysis.

Semi-leptonic W-pair decays, $\mathrm{W^+W^-} \to \mathrm{q\overline{q}e\nu_e}$, $\mathrm{W^+W^-} \to \mathrm{q\overline{q}}\mu\nu_\mu$ and $\mathrm{W^+W^-} \to \mathrm{q\overline{q}}\tau\nu_\tau$, are reconstructed as a pair of hadronic jets, possibly with a third jet from gluon radiation, and an isolated electron, muon or tau lepton. Photons from initial state radiation are detected in about 5% of the events and excluded from the jet clustering. The mass of the hadronically decaying W is determined directly from the jet system. In the leptonic $\mathrm{W} \to \mathrm{e}\nu_\mathrm{e}$ and $\mathrm{W} \to \mu\nu_\mu$ decays, the missing momentum vector is calculated applying total momentum conservation and is assigned to the momentum of the neutrino. The masses of both W decays can thus be reconstructed. In case of the $\mathrm{q\overline{q}}\tau\nu_\tau$ final state, only the hadronically decaying W contains useable W-mass information due to the presence of a second neutrino from the tau decay.

7.3.2 Kinematic Fitting

The di-jet mass resolution is mainly determined by the precision of jet energy measurements. The jet energy is carried by charged particles ($\sim$ 62% on average), photons ($\sim$ 27%) and neutral hadrons ($\sim$ 10%), which are measured using the tracking and calorimetric devices of the detectors. Even with the help of sophisticated energy-flow algorithms which combine tracks and calorimetric clusters in order to reduce effects of double counting of particles, the best jet energy resolutions achieved are typically $\Delta E/E \approx 60 - 80\%/\sqrt{E/\mathrm{GeV}}$. The corresponding di-jet mass resolution for W-boson decays is in the order of $8 - 9$ GeV.

The mass resolution is substantially improved by imposing the constraint that the total energy in the event should equal the known LEP centre-of-mass energy [246], or that the energy of each W boson should be equal to the LEP beam energy. In practice, this is most commonly implemented by means of a kinematic fit. In such a fit, the measured parameters of the jets and leptons are adjusted, taking account of their measurement uncertainties in such a

way as to satisfy the constraints of energy and momentum conservation. In case of hadronic jets, the jet three-momenta are varied while keeping the jet velocity constant, as systematic effects cancel in the ratio of jet momentum and jet energy. For leptons, the energy for electrons and momentum for muons, together with the polar and azimuthal angles, are considered in the fit. The lepton masses are set to their nominal values. For $q\overline{q}\tau\nu_\tau$ final states, an energy rescaling of the hadronic system to the beam energy is practically equivalent to a kinematic fit, due to the lack of further kinematic constraints.

In the $q\overline{q}q\overline{q}$ case, the improved kinematic reconstruction is referred to as a 4C fit, because there are four energy and momentum constraints. In the $q\overline{q}e\nu$ and $q\overline{q}\mu\nu_\mu$ channels it is referred to as a 1C or one constraint fit, because the three momentum components of the neutrino have to be determined, eliminating three of the constraints. It is often useful to impose the additional constraint that the masses of the two W bosons are equal, leading to a 5C or 2C fit, in which case the kinematic fit provides a single estimate of the average W mass in each event. Although the equal-mass assumption is not fulfilled in an individual event, it is valid on average. Since the intrinsic total width of the W is much smaller than the mass resolution, the equal-mass assumption further improves the mass resolution. The corresponding probabilities of fits in terms of a χ^2 variable are used to reject background and to resolve combinatorial ambiguities in the $q\overline{q}q\overline{q}$ channel.

The resolution on the W-boson mass varies slightly from experiment to experiment. Typical values[1], after use of kinematic fitting, are 2.5 GeV for the $W^+W^- \to q\overline{q}e\nu_e$ and $W^+W^- \to q\overline{q}\mu\nu_\mu$ channels, 3.1 GeV for the $W^+W^- \to q\overline{q}\tau\nu_\tau$ channel and 1.5 GeV for the $W^+W^- \to q\overline{q}q\overline{q}$ channel, at $\sqrt{s} = 189$ GeV. These resolutions increase to 2.9 GeV, 3.4 GeV and 1.7 GeV, respectively, at $\sqrt{s} = 207$ GeV.

The use of a kinematic fit or an equivalent kinematic constraint implies that the scale of the W mass measurement is directly linked to the knowledge of the LEP beam energy. Checks on the determination of the LEP energy are discussed in Appendix C. It should also be emphasised that the kinematic fit technique neglects the effects of initial-state radiation (ISR) if it is not measured directly in the detector. The average energy radiated in ISR in $e^+e^- \to W^+W^-$ events is 2.2 GeV at $\sqrt{s} = 189$ GeV, rising to ~ 3.5 GeV at $\sqrt{s} = 207$ GeV, which is substantially smaller than the intrinsic resolution of the jet energies and hence of the W mass, and therefore cannot be resolved by kinematic fitting. Any remaining bias due to unmeasured ISR photons is taken into account in the W mass and width extraction methods based on MC simulations of radiative effects.

7.3.3 Techniques for Determining the W-Boson Mass and Width

In the direct reconstruction method, the mass of the W boson is obtained by comparing data to simulated $e^+e^- \to W^+W^-$ event samples generated with known values of m_W and Γ_W, in order to obtain those which describe the data best. These Monte-Carlo samples are of large statistics, typically 10^6 events. Since the generation of event samples for all possible parameter values is very computing time intensive, different methods are used to perform the m_W and Γ_W extraction in a more efficient, but still precise way.

[1]The resolutions quoted here are estimated from the distributions of the difference between the fitted W mass and the average of the two true W masses in each event. These resolution functions are not Gaussian, and the values quoted represent RMS values computed in a range ± 10 GeV around zero. In order to estimate the intrinsic mass resolution, events with significant ISR are excluded, and Monte-Carlo information is used to identify the correct jet-pairings in the $q\overline{q}q\overline{q}$ channel.

The Monte-Carlo simulation programs used to generate the signal process, KandY [167], RACOONWW [168], and WPHACT [195], include all relevant diagrams leading to the same 4-fermion final state and full $O(\alpha)$ electroweak radiative corrections. Real ISR photons are calculated in $O(\alpha^3)$, and FSR photons to higher order leading-log approximation. The underlying mass and width of the W boson are defined using a relativistic Breit-Wigner propagator with s-dependent width which is also the convention adopted to quote the measured values. Tau decays are simulated using the TAUOLA [252] package. The fragmentation and hadronisation of quark and gluon jets is described by the JETSET [140], HERWIG [104], and ARIADNE [254] programs, which are compared to estimate the corresponding systematic uncertainties. The default fragmentation parameters exclude any FSI effects from Bose-Einstein correlations (BEC) or colour reconnection (CR). For the latter, a dedicated procedure is developed to suppress mass biases in the $\mathrm{W^+W^-} \to \mathrm{q\overline{q}q\overline{q}}$ channel, which is detailed below.

The background, mainly from $\mathrm{e^+e^-} \to \mathrm{q\overline{q}}(\gamma)$ with additional gluon radiation and pair production of Z bosons, amounts to $2-15\%$ in the $\mathrm{q\overline{q}}\ell\nu_\ell$ channels, depending on the selected $\mathrm{W^+W^-}$ final state, and about 30% in the $\mathrm{q\overline{q}q\overline{q}}$ channel. The background is simulated using Monte-Carlo programs which include radiative corrections with higher order ISR and FSR. Dedicated control samples of 2-fermion and 4-fermion events are studied by the LEP experiments to ensure the agreement of the Monte-Carlo simulations with data, concerning jet and lepton resolutions, event shape variables, and detector response. Any remaining differences are taken into account as systematic uncertainties.

The methods that are applied to extract the W mass and width results are based on unbinned maximum likelihood fits to the measured data. Different procedures are employed to construct the likelihood functions and to describe their dependence on the underlying m_W and Γ_W values. For the final results, ALEPH and L3 apply a reweighting method, while OPAL and DELPHI use a convolution technique. The OPAL collaboration also performs fits of an analytical description of the Breit-Wigner resonance curves and background shapes to data, in order to access systematic uncertainties of the mass and width extraction method. Since the W-boson width, Γ_W, depends on the mass m_W, the SM dependence of Γ_W on m_W is assumed when performing the fit to the data to determine m_W. In fits for Γ_W, both m_W and Γ_W are varied independently. The m_W values obtained in the two-parameter fits are consistent within the given uncertainty with the one-parameter fit for m_W only. The methods used are described in the following.

Monte-Carlo reweighting

In the reweighting method, a multi-dimensional probability density is calculated using different mass estimators. These estimators are the masses from the 5C and 4C kinematic fit in the $\mathrm{q\overline{q}q\overline{q}}$ channel, and those of the 2C and 1C fit for $\mathrm{q\overline{q}e\nu_e}$ and $\mathrm{q\overline{q}}\mu\nu_\mu$ events. To further improve the sensitivity, ALEPH also includes the uncertainty on the 5C and 2C masses. The $\mathrm{q\overline{q}}\tau\nu_\tau$ sample contributes only with the rescaled hadronic mass. The probability densities are determined from distributions of the corresponding multi-differential cross-sections, including m_W and Γ_W dependent signal predictions and background contributions. This is done either using binned distributions or a local sampling of the phase-space density determined from Monte-Carlo simulations. Since the signal Monte-Carlo sample is generated with pre-defined underlying W mass and width values, the m_W and Γ_W dependence is introduced by reweighting of Monte-Carlo events. Each signal event is given a weight according to the ratio of the absolute values of the matrix element squared for the $\mathrm{e^+e^-} \to \mathrm{W^+W^-} \to f\bar{f}f\bar{f}(\gamma)$ process, calculated for the m_W and Γ_W values that are to be determined and for the nominal m_W and Γ_W used in the

simulation. The total likelihood functions of the different data samples are maximised with respect to m_{W} and Γ_{W}. This method is applied for the final ALEPH and L3 results, and by the OPAL collaboration to evaluate systematic uncertainties of the extraction method.

Convolution method

In this method, a probability density function is computed for each event, giving the probability that this event, with a set of reconstructed mass estimators $m_{i,\mathrm{rec}}$ $(i = 1, \ldots, n)$, originated from a sample with true W mass and width, m_{W} and Γ_{W}, of the following schematic form:

$$P_s(m_{\mathrm{W}}, \Gamma_{\mathrm{W}}, m_{i,\mathrm{rec}}) = S(m_{\mathrm{W}}, \Gamma_{\mathrm{W}}, m_i, s') \otimes ISR(s', s) \otimes R(m_i, m_{i,\mathrm{rec}}) \tag{7.3}$$

In this expression, $S(m_{\mathrm{W}}, \Gamma_{\mathrm{W}}, m_i, s')$ is the true distribution of the mass estimators, folded with the radiator function $ISR(s', s)$ and the detector resolution function, $R(m, m_{\mathrm{rec}})$, which is determined from Monte-Carlo simulations and describes the probability that an event of true mass estimator m_i would be reconstructed with mass estimators $m_{i,\mathrm{rec}}$. The likelihood for the data is then constructed as the product of $f_s P_s(m_{\mathrm{W}}, \Gamma_{\mathrm{W}}, m_{i,\mathrm{rec}}) + f_b P_b(m_{i,\mathrm{rec}})$ over all events, where f_s and f_b are the probabilities that the event originates from signal and background processes, respectively, and $P_b(m_{i,\mathrm{rec}})$ is a parametrisation of the background distribution. The parameters of interest, m_{W} and Γ_{W}, are estimated by maximising the total likelihood. In this approach, the resolution function may take account of the uncertainties in the reconstructed mass, which are likely to vary from event to event, and thus better measured events are given greater weight. This procedure is used for the final OPAL and DELPHI results.

7.3.4 Combination Procedure

The maximum likelihood fits are performed for each of the data sets at the different centre-of-mass energies and for each W-pair decay channel separately. Table 7.2 shows the final results on m_{W} obtained by the four LEP experiments with the direct reconstruction method in the $\mathrm{W^+W^-} \to \mathrm{q\overline{q}}\ell\nu_\ell$ and $\mathrm{W^+W^-} \to \mathrm{q\overline{q}q\overline{q}}$ final states. For the LEP combination, each experiment individually combines the results of the three $\mathrm{q\overline{q}}\ell\nu_\ell$ channels. The OPAL collaboration also includes the $\ell\nu_\ell\ell\nu_\ell$ measurements in these results. Input to the combination procedure are thus the m_{W} and Γ_{W} central values and uncertainties from the four LEP experiments in the $\mathrm{q\overline{q}q\overline{q}}$ (4q) and $\mathrm{q\overline{q}}\ell\nu_\ell + \ell\nu_\ell\ell\nu_\ell$ (non-4q) final states for five centre-of-mass energy bins corresponding to the five years of data taking. These inputs combine the data collected in 1996 at 172 GeV, in 1997 at 183 GeV, in 1998 at 189 GeV, in 1999 at $192 - 202$ GeV, and in 2000 at $205 - 209$ GeV.

The combination of the measurements is performed and the evaluation of the components of the total measurement uncertainty is assessed using the Best Linear Unbiased Estimate (BLUE) technique [62]. In this way, statistical and systematic uncertainties of each measurement are properly taken into account, including correlations between them. The LEP combination procedure as described here is also applied to combine the measurements of each LEP experiment for comparison with the combined measurement published by each experiment in Table 7.2. The observed differences are mainly due to a different assessment of FSI uncertainties, which affects the fully hadronic channel, as discussed below. The changes of the semi-leptonic results are due to systematic uncertainties correlated between the $\mathrm{q\overline{q}q\overline{q}}$ and $\mathrm{q\overline{q}}\ell\nu_\ell$ channels.

Direct Reconstruction			
Experiment	$W^+W^- \to q\overline{q}\ell\nu_\ell$ m_W[GeV]	$W^+W^- \to q\overline{q}q\overline{q}$ m_W[GeV]	Combined m_W[GeV]
Published			
ALEPH	80.429 ± 0.060	80.475 ± 0.080	80.444 ± 0.051
DELPHI	80.339 ± 0.075	80.311 ± 0.137	80.336 ± 0.067
L3	80.212 ± 0.071	80.325 ± 0.080	80.270 ± 0.055
OPAL	80.449 ± 0.063	80.353 ± 0.083	80.416 ± 0.053
LEP combination			
ALEPH	80.429 ± 0.059	80.477 ± 0.082	80.444 ± 0.051
DELPHI	80.339 ± 0.076	80.310 ± 0.101	80.330 ± 0.064
L3	80.217 ± 0.071	80.324 ± 0.090	80.254 ± 0.058
OPAL	80.449 ± 0.062	80.353 ± 0.081	80.415 ± 0.052

Table 7.2: W mass measurements from direct reconstruction ($\sqrt{s} = 172 - 209$ GeV). Results are given for the semi-leptonic, fully-hadronic channels and the combined value. The top part of the table shows the results as published by the experiments [151, 152, 153, 154], using their individual evaluations of FSI effects; these results are final. The bottom part of the table shows the results of the experiments when propagating the common LEP estimates of FSI effects to the mass, which also affects the $W^+W^- \to q\overline{q}\ell\nu_\ell$ results through correlations due to other systematic uncertainties. The $W^+W^- \to q\overline{q}\ell\nu_\ell$ results from the OPAL collaboration include mass information from the $W^+W^- \to \ell\nu_\ell\ell\nu_\ell$ channel.

7.3.5 Overview of Systematic Uncertainties

There are several sources of systematic uncertainties affecting the measurements of m_W and Γ_W. Table 7.3 summarises the systematic and statistical uncertainties on the W mass and width measurements evaluated for the combined LEP data using the direct reconstruction method. For the W mass determination, the uncertainties are also given separately for the $q\overline{q}\ell\nu_\ell$ and $q\overline{q}q\overline{q}$ final states, and for their combination. The main contributions are discussed in the following.

LEP centre-of-mass energy

Since the LEP centre-of-mass energy is used as a constraint in order to improve the W mass resolution, uncertainties in the centre-of-mass energy translate directly into uncertainties on m_W. These can approximately be obtained by scaling the LEP centre-of-mass energy uncertainties with the ratio $m_W/(\sqrt{s}/2)$. The W width is less affected. At W-pair threshold energies, the calibration of the LEP centre-of-mass energy yields precisions of $25 - 27$ MeV, and at energies between 182.7 GeV up to 201.6 GeV the uncertainty is $20 - 24$ MeV. Since in the last LEP runs in the year 2000 horizontal corrector magnets were used to spread the magnetic field over a larger bending section in order to eventually increase the LEP beam energy to its absolute maximum, the related additional systematic effects reduced the centre-of-mass energy precision

Source	Systematic Uncertainty in MeV			
	on m_{W}			on Γ_{W}
	$\mathrm{q\overline{q}}\ell\nu_\ell$	$\mathrm{q\overline{q}q\overline{q}}$	Combined	
ISR/FSR	8	5	7	6
Hadronisation	13	19	14	40
Detector effects	10	8	9	23
LEP energy	9	9	9	5
Colour reconnection	–	35	8	27
Bose-Einstein Correlations	–	7	2	3
Other	3	10	3	12
Total systematic	21	44	22	55
Statistical	30	40	25	63
Statistical in absence of systematics	30	31	22	48
Total	36	59	34	83

Table 7.3: Error decomposition for the combined LEP W mass and width results using the direct reconstruction method. Information from cross-section measurements at the W-pair production threshold are not included in the W-mass uncertainties. Detector effects include uncertainties in the jet and lepton energy scales and resolution. The 'Other' category refers to errors, all of which are uncorrelated between experiments, arising from: simulation statistics, background estimation, four-fermion treatment, fitting method and event selection. The error decomposition in the $\mathrm{q\overline{q}}\ell\nu_\ell$ and $\mathrm{q\overline{q}q\overline{q}}$ channels refers to the independent fits to the results from the two channels separately. Large correlated uncertainties, mainly from FSI, lead to a reduced weight of measurements contributing to the average result and thus an increased statistical uncertainty both in the $\mathrm{q\overline{q}q\overline{q}}$ channel and for the LEP combination.

to $37 - 42$ MeV.

A cross-check of the LEP energy determination is performed by analysing $\mathrm{e^+e^-} \to \mathrm{Z} + \gamma \to \mathrm{f\overline{f}} + \gamma$ events with hard ISR photons, mostly emitted at small polar angles with respect to the beam directions. In these events with a so-called radiative return to the Z, the mass of the 2-fermion system is calculated from the fermion production angles only, assuming energy-momentum conservation. The mass spectrum exhibits a peak around the Z mass value. Comparing the Z mass, $m_{\mathrm{Z}}^{\mathrm{f\overline{f}}}$, determined from this spectrum with the precise value of m_{Z} measured at Z pole energies [4] is equivalent to a test of the LEP centre-of-mass energy (see Appendix C for further details):

$$\Delta\sqrt{s} = \sqrt{s} - \sqrt{s}_{LEP} = \sqrt{s}\frac{m_{\mathrm{Z}}^{\mathrm{f\overline{f}}} - m_{\mathrm{Z}}}{m_{\mathrm{Z}}} \,, \tag{7.4}$$

with the nominal value of $\sqrt{s}_{LEP}$ [246] provided by the LEP energy working group. When combining all available LEP data [151, 255, 256, 257] with Z decays to hadrons, and to electron,

	LEP energy correlations					
$\sqrt{s}$ [GeV]	161	172	183	189	192-202	205-209
161	1.00	1.00	0.57	0.56	0.58	0.36
172	1.00	1.00	0.58	0.57	0.58	0.37
183	0.57	0.58	1.00	0.94	0.95	0.53
189	0.56	0.57	0.94	1.00	0.94	0.53
192-202	0.58	0.58	0.95	0.94	1.00	0.55
205-209	0.36	0.37	0.53	0.53	0.55	1.00

Table 7.4: Correlation between the LEP centre-of-mass energy measurements in the six run periods [246].

muon, and tau pairs, the difference is found to be

$$\Delta\sqrt{s} = -54 \pm 54 \text{ MeV}\,, \tag{7.5}$$

in good agreement with no shift with respect to the more precise standard LEP energy calibration.

The properly calibrated LEP centre-of-mass energy is used in the W mass and width analysis on event-by-event basis. Uncertainties on m_{W} and Γ_{W} are determined by detailed Monte-Carlo studies, and also the effect of the LEP energy spread is taken into account. When combining the LEP W mass and width results the correlations between the LEP energy uncertainties at the different energies are properly included. They are derived from the LEP energy model [246] and listed in Table 7.4. The overall LEP energy uncertainty is 9 MeV on m_{W} and 5 MeV on Γ_{W}.

Detector effects

The effects of detector performance as well as of identification and reconstruction efficiencies for final state leptons, jets and photons are studied in dedicated control data samples. Energy and momentum calibration, as well as detector alignment and angular measurements, very important for the mass reconstructed, were studied [151, 152, 153, 154]. Since Monte-Carlo samples are compared to data to extract m_{W} and Γ_{W}, all effects are modelled in detail in the simulation and remaining differences to data result in corresponding systematic uncertainties. The LEP experiments provide separate uncertainties for lepton and jet measurements. These are considered uncorrelated between measurements from different experiments, but correlated for m_{W} and Γ_{W} measurements from the same experiment at different LEP energy points. The total systematic uncertainty from detector effects is 10 MeV and 8 MeV on m_{W} in the $\mathrm{q\overline{q}}\ell\nu_\ell$ and $\mathrm{q\overline{q}q\overline{q}}$ channels. The W width systematic uncertainties due to finite precision in modelling jet and lepton measurements is 23 MeV, combining all final states.

Fragmentation and hadronisation

Since the m_{W} and Γ_{W} extraction methods rely on the comparison of Monte-Carlo simulations to data the modelling of the fragmentation and hadronisation process subsequent to the $\mathrm{W} \to \mathrm{q\overline{q}}$

decay is essential. The calibration of the reconstructed jets is very sensitive to the fractions of the different final state hadrons inside the jets. Furthermore, the jet reconstruction usually can not resolve each individual hadron, so that the same particle masses are assumed (usually the pion mass) when tracks and clusters are combined to form quark and gluon jets. To assess systematic uncertainties due to fragmentation and hadronisation, different Monte-Carlo models are compared, whose parameters are adjusted to describe high-statistic data samples of $\mathrm{Z} \to \mathrm{q\overline{q}}$ decays at the Z pole. These Z decays are depleted in b-quarks, to resemble the hadronic decays of W bosons. The systematic uncertainty is derived from the relative shifts in W mass and width values determined in Monte-Carlo samples using the JETSET/PYTHIA [140], HERWIG [258], and ARIADNE [254] fragmentation models. In addition, the fraction of certain hadrons, like kaons and protons, is directly measured in $\mathrm{W} \to \mathrm{q\overline{q}}$ decays and compared to the fragmentation models. The measurement uncertainties on these fractions are also taken into account in the fragmentation and hadronisation systematic uncertainties for the m_{W} and Γ_{W} determination.

Since all four LEP experiments study the same fragmentation models, the systematic uncertainty is taken as fully correlated for all measurements of the W mass and width. Eventually, the systematic effect on m_{W} is estimated to be 13 MeV and 19 MeV in the $\mathrm{q\overline{q}}\ell\nu_\ell$ and $\mathrm{q\overline{q}q\overline{q}}$ final states. In the W width determination, the corresponding systematic uncertainties contribute with 40 MeV to the combined W width measurement.

Colour reconnection

A particular systematic uncertainty arises in the $\mathrm{W^+W^-} \to \mathrm{q\overline{q}q\overline{q}}$ channel, where the two W bosons decay close in phase space so that FSI effects may play a significant role. Indeed, colour reconnection (CR) effects leads to shifts of the extracted W mass up to about 100 MeV [151, 152, 153, 154] if nominal jet reconstruction is applied and data are compared to Monte-Carlo models with and without colour reconnection. These large shifts are observed even if the measured constraints on the reconnection parameters, which are discussed in section 4, are applied. The LEP collaborations therefore developed new techniques in the $\mathrm{q\overline{q}q\overline{q}}$ channel. It is observed that colour reconnection effects on m_{W} as implemented in the ARIADNE [103], SK [102], and HERWIG [104] models are reduced when the jet reconstruction is modified. This is achieved by either rejecting particles inside jets with energies or momenta lower than a given threshold or by reweighting their energies and momenta to suppress soft particles, which are mainly in the inter-jet and reconnection-sensitive region. The four LEP experiments applied thresholds and weights which are optimised individually for the colour reconnection constraints of the SK-I model [102] which are measured by each experiment separately. In the optimisation process the overall uncertainty on m_{W} is minimized, again individually, trading a reduced statistical precision due to a modified jet reconstruction for an improved FSI systematic uncertainty. For the LEP combined analysis, the threshold values and weights of each experiment are however not always optimal when the LEP combined upper limit on the SK-I parameter, $k_I < 2.10$, is used as reference for the CR uncertainty in the LEP m_{W} combination. Although this reduces the relative weight of some m_{W} measurements in the LEP combination, a further optimisation is not performed.

For the final LEP combination, the central value of the W mass is determined using Monte-Carlo samples without colour reconnection. The systematic uncertainties are evaluated from the mass differences observed when data is compared to the SK-I model with $k_I = 2.10$. The systematic uncertainties are evaluated at each centre-of-mass energy independently since the colour reconnection effects are energy dependent. The systematic uncertainties are taken as symmetric in the combination procedure and correlated between all measurements in the

$q\overline{q}q\overline{q}$ channel at the different centre-of-mass energies and by the four LEP experiments. They contribute 35 MeV to the total uncertainty in the fully hadronic final state.

When the W width is extracted, the optimisation of the jet reconstruction is not applied by the LEP collaborations, and the standard jet measurement is used. The reason is the relatively large statistical uncertainty of the W width measurement, which does not require a modification of the standard $q\overline{q}q\overline{q}$ analysis. The corresponding CR uncertainty is evaluated using the LEP upper limit on the SK-I parameter, $k_I < 2.10$, like in the W mass determination, and corresponds to 27 MeV on the combined width result.

Bose-Einstein correlations

A further source of uncertainty connected with FSI in the $W^+W^- \to q\overline{q}q\overline{q}$ channel is the possibility of Bose-Einstein correlations (BEC) between identical mesons in the decay of different W bosons. The measurement of these correlations is discussed in detail in section 4. For the final LEP results, Bose-Einstein correlations between particles from inside each hadronically decaying W are implemented in the Monte-Carlo simulation according to the BE_{32} model [140], which describes $W^+W^- \to q\overline{q}\ell\nu_\ell$ data well. However, the combined analysis of LEP data yields an upper limit on the strength of Bose-Einstein correlations between mesons from different W bosons of 30% of the full correlation in the BE_{32} model. The systematic effect on the W mass and width in the $W^+W^- \to q\overline{q}q\overline{q}$ channel is effectively reduced by the modified jet reconstruction algorithms, which were originally introduced for controlling systematic uncertainties from CR. Therefore, the uncertainties due to Bose-Einstein correlations on the W mass in $W^+W^- \to q\overline{q}q\overline{q}$ events is 7 MeV, while it is just 3 MeV on the combined witdth result.

Initial state radiation and $\mathcal{O}(\alpha)$ effects

Photon radiation influences the reconstructed W mass spectra. The Monte-Carlo programs used to extract m_W and Γ_W, KandY, RACOONWW and WPHACT, include ISR effects in the YFS exponentiation scheme to $O(\alpha^3)$, full $O(\alpha)$ electroweak corrections, including interference between ISR, FSR and photon radiation of the W boson, as well as screened Coulomb corrections. These describe Coulomb interactions between the W bosons, which are potentially large but screened due to the limited lifetime of the W bosons. Higher-order leading-log FSR corrections are included using PHOTOS for leptons and PYTHIA for quarks. ISR effects on m_W are estimated by comparing the $O(\alpha^3)$ with the $O(\alpha^2)$ calculation, yielding small shifts of about 1 MeV [259]. The effect of Coulomb screening are estimated by taking half of the difference between Monte-Carlo samples with screened Coulomb effect and without any Coulomb effect, which amounts to about 7 MeV. To evaluate the uncertainty on the non-leading $O(\alpha)$ electroweak corrections, a direct comparison of the RACOONWW and the KandY generators is performed. The observed differences are in the order of 10 MeV for $q\overline{q}\ell\nu_\ell$ and 5 MeV for $q\overline{q}q\overline{q}$. Some systematic studies overlap, however, and the experiments apply different strategies to assess them. The total LEP uncertainty on the W mass due to radiative corrections is 8 MeV in the semi-leptonic channel and 5 MeV in the fully hadronic channel. Full correlation between all data sets is assumed. In case of the W width, the corresponding uncertainties amount to 6 MeV when combining all final states.

Other sources of systematic uncertainties

The contribution of background to the selected W-pair samples arises mainly from 4-fermion and hadronic 2-fermion events. All LEP experiments study the event shapes of the different background contributions using control samples to best describe the data. The systematic effect of the background on m_{W} and Γ_{W} are derived by varying the overall scale on the production cross-sections of the background processes, mainly $\mathrm{e^+e^-} \to \mathrm{q\overline{q}}(\gamma, g)$ and $\mathrm{e^+e^-} \to \mathrm{ZZ}$, within the measured uncertainty. Effects on the mass spectrum which do not scale with the overall production rate are studied by varying, for example, the slope of the background spectra.

In addition, uncertainties due to limited Monte-Carlo statistics, from the mass and width extraction techniques, and due to the event selection are considered. Early analyses at LEP-II used Monte-Carlo simulations based on CC03 matrix elements to simulate $\mathrm{W^+W^-}$ production. In this case, systematic biases of the W mass and width may arise because four-fermion diagrams are neglected which might interfere with W-pair production.

All these categories of systematic uncertainties are taken as uncorrelated in the LEP combination and contribute on the mass with 3 MeV in the semi-leptonic channel and 10 MeV in the fully hadronic channel, and 12 MeV on Γ_{W}.

7.4 LEP Combined W-Boson Mass

The combined LEP W mass from direct reconstruction data alone is:

$$m_{\mathrm{W}}(\mathrm{direct}) = 80.375 \pm 0.025(\mathrm{stat.}) \pm 0.022(\mathrm{syst.})\ \mathrm{GeV}\,, \tag{7.6}$$

with a total uncertainty of 34 MeV. The combination has a χ^2/dof of 47.7/37, corresponding to a probability of 11.1%. The weight of the fully-hadronic channel in the combination amounts to just 22% due to significant FSI systematic uncertainties.

The largest contribution to the systematic error originates from hadronisation uncertainties, which are fully correlated between all measurements. In the absence of any systematic effects the current LEP statistical precision on m_{W} would be 22 MeV. The statistical error contribution in the LEP combination is larger than this, 25 MeV, due to the reduced weight of the fully-hadronic channel, mainly due to FSI systematic uncertainties.

When the threshold measurements (Section 7.2) are combined with the precise results obtained from direct reconstruction one achieves a W mass measurement of:

$$m_{\mathrm{W}} = 80.376 \pm 0.025(\mathrm{stat.}) \pm 0.022(\mathrm{syst.})\ \mathrm{GeV}\,, \tag{7.7}$$

with a slightly improved total uncertainty of 33 MeV. The combination has a χ^2/dof of 48.9/41, corresponding to a probability of 18.5%. The LEP energy uncertainty is the only correlated systematic error source between the threshold and direct reconstruction measurements. The threshold measurements have a weight of only 2% in the combined fit. This LEP combined result is compared with the final results of the four LEP experiments in Figure 7.1.

7.5 Consistency Checks

The masses from the two channels with all uncertainties and correlations included are:

$$m_{\mathrm{W}}(\mathrm{W^+W^-} \to \mathrm{q\overline{q}}\ell\nu_\ell) = 80.372 \pm 0.030(\mathrm{stat.}) \pm 0.021(\mathrm{syst.})\ \mathrm{GeV}, \tag{7.8}$$

$$m_{\mathrm{W}}(\mathrm{W^+W^-} \to \mathrm{q\overline{q}q\overline{q}}) = 80.387 \pm 0.040(\mathrm{stat.}) \pm 0.044(\mathrm{syst.})\ \mathrm{GeV}. \tag{7.9}$$

The two results are correlated with a correlation coefficient of 0.20. These results and the correlation between them can be used to combine the two measurements or to form the mass difference. The LEP combined results from the two channels are compared with those quoted by the individual experiments in Figure 7.2. When combining the m_{W} measurements in the $\mathrm{q\overline{q}}\ell\nu_\ell$ and $\mathrm{q\overline{q}q\overline{q}}$ channels separately and neglecting any correlations between these final states, results consistent within 2 MeV with the correlated averages above are obtained.

The difference between the combined W-boson mass measurements obtained from the fully-hadronic and semi-leptonic channels, $\Delta m_{\mathrm{W}}(\mathrm{q\overline{q}q\overline{q}} - \mathrm{q\overline{q}}\ell\nu_\ell)$ is also determined. Since Δm_{W} is primarily of interest as a check of the possible effects of final state interactions, the uncertainties from Bose-Einstein correlation and colour reconnection are set to zero in its determination. A fit imposing otherwise the same correlations as those for the results given in the previous sections yields:

$$\Delta m_{\mathrm{W}}(\mathrm{q\overline{q}q\overline{q}} - \mathrm{q\overline{q}}\ell\nu_\ell) = -12 \pm 45\ \mathrm{MeV}. \tag{7.10}$$

Note that this mass difference has a different value and opposite sign compared to the difference between the $\mathrm{q\overline{q}q\overline{q}}$ and $\mathrm{q\overline{q}}\ell\nu_\ell$ mass values presented above, because the BEC and CR uncertainties are not included in its determination. A significant non-zero value for Δm_{W} could indicate that such Bose-Einstein correlation or colour reconnection effects are biasing the value of m_{W} determined from $\mathrm{W^+W^-} \to \mathrm{q\overline{q}q\overline{q}}$ events. The consistency of the mass difference with zero shows that such FSI effects are well suppressed by the modified jet reconstruction in the fully hadronic channel.

7.6 LEP Combined W-Boson Width

The method of direct reconstruction is also well suited to the direct measurement of the total decay width of the W boson. The published results of the four LEP experiments are shown in Table 7.5 and in Figure 7.3.

For the LEP combination, each experiment provided a W width measurement for both $\mathrm{W^+W^-} \to \mathrm{q\overline{q}}\ell\nu_\ell$ and $\mathrm{W^+W^-} \to \mathrm{q\overline{q}q\overline{q}}$ channels for each of the data taking periods that were analysed, and using the same error categories as for the mass. The BEC and CR uncertainties supplied by the experiments were based on studies of phenomenological models of these effects, using the same estimates of such FSI effects as for the mass and propagating them to the width. Note that the W width results of the experiments do not use the techniques introduced to reduce sensitivity to FSI effects used for the mass analysis. A simultaneous fit to the results of the four LEP collaborations is performed in the same way as for the m_{W} measurement. Correlated systematic uncertainties are taken into account and the combination yields:

$$\Gamma_{\mathrm{W}} = 2.195 \pm 0.063(\mathrm{stat.}) \pm 0.055(\mathrm{syst.})\ \mathrm{GeV}, \tag{7.11}$$

Experiment	Published Γ_{W} [GeV]	LEP combination Γ_{W} [GeV]
ALEPH	2.14 ± 0.11	2.14 ± 0.11
DELPHI	2.40 ± 0.17	2.39 ± 0.17
L3	2.18 ± 0.14	2.24 ± 0.15
OPAL	2.00 ± 0.14	2.00 ± 0.14

Table 7.5: W width measurements ($\sqrt{s} = 172 - 209$ GeV) from the individual experiments. The column labelled "published" shows the results as published by the experiments, using their individual evaluations of FSI effects. The column labelled "LEP combination" shows the results of the experiments when propagating the LEP measurements of FSI effects to the W width.

for a total error of 83 MeV. The combination has a χ^2/dof of 37.4/33, corresponding to a probability of 27.3%.

7.7 Summary

The final results of the four LEP experiments on the mass and width of the W boson are combined taking into account correlated systematic uncertainties, with the result:

$$m_{\mathrm{W}} = 80.376 \pm 0.033 \text{ GeV}, \tag{7.12}$$

$$\Gamma_{\mathrm{W}} = 2.195 \pm 0.083 \text{ GeV}. \tag{7.13}$$

The correlations between mass and width are found to be less than 5% and thus negligible. These values correspond to the theoretical definition of a W-boson propagator with s-dependent width. The results of the mass and width determined by the LEP collaborations are in good agreement with the measurements at hadron colliders [239, 240, 241, 242]. Updated constraints on SM parameters using the mass and width results are presented in Appendix F.

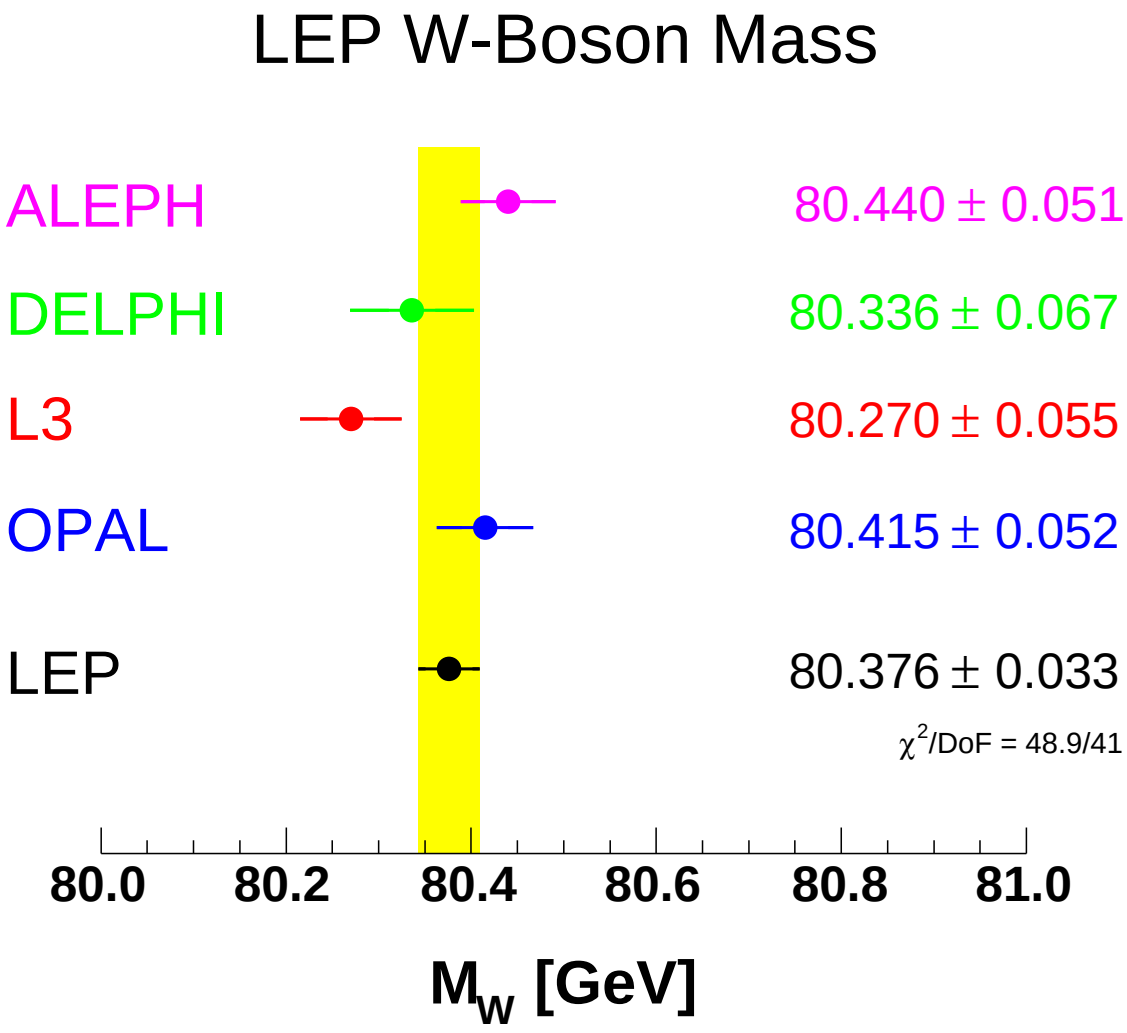


Figure 7.1: The measurements of the W-boson mass obtained by the four LEP collaborations (as published) together with the LEP combined result. The combined value includes correlations between experiments, between different energy points, and between the $q\bar{q}\ell\nu_\ell$ and $q\bar{q}q\bar{q}$ channels. A revised estimation of systematic uncertainties due to colour reconnection and Bose-Einstein correlations is applied to the input of the individual measurements to the LEP combined results in order to take the direct determination of FSI parameters into account.

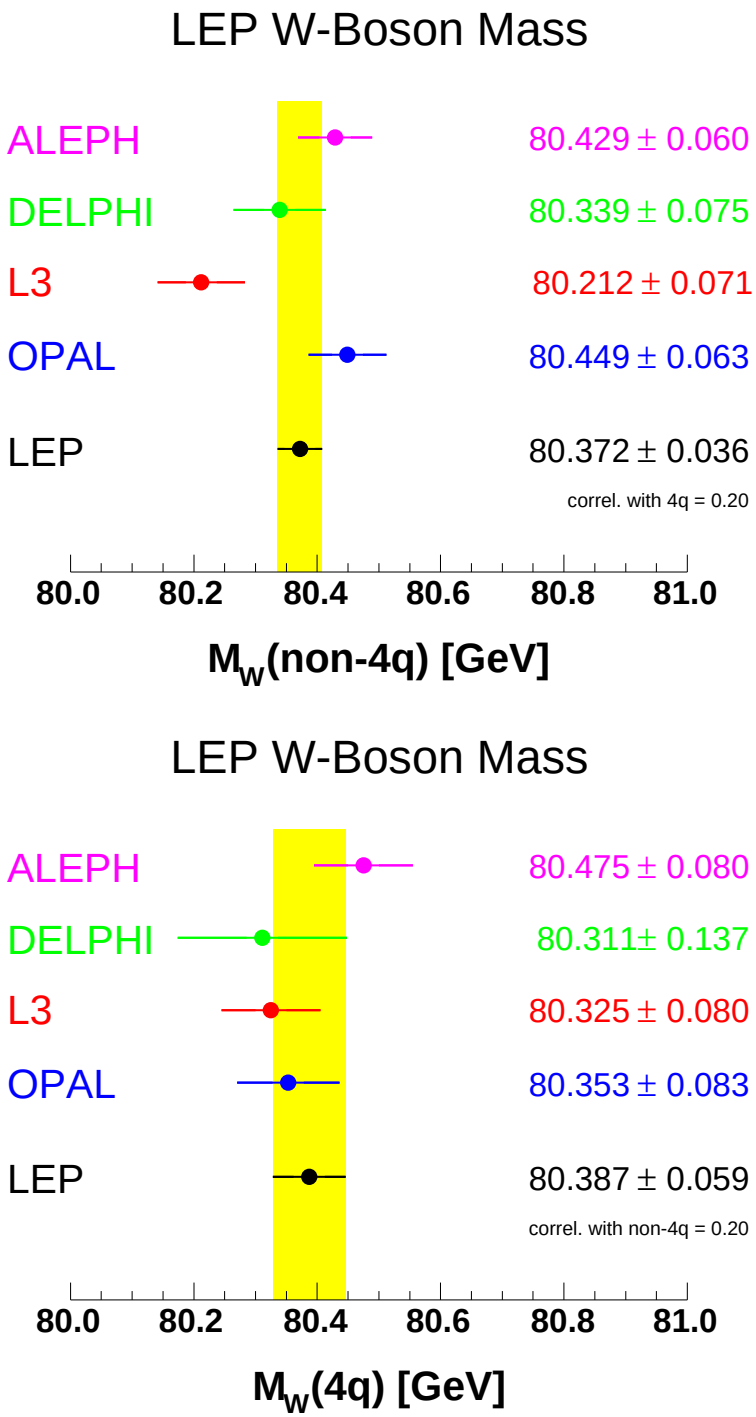


Figure 7.2: The W mass measurements in the $W^+W^- \to q\bar{q}\ell\nu_\ell$ channels (top), and the $W^+W^- \to q\bar{q}q\bar{q}$ channel (bottom) obtained by the four LEP collaborations (as published) compared to the combined value. Correlations between experiments and between measurements at different energy points are properly taken into account. The combined non-4q and 4q results are correlated since they are obtained from a fit to both channels taking into account inter-channel correlations. For the LEP combination, the assessment of systematic uncertainties due to colour reconnection and Bose-Einstein correlations for the individual measurements of the four experiments is revised with respect to the direct LEP measurements of FSI.

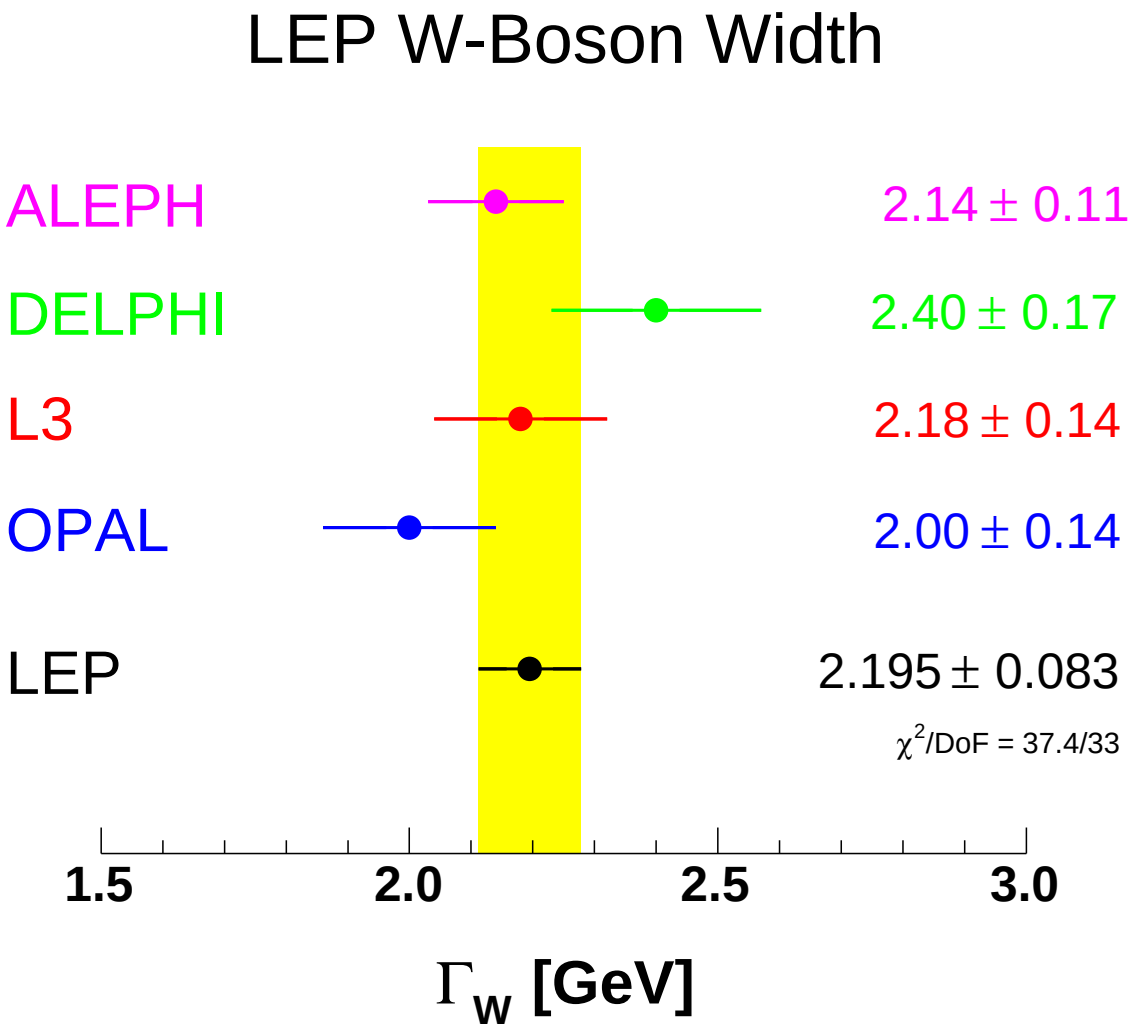


Figure 7.3: The measurements of the W-boson width obtained by the four LEP collaborations (as published) together with the LEP combined result. The combined value includes correlations between experiments, between different energy points, and between the $q\bar{q}\ell\nu_\ell$ and $q\bar{q}q\bar{q}$ channels. A revised estimation of systematic uncertainties due to colour reconnection and Bose-Einstein correlations is applied to the input of the individual measurements to the LEP combined results in order to take the direct determination of FSI parameters into account.

Chapter 8

Summary and Conclusions

The four LEP experiments ALEPH, DELPHI, L3 and OPAL performed measurements in electron-positron collisions at centre-of-mass energies above the mass of the Z boson, ranging from 130 GeV, crossing the W-pair production threshold at 160 GeV, up to 209 GeV. Based on about 0.75 fb^{-1} of luminosity collected by each experiment, yielding a total of 3 fb^{-1}, many precision measurements are summarised in this report.

The combinations of precise electroweak results yield stringent constraints on the Standard Model (SM) and its free parameters, for example:

$$\begin{aligned} m_{\mathrm{W}} &= 80.376 \pm 0.033 \text{ GeV} \\ \Gamma_{\mathrm{W}} &= 2.195 \pm 0.083 \text{ GeV} \\ B(W \to \mathrm{had}) &= 67.41 \pm 0.27 \text{ \%} \\ g_1^Z &= 0.984^{+0.018}_{-0.020} \\ \kappa_\gamma &= 0.982 \pm 0.042 \\ \lambda_\gamma &= -0.022 \pm 0.019\,. \end{aligned}$$

The results, together with measurements performed in electron-positron collisions at the Z-pole and in hadron collider experiments, test the SM with unprecedented precision at the highest interaction energies. The measurements agree well with the SM predictions.

Overall, the SM is verified to be a good theory up to the 200 GeV scale, see also the studies presented in Appendix F. The data impose very tight constraints on any new physics beyond the SM, and are well compatible with a $125-126$ GeV SM Higgs boson [260]. Any extended theory must be consistent with the SM or one or more Higgs doublet models such as super-symmetry.

Acknowledgements

We would like to thank the CERN accelerator divisions for the efficient operation of the LEP accelerator, the precise information on the beam energy scale and their close cooperation with the four experiments. We would also like to thank members of the SLD, CDF, DØ, NuTeV and E-158 collaborations for making results available to us and for useful discussions concerning their combination. Finally, the results and their interpretation within the SM would not have been possible without the close collaboration of many theorists.

Appendix A

S-Matrix

A.1 Introduction

The S-Matrix ansatz provides a coherent way of describing the measurements of the cross-section and forward-backward asymmetries in s-channel $e^+e^- \to f\bar{f}$ processes at centre-of-mass energies around the Z resonance and the measurements at centre-of-mass energies from 130 GeV to 209 GeV from the LEP-II program. This chapter describes the combination of results from the full LEP-I data sets of the four LEP experiments, to obtain a LEP combined result on the parameters of the S-Matrix ansatz describing the Z lineshape.

The standard description of the measurements at the Z resonance [4] makes use of nine parameters (m_Z, Γ_Z, σ^0_{had}, R^0_ℓ, $A^{0,\ell}_{FB}$, for $\ell = e, \mu, \tau$) which are reduced to five in case lepton universality is assumed. The S-Matrix formalism utilises an extra three parameters (assuming lepton universality) or seven parameters (not assuming lepton universality). The additional parameters describe the contributions to the cross-sections and forward-backward asymmetries of the interference between the exchange of a Z and a photon. The Z-pole data alone cannot tightly constrain these interference terms, in particular the interference term for cross-sections, since their contributions are small around the Z resonance and change sign at the pole. Owing to strong correlations between the size of the hadronic cross-section interference term and the mass of the Z, this leads to a larger error on the extracted mass of the Z compared to the standard five and nine parameter analyses where the hadronic interference term is fixed to the value predicted in the Standard Model (SM). However, using the LEP-II data leads to a significant improvement in the constraints on the interference terms and a corresponding reduction in the uncertainty on the mass of the Z, expected to result in a measurement of m_Z which is almost as precise but without having to constrain the γ/Z interference to the SM prediction.

The LEP combination is a two-step procedure: first a combination of the LEP-I based results, and then including the LEP-II data. For the LEP-I data, an average of the individual experiments' results on the S-Matrix parameters is made. Such a combination at parameter level, similar to the method used to combine the Z lineshape results in terms of the five and nine parameters [4], is presented here. To include the LEP-II data, a fit of the S-Matrix parameters to the combined LEP-II measurements of cross-sections and asymmetries as presented in Chapter 3 is envisaged, including in the χ^2 the LEP-I based combination of S-Matrix parameters with uncertainties and correlations as additional constraints.[1]

[1] Based on preliminary LEP measurements, Reference [262] contains a partial LEP-I+LEP-II combination along these lines, which shows the vast improvement made possible by including the LEP-II measurements.

In Section A.2 the parameters of the S-Matrix ansatz are explained in detail. In Section A.3 the average of the LEP-I data is described, preparing for the inclusion of the LEP-II measurements in the future. The results are discussed in Section A.4 while the detailed combination tables are listed in Section A.5.

A.2 The S-Matrix Ansatz

The S-Matrix ansatz [263] is a rigorous approach to describe the cross-sections and forward-backward asymmetries in s-channel e^+e^- annihilations under the basic assumption that the processes can be parametrised as the exchange of a massless and a massive vector boson, in which the couplings of the bosons including their interference are treated as free and independent parameters. In this model, the cross-sections are parametrised as follows:

$$\sigma^0_{\mathrm{tot,f}}(s) = \frac{4}{3}\pi\alpha^2 \left[\frac{g_{\mathrm{f}}^{tot}}{s} + \frac{j_{\mathrm{f}}^{tot}(s-\overline{m}_{\mathrm{Z}}^2) + r_{\mathrm{f}}^{tot}\, s}{(s-\overline{m}_{\mathrm{Z}}^2)^2 + \overline{m}_{\mathrm{Z}}^2\overline{\Gamma}_{\mathrm{Z}}^2} \right] \quad \text{with } \mathrm{f} = \mathrm{had}, \mathrm{e}, \mu, \tau\,, \tag{A.1}$$

while the forward-backward asymmetries are given by:

$$A^0_{\mathrm{fb,f}}(s) = \pi\alpha^2 \left[\frac{g_{\mathrm{f}}^{fb}}{s} + \frac{j_{\mathrm{f}}^{fb}(s-\overline{m}_{\mathrm{Z}}^2) + r_{\mathrm{f}}^{fb}\, s}{(s-\overline{m}_{\mathrm{Z}}^2)^2 + \overline{m}_{\mathrm{Z}}^2\overline{\Gamma}_{\mathrm{Z}}^2} \right] / \sigma^0_{\mathrm{tot,f}}(s)\,, \tag{A.2}$$

where $\sqrt{s}$ is the centre-of-mass energy. The parameters r_{f} and j_{f} scale the Z exchange and the γ/Z interference contributions to the total cross-section and forward-backward asymmetries. The contribution g_{f} of the pure γ exchange is fixed to the value predicted by QED. Neither the hadronic charge asymmetry nor the flavour-tagged quark forward-backward asymmetries are considered here, which leaves 16 S-Matrix parameters to describe the LEP data: the mass and total width of the Z resonance, and 14 r_{f} and j_{f} parameters. Applying the constraint of neutral-current lepton universality reduces the number of parameters from 16 to 8.

In the SM the Z exchange term, the γ/Z interference term and the photon exchange term are given in terms of the fermion charges and their effective vector and axial couplings to the Z by:

$$\begin{aligned}
r_{\mathrm{f}}^{\mathrm{tot}} &= \kappa^2 \left[g_{\mathrm{Ae}}^2 + g_{\mathrm{Ve}}^2\right]\left[g_{\mathrm{Af}}^2 + g_{\mathrm{Vf}}^2\right] - 2\kappa\, g_{\mathrm{Ve}}\, g_{\mathrm{Vf}} C_{Im} && \text{(A.3)}\\
j_{\mathrm{f}}^{\mathrm{tot}} &= 2\kappa\, g_{\mathrm{Ve}}\, g_{\mathrm{Vf}}\, (C_{Re} + C_{Im}) && \text{(A.4)}\\
g_{\mathrm{f}}^{\mathrm{tot}} &= Q_{\mathrm{e}}^2 Q_{\mathrm{f}}^2 \left|F_A(m_{\mathrm{Z}})\right|^2 && \text{(A.5)}\\
r_{\mathrm{f}}^{\mathrm{fb}} &= 4\kappa^2 g_{\mathrm{Ae}}\, g_{\mathrm{Ve}}\, g_{\mathrm{Af}}\, g_{\mathrm{Vf}} - 2\kappa\, g_{\mathrm{Ae}}\, g_{\mathrm{Af}} C_{Im} && \text{(A.6)}\\
j_{\mathrm{f}}^{\mathrm{fb}} &= 2\kappa\, g_{\mathrm{Ae}}\, g_{\mathrm{Af}}\, (C_{Re} + C_{Im}) && \text{(A.7)}\\
g_{\mathrm{f}}^{\mathrm{fb}} &= 0\,, && \text{(A.8)}
\end{aligned}$$

with the following definitions:

$$\kappa = \frac{G_F m_{\mathrm{Z}}^2}{2\sqrt{2}\,\pi\alpha} \approx 1.50 \tag{A.9}$$

$$C_{Im} = \frac{\Gamma_{\mathrm{Z}}}{m_{\mathrm{Z}}}\, Q_{\mathrm{e}} Q_{\mathrm{f}}\, \mathrm{Im}\left\{F_A(m_{\mathrm{Z}})\right\} \tag{A.10}$$

$$C_{Re} = Q_{\mathrm{e}} Q_{\mathrm{f}}\, \mathrm{Re}\left\{F_A(m_{\mathrm{Z}})\right\} \tag{A.11}$$

$$F_A(m_{\mathrm{Z}}) = \frac{\alpha(m_{\mathrm{Z}})}{\alpha}\,, \tag{A.12}$$

where $\alpha(m_{\mathrm{Z}})$ is the complex fine-structure constant, and $\alpha \equiv \alpha(0)$. The expressions of the S-Matrix parameters in terms of the effective vector and axial-vector couplings given above neglect the imaginary parts of the effective couplings. The photonic virtual and bremsstrahlung corrections are included through the convolution of Equations A.1 and A.2 with the same radiator functions as used in the five and nine parameter Z-lineshape fits [4].

In the S-Matrix framework, the parameters mass ($\overline{m}_{\mathrm{Z}}$)and total width ($\overline{\Gamma}_{\mathrm{Z}}$) of the Z boson are defined in terms of a relativistic Breit-Wigner with s-independent width. These definitions are related to the usual definitions of the mass m_{Z} and width Γ_{Z} of a Breit-Wigner resonance with s-dependent width, used in [4], as follows:

$$m_{\mathrm{Z}} \equiv \overline{m}_{\mathrm{Z}}\sqrt{1+\overline{\Gamma}_{\mathrm{Z}}^2/\overline{m}_{\mathrm{Z}}^2} \approx \overline{m}_{\mathrm{Z}} + 34.20\ \mathrm{MeV}\,, \tag{A.13}$$

$$\Gamma_{\mathrm{Z}} \equiv \overline{\Gamma}_{\mathrm{Z}}\sqrt{1+\overline{\Gamma}_{\mathrm{Z}}^2/\overline{m}_{\mathrm{Z}}^2} \approx \overline{\Gamma}_{\mathrm{Z}} + 0.94\ \mathrm{MeV}\,. \tag{A.14}$$

The predictions of the S-Matrix ansatz for cross-sections and asymmetries are calculated using SMATASY [267], which in turn uses ZFITTER [36] to calculate the QED convolution of the electroweak kernel. In case of the $\mathrm{e^+e^-}$ final state, t-channel and s/t interference contributions are added to the s-channel ansatz [4].

A.3 LEP-I Combination

The LEP experiments have determined the 16 S-Matrix parameters using their full LEP-I data set [268, 269, 270, 271]. These results are averaged using the BLUE technique [62]. Sources of systematic uncertainty correlated between the experiments have been investigated using techniques described in Reference [4] and are accounted for in the averaging procedure.

The main problem in the combination is the proper treatment of the common systematic uncertainties. The LEP experiments provide their results in terms of the standard S-Matrix parametrisation. This parameter set is not well suited for the determination of common systematic uncertainties since common errors such as the theory error for luminosity affect many parameters. Using a transformed parameter set, which is defined as similar as possible to the standard LEP nine parameter set, facilitates the study of common systematic errors as well as cross checks with the LEP nine-parameter combination [4]. The experiments' results are transformed to this parameter set, combined, and the final results transformed back to the standard S-Matrix parameter set. The transformed S-Matrix parameters are defined as follows:

$$S_{\mathrm{had}} \equiv \frac{r^{\mathrm{tot}}_{\mathrm{had}}}{\Gamma^2_{\mathrm{Z}}} \tag{A.15}$$

$$R^{\mathrm{smx}}_{\mathrm{e}} \equiv \frac{r^{\mathrm{tot}}_{\mathrm{had}}}{r^{\mathrm{tot}}_{\mathrm{e}}} \tag{A.16}$$

$$R^{\mathrm{smx}}_{\mu} \equiv \frac{r^{\mathrm{tot}}_{\mathrm{had}}}{r^{\mathrm{tot}}_{\mu}} \tag{A.17}$$

$$R^{\mathrm{smx}}_{\tau} \equiv \frac{r^{\mathrm{tot}}_{\mathrm{had}}}{r^{\mathrm{tot}}_{\tau}} \tag{A.18}$$

$$A^{\mathrm{smx,e}}_{\mathrm{FB}} \equiv \frac{3}{4}\frac{r^{\mathrm{fb}}_{\mathrm{e}}}{r^{\mathrm{tot}}_{\mathrm{e}}} \tag{A.19}$$

$$A^{\mathrm{smx},\mu}_{\mathrm{FB}} \equiv \frac{3}{4}\frac{r^{\mathrm{fb}}_{\mu}}{r^{\mathrm{tot}}_{\mu}} \tag{A.20}$$

$$A^{\mathrm{smx},\tau}_{\mathrm{FB}} \equiv \frac{3}{4}\frac{r^{\mathrm{fb}}_{\tau}}{r^{\mathrm{tot}}_{\tau}} \tag{A.21}$$

Table A.1 gives the input of the four LEP experiments for the 16 transformed S-Matrix parameters. The corresponding correlation matrices are given in Tables A.8, A.9, A.10 and A.11.

Table A.2 shows the common systematic uncertainty of the transformed S-Matrix parameters due to the uncertainties in the LEP centre-of-mass energy. The parameters m_{Z} and $j^{\mathrm{tot}}_{\mathrm{had}}$ are the most sensitive of all 16 S-Matrix parameters to the inclusion of the LEP-II data, and are also the most interesting ones in comparison to the five and nine parameter fits. For these parameters the most significant source of systematic error correlated between experiments arises from the uncertainty on the $\mathrm{e^+e^-}$ centre-of-mass energy. These errors amount to ± 3.2 MeV on m_{Z} and ± 0.16 on $j^{\mathrm{tot}}_{\mathrm{had}}$, with a correlation coefficient of -0.86. Table A.3 specifies the common uncertainties due to theoretical uncertainties in the calculation of the t-channel contributions for Bhabha scattering. In this case the determination of the common error was complicated by the fact that the experiments choose different procedures for the t-channel correction, which yield different common errors. We used the common t-channel errors as determined by ALEPH [4] as basis for the combination since these result in the smallest common errors. As a cross-check the combination was repeated with common t-channel errors based on OPAL's analysis which yields the largest common errors. The effect on the combined result is small, the shift of central values is below 20 % of its uncertainty. In this parametrisation, the luminosity theory uncertainty affects only the parameter S_{had}. The uncertainties are 0.061 % for ALEPH, DELPHI and L3, and 0.054 % for OPAL.

The result of the LEP-I combination in terms of the transformed S-Matrix parameters is listed in Table A.4, Table A.5 shows the corresponding correlation matrix. Transforming this result back to the standard S-Matrix parameter set, the combination is reported in Tables A.6 and A.7. The χ^2/dof for the average of all 16 parameters is 59.8/48, corresponding to a probability of 12%.

A.4 Discussion

In the LEP-I combination the measured values of the Z boson mass $m_{\mathrm{Z}} = 91.1929 \pm 0.0059$ GeV agrees well with the results of the standard nine parameter fit, 91.1876 ± 0.0021 GeV, albeit

with a significantly larger error, resulting from the correlation with the large uncertainty on $j^{\mathrm{tot}}_{\mathrm{had}}$. This uncertainty is the dominant source of uncertainty on m_{Z} in the S-Matrix fits. The measured value of $j^{\mathrm{tot}}_{\mathrm{had}} = -0.10 \pm 0.33$ also agrees with the prediction of the SM, $0.2201^{+0.0032}_{-0.0137}$.

Parameter	ALEPH	DELPHI	L3	OPAL
m_{Z} (GeV)	91.2143 ± 0.0120	91.1939 ± 0.0112	91.1893 ± 0.0112	91.1903 ± 0.0114
Γ_{Z} (GeV)	2.4900 ± 0.0052	2.4861 ± 0.0048	2.5028 ± 0.0046	2.4935 ± 0.0047
S_{had}	0.47736 ± 0.00068	0.47713 ± 0.00080	0.47660 ± 0.00063	0.47629 ± 0.00064
$j^{\mathrm{tot}}_{\mathrm{had}}$	-1.2618 ± 0.6500	-0.2067 ± 0.6364	0.2109 ± 0.6370	0.0017 ± 0.6419
$R^{\mathrm{smx}}_{\mathrm{e}}$	20.8010 ± 0.0830	20.9270 ± 0.1200	20.8528 ± 0.0977	20.9718 ± 0.0945
R^{smx}_{μ}	20.8360 ± 0.0580	20.6600 ± 0.0773	20.8790 ± 0.0982	20.8484 ± 0.0589
R^{smx}_{τ}	20.6860 ± 0.0640	20.8250 ± 0.1277	20.7546 ± 0.1339	20.8255 ± 0.0918
$j^{\mathrm{tot}}_{\mathrm{e}}$	-0.0531 ± 0.0500	-0.0939 ± 0.0750	-0.0293 ± 0.0542	-0.0856 ± 0.0528
j^{tot}_{μ}	-0.0646 ± 0.0430	0.0561 ± 0.0421	0.0355 ± 0.0459	-0.0131 ± 0.0415
j^{tot}_{τ}	-0.0449 ± 0.0440	0.0040 ± 0.0464	0.0729 ± 0.0476	-0.0073 ± 0.0442
$A^{\mathrm{smx,e}}_{\mathrm{FB}}$	0.0164 ± 0.0034	0.0163 ± 0.0048	0.0091 ± 0.0059	0.0071 ± 0.0046
$A^{\mathrm{smx},\mu}_{\mathrm{FB}}$	0.0178 ± 0.0027	0.0145 ± 0.0026	0.0179 ± 0.0034	0.0140 ± 0.0024
$A^{\mathrm{smx},\tau}_{\mathrm{FB}}$	0.0180 ± 0.0030	0.0215 ± 0.0038	0.0238 ± 0.0049	0.0126 ± 0.0031
$j^{\mathrm{fb}}_{\mathrm{e}}$	0.8599 ± 0.0570	0.8021 ± 0.0748	0.6983 ± 0.0797	0.7640 ± 0.0715
j^{fb}_{μ}	0.8196 ± 0.0400	0.7110 ± 0.0366	0.8192 ± 0.0474	0.7319 ± 0.0363
j^{fb}_{τ}	0.8481 ± 0.0430	0.7070 ± 0.0472	0.7536 ± 0.0550	0.7394 ± 0.0420

Table A.1: Transformed LEP-I S-Matrix input parameters of the four LEP experiments

	Parameters									
	1 m_{Z}	2 Γ_{Z}	3 S_{had}	4 $j^{\mathrm{tot}}_{\mathrm{had}}$	5 $R^{\mathrm{smx}}_{\mathrm{e}}$	8 $j^{\mathrm{tot}}_{\mathrm{e}}$	9 j^{tot}_{μ}	10 j^{tot}_{τ}	11 $A^{\mathrm{smx,e}}_{\mathrm{FB}}$	14 $j^{\mathrm{fb}}_{\mathrm{e}}$
1	3.2e-03	-1.4e-03	1.2e-04	-2.1e-02	5.1e-03	-4.4e-03	-4.4e-03	-4.5e-03	-8.3e-04	1.3e-03
2	-1.4e-03	1.4e-03	-3.2e-04	9.2e-03	-3.0e-03	1.8e-03	2.0e-03	2.0e-03	4.4e-04	-6.9e-04
3	1.2e-04	-3.2e-04	1.3e-04	-1.2e-03	9.7e-04	8.4e-05	-2.2e-04	-2.5e-04	-1.2e-04	2.0e-04
4	-2.1e-02	9.2e-03	-1.2e-03	1.6e-01	-3.6e-02	3.3e-02	3.3e-02	3.4e-02	5.7e-03	-9.3e-03
5	5.1e-03	-3.0e-03	9.7e-04	-3.6e-02	1.6e-02	-7.3e-03	-7.5e-03	-7.6e-03	-2.6e-03	3.5e-03
8	-4.4e-03	1.8e-03	8.4e-05	3.3e-02	-7.3e-03	7.0e-03	7.1e-03	7.2e-03	1.2e-03	-1.8e-03
9	-4.4e-03	2.0e-03	-2.2e-04	3.3e-02	-7.5e-03	7.1e-03	7.0e-03	7.2e-03	1.2e-03	-2.0e-03
10	-4.5e-03	2.0e-03	-2.5e-04	3.4e-02	-7.6e-03	7.2e-03	7.2e-03	7.3e-03	1.2e-03	-2.0e-03
11	-8.3e-04	4.4e-04	-1.2e-04	5.7e-03	-2.6e-03	1.2e-03	1.2e-03	1.2e-03	4.3e-04	-5.4e-04
14	1.3e-03	-6.9e-04	2.0e-04	-9.3e-03	3.5e-03	-1.8e-03	-2.0e-03	-2.0e-03	-5.4e-04	1.4e-03

Table A.2: Signed square-root of LEP-I covariance matrix for common energy errors

Parameters		5	8	11	14
5	$R_{\mathrm{e}}^{\mathrm{smx}}$	2.4e-02	-3.20e-03	-5.00e-03	-3.20e-03
8	$j_{\mathrm{e}}^{\mathrm{tot}}$	-3.20e-03	0.89e-02	0.00000	0.99e-02
11	$A_{\mathrm{FB}}^{\mathrm{smx,e}}$	-5.00e-03	0.00000	1.00e-03	-0.32e-03
14	$j_{\mathrm{e}}^{\mathrm{fb}}$	-3.20e-03	0.99e-02	-0.32e-03	1.10e-02

Table A.3: Signed square-root of LEP-I covariance matrix for common t-channel errors

Parameter	LEP-I
m_{Z} (GeV)	91.1929 ± 0.0059
Γ_{Z} (GeV)	2.4940 ± 0.0026
S_{had}	0.47676 ± 0.00043
$j_{\mathrm{had}}^{\mathrm{tot}}$	-0.10 ± 0.33
$R_{\mathrm{e}}^{\mathrm{smx}}$	20.865 ± 0.052
R_{μ}^{smx}	20.811 ± 0.034
R_{τ}^{smx}	20.746 ± 0.045
$j_{\mathrm{e}}^{\mathrm{tot}}$	-0.054 ± 0.029
j_{μ}^{tot}	0.013 ± 0.022
j_{τ}^{tot}	0.014 ± 0.023
$A_{\mathrm{FB}}^{\mathrm{smx,e}}$	0.0132 ± 0.0023
$A_{\mathrm{FB}}^{\mathrm{smx},\mu}$	0.0153 ± 0.0014
$A_{\mathrm{FB}}^{\mathrm{smx},\tau}$	0.0170 ± 0.0017
$j_{\mathrm{e}}^{\mathrm{fb}}$	0.792 ± 0.037
j_{μ}^{fb}	0.763 ± 0.020
j_{τ}^{fb}	0.766 ± 0.023
χ^2/dof	59.96/48

Table A.4: LEP-I combination result for transformed S-Matrix parameters

Parameters																
	1 m_{Z}	2 Γ_{Z}	3 S_{had}	4 $j^{\mathrm{tot}}_{\mathrm{had}}$	5 $R^{\mathrm{smx}}_{\mathrm{e}}$	6 R^{smx}_{μ}	7 R^{smx}_{τ}	8 $j^{\mathrm{tot}}_{\mathrm{e}}$	9 j^{tot}_{μ}	10 j^{tot}_{τ}	11 $A^{\mathrm{smx,e}}_{\mathrm{FB}}$	12 $A^{\mathrm{smx},\mu}_{\mathrm{FB}}$	13 $A^{\mathrm{smx},\tau}_{\mathrm{FB}}$	14 $j^{\mathrm{fb}}_{\mathrm{e}}$	15 j^{fb}_{μ}	16 j^{fb}_{τ}
1	1.000	-0.435	0.083	-0.936	0.330	-0.007	-0.006	-0.597	-0.665	-0.630	-0.128	0.221	0.182	-0.009	-0.006	0.005
2	-0.435	1.000	-0.307	0.442	-0.164	0.006	0.004	0.254	0.319	0.301	0.062	-0.096	-0.079	0.011	0.041	0.030
3	0.083	-0.307	1.000	-0.081	0.134	0.130	0.093	-0.056	-0.065	-0.063	-0.013	0.026	0.022	-0.003	-0.004	-0.002
4	-0.936	0.442	-0.081	1.000	-0.317	0.014	0.011	0.604	0.679	0.645	0.121	-0.221	-0.182	0.010	0.007	-0.004
5	0.330	-0.164	0.134	-0.317	1.000	0.053	0.035	-0.276	-0.228	-0.215	-0.407	0.082	0.067	-0.020	-0.002	0.002
6	-0.007	0.006	0.130	0.014	0.053	1.000	0.059	0.005	-0.128	0.005	0.002	-0.008	-0.002	-0.000	-0.045	-0.000
7	-0.006	0.004	0.093	0.011	0.035	0.059	1.000	0.005	0.005	-0.109	0.002	-0.002	0.000	0.000	-0.000	-0.057
8	-0.597	0.254	-0.056	0.604	-0.276	0.005	0.005	1.000	0.433	0.408	0.084	-0.148	-0.123	0.221	0.003	-0.004
9	-0.665	0.319	-0.065	0.679	-0.228	-0.128	0.005	0.433	1.000	0.460	0.086	-0.137	-0.131	0.007	-0.034	-0.003
10	-0.630	0.301	-0.063	0.645	-0.215	0.005	-0.109	0.408	0.460	1.000	0.081	-0.150	-0.107	0.007	0.005	-0.046
11	-0.128	0.062	-0.013	0.121	-0.407	0.002	0.002	0.084	0.086	0.081	1.000	-0.024	-0.019	0.092	0.001	-0.001
12	0.221	-0.096	0.026	-0.221	0.082	-0.008	-0.002	-0.148	-0.137	-0.150	-0.024	1.000	0.061	-0.005	0.198	0.002
13	0.182	-0.079	0.022	-0.182	0.067	-0.002	0.000	-0.123	-0.131	-0.107	-0.019	0.061	1.000	-0.004	-0.001	0.181
14	-0.009	0.011	-0.003	0.010	-0.020	-0.000	0.000	0.221	0.007	0.007	0.092	-0.005	-0.004	1.000	0.001	0.000
15	-0.006	0.041	-0.004	0.007	-0.002	-0.045	-0.000	0.003	-0.034	0.005	0.001	0.198	-0.001	0.001	1.000	0.002
16	0.005	0.030	-0.002	-0.004	0.002	-0.000	-0.057	-0.004	-0.003	-0.046	-0.001	0.002	0.181	0.000	0.002	1.000

Table A.5: Correlation matrix for transformed LEP-I S-Matrix parameters

Parameter	LEP-I
m_{Z} (GeV)	91.1929 ± 0.0059
Γ_{Z} (GeV)	2.4940 ± 0.0026
$r^{\mathrm{tot}}_{\mathrm{had}}$	2.9654 ± 0.0060
$j^{\mathrm{tot}}_{\mathrm{had}}$	-0.10 ± 0.33
$r^{\mathrm{tot}}_{\mathrm{e}}$	0.14214 ± 0.00049
r^{tot}_{μ}	0.14249 ± 0.00036
r^{tot}_{τ}	0.14294 ± 0.00042
$j^{\mathrm{tot}}_{\mathrm{e}}$	-0.054 ± 0.029
j^{tot}_{μ}	0.013 ± 0.022
j^{tot}_{τ}	0.014 ± 0.023
$r^{\mathrm{fb}}_{\mathrm{e}}$	0.00251 ± 0.00045
r^{fb}_{μ}	0.00291 ± 0.00026
r^{fb}_{τ}	0.00324 ± 0.00033
$j^{\mathrm{fb}}_{\mathrm{e}}$	0.792 ± 0.036
j^{fb}_{μ}	0.763 ± 0.020
j^{fb}_{τ}	0.766 ± 0.023
χ^2/dof	59.84/48

Table A.6: LEP-I combination result for standard S-Matrix parameters

Parameters																
	1	2	3	4	5	6	7	8	9	10	11	12	13	14	15	16
	m_{Z}	Γ_{Z}	$r_{\mathrm{had}}^{\mathrm{tot}}$	$j_{\mathrm{had}}^{\mathrm{tot}}$	$r_{\mathrm{e}}^{\mathrm{tot}}$	r_{μ}^{tot}	r_{τ}^{tot}	$j_{\mathrm{e}}^{\mathrm{tot}}$	j_{μ}^{tot}	j_{τ}^{tot}	$r_{\mathrm{e}}^{\mathrm{fb}}$	r_{μ}^{fb}	r_{τ}^{fb}	$j_{\mathrm{e}}^{\mathrm{fb}}$	j_{μ}^{fb}	j_{τ}^{fb}
1	1.000	-0.434	-0.416	-0.936	-0.493	-0.330	-0.285	-0.597	-0.664	-0.630	-0.138	0.212	0.174	-0.008	-0.006	0.005
2	-0.434	1.000	0.905	0.441	0.660	0.725	0.628	0.254	0.319	0.300	0.076	-0.075	-0.060	0.012	0.041	0.030
3	-0.416	0.905	1.000	0.424	0.678	0.764	0.663	0.240	0.303	0.285	0.073	-0.066	-0.053	0.011	0.041	0.031
4	-0.936	0.441	0.424	1.000	0.488	0.332	0.287	0.605	0.678	0.645	0.131	-0.212	-0.174	0.009	0.007	-0.004
5	-0.493	0.660	0.678	0.488	1.000	0.546	0.472	0.347	0.349	0.329	0.356	-0.098	-0.079	0.022	0.026	0.017
6	-0.330	0.725	0.764	0.332	0.546	1.000	0.534	0.190	0.327	0.226	0.058	-0.037	-0.041	0.009	0.062	0.025
7	-0.285	0.628	0.663	0.287	0.472	0.534	1.000	0.163	0.207	0.280	0.049	-0.045	-0.021	0.007	0.028	0.064
8	-0.597	0.254	0.240	0.605	0.347	0.190	0.163	1.000	0.433	0.408	0.091	-0.143	-0.118	0.219	0.003	-0.004
9	-0.664	0.319	0.303	0.678	0.349	0.327	0.207	0.433	1.000	0.460	0.093	-0.128	-0.125	0.007	-0.034	-0.003
10	-0.630	0.300	0.285	0.645	0.329	0.226	0.280	0.408	0.460	1.000	0.087	-0.143	-0.099	0.007	0.005	-0.046
11	-0.138	0.076	0.073	0.131	0.356	0.058	0.049	0.091	0.093	0.087	1.000	-0.025	-0.020	0.093	0.001	-0.000
12	0.212	-0.075	-0.066	-0.212	-0.098	-0.037	-0.045	-0.143	-0.128	-0.143	-0.025	1.000	0.059	-0.005	0.200	0.003
13	0.174	-0.060	-0.053	-0.174	-0.079	-0.041	-0.021	-0.118	-0.125	-0.099	-0.020	0.059	1.000	-0.004	0.000	0.183
14	-0.008	0.012	0.011	0.009	0.022	0.009	0.007	0.219	0.007	0.007	0.093	-0.005	-0.004	1.000	0.001	0.000
15	-0.006	0.041	0.041	0.007	0.026	0.062	0.028	0.003	-0.034	0.005	0.001	0.200	0.000	0.001	1.000	0.002
16	0.005	0.030	0.031	-0.004	0.017	0.025	0.064	-0.004	-0.003	-0.046	-0.000	0.003	0.183	0.000	0.002	1.000

Table A.7: Correlation matrix for standard LEP-I S-Matrix parameters

A.5 S-Matrix Combination Tables

Parameters																
	1 m_{Z}	2 Γ_{Z}	3 S_{had}	4 $j_{\mathrm{had}}^{\mathrm{tot}}$	5 $R_{\mathrm{e}}^{\mathrm{smx}}$	6 R_{μ}^{smx}	7 R_{τ}^{smx}	8 $j_{\mathrm{e}}^{\mathrm{tot}}$	9 j_{μ}^{tot}	10 j_{τ}^{tot}	11 $A_{\mathrm{FB}}^{\mathrm{smx,e}}$	12 $A_{\mathrm{FB}}^{\mathrm{smx},\mu}$	13 $A_{\mathrm{FB}}^{\mathrm{smx},\tau}$	14 $j_{\mathrm{e}}^{\mathrm{fb}}$	15 j_{μ}^{fb}	16 j_{τ}^{fb}
1	1.000	-0.537	0.243	-0.963	0.449	-0.004	-0.015	-0.592	-0.685	-0.676	-0.209	0.313	0.296	0.005	-0.023	0.003
2	-0.537	1.000	-0.436	0.547	-0.234	0.008	0.008	0.324	0.391	0.385	0.106	-0.169	-0.160	0.014	0.056	0.040
3	0.243	-0.436	1.000	-0.225	0.219	0.160	0.143	-0.144	-0.171	-0.168	-0.041	0.087	0.082	0.000	-0.012	-0.005
4	-0.963	0.547	-0.225	1.000	-0.426	0.011	0.021	0.593	0.685	0.676	0.197	-0.307	-0.290	-0.003	0.024	-0.002
5	0.449	-0.234	0.219	-0.426	1.000	0.070	0.051	-0.400	-0.307	-0.301	-0.413	0.139	0.131	-0.047	-0.011	0.001
6	-0.004	0.008	0.160	0.011	0.070	1.000	0.089	0.002	-0.171	0.003	0.001	-0.008	-0.001	-0.001	-0.036	0.000
7	-0.015	0.008	0.143	0.021	0.051	0.089	1.000	0.011	0.011	-0.142	0.003	-0.005	-0.007	0.000	0.000	-0.038
8	-0.592	0.324	-0.144	0.593	-0.400	0.002	0.011	1.000	0.422	0.411	0.133	-0.189	-0.179	0.159	0.014	-0.002
9	-0.685	0.391	-0.171	0.685	-0.307	-0.171	0.011	0.422	1.000	0.481	0.141	-0.198	-0.206	-0.002	-0.015	-0.002
10	-0.676	0.385	-0.168	0.676	-0.301	0.003	-0.142	0.411	0.481	1.000	0.139	-0.215	-0.193	-0.002	0.017	-0.050
11	-0.209	0.106	-0.041	0.197	-0.413	0.001	0.003	0.133	0.141	0.139	1.000	-0.055	-0.053	0.159	0.005	0.000
12	0.313	-0.169	0.087	-0.307	0.139	-0.008	-0.005	-0.189	-0.198	-0.215	-0.055	1.000	0.105	0.000	0.231	0.002
13	0.296	-0.160	0.082	-0.290	0.131	-0.001	-0.007	-0.179	-0.206	-0.193	-0.053	0.105	1.000	0.000	-0.006	0.202
14	0.005	0.014	0.000	-0.003	-0.047	-0.001	0.000	0.159	-0.002	-0.002	0.159	0.000	0.000	1.000	0.001	0.001
15	-0.023	0.056	-0.012	0.024	-0.011	-0.036	0.000	0.014	-0.015	0.017	0.005	0.231	-0.006	0.001	1.000	0.003
16	0.003	0.040	-0.005	-0.002	0.001	0.000	-0.038	-0.002	-0.002	-0.050	0.000	0.002	0.202	0.001	0.003	1.000

Table A.8: Correlation matrix of transformed LEP-I S-Matrix input parameters for ALEPH.

Parameters																
	1 m_{Z}	2 Γ_{Z}	3 S_{had}	4 $j_{\mathrm{had}}^{\mathrm{tot}}$	5 $R_{\mathrm{e}}^{\mathrm{smx}}$	6 R_{μ}^{smx}	7 R_{τ}^{smx}	8 $j_{\mathrm{e}}^{\mathrm{tot}}$	9 j_{μ}^{tot}	10 j_{τ}^{tot}	11 $A_{\mathrm{FB}}^{\mathrm{smx,e}}$	12 $A_{\mathrm{FB}}^{\mathrm{smx},\mu}$	13 $A_{\mathrm{FB}}^{\mathrm{smx},\tau}$	14 $j_{\mathrm{e}}^{\mathrm{fb}}$	15 j_{μ}^{fb}	16 j_{τ}^{fb}
1	1.000	-0.504	0.123	-0.966	0.034	-0.030	0.002	-0.804	-0.702	-0.640	0.133	0.253	0.173	-0.029	-0.002	-0.003
2	-0.504	1.000	-0.285	0.528	-0.018	0.008	-0.004	0.403	0.385	0.350	-0.069	-0.125	-0.086	0.040	0.043	0.034
3	0.123	-0.285	1.000	-0.112	0.124	0.185	0.113	-0.098	-0.092	-0.085	0.018	0.033	0.022	-0.003	0.003	0.002
4	-0.966	0.528	-0.112	1.000	-0.027	0.037	0.002	0.786	0.695	0.634	-0.131	-0.247	-0.169	0.030	0.004	0.005
5	0.034	-0.018	0.124	-0.027	1.000	0.053	0.033	-0.061	-0.023	-0.021	-0.100	0.009	0.006	-0.066	-0.000	-0.000
6	-0.030	0.008	0.185	0.037	0.053	1.000	0.051	0.025	-0.086	0.019	-0.005	-0.013	-0.006	0.001	-0.056	-0.000
7	0.002	-0.004	0.113	0.002	0.033	0.051	1.000	-0.002	-0.001	-0.089	0.000	0.000	-0.002	-0.000	-0.000	-0.079
8	-0.804	0.403	-0.098	0.786	-0.061	0.025	-0.002	1.000	0.571	0.521	-0.081	-0.205	-0.140	0.102	0.001	0.003
9	-0.702	0.385	-0.092	0.695	-0.023	-0.086	-0.001	0.571	1.000	0.461	-0.095	-0.158	-0.123	0.022	-0.038	0.004
10	-0.640	0.350	-0.085	0.634	-0.021	0.019	-0.089	0.521	0.461	1.000	-0.086	-0.164	-0.090	0.020	0.003	-0.035
11	0.133	-0.069	0.018	-0.131	-0.100	-0.005	0.000	-0.081	-0.095	-0.086	1.000	0.044	0.029	0.087	0.001	-0.000
12	0.253	-0.125	0.033	-0.247	0.009	-0.013	0.000	-0.205	-0.158	-0.164	0.044	1.000	0.053	-0.008	0.196	-0.000
13	0.173	-0.086	0.022	-0.169	0.006	-0.006	-0.002	-0.140	-0.123	-0.090	0.029	0.053	1.000	-0.005	0.001	0.176
14	-0.029	0.040	-0.003	0.030	-0.066	0.001	-0.000	0.102	0.022	0.020	0.087	-0.008	-0.005	1.000	0.002	0.001
15	-0.002	0.043	0.003	0.004	-0.000	-0.056	-0.000	0.001	-0.038	0.003	0.001	0.196	0.001	0.002	1.000	0.002
16	-0.003	0.034	0.002	0.005	-0.000	-0.000	-0.079	0.003	0.004	-0.035	-0.000	-0.000	0.176	0.001	0.002	1.000

Table A.9: Correlation matrix of transformed LEP-I S-Matrix input parameters for DELPHI.

Parameters																
	1 m_{Z}	2 Γ_{Z}	3 S_{had}	4 $j^{\mathrm{tot}}_{\mathrm{had}}$	5 $R^{\mathrm{smx}}_{\mathrm{e}}$	6 R^{smx}_{μ}	7 R^{smx}_{τ}	8 $j^{\mathrm{tot}}_{\mathrm{e}}$	9 j^{tot}_{μ}	10 j^{tot}_{τ}	11 $A^{\mathrm{smx,e}}_{\mathrm{FB}}$	12 $A^{\mathrm{smx},\mu}_{\mathrm{FB}}$	13 $A^{\mathrm{smx},\tau}_{\mathrm{FB}}$	14 $j^{\mathrm{fb}}_{\mathrm{e}}$	15 j^{fb}_{μ}	16 j^{fb}_{τ}
1	1.000	-0.378	0.024	-0.959	0.418	-0.010	-0.013	-0.528	-0.627	-0.600	-0.200	0.226	0.150	0.011	-0.006	0.008
2	-0.378	1.000	-0.331	0.410	-0.165	0.002	0.006	0.196	0.271	0.262	0.076	-0.087	-0.057	-0.009	0.042	0.028
3	0.024	-0.331	1.000	-0.020	0.076	0.079	0.055	-0.029	-0.025	-0.025	0.010	0.011	0.007	-0.008	-0.002	-0.001
4	-0.959	0.410	-0.020	1.000	-0.403	0.015	0.017	0.528	0.627	0.600	0.195	-0.220	-0.146	-0.009	0.007	-0.006
5	0.418	-0.165	0.076	-0.403	1.000	0.024	0.016	-0.274	-0.267	-0.256	-0.202	0.107	0.070	0.027	-0.003	0.003
6	-0.010	0.002	0.079	0.015	0.024	1.000	0.021	0.006	-0.104	0.006	0.002	-0.007	-0.002	0.000	-0.068	-0.001
7	-0.013	0.006	0.055	0.017	0.016	0.021	1.000	0.007	0.008	-0.078	0.002	-0.003	-0.004	0.000	-0.000	-0.080
8	-0.528	0.196	-0.029	0.528	-0.274	0.006	0.007	1.000	0.346	0.331	0.097	-0.121	-0.080	0.166	0.002	-0.005
9	-0.627	0.271	-0.025	0.627	-0.267	-0.104	0.008	0.346	1.000	0.393	0.127	-0.119	-0.096	-0.006	-0.041	-0.004
10	-0.600	0.262	-0.025	0.600	-0.256	0.006	-0.078	0.331	0.393	1.000	0.122	-0.138	-0.075	-0.006	0.005	-0.039
11	-0.200	0.076	0.010	0.195	-0.202	0.002	0.002	0.097	0.127	0.122	1.000	-0.051	-0.034	0.026	0.001	-0.002
12	0.226	-0.087	0.011	-0.220	0.107	-0.007	-0.003	-0.121	-0.119	-0.138	-0.051	1.000	0.038	0.003	0.170	0.002
13	0.150	-0.057	0.007	-0.146	0.070	-0.002	-0.004	-0.080	-0.096	-0.075	-0.034	0.038	1.000	0.002	-0.001	0.150
14	0.011	-0.009	-0.008	-0.009	0.027	0.000	0.000	0.166	-0.006	-0.006	0.026	0.003	0.002	1.000	-0.001	-0.000
15	-0.006	0.042	-0.002	0.007	-0.003	-0.068	-0.000	0.002	-0.041	0.005	0.001	0.170	-0.001	-0.001	1.000	0.002
16	0.008	0.028	-0.001	-0.006	0.003	-0.001	-0.080	-0.005	-0.004	-0.039	-0.002	0.002	0.150	-0.000	0.002	1.000

Table A.10: Correlation matrix of transformed LEP-I S-Matrix input parameters for L3.

Parameters																
	1 m_{Z}	2 Γ_{Z}	3 S_{had}	4 $j_{\mathrm{had}}^{\mathrm{tot}}$	5 $R_{\mathrm{e}}^{\mathrm{smx}}$	6 R_{μ}^{smx}	7 R_{τ}^{smx}	8 $j_{\mathrm{e}}^{\mathrm{tot}}$	9 j_{μ}^{tot}	10 j_{τ}^{tot}	11 $A_{\mathrm{FB}}^{\mathrm{smx,e}}$	12 $A_{\mathrm{FB}}^{\mathrm{smx},\mu}$	13 $A_{\mathrm{FB}}^{\mathrm{smx},\tau}$	14 $j_{\mathrm{e}}^{\mathrm{fb}}$	15 j_{μ}^{fb}	16 j_{τ}^{fb}
1	1.000	-0.446	0.120	-0.963	0.442	0.012	0.013	-0.525	-0.703	-0.651	-0.244	0.299	0.262	0.025	0.001	0.013
2	-0.446	1.000	-0.360	0.462	-0.194	0.008	0.001	0.224	0.338	0.315	0.110	-0.131	-0.114	-0.012	0.043	0.032
3	0.120	-0.360	1.000	-0.110	0.188	0.221	0.141	-0.067	-0.090	-0.084	-0.018	0.039	0.037	-0.002	-0.007	-0.004
4	-0.963	0.462	-0.110	1.000	-0.428	-0.005	-0.009	0.525	0.701	0.650	0.239	-0.293	-0.256	-0.024	0.000	-0.012
5	0.442	-0.194	0.188	-0.428	1.000	0.085	0.043	-0.278	-0.315	-0.292	-0.298	0.151	0.131	0.023	0.001	0.008
6	0.012	0.008	0.221	-0.005	0.085	1.000	0.056	-0.006	-0.133	-0.007	-0.004	-0.002	0.004	0.001	-0.037	0.002
7	0.013	0.001	0.141	-0.009	0.043	0.056	1.000	-0.008	-0.009	-0.100	-0.003	0.004	0.017	-0.000	0.001	-0.060
8	-0.525	0.224	-0.067	0.525	-0.278	-0.006	-0.008	1.000	0.383	0.354	0.125	-0.160	-0.140	0.218	-0.002	-0.008
9	-0.703	0.338	-0.090	0.701	-0.315	-0.133	-0.009	0.383	1.000	0.473	0.174	-0.193	-0.187	-0.017	-0.041	-0.009
10	-0.651	0.315	-0.084	0.650	-0.292	-0.007	-0.100	0.354	0.473	1.000	0.161	-0.198	-0.157	-0.016	0.001	-0.056
11	-0.244	0.110	-0.018	0.239	-0.298	-0.004	-0.003	0.125	0.174	0.161	1.000	-0.083	-0.072	0.056	-0.000	-0.004
12	0.299	-0.131	0.039	-0.293	0.151	-0.002	0.004	-0.160	-0.193	-0.198	-0.083	1.000	0.090	0.008	0.179	0.005
13	0.262	-0.114	0.037	-0.256	0.131	0.004	0.017	-0.140	-0.187	-0.157	-0.072	0.090	1.000	0.007	0.001	0.175
14	0.025	-0.012	-0.002	-0.024	0.023	0.001	-0.000	0.218	-0.017	-0.016	0.056	0.008	0.007	1.000	-0.000	0.000
15	0.001	0.043	-0.007	0.000	0.001	-0.037	0.001	-0.002	-0.041	0.001	-0.000	0.179	0.001	-0.000	1.000	0.002
16	0.013	0.032	-0.004	-0.012	0.008	0.002	-0.060	-0.008	-0.009	-0.056	-0.004	0.005	0.175	0.000	0.002	1.000

Table A.11: Correlation matrix of transformed LEP-I S-Matrix input parameters for OPAL.

Appendix B

Two-Fermion Combination Details

B.1 Input Measurements

In this Section, the experimental measurements of total cross-sections and forward-backward asymmetries as used in the combination are reported. For each result, the ZFITTER prediction, followed by the measured value and the six error components as described in Section 3.2, are listed. The results are extrapolated to 4π acceptance ($|\cos\theta| \leq 1$) except for ALEPH ($|\cos\theta| < 0.95$).

ALEPH

ALEPH results at 130 GeV

```
* E_CM = 130.200 GeV
*
XSEC_QQ       71.15    71.6    3.8     0.64      0.82      0.29     0.19  0.22
XSEC_MUMU      6.987    7.9    1.22    0.041     0.008     0.04     0.02  0.077
XSEC_TAUTAU    7.234   10.9    1.79    0.152     0.22      0.29     0.03  0.137
AFB_MUMU       0.698    0.83   0.09    0.004     0.026     0.004    0.0   0.01
AFB_TAUTAU     0.697    0.56   0.12    0.011     0.035     0.004    0.0   0.01
```

ALEPH results at 136 GeV

```
* E_CM = 136.200 GeV
*
XSEC_QQ       57.64     58.8    3.5     0.53      0.67      0.23     0.15  0.18
XSEC_MUMU      6.053     6.9    1.1     0.04      0.007     0.034    0.02  0.076
XSEC_TAUTAU    6.267     5.6    1.3     0.073     0.11      0.15     0.01  0.1
AFB_MUMU       0.678     0.63   0.105   0.004     0.024     0.004    0.0   0.01
AFB_TAUTAU     0.677     0.65   0.14    0.009     0.028     0.004    0.0   0.012
```

ALEPH results at 161 GeV

```
* E_CM = 161.314 GeV
*
XSEC_QQ       30.88     29.9    1.8     0.21      0.29      0.16     0.08  0.09
XSEC_MUMU      3.857     4.5    0.69    0.03      0.008     0.027    0.01  0.06
XSEC_TAUTAU    3.992     5.75   0.94    0.08      0.13      0.17     0.01  0.17
AFB_MUMU       0.609     0.63   0.11    0.004     0.026     0.004    0.0   0.009
AFB_TAUTAU     0.608     0.48   0.14    0.009     0.029     0.004    0.0   0.008
```

ALEPH results at 172 GeV

```
* E_CM = 172.086 GeV
*
XSEC_QQ       25.22    26.4    1.7     0.18      0.30      0.18     0.06  0.08
XSEC_MUMU      3.30     2.64   0.53    0.042     0.008     0.021    0.006 0.04
XSEC_TAUTAU    3.415    3.26   0.74    0.04      0.07      0.04     0.008 0.07
AFB_MUMU       0.593    0.72   0.14    0.005     0.034     0.005    0.0   0.01
AFB_TAUTAU     0.592    0.44   0.16    0.009     0.029     0.004    0.0   0.01
```

ALEPH results at 183 GeV

```
* E_CM = 183.00  GeV
*
XSEC_QQ       21.24    21.71   0.70    0.13      0.12    0.126   0.06   0.07
XSEC_MUMU      2.871    2.98   0.24    0.045     0.004   0.019   0.012  0.05
XSEC_TAUTAU    2.974    2.90   0.29    0.048     0.067   0.011   0.012  0.06
AFB_MUMU       0.579    0.54   0.06    0.02      0.01    0.004   0.0    0.008
AFB_TAUTAU     0.579    0.52   0.08    0.03      0.02    0.004   0.0    0.009
```

ALEPH results at 189 GeV

```
* E_CM = 189 GeV
*
XSEC_QQ       20.580  20.800   0.380   0.156  0.108  0.021  0.052  0.021
XSEC_MUMU      2.831   2.879   0.134   0.007  0.014  0.000  0.007  0.004
XSEC_TAUTAU    2.910   2.787   0.198   0.020  0.014  0.000  0.007  0.020
AFB_MUMU       0.570   0.576   0.036   0.001  0.000  0.000  0.000  0.009
AFB_TAUTAU     0.570   0.598   0.046   0.007  0.000  0.000  0.000  0.010
```

ALEPH results at 192 GeV

```
* E_CM = 192 GeV
*
XSEC_QQ       19.720   20.070  0.920   0.151  0.111  0.020  0.050  0.040
XSEC_MUMU      2.729   2.862   0.333   0.008  0.013  0.000  0.004  0.004
XSEC_TAUTAU    2.811   2.600   0.467   0.062  0.011  0.000  0.003  0.020
AFB_MUMU       0.567   0.580   0.088   0.001  0.000  0.000  0.000  0.009
AFB_TAUTAU     0.567   0.490   0.124   0.006  0.000  0.000  0.000  0.009
```

ALEPH results at 196 GeV

```
* E_CM = 196 GeV
*
XSEC_QQ       18.670  18.930   0.540   0.144  0.115  0.015  0.047  0.038
XSEC_MUMU      2.611   2.704   0.193   0.014  0.012  0.000  0.003  0.004
XSEC_TAUTAU    2.69    2.551   0.289   0.012  0.012  0.000  0.003  0.020
AFB_MUMU       0.563   0.553   0.057   0.001  0.000  0.000  0.000  0.006
AFB_TAUTAU     0.563   0.543   0.075   0.007  0.000  0.000  0.000  0.010
```

ALEPH results at 200 GeV

```
* E_CM = 200 GeV
*
XSEC_QQ       17.690  17.940   0.510   0.138  0.113  0.014  0.045  0.036
XSEC_MUMU      2.502   2.991   0.195   0.015  0.012  0.000  0.004  0.005
XSEC_TAUTAU    2.571   2.881   0.293   0.012  0.012  0.000  0.003  0.021
AFB_MUMU       0.560   0.442   0.056   0.003  0.000  0.000  0.000  0.006
AFB_TAUTAU     0.560   0.445   0.073   0.005  0.000  0.000  0.000  0.009
```

ALEPH results at 202 GeV

```
*E_CM = 202 GeV
*
XSEC_QQ       17.210  17.560   0.710   0.137  0.133  0.012  0.044  0.035
XSEC_MUMU      2.442   2.639   0.262   0.015  0.011  0.000  0.003  0.005
XSEC_TAUTAU    2.512   2.832   0.411   0.012  0.011  0.000  0.003  0.021
AFB_MUMU       0.558   0.573   0.078   0.001  0.000  0.000  0.000  0.010
AFB_TAUTAU     0.557   0.654   0.090   0.008  0.000  0.000  0.000  0.012
```

ALEPH results at 205 GeV

```
*E_CM = 205 GeV
*
XSEC_QQ       16.510  16.940   0.520   0.129  0.100  0.012  0.042  0.034
XSEC_MUMU      2.358   1.918   0.162   0.014  0.011  0.000  0.003  0.005
XSEC_TAUTAU    2.434   2.430   0.290   0.016  0.010  0.000  0.003  0.020
AFB_MUMU       0.555   0.572   0.066   0.003  0.000  0.000  0.000  0.008
AFB_TAUTAU     0.555   0.593   0.075   0.007  0.000  0.000  0.000  0.011
```

ALEPH results at 207 GeV

```
*E_CM = 207 GeV
*
XSEC_QQ       16.160  16.340   0.380   0.124  0.087  0.011  0.041  0.033
XSEC_MUMU      2.318   2.458   0.143   0.014  0.010  0.000  0.003  0.005
XSEC_TAUTAU    2.383   2.101   0.212   0.015  0.010  0.000  0.003  0.021
AFB_MUMU       0.554   0.572   0.066   0.001  0.000  0.000  0.000  0.009
AFB_TAUTAU     0.554   0.568   0.062   0.007  0.000  0.000  0.000  0.011
```

DELPHI

DELPHI results at 130 GeV

```
* Centre-of-mass energy used: 130.200 GeV
*
XSEC_QQ       82.506   82.400   5.200   0.411     0.296     0.000    0.098  2.509
XSEC_MUMU      8.107    9.700   1.900   0.015     0.000     0.000    0.000  0.359
XSEC_TAUTAU    8.312   10.200   3.100   0.009     0.037     0.000    0.012  0.714
AFB_MUMU       0.719    0.670   0.150   0.000     0.000     0.000    0.000  0.003
AFB_TAUTAU     0.719    0.730   0.170   0.000     0.000     0.000    0.000  0.020
```

DELPHI results at 136 GeV

```
* Centre-of-mass energy used: 136.20 GeV
*
XSEC_QQ       66.362   65.300   4.700   0.326     0.241     0.000    0.078  2.010
XSEC_MUMU      6.997    6.600   1.600   0.010     0.000     0.000    0.000  0.244
XSEC_TAUTAU    7.173    8.800   3.000   0.008     0.033     0.000    0.011  0.616
```

```
AFB_MUMU        0.699    0.740   0.160   0.000     0.000     0.000     0.000  0.003
AFB_TAUTAU      0.699    0.490   0.230   0.000     0.000     0.000     0.000  0.020
```

DELPHI results at 161 GeV

```
* Centre-of-mass energy used: 161.30 GeV
*
XSEC_QQ        35.119   41.000   2.100   0.215     0.162     0.000     0.051  1.223
XSEC_MUMU       4.426    3.600   0.700   0.019     0.000     0.000     0.000  0.126
XSEC_TAUTAU     4.538    5.100   1.200   0.025     0.016     0.000     0.006  0.357
AFB_MUMU        0.629    0.430   0.160   0.000     0.000     0.000     0.000  0.003
AFB_TAUTAU      0.628    0.920   0.080   0.000     0.000     0.000     0.000  0.020
```

DELPHI results at 172 GeV

```
* Centre-of-mass energy used: 172.10 GeV
*
XSEC_QQ        28.745   30.400   1.900   0.176     0.159     0.000     0.042  0.932
XSEC_MUMU       3.790    3.600   0.700   0.019     0.000     0.000     0.000  0.122
XSEC_TAUTAU     3.886    4.500   1.100   0.023     0.020     0.000     0.005  0.315
AFB_MUMU        0.610    0.940   0.140   0.000     0.000     0.000     0.000  0.003
AFB_TAUTAU      0.610    0.130   0.200   0.000     0.000     0.000     0.000  0.020
```

DELPHI results at 183 GeV

```
* Centre-of-mass energy used: 182.65 GeV
*
XSEC_QQ        24.154   25.500   0.796   0.272     0.057     0.026     0.137  0.056
XSEC_MUMU       3.304    3.605   0.284   0.027     0.000     0.000     0.000  0.011
XSEC_TAUTAU     3.387    3.292   0.376   0.071     0.006     0.011     0.013  0.000
AFB_MUMU        0.596    0.588   0.064   0.001     0.000     0.000     0.000  0.001
AFB_TAUTAU      0.596    0.671   0.080   0.011     0.000     0.002     0.002  0.000
```

DELPHI results at 189 GeV

```
* Centre-of-mass energy used: 188.63 GeV
*
XSEC_QQ        22.099   22.630   0.452   0.257     0.034     0.023     0.136  0.040
XSEC_MUMU       3.072    3.071   0.150   0.023     0.000     0.000     0.000  0.008
XSEC_TAUTAU     3.150    3.105   0.215   0.065     0.003     0.011     0.013  0.000
AFB_MUMU        0.589    0.600   0.039   0.001     0.000     0.000     0.000  0.001
AFB_TAUTAU      0.589    0.697   0.048   0.011     0.000     0.002     0.002  0.000
```

DELPHI results at 192 GeV

```
* Centre-of-mass energy used: 191.58 GeV
*
XSEC_QQ        21.191   22.140   1.119   0.255     0.098     0.022     0.136  0.072
XSEC_MUMU       2.967    2.822   0.357   0.021     0.000     0.000     0.000  0.006
```

```
XSEC_TAUTAU     3.042    2.497   0.479   0.053     0.007     0.008    0.011  0.000
AFB_MUMU        0.586    0.636   0.098   0.001     0.000     0.000    0.000  0.001
AFB_TAUTAU      0.586    0.578   0.150   0.011     0.000     0.002    0.002  0.000
```

DELPHI results at 196 GeV

```
* Centre-of-mass energy used: 195.51 GeV
*
XSEC_QQ        20.075   21.180   0.634   0.249     0.058     0.021    0.136  0.053
XSEC_MUMU       2.837    2.763   0.207   0.020     0.000     0.000    0.000  0.006
XSEC_TAUTAU     2.908    2.895   0.301   0.062     0.006     0.010    0.012  0.000
AFB_MUMU        0.582    0.586   0.061   0.001     0.000     0.000    0.000  0.000
AFB_TAUTAU      0.582    0.465   0.083   0.011     0.000     0.002    0.002  0.000
```

DELPHI results at 200 GeV

```
* Centre-of-mass energy used: 199.51 GeV
*
XSEC_QQ        19.035   19.450   0.591   0.240     0.054     0.020    0.135  0.051
XSEC_MUMU       2.713    3.080   0.207   0.023     0.000     0.000    0.000  0.007
XSEC_TAUTAU     2.781    2.614   0.270   0.056     0.005     0.009    0.011  0.000
AFB_MUMU        0.578    0.548   0.056   0.001     0.000     0.000    0.000  0.000
AFB_TAUTAU      0.578    0.540   0.080   0.011     0.000     0.002    0.002  0.000
```

DELPHI results at 202 GeV

```
* Centre-of-mass energy used: 201.64 GeV
*
XSEC_QQ        18.517   18.880   0.843   0.237     0.077     0.019    0.135  0.066
XSEC_MUMU       2.650    2.464   0.268   0.018     0.000     0.000    0.000  0.005
XSEC_TAUTAU     2.717    2.550   0.380   0.054     0.007     0.009    0.011  0.000
AFB_MUMU        0.577    0.544   0.090   0.001     0.000     0.000    0.000  0.001
AFB_TAUTAU      0.576    0.464   0.122   0.011     0.000     0.002    0.002  0.000
```

DELPHI results at 205 GeV

```
* Centre-of-mass energy used: 204.87 GeV
*
XSEC_QQ        17.775   17.670   0.580   0.230     0.053     0.018    0.135  0.042
XSEC_MUMU       2.560    2.345   0.188   0.017     0.000     0.000    0.000  0.005
XSEC_TAUTAU     2.625    2.803   0.282   0.059     0.006     0.010    0.012  0.000
AFB_MUMU        0.574    0.642   0.061   0.001     0.000     0.000    0.000  0.001
AFB_TAUTAU      0.574    0.709   0.068   0.011     0.000     0.002    0.002  0.000
```

DELPHI results at 207 GeV

```
* Centre-of-mass energy used: 206.55 GeV
*
XSEC_QQ        17.408   17.040   0.444   0.228     0.040     0.017    0.135  0.033
```

XSEC_MUMU	2.515	2.475	0.145	0.018	0.000	0.000	0.000	0.004
XSEC_TAUTAU	2.578	2.534	0.210	0.055	0.004	0.009	0.011	0.000
AFB_MUMU	0.573	0.558	0.048	0.001	0.000	0.000	0.000	0.001
AFB_TAUTAU	0.572	0.666	0.059	0.011	0.000	0.002	0.002	0.000

L3

L3 results at 130 GeV

```
* Exact centre-of-mass energy: 130.0  GeV
*
```

XSEC_QQ	83.5	84.2	4.4	0.96	0.05	0.27	0.03	0.0
XSEC_MUMU	8.5	8.2	1.4	0.200	0.006	0.012	0.004	0.0
XSEC_TAUTAU	8.5	9.8	1.9	0.300	0.006	0.010	0.004	0.0
AFB_MUMU	0.707	0.67	0.11	0.020	0.0	0.004	0.0	0.0
AFB_TAUTAU	0.707	0.78	0.16	0.020	0.0	0.004	0.0	0.0

L3 results at 136 GeV

```
* Exact centre-of-mass energy: 136.1  GeV
*
```

XSEC_QQ	66.9	66.6	3.9	0.77	0.05	0.22	0.03	0.0
XSEC_MUMU	7.3	6.9	1.4	0.300	0.006	0.012	0.004	0.0
XSEC_TAUTAU	7.3	7.5	1.8	0.300	0.006	0.010	0.004	0.0
AFB_MUMU	0.686	0.75	0.11	0.050	0.0	0.004	0.0	0.0
AFB_TAUTAU	0.686	0.96	0.17	0.030	0.0	0.004	0.0	0.0

L3 results at 161 GeV

```
* Exact centre-of-mass energy: 161.3  GeV
*
```

XSEC_QQ	35.4	37.3	2.2	0.69	0.05	0.12	0.03	0.0
XSEC_MUMU	4.70	4.59	0.84	0.180	0.006	0.012	0.004	0.0
XSEC_TAUTAU	4.7	4.6	1.1	0.300	0.006	0.010	0.004	0.0
AFB_MUMU	0.619	0.59	0.15	0.050	0.0	0.004	0.0	0.0
AFB_TAUTAU	0.619	0.97	0.25	0.020	0.0	0.004	0.0	0.0

L3 results at 172 GeV

```
* Exact centre-of-mass energy: 172.1  GeV
*
```

XSEC_QQ	28.8	28.2	2.2	0.59	0.05	0.09	0.03	0.0
XSEC_MUMU	4.00	3.60	0.75	0.140	0.006	0.012	0.004	0.0
XSEC_TAUTAU	4.0	4.3	1.1	0.300	0.006	0.010	0.004	0.0
AFB_MUMU	0.598	0.31	0.195	0.050	0.0	0.004	0.0	0.0
AFB_TAUTAU	0.598	0.18	0.27	0.020	0.0	0.004	0.0	0.0

L3 results at 183 GeV

```
* Exact centre-of-mass energy: 182.7  GeV
*
XSEC_QQ       24.3    24.7     0.8    0.38   0.05   0.08   0.03   0.0
XSEC_MUMU      3.47    3.09    0.35   0.059  0.006  0.012  0.004  0.0
XSEC_TAUTAU    3.47    3.62    0.40   0.059  0.006  0.010  0.004  0.0
AFB_MUMU       0.582   0.62    0.08   0.020  0.0    0.004  0.0    0.0
AFB_TAUTAU     0.582   0.53    0.105  0.020  0.0    0.004  0.0    0.0
```

L3 results at 189 GeV

```
* Exact centre-of-mass energy: 188.7  GeV
*
XSEC_QQ       22.2    23.1     0.4    0.28   0.05   0.07   0.03   0.0
XSEC_MUMU      3.22    2.92    0.16   0.059  0.006  0.012  0.004  0.0
XSEC_TAUTAU    3.22    3.18    0.21   0.069  0.006  0.010  0.004  0.0
AFB_MUMU       0.573   0.58    0.04   0.020  0.0    0.004  0.0    0.0
AFB_TAUTAU     0.573   0.44    0.06   0.020  0.0    0.004  0.0    0.0
```

L3 results at 192 GeV

```
* Exact centre-of-mass energy: 191.6 GeV
*
XSEC_QQ       21.334  22.38    1.020  0.180  0.032  0.045  0.019  0.010
XSEC_MUMU      3.112   2.54    0.390  0.087  0.009  0.018  0.006  0.004
XSEC_TAUTAU    3.112   2.93    0.480  0.059  0.005  0.009  0.003  0.003
AFB_MUMU       0.571   0.69    0.120  0.069  0.000  0.014  0.000  0.004
AFB_TAUTAU     0.571   0.52    0.120  0.049  0.000  0.010  0.000  0.003
```

L3 results at 196 GeV

```
* Exact centre-of-mass energy: 195.5 GeV
*
XSEC_QQ       20.212  20.14    0.580  0.152  0.027  0.038  0.016  0.008
XSEC_MUMU      2.972   3.05    0.250  0.097  0.010  0.020  0.007  0.005
XSEC_TAUTAU    2.972   3.22    0.300  0.069  0.006  0.010  0.004  0.004
AFB_MUMU       0.566   0.53    0.070  0.039  0.000  0.008  0.000  0.002
AFB_TAUTAU     0.566   0.44    0.090  0.049  0.000  0.010  0.000  0.003
```

L3 results at 200 GeV

```
* Exact centre-of-mass energy: 199.6 GeV
*
XSEC_QQ       19.133  19.09    0.570  0.152  0.027  0.038  0.016  0.008
XSEC_MUMU      2.837   2.85    0.240  0.087  0.009  0.018  0.006  0.004
XSEC_TAUTAU    2.836   2.97    0.300  0.069  0.006  0.010  0.004  0.004
AFB_MUMU       0.561   0.44    0.080  0.039  0.000  0.008  0.000  0.002
AFB_TAUTAU     0.561   0.46    0.100  0.049  0.000  0.010  0.000  0.003
```

L3 results at 202 GeV

```
* Exact centre-of-mass energy: 201.8 GeV
*
XSEC_QQ       18.593  19.33    0.890  0.152  0.027  0.038  0.016  0.008
XSEC_MUMU      2.768   2.97    0.350  0.097  0.010  0.020  0.007  0.005
XSEC_TAUTAU    2.767   2.81    0.420  0.007  0.001  0.001  0.000  0.000
AFB_MUMU       0.559   0.59    0.090  0.020  0.000  0.004  0.000  0.001
AFB_TAUTAU     0.559   0.47    0.130  0.078  0.000  0.016  0.000  0.004
```

L3 results at 205 GeV

```
* Exact centre-of-mass energy: 204.9 GeV
*
XSEC_QQ       17.872  18.46    0.590  0.133  0.024  0.033  0.014  0.007
XSEC_MUMU      2.675   2.37    0.220  0.068  0.007  0.014  0.005  0.004
XSEC_TAUTAU    2.675   2.93    0.320  0.069  0.006  0.010  0.004  0.004
AFB_MUMU       0.556   0.48    0.090  0.029  0.000  0.006  0.000  0.002
AFB_TAUTAU     0.556   0.56    0.090  0.049  0.000  0.010  0.000  0.003
```

L3 results at 207 GeV

```
* Exact centre-of-mass energy: 206.5 GeV
*
XSEC_QQ       17.518  17.87    0.440  0.123  0.022  0.031  0.013  0.007
XSEC_MUMU      2.629   2.24    0.170  0.058  0.006  0.012  0.004  0.003
XSEC_TAUTAU    2.629   2.34    0.210  0.079  0.007  0.011  0.005  0.004
AFB_MUMU       0.554   0.54    0.060  0.020  0.000  0.004  0.000  0.001
AFB_TAUTAU     0.554   0.61    0.070  0.088  0.000  0.018  0.000  0.004
```

OPAL

OPAL results at 130 GeV

```
* Exact centre-of-mass energy: 130.12 GeV
*
XSEC_QQ       83.078  79.30    3.8    1.25   0.52   0.47   0.20   0.54
XSEC_MUMU      8.453   7.63    1.14   0.16   0.05   0.03   0.02   0.26
XSEC_TAUTAU    8.450   6.83    1.40   0.18   0.05   0.03   0.02   0.16
AFB_MUMU       0.705   0.40    0.15   0.02   0.0    0.004  0.0    0.0
AFB_TAUTAU     0.705   0.80    0.22   0.01   0.0    0.004  0.0    0.0
```

OPAL results at 136 GeV

```
* Exact centre-of-mass energy: 136.08 GeV
*
XSEC_QQ       66.875  66.30    3.3    1.04   0.43   0.40   0.17   0.47
XSEC_MUMU      7.298  10.37    1.31   0.16   0.07   0.03   0.03   0.23
XSEC_TAUTAU    7.295   7.32    1.39   0.19   0.05   0.02   0.02   0.15
```

```
AFB_MUMU       0.685   0.71    0.12   0.01   0.0    0.002  0.0    0.0
AFB_TAUTAU     0.684   0.86    0.20   0.01   0.0    0.003  0.0    0.0
```

OPAL results at 161 GeV

```
* Exact centre-of-mass energy: 161.34 GeV
*
XSEC_QQ       33.606  35.20    2.00   0.73   0.16   0.22   0.09   0.07
XSEC_MUMU      4.419   4.49    0.67   0.07   0.02   0.02   0.01   0.11
XSEC_TAUTAU    4.418   6.22    1.01   0.17   0.03   0.02   0.02   0.05
AFB_MUMU       0.609   0.45    0.14   0.01   0.0    0.005  0.0    0.0
AFB_TAUTAU     0.609   0.56    0.14   0.01   0.0    0.005  0.0    0.0
```

OPAL results at 172 GeV

```
* Exact centre-of-mass energy: 172.12 GeV
*
XSEC_QQ       27.566  26.80    1.80   0.57   0.13   0.16   0.07   0.05
XSEC_MUMU      3.790   3.56    0.59   0.08   0.02   0.02   0.01   0.11
XSEC_TAUTAU    3.789   3.85    0.78   0.11   0.02   0.02   0.01   0.06
AFB_MUMU       0.590   0.55    0.15   0.01   0.0    0.005  0.0    0.0
AFB_TAUTAU     0.590   0.56    0.19   0.01   0.0    0.005  0.0    0.0
```

OPAL results at 183 GeV

```
* Exact centre-of-mass energy: 182.69 GeV
*
XSEC_QQ       24.237  23.50    0.72   0.35   0.08   0.15   0.06   0.06
XSEC_MUMU      3.445   3.463   0.264  0.045  0.012  0.013  0.009  0.105
XSEC_TAUTAU    3.445   3.315   0.301  0.103  0.012  0.011  0.008  0.028
AFB_MUMU       0.576   0.543   0.071  0.011  0.0    0.004  0.0    0.0
AFB_TAUTAU     0.576   0.683   0.088  0.002  0.0    0.004  0.0    0.0
```

OPAL results at 189 GeV

```
* Exact centre-of-mass energy: 188.635 GeV
*
XSEC_QQ       22.188  21.99    0.37   0.09   0.04   0.09   0.03   0.03
XSEC_MUMU      3.206   3.142   0.145  0.033  0.005  0.005  0.004  0.007
XSEC_TAUTAU    3.206   3.445   0.211  0.085  0.006  0.002  0.004  0.020
AFB_MUMU       0.569   0.548   0.039  0.004  0.0    0.002  0.0    0.002
AFB_TAUTAU     0.569   0.591   0.054  0.008  0.0    0.001  0.0    0.010
```

OPAL results at 192 GeV

```
* Exact centre-of-mass energy: 191.590 GeV
*
XSEC_QQ       21.276  22.23    0.94   0.08   0.07   0.08   0.03   0.02
XSEC_MUMU      3.097   2.857   0.344  0.030  0.008  0.004  0.003  0.005
```

```
XSEC_TAUTAU    3.097   3.167   0.503  0.078  0.009  0.001  0.004  0.015
AFB_MUMU       0.566   0.341   0.102  0.004  0.0    0.002  0.0    0.002
AFB_TAUTAU     0.566   0.813   0.138  0.005  0.0    0.001  0.0    0.012
```

OPAL results at 196 GeV

```
* Exact centre-of-mass energy: 195.526 GeV
*
XSEC_QQ       20.154  19.78    0.55   0.08   0.04   0.07   0.02   0.02
XSEC_MUMU      2.961   2.932   0.215  0.031  0.007  0.004  0.004  0.004
XSEC_TAUTAU    2.961   2.893   0.298  0.072  0.007  0.001  0.003  0.011
AFB_MUMU       0.562   0.683   0.055  0.004  0.0    0.002  0.0    0.002
AFB_TAUTAU     0.562   0.373   0.103  0.013  0.0    0.001  0.0    0.005
```

OPAL results at 200 GeV

```
* Exact centre-of-mass energy: 199.522 GeV
*
XSEC_QQ       19.112  18.89    0.54   0.08   0.05   0.06   0.02   0.01
XSEC_MUMU      2.833   2.772   0.207  0.029  0.007  0.004  0.003  0.003
XSEC_TAUTAU    2.833   3.136   0.304  0.077  0.007  0.001  0.004  0.010
AFB_MUMU       0.558   0.637   0.059  0.004  0.0    0.002  0.0    0.001
AFB_TAUTAU     0.558   0.700   0.077  0.006  0.0    0.001  0.0    0.006
```

OPAL results at 202 GeV

```
* Exact centre-of-mass energy: 201.636 GeV
*
XSEC_QQ       18.596  18.54    0.77   0.08   0.05   0.05   0.02   0.01
XSEC_MUMU      2.768   2.363   0.280  0.025  0.006  0.004  0.003  0.003
XSEC_TAUTAU    2.768   2.954   0.430  0.072  0.008  0.001  0.004  0.009
AFB_MUMU       0.556   0.489   0.100  0.004  0.0    0.002  0.0    0.001
AFB_TAUTAU     0.556   0.440   0.130  0.010  0.0    0.001  0.0    0.004
```

OPAL results at 205 GeV

```
* Exact centre-of-mass energy: 204.881 GeV
*
XSEC_QQ       17.847  18.18    0.52   0.08   0.04   0.05   0.02   0.01
XSEC_MUMU      2.674   2.885   0.210  0.030  0.007  0.004  0.003  0.004
XSEC_TAUTAU    2.674   2.721   0.283  0.067  0.006  0.001  0.003  0.011
AFB_MUMU       0.553   0.512   0.063  0.004  0.0    0.002  0.0    0.002
AFB_TAUTAU     0.553   0.575   0.092  0.009  0.0    0.001  0.0    0.006
```

OPAL results at 207 GeV

```
* Exact centre-of-mass energy: 206.561 GeV
*
XSEC_QQ       17.479  16.81    0.39   0.08   0.04   0.04   0.02   0.02
```

XSEC_MUMU	2.627	2.766	0.158	0.029	0.006	0.004	0.003	0.005
XSEC_TAUTAU	2.627	2.782	0.219	0.068	0.006	0.001	0.003	0.013
AFB_MUMU	0.552	0.508	0.050	0.004	0.0	0.002	0.0	0.002
AFB_TAUTAU	0.552	0.472	0.075	0.010	0.0	0.001	0.0	0.005

B.2 Differential Cross-Section for Muon- and Tau-Pair Final States

The following lists show for each centre-of-mass energy point (rounded in GeV) the LEP-combined differential lepton-pair cross-sections (DC) for $\mu^+\mu^-$ (MM) and $\tau^+\tau^-$ (TT) final states in 10 $\cos\theta$-bins $(1-10)$ of constant width 0.2, comparing the LEP average value and its total error with the SM prediction. Also shown is the overall χ^2/dof and the bin-by-bin χ^2/dof contribution. The overall matrix of correlation coefficients and inverse covariance matrix are available at the LEPEWWG web site: `http://www.cern.ch/LEPEWWG`.

```
Total chi2/NDF =  352.156/320
183_DC_MM_1     average =  0.197 +-  0.183   SM=  0.547   chi2/NDF =   0.688/1
183_DC_MM_2     average =  0.589 +-  0.163   SM=  0.534   chi2/NDF =   0.717/1
183_DC_MM_3     average =  0.807 +-  0.174   SM=  0.627   chi2/NDF =   2.204/1
183_DC_MM_4     average =  1.033 +-  0.197   SM=  0.823   chi2/NDF =   0.211/1
183_DC_MM_5     average =  1.178 +-  0.236   SM=  1.121   chi2/NDF =   0.014/1
183_DC_MM_6     average =  1.778 +-  0.276   SM=  1.521   chi2/NDF =   0.007/1
183_DC_MM_7     average =  2.143 +-  0.315   SM=  2.020   chi2/NDF =   0.777/1
183_DC_MM_8     average =  2.690 +-  0.367   SM=  2.619   chi2/NDF =   4.165/1
183_DC_MM_9     average =  2.916 +-  0.420   SM=  3.314   chi2/NDF =   1.199/1
183_DC_MM_10    average =  4.368 +-  0.529   SM=  4.096   chi2/NDF =   0.254/1
183_DC_TT_1     average =  0.302 +-  0.351   SM=  0.548   chi2/NDF =   1.439/1
183_DC_TT_2     average =  0.206 +-  0.240   SM=  0.535   chi2/NDF =   1.677/1
183_DC_TT_3     average =  0.198 +-  0.230   SM=  0.627   chi2/NDF =   1.127/1
183_DC_TT_4     average =  0.542 +-  0.254   SM=  0.823   chi2/NDF =   0.176/1
183_DC_TT_5     average =  1.364 +-  0.302   SM=  1.121   chi2/NDF =   0.206/1
183_DC_TT_6     average =  1.519 +-  0.350   SM=  1.521   chi2/NDF =   0.045/1
183_DC_TT_7     average =  1.583 +-  0.389   SM=  2.020   chi2/NDF =   0.403/1
183_DC_TT_8     average =  2.296 +-  0.450   SM=  2.619   chi2/NDF =   0.095/1
183_DC_TT_9     average =  3.954 +-  0.574   SM=  3.313   chi2/NDF =   0.321/1
183_DC_TT_10    average =  4.156 +-  0.919   SM=  4.095   chi2/NDF =   0.263/1
189_DC_MM_1     average =  0.614 +-  0.080   SM=  0.532   chi2/NDF =   4.079/3
189_DC_MM_2     average =  0.420 +-  0.065   SM=  0.514   chi2/NDF =   1.836/3
189_DC_MM_3     average =  0.530 +-  0.069   SM=  0.595   chi2/NDF =   0.702/3
189_DC_MM_4     average =  0.651 +-  0.077   SM=  0.772   chi2/NDF =   2.544/3
189_DC_MM_5     average =  1.064 +-  0.089   SM=  1.044   chi2/NDF =  10.239/3
189_DC_MM_6     average =  1.313 +-  0.111   SM=  1.411   chi2/NDF =   1.906/3
189_DC_MM_7     average =  2.038 +-  0.123   SM=  1.872   chi2/NDF =   1.168/3
189_DC_MM_8     average =  2.158 +-  0.139   SM=  2.426   chi2/NDF =   0.374/3
189_DC_MM_9     average =  2.954 +-  0.158   SM=  3.072   chi2/NDF =   2.558/3
189_DC_MM_10    average =  3.795 +-  0.216   SM=  3.799   chi2/NDF =   0.853/3
189_DC_TT_1     average =  0.389 +-  0.123   SM=  0.532   chi2/NDF =   7.662/3
189_DC_TT_2     average =  0.379 +-  0.093   SM=  0.515   chi2/NDF =   5.211/3
189_DC_TT_3     average =  0.485 +-  0.089   SM=  0.595   chi2/NDF =  10.195/3
189_DC_TT_4     average =  0.809 +-  0.100   SM=  0.772   chi2/NDF =   0.944/3
189_DC_TT_5     average =  0.848 +-  0.118   SM=  1.044   chi2/NDF =   0.139/3
189_DC_TT_6     average =  1.323 +-  0.139   SM=  1.411   chi2/NDF =   7.994/3
```

```
189_DC_TT_7     average =  1.989 +-  0.154   SM=  1.872   chi2/NDF =   2.494/3
189_DC_TT_8     average =  2.445 +-  0.179   SM=  2.426   chi2/NDF =   0.841/3
189_DC_TT_9     average =  2.467 +-  0.225   SM=  3.071   chi2/NDF =   2.313/3
189_DC_TT_10    average =  4.111 +-  0.357   SM=  3.798   chi2/NDF =   7.763/3
192_DC_MM_1     average =  0.481 +-  0.198   SM=  0.524   chi2/NDF =   6.372/2
192_DC_MM_2     average =  0.384 +-  0.173   SM=  0.504   chi2/NDF =   1.804/2
192_DC_MM_3     average =  0.788 +-  0.186   SM=  0.579   chi2/NDF =   2.816/2
192_DC_MM_4     average =  0.581 +-  0.212   SM=  0.748   chi2/NDF =   0.388/2
192_DC_MM_5     average =  1.324 +-  0.248   SM=  1.008   chi2/NDF =   2.698/2
192_DC_MM_6     average =  1.187 +-  0.292   SM=  1.360   chi2/NDF =   3.178/2
192_DC_MM_7     average =  1.932 +-  0.334   SM=  1.803   chi2/NDF =   6.530/2
192_DC_MM_8     average =  2.080 +-  0.379   SM=  2.337   chi2/NDF =   0.245/2
192_DC_MM_9     average =  3.003 +-  0.429   SM=  2.960   chi2/NDF =   2.441/2
192_DC_MM_10    average =  3.083 +-  0.552   SM=  3.662   chi2/NDF =   2.378/2
192_DC_TT_1     average =  0.014 +-  0.325   SM=  0.524   chi2/NDF =   1.103/2
192_DC_TT_2     average =  0.355 +-  0.247   SM=  0.505   chi2/NDF =   2.256/2
192_DC_TT_3     average =  0.479 +-  0.245   SM=  0.580   chi2/NDF =   1.130/2
192_DC_TT_4     average =  0.762 +-  0.278   SM=  0.748   chi2/NDF =   2.704/2
192_DC_TT_5     average =  0.816 +-  0.331   SM=  1.008   chi2/NDF =   0.540/2
192_DC_TT_6     average =  1.609 +-  0.385   SM=  1.360   chi2/NDF =   0.055/2
192_DC_TT_7     average =  1.810 +-  0.433   SM=  1.803   chi2/NDF =   0.026/2
192_DC_TT_8     average =  2.059 +-  0.491   SM=  2.337   chi2/NDF =   0.688/2
192_DC_TT_9     average =  2.643 +-  0.599   SM=  2.959   chi2/NDF =   1.439/2
192_DC_TT_10    average =  2.575 +-  0.935   SM=  3.661   chi2/NDF =   6.306/2
196_DC_MM_1     average =  0.535 +-  0.119   SM=  0.512   chi2/NDF =   3.633/2
196_DC_MM_2     average =  0.485 +-  0.103   SM=  0.491   chi2/NDF =   1.848/2
196_DC_MM_3     average =  0.668 +-  0.111   SM=  0.560   chi2/NDF =   0.766/2
196_DC_MM_4     average =  0.484 +-  0.126   SM=  0.718   chi2/NDF =   1.473/2
196_DC_MM_5     average =  0.802 +-  0.147   SM=  0.964   chi2/NDF =   1.659/2
196_DC_MM_6     average =  1.507 +-  0.172   SM=  1.298   chi2/NDF =   2.480/2
196_DC_MM_7     average =  1.657 +-  0.197   SM=  1.720   chi2/NDF =   1.467/2
196_DC_MM_8     average =  2.303 +-  0.223   SM=  2.229   chi2/NDF =   0.450/2
196_DC_MM_9     average =  2.949 +-  0.253   SM=  2.824   chi2/NDF =   0.068/2
196_DC_MM_10    average =  3.272 +-  0.325   SM=  3.495   chi2/NDF =   1.622/2
196_DC_TT_1     average =  0.810 +-  0.211   SM=  0.513   chi2/NDF =   2.172/2
196_DC_TT_2     average =  0.738 +-  0.147   SM=  0.491   chi2/NDF =   2.311/2
196_DC_TT_3     average =  0.524 +-  0.141   SM=  0.560   chi2/NDF =   9.697/2
196_DC_TT_4     average =  0.688 +-  0.162   SM=  0.718   chi2/NDF =   0.718/2
196_DC_TT_5     average =  0.976 +-  0.195   SM=  0.964   chi2/NDF =   1.445/2
196_DC_TT_6     average =  0.977 +-  0.225   SM=  1.298   chi2/NDF =   0.257/2
196_DC_TT_7     average =  1.648 +-  0.252   SM=  1.719   chi2/NDF =   3.406/2
196_DC_TT_8     average =  1.965 +-  0.289   SM=  2.228   chi2/NDF =   0.535/2
196_DC_TT_9     average =  2.269 +-  0.357   SM=  2.823   chi2/NDF =   1.278/2
196_DC_TT_10    average =  3.346 +-  0.557   SM=  3.494   chi2/NDF =   0.714/2
200_DC_MM_1     average =  0.558 +-  0.113   SM=  0.501   chi2/NDF =   1.899/2
200_DC_MM_2     average =  0.376 +-  0.098   SM=  0.478   chi2/NDF =   3.670/2
200_DC_MM_3     average =  0.799 +-  0.105   SM=  0.541   chi2/NDF =   2.306/2
```

```
200_DC_MM_4     average =  0.817 +-  0.118   SM=  0.689   chi2/NDF =   2.762/2
200_DC_MM_5     average =  1.105 +-  0.139   SM=  0.922   chi2/NDF =   1.269/2
200_DC_MM_6     average =  1.462 +-  0.162   SM=  1.239   chi2/NDF =   0.517/2
200_DC_MM_7     average =  1.849 +-  0.185   SM=  1.640   chi2/NDF =   0.217/2
200_DC_MM_8     average =  2.122 +-  0.211   SM=  2.126   chi2/NDF =   5.430/2
200_DC_MM_9     average =  2.947 +-  0.239   SM=  2.694   chi2/NDF =   0.365/2
200_DC_MM_10    average =  3.474 +-  0.306   SM=  3.336   chi2/NDF =   0.435/2
200_DC_TT_1     average =  0.489 +-  0.201   SM=  0.501   chi2/NDF =   0.340/2
200_DC_TT_2     average =  0.619 +-  0.141   SM=  0.478   chi2/NDF =   7.623/2
200_DC_TT_3     average =  0.528 +-  0.137   SM=  0.541   chi2/NDF =   0.040/2
200_DC_TT_4     average =  0.628 +-  0.155   SM=  0.689   chi2/NDF =   0.631/2
200_DC_TT_5     average =  1.067 +-  0.186   SM=  0.922   chi2/NDF =   2.966/2
200_DC_TT_6     average =  1.130 +-  0.214   SM=  1.239   chi2/NDF =   1.361/2
200_DC_TT_7     average =  1.871 +-  0.240   SM=  1.640   chi2/NDF =   0.687/2
200_DC_TT_8     average =  2.043 +-  0.274   SM=  2.125   chi2/NDF =   0.684/2
200_DC_TT_9     average =  2.777 +-  0.339   SM=  2.694   chi2/NDF =   1.916/2
200_DC_TT_10    average =  3.437 +-  0.523   SM=  3.336   chi2/NDF =   0.841/2
202_DC_MM_1     average =  1.137 +-  0.162   SM=  0.495   chi2/NDF =   3.111/2
202_DC_MM_2     average =  0.295 +-  0.139   SM=  0.471   chi2/NDF =   2.215/2
202_DC_MM_3     average =  0.506 +-  0.149   SM=  0.531   chi2/NDF =   3.903/2
202_DC_MM_4     average =  0.455 +-  0.169   SM=  0.674   chi2/NDF =   0.372/2
202_DC_MM_5     average =  0.860 +-  0.197   SM=  0.900   chi2/NDF =   1.540/2
202_DC_MM_6     average =  1.010 +-  0.230   SM=  1.208   chi2/NDF =   0.967/2
202_DC_MM_7     average =  1.749 +-  0.264   SM=  1.599   chi2/NDF =   6.636/2
202_DC_MM_8     average =  1.844 +-  0.299   SM=  2.072   chi2/NDF =   2.847/2
202_DC_MM_9     average =  2.268 +-  0.339   SM=  2.627   chi2/NDF =   0.898/2
202_DC_MM_10    average =  3.396 +-  0.435   SM=  3.254   chi2/NDF =   0.873/2
202_DC_TT_1     average =  0.968 +-  0.287   SM=  0.495   chi2/NDF =  10.336/2
202_DC_TT_2     average =  0.322 +-  0.189   SM=  0.471   chi2/NDF =   2.713/2
202_DC_TT_3     average =  0.420 +-  0.194   SM=  0.531   chi2/NDF =   0.236/2
202_DC_TT_4     average =  0.731 +-  0.220   SM=  0.674   chi2/NDF =   1.905/2
202_DC_TT_5     average =  0.922 +-  0.263   SM=  0.900   chi2/NDF =   2.804/2
202_DC_TT_6     average =  0.789 +-  0.300   SM=  1.208   chi2/NDF =   0.094/2
202_DC_TT_7     average =  1.953 +-  0.341   SM=  1.599   chi2/NDF =   2.468/2
202_DC_TT_8     average =  1.838 +-  0.386   SM=  2.072   chi2/NDF =   4.162/2
202_DC_TT_9     average =  3.129 +-  0.479   SM=  2.626   chi2/NDF =   9.918/2
202_DC_TT_10    average =  3.186 +-  0.747   SM=  3.254   chi2/NDF =   1.368/2
205_DC_MM_1     average =  0.621 +-  0.113   SM=  0.485   chi2/NDF =   2.027/2
205_DC_MM_2     average =  0.385 +-  0.098   SM=  0.461   chi2/NDF =   0.169/2
205_DC_MM_3     average =  0.382 +-  0.104   SM=  0.517   chi2/NDF =   4.554/2
205_DC_MM_4     average =  0.443 +-  0.118   SM=  0.654   chi2/NDF =   0.774/2
205_DC_MM_5     average =  0.891 +-  0.137   SM=  0.870   chi2/NDF =   1.913/2
205_DC_MM_6     average =  1.205 +-  0.160   SM=  1.166   chi2/NDF =   1.383/2
205_DC_MM_7     average =  1.614 +-  0.183   SM=  1.542   chi2/NDF =   5.186/2
205_DC_MM_8     average =  1.663 +-  0.209   SM=  1.998   chi2/NDF =   0.393/2
205_DC_MM_9     average =  2.097 +-  0.237   SM=  2.534   chi2/NDF =   0.449/2
205_DC_MM_10    average =  3.318 +-  0.306   SM=  3.140   chi2/NDF =   6.351/2
```

```
205_DC_TT_1     average =  0.363 +-  0.203   SM=  0.486   chi2/NDF =   6.520/2
205_DC_TT_2     average =  0.562 +-  0.137   SM=  0.461   chi2/NDF =   0.697/2
205_DC_TT_3     average =  0.603 +-  0.135   SM=  0.517   chi2/NDF =   4.695/2
205_DC_TT_4     average =  0.443 +-  0.154   SM=  0.654   chi2/NDF =   0.276/2
205_DC_TT_5     average =  0.397 +-  0.179   SM=  0.870   chi2/NDF =   0.237/2
205_DC_TT_6     average =  1.242 +-  0.209   SM=  1.166   chi2/NDF =   0.132/2
205_DC_TT_7     average =  1.522 +-  0.237   SM=  1.542   chi2/NDF =   0.804/2
205_DC_TT_8     average =  1.846 +-  0.268   SM=  1.998   chi2/NDF =   1.367/2
205_DC_TT_9     average =  2.045 +-  0.330   SM=  2.533   chi2/NDF =   3.717/2
205_DC_TT_10    average =  4.671 +-  0.520   SM=  3.140   chi2/NDF =   1.658/2
207_DC_MM_1     average =  0.518 +-  0.087   SM=  0.481   chi2/NDF =   0.388/2
207_DC_MM_2     average =  0.496 +-  0.075   SM=  0.456   chi2/NDF =   0.051/2
207_DC_MM_3     average =  0.473 +-  0.079   SM=  0.510   chi2/NDF =   5.634/2
207_DC_MM_4     average =  0.781 +-  0.089   SM=  0.643   chi2/NDF =   5.052/2
207_DC_MM_5     average =  0.795 +-  0.104   SM=  0.855   chi2/NDF =   2.185/2
207_DC_MM_6     average =  0.995 +-  0.121   SM=  1.145   chi2/NDF =   0.627/2
207_DC_MM_7     average =  1.630 +-  0.139   SM=  1.515   chi2/NDF =   0.808/2
207_DC_MM_8     average =  2.247 +-  0.159   SM=  1.963   chi2/NDF =   4.025/2
207_DC_MM_9     average =  2.491 +-  0.179   SM=  2.489   chi2/NDF =   4.407/2
207_DC_MM_10    average =  2.995 +-  0.231   SM=  3.086   chi2/NDF =   1.136/2
207_DC_TT_1     average =  0.272 +-  0.145   SM=  0.481   chi2/NDF =   0.134/2
207_DC_TT_2     average =  0.412 +-  0.106   SM=  0.456   chi2/NDF =   6.521/2
207_DC_TT_3     average =  0.534 +-  0.104   SM=  0.510   chi2/NDF =   0.745/2
207_DC_TT_4     average =  0.563 +-  0.118   SM=  0.644   chi2/NDF =   0.133/2
207_DC_TT_5     average =  0.683 +-  0.140   SM=  0.855   chi2/NDF =   5.976/2
207_DC_TT_6     average =  1.443 +-  0.161   SM=  1.145   chi2/NDF =   1.658/2
207_DC_TT_7     average =  1.351 +-  0.181   SM=  1.514   chi2/NDF =   1.519/2
207_DC_TT_8     average =  1.761 +-  0.207   SM=  1.962   chi2/NDF =   6.867/2
207_DC_TT_9     average =  1.655 +-  0.255   SM=  2.489   chi2/NDF =   0.561/2
207_DC_TT_10    average =  3.597 +-  0.399   SM=  3.085   chi2/NDF =   3.709/2
```

B.3 Differential Cross-Section for Electron-Positron Final States

The following lists show for each centre-of-mass energy point (rounded in GeV) the LEP-combined differential cross-sections (DC) for e^+e^- (EE) final states in 15 $\cos\theta$-bins ($1-15$ with bin boundaries as defined in Tables 3.11 and 3.12), comparing the LEP average value and its total error with the SM prediction. Also shown is the overall χ^2/dof and the bin-by-bin χ^2/dof contribution. The overall matrix of correlation coefficients and inverse covariance matrix are available at the LEPEWWG web site: `http://www.cern.ch/LEPEWWG`.

```
Total chi2/NDF =  199.402/189
189_DC_EE_1     average =  1.401 +-  0.161   SM=  1.590   chi2/NDF =   1.576/1
189_DC_EE_2     average =  2.030 +-  0.160   SM=  1.816   chi2/NDF =   6.274/2
189_DC_EE_3     average =  2.162 +-  0.170   SM=  2.162   chi2/NDF =   1.237/2
189_DC_EE_4     average =  2.298 +-  0.186   SM=  2.681   chi2/NDF =   0.654/2
189_DC_EE_5     average =  4.321 +-  0.230   SM=  3.906   chi2/NDF =   4.262/2
189_DC_EE_6     average =  4.898 +-  0.348   SM=  5.372   chi2/NDF =   2.403/2
189_DC_EE_7     average =  6.090 +-  0.404   SM=  6.892   chi2/NDF =   6.751/2
189_DC_EE_8     average =  8.838 +-  0.476   SM=  9.610   chi2/NDF =   2.341/2
189_DC_EE_9     average = 12.781 +-  0.576   SM= 13.345   chi2/NDF =   3.970/2
189_DC_EE_10    average = 19.586 +-  0.707   SM= 19.445   chi2/NDF =   0.115/2
189_DC_EE_11    average = 30.598 +-  0.895   SM= 30.476   chi2/NDF =   2.386/2
189_DC_EE_12    average = 50.488 +-  1.135   SM= 51.012   chi2/NDF =   2.339/2
189_DC_EE_13    average = 95.178 +-  1.520   SM= 95.563   chi2/NDF =   0.211/2
189_DC_EE_14    average =211.427 +-  2.900   SM=212.390   chi2/NDF =   2.620/1
189_DC_EE_15    average =679.146 +-  5.773   SM=689.989   chi2/NDF =   1.921/1
192_DC_EE_1     average =  1.300 +-  0.364   SM=  1.539   chi2/NDF =   0.051/1
192_DC_EE_2     average =  2.099 +-  0.419   SM=  1.754   chi2/NDF =   0.462/2
192_DC_EE_3     average =  1.871 +-  0.385   SM=  2.091   chi2/NDF =   1.602/2
192_DC_EE_4     average =  1.808 +-  0.422   SM=  2.604   chi2/NDF =   1.619/2
192_DC_EE_5     average =  3.800 +-  0.519   SM=  3.778   chi2/NDF =   3.179/2
192_DC_EE_6     average =  5.015 +-  0.891   SM=  5.205   chi2/NDF =   1.897/2
192_DC_EE_7     average =  5.695 +-  0.976   SM=  6.692   chi2/NDF =   9.314/2
192_DC_EE_8     average =  9.239 +-  1.175   SM=  9.242   chi2/NDF =   0.003/2
192_DC_EE_9     average = 12.941 +-  1.414   SM= 12.800   chi2/NDF =   0.749/2
192_DC_EE_10    average = 20.761 +-  1.807   SM= 18.776   chi2/NDF =   0.371/2
192_DC_EE_11    average = 26.466 +-  2.074   SM= 29.471   chi2/NDF =   4.398/2
192_DC_EE_12    average = 49.382 +-  2.671   SM= 49.338   chi2/NDF =   1.721/2
192_DC_EE_13    average = 89.676 +-  3.615   SM= 92.079   chi2/NDF =   2.159/2
192_DC_EE_14    average =204.579 +-  6.760   SM=206.087   chi2/NDF =   0.054/1
192_DC_EE_15    average =655.724 +- 12.588   SM=669.173   chi2/NDF =   0.482/1
196_DC_EE_1     average =  1.470 +-  0.261   SM=  1.483   chi2/NDF =   1.887/1
196_DC_EE_2     average =  1.527 +-  0.221   SM=  1.695   chi2/NDF =   0.421/2
196_DC_EE_3     average =  2.058 +-  0.250   SM=  2.000   chi2/NDF =   0.865/2
196_DC_EE_4     average =  2.788 +-  0.284   SM=  2.498   chi2/NDF =   0.014/2
196_DC_EE_5     average =  3.646 +-  0.318   SM=  3.610   chi2/NDF =   0.212/2
196_DC_EE_6     average =  5.887 +-  0.521   SM=  4.999   chi2/NDF =   1.809/2
```

```
196_DC_EE_7     average =  6.233 +-  0.591   SM=  6.406   chi2/NDF =   1.078/2
196_DC_EE_8     average =  9.016 +-  0.694   SM=  8.832   chi2/NDF =   2.379/2
196_DC_EE_9     average = 13.444 +-  0.856   SM= 12.326   chi2/NDF =   0.593/2
196_DC_EE_10    average = 18.568 +-  0.977   SM= 18.039   chi2/NDF =  11.452/2
196_DC_EE_11    average = 27.056 +-  1.223   SM= 28.300   chi2/NDF =   0.962/2
196_DC_EE_12    average = 49.391 +-  1.619   SM= 47.362   chi2/NDF =   0.784/2
196_DC_EE_13    average = 88.163 +-  2.154   SM= 88.473   chi2/NDF =   0.982/2
196_DC_EE_14    average =197.369 +-  4.121   SM=198.250   chi2/NDF =   0.438/1
196_DC_EE_15    average =637.846 +-  8.003   SM=642.688   chi2/NDF =   0.118/1
200_DC_EE_1     average =  1.483 +-  0.245   SM=  1.420   chi2/NDF =   0.002/1
200_DC_EE_2     average =  1.638 +-  0.214   SM=  1.623   chi2/NDF =   0.802/2
200_DC_EE_3     average =  2.068 +-  0.227   SM=  1.885   chi2/NDF =   3.449/2
200_DC_EE_4     average =  2.362 +-  0.250   SM=  2.409   chi2/NDF =   0.753/2
200_DC_EE_5     average =  4.251 +-  0.313   SM=  3.435   chi2/NDF =   1.068/2
200_DC_EE_6     average =  5.244 +-  0.506   SM=  4.770   chi2/NDF =   1.098/2
200_DC_EE_7     average =  5.888 +-  0.571   SM=  6.157   chi2/NDF =   0.142/2
200_DC_EE_8     average =  8.244 +-  0.667   SM=  8.471   chi2/NDF =   3.666/2
200_DC_EE_9     average =  9.506 +-  0.736   SM= 11.773   chi2/NDF =   8.162/2
200_DC_EE_10    average = 16.376 +-  0.920   SM= 17.262   chi2/NDF =   3.021/2
200_DC_EE_11    average = 27.000 +-  1.214   SM= 27.117   chi2/NDF =   2.513/2
200_DC_EE_12    average = 44.614 +-  1.537   SM= 45.607   chi2/NDF =   5.241/2
200_DC_EE_13    average = 86.454 +-  2.060   SM= 85.143   chi2/NDF =   0.582/2
200_DC_EE_14    average =190.962 +-  3.941   SM=190.786   chi2/NDF =   0.760/1
200_DC_EE_15    average =604.986 +-  7.608   SM=617.718   chi2/NDF =   0.059/1
202_DC_EE_1     average =  1.568 +-  0.368   SM=  1.401   chi2/NDF =   2.070/1
202_DC_EE_2     average =  1.344 +-  0.276   SM=  1.579   chi2/NDF =   0.070/2
202_DC_EE_3     average =  2.107 +-  0.345   SM=  1.836   chi2/NDF =   1.503/2
202_DC_EE_4     average =  3.240 +-  0.406   SM=  2.361   chi2/NDF =   1.130/2
202_DC_EE_5     average =  2.911 +-  0.394   SM=  3.356   chi2/NDF =   3.574/2
202_DC_EE_6     average =  4.603 +-  0.628   SM=  4.669   chi2/NDF =   0.358/2
202_DC_EE_7     average =  6.463 +-  0.861   SM=  6.017   chi2/NDF =   1.590/2
202_DC_EE_8     average =  7.457 +-  0.957   SM=  8.320   chi2/NDF =   3.276/2
202_DC_EE_9     average = 11.032 +-  1.113   SM= 11.554   chi2/NDF =   0.602/2
202_DC_EE_10    average = 16.428 +-  1.338   SM= 16.891   chi2/NDF =   1.489/2
202_DC_EE_11    average = 27.153 +-  1.643   SM= 26.583   chi2/NDF =   4.350/2
202_DC_EE_12    average = 46.490 +-  2.214   SM= 44.786   chi2/NDF =   0.246/2
202_DC_EE_13    average = 87.253 +-  2.887   SM= 83.473   chi2/NDF =   1.047/2
202_DC_EE_14    average =189.026 +-  5.516   SM=186.904   chi2/NDF =   0.626/1
202_DC_EE_15    average =599.860 +- 10.339   SM=605.070   chi2/NDF =   0.476/1
205_DC_EE_1     average =  1.102 +-  0.205   SM=  1.355   chi2/NDF =   3.910/1
205_DC_EE_2     average =  1.470 +-  0.195   SM=  1.539   chi2/NDF =   4.105/2
205_DC_EE_3     average =  2.050 +-  0.231   SM=  1.786   chi2/NDF =   0.679/2
205_DC_EE_4     average =  2.564 +-  0.255   SM=  2.280   chi2/NDF =   0.611/2
205_DC_EE_5     average =  3.410 +-  0.300   SM=  3.253   chi2/NDF =   1.269/2
205_DC_EE_6     average =  5.308 +-  0.472   SM=  4.479   chi2/NDF =   1.159/2
205_DC_EE_7     average =  5.836 +-  0.571   SM=  5.820   chi2/NDF =   1.925/2
205_DC_EE_8     average =  7.996 +-  0.635   SM=  8.077   chi2/NDF =   0.869/2
```

```
205_DC_EE_9     average = 10.607 +-  0.764   SM= 11.200   chi2/NDF =   0.581/2
205_DC_EE_10    average = 14.729 +-  0.874   SM= 16.322   chi2/NDF =   1.139/2
205_DC_EE_11    average = 26.189 +-  1.157   SM= 25.722   chi2/NDF =   0.829/2
205_DC_EE_12    average = 43.124 +-  1.497   SM= 43.217   chi2/NDF =   0.942/2
205_DC_EE_13    average = 79.255 +-  1.976   SM= 80.939   chi2/NDF =   0.758/2
205_DC_EE_14    average =179.842 +-  3.838   SM=180.878   chi2/NDF =   3.902/1
205_DC_EE_15    average =587.999 +-  7.527   SM=586.205   chi2/NDF =   2.437/1
207_DC_EE_1     average =  1.440 +-  0.196   SM=  1.339   chi2/NDF =   0.019/1
207_DC_EE_2     average =  1.426 +-  0.163   SM=  1.517   chi2/NDF =   1.800/2
207_DC_EE_3     average =  1.889 +-  0.177   SM=  1.745   chi2/NDF =   0.809/2
207_DC_EE_4     average =  2.156 +-  0.198   SM=  2.240   chi2/NDF =   4.511/2
207_DC_EE_5     average =  3.215 +-  0.233   SM=  3.194   chi2/NDF =   2.133/2
207_DC_EE_6     average =  4.434 +-  0.357   SM=  4.380   chi2/NDF =   4.019/2
207_DC_EE_7     average =  6.393 +-  0.463   SM=  5.729   chi2/NDF =   1.649/2
207_DC_EE_8     average =  6.951 +-  0.481   SM=  7.972   chi2/NDF =   1.727/2
207_DC_EE_9     average = 11.221 +-  0.615   SM= 11.019   chi2/NDF =   1.981/2
207_DC_EE_10    average = 15.933 +-  0.739   SM= 16.053   chi2/NDF =   1.275/2
207_DC_EE_11    average = 25.676 +-  0.923   SM= 25.254   chi2/NDF =   5.712/2
207_DC_EE_12    average = 42.075 +-  1.188   SM= 42.456   chi2/NDF =   0.527/2
207_DC_EE_13    average = 77.611 +-  1.569   SM= 79.639   chi2/NDF =   0.550/2
207_DC_EE_14    average =173.825 +-  3.002   SM=178.042   chi2/NDF =   0.026/1
207_DC_EE_15    average =573.637 +-  6.024   SM=576.688   chi2/NDF =   3.200/1
```

Appendix C

Determination of the LEP Centre-of-Mass Energy Using Radiative-Return Events

The LEP collaborations performed measurements of radiative Z boson production, $e^+e^- \to Z + \gamma \to f\bar{f} + \gamma$, at centre-of-mass energies well above the Z peak, $\sqrt{s} = 161 - 209$ GeV [151, 255, 256, 257]. Events with pairs of electrons, muons, taus, and hadronic jets were selected. The presence of hard ISR photons, mostly emitted at small polar angles with respect to the beam directions and recoiling against the di-fermion system, led to typical event topologies with acollinear fermions measured in the detector. Due to the photon emission, the mass of the two-fermion system, $\sqrt{s'}$, is reduced to values less than $\sqrt{s}$. The spectrum of $\sqrt{s'}$ exhibits a resonance peak around the Z boson mass and allows a determination of m_Z. The determination of $\sqrt{s'}$ furthermore involves the knowledge of the e^+e^- centre-of-mass mass energy, because in the kinematic reconstruction of the $Z + \gamma \to f\bar{f} + \gamma$ events, energy-momentum conservation is imposed. Thus, a measurement of the Z boson mass in radiative-return events, $m_Z^{f\bar{f}}$, is equivalent to determining the average $\sqrt{s}$ of each analysed data set. Figure C.1 shows two examples of the two-fermion mass spectra measured by the LEP experiments.

The ISR photons are either detected as isolated energy depositions in the calorimeters compatible with an electromagnetic shower or as missing momentum pointing along the beam directions. Typically, the energy of the calorimeter shower is required to be larger than $30 - 60$ GeV. For hadronic final states, a kinematic fit is applied to the event imposing energy and momentum conservation. In case the ISR photons are not observed in the detector, the sum of the photon momenta is assumed to either point along only one beam direction or along both beam axes. In the kinematic fit, usually both possibilities are tested and the one obtaining the best fit results is eventually chosen. In this way, the mass of the two-fermion system is reconstructed with optimised precision. In leptonic final states, $\sqrt{s'}$ is determined using the well-measured polar angles of the leptons, according to the following equation:

$$\sqrt{s'} = \sqrt{1 - \frac{2E_{\mathrm{ISR}}}{\sqrt{s}}}\ , \text{ with} \tag{C.1}$$

$$E_{\mathrm{ISR}} = \sqrt{s}\frac{|\sin(\theta_1 + \theta_2)|}{\sin\theta_1 + \sin\theta_2 + |\sin(\theta_1 + \theta_2)|}\ . \tag{C.2}$$

The leptonic polar angles θ_1 and θ_2 are determined either relative to the beam axis if no photon

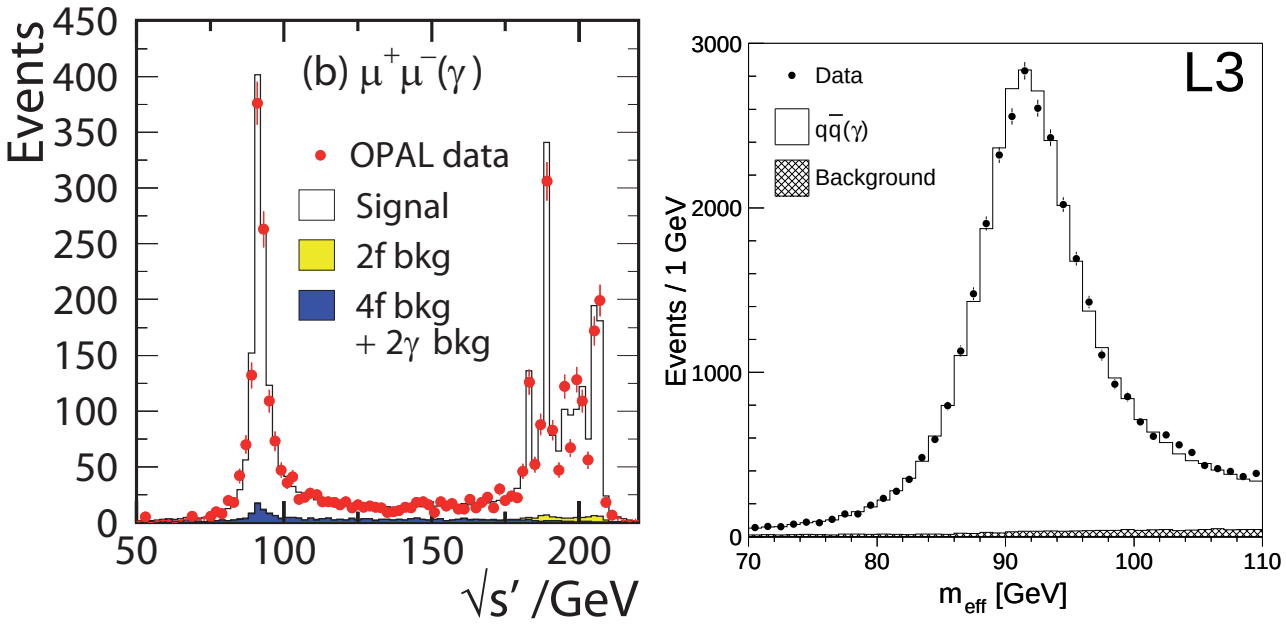


Figure C.1: Examples of reconstructed two-fermion mass spectra in the $Z + \gamma \to \mu^+\mu^- + \gamma$ channel (left) and in the hadronic channel (right), as measured by OPAL and by L3, respectively [257]. The data collected at different centre-of-mass energies is combined and compared to Monte-Carlo predictions using the nominal Z bosons mass [4]. The Z resonance peak is clearly visible.

is measured in the detector, or relative to the direction of the measured ISR photon.

After correcting for remaining background, the mass of the Z boson is extracted either by applying a Monte-Carlo event reweighting based on the corresponding matrix element of the signal process or by fitting an analytical function describing the signal spectrum to the data. The measured Z mass, $m_{\mathrm{Z}}^{\mathrm{f\bar{f}}}$, is then compared to the Z mass determined in precision measurements at Z-pole energies [4], $m_{\mathrm{Z}} = 91.1875 \pm 0.0021$ GeV. The comparison is converted into a difference in terms of the centre-of-mass energy, $\Delta\sqrt{s}$, between $\sqrt{s}$ derived from radiative return events and the nominal centre-of-mass energy, $\sqrt{s}_{\mathrm{LEP}}$, determined by the precise LEP energy calibration [246]:

$$\Delta\sqrt{s} = \sqrt{s} - \sqrt{s}_{\mathrm{LEP}} = \sqrt{s}\frac{m_{\mathrm{Z}}^{\mathrm{f\bar{f}}} - m_{\mathrm{Z}}}{m_{\mathrm{Z}}}\,. \tag{C.3}$$

This observable is eventually used to combine the results of the four LEP experiments.

Various sources of systematic uncertainties are studied and possible correlations between them are taken into account in the combination procedure. The dominant uncertainty is due to the modelling of the fragmentation process in hadronic Z decays. An uncertainty of 22 MeV on $\Delta\sqrt{s}$ is derived from a comparison of different fragmentation models implemented in the PYTHIA [140], HERWIG [258], and ARIADNE [254] software packages. The Monte-Carlo predictions of the $\mathrm{e^+e^-} \to \mathrm{f\bar{f}} + \gamma$ process are calculated using the KK v4.02 [60] Monte-Carlo generator. Theoretical uncertainties in the description of ISR and FSR and missing higher order corrections are estimated by reweighting events applying different orders of α in the prediction and comparing it to the $\mathcal{O}(\alpha^2)$ calculations in the Coherent Exclusive Exponentiation scheme. Furthermore, the effect of neglecting the interference between ISR and FSR was studied. The

Source	Uncertainty on $\Delta\sqrt{s}$ [MeV]
Fragmentation	22
ISR/FSR Modelling	7
Four Fermion Background	6
Z Mass	1
LEP Parameters	3
Total Correlated	23
Monte-Carlo Statistics	7
Detector Bias and Resolution	28
Total Uncorrelated	29
Total Systematics	37
Total Statistical	40
Total	54

Table C.1: Systematic and statistical uncertainties on the measurement of the LEP centre-of-mass energy shift, $\Delta\sqrt{s}$.

total systematic uncertainties due to modelling of ISR and FSR amounts to 7 MeV. The uncertainty due to the prediction of the four-fermion background using measured cross-sections as input is estimated to be 6 MeV. The operational parameters of the LEP collider may also influence the reconstruction of the two-fermion mass. In particular, the effects of beam energy spread and a possible asymmetry in beam energy were studied and found to influence $\Delta\sqrt{s}$ by less than 3 MeV. The uncertainty on the nominal Z boson mass contributes with less than 1 MeV. All these sources of systematic uncertainties are assumed to be fully correlated between experiments.

Each experiment determined the influence of detector alignment, bias in angular measurements, uncertainty of energy and momentum scale and resolution in great detail. Control samples were selected in data to measure the various detector and resolution effects. These uncertainties are treated as uncorrelated between experiments. Uncertainties from limited Monte-Carlo statistics also contribute. If sources of systematic uncertainties affect data from different data taking periods or different channels similarly also the corresponding correlations are taken into account. A summary of the different sources of systematic uncertainties is listed in Table C.1. The uncertainties due to Monte-Carlo statistics and detector bias and resolution are uncorrelated between experiments. Details of the systematic effects due to detector bias and resolution combine several individual sources of uncertainty and are discussed in the publications by the experiments [151, 255, 256, 257]. The total statistical and systematic uncertainties on the LEP average for $\Delta\sqrt{s}$ are 40 MeV and 36 MeV, respectively.

When combining all available LEP data [151, 255, 256, 257] with Z decays to hadrons, and to electron, muon, and tau pairs, the difference is found to be:

$$\Delta\sqrt{s} = -54 \pm 54 \text{ MeV}\,, \tag{C.4}$$

in good agreement with no shift with respect to the more precise standard LEP energy calibration. There is also no significant shift observed when analysing the leptonic and hadronic

Data set	$\Delta\sqrt{s}$ [MeV]
$e^+e^- \to \text{hadrons} + \gamma$	-88 ± 40 ± 56
$e^+e^- \to \ell^+\ell^- + \gamma$	-10 ± 80 ± 26
$\sqrt{s} = 183$ GeV	70 ± 98 ± 50
$\sqrt{s} = 189$ GeV	-86 ± 60 ± 46
$\sqrt{s} = 192 - 202$ GeV	-66 ± 62 ± 44
$\sqrt{s} = 205 - 209$ GeV	-140 ± 70 ± 52
All LEP data	-54 ± 40 ± 36

Table C.2: Combined results of ALEPH, DELPHI, L3, and OPAL on the determination of the LEP centre-of-mass energy shift, $\Delta\sqrt{s}$, with respect to the nominal value of $\sqrt{s}$. The results are shown for the leptonic and hadronic final states, as well as for the different data taking periods, together with the LEP combined value. Statistical and systematic uncertainties are given separately.

decay channels separately. Furthermore, there is no significant dependence on the LEP beam energy, respectively data taking periods, as illustrated in Figure C.2 and Table C.2.

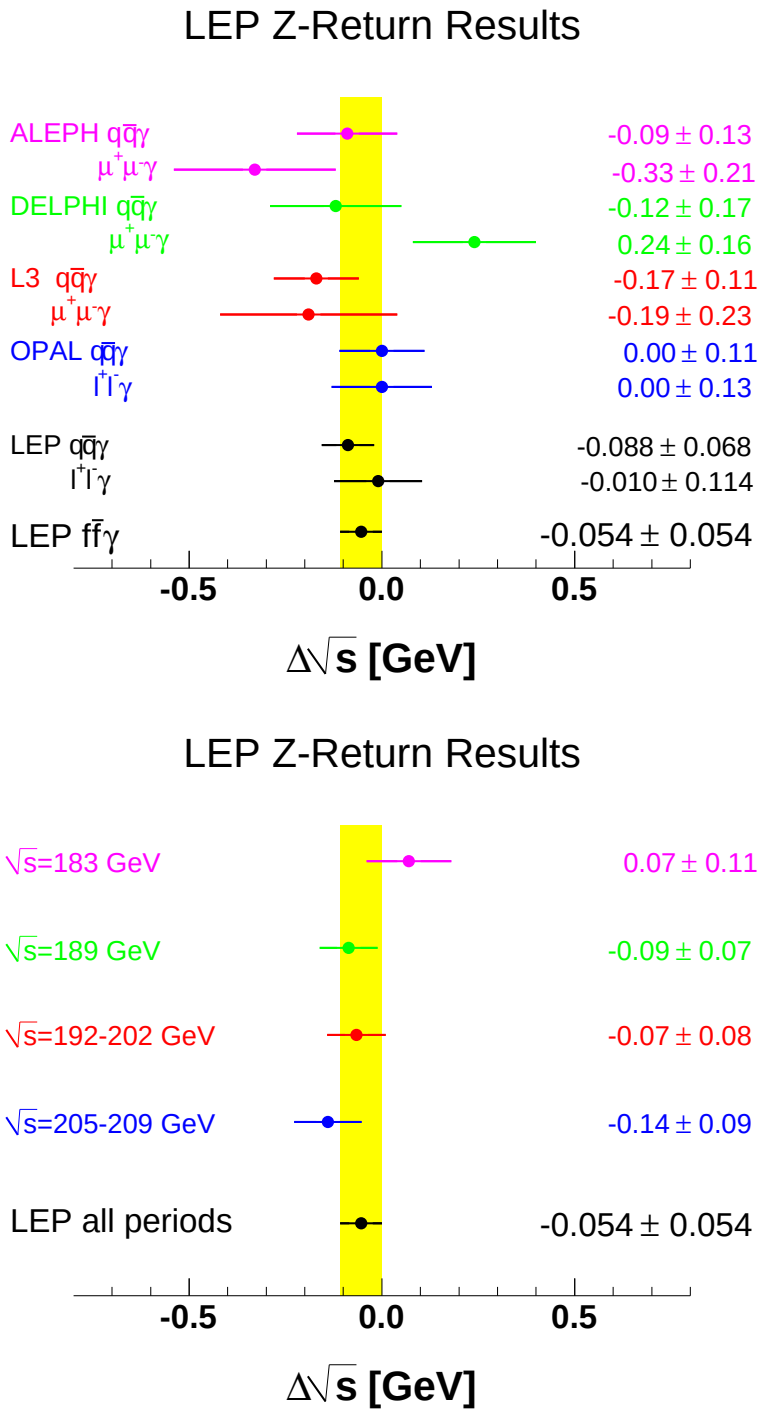


Figure C.2: Difference between the energy determined in Z-return events and the nominal LEP centre-of-mass energy, $\Delta\sqrt{s}$, for the different experiments and final states (top), and for the data taking periods with energies well above the W-pair threshold (bottom). The individual measurements as well as the LEP combined values take systematic uncertainties and their correlations into account.

Appendix D

Tests of the Colour-Reconnection Combination Procedure

Here we report on the tests of the LEP combination procedure used to combine the measurements of the LEP experiments on colour-reconnection (CR). It is shown that the LEP combination procedure is able to reproduce the combination of each experiment separately.

For each measurement, the dependence of the measured observable on the model parameter k_I is determined based on Monte-Carlo simulations. For the particle-flow based measurements, the results are reported in Table D.1. The corresponding parameter values for the phenomenological function shown in Equation 4.4 are listed in Table D.2. The parametrisations of $\delta_{\Delta m_{\mathrm{W}},i}(k_I)$ which are used to introduce systematic uncertainties for the likelihood functions of the CR measurements from Δm_{W} by ALEPH, DELPHI, and OPAL are given by:

$$\delta_{\Delta m_{\mathrm{W}},A}(k_I) = \begin{cases} 0.416408 + (0.624184)^2 \cdot k_I & , k_I \in [0.0, 1.3) \\ 1.227847 + (0.251441)^2 \cdot (k_I - 1.3) & , k_I \in [1.3, 2.5) \\ 1.529576 + (0.750313)^2 \cdot (k_I - 2.5) & , k_I \in [2.5, 4.5) \\ 3.030202 + (0.279341)^2 \cdot (k_I - 4.5) & , k_I \in [4.5, 6.0) \\ 3.449214 + (0.600389)^2 \cdot (k_I - 6.0) & , k_I \in [6.0, \infty) \end{cases} \tag{D.1}$$

$$\delta_{\Delta m_{\mathrm{W}},D}(k_I) = 0.233054 + (0.486925)^2 \cdot k_I \tag{D.2}$$

$$\delta_{\Delta m_{\mathrm{W}},O}(k_I) = 0.666308 + (0.483630)^2 \cdot k_I \,. \tag{D.3}$$

A graphical comparison of the original input and the parametrised $\Delta\chi^2$ distributions is displayed in Figure 4.2 and shows good agreement.

The ALEPH input is available as a set of $\Delta\chi^2(k_I)$ values including systematic uncertainties, which can be evaluated directly. The result is shown in Figure D.1 and the numerical analysis yields:

$$k_I = 0.33^{+1.82}_{-0.33} \,. \tag{D.4}$$

By construction, this agrees well with the original ALEPH result [111]. However, the ALEPH input does not include BEC systematic uncertainties. To incorporate also this effect, the correlated part of the systematic uncertainties is increased by 11%. This value is derived from

k_I	$R_N(k_I)$ for SK1 Model L3	OPAL
0.10	0.8613 ± 0.0037	1.2816 ± 0.0028
0.15	0.8598 ± 0.0037	1.2792 ± 0.0028
0.20	0.8585 ± 0.0037	1.2759 ± 0.0028
0.25	0.8561 ± 0.0037	1.2738 ± 0.0028
0.35	0.8551 ± 0.0037	1.2683 ± 0.0028
0.45	0.8509 ± 0.0036	1.2643 ± 0.0028
0.60	0.8482 ± 0.0036	1.2575 ± 0.0028
0.80	0.8414 ± 0.0037	1.2495 ± 0.0028
0.90	–	1.2464 ± 0.0028
1.00	0.8381 ± 0.0036	1.2420 ± 0.0028
1.10	–	1.2389 ± 0.0028
1.20	–	1.2355 ± 0.0028
1.30	–	1.2326 ± 0.0028
1.50	0.8318 ± 0.0036	1.2265 ± 0.0028
1.75	–	1.2201 ± 0.0028
2.00	–	1.2133 ± 0.0028
2.50	–	1.2029 ± 0.0028
3.00	0.8135 ± 0.0036	1.1942 ± 0.0028
5.00	0.7989 ± 0.0035	1.1705 ± 0.0028
10.00	–	1.1413 ± 0.0028
30.00	–	1.1101 ± 0.0028
60.00	–	1.0997 ± 0.0028
100.00	–	1.0918 ± 0.0028
10000.00	0.7482 ± 0.0033	1.0780 ± 0.0028

Table D.1: Monte-Carlo predictions for the particle-flow parameter $R_N(k_I)$ provided for the SK1 model by L3 and OPAL.

Experiment	a_1	a_2	a_3	a_4	b
L3	-12.1076	2.03107	-0.23384	-10.1780	1.18954
OPAL	-0.26969	0.20543	-0.06698	0.03388	10.8576

Table D.2: Parameter sets used for the functional description of the particle-flow input provided for the SK1 model by L3 and OPAL.

a dedicated study, not included in the ALEPH publication. The final result using only ALEPH data and including BEC uncertainties is

$$k_I = 0.34^{+1.86}_{-0.34}\,. \tag{D.5}$$

The 68% upper limit is about 3% higher compared to the original ALEPH input.

DELPHI provides $\Delta\chi^2(k_I)$ inputs from their ΔM_W and particle-flow analyses. In the DELPHI publication, both curves are simply added neglecting correlations, yielding [128]:

$$k_I = 2.2^{+2.5}_{-1.3}\,. \tag{D.6}$$

As a cross-check, the same combination strategy is applied, i.e., assuming no correlations. When using a total $\chi^2(k_I)$ of:

$$\chi^2(k_I, c) = \Delta\chi^2_{\Delta m_{\mathrm{W}},D,\mathrm{full}}(k_I) + \Delta\chi^2_{\mathrm{p-flow},D,\mathrm{full}}(k_I)\,, \tag{D.7}$$

the following result is obtained:

$$k_I = 2.17^{+2.55}_{-1.33}\,, \tag{D.8}$$

which is consistent with the combination performed by DELPHI. The LEP combination procedure allows a more refined treatment of correlations. Using a correlation coefficient of 0.50 between the measurements, motivated by the full covariance matrix for the particle-flow combination, the fit obtains:

$$k_I = 2.12^{+2.61}_{-1.33}\,. \tag{D.9}$$

This corresponds to a 5% increase of the positive uncertainty and a small shift of the minimum. The result is shown in Figure D.1.

The L3 input is provided in terms of $r(k_I)$ derived from Monte-Carlo simulations and the measured r_{data} together with measurement uncertainties. The fit results in:

$$k_I = 0.76^{+1.89}_{-1.22}\,, \tag{D.10}$$

and the corresponding $\Delta\chi^2$ curve is shown in Figure D.1. The result obtained is different from the L3 paper on CR [129], where a value of $k_I = 0.08^{+1.02}_{-0.08}$ is derived. This is due to the difference between the non-CR reference Monte-Carlo simulation used by L3 and the common LEP Monte-Carlo sample used in this combination. These Monte-Carlo samples were generated with different fragmentation and hadronisation parameters; the former was tuned to describe L3 data best. The difference in the k_I result is fully compatible with the systematic uncertainty assigned to hadronisation and fragmentation effects.

OPAL measures k_I in W-mass shift and particle-flow analyses. As for DELPHI, a correlation coefficient of 0.50 is assumed between the correlated uncertainties in both inputs. Both $\Delta\chi^2$ curves and their combination are shown in Figure D.1. The combined fit yields

$$k_I = 1.24^{+1.13}_{-0.77}\,. \tag{D.11}$$

The 68% C.L. upper limit of 2.37 is in good agreement with the OPAL result $k_I < 2.3$ at 68% C.L. [114]. OPAL presents the results in terms of $p_{\rm reco} = 0.43^{+0.15}_{-0.20}$ which translates into $k_I \approx 1.3^{+1.1}_{-0.8}$, using the conversion from $p_{\rm reco}$ to k_I based on OPAL's Monte-Carlo simulation. Using only information from ΔM_W, the fit obtains $k_I = 1.75^{+1.99}_{-1.28}$, also agreeing well with the OPAL publication: $k_I = 1.7^{+2.0}_{-1.2}$.

In summary, the LEP combination procedure reproduces well the results obtained by each collaboration, with the observed differences explained by known systematic effects.

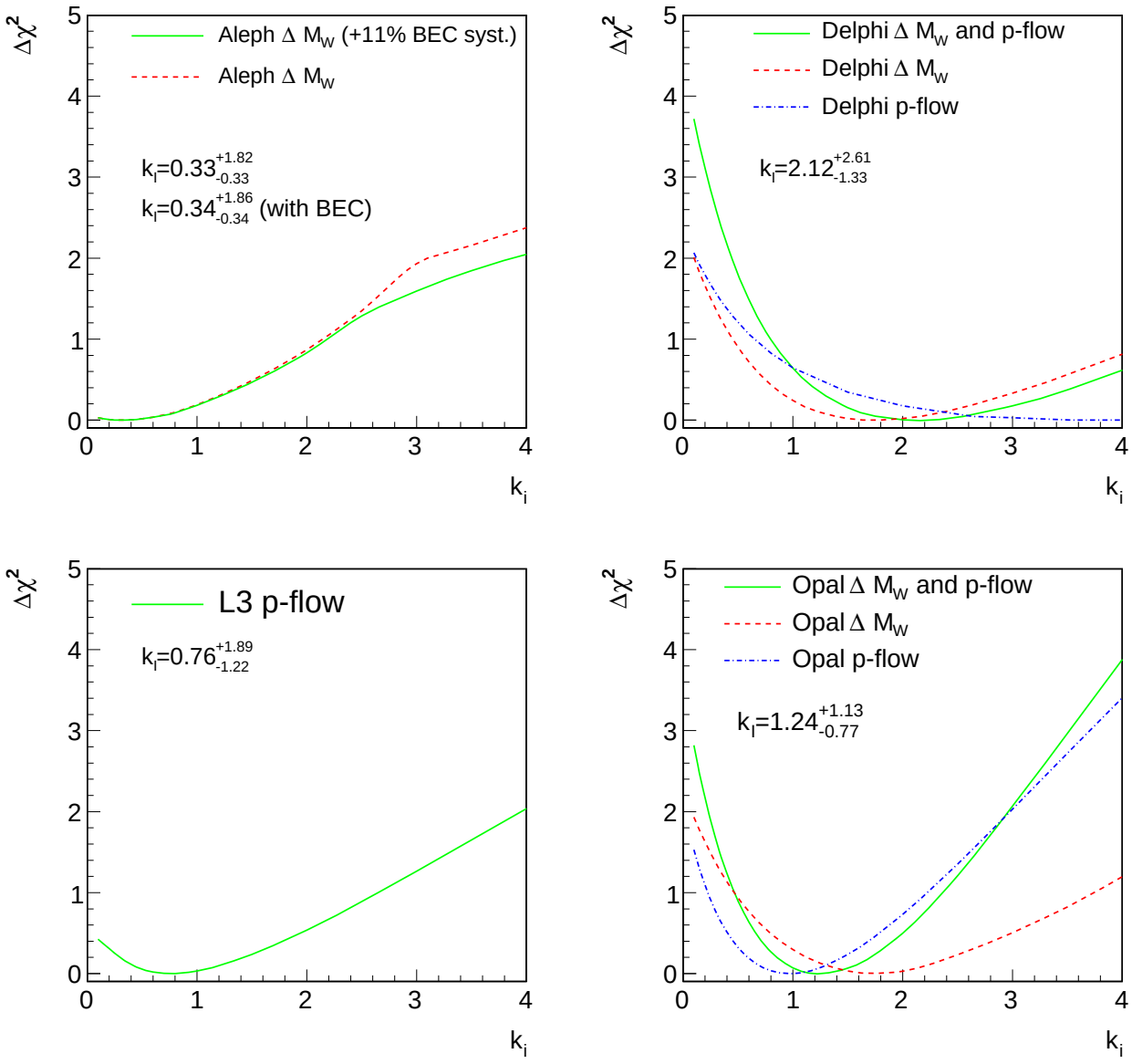


Figure D.1: LEP input to the CR measurement in terms of $\Delta\chi^2$ curves. The input data provided by the ALEPH experiment are shown as a dashed line and are compared to the data used in the LEP combination, where additional BEC systematic uncertainties are taken into account. The DELPHI and OPAL results from the analysis of the W-mass shift, Δm_{W}, and from the measurement of particle-flow are shown as dashed and dotted lines, respectively. The solid line represents the combined results taking correlations into account. The L3 experiment provided input from the particle-flow measurement, also shown as a solid line.

Appendix E

Detailed Inputs and Results of LEP Four-Fermion Averages

Tables E.1 - E.21 give the details of the inputs and of the results for the calculation of LEP averages of the measured four-fermion cross-sections and the corresponding ratios of measured cross-sections to the theoretical predictions. For both inputs and results, whenever relevant, the breakdown of the errors into their various components is given in the tables.

For each measurement, the collaborations have privately provided unpublished information which is necessary for the combination of the LEP results, such as the expected statistical error or the split of the total systematic uncertainty into correlated and uncorrelated components. Where necessary, minor re-arrangements with respect to published results across error categories have been applied.

$\sqrt{s}$ (GeV)	σ_{WW}	$\Delta\sigma^{\mathrm{stat}}_{\mathrm{WW}}$	(LCEC) $\Delta\sigma^{\mathrm{syst}}_{\mathrm{WW}}$	(LUEU) $\Delta\sigma^{\mathrm{syst}}_{\mathrm{WW}}$	(LUEC) $\Delta\sigma^{\mathrm{syst}}_{\mathrm{WW}}$	$\Delta\sigma^{\mathrm{syst}}_{\mathrm{WW}}$	$\Delta\sigma_{\mathrm{WW}}$
ALEPH [157]							
182.7	15.86	±0.61	±0.08	±0.08	±0.09	±0.14	±0.63
188.6	15.78	±0.34	±0.07	±0.05	±0.09	±0.12	±0.36
191.6	17.10	±0.90	±0.07	±0.07	±0.09	±0.14	±0.90
195.5	16.60	±0.52	±0.07	±0.06	±0.09	±0.12	±0.54
199.5	16.93	±0.50	±0.07	±0.06	±0.09	±0.12	±0.52
201.6	16.63	±0.70	±0.07	±0.07	±0.09	±0.13	±0.71
204.9	16.84	±0.53	±0.07	±0.06	±0.09	±0.13	±0.54
206.6	17.42	±0.41	±0.07	±0.06	±0.09	±0.13	±0.43
DELPHI [158]							
182.7	16.07	±0.68	±0.09	±0.09	±0.08	±0.15	±0.70
188.6	16.09	±0.39	±0.08	±0.09	±0.09	±0.15	±0.42
191.6	16.64	±0.99	±0.09	±0.10	±0.09	±0.16	±1.00
195.5	17.04	±0.58	±0.09	±0.10	±0.09	±0.16	±0.60
199.5	17.39	±0.55	±0.09	±0.10	±0.09	±0.16	±0.57
201.6	17.37	±0.80	±0.10	±0.10	±0.09	±0.17	±0.82
204.9	17.56	±0.57	±0.10	±0.10	±0.09	±0.17	±0.59
206.6	16.35	±0.44	±0.10	±0.10	±0.09	±0.17	±0.47
L3 [159]							
182.7	16.53	±0.67	±0.19	±0.13	±0.12	±0.26	±0.72
188.6	16.17	±0.37	±0.11	±0.06	±0.11	±0.17	±0.41
191.6	16.11	±0.90	±0.11	±0.07	±0.11	±0.17	±0.92
195.5	16.22	±0.54	±0.11	±0.06	±0.10	±0.16	±0.57
199.5	16.49	±0.56	±0.11	±0.07	±0.11	±0.17	±0.58
201.6	16.01	±0.82	±0.11	±0.06	±0.12	±0.17	±0.84
204.9	17.00	±0.58	±0.12	±0.06	±0.11	±0.17	±0.60
206.6	17.33	±0.44	±0.12	±0.04	±0.11	±0.17	±0.47
OPAL [160]							
182.7	15.45	±0.61	±0.10	±0.04	±0.05	±0.12	±0.62
188.6	16.24	±0.35	±0.10	±0.04	±0.03	±0.11	±0.37
191.6	15.93	±0.86	±0.10	±0.04	±0.03	±0.11	±0.86
195.5	18.27	±0.57	±0.11	±0.05	±0.04	±0.12	±0.58
199.5	16.29	±0.54	±0.11	±0.04	±0.03	±0.12	±0.55
201.6	18.01	±0.81	±0.11	±0.05	±0.04	±0.13	±0.82
204.9	16.05	±0.52	±0.11	±0.04	±0.04	±0.12	±0.53
206.6	17.64	±0.42	±0.11	±0.05	±0.04	±0.13	±0.44

Table E.1: W-pair production cross-section (in pb) for different centre–of–mass energies from the four LEP experiments. The first column contains the centre–of–mass energy and the second the measurements. Observed statistical uncertainties are used in the fit and are listed in the third column; when asymmetric errors are quoted by the collaborations, the positive error is listed in the table and used in the fit. The fourth, fifth and sixth columns contain the components of the systematic errors, as subdivided by the collaborations into LEP-correlated energy-correlated (LCEC), LEP-uncorrelated energy-uncorrelated (LUEU), LEP-uncorrelated energy-correlated (LUEC). The total systematic error is given in the seventh column, the total error in the eighth.

LEP Averages								
$\sqrt{s}$ (GeV)	σ_{WW}	$\Delta\sigma^{\mathrm{stat}}_{\mathrm{WW}}$	(LCEC) $\Delta\sigma^{\mathrm{syst}}_{\mathrm{WW}}$	(LUEU) $\Delta\sigma^{\mathrm{syst}}_{\mathrm{WW}}$	(LUEC) $\Delta\sigma^{\mathrm{syst}}_{\mathrm{WW}}$	$\Delta\sigma^{\mathrm{syst}}_{\mathrm{WW}}$	$\Delta\sigma_{\mathrm{WW}}$	χ^2/dof
182.7	15.92	±0.33	±0.10	±0.04	±0.04	±0.11	±0.34	26.6/24
188.6	16.05	±0.18	±0.08	±0.03	±0.04	±0.10	±0.21	
191.6	16.42	±0.46	±0.08	±0.04	±0.04	±0.10	±0.47	
195.5	16.99	±0.28	±0.08	±0.03	±0.04	±0.10	±0.29	
199.5	16.77	±0.27	±0.08	±0.03	±0.04	±0.10	±0.29	
201.6	16.98	±0.39	±0.08	±0.04	±0.04	±0.10	±0.40	
204.9	16.81	±0.27	±0.08	±0.03	±0.04	±0.10	±0.29	
206.6	17.20	±0.21	±0.09	±0.03	±0.04	±0.11	±0.24	

Table E.2: LEP combined W-pair production cross-section (in pb) for different centre–of–mass energies. The first column contains the centre–of–mass energy and the second the measurements. Observed statistical uncertainties are used in the fit and are listed in the third column; when asymmetric errors are quoted by the collaborations, the positive error is listed in the table and used in the fit. The fourth, fifth and sixth columns contain the components of the systematic errors, as subdivided by the collaborations into LEP-correlated energy-correlated (LCEC), LEP-uncorrelated energy-uncorrelated (LUEU), LEP-uncorrelated energy-correlated (LUEC). The total systematic error is given in the seventh column, the total error in the eighth. The χ^2/dof of the fit is also given in the ninth column.

$\sqrt{s}$(GeV)	182.7	188.6	191.6	195.5	199.5	201.6	204.9	206.6
182.7	1.000	0.145	0.065	0.104	0.105	0.076	0.104	0.130
188.6	0.145	1.000	0.093	0.148	0.149	0.108	0.148	0.186
191.6	0.065	0.093	1.000	0.066	0.067	0.048	0.066	0.083
195.5	0.104	0.148	0.066	1.000	0.107	0.077	0.106	0.133
199.5	0.105	0.149	0.067	0.107	1.000	0.078	0.106	0.134
201.6	0.076	0.108	0.048	0.077	0.078	1.000	0.077	0.097
204.9	0.104	0.148	0.066	0.106	0.106	0.077	1.000	0.132
206.6	0.130	0.186	0.083	0.133	0.134	0.097	0.132	1.000

Table E.3: Correlation matrix for the LEP combined W-pair cross-sections listed in Table E.2. Correlations are all positive and range from 5% to 19%.

$\sqrt{s}$ (GeV)	WW cross-section (pb)	
	$\sigma_{\mathrm{WW}}^{\mathrm{YFSWW}}$	$\sigma_{\mathrm{WW}}^{\mathrm{RACOONWW}}$
182.7	15.361 ± 0.005	15.368 ± 0.008
188.6	16.266 ± 0.005	16.249 ± 0.011
191.6	16.568 ± 0.006	16.519 ± 0.009
195.5	16.841 ± 0.006	16.801 ± 0.009
199.5	17.017 ± 0.007	16.979 ± 0.009
201.6	17.076 ± 0.006	17.032 ± 0.009
204.9	17.128 ± 0.006	17.079 ± 0.009
206.6	17.145 ± 0.006	17.087 ± 0.009

Table E.4: W-pair cross-section predictions (in pb) for different centre–of–mass energies, according to YFSWW [161, 167] and RACOONWW [168], for $m_{\mathrm{W}} = 80.35$ GeV. The errors listed in the table are only the statistical errors from the numerical integration of the cross-section.

$\sqrt{s}$ (GeV)	$\mathcal{R}_{\mathrm{WW}}$	$\Delta\mathcal{R}^{\mathrm{stat}}_{\mathrm{WW}}$	(LCEU) $\Delta\mathcal{R}^{\mathrm{syst}}_{\mathrm{WW}}$	(LCEC) $\Delta\mathcal{R}^{\mathrm{syst}}_{\mathrm{WW}}$	(LUEU) $\Delta\mathcal{R}^{\mathrm{syst}}_{\mathrm{WW}}$	(LUEC) $\Delta\mathcal{R}^{\mathrm{syst}}_{\mathrm{WW}}$	$\Delta\mathcal{R}_{\mathrm{WW}}$	χ^2/dof
YFSWW [161, 167]								
182.7	1.037	±0.021	±0.000	±0.006	±0.003	±0.003	±0.022	26.6/24
188.6	0.987	±0.011	±0.000	±0.005	±0.002	±0.003	±0.013	
191.6	0.991	±0.028	±0.000	±0.005	±0.002	±0.002	±0.028	
195.5	1.009	±0.016	±0.000	±0.005	±0.002	±0.002	±0.018	
199.5	0.985	±0.016	±0.000	±0.005	±0.002	±0.003	±0.017	
201.6	0.994	±0.023	±0.000	±0.005	±0.002	±0.003	±0.023	
204.9	0.982	±0.016	±0.000	±0.005	±0.002	±0.002	±0.017	
206.6	1.003	±0.013	±0.000	±0.005	±0.002	±0.002	±0.014	
Average	0.995	±0.006	±0.000	±0.005	±0.001	±0.003	±0.008	32.2/31
RACOONWW [168]								
182.7	1.036	±0.021	±0.001	±0.007	±0.003	±0.003	±0.022	26.6/24
188.6	0.988	±0.011	±0.001	±0.005	±0.002	±0.003	±0.013	
191.6	0.994	±0.028	±0.001	±0.005	±0.002	±0.002	±0.028	
195.5	1.011	±0.017	±0.001	±0.005	±0.002	±0.003	±0.018	
199.5	0.987	±0.016	±0.001	±0.005	±0.002	±0.003	±0.017	
201.6	0.997	±0.023	±0.001	±0.005	±0.002	±0.003	±0.024	
204.9	0.984	±0.016	±0.001	±0.005	±0.002	±0.002	±0.017	
206.6	1.007	±0.013	±0.001	±0.005	±0.002	±0.002	±0.014	
Average	0.997	±0.006	±0.000	±0.005	±0.001	±0.003	±0.008	32.0/31

Table E.5: Ratios of LEP combined W-pair cross-section measurements to the expectations of the considered theoretical models, for different centre–of–mass energies and for all energies combined. The first column contains the centre–of–mass energy, the second the combined ratios, the third the statistical errors. The fourth, fifth, sixth and seventh columns contain the sources of systematic errors that are considered as LEP-correlated energy-uncorrelated (LCEU), LEP-correlated energy-correlated (LCEC), LEP-uncorrelated energy-uncorrelated (LUEU), LEP-uncorrelated energy-correlated (LUEC). The total error is given in the eighth column. The only LCEU systematic sources considered are the statistical errors on the cross-section theoretical predictions, while the LCEC, LUEU and LUEC sources are those coming from the corresponding errors on the cross-section measurements. For the LEP averages, the χ^2/dof of the fit is also given in the ninth column.

Decay channel	$\mathcal{B}$	$\Delta\mathcal{B}^{\text{stat}}$	$\Delta\mathcal{B}^{\text{syst}}$ (unc)	$\Delta\mathcal{B}^{\text{syst}}$ (cor)	$\Delta\mathcal{B}^{\text{syst}}$	$\Delta\mathcal{B}$	3×3 correlation for $\Delta\mathcal{B}$
ALEPH [157]							
$\mathcal{B}(\text{W} \to \text{e}\overline{\nu}_{\text{e}})$	10.78	±0.27	±0.09	±0.04	±0.10	±0.29	1.000 -0.009 -0.332
$\mathcal{B}(\text{W} \to \mu\overline{\nu}_{\mu})$	10.87	±0.25	±0.07	±0.04	±0.08	±0.26	-0.009 1.000 -0.268
$\mathcal{B}(\text{W} \to \tau\overline{\nu}_{\tau})$	11.25	±0.32	±0.19	±0.05	±0.20	±0.38	-0.332 -0.268 1.000
DELPHI [158]							
$\mathcal{B}(\text{W} \to \text{e}\overline{\nu}_{\text{e}})$	10.55	±0.31	±0.13	±0.05	±0.14	±0.34	1.000 0.030 -0.340
$\mathcal{B}(\text{W} \to \mu\overline{\nu}_{\mu})$	10.65	±0.26	±0.06	±0.05	±0.08	±0.27	0.030 1.000 -0.170
$\mathcal{B}(\text{W} \to \tau\overline{\nu}_{\tau})$	11.46	±0.39	±0.17	±0.09	±0.19	±0.43	-0.340 -0.170 1.000
L3 [159]							
$\mathcal{B}(\text{W} \to \text{e}\overline{\nu}_{\text{e}})$	10.78	±0.29	±0.10	±0.08	±0.13	±0.32	1.000 -0.016 -0.279
$\mathcal{B}(\text{W} \to \mu\overline{\nu}_{\mu})$	10.03	±0.29	±0.10	±0.07	±0.12	±0.31	-0.016 1.000 -0.295
$\mathcal{B}(\text{W} \to \tau\overline{\nu}_{\tau})$	11.89	±0.40	±0.17	±0.11	±0.20	±0.45	-0.279 -0.295 1.000
OPAL [160]							
$\mathcal{B}(\text{W} \to \text{e}\overline{\nu}_{\text{e}})$	10.71	±0.25	±0.09	±0.06	±0.11	±0.27	1.000 0.135 -0.303
$\mathcal{B}(\text{W} \to \mu\overline{\nu}_{\mu})$	10.78	±0.24	±0.07	±0.07	±0.10	±0.26	0.135 1.000 -0.230
$\mathcal{B}(\text{W} \to \tau\overline{\nu}_{\tau})$	11.14	±0.31	±0.16	±0.06	±0.17	±0.35	-0.303 -0.230 1.000
LEP Average (without lepton universality assumption)							
$\mathcal{B}(\text{W} \to \text{e}\overline{\nu}_{\text{e}})$	10.71	±0.14	±0.05	±0.05	±0.07	±0.16	1.000 0.136 -0.201
$\mathcal{B}(\text{W} \to \mu\overline{\nu}_{\mu})$	10.63	±0.13	±0.04	±0.05	±0.07	±0.15	0.136 1.000 -0.122
$\mathcal{B}(\text{W} \to \tau\overline{\nu}_{\tau})$	11.38	±0.17	±0.09	±0.07	±0.11	±0.21	-0.201 -0.122 1.000
χ^2/dof	6.3/9						
LEP Average (with lepton universality assumption)							
$\mathcal{B}(\text{W} \to \ell\overline{\nu}_{\ell})$	10.86	±0.06	±0.03	±0.06	±0.07	±0.09	
$\mathcal{B}(\text{W} \to \text{had.})$	67.41	±0.18	±0.10	±0.17	±0.20	±0.27	
χ^2/dof	15.4/11						

Table E.6: W branching fraction measurements (in %). The first column contains the decay channel, the second the measurements, the third the statistical uncertainty. The fourth and fifth column list the uncorrelated and correlated components of the systematic errors, as provided by the collaborations. The total systematic error is given in the sixth column and the total error in the seventh. Correlation matrices for the three leptonic branching fractions are given in the last column.

ALEPH [157]

$\sqrt{s}$ interval (GeV)	Luminosity (pb^{-1})	Luminosity weighted $\sqrt{s}$ (GeV)
180-184	56.81	182.65

$\cos\theta_{W^-}$ bin i	1	2	3	4	5	6	7	8	9	10
σ_i (pb)	0.216	0.498	0.696	1.568	1.293	1.954	2.486	2.228	4.536	6.088
$\delta\sigma_i$(stat) (pb)	0.053	0.137	0.185	0.517	0.319	0.481	0.552	0.363	0.785	0.874
$\delta\sigma_i$(stat,exp.) (pb)	0.263	0.276	0.309	0.341	0.376	0.415	0.459	0.523	0.597	0.714
$\delta\sigma_i$(syst,unc) (pb)	0.012	0.018	0.017	0.025	0.023	0.021	0.036	0.047	0.047	0.066
$\delta\sigma_i$(syst,cor) (pb)	0.004	0.003	0.003	0.003	0.003	0.004	0.004	0.003	0.004	0.006

$\sqrt{s}$ interval (GeV)	Luminosity (pb^{-1})	Luminosity weighted $\sqrt{s}$ (GeV)
184-194	203.14	189.05

$\cos\theta_{W^-}$ bin i	1	2	3	4	5	6	7	8	9	10
σ_i (pb)	0.665	0.743	0.919	0.990	1.156	2.133	2.795	3.070	3.851	5.772
$\delta\sigma_i$(stat) (pb)	0.148	0.140	0.158	0.142	0.144	0.287	0.337	0.297	0.300	0.366
$\delta\sigma_i$(stat,exp.) (pb)	0.132	0.147	0.157	0.175	0.196	0.223	0.246	0.282	0.332	0.408
$\delta\sigma_i$(syst,unc) (pb)	0.010	0.016	0.015	0.024	0.021	0.020	0.035	0.047	0.049	0.075
$\delta\sigma_i$(syst,cor) (pb)	0.003	0.003	0.003	0.002	0.002	0.003	0.003	0.003	0.005	0.005

$\sqrt{s}$ interval (GeV)	Luminosity (pb^{-1})	Luminosity weighted $\sqrt{s}$ (GeV)
194-204	208.03	198.42

$\cos\theta_{W^-}$ bin i	1	2	3	4	5	6	7	8	9	10
σ_i (pb)	0.802	0.475	0.886	0.972	1.325	1.889	2.229	3.581	4.428	6.380
$\delta\sigma_i$(stat) (pb)	0.225	0.082	0.162	0.147	0.186	0.248	0.245	0.363	0.343	0.368
$\delta\sigma_i$(stat,exp.) (pb)	0.124	0.134	0.149	0.167	0.188	0.214	0.241	0.281	0.338	0.433
$\delta\sigma_i$(syst,unc) (pb)	0.007	0.013	0.012	0.021	0.018	0.016	0.032	0.046	0.049	0.082
$\delta\sigma_i$(syst,cor) (pb)	0.003	0.002	0.002	0.002	0.002	0.002	0.002	0.003	0.003	0.004

$\sqrt{s}$ interval (GeV)	Luminosity (pb^{-1})	Luminosity weighted $\sqrt{s}$ (GeV)
204-210	214.62	205.90

$\cos\theta_{W^-}$ bin i	1	2	3	4	5	6	7	8	9	10
σ_i (pb)	0.334	0.637	0.800	1.229	1.229	1.789	2.810	2.740	4.192	8.005
$\delta\sigma_i$(stat) (pb)	0.072	0.136	0.148	0.224	0.176	0.237	0.351	0.246	0.306	0.474
$\delta\sigma_i$(stat,exp.) (pb)	0.114	0.126	0.143	0.155	0.180	0.206	0.234	0.273	0.338	0.443
$\delta\sigma_i$(syst,unc) (pb)	0.008	0.013	0.013	0.020	0.018	0.017	0.033	0.046	0.052	0.089
$\delta\sigma_i$(syst,cor) (pb)	0.003	0.003	0.003	0.002	0.002	0.003	0.003	0.003	0.004	0.005

Table E.7: W^- differential angular cross-section in the 10 angular bins for the four chosen energy intervals for the ALEPH experiment. For each energy range, the measured integrated luminosity and the luminosity-weighted centre-of-mass energy is reported. The results per angular bin in each energy interval are then presented: σ_i indicates the average of $d[\sigma_{WW}(BR_{e\nu}+BR_{\mu\nu})]/d\cos\theta_{W^-}$ in the i-th bin of $\cos\theta_{W^-}$ with width 0.2. The values in each bin of the measured and expected statistical error and of the systematic errors, LEP uncorrelated and correlated, are reported as well. All values are expressed in pb.

DELPHI [158]

$\sqrt{s}$ interval (GeV)	Luminosity (pb^{-1})	Luminosity weighted $\sqrt{s}$ (GeV)
180-184	51.63	182.65

$\cos\theta_{W^-}$ bin i	1	2	3	4	5	6	7	8	9	10
σ_i (pb)	0.715	0.795	1.175	1.365	1.350	1.745	1.995	2.150	4.750	6.040
$\delta\sigma_i$(stat) (pb)	0.320	0.315	0.380	0.400	0.400	0.450	0.485	0.510	0.775	0.895
$\delta\sigma_i$(stat,exp.) (pb)	0.320	0.315	0.350	0.370	0.405	0.450	0.505	0.580	0.695	0.850
$\delta\sigma_i$(syst,unc) (pb)	0.020	0.025	0.035	0.035	0.040	0.085	0.050	0.065	0.095	0.075
$\delta\sigma_i$(syst,cor) (pb)	0.045	0.025	0.020	0.015	0.015	0.025	0.015	0.015	0.030	0.035

$\sqrt{s}$ interval (GeV)	Luminosity (pb^{-1})	Luminosity weighted $\sqrt{s}$ (GeV)
184-194	178.32	189.03

$\cos\theta_{W^-}$ bin i	1	2	3	4	5	6	7	8	9	10
σ_i (pb)	0.865	0.760	0.990	0.930	1.330	1.460	1.675	2.630	4.635	5.400
$\delta\sigma_i$(stat) (pb)	0.180	0.170	0.185	0.180	0.215	0.225	0.240	0.300	0.405	0.455
$\delta\sigma_i$(stat,exp.) (pb)	0.165	0.170	0.180	0.200	0.215	0.240	0.270	0.320	0.385	0.490
$\delta\sigma_i$(syst,unc) (pb)	0.020	0.020	0.035	0.035	0.040	0.085	0.050	0.060	0.100	0.085
$\delta\sigma_i$(syst,cor) (pb)	0.040	0.020	0.020	0.015	0.015	0.020	0.015	0.015	0.025	0.035

$\sqrt{s}$ interval (GeV)	Luminosity (pb^{-1})	Luminosity weighted $\sqrt{s}$ (GeV)
194-204	193.52	198.46

$\cos\theta_{W^-}$ bin i	1	2	3	4	5	6	7	8	9	10
σ_i (pb)	0.600	0.675	1.510	1.150	1.055	1.635	2.115	3.175	4.470	7.140
$\delta\sigma_i$(stat) (pb)	0.155	0.160	0.215	0.190	0.185	0.225	0.255	0.320	0.385	0.500
$\delta\sigma_i$(stat,exp.) (pb)	0.150	0.160	0.170	0.180	0.200	0.230	0.260	0.310	0.380	0.505
$\delta\sigma_i$(syst,unc) (pb)	0.015	0.020	0.030	0.035	0.035	0.085	0.045	0.055	0.105	0.100
$\delta\sigma_i$(syst,cor) (pb)	0.025	0.015	0.015	0.015	0.015	0.015	0.010	0.015	0.025	0.030

$\sqrt{s}$ interval (GeV)	Luminosity (pb^{-1})	Luminosity weighted $\sqrt{s}$ (GeV)
204-210	198.59	205.91

$\cos\theta_{W^-}$ bin i	1	2	3	4	5	6	7	8	9	10
σ_i (pb)	0.275	0.590	0.575	0.930	1.000	1.190	2.120	2.655	4.585	7.290
$\delta\sigma_i$(stat) (pb)	0.120	0.145	0.140	0.170	0.175	0.195	0.255	0.290	0.385	0.505
$\delta\sigma_i$(stat,exp.) (pb)	0.145	0.150	0.160	0.175	0.195	0.220	0.250	0.300	0.380	0.520
$\delta\sigma_i$(syst,unc) (pb)	0.015	0.020	0.025	0.035	0.035	0.085	0.045	0.055	0.110	0.110
$\delta\sigma_i$(syst,cor) (pb)	0.020	0.015	0.010	0.010	0.015	0.010	0.010	0.010	0.020	0.030

Table E.8: W^- differential angular cross-section in the 10 angular bins for the four chosen energy intervals for the DELPHI experiment. For each energy range, the measured integrated luminosity and the luminosity-weighted centre-of-mass energy is reported. The results per angular bin in each energy interval are then presented: σ_i indicates the average of $d[\sigma_{WW}(BR_{e\nu}+BR_{\mu\nu})]/d\cos\theta_{W^-}$ in the i-th bin of $\cos\theta_{W^-}$ with width 0.2. The values in each bin of the measured and expected statistical error and of the systematic errors, LEP uncorrelated and correlated, are reported as well. All values are expressed in pb.

L3 [159]

$\sqrt{s}$ interval (GeV)	Luminosity (pb^{-1})	Luminosity weighted $\sqrt{s}$ (GeV)
180-184	55.46	182.68

$\cos\theta_{W^-}$ bin i	1	2	3	4	5	6	7	8	9	10
σ_i (pb)	0.691	0.646	0.508	0.919	1.477	2.587	3.541	3.167	3.879	4.467
$\delta\sigma_i$(stat) (pb)	0.270	0.265	0.243	0.322	0.407	0.539	0.640	0.619	0.708	0.801
$\delta\sigma_i$(stat,exp.) (pb)	0.269	0.290	0.329	0.364	0.404	0.453	0.508	0.591	0.704	0.877
$\delta\sigma_i$(syst,unc) (pb)	0.016	0.009	0.007	0.011	0.018	0.031	0.043	0.039	0.048	0.058
$\delta\sigma_i$(syst,cor) (pb)	0.002	0.002	0.002	0.003	0.005	0.009	0.012	0.011	0.013	0.015

$\sqrt{s}$ interval (GeV)	Luminosity (pb^{-1})	Luminosity weighted $\sqrt{s}$ (GeV)
184-194	206.49	189.16

$\cos\theta_{W^-}$ bin i	1	2	3	4	5	6	7	8	9	10
σ_i (pb)	0.759	0.902	1.125	1.320	1.472	1.544	2.085	2.870	4.144	6.022
$\delta\sigma_i$(stat) (pb)	0.128	0.151	0.173	0.190	0.209	0.213	0.254	0.303	0.370	0.459
$\delta\sigma_i$(stat,exp.) (pb)	0.115	0.137	0.160	0.180	0.205	0.223	0.262	0.304	0.367	0.461
$\delta\sigma_i$(syst,unc) (pb)	0.017	0.013	0.015	0.015	0.017	0.018	0.024	0.034	0.048	0.074
$\delta\sigma_i$(syst,cor) (pb)	0.003	0.003	0.004	0.005	0.005	0.005	0.007	0.010	0.014	0.021

$\sqrt{s}$ interval (GeV)	Luminosity (pb^{-1})	Luminosity weighted $\sqrt{s}$ (GeV)
194-204	203.50	198.30

$\cos\theta_{W^-}$ bin i	1	2	3	4	5	6	7	8	9	10
σ_i (pb)	0.652	0.709	0.880	0.859	1.140	1.295	2.114	2.334	3.395	5.773
$\delta\sigma_i$(stat) (pb)	0.105	0.123	0.146	0.155	0.179	0.192	0.255	0.264	0.333	0.442
$\delta\sigma_i$(stat,exp.) (pb)	0.092	0.117	0.140	0.164	0.184	0.209	0.245	0.288	0.354	0.459
$\delta\sigma_i$(syst,unc) (pb)	0.014	0.010	0.011	0.010	0.013	0.015	0.024	0.027	0.040	0.071
$\delta\sigma_i$(syst,cor) (pb)	0.002	0.002	0.003	0.003	0.004	0.004	0.007	0.008	0.012	0.020

$\sqrt{s}$ interval (GeV)	Luminosity (pb^{-1})	Luminosity weighted $\sqrt{s}$ (GeV)
204-210	217.30	205.96

$\cos\theta_{W^-}$ bin i	1	2	3	4	5	6	7	8	9	10
σ_i (pb)	0.678	0.578	0.768	1.052	1.620	1.734	1.873	2.903	4.638	7.886
$\delta\sigma_i$(stat) (pb)	0.111	0.114	0.140	0.168	0.212	0.226	0.238	0.302	0.394	0.534
$\delta\sigma_i$(stat,exp.) (pb)	0.089	0.117	0.141	0.164	0.186	0.216	0.251	0.303	0.387	0.528
$\delta\sigma_i$(syst,unc) (pb)	0.015	0.008	0.010	0.012	0.019	0.020	0.021	0.034	0.054	0.097
$\delta\sigma_i$(syst,cor) (pb)	0.002	0.002	0.003	0.004	0.006	0.006	0.006	0.010	0.016	0.027

Table E.9: W^- differential angular cross-section in the 10 angular bins for the four chosen energy intervals for the L3 experiment. For each energy range, the measured integrated luminosity and the luminosity-weighted centre-of-mass energy is reported. The results per angular bin in each energy interval are then presented: σ_i indicates the average of $d[\sigma_{WW}(BR_{e\nu}+BR_{\mu\nu})]/d\cos\theta_{W^-}$ in the i-th bin of $\cos\theta_{W^-}$ with width 0.2. The values in each bin of the measured and expected statistical error and of the systematic errors, LEP uncorrelated and correlated, are reported as well. All values are expressed in pb.

OPAL [160]

$\sqrt{s}$ interval (GeV)	Luminosity (pb^{-1})	Luminosity weighted $\sqrt{s}$ (GeV)
180-184	57.38	182.68

$\cos\theta_{W^-}$ bin i	1	2	3	4	5	6	7	8	9	10
σ_i (pb)	0.462	0.910	1.101	1.247	1.910	2.291	2.393	2.871	3.851	4.746
$\delta\sigma_i$(stat) (pb)	0.228	0.298	0.313	0.333	0.408	0.451	0.461	0.507	0.602	0.689
$\delta\sigma_i$(stat,exp.) (pb)	0.276	0.286	0.296	0.328	0.353	0.396	0.444	0.502	0.599	0.735
$\delta\sigma_i$(syst,unc) (pb)	0.008	0.013	0.013	0.020	0.018	0.017	0.033	0.046	0.052	0.089
$\delta\sigma_i$(syst,cor) (pb)	0.003	0.003	0.003	0.002	0.002	0.003	0.003	0.003	0.004	0.005

$\sqrt{s}$ interval (GeV)	Luminosity (pb^{-1})	Luminosity weighted $\sqrt{s}$ (GeV)
184-194	212.37	189.04

$\cos\theta_{W^-}$ bin i	1	2	3	4	5	6	7	8	9	10
σ_i (pb)	0.621	0.980	1.004	1.125	1.193	1.944	2.190	2.696	3.622	5.798
$\delta\sigma_i$(stat) (pb)	0.135	0.160	0.158	0.165	0.168	0.213	0.228	0.256	0.305	0.401
$\delta\sigma_i$(stat,exp.) (pb)	0.139	0.145	0.154	0.167	0.180	0.202	0.230	0.267	0.326	0.417
$\delta\sigma_i$(syst,unc) (pb)	0.008	0.013	0.013	0.020	0.018	0.017	0.033	0.046	0.052	0.089
$\delta\sigma_i$(syst,cor) (pb)	0.003	0.003	0.003	0.002	0.002	0.003	0.003	0.003	0.004	0.005

$\sqrt{s}$ interval (GeV)	Luminosity (pb^{-1})	Luminosity weighted $\sqrt{s}$ (GeV)
194-204	190.67	198.35

$\cos\theta_{W^-}$ bin i	1	2	3	4	5	6	7	8	9	10
σ_i (pb)	0.651	0.678	0.834	1.397	1.543	1.994	1.844	2.422	4.168	7.044
$\delta\sigma_i$(stat) (pb)	0.147	0.145	0.153	0.191	0.200	0.224	0.219	0.256	0.344	0.472
$\delta\sigma_i$(stat,exp.) (pb)	0.140	0.148	0.156	0.168	0.185	0.204	0.238	0.282	0.353	0.478
$\delta\sigma_i$(syst,unc) (pb)	0.008	0.013	0.013	0.020	0.018	0.017	0.033	0.046	0.052	0.089
$\delta\sigma_i$(syst,cor) (pb)	0.003	0.003	0.003	0.002	0.002	0.003	0.003	0.003	0.004	0.005

$\sqrt{s}$ interval (GeV)	Luminosity (pb^{-1})	Luminosity weighted $\sqrt{s}$ (GeV)
204-210	220.45	205.94

$\cos\theta_{W^-}$ bin i	1	2	3	4	5	6	7	8	9	10
σ_i (pb)	0.496	0.606	0.453	0.989	1.116	1.919	2.303	2.874	4.573	7.129
$\delta\sigma_i$(stat) (pb)	0.122	0.129	0.111	0.151	0.158	0.206	0.227	0.256	0.335	0.442
$\delta\sigma_i$(stat,exp.) (pb)	0.123	0.133	0.140	0.149	0.164	0.185	0.215	0.258	0.331	0.458
$\delta\sigma_i$(syst,unc) (pb)	0.008	0.013	0.013	0.020	0.018	0.017	0.033	0.046	0.052	0.089
$\delta\sigma_i$(syst,cor) (pb)	0.003	0.003	0.003	0.002	0.002	0.003	0.003	0.003	0.004	0.005

Table E.10: W^- differential angular cross-section in the 10 angular bins for the four chosen energy intervals for the OPAL experiment. For each energy range, the measured integrated luminosity and the luminosity-weighted centre-of-mass energy is reported. The results per angular bin in each energy interval are then presented: σ_i indicates the average of $d[\sigma_{WW}(BR_{e\nu}+BR_{\mu\nu})]/d\cos\theta_{W^-}$ in the i-th bin of $\cos\theta_{W^-}$ with width 0.2. The values in each bin of the measured and expected statistical error and of the systematic errors, LEP uncorrelated and correlated, are reported as well. All values are expressed in pb.

$\sqrt{s}$ (GeV)	σ_{ZZ}	$\Delta\sigma_{ZZ}^{stat}$	(LCEC) $\Delta\sigma_{ZZ}^{syst}$	(LUEU) $\Delta\sigma_{ZZ}^{syst}$	(LUEC) $\Delta\sigma_{ZZ}^{syst}$	$\Delta\sigma_{ZZ}$	$\Delta\sigma_{ZZ}^{stat\,(exp)}$
ALEPH [179]							
182.7	0.11	$^{+0.16}_{-0.11}$	±0.01	±0.03	±0.03	$^{+0.16}_{-0.12}$	±0.14
188.6	0.67	$^{+0.13}_{-0.12}$	±0.01	±0.03	±0.03	$^{+0.14}_{-0.13}$	±0.13
191.6	0.62	$^{+0.40}_{-0.32}$	±0.01	±0.06	±0.01	$^{+0.40}_{-0.33}$	±0.36
195.5	0.73	$^{+0.24}_{-0.21}$	±0.01	±0.06	±0.01	$^{+0.25}_{-0.22}$	±0.23
199.5	0.91	$^{+0.24}_{-0.21}$	±0.01	±0.08	±0.01	$^{+0.25}_{-0.22}$	±0.23
201.6	0.71	$^{+0.31}_{-0.26}$	±0.01	±0.08	±0.01	$^{+0.32}_{-0.27}$	±0.29
204.9	1.20	$^{+0.27}_{-0.25}$	±0.01	±0.07	±0.02	$^{+0.28}_{-0.26}$	±0.26
206.6	1.05	$^{+0.21}_{-0.20}$	±0.01	±0.06	±0.01	$^{+0.22}_{-0.21}$	±0.21
DELPHI [180]							
182.7	0.35	$^{+0.20}_{-0.15}$	±0.01	±0.00	±0.02	$^{+0.20}_{-0.15}$	±0.16
188.6	0.52	$^{+0.12}_{-0.11}$	±0.01	±0.00	±0.02	$^{+0.12}_{-0.11}$	±0.13
191.6	0.63	$^{+0.36}_{-0.30}$	±0.01	±0.01	±0.02	$^{+0.36}_{-0.30}$	±0.35
195.5	1.05	$^{+0.25}_{-0.22}$	±0.01	±0.01	±0.02	$^{+0.25}_{-0.22}$	±0.21
199.5	0.75	$^{+0.20}_{-0.18}$	±0.01	±0.01	±0.01	$^{+0.20}_{-0.18}$	±0.21
201.6	0.85	$^{+0.33}_{-0.28}$	±0.01	±0.01	±0.01	$^{+0.33}_{-0.28}$	±0.32
204.9	1.03	$^{+0.23}_{-0.20}$	±0.02	±0.01	±0.01	$^{+0.23}_{-0.20}$	±0.23
206.6	0.96	$^{+0.16}_{-0.15}$	±0.02	±0.01	±0.01	$^{+0.16}_{-0.15}$	±0.17
L3 [181]							
182.7	0.31	±0.16	±0.05	±0.00	±0.01	±0.17	±0.16
188.6	0.73	±0.15	±0.02	±0.02	±0.02	±0.15	±0.15
191.6	0.29	±0.22	±0.01	±0.01	±0.02	±0.22	±0.34
195.5	1.18	±0.24	±0.04	±0.05	±0.06	±0.26	±0.22
199.5	1.25	±0.25	±0.04	±0.05	±0.07	±0.27	±0.24
201.6	0.95	±0.38	±0.03	±0.04	±0.05	±0.39	±0.35
204.9	0.77	$^{+0.21}_{-0.19}$	±0.01	±0.01	±0.04	$^{+0.21}_{-0.19}$	±0.22
206.6	1.09	$^{+0.17}_{-0.16}$	±0.02	±0.02	±0.06	$^{+0.18}_{-0.17}$	±0.17
OPAL [182]							
182.7	0.12	$^{+0.20}_{-0.18}$	±0.00	±0.03	±0.00	$^{+0.20}_{-0.18}$	±0.19
188.6	0.80	$^{+0.14}_{-0.13}$	±0.01	±0.05	±0.03	$^{+0.15}_{-0.14}$	±0.14
191.6	1.29	$^{+0.47}_{-0.40}$	±0.02	±0.09	±0.05	$^{+0.48}_{-0.41}$	±0.36
195.5	1.13	$^{+0.26}_{-0.24}$	±0.02	±0.06	±0.05	$^{+0.27}_{-0.25}$	±0.25
199.5	1.05	$^{+0.25}_{-0.22}$	±0.02	±0.05	±0.04	$^{+0.26}_{-0.23}$	±0.25
201.6	0.79	$^{+0.35}_{-0.29}$	±0.02	±0.05	±0.03	$^{+0.36}_{-0.30}$	±0.37
204.9	1.07	$^{+0.27}_{-0.24}$	±0.02	±0.06	±0.04	$^{+0.28}_{-0.25}$	±0.26
206.6	0.97	$^{+0.19}_{-0.18}$	±0.02	±0.05	±0.04	$^{+0.20}_{-0.19}$	±0.20

Table E.11: Z-pair production cross-section (in pb) at different energies from the four LEP experiments. The first column contains the LEP centre–of–mass energy, the second the measurements and the third the statistical uncertainty. The fourth, the fifth and the sixth columns list the different components of the systematic errors as defined in Table E.5. The total error is given in the seventh column, and the eighth column lists the symmetrised expected statistical error for each of the four experiments.

LEP							
$\sqrt{s}$ (GeV)	σ_{ZZ}	$\Delta\sigma_{ZZ}^{stat}$	(LCEC) $\Delta\sigma_{ZZ}^{syst}$	(LUEU) $\Delta\sigma_{ZZ}^{syst}$	(LUEC) $\Delta\sigma_{ZZ}^{syst}$	$\Delta\sigma_{ZZ}$	χ^2/dof
182.7	0.22	$\pm$0.08	$\pm$0.02	$\pm$0.01	$\pm$0.01	$\pm$0.08	14.5/24
188.6	0.66	$\pm$0.07	$\pm$0.01	$\pm$0.01	$\pm$0.01	$\pm$0.07	
191.6	0.67	$\pm$0.17	$\pm$0.01	$\pm$0.03	$\pm$0.01	$\pm$0.18	
195.5	1.00	$\pm$0.11	$\pm$0.02	$\pm$0.02	$\pm$0.02	$\pm$0.12	
199.5	0.95	$\pm$0.12	$\pm$0.02	$\pm$0.02	$\pm$0.02	$\pm$0.12	
201.6	0.81	$\pm$0.17	$\pm$0.02	$\pm$0.02	$\pm$0.01	$\pm$0.18	
204.9	0.98	$\pm$0.12	$\pm$0.01	$\pm$0.02	$\pm$0.02	$\pm$0.13	
206.6	1.00	$\pm$0.09	$\pm$0.02	$\pm$0.02	$\pm$0.02	$\pm$0.09	

Table E.12: LEP combined Z-pair production cross-section (in pb) at different energies. The first column contains the LEP centre–of–mass energy, the second the measurements and the third the statistical uncertainty. The fourth, the fifth and the sixth columns list the different components of the systematic errors as defined in Table E.5. The total error is given in the seventh column, and the eighth column lists the χ^2/dof of the fit.

$\sqrt{s}$ (GeV)	ZZ cross-section (pb)	
	σ_{ZZ}^{YFSZZ}	σ_{ZZ}^{ZZTO}
182.7	0.254[1]	0.25425[2]
188.6	0.655[2]	0.64823[1]
191.6	0.782[2]	0.77670[1]
195.5	0.897[3]	0.89622[1]
199.5	0.981[2]	0.97765[1]
201.6	1.015[1]	1.00937[1]
204.9	1.050[1]	1.04335[1]
206.6	1.066[1]	1.05535[1]

Table E.13: Z-pair cross-section predictions (in pb) interpolated at the data centre–of–mass energies, according to the YFSZZ [183] and ZZTO [184] predictions. The numbers in brackets are the errors on the last digit and arise from the numerical integration of the cross-section only.

$\sqrt{s}$ (GeV)	$\mathcal{R}_{ZZ}$	$\Delta\mathcal{R}_{ZZ}^{stat}$	(LCEU) $\Delta\mathcal{R}_{ZZ}^{syst}$	(LCEC) $\Delta\mathcal{R}_{ZZ}^{syst}$	(LUEU) $\Delta\mathcal{R}_{ZZ}^{syst}$	(LUEC) $\Delta\mathcal{R}_{ZZ}^{syst}$	$\Delta\mathcal{R}_{ZZ}$	χ^2/dof
YFSZZ [183]								
182.7	0.857	±0.307	±0.018	±0.068	±0.041	±0.040	±0.320	
188.6	1.007	±0.104	±0.020	±0.019	±0.022	±0.018	±0.111	
191.6	0.859	±0.220	±0.017	±0.013	±0.032	±0.016	±0.224	
195.5	1.118	±0.127	±0.023	±0.021	±0.025	±0.019	±0.134	14.5/24
199.5	0.970	±0.119	±0.020	±0.018	±0.025	±0.016	±0.126	
201.6	0.800	±0.170	±0.016	±0.016	±0.023	±0.012	±0.174	
204.9	0.928	±0.116	±0.019	±0.013	±0.019	±0.014	±0.121	
206.6	0.938	±0.085	±0.019	±0.014	±0.017	±0.016	±0.091	
Average	0.960	±0.045	±0.008	±0.017	±0.009	±0.015	±0.052	17.4/31
ZZTO [184]								
182.7	0.857	±0.307	±0.018	±0.068	±0.041	±0.040	±0.320	
188.6	1.017	±0.105	±0.021	±0.019	±0.022	±0.019	±0.113	
191.6	0.865	±0.222	±0.018	±0.014	±0.033	±0.016	±0.226	
195.5	1.118	±0.127	±0.023	±0.021	±0.025	±0.019	±0.134	14.5/24
199.5	0.974	±0.120	±0.020	±0.018	±0.025	±0.016	±0.126	
201.6	0.805	±0.171	±0.016	±0.016	±0.023	±0.012	±0.174	
204.9	0.934	±0.117	±0.019	±0.013	±0.019	±0.013	±0.122	
206.6	0.948	±0.085	±0.019	±0.014	±0.017	±0.016	±0.092	
Average	0.966	±0.046	±0.008	±0.017	±0.009	±0.015	±0.052	17.4/31

Table E.14: Ratios of LEP combined Z-pair cross-section measurements to the expectations, for different centre–of–mass energies and for all energies combined. The first column contains the centre–of–mass energy, the second the combined ratios, the third the statistical errors. The fourth to seventh columns contain the sources of systematic errors as defined in Table E.5. The total error is given in the eighth column. The only LCEU systematic sources considered are the statistical errors on the cross-section theoretical predictions, while the LCEC, LUEU and LUEC sources are those coming from the corresponding errors on the cross-section measurements. For the LEP averages, the χ^2/dof of the fit is also given in the ninth column.

$\sqrt{s}$ (GeV)	$\sigma_{\mathrm{We\nu\,had}}$	$\Delta\sigma^{\mathrm{stat}}_{\mathrm{We\nu\,had}}$	(LCEC) $\Delta\sigma^{\mathrm{syst}}_{\mathrm{We\nu\,had}}$	(LUEU) $\Delta\sigma^{\mathrm{syst}}_{\mathrm{We\nu\,had}}$	(LUEC) $\Delta\sigma^{\mathrm{syst}}_{\mathrm{We\nu\,had}}$	$\Delta\sigma_{\mathrm{We\nu\,had}}$	$\Delta\sigma^{\mathrm{stat\,(exp)}}_{\mathrm{We\nu\,had}}$
ALEPH [190]							
182.7	0.44	$^{+0.29}_{-0.24}$	±0.01	±0.01	±0.01	$^{+0.29}_{-0.24}$	±0.26
188.6	0.33	$^{+0.16}_{-0.14}$	±0.02	±0.01	±0.01	$^{+0.16}_{-0.15}$	±0.16
191.6	0.52	$^{+0.52}_{-0.40}$	±0.02	±0.01	±0.01	$^{+0.52}_{-0.40}$	±0.45
195.5	0.61	$^{+0.28}_{-0.25}$	±0.02	±0.01	±0.01	$^{+0.28}_{-0.25}$	±0.25
199.5	1.06	$^{+0.30}_{-0.27}$	±0.02	±0.01	±0.01	$^{+0.30}_{-0.27}$	±0.24
201.6	0.72	$^{+0.39}_{-0.33}$	±0.02	±0.01	±0.02	$^{+0.39}_{-0.33}$	±0.34
204.9	0.34	$^{+0.24}_{-0.21}$	±0.02	±0.01	±0.02	$^{+0.24}_{-0.21}$	±0.25
206.6	0.64	$^{+0.21}_{-0.19}$	±0.02	±0.01	±0.02	$^{+0.21}_{-0.19}$	±0.19
DELPHI [191]							
182.7	0.11	$^{+0.30}_{-0.11}$	±0.02	±0.03	±0.08	$^{+0.31}_{-0.14}$	±0.30
188.6	0.57	$^{+0.19}_{-0.18}$	±0.02	±0.04	±0.08	$^{+0.21}_{-0.20}$	±0.18
191.6	0.30	$^{+0.47}_{-0.30}$	±0.02	±0.03	±0.08	$^{+0.48}_{-0.31}$	±0.43
195.5	0.50	$^{+0.29}_{-0.26}$	±0.02	±0.03	±0.08	$^{+0.30}_{-0.27}$	±0.27
199.5	0.57	$^{+0.27}_{-0.25}$	±0.02	±0.02	±0.08	$^{+0.28}_{-0.26}$	±0.25
201.6	0.67	$^{+0.39}_{-0.35}$	±0.02	±0.03	±0.08	$^{+0.40}_{-0.36}$	±0.35
204.9	0.99	$^{+0.32}_{-0.30}$	±0.02	±0.05	±0.08	$^{+0.33}_{-0.31}$	±0.28
206.6	0.81	$^{+0.22}_{-0.20}$	±0.02	±0.04	±0.08	$^{+0.23}_{-0.22}$	±0.20
L3 [192, 193, 194]							
182.7	0.58	$^{+0.23}_{-0.20}$	±0.03	±0.03	±0.00	$^{+0.23}_{-0.20}$	±0.21
188.6	0.52	$^{+0.14}_{-0.13}$	±0.02	±0.02	±0.00	$^{+0.14}_{-0.13}$	±0.14
191.6	0.84	$^{+0.44}_{-0.37}$	±0.03	±0.03	±0.00	$^{+0.44}_{-0.37}$	±0.41
195.5	0.66	$^{+0.24}_{-0.22}$	±0.02	±0.03	±0.00	$^{+0.25}_{-0.23}$	±0.21
199.5	0.37	$^{+0.22}_{-0.20}$	±0.01	±0.02	±0.00	$^{+0.22}_{-0.20}$	±0.22
201.6	1.10	$^{+0.40}_{-0.35}$	±0.05	±0.05	±0.00	$^{+0.40}_{-0.35}$	±0.35
204.9	0.42	$^{+0.25}_{-0.21}$	±0.02	±0.03	±0.00	$^{+0.25}_{-0.21}$	±0.25
206.6	0.66	$^{+0.19}_{-0.17}$	±0.02	±0.03	±0.00	$^{+0.20}_{-0.18}$	±0.20
LEP							χ^2/dof
182.7	0.42	±0.15	±0.02	±0.02	±0.01	±0.15	13.2/16
188.6	0.47	±0.09	±0.02	±0.01	±0.01	±0.09	
191.6	0.56	±0.25	±0.02	±0.02	±0.02	±0.25	
195.5	0.60	±0.14	±0.02	±0.01	±0.02	±0.14	
199.5	0.65	±0.14	±0.02	±0.01	±0.02	±0.14	
201.6	0.82	±0.20	±0.03	±0.02	±0.02	±0.20	
204.9	0.54	±0.15	±0.02	±0.02	±0.02	±0.15	
206.6	0.69	±0.11	±0.02	±0.02	±0.02	±0.12	

Table E.15: Single-W hadronic production cross-section (in pb) at different energies. The first column contains the LEP centre–of–mass energy, and the second the measurements. The third column reports the statistical error, and the fourth to the sixth columns list the different systematic uncertainties. The labels LCEC, LUEU and LUEC are defined in Table E.5. The seventh column contains the total error and the eighth lists the symmetrised expected statistical error for the three LEP measurements, and, for the LEP combined value, the χ^2/dof of the fit.

$\sqrt{s}$ (GeV)	$\sigma_{We\nu\,tot}$	$\Delta\sigma^{stat}_{We\nu\,tot}$	(LCEC) $\Delta\sigma^{syst}_{We\nu\,tot}$	(LUEU) $\Delta\sigma^{syst}_{We\nu\,tot}$	(LUEC) $\Delta\sigma^{syst}_{We\nu\,tot}$	$\Delta\sigma_{We\nu\,tot}$	$\Delta\sigma^{stat\,(exp)}_{We\nu\,tot}$
ALEPH [190]							
182.7	0.60	$^{+0.32}_{-0.26}$	±0.02	±0.01	±0.01	$^{+0.32}_{-0.26}$	±0.29
188.6	0.55	$^{+0.18}_{-0.16}$	±0.02	±0.01	±0.01	$^{+0.18}_{-0.16}$	±0.18
191.6	0.89	$^{+0.58}_{-0.44}$	±0.02	±0.01	±0.02	$^{+0.58}_{-0.44}$	±0.48
195.5	0.87	$^{+0.31}_{-0.27}$	±0.03	±0.01	±0.02	$^{+0.31}_{-0.27}$	±0.28
199.5	1.31	$^{+0.32}_{-0.29}$	±0.03	±0.01	±0.02	$^{+0.32}_{-0.29}$	±0.26
201.6	0.80	$^{+0.42}_{-0.35}$	±0.03	±0.01	±0.02	$^{+0.42}_{-0.35}$	±0.38
204.9	0.65	$^{+0.27}_{-0.23}$	±0.03	±0.02	±0.02	$^{+0.27}_{-0.23}$	±0.27
206.6	0.81	$^{+0.22}_{-0.20}$	±0.03	±0.02	±0.02	$^{+0.22}_{-0.20}$	±0.22
DELPHI [191]							
182.7	0.69	$^{+0.41}_{-0.23}$	±0.02	±0.04	±0.08	$^{+0.42}_{-0.25}$	±0.33
188.6	0.75	$^{+0.22}_{-0.20}$	±0.02	±0.04	±0.08	$^{+0.23}_{-0.22}$	±0.20
191.6	0.40	$^{+0.54}_{-0.31}$	±0.02	±0.03	±0.08	$^{+0.55}_{-0.33}$	±0.48
195.5	0.68	$^{+0.33}_{-0.28}$	±0.02	±0.03	±0.08	$^{+0.34}_{-0.38}$	±0.30
199.5	0.95	$^{+0.33}_{-0.29}$	±0.02	±0.03	±0.08	$^{+0.34}_{-0.30}$	±0.29
201.6	1.24	$^{+0.51}_{-0.42}$	±0.02	±0.04	±0.08	$^{+0.52}_{-0.43}$	±0.41
204.9	1.06	$^{+0.36}_{-0.30}$	±0.02	±0.05	±0.08	$^{+0.37}_{-0.32}$	±0.33
206.6	1.14	$^{+0.26}_{-0.23}$	±0.02	±0.04	±0.08	$^{+0.28}_{-0.25}$	±0.23
L3 [192, 193, 194]							
182.7	0.80	$^{+0.28}_{-0.25}$	±0.04	±0.04	±0.01	$^{+0.28}_{-0.25}$	±0.26
188.6	0.69	$^{+0.16}_{-0.14}$	±0.03	±0.03	±0.01	$^{+0.16}_{-0.15}$	±0.15
191.6	1.11	$^{+0.48}_{-0.41}$	±0.02	±0.04	±0.01	$^{+0.48}_{-0.41}$	±0.46
195.5	0.97	$^{+0.27}_{-0.25}$	±0.02	±0.02	±0.01	$^{+0.27}_{-0.25}$	±0.25
199.5	0.88	$^{+0.26}_{-0.24}$	±0.02	±0.03	±0.01	$^{+0.26}_{-0.24}$	±0.25
201.6	1.50	$^{+0.45}_{-0.40}$	±0.03	±0.04	±0.02	$^{+0.45}_{-0.40}$	±0.38
204.9	0.78	$^{+0.29}_{-0.25}$	±0.02	±0.03	±0.01	$^{+0.29}_{-0.25}$	±0.29
206.6	1.08	$^{+0.21}_{-0.20}$	±0.02	±0.03	±0.01	$^{+0.21}_{-0.20}$	±0.23
LEP							χ^2/dof
182.7	0.70	±0.17	±0.03	±0.02	±0.02	±0.17	
188.6	0.66	±0.10	±0.02	±0.02	±0.01	±0.10	
191.6	0.81	±0.27	±0.02	±0.02	±0.02	±0.28	
195.5	0.85	±0.16	±0.02	±0.01	±0.02	±0.16	8.1/16
199.5	1.05	±0.15	±0.02	±0.01	±0.02	±0.16	
201.6	1.17	±0.23	±0.03	±0.02	±0.02	±0.23	
204.9	0.80	±0.17	±0.02	±0.02	±0.02	±0.17	
206.6	1.00	±0.13	±0.03	±0.02	±0.02	±0.14	

Table E.16: Single-W total production cross-section (in pb) at different energies. The first column contains the LEP centre–of–mass energy, and the second the measurements. The third column reports the statistical error, and the fourth to the sixth columns list the different systematic uncertainties. The labels LCEC, LUEU and LUEC are defined in Table E.5. The seventh column contains the total error and the eighth lists the symmetrised expected statistical error for the three LEP measurements, and, for the LEP combined values, the χ^2/dof of the fit.

$\sqrt{s}$	Weν $\rightarrow$qqeν cross-section (pb)			Weν total cross-section (pb)	
(GeV)	$\sigma^{\texttt{grc4f}}_{\mathrm{We}\nu\,\mathrm{had}}$	$\sigma^{\mathrm{WPHACT}}_{\mathrm{We}\nu\,\mathrm{had}}$	$\sigma^{\mathrm{WTO}}_{\mathrm{We}\nu\,\mathrm{had}}$	$\sigma^{\texttt{grc4f}}_{\mathrm{We}\nu\,\mathrm{tot}}$	$\sigma^{\mathrm{WPHACT}}_{\mathrm{We}\nu\,\mathrm{tot}}$
182.7	0.4194[1]	0.4070[2]	0.40934[8]	0.6254[1]	0.6066[2]
188.6	0.4699[1]	0.4560[2]	0.45974[9]	0.6999[1]	0.6796[2]
191.6	0.4960[1]	0.4810[2]	0.4852[1]	0.7381[2]	0.7163[2]
195.5	0.5308[2]	0.5152[2]	0.5207[1]	0.7896[2]	0.7665[3]
199.5	0.5673[2]	0.5509[3]	0.5573[1]	0.8431[2]	0.8182[3]
201.6	0.5870[2]	0.5704[4]	0.5768[1]	0.8718[2]	0.8474[4]
204.9	0.6196[2]	0.6021[4]	0.6093[2]	0.9185[3]	0.8921[4]
206.6	0.6358[2]	0.6179[4]	0.6254[2]	0.9423[3]	0.9157[5]

Table E.17: Single-W hadronic and total cross-section predictions (in pb) interpolated at the data centre–of–mass energies, according to the `grc4f` [187], WPHACT [195] and WTO [198] predictions. The numbers in brackets are the errors on the last digit and arise from the numerical integration of the cross-section only.

$\sqrt{s}$ (GeV)	$\mathcal{R}_{\mathrm{We}\nu}$	$\Delta\mathcal{R}^{\mathrm{stat}}_{\mathrm{We}\nu}$	(LCEU) $\Delta\mathcal{R}^{\mathrm{syst}}_{\mathrm{We}\nu}$	(LCEC) $\Delta\mathcal{R}^{\mathrm{syst}}_{\mathrm{We}\nu}$	(LUEU) $\Delta\mathcal{R}^{\mathrm{syst}}_{\mathrm{We}\nu}$	(LUEC) $\Delta\mathcal{R}^{\mathrm{syst}}_{\mathrm{We}\nu}$	$\Delta\mathcal{R}_{\mathrm{We}\nu}$	χ^2/dof
`grc4f` [187]								
182.7	1.122	±0.266	±0.001	±0.041	±0.029	±0.026	±0.272	8.1/16
188.6	0.936	±0.142	±0.001	±0.033	±0.022	±0.024	±0.149	
191.6	1.094	±0.370	±0.001	±0.030	±0.026	±0.028	±0.373	
195.5	1.081	±0.199	±0.001	±0.028	±0.017	±0.023	±0.203	
199.5	1.242	±0.183	±0.001	±0.028	±0.017	±0.022	±0.187	
201.6	1.340	±0.258	±0.001	±0.031	±0.021	±0.023	±0.261	
204.9	0.873	±0.185	±0.001	±0.025	±0.020	±0.020	±0.189	
206.6	1.058	±0.138	±0.001	±0.026	±0.019	±0.021	±0.143	
Average	1.058	±0.068	±0.000	±0.029	±0.008	±0.022	±0.078	12.2/24
WPHACT [195]								
182.7	1.157	±0.274	±0.001	±0.043	±0.030	±0.027	±0.281	8.1/16
188.6	0.965	±0.146	±0.001	±0.034	±0.023	±0.024	±0.154	
191.6	1.128	±0.382	±0.001	±0.031	±0.027	±0.029	±0.385	
195.5	1.115	±0.206	±0.001	±0.029	±0.017	±0.023	±0.210	
199.5	1.280	±0.188	±0.001	±0.029	±0.018	±0.022	±0.193	
201.6	1.380	±0.265	±0.001	±0.032	±0.022	±0.024	±0.269	
204.9	0.899	±0.191	±0.001	±0.026	±0.020	±0.020	±0.195	
206.6	1.089	±0.142	±0.001	±0.027	±0.020	±0.022	±0.148	
Average	1.090	±0.070	±0.000	±0.030	±0.008	±0.023	±0.080	12.2/24

Table E.18: Ratios of LEP combined total single-W cross-section measurements to the expectations, for different centre–of–mass energies and for all energies combined. The first column contains the centre–of–mass energy, the second the combined ratios, the third the statistical errors. The fourth to seventh columns contain the sources of systematic errors, as defined in Table E.5. The total error is given in the eighth column. The only LCEU systematic sources considered are the statistical errors on the cross-section theoretical predictions, while the LCEC, LUEU and LUEC sources are those arising from the corresponding errors on the cross-section measurements.

$\sqrt{s}$ (GeV)	σ_{Zee}	$\Delta\sigma^{\mathrm{stat}}_{\mathrm{Zee}}$	(LCEC) $\Delta\sigma^{\mathrm{syst}}_{\mathrm{Zee}}$	(LUEU) $\Delta\sigma^{\mathrm{syst}}_{\mathrm{Zee}}$	(LUEC) $\Delta\sigma^{\mathrm{syst}}_{\mathrm{Zee}}$	$\Delta\sigma_{\mathrm{Zee}}$	$\Delta\sigma^{\mathrm{stat\,(exp)}}_{\mathrm{Zee}}$
ALEPH [190]							
182.7	0.27	$^{+0.21}_{-0.16}$	±0.01	±0.02	±0.01	$^{+0.21}_{-0.16}$	±0.20
188.6	0.42	$^{+0.14}_{-0.12}$	±0.01	±0.03	±0.01	$^{+0.14}_{-0.12}$	±0.12
191.6	0.61	$^{+0.39}_{-0.29}$	±0.01	±0.03	±0.01	$^{+0.39}_{-0.29}$	±0.29
195.5	0.72	$^{+0.24}_{-0.20}$	±0.01	±0.03	±0.01	$^{+0.24}_{-0.20}$	±0.18
199.5	0.60	$^{+0.21}_{-0.18}$	±0.01	±0.03	±0.01	$^{+0.21}_{-0.18}$	±0.17
201.6	0.89	$^{+0.35}_{-0.28}$	±0.01	±0.03	±0.01	$^{+0.35}_{-0.28}$	±0.24
204.9	0.42	$^{+0.17}_{-0.14}$	±0.01	±0.03	±0.01	$^{+0.17}_{-0.15}$	±0.17
206.6	0.70	$^{+0.17}_{-0.15}$	±0.01	±0.03	±0.01	$^{+0.17}_{-0.15}$	±0.14
DELPHI [191]							
182.7	0.56	$^{+0.27}_{-0.22}$	±0.01	±0.06	±0.02	$^{+0.28}_{-0.23}$	±0.24
188.6	0.64	$^{+0.15}_{-0.14}$	±0.01	±0.03	±0.02	$^{+0.16}_{-0.14}$	±0.14
191.6	0.63	$^{+0.40}_{-0.30}$	±0.01	±0.03	±0.03	$^{+0.40}_{-0.30}$	±0.32
195.5	0.66	$^{+0.22}_{-0.18}$	±0.01	±0.02	±0.03	$^{+0.22}_{-0.19}$	±0.19
199.5	0.57	$^{+0.20}_{-0.17}$	±0.01	±0.02	±0.02	$^{+0.20}_{-0.17}$	±0.18
201.6	0.19	$^{+0.21}_{-0.16}$	±0.01	±0.02	±0.01	$^{+0.21}_{-0.16}$	±0.25
204.9	0.37	$^{+0.18}_{-0.15}$	±0.01	±0.02	±0.02	$^{+0.18}_{-0.15}$	±0.19
206.6	0.69	$^{+0.16}_{-0.14}$	±0.01	±0.01	±0.03	$^{+0.16}_{-0.14}$	±0.14
L3 [203]							
182.7	0.51	$^{+0.19}_{-0.16}$	±0.02	±0.01	±0.03	$^{+0.19}_{-0.16}$	±0.16
188.6	0.55	$^{+0.10}_{-0.09}$	±0.02	±0.01	±0.03	$^{+0.11}_{-0.10}$	±0.09
191.6	0.60	$^{+0.26}_{-0.21}$	±0.01	±0.01	±0.03	$^{+0.26}_{-0.21}$	±0.21
195.5	0.40	$^{+0.13}_{-0.11}$	±0.01	±0.01	±0.03	$^{+0.13}_{-0.11}$	±0.13
199.5	0.33	$^{+0.12}_{-0.10}$	±0.01	±0.01	±0.03	$^{+0.13}_{-0.11}$	±0.14
201.6	0.81	$^{+0.27}_{-0.23}$	±0.02	±0.02	±0.03	$^{+0.27}_{-0.23}$	±0.19
204.9	0.56	$^{+0.16}_{-0.14}$	±0.01	±0.01	±0.03	$^{+0.16}_{-0.14}$	±0.14
206.6	0.59	$^{+0.12}_{-0.10}$	±0.01	±0.01	±0.03	$^{+0.12}_{-0.11}$	±0.11
LEP							χ^2/dof
182.7	0.45	±0.11	±0.01	±0.02	±0.01	±0.11	
188.6	0.53	±0.07	±0.01	±0.01	±0.01	±0.07	
191.6	0.61	±0.15	±0.01	±0.02	±0.01	±0.15	
195.5	0.55	±0.09	±0.01	±0.01	±0.01	±0.10	
199.5	0.47	±0.09	±0.01	±0.02	±0.01	±0.10	13.0/16
201.6	0.67	±0.13	±0.01	±0.01	±0.01	±0.13	
204.9	0.47	±0.10	±0.01	±0.01	±0.01	±0.10	
206.6	0.65	±0.07	±0.01	±0.01	±0.01	±0.08	

Table E.19: Single-Z hadronic production cross-section (in pb) at different energies. The first column contains the LEP centre–of–mass energy, and the second the measurements. The third column reports the statistical error, and the fourth to the sixth columns list the different systematic uncertainties. The labels LCEC, LUEU and LUEC are defined in Table E.5. The seventh column contains the total error and the eighth lists the symmetrised expected statistical error for each of the three LEP experiments, and, for the LEP combined value, the χ^2/dof of the fit.

$\sqrt{s}$	Zee cross-section (pb)	
(GeV)	$\sigma_{\mathrm{Zee}}^{\mathrm{WPHACT}}$	$\sigma_{\mathrm{Zee}}^{\texttt{grc4f}}$
182.7	0.51275[4]	0.51573[4]
188.6	0.53686[4]	0.54095[5]
191.6	0.54883[4]	0.55314[5]
195.5	0.56399[5]	0.56891[4]
199.5	0.57935[5]	0.58439[4]
201.6	0.58708[4]	0.59243[4]
204.9	0.59905[4]	0.60487[4]
206.6	0.61752[4]	0.60819[4]

Table E.20: Zee hadronic cross-section predictions (in pb) interpolated at the data centre–of–mass energies, according to the WPHACT [195] and `grc4f` [187] predictions. The numbers in brackets are the errors on the last digit and arise from the numerical integration of the cross-section only.

$\sqrt{s}$ (GeV)	$\mathcal{R}_{\mathrm{Zee}}$	$\Delta\mathcal{R}^{\mathrm{stat}}_{\mathrm{Zee}}$	(LCEU) $\Delta\mathcal{R}^{\mathrm{syst}}_{\mathrm{Zee}}$	(LCEC) $\Delta\mathcal{R}^{\mathrm{syst}}_{\mathrm{Zee}}$	(LUEU) $\Delta\mathcal{R}^{\mathrm{syst}}_{\mathrm{Zee}}$	(LUEC) $\Delta\mathcal{R}^{\mathrm{syst}}_{\mathrm{Zee}}$	$\Delta\mathcal{R}_{\mathrm{Zee}}$	χ^2/dof
`grc4f` [187]								
182.7	0.871	±0.214	±0.000	±0.020	±0.035	±0.025	±0.219	13.0/16
188.6	0.982	±0.120	±0.000	±0.022	±0.023	±0.024	±0.126	
191.6	1.104	±0.272	±0.000	±0.019	±0.027	±0.025	±0.276	
195.5	0.964	±0.163	±0.000	±0.016	±0.024	±0.025	±0.167	
199.5	0.809	±0.160	±0.000	±0.018	±0.030	±0.023	±0.165	
201.6	1.126	±0.219	±0.000	±0.023	±0.024	±0.021	±0.222	
204.9	0.769	±0.157	±0.000	±0.019	±0.019	±0.021	±0.160	
206.6	1.062	±0.119	±0.000	±0.018	±0.018	±0.024	±0.124	
Average	0.955	±0.057	±0.000	±0.019	±0.009	±0.023	±0.065	17.1/23
WPHACT [195]								
182.7	0.876	±0.215	±0.000	±0.020	±0.035	±0.025	±0.220	13.0/16
188.6	0.990	±0.120	±0.000	±0.022	±0.023	±0.025	±0.127	
191.6	1.112	±0.274	±0.000	±0.020	±0.027	±0.026	±0.277	
195.5	0.972	±0.164	±0.000	±0.016	±0.025	±0.025	±0.168	
199.5	0.816	±0.161	±0.000	±0.019	±0.030	±0.023	±0.167	
201.6	1.135	±0.221	±0.000	±0.023	±0.024	±0.021	±0.224	
204.9	0.776	±0.158	±0.000	±0.019	±0.019	±0.021	±0.162	
206.6	1.067	±0.120	±0.000	±0.018	±0.018	±0.024	±0.125	
Average	0.962	±0.057	±0.000	±0.020	±0.009	±0.024	±0.065	17.0/23

Table E.21: Ratios of LEP combined single-Z hadronic cross-section measurements to the expectations, for different centre–of–mass energies and for all energies combined. The first column contains the centre–of–mass energy, the second the combined ratios, the third the statistical errors. The fourth to seventh columns contain the sources of systematic errors as defined in Table E.5. The total error is given in the eighth column. The only LCEU systematic sources considered are the statistical errors on the cross-section theoretical predictions, while the LCEC, LUEU and LUEC sources are those arising from the corresponding errors on the cross-section measurements. For the LEP averages, the χ^2/dof of the fit is also given in the ninth column.

Appendix F

Constraints on the Standard Model

F.1 Introduction

The experimental measurements used here to place constraints on the Standard Model (SM) consist of three groups: (i) the final Z-pole results measured in electron-positron collisions by the ALEPH, DELPHI, L3, OPAL and SLD experiments, as combined in Reference [4]; (ii) the mass and width of the W boson measured at LEP-II and described earlier in this report; and (iii) the measurements of the mass of the top quark and the mass and width of the W boson at the Tevatron collider.

The measurements allow checks of the validity of the SM and, within its framework, to infer valuable information about its fundamental parameters. The accuracy of the Z-boson and W-boson measurements makes them sensitive to the mass of the top quark m_{t}, and to the mass of the Higgs boson m_{H} through electroweak loop corrections. While the leading m_{t} dependence is quadratic, the leading m_{H} dependence is logarithmic. Therefore, the inferred constraints on m_{t} are much stronger than those on m_{H}.

In a first step, the predictions for the mass and width of the W boson based on measurements performed at lower Z-pole centre-of-mass energies (LEP-I, SLC, etc) [4] are compared to the direct measurements performed at LEP-II and the Tevatron. The comparison between prediction and direct measurement is also performed for the mass of the top quark. Finally, all measurements are used to infer constraints on the Higgs boson of the minimal SM.

This analysis updates our previous analysis [4]. Similar analyses of this type are presented in References [178, 272], obtaining equivalent results when accounting for the different sets of measurements considered.

F.2 Measurements

The measured quantities considered here are summarised in Table F.1. The predictions of these observables are also shown in this table, derived from the results of the SM fit to the combined high-Q^2 measurements described in the last column of Table F.2. The measurements obtained at the Z pole by the LEP and SLC experiments ALEPH, DELPHI, L3, OPAL and SLD and their combinations, reported in parts a), b) and c) of Table F.1, are final and published [4].

The measurements of the W-boson mass published by CDF [274, 241] and D0 [281, 242], and on the W-boson width published by CDF [289, 239] and D0 [290, 240] are combined by the Tevatron Electroweak Working Group, based on a detailed treatment of correlated systematic uncertainties, with the result: $m_{\mathrm{W}} = 80.387 \pm 0.016$ GeV [291] and $\Gamma_{\mathrm{W}} = 2.050 \pm 0.058$ GeV [292].

Combining these Tevatron results with the final LEP-II results presented in Chapter 7 of this report, $m_{\rm W} = 80.376 \pm 0.033$ GeV and $\Gamma_{\rm W} = 2.195 \pm 0.083$ GeV, the resulting world averages are:

$$m_{\rm W} = 80.385 \pm 0.015 \text{ GeV} \quad \text{(F.1)}$$
$$\Gamma_{\rm W} = 2.085 \pm 0.042 \text{ GeV}\,, \quad \text{(F.2)}$$

and are used in the following.

For the mass of the top quark, $m_{\rm t}$, the published results from CDF [293] and D0 [301] are combined by the Tevatron Electroweak Working Group with the result: $m_{\rm t} = 173.2 \pm 0.9$ GeV [307].

In addition to these high-Q^2 results, the following results measured in low-Q^2 interactions and reported in Table F.3 are considered: (i) the measurements of atomic parity violation in caesium[309], with the numerical result[312] based on a revised analysis of QED radiative corrections applied to the raw measurement; (ii) the result of the E-158 collaboration on the electroweak mixing angle[1] measured in Møller scattering [313]; and (iii) the final result of the NuTeV collaboration on neutrino-nucleon neutral to charged current cross-section ratios [315].

Using neutrino-nucleon data with an average $Q^2 \simeq 20$ GeV^2, the NuTeV collaboration has extracted the left- and right-handed couplings combinations $g^2_{\nu\rm Lud} = 4g^2_{\rm L\nu}(g^2_{\rm Lu} + g^2_{\rm Ld}) = [1/2 - \sin^2\theta_{\rm eff} + (5/9)\sin^4\theta_{\rm eff}]\rho_\nu\rho_{\rm ud}$ and $g^2_{\nu\rm Rud} = 4g^2_{\rm L\nu}(g^2_{\rm Ru} + g^2_{\rm Rd}) = (5/9)\sin^4\theta_{\rm eff}\rho_\nu\rho_{\rm ud}$, with the ρ parameters for example defined in [317]. The NuTeV results for the effective couplings are: $g^2_{\nu\rm Lud} = 0.30005 \pm 0.00137$ and $g^2_{\nu\rm Rud} = 0.03076 \pm 0.00110$, with a correlation of -0.017. While the result on $g_{\nu\rm Rud}$ agrees with the SM expectation, the result on $g_{\nu\rm Lud}$, relatively measured nearly eight times more precisely than $g_{\nu\rm Rud}$, shows a deficit with respect to the expectation at the level of 2.9 standard deviations [315]. A recent study finds that EMC-like isovector effects are able to explain this difference [318].

An important quantity in electroweak analyses is given by the running electromagnetic fine-structure constant, $\alpha(m^2_{\rm Z})$. The uncertainty in $\alpha(m^2_{\rm Z})$ arises from the contribution of light quarks to the photon vacuum polarisation, $\Delta\alpha^{(5)}_{\rm had}(m^2_{\rm Z})$:

$$\alpha(m^2_{\rm Z}) = \frac{\alpha(0)}{1 - \Delta\alpha_\ell(m^2_{\rm Z}) - \Delta\alpha^{(5)}_{\rm had}(m^2_{\rm Z}) - \Delta\alpha_{\rm top}(m^2_{\rm Z})}\,, \quad \text{(F.3)}$$

where $\alpha(0) = 1/137.036$. The top contribution, $-0.00007(1)$, depends on the mass of the top quark. The leptonic contribution is calculated to third order [320] to be 0.03150, with negligible uncertainty. For the hadronic contribution $\Delta\alpha^{(5)}_{\rm had}(m^2_{\rm Z})$, we use the new result 0.02750 ± 0.00033 [321] listed in the first row of Table F.1, which takes into account recent results on electron-positron annihilations into hadrons at low centre-of-mass energies measured by the BES, CMD-2, KLOE and BABAR collaborations. The reduced uncertainty of 0.00033 still causes an error of 0.00012 on the SM prediction of $\sin^2\theta^{\rm lept}_{\rm eff}$ and of 0.08 on the fitted value of $\log(m_{\rm H})$, while the $\alpha_{\rm S}(m^2_{\rm Z})$ values presented here are stable against a variation of $\alpha(m^2_{\rm Z})$ in the interval quoted. Several evaluations of $\Delta\alpha^{(5)}_{\rm had}(m^2_{\rm Z})$ exist which are more theory driven [322, 335], resulting in a much reduced uncertainty. To show the effect of the $\alpha(m^2_{\rm Z})$ uncertainty on the results, we also use the most recent of these evaluations, 0.02757 ± 0.00010 [335].

[1] E-158 quotes in the $\overline{\rm MS}$ scheme, evolved to $Q^2 = m^2_{\rm Z}$. We add 0.00029 to the quoted value in order to obtain the effective electroweak mixing angle [178].

	Measurement with Total Error	Systematic Error	Standard-Model fit	Pull
$\Delta\alpha^{(5)}_{\rm had}(m^2_{\rm Z})$[321]	0.02750 ± 0.00033		0.02759	-0.3
a) LEP-I				
line-shape and				
lepton asymmetries:				
$m_{\rm Z}$ [GeV]	91.1875 ± 0.0021	[a] 0.0017	91.1874	0.0
$\Gamma_{\rm Z}$ [GeV]	2.4952 ± 0.0023	[a] 0.0012	2.4959	-0.3
$\sigma^0_{\rm had}$ [nb]	41.540 ± 0.037	[b] 0.028	41.478	1.7
R^0_ℓ	20.767 ± 0.025	[b] 0.007	20.742	1.0
$A^{0,\ell}_{\rm FB}$	0.0171 ± 0.0010	[b] 0.0003	0.0164	0.7
+ correlation matrix [4]				
τ polarisation:				
$\mathcal{A}_\ell$ ($\mathcal{P}_\tau$)	0.1465 ± 0.0033	0.0016	0.1481	-0.5
$q\overline{q}$ charge asymmetry:				
$\sin^2\theta^{\rm lept}_{\rm eff}(Q^{\rm had}_{\rm FB})$	0.2324 ± 0.0012	0.0010	0.231439	0.8
b) SLD				
$\mathcal{A}_\ell$ (SLD)	0.1513 ± 0.0021	0.0010	0.1481	1.6
c) LEP-I/SLD Heavy Flavour				
$R^0_{\rm b}$	0.21629 ± 0.00066	0.00050	0.21579	0.8
$R^0_{\rm c}$	0.1721 ± 0.0030	0.0019	0.1723	-0.1
$A^{0,{\rm b}}_{\rm FB}$	0.0992 ± 0.0016	0.0007	0.1038	-2.9
$A^{0,{\rm c}}_{\rm FB}$	0.0707 ± 0.0035	0.0017	0.0742	-1.0
$\mathcal{A}_{\rm b}$	0.923 ± 0.020	0.013	0.935	-0.6
$\mathcal{A}_{\rm c}$	0.670 ± 0.027	0.015	0.668	0.1
+ correlation matrix [4]				
d) LEP-II and Tevatron				
$m_{\rm W}$ [GeV] (LEP-II, Tevatron)	80.385 ± 0.015		80.377	0.5
$\Gamma_{\rm W}$ [GeV] (LEP-II, Tevatron)	2.085 ± 0.042		2.092	-0.2
$m_{\rm t}$ [GeV] (Tevatron [307])	173.2 ± 0.9		173.3	-0.1

Table F.1: Summary of high-Q^2 measurements included in the combined analysis of SM parameters. Section a) summarises LEP-I averages, Section b) SLD results ($\mathcal{A}_\ell$ includes $A_{\rm LR}$ and the polarised lepton asymmetries), Section c) the LEP-I and SLD heavy flavour results, and Section d) electroweak measurements from LEP-II and the Tevatron. The total errors in column 2 include the systematic errors listed in column 3; the determination of the systematic part of each error is approximate. The SM results in column 4 and the pulls (difference between measurement and fit in units of the total measurement error) in column 5 are derived from the SM fit to all high-Q^2 data, see Table F.2 column 4.

[a] The systematic errors on $m_{\rm Z}$ and $\Gamma_{\rm Z}$ contain the errors arising from the uncertainties in the LEP-I beam energy only.

[b] Only common systematic errors are indicated.

An additional input parameter, not shown in Table F.1, is the Fermi constant G_F, determined from the μ lifetime: $G_F = 1.16637(1) \cdot 10^{-5}$ GeV^{-2}[337]. New measurements of G_F yield values which are in good agreement [340]. The relative error of G_F is comparable to that of m_{Z}; both uncertainties have negligible effects on the fit results.

F.3 Theoretical Uncertainties

Detailed studies of the theoretical uncertainties in the SM predictions due to missing higher-order electroweak corrections and their interplay with QCD corrections had been carried out by the working group on 'Precision calculations for the Z resonance'[317], and later in References [343] and [344]. Theoretical uncertainties are evaluated by comparing different but, within our present knowledge, equivalent treatments of aspects such as resummation techniques, momentum transfer scales for vertex corrections and factorisation schemes. The effects of these theoretical uncertainties are reduced by the inclusion of higher-order corrections[345, 349] in the electroweak libraries TOPAZ0 [351] and ZFITTER [36].

The use of the higher-order QCD corrections[349] increases the value of $\alpha_{\mathrm{S}}(m_{\mathrm{Z}}^2)$ by 0.001, as expected. The effect of missing higher-order QCD corrections on $\alpha_{\mathrm{S}}(m_{\mathrm{Z}}^2)$ dominates missing higher-order electroweak corrections and uncertainties in the interplay of electroweak and QCD corrections. A discussion of theoretical uncertainties in the determination of α_{S} can be found in References [317] and [355], with a more recent analysis in Reference [358] where the theoretical uncertainty is estimated to be about 0.001 for the analyses presented in the following.

The complete (fermionic and bosonic) two-loop corrections for the calculation of m_{W} [359], and the complete fermionic two-loop corrections for the calculation of $\sin^2\theta_{\mathrm{eff}}^{\mathrm{lept}}$ [360] have been calculated. Including three-loop top-quark contributions to the ρ parameter in the limit of large m_{t} [361], efficient routines for evaluating these corrections have been implemented since version 6.40 in the semi-analytical program ZFITTER. The remaining theoretical uncertainties are estimated to be 4 MeV on m_{W} and 0.000049 on $\sin^2\theta_{\mathrm{eff}}^{\mathrm{lept}}$. The latter uncertainty dominates the theoretical uncertainty in the SM fits and the extraction of constraints on the mass of the Higgs boson presented below. For a consistent treatment, the complete two-loop calculation for the partial Z decay widths should be calculated.

The theoretical uncertainties discussed above are not included in the results presented in Tables F.2 and F.3. At present the impact of theoretical uncertainties on the determination of SM parameters from the precise electroweak measurements is small compared to the error due to the uncertainty in the value of $\alpha(m_{\mathrm{Z}}^2)$, which is included in the results.

F.4 Standard-Model Analyses

Strong Coupling Constant

Of the measurements listed in Table F.1, R_ℓ^0 is the one most sensitive to QCD corrections. For $m_{\mathrm{Z}} = 91.1875$ GeV and imposing $m_{\mathrm{t}} = 173.2 \pm 0.9$ GeV [307] as a constraint, $\alpha_{\mathrm{S}} = 0.1223 \pm 0.0038$ is obtained. Alternatively, $\sigma_{\mathrm{lep}}^0 \equiv \sigma_{\mathrm{had}}^0 / R_\ell^0 = 2.0003 \pm 0.0027$ nb [4], which has higher sensitivity to QCD corrections and less dependence on m_{H}, yields: $\alpha_{\mathrm{S}} = 0.1179 \pm 0.0030$. The central values obtained increase by 0.0013 and 0.0010, respectively, when changing m_{H} from 100 GeV to 300 GeV. These results on α_{S}, as well as those reported in the next section, are in good agreement with both independent measurements of α_{S} and the world average $\alpha_{\mathrm{S}}(m_{\mathrm{Z}}^2) = 0.1184 \pm 0.0007$ [362].

Electroweak Analyses

In the following, several different SM analyses as reported in Table F.2 are discussed. The χ^2 minimisation is performed with the program MINUIT [155], and the predictions are calculated with ZFITTER 6.43 as a function of the five SM input parameters $\Delta\alpha^{(5)}_{\rm had}(m^2_{\rm Z})$, $\alpha_{\rm S}(m^2_{\rm Z})$, $m_{\rm Z}$, $m_{\rm t}$ and $\log_{10}(m_{\rm H}/{\rm GeV})$ which are varied simultaneously in the fits; see [4] for details on the fit procedure. The somewhat large χ^2/dof for all of these fits is caused by the large dispersion in the values of the leptonic effective electroweak mixing angle measured through the various asymmetries at LEP-I and SLD [4]. Following [4] for the analyses presented here, this dispersion is interpreted as a fluctuation in one or more of the input measurements, and thus we neither modify nor exclude any of them. A further significant increase in χ^2/dof is observed when the low-Q^2 NuTeV results are included in the analysis.

To test the agreement between the Z-pole data [4] (LEP-I and SLD) and the SM, a fit to these data is performed. This fit differs from the corresponding analysis reported in Reference [4] in that the new result for $\Delta\alpha^{(5)}_{\rm had}(m^2_{\rm Z})$ [321], reported in Table F.1, is used. The result is shown in Table F.2, column 1. The indirect constraints on $m_{\rm W}$ and $m_{\rm t}$ are shown in Figure F.1, compared with the direct measurements. Also shown are the SM predictions for Higgs masses between 114 and 1000 GeV. The indirect and direct results on $m_{\rm W}$ and $m_{\rm t}$ are in good agreement. In both cases, a low value of the Higgs-boson mass is preferred.

For the fit shown in column 2 of Table F.2, the direct measurement of $m_{\rm t}$ from the Tevatron experiments is included, in order to obtain the best indirect determination of $m_{\rm W}$. The result is also shown in Figure F.2. The indirect determination of the W-boson mass, 80.363 ± 0.020 GeV, is in good agreement with the direct measurements at LEP-II and the Tevatron, $m_{\rm W} = 80.385 \pm 0.015$ GeV. For the fit shown in column 3 of Table F.2 and Figure F.3, the direct $m_{\rm W}$ and $\Gamma_{\rm W}$ measurements from LEP-II and the Tevatron are included instead of the direct $m_{\rm t}$ measurement, in order to obtain the constraint $m_{\rm t} = 178^{+11}_{-8}$ GeV, in good agreement with the much more precise direct measurement of $m_{\rm t} = 173.2 \pm 0.9$ GeV.

The best constraints on $m_{\rm H}$ are obtained when all high-Q^2 measurements are used in the fit. The results of this fit are shown in column 4 of Table F.2. The predictions of this fit for observables measured in high-Q^2 and low-Q^2 reactions are listed in Tables F.1 and F.3, respectively. In Figure F.4 the observed value of $\Delta\chi^2 \equiv \chi^2 - \chi^2_{\rm min}$ as a function of $m_{\rm H}$ is plotted for this fit including all high-Q^2 results. The solid curve is the result using ZFITTER, and corresponds to the last column of Table F.2. The shaded band represents the uncertainty due to uncalculated higher-order corrections, as estimated by ZFITTER. Also shown is the result (dashed curve) obtained when using $\Delta\alpha^{(5)}_{\rm had}(m^2_{\rm Z})$ of Reference [335].

The 95% one-sided confidence level upper limit on $m_{\rm H}$ (taking the band into account) is 152 GeV. When the 95% C.L. lower limit on $m_{\rm H}$ of 114.4 GeV obtained from direct searches at LEP-II [363] is included, the upper limit increases from 152 GeV to 171 GeV.

Given the direct measurements of the other four SM input parameters, each observable is equivalent to a constraint on the mass of the SM Higgs boson. These constraints are compared in Figure F.5. For very low Higgs-masses, the constraints are qualitative only as the effects of real Higgs-strahlung, neither included in the experimental analyses nor in the SM calculations of expectations, may become sizeable [364]. Besides the measurement of the W mass, the most sensitive measurements are the asymmetries, *i.e.*, $\sin^2\theta^{\rm lept}_{\rm eff}$. A reduced uncertainty for the value of $\alpha(m^2_{\rm Z})$ would therefore result in an improved constraint on $\log m_{\rm H}$ and thus $m_{\rm H}$, as already shown in Figure F.4.

Direct searches for the Higgs boson of the SM are currently performed at the Tevatron and

	- 1 - all Z-pole data	- 2 - all Z-pole data plus $m_{\rm t}$	- 3 - all Z-pole data plus $m_{\rm W}$, $\Gamma_{\rm W}$	- 4 - all Z-pole data plus $m_{\rm t}, m_{\rm W}, \Gamma_{\rm W}$
$m_{\rm t}$ [GeV]	173^{+13}_{-10}	$173.2^{+0.9}_{-0.9}$	$178.1^{+10.9}_{-7.8}$	$173.3^{+0.9}_{-0.9}$
$m_{\rm H}$ [GeV]	118^{+203}_{-64}	122^{+59}_{-41}	148^{+237}_{-81}	94^{+29}_{-24}
$\log_{10}(m_{\rm H}/{\rm GeV})$	$2.07^{+0.43}_{-0.34}$	$2.09^{+0.17}_{-0.18}$	$2.17^{+0.41}_{-0.35}$	$1.97^{+0.12}_{-0.13}$
$\alpha_{\rm S}(m_{\rm Z}^2)$	0.1190 ± 0.0027	0.1191 ± 0.0027	0.1190 ± 0.0028	0.1185 ± 0.0026
χ^2/dof (P)	16.0/10 (9.9%)	16.0/11 (14%)	16.5/12 (17%)	16.9/13 (21%)
$\sin^2\theta^{\rm lept}_{\rm eff}$	0.23149 $\pm$0.00016	0.23149 $\pm$0.00016	0.23144 $\pm$0.00014	0.23139 $\pm$0.00011
$\sin^2\theta_{\rm W}$	0.22334 $\pm$0.00062	0.22332 $\pm$0.00039	0.22298 $\pm$0.00026	0.22305 $\pm$0.00023
$m_{\rm W}$ [GeV]	80.362 ± 0.032	80.363 ± 0.020	80.381 ± 0.013	80.377 ± 0.012

Table F.2: Results of the fits to: (1) all Z-pole data (LEP-I and SLD), (2) all Z-pole data plus the direct $m_{\rm t}$ determination, (3) all Z-pole data plus the direct $m_{\rm W}$ and $\Gamma_{\rm W}$ determinations, (4) all Z-pole data plus the direct $m_{\rm t}, m_{\rm W}, \Gamma_{\rm W}$ determinations (i.e., all high-Q^2 results). As the sensitivity to $m_{\rm H}$ is logarithmic, both $m_{\rm H}$ as well as $\log_{10}(m_{\rm H}/{\rm GeV})$ are quoted. The bottom part of the table lists derived results for $\sin^2\theta^{\rm lept}_{\rm eff}$, $\sin^2\theta_{\rm W}$ and $m_{\rm W}$. See text for a discussion of theoretical errors not included in the errors above.

	Measurement with Total Error	Standard-Model High-Q^2 Fit	Pull
APV [312]			
$Q_{\rm W}$(Cs)	-72.74 ± 0.46	-72.909 ± 0.025	0.4
Møller [313]			
$\sin^2\theta_{\overline{\rm MS}}(m_{\rm Z})$	0.2330 ± 0.0015	0.23110 ± 0.00011	1.3
νN [315]			
$g^2_{\nu{\rm Lud}}$	0.30005 ± 0.00137	0.30397 ± 0.00013	2.9
$g^2_{\nu{\rm Rud}}$	0.03076 ± 0.00110	0.03011 ± 0.00002	0.6

Table F.3: Summary of measurements performed in low-Q^2 reactions: atomic parity violation, e^-e^- Møller scattering and neutrino-nucleon scattering. The SM results and the pulls (difference between measurement and fit in units of the total measurement error) are derived from the SM fit including all high-Q^2 data (Table F.2, column 4) with the Higgs mass treated as a free parameter.

the LHC. In summer 2012, the combined Higgs-boson analyses of the Tevatron experiments CDF and D0 excluded the mass ranges of $100 - 103$ GeV and $147 - 180$ GeV and reported evidence for a new particle with a combined significance of about three standard deviations [365]. At the same time, using both 2011 and some 2012 data, the LHC collaborations ATLAS and CMS excluded the mass regions of $110 - 122$ GeV and $128 - 600$ GeV and both reported independently the observation of a new particle in Higgs-boson searches with a significance of five or more standard deviations [260]. The electroweak precision data are well compatible with the hypothesis that the new particle, observed with a mass in the range of $125 - 126$ GeV, is the Higgs boson of the SM, as is also evident from Figures F.1 to F.5. If the new particle is not the Higgs boson of the SM, the results of electroweak fits such as those presented here may be unreliable because in that case the new particle is not considered in the calculation of electroweak radiative corrections.

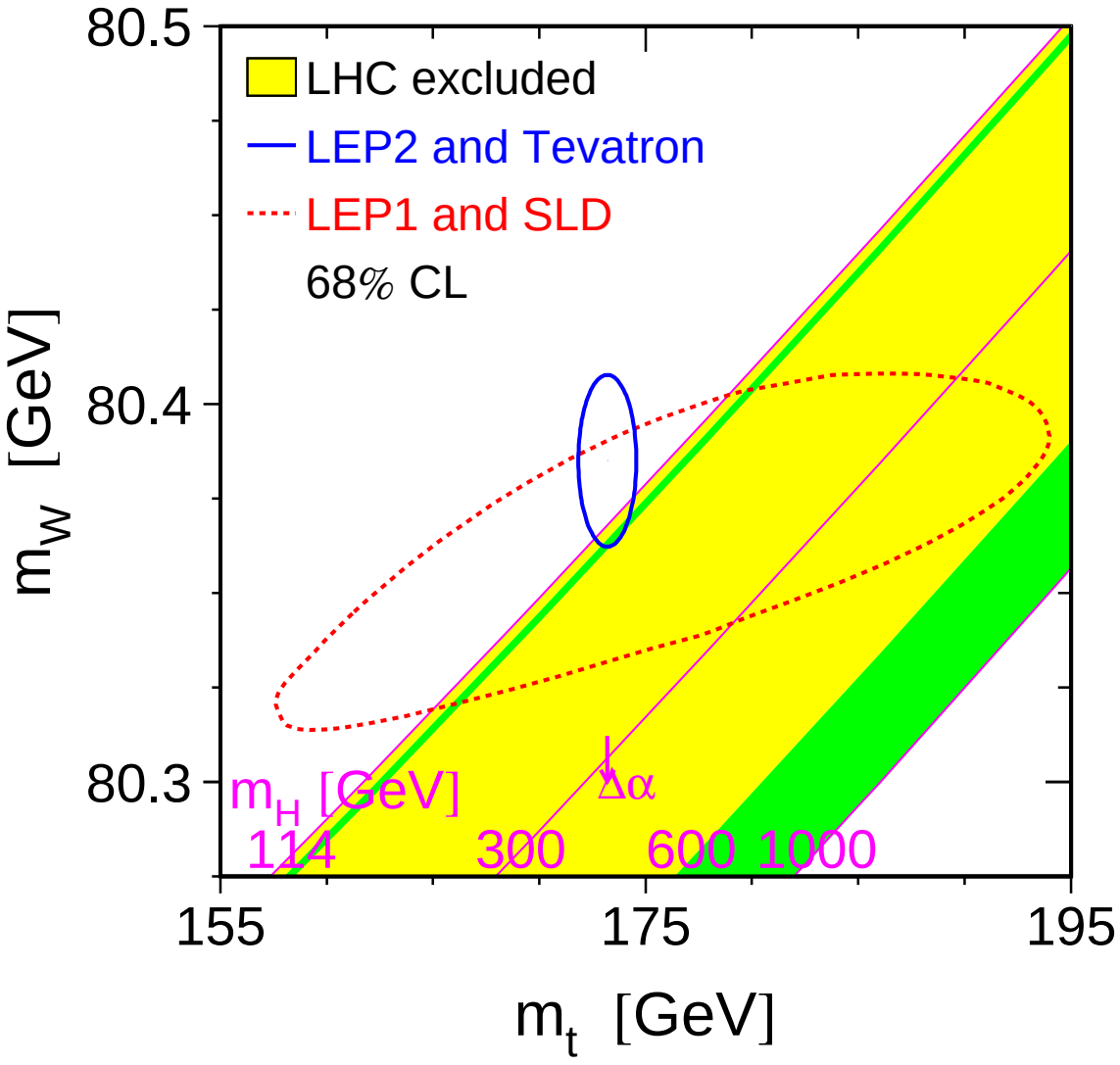


Figure F.1: The comparison of the indirect constraints on $m_{\rm W}$ and $m_{\rm t}$ based on LEP-I/SLD data (dashed contour) and the direct measurements from the LEP-II/Tevatron experiments (solid contour). In both cases the 68% CL contours are plotted. Also shown is the SM relationship for the masses as a function of the Higgs mass in the region favoured by theory ($<$ 1000 GeV) and allowed by direct searches (dark green bands). The arrow labelled $\Delta\alpha$ shows the variation of this relation if $\alpha(m_{\rm Z}^2)$ is changed by plus/minus one standard deviation. This variation gives an additional uncertainty to the SM band shown in the figure.

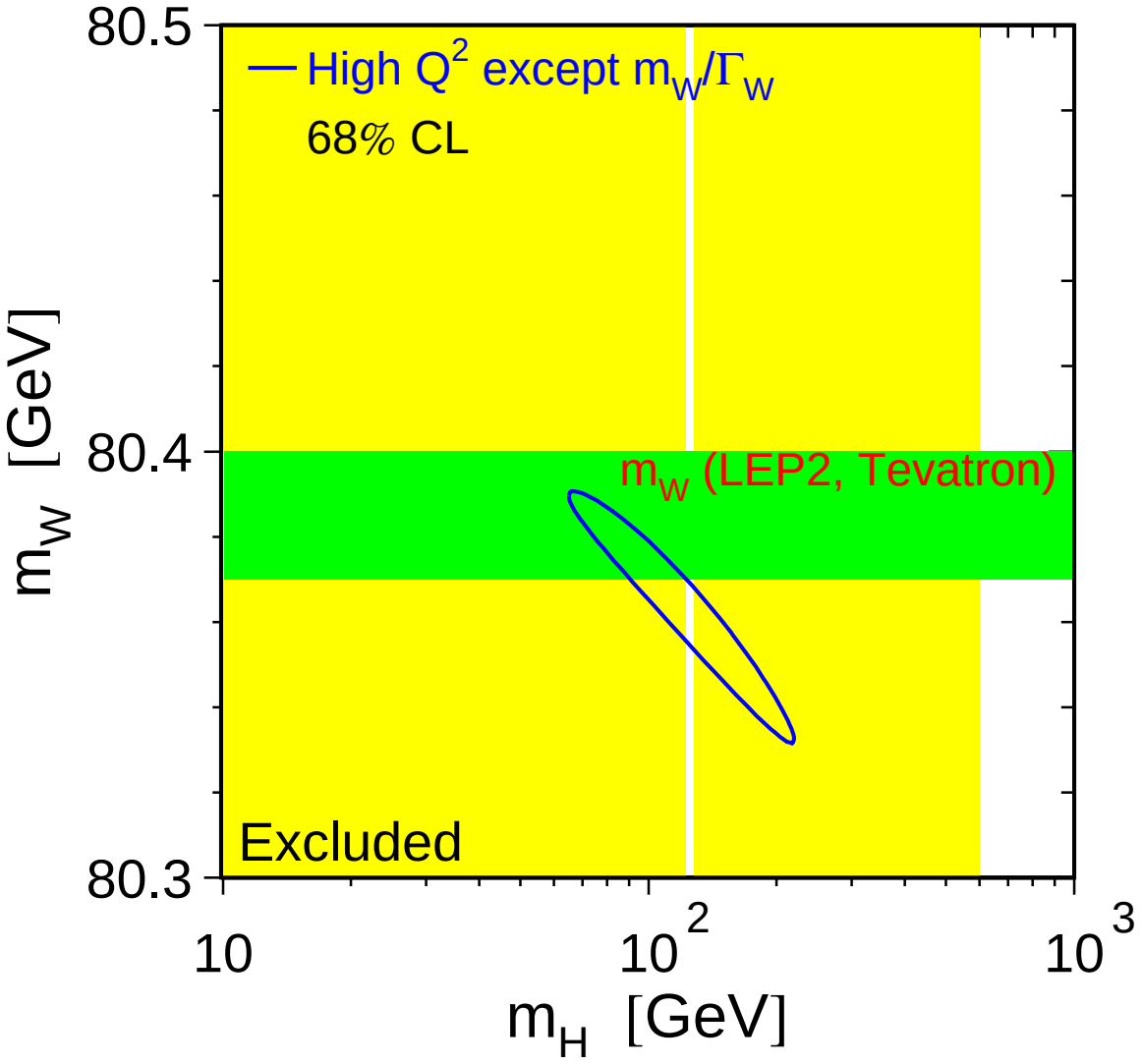


Figure F.2: The 68% confidence level contour in m_{W} and m_{H} for the fit to all data except the direct measurement of m_{W}, indicated by the shaded horizontal band of ± 1 sigma width. The vertical bands show the 95% CL exclusion ranges on m_{H} from the direct searches.

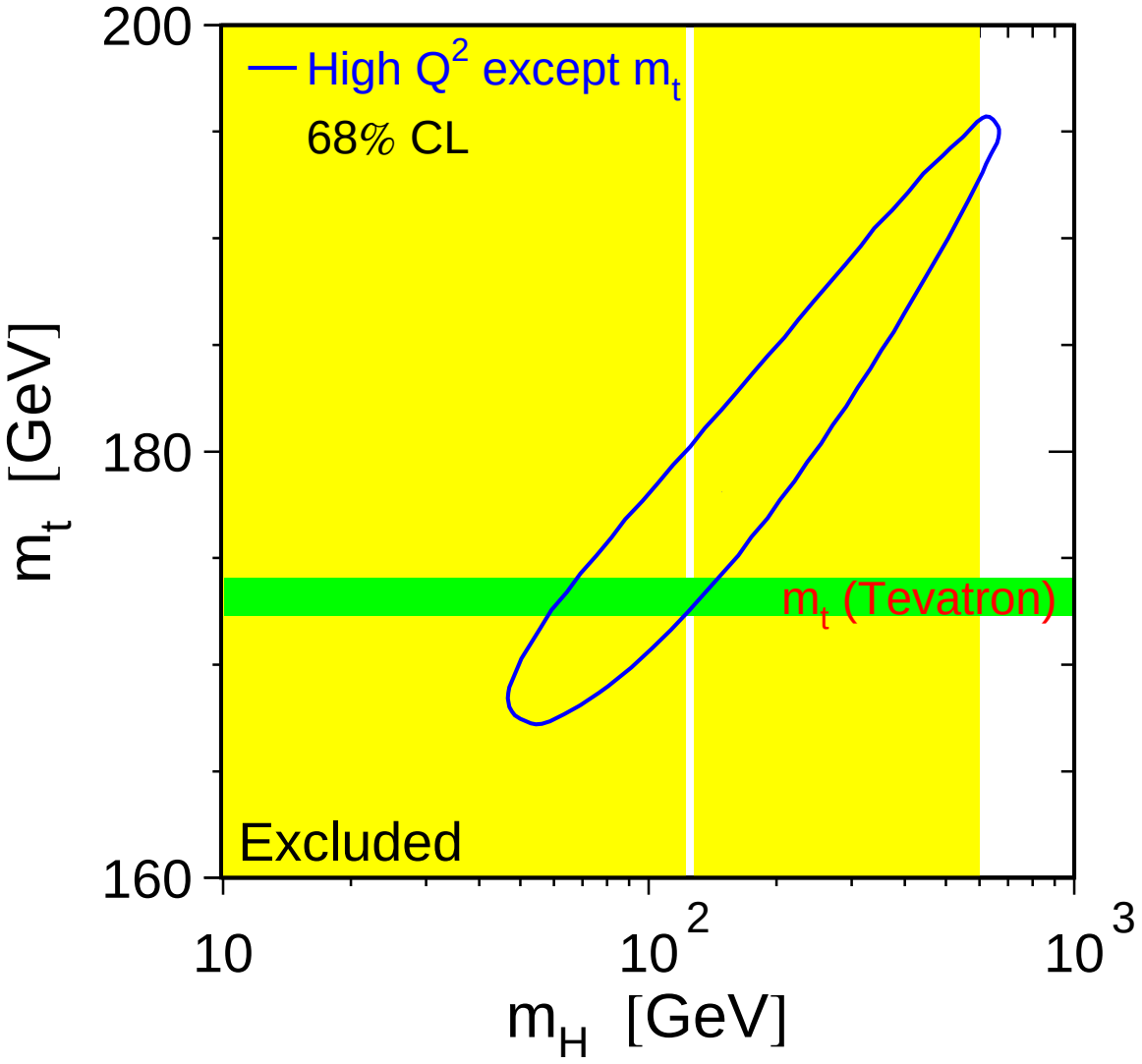


Figure F.3: The 68% confidence level contour in $m_{\rm t}$ and $m_{\rm H}$ for the fit to all data except the direct measurement of $m_{\rm t}$, indicated by the shaded horizontal band of ± 1 sigma width. The vertical bands show the 95% CL exclusion ranges on $m_{\rm H}$ from the direct searches.

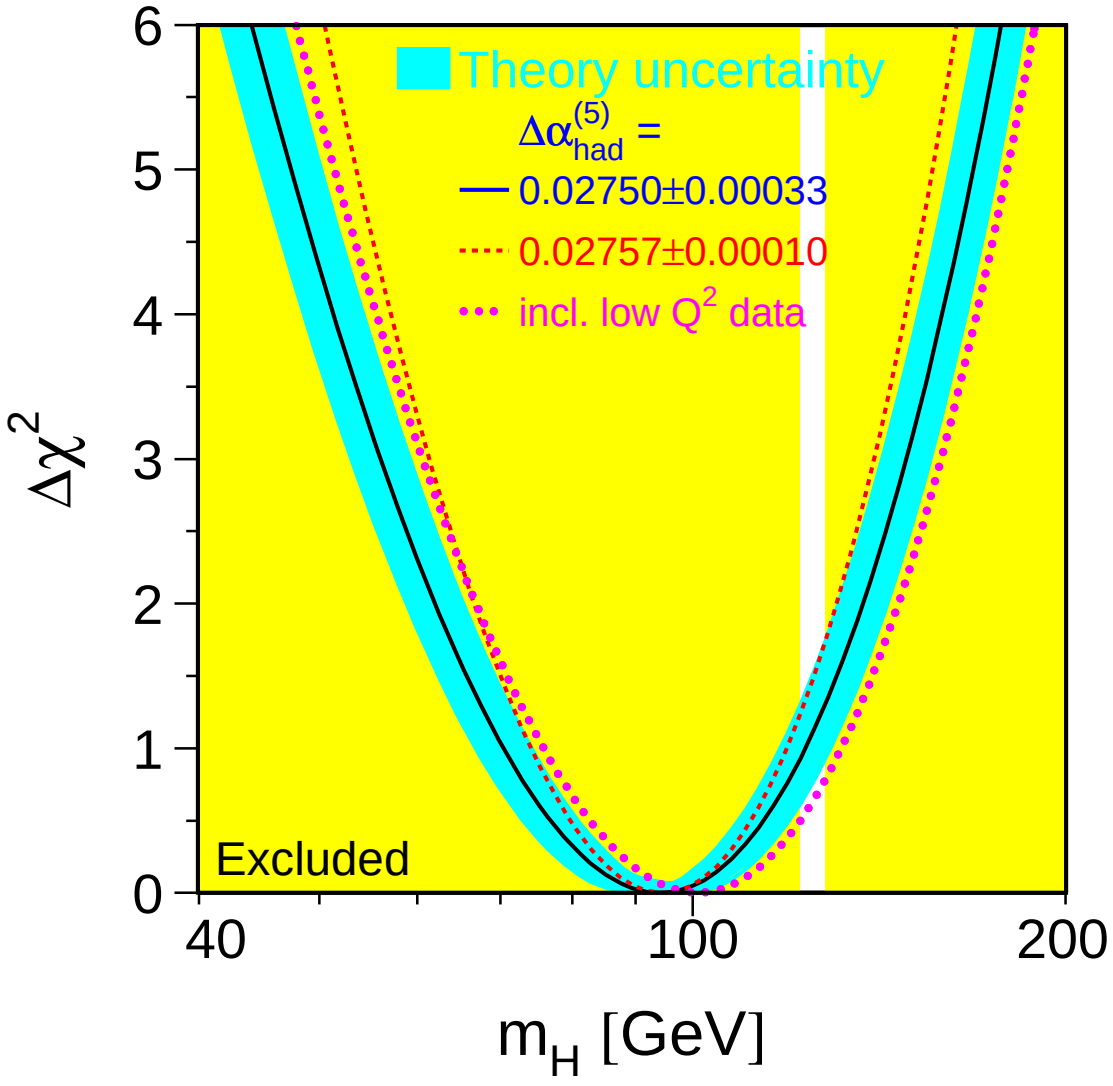


Figure F.4: $\Delta\chi^2 = \chi^2 - \chi^2_{min}$ *vs.* $m_{\rm H}$ curve. The line is the result of the fit using all high-Q^2 data (last column of Table F.2); the band represents an estimate of the theoretical error due to missing higher order corrections. The vertical bands show the 95% CL exclusion ranges on $m_{\rm H}$ from the direct searches. The dashed curve is the result obtained using the evaluation of $\Delta\alpha^{(5)}_{\rm had}(m^2_{\rm Z})$ from Reference [335]. The dotted curve corresponds to a fit including also the low-Q^2 data from Table F.3.

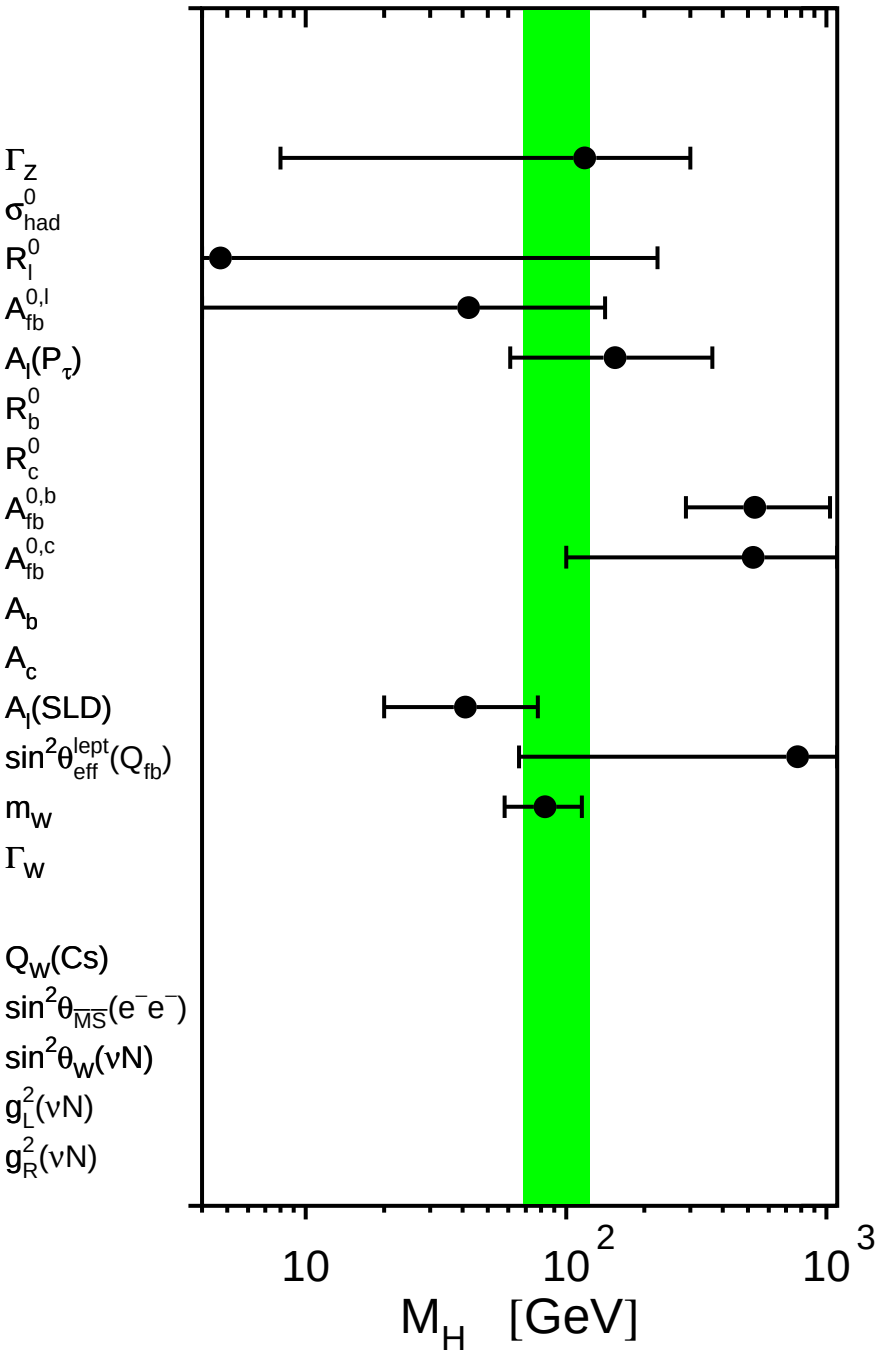


Figure F.5: Constraints on the mass of the Higgs boson from each observable. The Higgs-boson mass and its 68% CL uncertainty is obtained from a five-parameter SM fit to the observable, constraining $\Delta\alpha^{(5)}_{\rm had}(m^2_{\rm Z}) = 0.02750 \pm 0.00033$, $\alpha_{\rm S}(m^2_{\rm Z}) = 0.118 \pm 0.003$, $m_{\rm Z} = 91.1875 \pm 0.0021$ GeV and $m_{\rm t} = 173.2 \pm 0.9$ GeV. Because of these four common constraints the resulting Higgs-boson mass values are highly correlated. The shaded band denotes the overall constraint on the mass of the Higgs boson derived from all observables including the above four SM parameters as reported in the last column of Table F.2. Results are only shown for observables whose measurement accuracy allows to constrain the Higgs-boson mass on the scale of the figure.

Bibliography

[1] S. Glashow, Nucl.Phys. **22** (1961) 579–588

[2] S. Weinberg, Phys.Rev.Lett. **19** (1967) 1264–1266

[3] A. Salam, Conf.Proc. **C680519** (1968) 367–377

[4] ALEPH Collaboration, DELPHI Collaboration, L3 Collaboration, OPAL Collaboration, SLD Collaboration, LEP Electroweak Working Group, SLD Electroweak and Heavy Flavour Groups, Phys.Rept. **427** (2006) 257–454

[5] ALEPH Collaboration, A. Heister *et al.*, Eur.Phys.J. **C28** (2003) 1–13

[6] DELPHI Collaboration, J. Abdallah *et al.*, Eur.Phys.J. **C37** (2004) 405–419

[7] L3 Collaboration, P. Achard *et al.*, Phys.Lett. **B531** (2002) 28–38

[8] OPAL Collaboration, G. Abbiendi *et al.*, Eur.Phys.J. **C26** (2003) 331–344

[9] W. Heitler, Quantum Theory of Radiation, (Oxford University Press, second edition, 1944), pages 204–207

[10] M. Capdequi Peyranere, Y. Loubatieres, and M. Talon, Nucl.Phys. **B249** (1985) 61

[11] J. Fujimoto, M. Igarashi, and Y. Shimizu, Prog.Theor.Phys. **77** (1987) 118

[12] S. Drell, Annals Phys. **4** (1958) 75–80

[13] F. Low, Phys.Rev.Lett. **14** (1965) 238–239

[14] O. J. Eboli, A. Natale, and S. Novaes, Phys.Lett. **B271** (1991) 274–276

[15] I. Antoniadis *et al.*, Phys.Lett. **B436** (1998) 257–263

[16] K. Agashe and N. Deshpande, Phys.Lett. **B456** (1999) 60–67

[17] P. Mery, M. Perrottet, and F. Renard, Z.Phys. **C38** (1988) 579

[18] S. J. Brodsky and S. Drell, Phys.Rev. **D22** (1980) 2236

[19] F. Renard, Phys.Lett. **B116** (1982) 264

[20] B. Vachon, Search for excited charged leptons in electron positron collisions, Ph.D. thesis, Victoria University, 2002, UMI-NQ-74948

[21] B. Vachon, *Excited electron contribution to the* $e^+e^- \to \gamma\gamma$ *cross-section*, Eprint hep-ph/0103132v2, 2004

[22] F. A. Berends and R. Kleiss, Nucl.Phys. **B186** (1981) 22

[23] VENUS Collaboration, K. Abe *et al.*, Z.Phys. **C45** (1989) 175–191

[24] ALEPH Collaboration, D. Buskulic *et al.*, Z.Phys. **C59** (1993) 215–230

[25] DELPHI Collaboration, P. Abreu *et al.*, Phys.Lett. **B327** (1994) 386–396

[26] L3 Collaboration, B. Adeva *et al.*, Phys.Lett. **B250** (1990) 199–204

[27] L3 Collaboration, O. Adriani *et al.*, Phys.Lett. **B288** (1992) 404–411

[28] L3 Collaboration, M. Acciarri *et al.*, Phys.Lett. **B353** (1995) 136–144

[29] OPAL Collaboration, M. Akrawy *et al.*, Phys.Lett. **B241** (1990) 133

[30] OPAL Collaboration, M. Akrawy *et al.*, Phys.Lett. **B257** (1991) 531–540

[31] O. J. Eboli, A. Natale, and S. Novaes, Phys.Lett. **B271** (1991) 274–276

[32] ALEPH Collaboration, S. Schael *et al.*, Eur.Phys.J. **C49** (2007) 411–437

[33] DELPHI Collaboration, J. Abdallah *et al.*, Eur.Phys.J. **C45** (2006) 589–632

[34] L3 Collaboration, P. Achard *et al.*, Eur.Phys.J. **C47** (2006) 1–19

[35] OPAL Collaboration, G. Abbiendi *et al.*, Eur.Phys.J. **C33** (2004) 173–212

[36] D. Y. Bardin *et al.*, Z.Phys. **C44** (1989) 493

[37] D. Y. Bardin *et al.*, Comput.Phys.Commun. **59** (1990) 303–312

[38] D. Y. Bardin *et al.*, Nucl.Phys. **B351** (1991) 1–48

[39] D. Y. Bardin *et al.*, Phys.Lett. **B255** (1991) 290–296

[40] D. Y. Bardin *et al.*, *ZFITTER: An Analytical program for fermion pair production in* e^+e^- *annihilation*, Eprint hep-ph/9412201, 1992

[41] D. Y. Bardin *et al.*, Comput.Phys.Commun. **133** (2001) 229–395

[42] A. Arbuzov, *Light pair corrections to electron positron annihilation at LEP / SLC*, Eprint hep-ph/9907500, 1999

[43] A. Arbuzov, JHEP **0107** (2001) 043

[44] A. Arbuzov *et al.*, Comput.Phys.Commun. **174** (2006) 728–758

[45] ZFITTER support group, `ZFITTER 6.43`, June 2008, `http://zfitter.desy.de`

[46] ALEPH Collaboration, R. Barate *et al.*, Eur.Phys.J. **C12** (2000) 183–207

[47] ALEPH Collaboration, S. Schael *et al.*, Eur.Phys.J. **C49** (2007) 411–437

[48] DELPHI Collaboration, P. Abreu *et al.*, Eur.Phys.J. **C11** (1999) 383–407

[49] DELPHI Collaboration, P. Abreu *et al.*, Phys.Lett. **B485** (2000) 45–61

[50] DELPHI Collaboration, J. Abdallah *et al.*, Eur.Phys.J. **C45** (2006) 589–632

[51] L3 Collaboration, M. Acciarri *et al.*, Phys.Lett. **B407** (1997) 361–376

[52] L3 Collaboration, M. Acciarri *et al.*, Phys.Lett. **B479** (2000) 101–117

[53] L3 Collaboration, P. Achard *et al.*, Eur.Phys.J. **C47** (2006) 1–19

[54] OPAL Collaboration, K. Ackerstaff *et al.*, Phys.Lett. **B391** (1997) 221–234

[55] OPAL Collaboration, K. Ackerstaff *et al.*, Eur.Phys.J. **C2** (1998) 441–472

[56] OPAL Collaboration, G. Abbiendi *et al.*, Eur.Phys.J. **C6** (1999) 1–18

[57] OPAL Collaboration, G. Abbiendi *et al.*, Eur.Phys.J. **C13** (2000) 553–572

[58] OPAL Collaboration, G. Abbiendi *et al.*, Eur.Phys.J. **C33** (2004) 173–212

[59] Two Fermion Working Group, M. Kobel *et al.*, *Reports of the Working Groups on Precision Calculations for LEP2 Physics: Proceedings. Two fermion production in electron positron collisions*, Eprint hep-ph/0007180, 2000

[60] S. Jadach, B. Ward, and Z. Was, Comput.Phys.Commun. **130** (2000) 260–325

[61] S. Jadach, B. Ward, and Z. Was, Phys.Rev. **D63** (2001) 113009

[62] L. Lyons, D. Gibaut, and P. Clifford, Nucl.Instrum.Meth. **A270** (1988) 110

[63] A. Valassi, Nucl.Instrum.Meth. **A500** (2003) 391–405

[64] S. Jadach, W. Placzek, and B. Ward, Phys.Lett. **B390** (1997) 298–308

[65] P. Langacker, AIP Conf.Proc. **1200** (2010) 55–63

[66] P. Langacker, Rev.Mod.Phys. **81** (2009) 1199–1228

[67] A. Leike, Phys.Rept. **317** (1999) 143–250

[68] J. L. Hewett and T. G. Rizzo, Phys.Rept. **183** (1989) 193

[69] P. Langacker, R. W. Robinett, and J. L. Rosner, Phys.Rev. **D30** (1984) 1470

[70] D. London and J. L. Rosner, Phys.Rev. **D34** (1986) 1530

[71] J. C. Pati and A. Salam, Phys.Rev. **D10** (1974) 275–289

[72] J. C. Pati and A. Salam, Phys.Rev. **D11** (1974) 703–703

[73] R. N. Mohapatra and J. C. Pati, Phys.Rev. **D11** (1975) 566–571

[74] G. Altarelli, B. Mele, and M. Ruiz-Altaba, Z.Phys. **C45** (1989) 109

[75] G. Altarelli, B. Mele, and M. Ruiz-Altaba, Z.Phys. **C47** (1990) 676

[76] DELPHI Collaboration, P. Abreu *et al.*, Z.Phys. **C65** (1995) 603–618

[77] A. Leike, S. Riemann, and T. Riemann, *Z Z-prime mixing in presence of standard weak loop corrections*, Eprint hep-ph/9808374, 1991

[78] A. Leike, S. Riemann, and T. Riemann, Phys.Lett. **B291** (1992) 187–194

[79] E. Eichten, K. D. Lane, and M. E. Peskin, Phys.Rev.Lett. **50** (1983) 811–814

[80] H. Kroha, Phys.Rev. **D46** (1992) 58–69

[81] D. Bourilkov, JHEP **9908** (1999) 006

[82] D. Bourilkov, Phys.Rev. **D62** (2000) 076005

[83] D. Bourilkov, Phys.Rev. **D64** (2001) 071701

[84] N. Arkani-Hamed, S. Dimopoulos, and G. Dvali, Phys.Lett. **B429** (1998) 263–272

[85] I. Antoniadis *et al.*, Phys.Lett. **B436** (1998) 257–263

[86] N. Arkani-Hamed, S. Dimopoulos, and G. Dvali, Phys.Rev. **D59** (1999) 086004

[87] J. L. Hewett, Phys.Rev.Lett. **82** (1999) 4765–4768

[88] T. G. Rizzo, Phys.Rev. **D59** (1999) 115010

[89] G. F. Giudice, R. Rattazzi, and J. D. Wells, Nucl.Phys. **B544** (1999) 3–38

[90] T. Han, J. D. Lykken, and R.-J. Zhang, Phys.Rev. **D59** (1999) 105006

[91] S. Nussinov and R. Shrock, Phys.Rev. **D59** (1999) 105002

[92] W. Buchmuller, R. Ruckl, and D. Wyler, Phys.Lett. **B191** (1987) 442–448

[93] W. Buchmuller, R. Ruckl, and D. Wyler, Phys.Lett. **B448** (1999) 320

[94] J. Kalinowski *et al.*, Z.Phys. **C74** (1997) 595–603

[95] R. Hanbury Brown and R. Twiss, Nature **178** (1956) 1046–1048

[96] G. Goldhaber *et al.*, Phys.Rev.Lett. **3** (1959) 181–183

[97] D. Boal, C. Gelbke, and B. Jennings, Rev.Mod.Phys. **62** (1990) 553–602

[98] G. Baym, Acta Phys.Polon. **B29** (1998) 1839–1884

[99] ARGUS Collaboration, H. Albrecht *et al.*, Phys.Lett. **B162** (1985) 395

[100] CLEO Collaboration, P. Haas *et al.*, Phys.Rev.Lett. **55** (1985) 1248

[101] G. Gustafson, U. Pettersson, and P. Zerwas, Phys.Lett. **B209** (1988) 90

[102] T. Sjöstrand and V. A. Khoze, Z.Phys. **C62** (1994) 281–310

[103] L. Lonnblad, Z.Phys. **C70** (1996) 107–114

[104] G. Corcella *et al.*, JHEP **0101** (2001) 010

[105] G. Gustafson and J. Hakkinen, Z.Phys. **C64** (1994) 659–664

[106] J. R. Ellis and K. Geiger, Phys.Rev. **D54** (1996) 1967–1990

[107] J. Rathsman, Phys.Lett. **B452** (1999) 364–371

[108] ALEPH Collaboration, S. Schael *et al.*, Eur.Phys.J. **C48** (2006) 685–698

[109] L3 Collaboration, P. Achard *et al.*, Phys.Lett. **B581** (2004) 19–30

[110] OPAL Collaboration, G. Abbiendi *et al.*, Eur.Phys.J. **C35** (2004) 293–312

[111] ALEPH Collaboration, S. Schael *et al.*, Eur.Phys.J. **C47** (2006) 309–335

[112] DELPHI Collaboration, J. Abdallah *et al.*, Eur.Phys.J. **C55** (2008) 1–38

[113] L3 Collaboration, P. Achard *et al.*, Eur.Phys.J. **C45** (2006) 569–587

[114] OPAL Collaboration, G. Abbiendi *et al.*, Eur.Phys.J. **C45** (2006) 307–335

[115] OPAL Collaboration, G. Abbiendi *et al.*, Eur.Phys.J. **C45** (2006) 291–305

[116] DELPHI Collaboration, P. Abreu *et al.*, Eur.Phys.J. **C18** (2000) 203–228

[117] V. A. Khoze and T. Sjöstrand, Eur.Phys.J. **C6** (1999) 271–284

[118] D. Duchesneau, *New method based on energy and particle flow in* $e^+e^- \to W^+W^- \to$ *hadrons events for color reconnection studies*, LAPP-EXP-2000-02, 2000

[119] D. Duchesneau, Nucl.Phys.Proc.Suppl. **96** (2001) 13–22

[120] A. Ballestrero *et al.*, J.Phys.G **G24** (1998) 365–403

[121] JADE Collaboration, W. Bartel *et al.*, Phys.Lett. **B101** (1981) 129

[122] JADE Collaboration, W. Bartel *et al.*, Z.Phys. **C21** (1983) 37

[123] JADE Collaboration, W. Bartel *et al.*, Phys.Lett. **B134** (1984) 275

[124] JADE Collaboration, W. Bartel *et al.*, Phys.Lett. **B157** (1985) 340

[125] TPC/Two Gamma Collaboration, H. Aihara *et al.*, Z.Phys. **C28** (1985) 31

[126] TPC/Two Gamma Collaboration, H. Aihara *et al.*, Phys.Rev.Lett. **57** (1986) 945

[127] TASSO Collaboration, M. Althoff *et al.*, Z.Phys. **C29** (1985) 29

[128] DELPHI Collaboration, J. Abdallah *et al.*, Eur.Phys.J. **C51** (2007) 249–269

[129] L3 Collaboration, P. Achard *et al.*, Phys.Lett. **B561** (2003) 202–212

[130] S. Catani *et al.*, Phys.Lett. **B269** (1991) 432–438

[131] Y. L. Dokshitzer, V. A. Khoze, and S. Troian, J.Phys.G **G17** (1991) 1481–1492

[132] S. Bethke *et al.*, Nucl.Phys. **B370** (1992) 310–334

[133] S. Bethke *et al.*, Nucl.Phys. **B523** (1998) 681

[134] T. Sjöstrand, Comput.Phys.Commun. **27** (1982) 243

[135] T. Sjöstrand, Comput.Phys.Commun. **28** (1983) 229

[136] T. Sjöstrand, Comput.Phys.Commun. **39** (1986) 347–407

[137] T. Sjöstrand and M. Bengtsson, Comput.Phys.Commun. **43** (1987) 367

[138] M. Bengtsson and T. Sjöstrand, Nucl.Phys. **B289** (1987) 810

[139] S. Jadach *et al.*, Comput.Phys.Commun. **140** (2001) 475–512

[140] T. Sjöstrand, Comput.Phys.Commun. **82** (1994) 74–90

[141] W. A. Rolke, A. M. Lopez, and J. Conrad, Nucl.Instrum.Meth. **A551** (2005) 493–503

[142] S. Chekanov, E. De Wolf, and W. Kittel, Eur.Phys.J. **C6** (1999) 403–411

[143] DELPHI Collaboration, P. Abreu *et al.*, Phys.Lett. **B401** (1997) 181–191

[144] E. De Wolf, *Correlations in $e^+e^- \to W^+W^-$ hadronic decays*, Eprint hep-ph/0101243, 2001

[145] ALEPH Collaboration, R. Barate *et al.*, Phys.Lett. **B478** (2000) 50–64

[146] ALEPH Collaboration, S. Schael *et al.*, Phys.Lett. **B606** (2005) 265–275

[147] DELPHI Collaboration, J. Abdallah *et al.*, Eur.Phys.J. **C44** (2005) 161–174

[148] L3 Collaboration, P. Achard *et al.*, Phys.Lett. **B547** (2002) 139–150

[149] OPAL Collaboration, G. Abbiendi *et al.*, Eur.Phys.J. **C36** (2004) 297–308

[150] L. Lonnblad and T. Sjöstrand, Eur.Phys.J. **C2** (1998) 165–180

[151] ALEPH Collaboration, S. Schael *et al.*, Eur.Phys.J. **C47** (2006) 309–335

[152] DELPHI Collaboration, J. Abdallah *et al.*, Eur.Phys.J. **C55** (2008) 1–38

[153] L3 Collaboration, P. Achard *et al.*, Eur.Phys.J. **C45** (2006) 569–587

[154] OPAL Collaboration, G. Abbiendi *et al.*, Eur.Phys.J. **C45** (2006) 307–335

[155] F. James and M. Roos, Comput.Phys.Commun. **10** (1975) 343–367

[156] M. W. Grünewald *et al.*, *Reports of the Working Groups on Precision Calculations for LEP2 Physics: Proceedings. Four fermion production in electron positron collisions*, Eprint hep-ph/0005309, 2000

[157] ALEPH Collaboration, A. Heister *et al.*, Eur.Phys.J. **C38** (2004) 147–160

[158] DELPHI Collaboration, J. Abdallah *et al.*, Eur.Phys.J. **C34** (2004) 127–144

[159] L3 Collaboration, P. Achard *et al.*, Phys.Lett. **B600** (2004) 22–40

[160] OPAL Collaboration, G. Abbiendi *et al.*, Eur.Phys.J. **C52** (2007) 767–785

[161] S. Jadach *et al.*, Phys.Rev. **D54** (1996) 5434–5442

[162] S. Jadach *et al.*, Phys.Lett. **B417** (1998) 326–336

[163] S. Jadach *et al.*, Phys.Rev. **D61** (2000) 113010

[164] S. Jadach *et al.*, Phys.Rev. **D65** (2002) 093010

[165] S. Jadach *et al.*, Comput.Phys.Commun. **140** (2001) 432–474

[166] The YFSWW cross-sections at 155–215 GeV have been kindly provided by the authors

[167] S. Jadach *et al.*, Comput.Phys.Commun. **140** (2001) 475–512

[168] A. Denner *et al.*, Nucl.Phys. **B560** (1999) 33–65

[169] A. Denner *et al.*, Phys.Lett. **B475** (2000) 127–134

[170] A. Denner *et al.*, Nucl.Phys. **B587** (2000) 67–117

[171] A. Denner *et al.*, *Off-shell W pair production: Universal versus nonuniversal corrections*, Eprint hep-ph/0101257, 2001

[172] The RACOONWW cross-sections at 155–215 GeV have been kindly provided by the authors

[173] D. Y. Bardin *et al.*, Comput.Phys.Commun. **104** (1997) 161–187

[174] M. Skrzypek *et al.*, Phys.Lett. **B372** (1996) 289–298

[175] M. Skrzypek *et al.*, Comput.Phys.Commun. **94** (1996) 216–248

[176] S. Jadach *et al.*, Comput.Phys.Commun. **119** (1999) 272–311

[177] The KORALW cross-sections at 155–215 GeV have been kindly provided by the authors. They have actually been computed using YFSWW [161, 167], switching off non-leading $\mathcal{O}(\alpha)$ radiative corrections and the screening of the Coulomb correction, to reproduce the calculation from KORALW

[178] Particle Data Group, K. Nakamura *et al.*, J.Phys.G **G37** (2010) 075021

[179] ALEPH Collaboration, S. Schael *et al.*, JHEP **0904** (2009) 124

[180] DELPHI Collaboration, J. Abdallah *et al.*, Eur.Phys.J. **C30** (2003) 447–466

[181] L3 Collaboration, P. Achard *et al.*, Phys.Lett. **B572** (2003) 133–144

[182] OPAL Collaboration, G. Abbiendi *et al.*, Eur.Phys.J. **C32** (2003) 303–322

[183] S. Jadach, W. Placzek, and B. Ward, Phys.Rev. **D56** (1997) 6939–6941

[184] G. Passarino, ZZTO, in [156], pages 134–140

[185] DELPHI Collaboration, J. Abdallah *et al.*, Eur.Phys.J. **C51** (2007) 503–523

[186] L3 Collaboration, P. Achard *et al.*, Phys.Lett. **B616** (2005) 159–173

[187] J. Fujimoto *et al.*, *grc4f v1.0: A Four fermion event generator for e^+e^- collisions*, Eprint hep-ph/9603394, 1996

[188] J. Fujimoto *et al.*, Comput.Phys.Commun. **100** (1997) 128–156

[189] Y. Kurihara *et al.*, Prog.Theor.Phys. **103** (2000) 1199–1211

[190] ALEPH Collaboration, S. Schael *et al.*, Phys.Lett. **B605** (2005) 49–62

[191] DELPHI Collaboration, J. Abdallah *et al.*, Eur.Phys.J. **C45** (2006) 273–289

[192] L3 Collaboration, M. Acciarri *et al.*, Phys.Lett. **B436** (1998) 417–427

[193] L3 Collaboration, M. Acciarri *et al.*, Phys.Lett. **B487** (2000) 229–240

[194] L3 Collaboration, P. Achard *et al.*, Phys.Lett. **B547** (2002) 151–163

[195] E. Accomando and A. Ballestrero, Comput.Phys.Commun. **99** (1997) 270–296

[196] E. Accomando, A. Ballestrero, and E. Maina, Comput.Phys.Commun. **150** (2003) 166–196

[197] The WPHACT cross-sections at 160–210 GeV have been kindly provided by A. Ballestrero

[198] G. Passarino, Comput.Phys.Commun. **97** (1996) 261–303

[199] G. Passarino, Nucl.Phys. **B574** (2000) 451–494

[200] G. Passarino, Nucl.Phys. **B578** (2000) 3–26

[201] The WTO cross-sections at 160–210 GeV have been kindly provided by the author

[202] G. Montagna *et al.*, Eur.Phys.J. **C20** (2001) 217–225

[203] L3 Collaboration, P. Achard *et al.*, Phys.Lett. **B561** (2003) 202–212

[204] OPAL Collaboration, G. Abbiendi *et al.*, Phys.Lett. **B438** (1998) 391–404

[205] OPAL Collaboration, G. Abbiendi *et al.*, Eur.Phys.J. **C24** (2002) 1–15

[206] DELPHI Collaboration, J. Abdallah *et al.*, Eur.Phys.J. **C31** (2003) 139–147

[207] L3 Collaboration, P. Achard *et al.*, Phys.Lett. **B527** (2002) 29–38

[208] OPAL Collaboration, G. Abbiendi *et al.*, Phys.Lett. **B580** (2004) 17–36

[209] W. J. Stirling and A. Werthenbach, Eur.Phys.J. **C14** (2000) 103–110

[210] G. Altarelli *et al.*, *Physics at LEP2: Vol. 1*, Eprint CERN Yellow Report CERN-96-01-V-1, 1996

[211] ALEPH Collaboration, S. Schael *et al.*, Phys.Lett. **B614** (2005) 7–26

[212] DELPHI Collaboration, J. Abdallah *et al.*, Eur.Phys.J. **C66** (2010) 35–56

[213] L3 Collaboration, P. Achard *et al.*, Phys.Lett. **B586** (2004) 151–166

[214] OPAL Collaboration, G. Abbiendi *et al.*, Eur.Phys.J. **C33** (2004) 463–476

[215] K. Gaemers and G. Gounaris, Z.Phys. **C1** (1979) 259

[216] K. Hagiwara *et al.*, Nucl.Phys. **B282** (1987) 253

[217] K. Hagiwara *et al.*, Phys.Lett. **B283** (1992) 353–359

[218] K. Hagiwara *et al.*, Phys.Rev. **D48** (1993) 2182–2203

[219] K. Hagiwara *et al.*, Nucl.Phys. **B496** (1997) 66–102

[220] M. S. Bilenky *et al.*, Nucl.Phys. **B409** (1993) 22–68

[221] M. S. Bilenky *et al.*, Nucl.Phys. **B419** (1994) 240–253

[222] I. Kuss and D. Schildknecht, Phys.Lett. **B383** (1996) 470–474

[223] G. Gounaris and C. G. Papadopoulos, Eur.Phys.J. **C2** (1998) 365–372

[224] G. Gounaris, J. Layssac, and F. Renard, Phys.Rev. **D62** (2000) 073013

[225] R. Brunelière *et al.*, Phys.Lett. **B533** (2002) 75–84

[226] J. Alcaraz, *A proposal for the combination of TGC measurements*, L3 Note 2718

[227] R. Brunelière, *Tests on the LEP TGC combination procedures*, ALEPH 2002-008 PHYS-2002-007 (2002)

[228] L3 Collaboration, M. Acciarri *et al.*, Phys.Lett. **B467** (1999) 171–184

[229] L3 Collaboration, P. Achard *et al.*, Phys.Lett. **B586** (2004) 151–166

[230] L3 Collaboration, P. Achard *et al.*, Phys.Lett. **B547** (2002) 151–163

[231] ALEPH Collaboration, S. Schael *et al.*, JHEP **0904** (2009) 124

[232] DELPHI Collaboration, J. Abdallah *et al.*, Eur.Phys.J. **C51** (2007) 525–542

[233] L3 Collaboration, P. Achard *et al.*, Phys.Lett. **B597** (2004) 119–130

[234] OPAL Collaboration, G. Abbiendi *et al.*, Eur.Phys.J. **C17** (2000) 553–566

[235] L3 Collaboration, P. Achard *et al.*, Phys.Lett. **B572** (2003) 133–144

[236] OPAL Collaboration, G. Abbiendi *et al.*, Eur.Phys.J. **C32** (2003) 303–322

[237] O. Klein, Surveys High Energ.Phys. **5** (1986) 269–285

[238] L.Maiani and P.M.Zerwas, *W Static ELM Parameters*, Memorandum to the TGC Combination Group (1998)

[239] CDF Collaboration, T. Aaltonen *et al.*, Phys.Rev.Lett. **100** (2008) 071801

[240] D0 Collaboration, V. Abazov *et al.*, Phys.Rev.Lett. **103** (2009) 231802

[241] CDF Collaboration, T. Aaltonen *et al.*, Phys.Rev.Lett. **108** (2012) 151803

[242] D0 Collaboration, V. M. Abazov *et al.*, Phys.Rev.Lett. **108** (2012) 151804

[243] ALEPH Collaboration, R. Barate *et al.*, Phys.Lett. **B415** (1997) 435–444

[244] L3 Collaboration, M. Acciarri *et al.*, Phys.Lett. **B407** (1997) 419–431

[245] OPAL Collaboration, K. Ackerstaff *et al.*, Phys.Lett. **B389** (1996) 416–428

[246] LEP Energy Working Group, R. Assmann *et al.*, Eur.Phys.J. **C6** (1999) 187–223

[247] LEP Energy Working Group, R. Assmann *et al.*, Eur.Phys.J. **C39** (2005) 253–292

[248] OPAL Collaboration, G. Abbiendi *et al.*, Eur.Phys.J. **C26** (2003) 321–330

[249] L. Lonnblad, Z.Phys. **C58** (1993) 471–478

[250] Y. L. Dokshitzer *et al.*, JHEP **9708** (1997) 001

[251] S. Bentvelsen and I. Meyer, Eur.Phys.J. **C4** (1998) 623–629

[252] S. Jadach, J. H. Kuhn, and Z. Was, Comput.Phys.Commun. **64** (1990) 275–299

[253] S. Jadach *et al.*, Comput.Phys.Commun. **76** (1993) 361–380

[254] L. Lonnblad, Comput.Phys.Commun. **71** (1992) 15–31

[255] DELPHI Collaboration, J. Abdallah *et al.*, Eur.Phys.J. **C46** (2006) 295–305

[256] L3 Collaboration, P. Achard *et al.*, Phys.Lett. **B585** (2004) 42–52

[257] OPAL Collaboration, G. Abbiendi *et al.*, Phys.Lett. **B604** (2004) 31–47

[258] G. Marchesini *et al.*, Comput.Phys.Commun. **67** (1992) 465–508

[259] F. Cossutti, Eur.Phys.J. **C44** (2005) 383–393

[260] ATLAS Collaboration, G. Aad *et al.*, Phys.Lett.B **716** (2012) 1–29

[261] CMS Collaboration, S. Chatrchyan *et al.*, Phys.Lett.B **716** (2012) 30–61

[262] The LEP Collaborations ALEPH, DELPHI, L3, OPAL, and the LEP Electroweak Working Group, *A Combination of Preliminary Electroweak Measurements and Constraints on the Standard Model*, Eprint hep-ex/0612034, CERN, 2006

[263] A. Borrelli *et al.*, Nucl.Phys. **B333** (1990) 357

[264] R. G. Stuart, Phys.Lett. **B272** (1991) 353–358

[265] A. Leike, T. Riemann, and J. Rose, Phys.Lett. **B273** (1991) 513–518

[266] T. Riemann, Phys.Lett. **B293** (1992) 451–456

[267] S. Kirsch and T. Riemann, Comput.Phys.Commun. **88** (1995) 89–108

[268] The ALEPH Collaboration, *S-Matrix fits to cross-section and forward-backward asymmetry measurements at LEP 1 and 2*, ALEPH 2000-042 PHYSICS 2000-015 (2002)

[269] DELPHI Collaboration, J. Abdallah *et al.*, Eur.Phys.J. **C45** (2006) 589–632

[270] L3 Collaboration, M. Acciarri *et al.*, Eur.Phys.J. **C16** (2000) 1–40

[271] OPAL Collaboration, G. Abbiendi *et al.*, Eur.Phys.J. **C19** (2001) 587–651

[272] H. Flacher *et al.*, Eur.Phys.J. **C60** (2009) 543–583

[273] M. Baak *et al.*, Eur.Phys.J. **C72** (2012) 2003

[274] CDF Collaboration, F. Abe *et al.*, Phys.Rev.Lett. **65** (1990) 2243–2246

[275] CDF Collaboration, F. Abe *et al.*, Phys.Rev. **D43** (1991) 2070–2093

[276] CDF Collaboration, F. Abe *et al.*, Phys.Rev.Lett. **75** (1995) 11–16

[277] CDF Collaboration, F. Abe *et al.*, Phys.Rev. **D52** (1995) 4784–4827

[278] CDF Collaboration, T. Affolder *et al.*, Phys.Rev. **D64** (2001) 052001

[279] CDF Collaboration, T. Aaltonen *et al.*, Phys.Rev.Lett. **99** (2007) 151801

[280] CDF Collaboration, T. Aaltonen *et al.*, Phys.Rev. **D77** (2008) 112001

[281] D0 Collaboration, S. Abachi *et al.*, Phys.Rev.Lett. **77** (1996) 3309–3314

[282] D0 Collaboration, B. Abbott *et al.*, Phys.Rev. **D58** (1998) 012002

[283] D0 Collaboration, B. Abbott *et al.*, Phys.Rev.Lett. **80** (1998) 3008

[284] D0 Collaboration, B. Abbott *et al.*, Phys.Rev. **D58** (1998) 092003

[285] D0 Collaboration, B. Abbott *et al.*, Phys.Rev. **D62** (2000) 092006

[286] D0 Collaboration, B. Abbott *et al.*, Phys.Rev.Lett. **84** (2000) 222–227

[287] D0 Collaboration, V. Abazov *et al.*, Phys.Rev. **D66** (2002) 012001

[288] D0 Collaboration, V. M. Abazov *et al.*, Phys.Rev.Lett. **103** (2009) 141801

[289] CDF Collaboration, T. Affolder *et al.*, Phys.Rev.Lett. **85** (2000) 3347–3352

[290] D0 Collaboration, V. Abazov *et al.*, Phys.Rev. **D66** (2002) 032008

[291] The Tevatron Electroweak Working Group for the CDF and D0 Collaborations, *2012 Update of the Combination of CDF and D0 Results for the Mass of the W Boson*, Eprint 1204.0042, FERMILAB, 2012

[292] The Tevatron Electroweak Working Group for the CDF and D0 Collaborations, *Combination of CDF and D0 Results on the Width of the W boson*, Eprint 1003.2826, FERMILAB, 2010

[293] CDF Collaboration, T. Aaltonen *et al.*, Phys.Rev.Lett. **105** (2010) 252001

[294] CDF Collaboration, T. Affolder *et al.*, Phys.Rev. **D63** (2001) 032003

[295] CDF Collaboration, T. Aaltonen *et al.*, Phys.Lett. **B714** (2012) 24–31

[296] CDF Collaboration, T. Aaltonen *et al.*, Phys.Rev. **D83** (2011) 111101

[297] CDF Collaboration, F. Abe *et al.*, Phys.Rev.Lett. **82** (1999) 271–276

[298] CDF Collaboration, F. Abe *et al.*, Phys.Rev.Lett. **82** (1999) 2808–2809

[299] CDF Collaboration, T. Aaltonen *et al.*, Phys.Rev.Lett. **107** (2011) 232002

[300] CDF Collaboration, T. Aaltonen *et al.*, Phys.Rev. **D81** (2010) 032002

[301] D0 Collaboration, V. M. Abazov *et al.*, Phys.Rev. **D84** (2011) 032004

[302] D0 Collaboration, V. Abazov *et al.*, Nature **429** (2004) 638–642

[303] D0 Collaboration, S. Abachi *et al.*, Phys.Rev.Lett. **79** (1997) 1197–1202

[304] D0 Collaboration, V. M. Abazov *et al.*, Phys.Rev. **D86** (2012) (R)

[305] D0 Collaboration, B. Abbott *et al.*, Phys.Rev.Lett. **80** (1998) 2063–2068

[306] D0 Collaboration, B. Abbott *et al.*, Phys.Rev. **D60** (1999) 052001

[307] The Tevatron Electroweak Working Group, for the CDF and D0 Collaborations, *Combination of CDF and D0 results on the mass of the top quark using up to 5.8/fb of data*, Eprint 1107.5255, 2011

[308] CDF Collaboration, D0 Collaboration, T. Aaltonen *et al.*, Phys.Rev. **D86** (2012) 092003

[309] C. Wood *et al.*, Science **275** (1997) 1759–1763

[310] S. Bennett and C. E. Wieman, Phys.Rev.Lett. **82** (1999) 2484–2487

[311] S. Bennett and C. Wieman, Phys.Rev.Lett. **82** (1999) 4153–4153

[312] J. Ginges and V. Flambaum, Phys.Rept. **397** (2004) 63–154

[313] SLAC E158 Collaboration, P. Anthony *et al.*, Phys.Rev.Lett. **92** (2004) 181602

[314] SLAC E158 Collaboration, P. Anthony *et al.*, Phys.Rev.Lett. **95** (2005) 081601

[315] NuTeV Collaboration, G. Zeller *et al.*, Phys.Rev.Lett. **88** (2002) 091802

[316] NuTeV Collaboration, G. Zeller *et al.*, Phys.Rev.Lett. **90** (2003) 239902(E)

[317] D. Y. Bardin *et al.*, *Electroweak working group report*, Eprint hep-ph/9709229, 1997

[318] I. Cloet, W. Bentz, and A. Thomas, Phys.Rev.Lett. **102** (2009) 252301

[319] W. Bentz *et al.*, Phys.Lett. **B693** (2010) 462–466

[320] M. Steinhauser, Phys.Lett. **B429** (1998) 158–161

[321] H. Burkhardt and B. Pietrzyk, Phys.Rev. **D84** (2011) 037502

[322] M. L. Swartz, Phys.Rev. **D53** (1996) 5268–5282

[323] A. D. Martin and D. Zeppenfeld, Phys.Lett. **B345** (1995) 558–563

[324] R. Alemany, M. Davier, and A. Hocker, Eur.Phys.J. **C2** (1998) 123–135

[325] M. Davier and A. Hocker, Phys.Lett. **B419** (1998) 419–431

[326] J. H. Kuhn and M. Steinhauser, Phys.Lett. **B437** (1998) 425–431

[327] F. Jegerlehner, *Hadronic effects in (g - 2)(mu) and alpha(QED)(M(Z)): Status and perspectives*, Eprint hep-ph/9901386, 1999

[328] J. Erler, Phys.Rev. **D59** (1999) 054008

[329] A. D. Martin, J. Outhwaite, and M. Ryskin, Phys.Lett. **B492** (2000) 69–73

[330] J. de Troconiz and F. Yndurain, Phys.Rev. **D65** (2002) 093002

[331] K. Hagiwara *et al.*, Phys.Rev. **D69** (2004) 093003

[332] J. de Troconiz and F. Yndurain, Phys.Rev. **D71** (2005) 073008

[333] T. Teubner *et al.*, *Update of g-2 of the Muon and Delta Alpha*, Eprint 1001.5401, 2010

[334] K. Hagiwara *et al.*, J.Phys.G **G38** (2011) 085003

[335] M. Davier *et al.*, Eur.Phys.J. **C71** (2011) 1515

[336] M. Davier *et al.*, Eur.Phys.J. **C72** (2012) 1874

[337] T. van Ritbergen and R. G. Stuart, Phys.Rev.Lett. **82** (1999) 488–491

[338] T. van Ritbergen and R. G. Stuart, Nucl.Phys. **B564** (2000) 343–390

[339] M. Steinhauser and T. Seidensticker, Phys.Lett. **B467** (1999) 271–278

[340] MuLan Collaboration, D. Chitwood *et al.*, Phys.Rev.Lett. **99** (2007) 032001

[341] FAST Collaboration, A. Barczyk *et al.*, Phys.Lett. **B663** (2008) 172–180

[342] MuLan Collaboration, D. Webber *et al.*, Phys.Rev.Lett. **106** (2011) 041803

[343] D. Y. Bardin and G. Passarino, *Upgrading of precision calculations for electroweak observables*, Eprint hep-ph/9803425, 1998

[344] D. Y. Bardin, M. W. Grünewald, and G. Passarino, *Precision calculation project report*, Eprint hep-ph/9902452, 1999

[345] G. Degrassi, S. Fanchiotti, and A. Sirlin, Nucl.Phys. **B351** (1991) 49–69

[346] G. Degrassi and A. Sirlin, Nucl.Phys. **B352** (1991) 342–366

[347] G. Degrassi, P. Gambino, and A. Vicini, Phys.Lett. **B383** (1996) 219–226

[348] G. Degrassi, P. Gambino, and A. Sirlin, Phys.Lett. **B394** (1997) 188–194

[349] A. Czarnecki and J. H. Kuhn, Phys.Rev.Lett. **77** (1996) 3955–3958

[350] R. Harlander, T. Seidensticker, and M. Steinhauser, Phys.Lett. **B426** (1998) 125–132

[351] G. Montagna *et al.*, Nucl.Phys. **B401** (1993) 3–66

[352] G. Montagna *et al.*, Comput.Phys.Commun. **76** (1993) 328–360

[353] G. Montagna *et al.*, Comput.Phys.Commun. **93** (1996) 120–126

[354] G. Montagna *et al.*, Comput.Phys.Commun. **117** (1999) 278–289, updated to include initial state pair radiation (G. Passarino, priv. comm.)

[355] T. Hebbeker *et al.*, Phys.Lett. **B331** (1994) 165–170

[356] P. A. Raczka and A. Szymacha, Phys.Rev. **D54** (1996) 3073–3084

[357] D. E. Soper and L. R. Surguladze, Phys.Rev. **D54** (1996) 4566–4577

[358] H. Stenzel, JHEP **0507** (2005) 0132

[359] M. Awramik *et al.*, Phys.Rev. **D69** (2004) 053006

[360] M. Awramik *et al.*, Phys.Rev.Lett. **93** (2004) 201805

[361] M. Faisst *et al.*, Nucl.Phys. **B665** (2003) 649–662

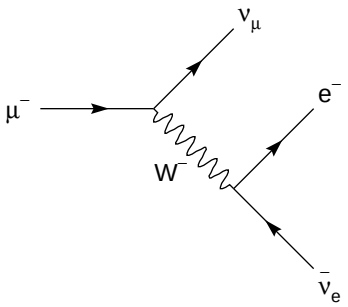
[362] S. Bethke, Eur.Phys.J. **C64** (2009) 689–703

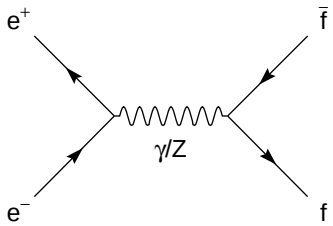
[363] ALEPH, DELPHI, L3, and OPAL Collaborations, The LEP Working Group for Higgs Boson Searches, Phys.Lett. **B565** (2003) 61–75

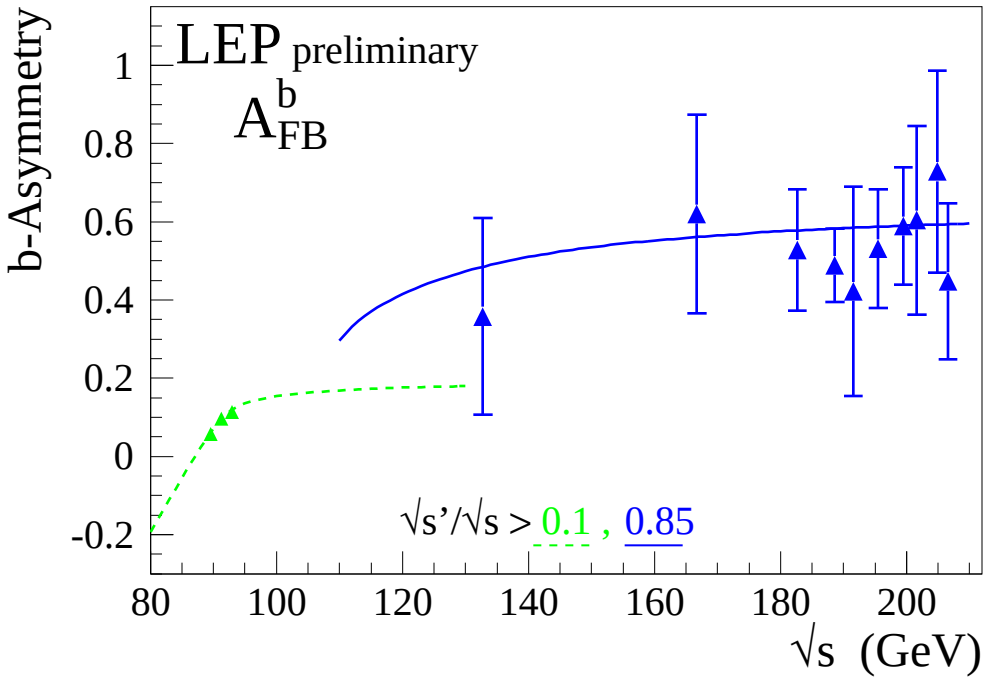
[364] T. Kawamoto and R. Kellogg, Phys.Rev. **D69** (2004) 113008

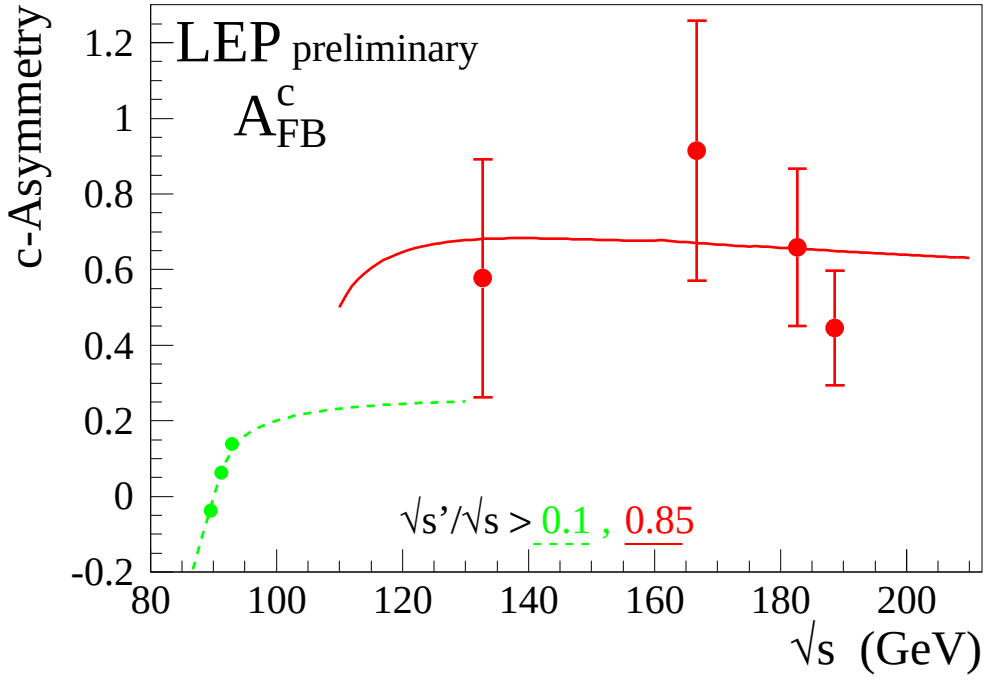
[365] Tevatron New Physics Higgs Working Group, CDF Collaboration, D0 Collaboration, *Updated Combination of CDF and D0 Searches for Standard Model Higgs Boson Production with up to 10.0 fb^{-1} of Data*, Eprint 1207.0449, 2012

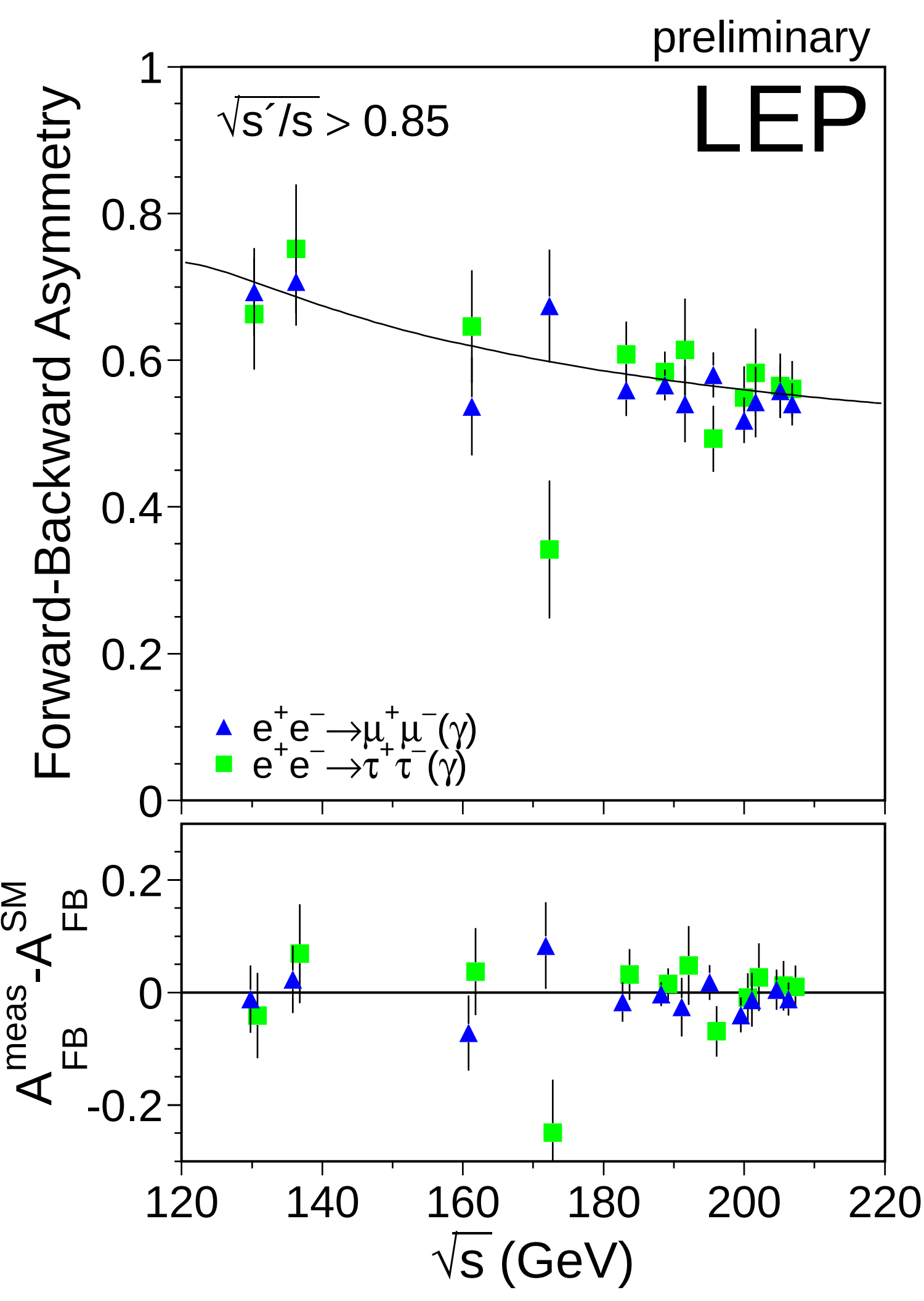
[366] CDF Collaboration, D0 Collaboration, T. Aaltonen *et al.*, Phys.Rev.Lett. **109** (2012) 071804.

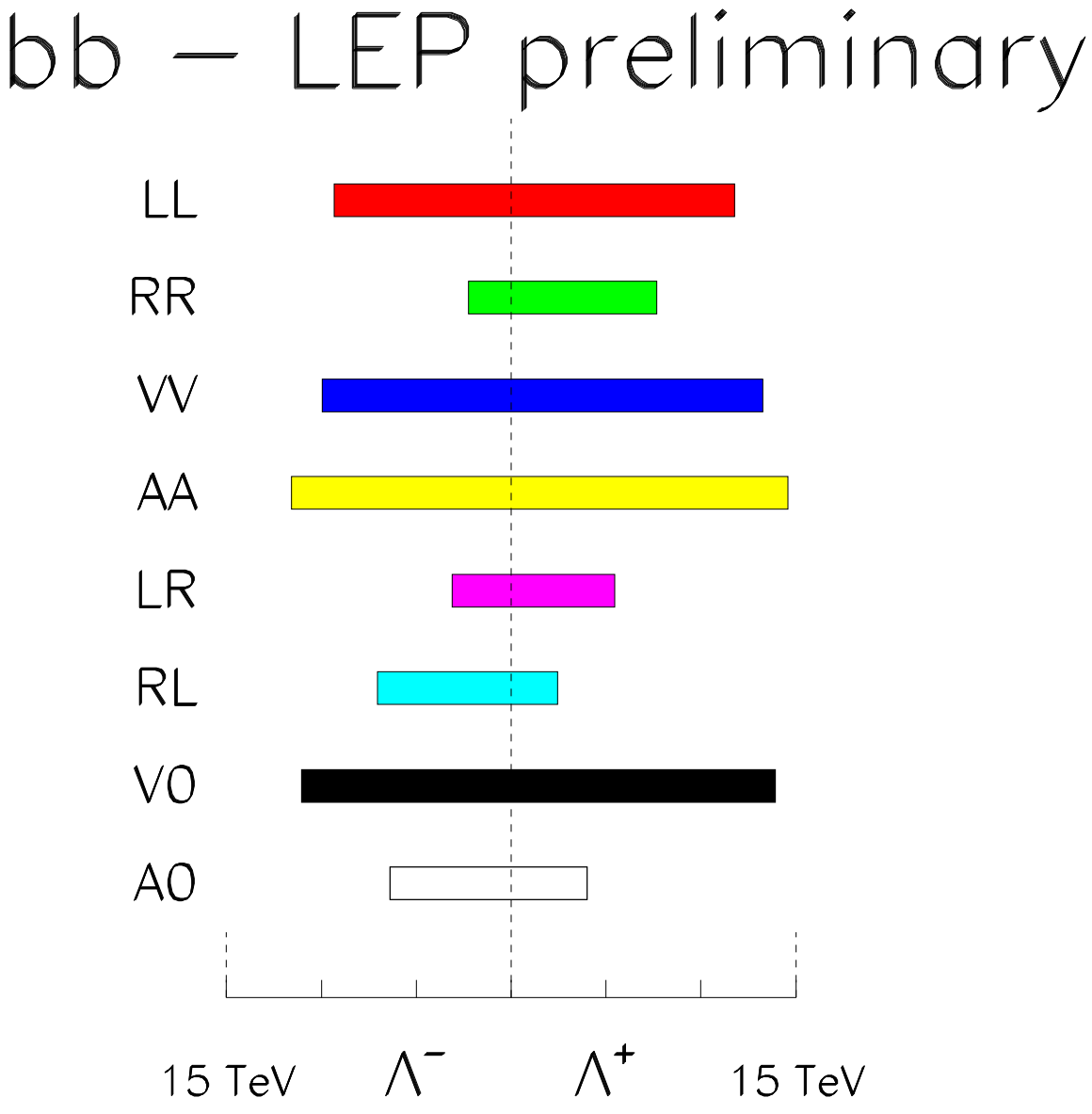

ν_μ
μ^-
e^-
W^-
$\bar{\nu}_e$

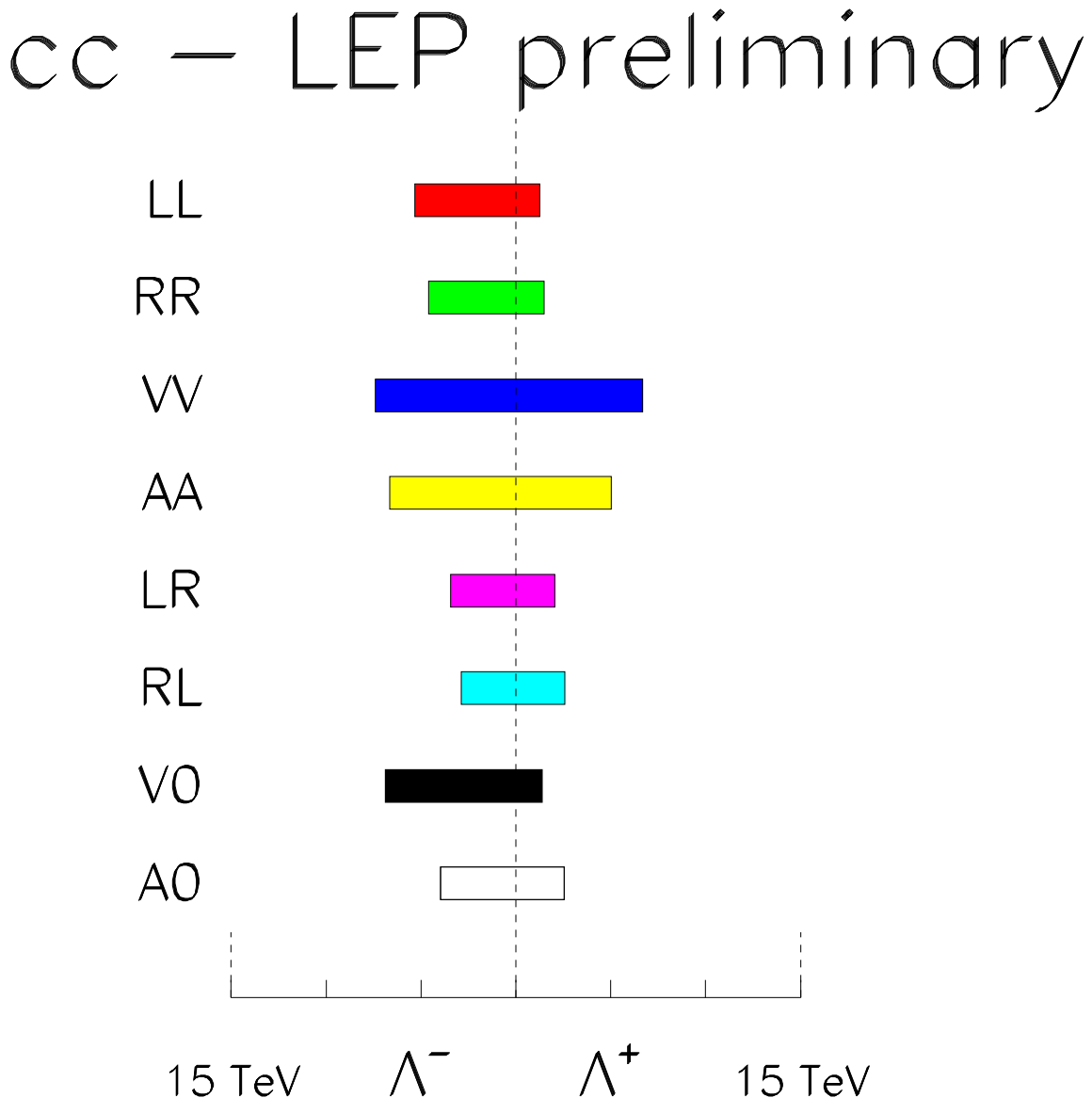

e^+
$\bar{f}$
γ/Z
e^-
f


LEP preliminary
A_{FB}^{b}
b-Asymmetry
1
0.8
0.6
0.4
0.2
0
-0.2
80
100
120
140
160
180
200
√s (GeV)
√s'/√s > 0.1 , 0.85


LEP preliminary
A_{FB}^{c}
c-Asymmetry
1.2
1
0.8
0.6
0.4
0.2
0
-0.2
80
100
120
140
160
180
200
√s (GeV)
√s'/√s > 0.1 , 0.85


preliminary
LEP
$\sqrt{s'/s} > 0.85$
Forward-Backward Asymmetry
$e^+e^- \to \mu^+\mu^-(\gamma)$
$e^+e^- \to \tau^+\tau^-(\gamma)$
$A_{FB}^{meas} - A_{FB}^{SM}$
$\sqrt{s}$ (GeV)
1
0.8
0.6
0.4
0.2
0
0.2
0
-0.2
120
140
160
180
200
220

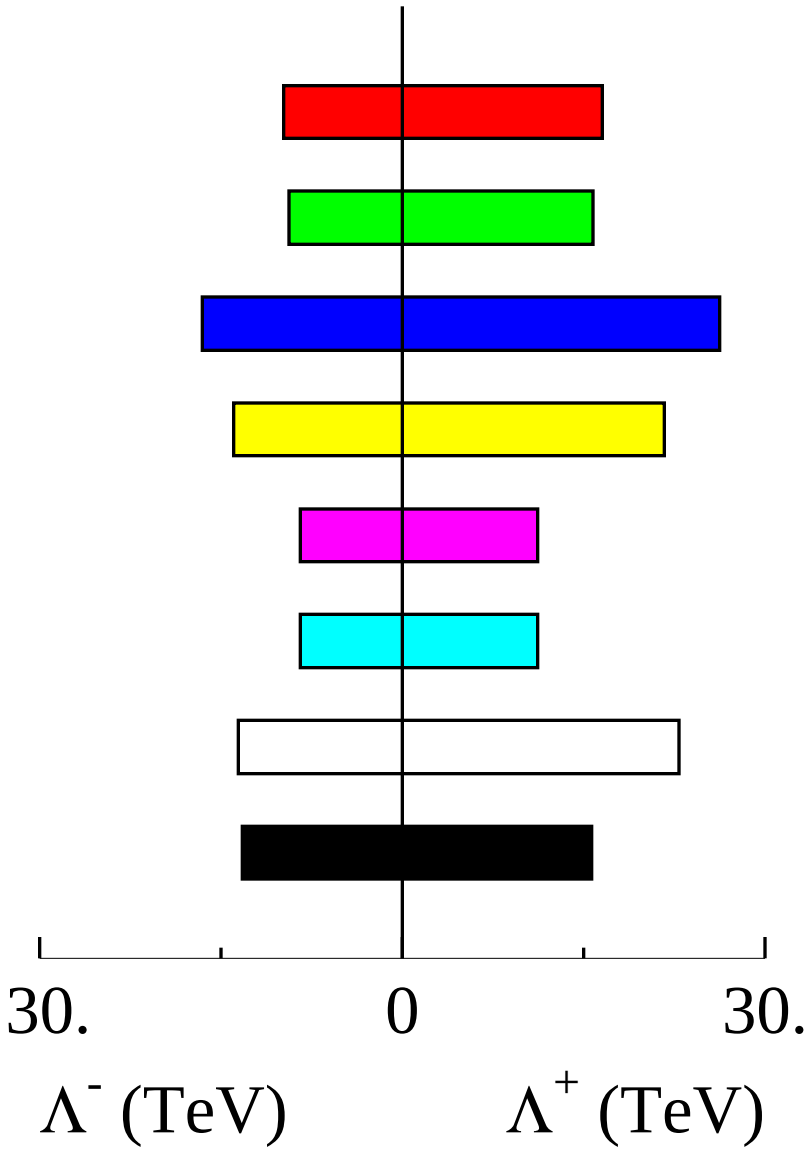

bb — LEP preliminary
LL
RR
VV
AA
LR
RL
V0
A0
15 TeV
Λ⁻
Λ⁺
15 TeV

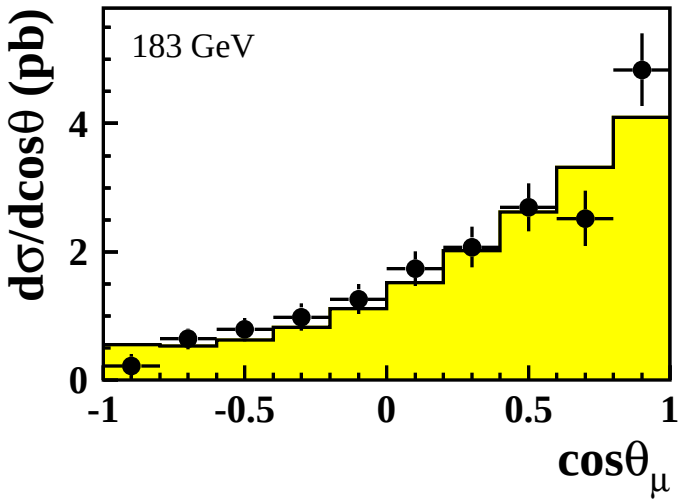

cc — LEP preliminary
LL
RR
VV
AA
LR
RL
V0
A0
15 TeV
Λ⁻
Λ⁺
15 TeV

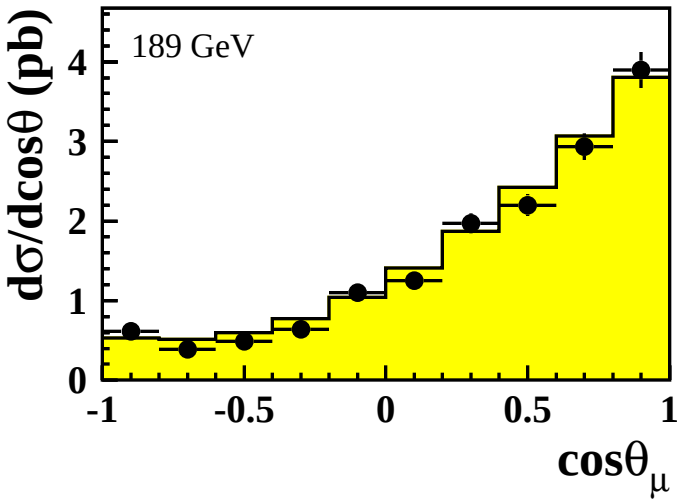
Preliminary LEP Combined

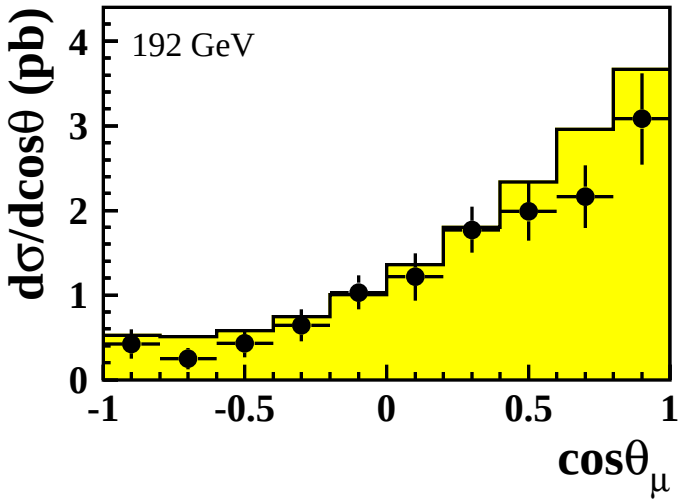
	Λ^-	Λ^+
LL	9.8	16.5
RR	9.4	15.8
VV	16.5	26.2
AA	14.0	21.7
LR	8.5	11.2
RL	8.5	11.2
V0	13.5	22.9
A0	13.2	15.6

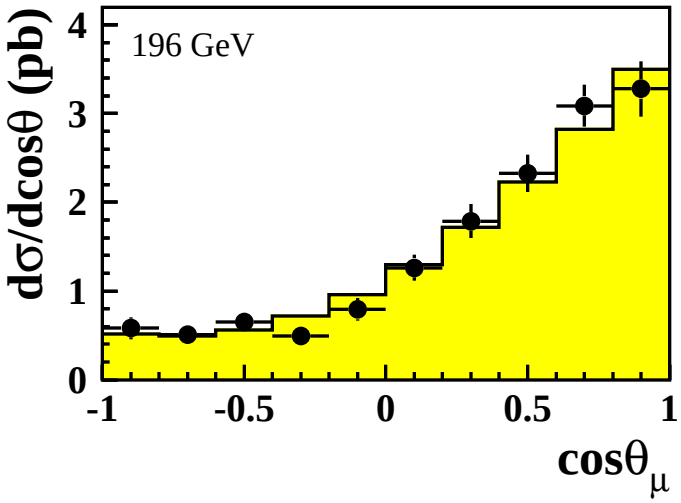
l^+l^-

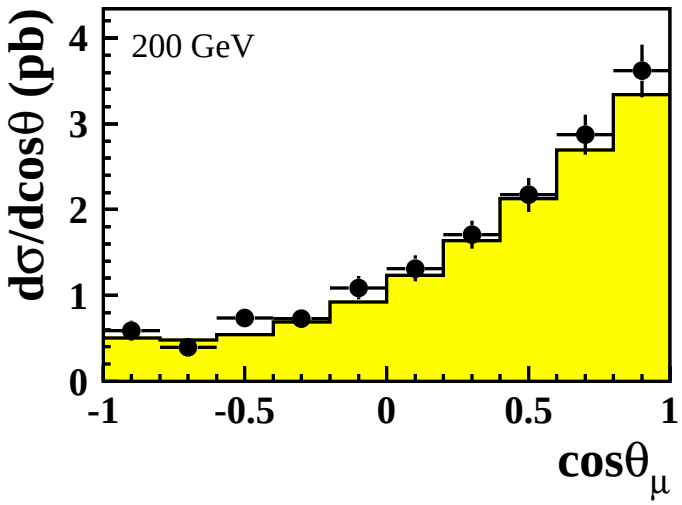


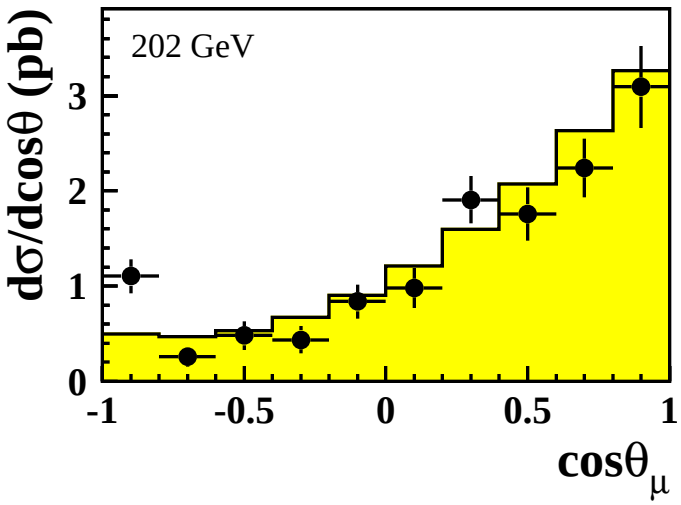

183 GeV
dσ/dcosθ (pb)
cosθμ

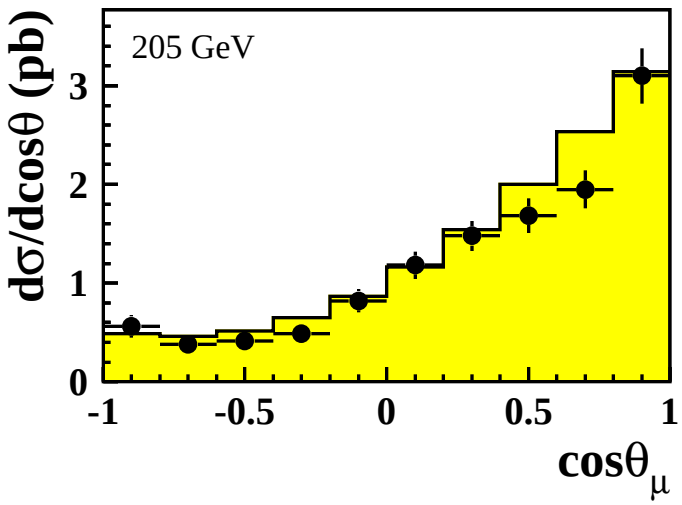

189 GeV
dσ/dcosθ (pb)
cosθμ

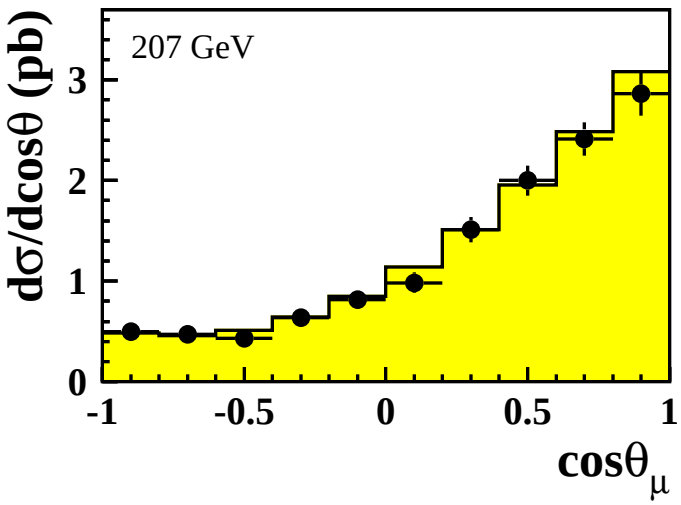

192 GeV
dσ/dcosθ (pb)
cosθμ

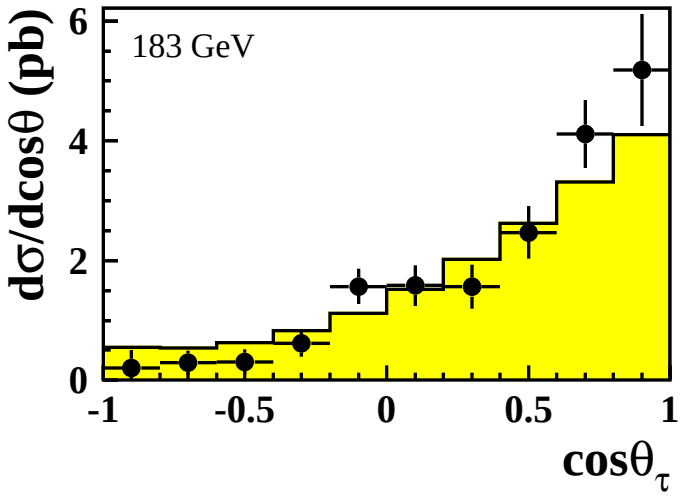

196 GeV
dσ/dcosθ (pb)
cosθμ

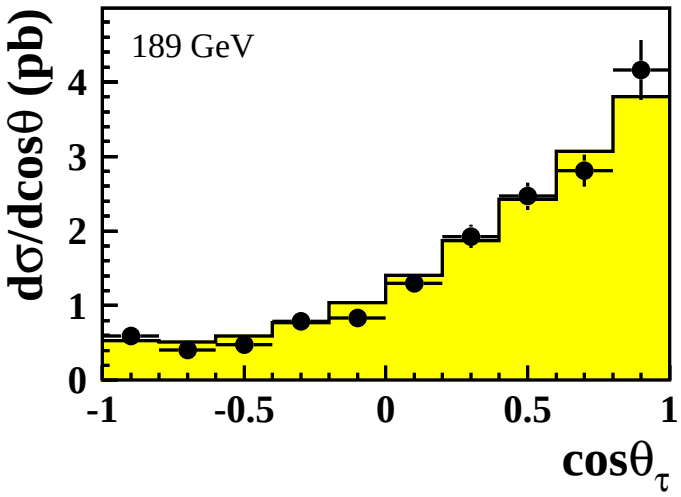

200 GeV
dσ/dcosθ (pb)
cosθμ

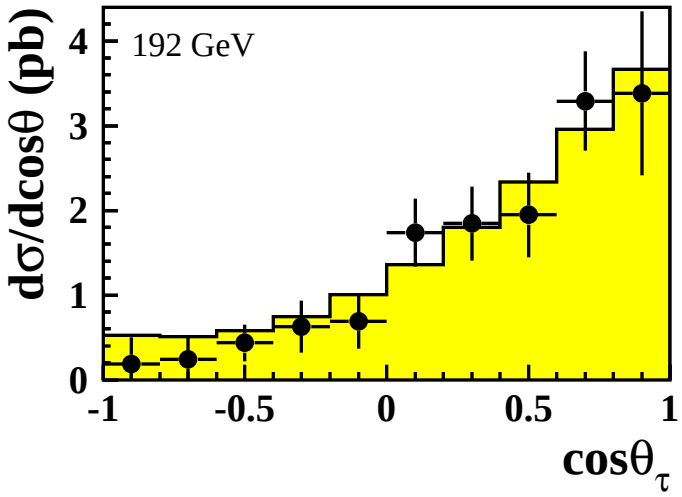

202 GeV
dσ/dcosθ (pb)
cosθμ

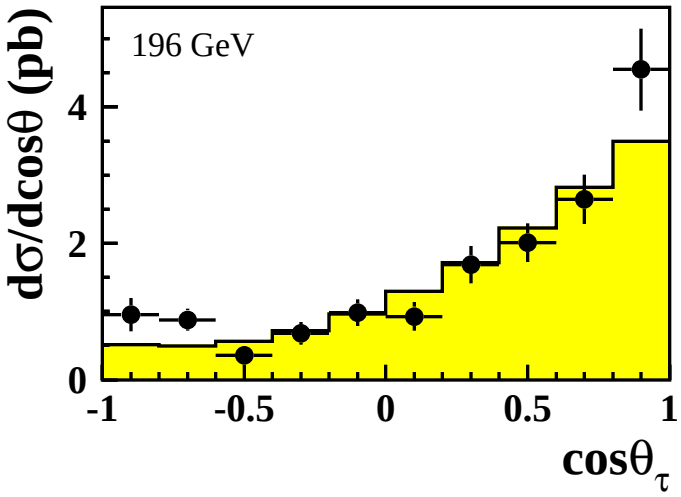

205 GeV
dσ/dcosθ (pb)
cosθμ

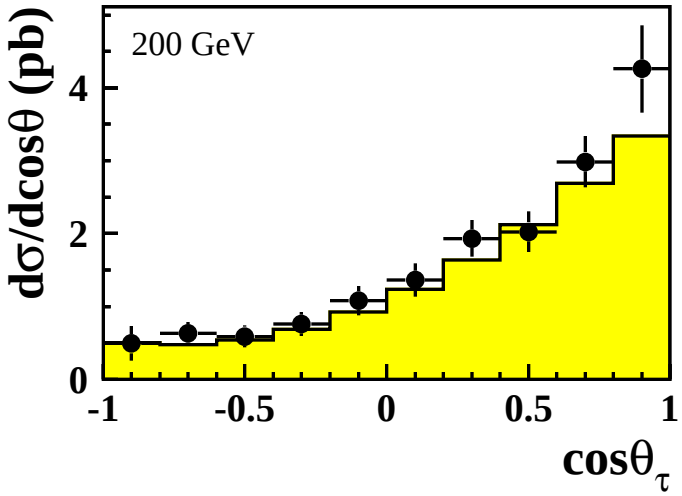

207 GeV
dσ/dcosθ (pb)
cosθμ

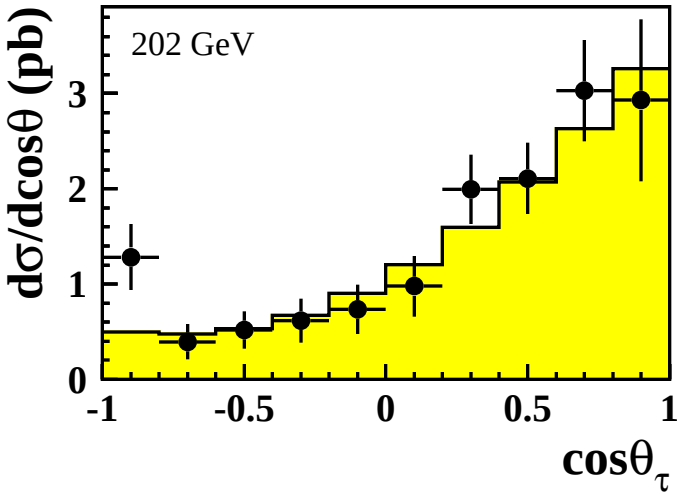

183 GeV
dσ/dcosθ (pb)
cosθτ

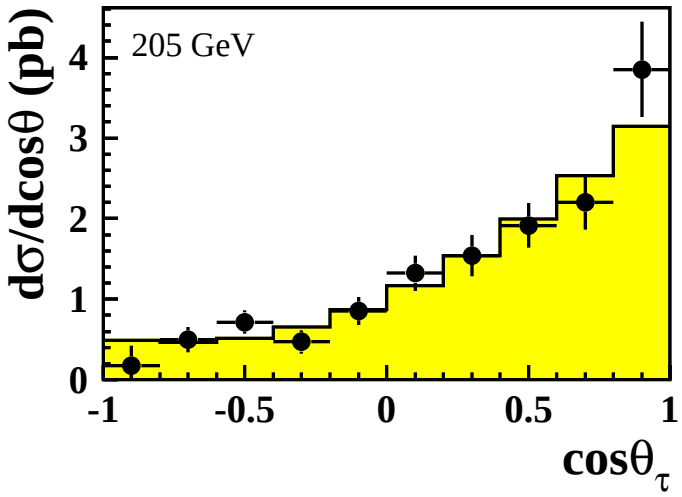

189 GeV
dσ/dcosθ (pb)
cosθτ

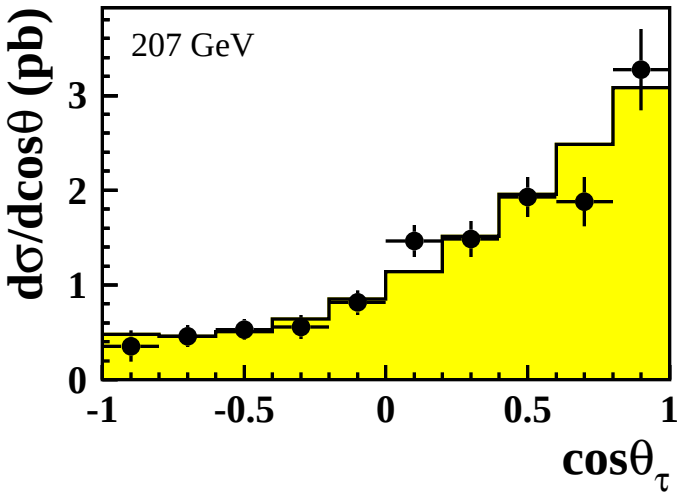

192 GeV
dσ/dcosθ (pb)
cosθτ

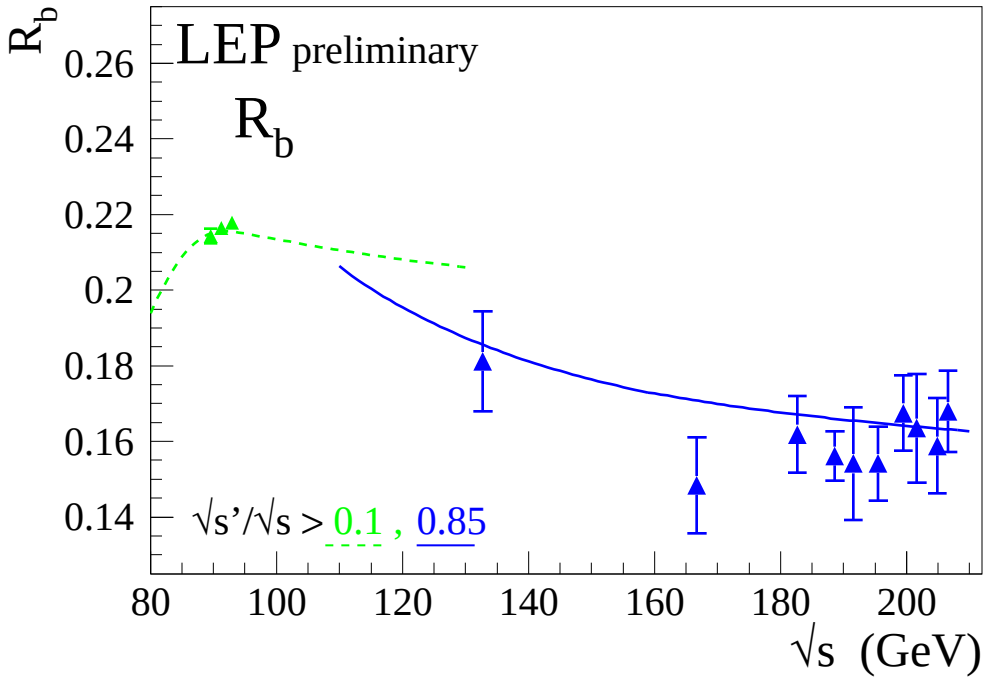

196 GeV
dσ/dcosθ (pb)
cosθτ

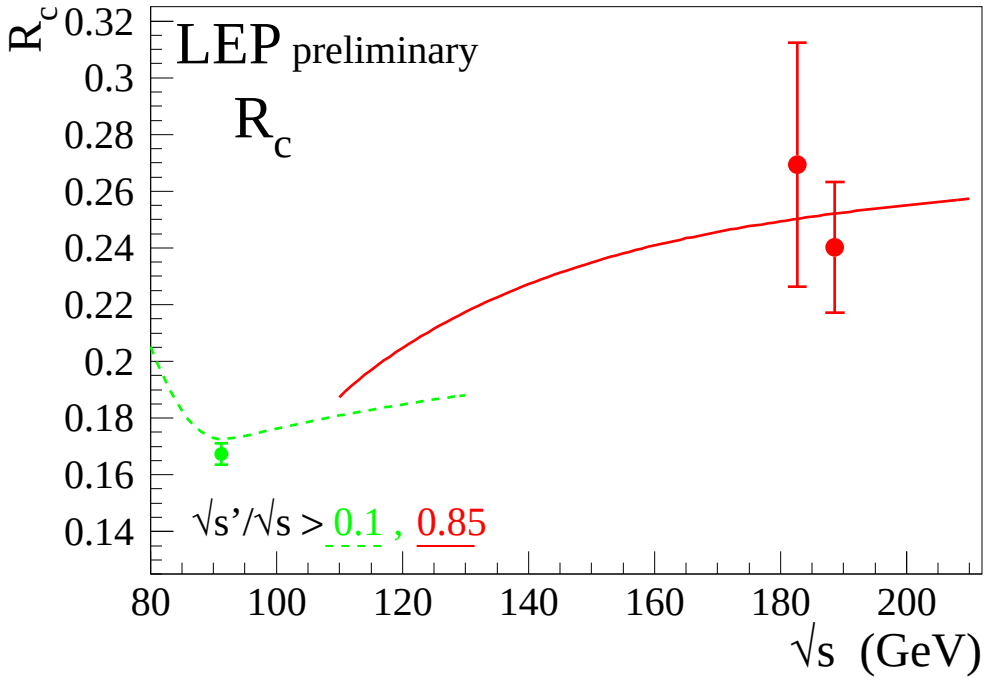

200 GeV
dσ/dcosθ (pb)
cosθτ

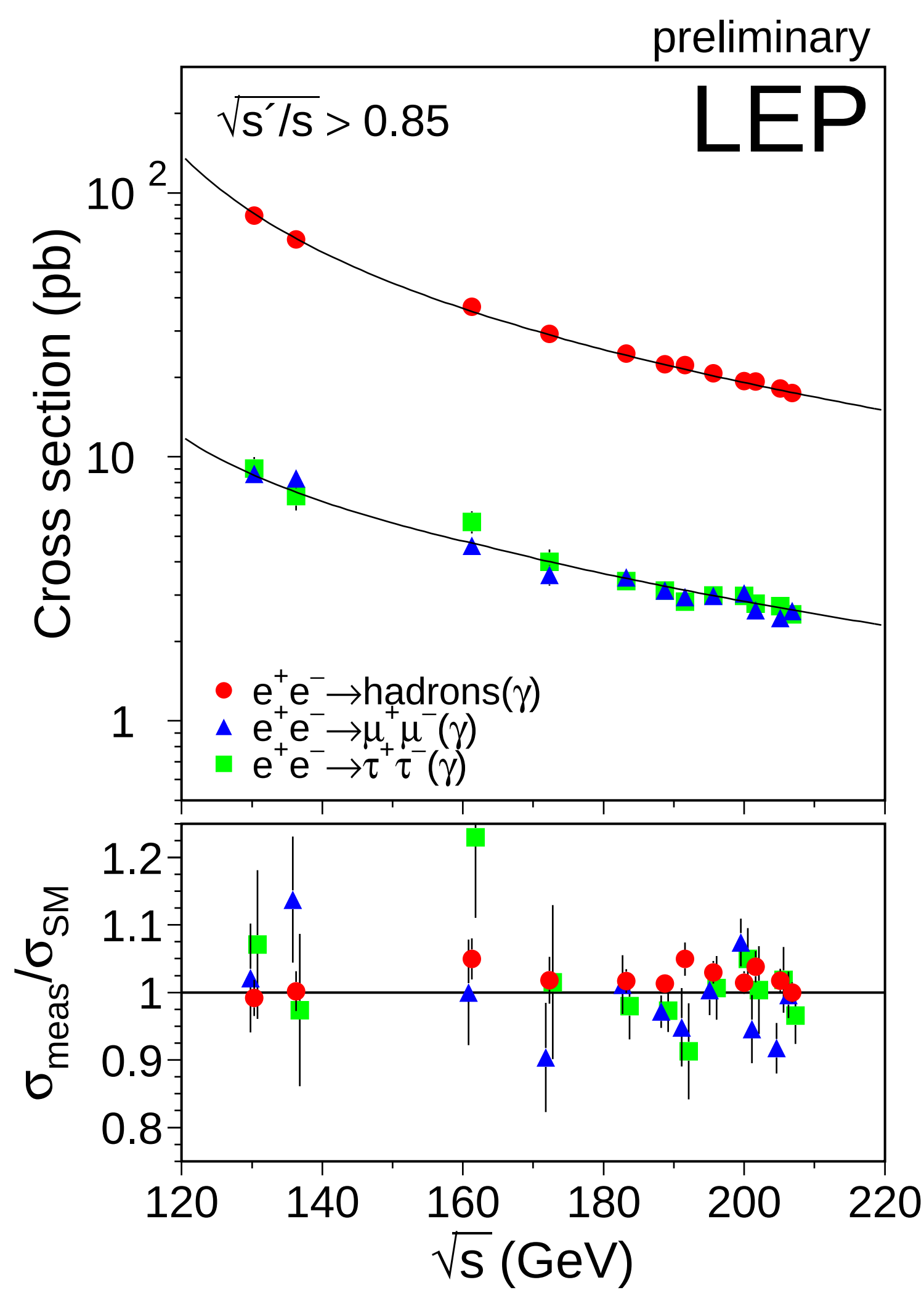

202 GeV
dσ/dcosθ (pb)
cosθτ

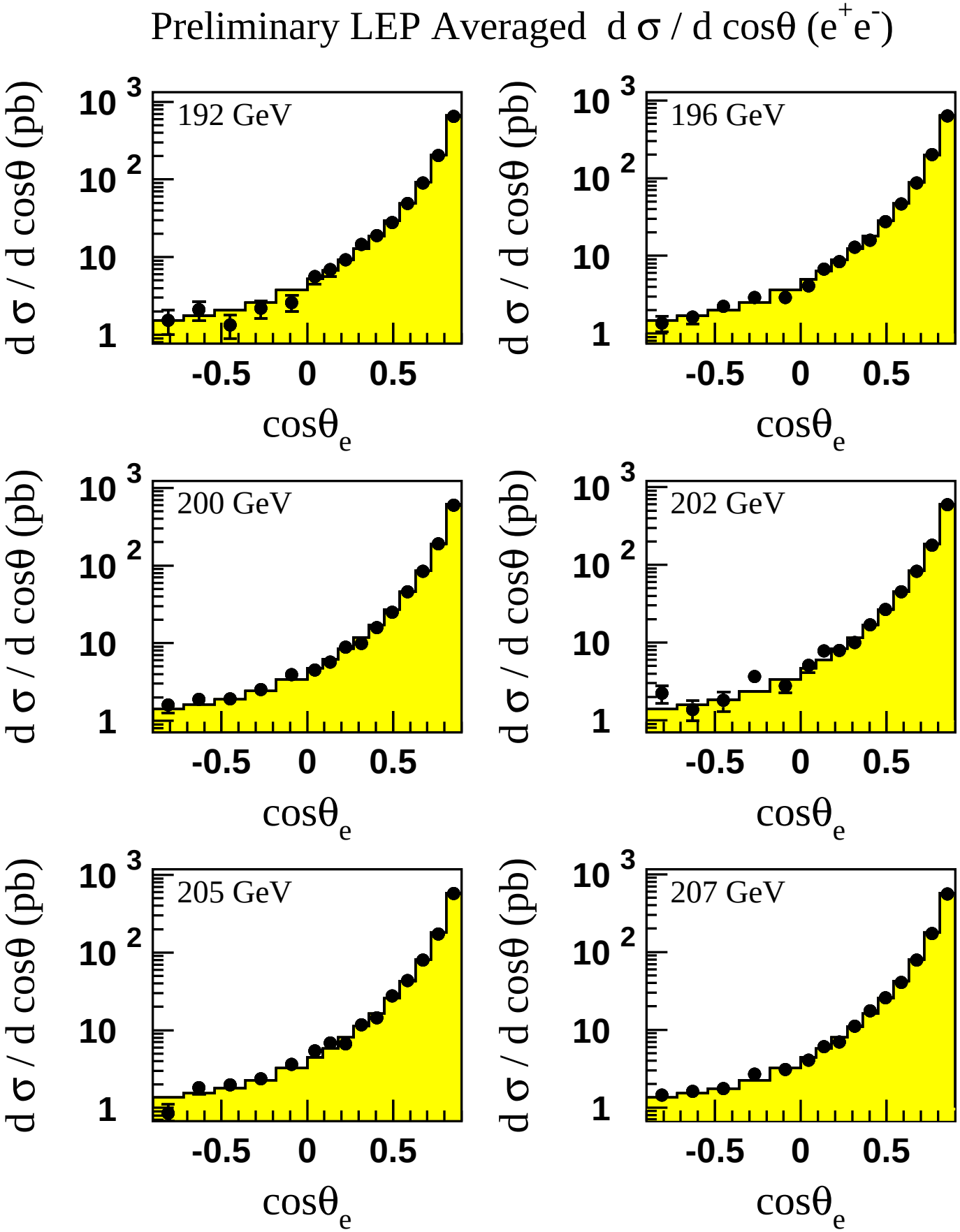

205 GeV
dσ/dcosθ (pb)
cosθτ

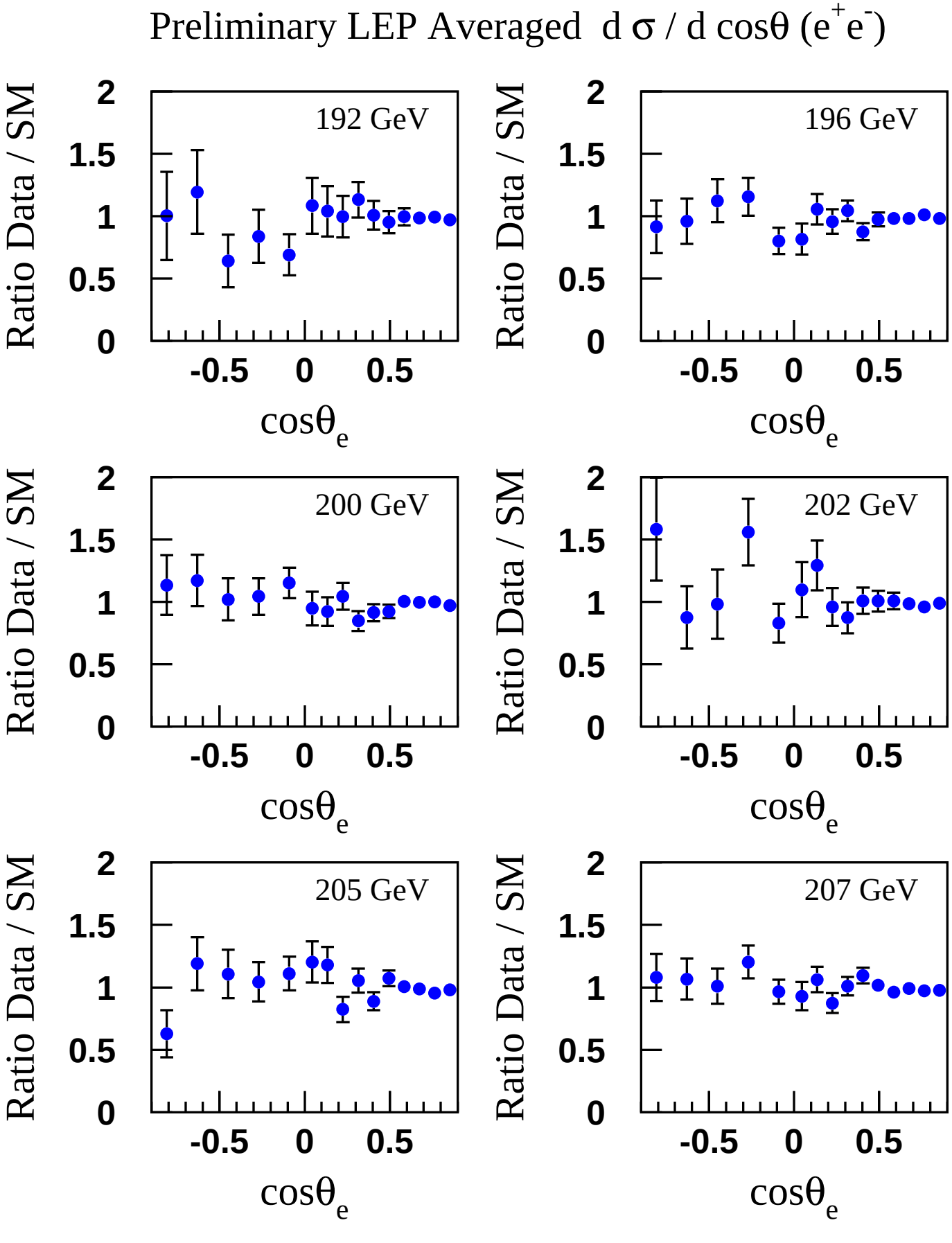

207 GeV
dσ/dcosθ (pb)
cosθτ

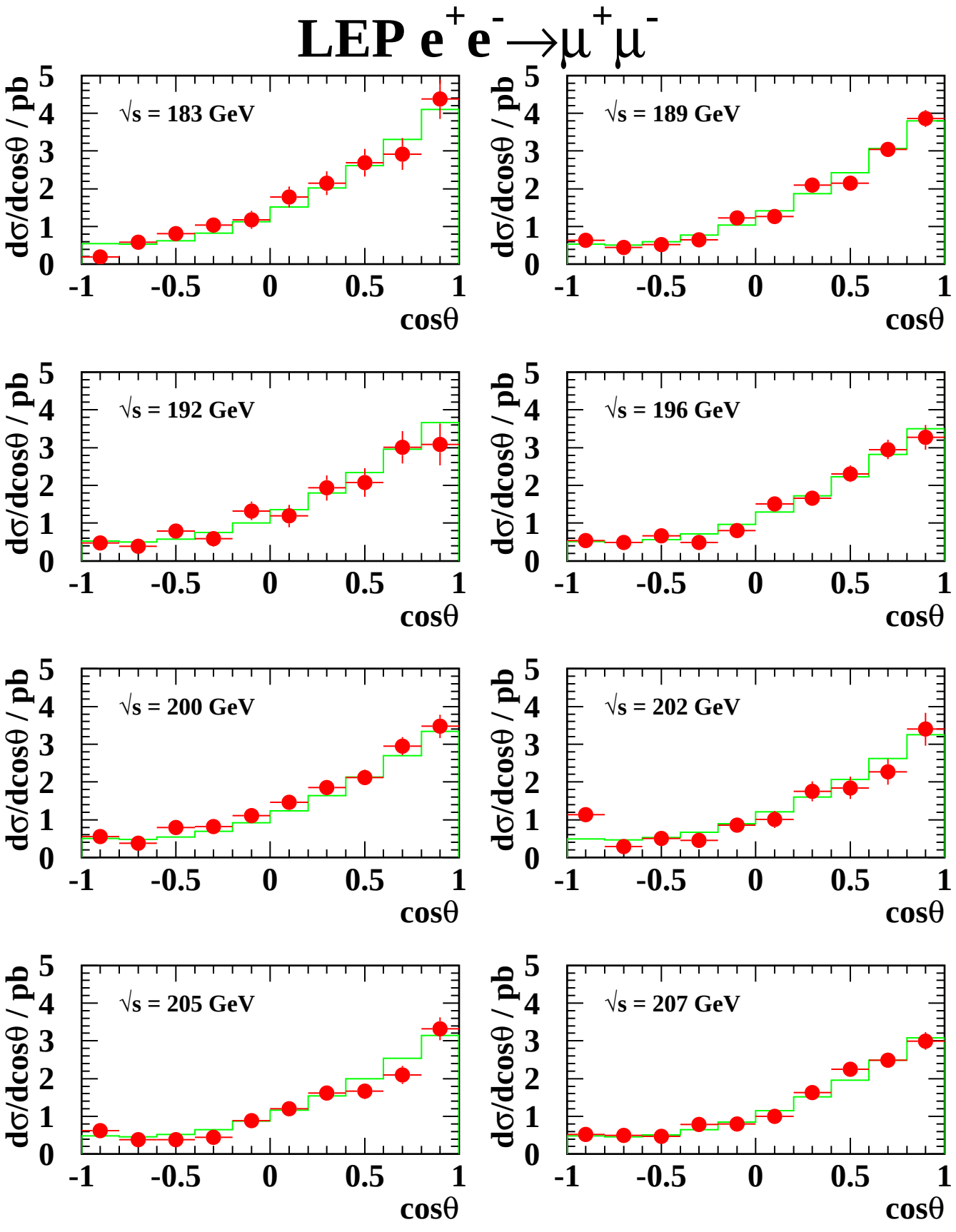

LEP preliminary
R_b
R_b
0.26
0.24
0.22
0.2
0.18
0.16
0.14
√s'/√s > 0.1 , 0.85
80
100
120
140
160
180
200
√s (GeV)

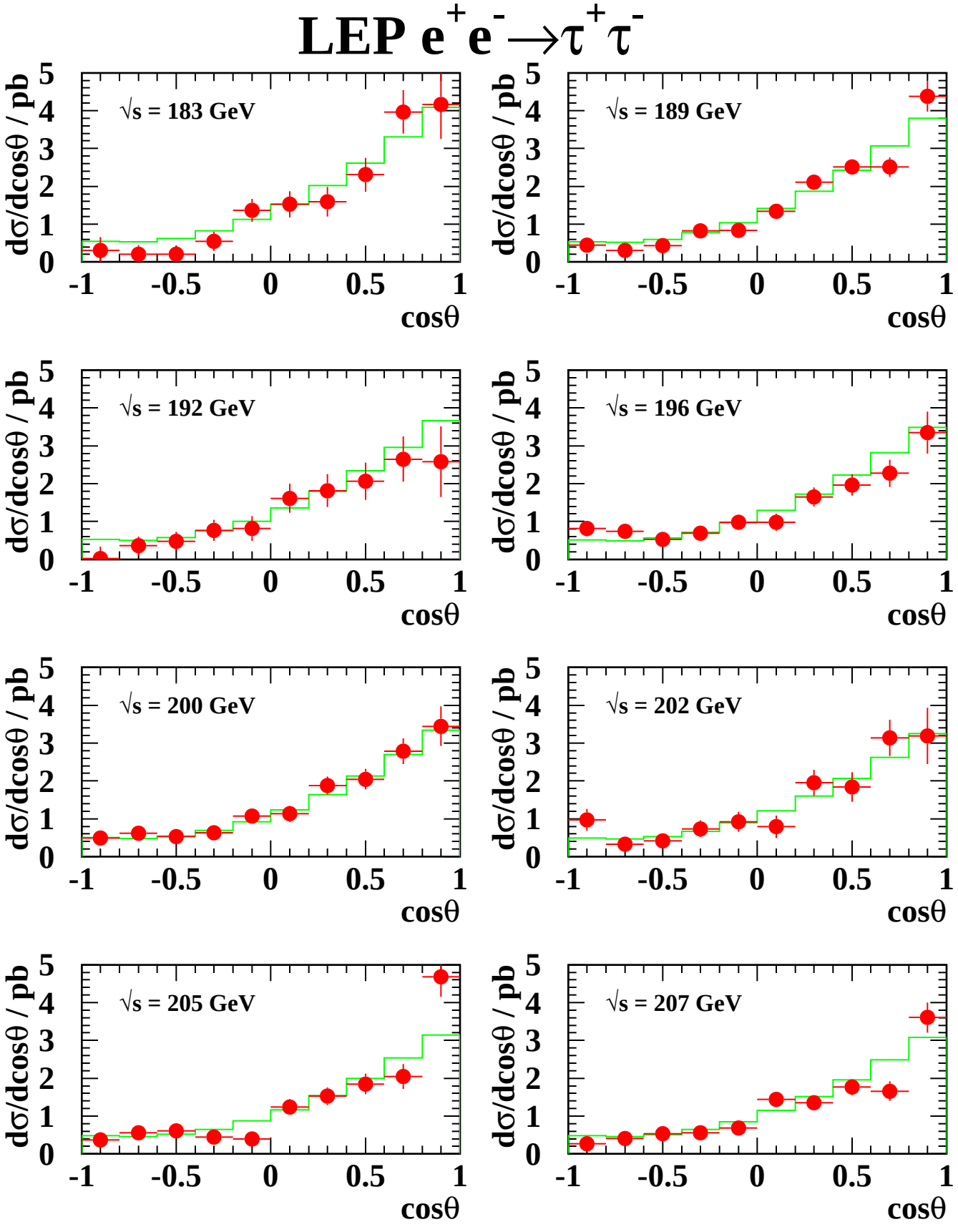

LEP preliminary
R_c
R_c
0.32
0.3
0.28
0.26
0.24
0.22
0.2
0.18
0.16
0.14
√s'/√s > 0.1 , 0.85
80
100
120
140
160
180
200
√s (GeV)

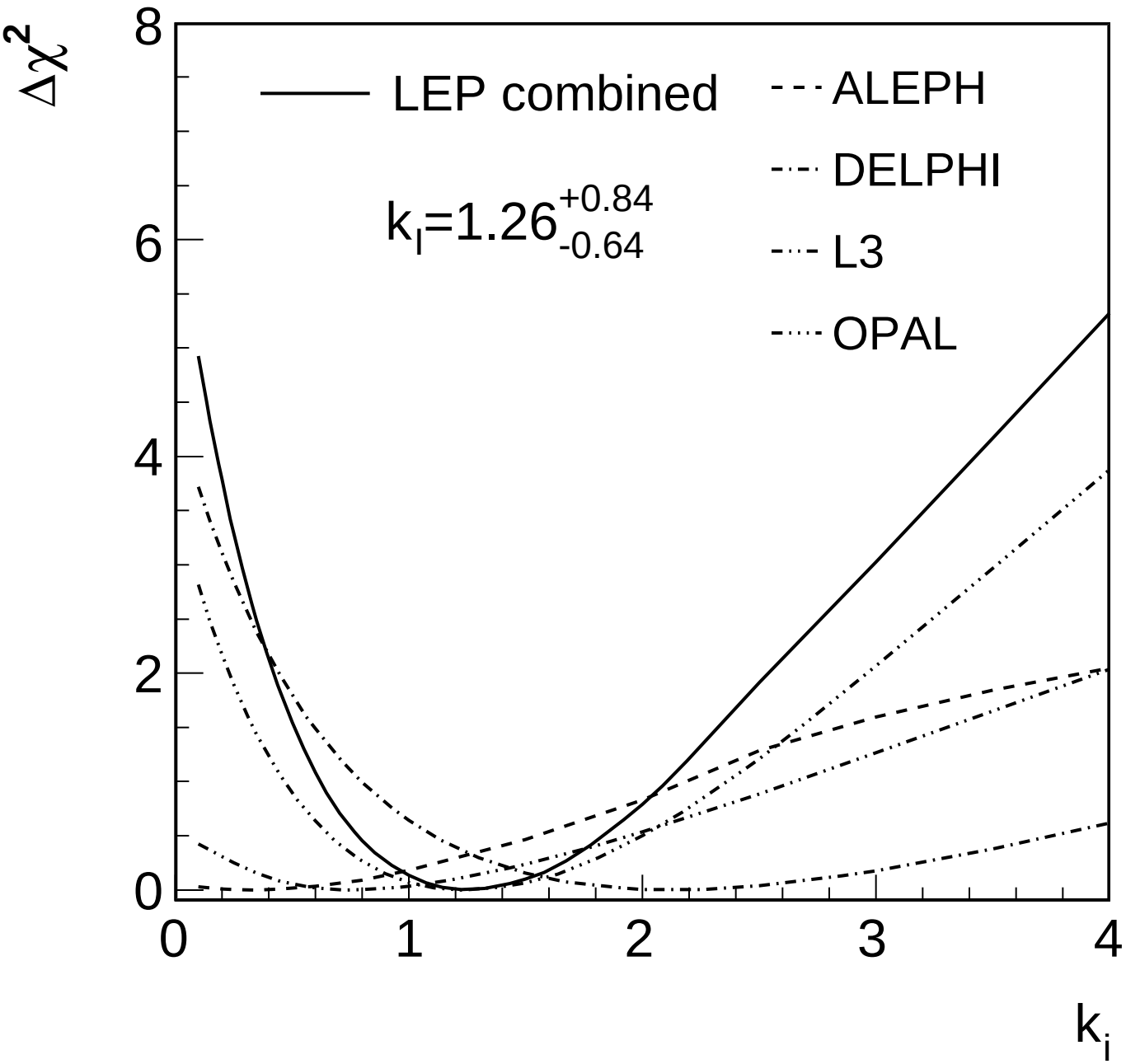

preliminary
LEP
$\sqrt{s'/s} > 0.85$
Cross section (pb)
10^2
10
1
$e^+e^- \to \text{hadrons}(\gamma)$
$e^+e^- \to \mu^+\mu^-(\gamma)$
$e^+e^- \to \tau^+\tau^-(\gamma)$
$\sigma_{meas}/\sigma_{SM}$
1.2
1.1
1
0.9
0.8
120
140
160
180
200
220
$\sqrt{s}$ (GeV)

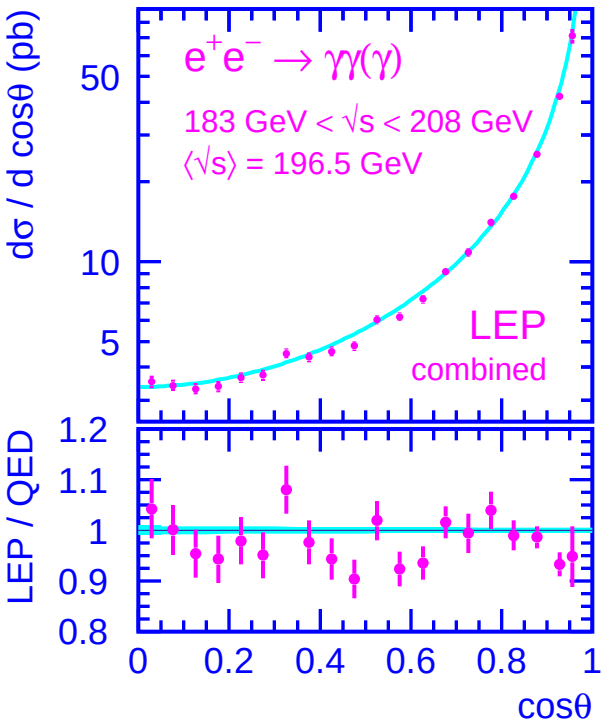

Preliminary LEP Averaged d σ / d cosθ (e+e-)
d σ / d cosθ (pb)
192 GeV
196 GeV
200 GeV
202 GeV
205 GeV
207 GeV
cosθe
10 3
10 2
10
1
-0.5
0
0.5

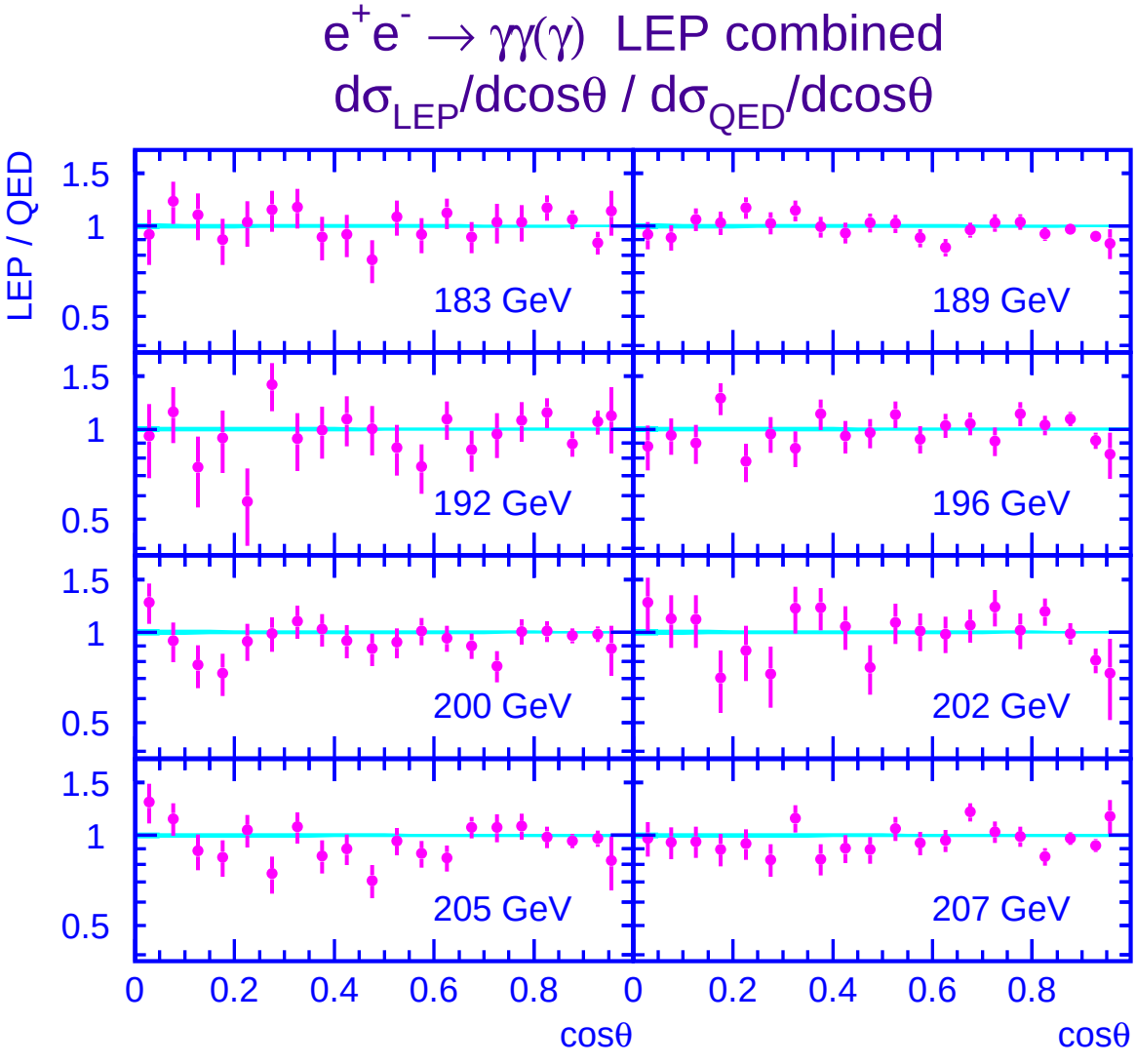

Preliminary LEP Averaged d σ / d cosθ (e+e-)
Ratio Data / SM
192 GeV
196 GeV
200 GeV
202 GeV
205 GeV
207 GeV
cosθe
2
1.5
1
0.5
0
-0.5
0
0.5

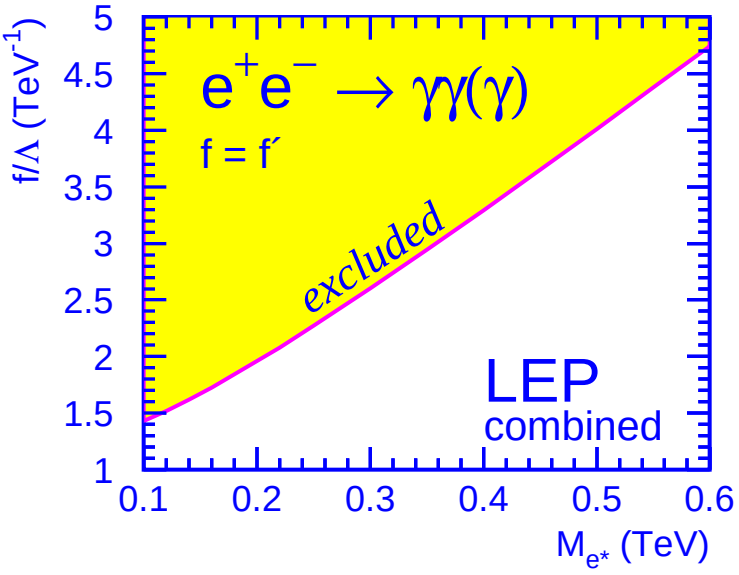

LEP e+e-→μ+μ-
√s = 183 GeV
√s = 189 GeV
√s = 192 GeV
√s = 196 GeV
√s = 200 GeV
√s = 202 GeV
√s = 205 GeV
√s = 207 GeV
dσ/dcosθ / pb
cosθ
0
1
2
3
4
5
-1
-0.5
0
0.5
1

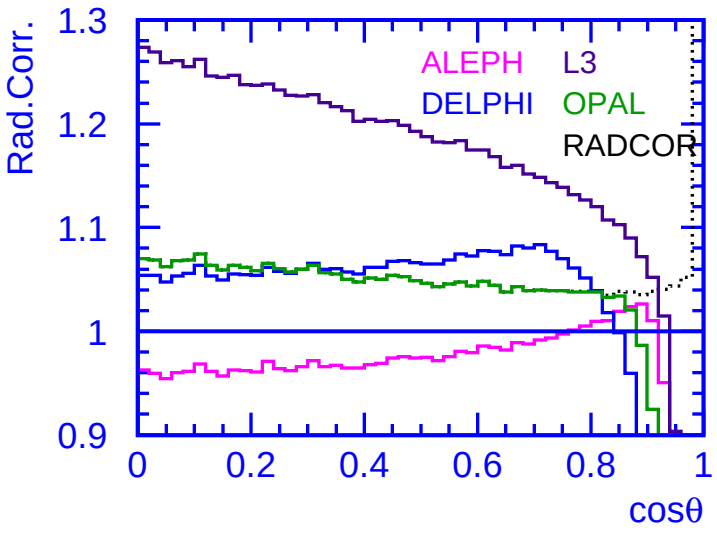

LEP e+e-→τ+τ-
√s = 183 GeV
√s = 189 GeV
√s = 192 GeV
√s = 196 GeV
√s = 200 GeV
√s = 202 GeV
√s = 205 GeV
√s = 207 GeV
dσ/dcosθ / pb
cosθ
0
1
2
3
4
5
-1
-0.5
0
0.5
1

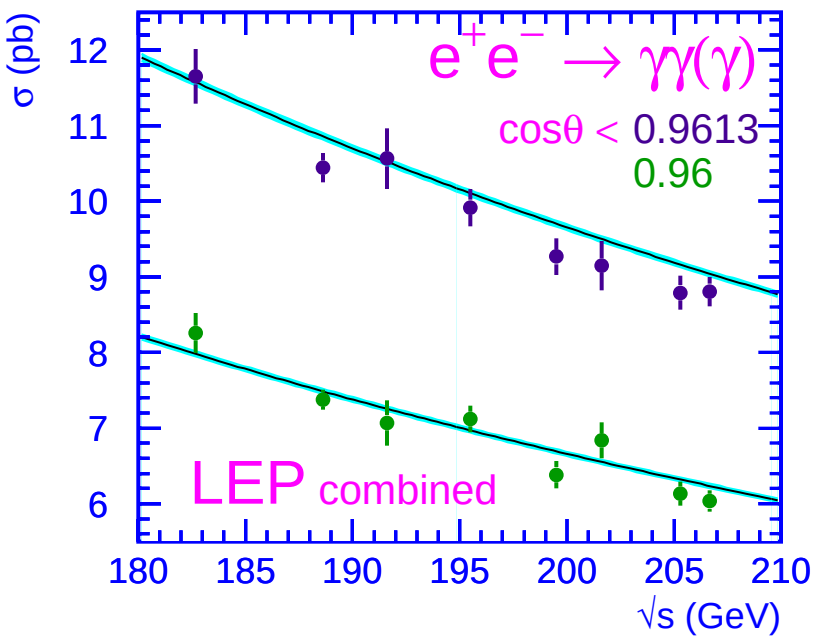

$\Delta\chi^2$
8
6
4
2
0
0
1
2
3
4
k_i
LEP combined
$k_l=1.26^{+0.84}_{-0.64}$
ALEPH
DELPHI
L3
OPAL

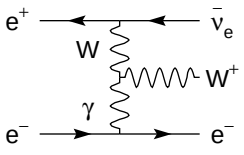

$e^+e^- \to \gamma\gamma(\gamma)$
183 GeV < √s < 208 GeV
⟨√s⟩ = 196.5 GeV
LEP
combined
dσ / d cosθ (pb)
50
10
5
LEP / QED
1.2
1.1
1
0.9
0.8
0
0.2
0.4
0.6
0.8
1
cosθ

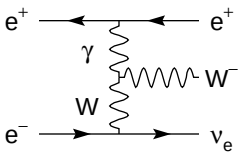

$e^+e^- \to \gamma\gamma(\gamma)$ LEP combined
$d\sigma_{LEP}/d\cos\theta$ / $d\sigma_{QED}/d\cos\theta$
LEP / QED
183 GeV
189 GeV
192 GeV
196 GeV
200 GeV
202 GeV
205 GeV
207 GeV
cosθ
cosθ


$e^+e^- \to \gamma\gamma(\gamma)$
f = f´
excluded
LEP
combined
f/Λ (TeV^{-1})
M_{e^*} (TeV)
5
4.5
4
3.5
3
2.5
2
1.5
1
0.1
0.2
0.3
0.4
0.5
0.6


Rad.Corr.
1.3
1.2
1.1
1
0.9
0
0.2
0.4
0.6
0.8
1
cosθ
ALEPH
L3
DELPHI
OPAL
RADCOR


σ (pb)
12
11
10
9
8
7
6
180
185
190
195
200
205
210
√s (GeV)
e+e− → γγ(γ)
cosθ < 0.9613
0.96
LEP combined


e+
ν̄e
W
W+
γ
e−
e−


e+
e+
γ
W−
W
e−
νe